Springer Proceedings in Physics 219

Alba Formicola
Matthias Junker
Lucio Gialanella
Gianluca Imbriani *Editors*

Nuclei in the Cosmos XV

Springer

Springer Proceedings in Physics

Volume 219

Indexed by Scopus. The series Springer Proceedings in Physics, founded in 1984, is devoted to timely reports of state-of-the-art developments in physics and related sciences. Typically based on material presented at conferences, workshops and similar scientific meetings, volumes published in this series will constitute a comprehensive up-to-date source of reference on a field or subfield of relevance in contemporary physics. Proposals must include the following:

- name, place and date of the scientific meeting
- a link to the committees (local organization, international advisors etc.)
- scientific description of the meeting
- list of invited/plenary speakers
- an estimate of the planned proceedings book parameters (number of pages/articles, requested number of bulk copies, submission deadline).

More information about this series at http://www.springer.com/series/361

Alba Formicola · Matthias Junker ·
Lucio Gialanella · Gianluca Imbriani
Editors

Nuclei in the Cosmos XV

Springer

Editors
Alba Formicola
Laboratori Nazionali del Gran Sasso
Istituto Nazionale di Fisica Nucleare
L'Aquila, Italy

Matthias Junker
Laboratori Nazionali del Gran Sasso
Istituto Nazionale di Fisica Nucleare
L'Aquila, Italy

Lucio Gialanella
Dipartimento di Matematica e Fisica
Università degli Studi della Campania
"Luigi Vanvitelli"
Caserta, Italy

Gianluca Imbriani
Dipartimento di Fisica "E. Pancini"
Università degli Studi di Napoli "Federico II"
Napoli, Italy

ISSN 0930-8989 ISSN 1867-4941 (electronic)
Springer Proceedings in Physics
ISBN 978-3-030-13875-2 ISBN 978-3-030-13876-9 (eBook)
https://doi.org/10.1007/978-3-030-13876-9

Library of Congress Control Number: 2019935995

This Springer imprint is published by the registered company Springer Nature Switzerland AG
The registered company address is: Gewerbestrasse 11, 6330 Cham, Switzerland

Committees

International Advisory Committee

A. Aprahamian, University of Notre Dame, USA
C. Brofferio, University of Milano-Bicocca and INFN, Italy
M. Busso, University of Perugia and INFN, Italy
S. DeglInnocenti, University of Pisa and INFN, Italy
R. Diehl, MPE-MPG, Germany
A. L. Frebel, Massachusetts Institute of Technology, USA
Z. Flp, MTA ATOMKI, Hungary
L. Gialanella, University of Campania Luigi Vanvitelli and INFN, Italy
A. Guglielmetti, University of Milano-Bicocca and INFN, Italy
J. José, Universitat Politècnica de Catalunya, Spain
M. Junker, INFN LNGS, Italy
T. Kajino, NAO, University of Tokyo, Japan
W. Liu, China Institute of Atomic Energy, China
M. Lugaro, Konkoly Observatory, Hungary
F. Matteucci, INAF-OATs, Italy
R. Reifarth, Goethe University Frankfurt, Germany
H. Schatz, Michigan State University, USA
C. Spitaleri, University of Catania and INFN, Italy
O. Straniero, INAF-OATe, Italy
F. K. Thielemann, University of Basel, Switzerland
C. Travaglio, INAF-OATo, Italy
R. Tribble, Texas A&M University, USA
M. Wiescher, University of Notre Dame, USA
P. J. Woods, University of Edinburgh, UK

International Program Committee

N. Colonna, INFN-Bari, Italy
M. Couder, University of Notre Dame, USA
P. Descouvemont, Université Libre de Bruxelles, Belgium
A. Di Leva, University of Naples Federico II and INFN, Italy
I. Dillmann, TRIUMF, Canada
I. Domnguez, Universidad de Granada, Spain
A. Formicola, INFN LNGS, Italy
S. Kubono, RIKEN Nishina Center, Japan
L. E. Marcucci, University of Pisa and INFN, Italy
O. Sorlin, GANIL, France
F. Strieder, South Dakota School of Mines & Technology, USA
A. Tumino, Kore University of Enna and INFN, Italy

Organizing Committee

A. Formicola, Chair, INFN LNGS
M. Junker, Vice-chair, INFN LNGS
F. Cavanna, INFN Genova
G. F. Ciani, GSSI
L. Csedreki, INFN LNGS
R. Depalo, INFN Padova
L. Gialanella, University of Campania Luigi Vanvitelli and INFN
I. Kochanek, INFN LNGS
G. Imbriani, University of Naples Federico II and INFN
F. Chiarizia, Secretary, INFN LNGS

Foreword

The symposium *NUCLEI IN THE COSMOS 2018* was held at the Laboratori Nazionali del Gran Sasso (LNGS), L'Aquila—Assergi, Italy, from June 24 to 29, 2018. Already in 1994, LNGS had hosted a *NUCLEI IN THE COSMOS* symposium. So, LNGS is honored to be the first location chosen to host this conference two times. Starting from the pilot meeting in Greece (1988), the series of international conference on *NUCLEI IN THE COSMOS* has been organized in Australia, Austria, Denmark, Hungary, Italy, Japan, Germany, Greece and Switzerland to discuss topics at the crossroads of astronomy, astrophysics and nuclear physics. In this XV edition, 197 researches from 29 countries participated to conference, 153 of which traveled in from outside the host country. Thus, the NIC XV program consisted of 25 invited review talks, 48 selected oral and 110 poster contributions on important experimental and theoretical results in nuclear, particle and astrophysics researches, as well as a detailed and thorough exposition of the modern challenges in nuclear astrophysical scenarios.

The conference program aimed to address the current major achievements in nuclear physics, astrophysics, astronomy, cosmochemistry and neutrino physics that provide the necessary framework for any microscopic understanding of astrophysical processes, as well as for discussing the future directions and perspectives in the various fields of nuclear astrophysics research. The scientific program covered specific sessions on cosmology and Big Bang nucleosynthesis, stellar contributions to the chemical evolution, hydrostatic and explosive nucleosynthesis, neutrino and nucleus interaction in the cosmos, physics of nuclei far from stability, synthesis of heavy elements, direct observation of nucleosynthesis in stars, study of extraterrestrial materials, nucleosynthesis in extreme environments, techniques, tools and facilities for nuclear astrophysics and nuclear data for astrophysical applications.

In addition, a limited number of contributions on the special topic "particle astrophysics and rare events in cosmos" provided the possibility to explore the interface between nuclear astrophysics and astroparticle physics.

To encourage the attendance of young physicists, the support was granted to 19 undergraduate and graduate students without Ph.D. status or young postdocs. The five best poster presentations delivered by graduate and undergraduate students were selected and rewarded during the conference by a dedicated committee.

NUCLEI IN THE COSMOS 2018 was the fifteenth symposium of the series, and Prof. Karl-Friedel Thielemann contributed with Special Lecture entitled "explosive nucleosynthesis: what we learned and what we still did not understand" to review the incredible story of success of this series of conferences.

As in previous editions, also *NUCLEI IN THE COSMOS 2018* was complemented by two dedicated satellite events: the NIC XV "School on Experimental and Theoretical Methods in Nuclear Astrophysics with Applications" and the NIC XV Workshop "Core-collapse Supernovae in the Multi-messenger Era (CCSN 2018)."

The "*School on Experimental and Theoretical Methods in Nuclear Astrophysics with Applications*" (http://www.circe.unicampania.it/index.php/special-events/nic-2018-satellite-school) was held in Caserta, Italy, from June 18 to 22, 2018. It was geared toward graduate students, but advanced undergraduate students as well as postdocs were also admitted. A total of 26 students from 10 countries and 3 continents attended the school.

The first two days were devoted to introductory lectures. In the following days, students split in groups to perform one out of four possible hands-on stages on nuclear reaction cross sections using ERNA ("European Recoil Separator for Nuclear Astrophysics") at the 3MV tandem laboratory (convener: R. Buompane), measurements of isotopic ratios in meteorites at the ICP-MS laboratory (convener: S. Palmerini), model calculations, nuclear cross sections and comparison to observations in stellar evolution and nucleosynthesis (convener: L. Piersanti) and data analysis in the context of the Trojan Horse method (convener: M. La Cognata).

The school took place in a constructive atmosphere, where the different scientific backgrounds and even cultural diversity became opportunities for mutual enrichment. The dedicated Scientific Committee included A. Di Leva, A. Formicola, L. Gialanella (Chair), F. Marzaioli, P. Migliozzi, H. Schatz, O. Straniero, F. Strieder and A. Tumino. It was organized by the University of Campania "Luigi Vanvitelli," supported by INFN and JINA and sponsored by CAEN. Lectures and hands-on stages were held by the staff of different universities/research institutes: INAF, INFN, South Dakota School of Mines & Technology, universities of Bologna, Campania, Catania, Naples and Perugia.

The workshop "*Core-collapse Supernovae in the Multi-messenger Era (CCSN 2018)*" was organized from July 2 to 3, 2018, at the GSSI as a second satellite event of the NIC XV conference (http://ccsn2018.0a-teramo.inaf.it). It has been planned considering that even though core-collapse supernovae are events of key relevance in the cosmos their understanding is still rather limited. This poses many unanswered questions with multidisciplinary character to the scientific community.

The workshop was enthusiastically attended by a very wide and varied scientific community, including astronomers and astrophysicists, particle and nuclear physicists, experimentalists and theorists. The field has shown to be lively, and the debates have seen intense participation. It offered occasions of new collaborations

and works and important progresses have been announced. *CCSN 2018* was organized jointly by the GSSI—Gran Sasso Science Institute, INAF—Osservatorio Astronomico d'Abruzzo and INFN—Laboratori Nazionali del Gran Sasso. The Organizing Committee of the workshop was chaired by Oscar Straniero and Francesco Vissani and included Marica Branchesi, Marco Drago, Matthias Junker, Chris Fryer, Ewald Muller, Massimo della Valle and Diego Vescovi.

NUCLEI IN THE COSMOS 2018 has been made possible thanks to the engagement of all those colleagues who served in the International Advisory and Program Committees as well of the Organizing Committee. A special thank is addressed to Fausto Chiarizia for his efficiency in the logistic and the secretary organization, we are also like to thank Alessio Attardi, as well as Aurora Galimi, Valeria La Speme, Chiara Ruggeri and Alessandro Serafini ("Liceo Pasteur" high school in Rome).

The conference and satellite events received support by INFN, Università degli Studi della Campania "Luigi Vanvitelli," GSSI, JINA-CEE, IUPAP and EPS. We are grateful to High Voltage Engineering Europe and Springer Nature who sponsored the conference, too.

L'Aquila, Italy — Alba Formicola
L'Aquila, Italy — Matthias Junker
Caserta, Italy — Lucio Gialanella
Napoli, Italy — Gianluca Imbriani

Contents

Contributors

K. Abe Center for Nuclear Study, University of Tokyo, Wako, Japan

O. Aberle European Organization for Nuclear Research (CERN), Meyrin, Switzerland

Carlos Abia Dpto. Física Teórica y del Cosmos, Universidad de Granada, Granada, Spain

P. Adsley Institut de Physique Nucléaire, IN2P3/CNRS-Université de Paris XI, Orsay Cedex, France;
Institut Physique Nucléaire dOrsay, UMR8608, CNRS-IN2P3, Universite Paris Sud 11, Orsay, France

J. Agramunt Instituto de Fisica Corpuscular (CSIC-Univ. de Valencia), Paterna, Spain

D. S. Ahn RIKEN Nishina Center, Wako, Saitama, Japan

V. Alcayne Centro de Investigaciones Energéticas Medioambientales y Tecnológicas (CIEMAT), Madrid, Spain

B. Alex Brown National Superconducting Cyclotron Laboratory, Michigan State University, East Lansing, MI, USA;
Joint Institute for Nuclear Astrophysics: Center for the Evolution of the Elements, Michigan State University, East Lansing, MI, USA;
Department of Physics and Astronomy, Michigan State University, East Lansing, MI, USA

A. Algora Instituto de Fisica Corpuscular (CSIC-Univ. de Valencia), Paterna, Spain;
Institute of Nuclear Research of the Hungarian Academy of Sciences, Debrecen, Hungary

Marialuisa Aliotta SUPA, School of Physics and Astronomy, University of Edinburgh, Edinburgh, UK

S. Altstadt Johann-Wolfgang-Goethe Universitat, Frankfurt, Germany

S. Amari McDonnell Center for the Space Sciences and Physics Department, Washington University, St. Louis, MO, USA

Robert Andrassy Joint Institute for Nuclear Astrophysics, Center for the Evolution of the Elements, Michigan State University, East Lansing, MI, USA; Heidelberg Institute for Theoretical Studies, Heidelberg, Germany

J. Andrzejewski University of Lodz, Lodz, Poland

M. Anger Department of Physics, Technical University Munich, Garching, Germany

W. David Arnett Steward Observatory, University of Arizona, Tuscon, USA

Chris Ashall Florida State University, Tallahassee, FL, USA

M. Assié Institut de Physique Nucléaire, IN2P3/CNRS-Université de Paris XI, Orsay Cedex, France;
Institut Physique Nucléaire dOrsay, UMR8608, CNRS-IN2P3, Universite Paris Sud 11, Orsay, France

E.-M. Assimakopoulou Department of Physics, University of Athens, Athens, Greece

M. Assunção Instituto de Física, Universidade de São Paulo, São Paulo, Brazil

L. Audouin Institut de Physique Nucléaire, CNRS-IN2P3, Univ. Paris-Sud, Université Paris-Saclay, Orsay Cedex, France;
Centre National de la Recherche Scientifique/IN2P3 - IPN, Orsay, France

J. Austin Harris National Center for Computational Sciences, Oak Ridge National Laboratory, Oak Ridge, TN, USA

M. Ayranov European Commission, DG-Energy, Luxembourg, Belgium

H. Baba RIKEN Nishina Center, Wako, Saitama, Japan

V. Babiano-Suarez Instituto de Física Corpuscular, CSIC - Universidad de Valencia, Valencia, Spain

A. Babounis Department of Physics, University of Athens, Athens, Greece

M. Bacak European Organization for Nuclear Research (CERN), Meyrin, Switzerland;
CEA Irfu, Université Paris-Saclay, Gif-sur-Yvette, France;
Atominstitut der Osterreichischen Universitaten, Technische Universitat Wien, Vienna, Austria

S. Bae Department of Physics, Seoul National University, Seoul, Republic of Korea

D. Balabanski ELI-NP/IFIN-HH, Bucharest, Romania

J. Balibrea-Correa Università di Napoli "Federico II", and INFN, Napoli, Italy;
Universit degli Studi di Napoli Federico II, Naples, Italy;
Università di Napoli Federico II and INFN, Naples, Italy;
Centro de Investigaciones Energeticas Medioambientales y Tecnolgicas (CIEMAT), Madrid, Spain

J. Ballof European Organization for Nuclear Research (CERN), Meyrin, Switzerland

A. Banu Department of Physics and Astronomy, James Madison University, Harrisonburg, VA, USA

M. Barbagallo European Organization for Nuclear Research (CERN), Meyrin, Switzerland;
Istituto Nazionale di Fisica Nucleare, Sezione di Bari, Italy;
INFN, Sezione di Bari, Dipartimento di Fisica, Bari, Italy

B. Bastin Grand Accélérateur National d'Ions Lourds (GANIL), CEA/DRFCNRS/IN2P3, Bvd. Henri Becquerel, Caen, France

Umberto Battino University of Edinburgh, Edinburgh, UK

V. Bcares Centro de Investigaciones Energeticas Medioambientales y Tecnolgicas (CIEMAT), Madrid, Spain

D. Beaumel Institut de Physique Nucléaire, IN2P3/CNRS-Université de Paris XI, Orsay Cedex, France;
Institut Physique Nucléaire dOrsay, UMR8608, CNRS-IN2P3, Universite Paris Sud 11, Orsay, France

V. Bécares Centro de Investigaciones Energéticas Medioambientales y Tecnológicas (CIEMAT), Madrid, Spain

B. Becherini Department of Physics and Geology, University of Perugia, Perugia, Italy;
Section of Perugia, INFN, Perugia, Italy

F. Bečvař Charles University, Prague, Czech Republic

C. Beinrucker Johann-Wolfgang-Goethe Universitat, Frankfurt, Germany

O. Beliuskina Center for Nuclear Study, University of Tokyo, Wako, Japan

G. Bellia INFN - Laboratori Nazionali del Sud, Catania, Italy;
Dipartimento di Fisica e Astronomia, Universit di Catania, Catania, Italy

F. L. Bello Garrote Department of Physics, University of Oslo, Oslo, Norway

D. Bemmerer Helmholtz-Zentrum Dresden-Rossendorf (HZDR), Dresden, Germany

Th. Benedikt Goethe University Frankfurt, Frankfurt, Germany

Á. M. Sánchez Benítez Grand Accélérateur National d'Ions Lourds (GANIL), CEA/DRFCNRS/IN2P3, Bvd. Henri Becquerel, Caen, France;
Departamento de Ciencias Integradas, University of Huelva, Huelva, Spain

S. Bennett University of Manchester, Manchester, UK

A. P. Bernardes European Organization for Nuclear Research (CERN), Meyrin, Switzerland

K. Béroff Institut des Sciences Moléculaires d'Orsay (ISMO), UMR 8214, CNRS, Université Paris Sud, Orsay, France

E. Berthoumieux CEA Irfu, Université Paris-Saclay, Gif-sur-Yvette, France;
CEA/Saclay - IRFU, Gif-sur-Yvette, France

C. A. Bertulani Department of Physics, Tohoku University, Sendai, Japan;
Texas A&M University-Commerce, Commerce, TX, USA

A. Best Università di Napoli "Federico II", and INFN, Napoli, Italy;
Universit degli Studi di Napoli Federico II, Naples, Italy;
Università di Napoli Federico II and INFN, Sezione di Napoli, Strada Comunale Cinthia, Napoli, Italy

J. Billowes University of Manchester, Manchester, UK

S. Bishop Department of Physics, Technical University Munich, Garching, Germany

Axel Boeltzig Department of Physics, University of Notre Dame, Notre Dame, IN, USA

A. Boiano INFN-Sezione di Napoli, Napoli, Italy

C. Boiano Center for Nuclear Study, University of Tokyo, Tokyo, Japan

M. J. G. Borge European Organization for Nuclear Research (CERN), Meyrin, Switzerland

Tyler Borgwardt Department of Physics, South Dakota School of Mines & Technology, Rapid City, SD, USA

D. Bosnar Department of Physics, Faculty of Science, University of Zagreb, Zagreb, Croatia

Lukas Bott Goethe University Frankfurt, Frankfurt, Germany

N. T. Brewer Physics Division, Oak Ridge National Laboratory, Oak Ridge, TN, USA

H. E. Brinkman Konkoly Observatory, Research Centre for Astronomy and Earth Sciences, Hungarian Academy of Sciences, Budapest, Hungary

Carlo Broggini INFN - Sezione di Padova, Padova, Italy

O. E. Bronson Messer Physics Division, Oak Ridge National Laboratory, Oak Ridge, TN, USA;
National Center for Computational Sciences, Oak Ridge National Laboratory, Oak Ridge, TN, USA

A. Brown University of York, York, UK

Benjamin Brückner Goethe University Frankfurt, Frankfurt, Germany

Stephen Bruenn Department of Physics, Florida Atlantic University, Boca Raton, FL, USA

M. Brugger European Organization for Nuclear Research (CERN), Meyrin, Switzerland

C. Bruno University of Edinburgh, Edinburgh, United Kingdom

V. Burjan Ústav jaderné fyziky AV ČR, v.v.i, Řež, Czech Republic

Maurizio Busso Istituto Nazionale di Fisica Nucleare, Sezione di Perugia, Italy;
Dipartimento di Fisica e Geologia, Università di Perugia, Perugia, Italy

M. Caamaño Universidade de Santiago de Compostela, A Coruña, Spain

R. Caballero Folch TRIUMF, Vancouver, BC, Canada

L. Caballero-Ontanaya Instituto de Física Corpuscular, CSIC - Universidad de Valencia, Valencia, Spain

R. M. Cabezón sciCORE, Universität Basel, Basel, Switzerland

Antonio Caciolli INFN - Sezione di Padova, Padova, Italy;
Dipartimento di Fisica eAstronomia, Università degli Studi di Padova, Padova, Italy

M. Calviani European Organization for Nuclear Research (CERN), Meyrin, Switzerland

F. Calviño Universitat Politecnica de Catalunya (UPC), Barcelona, Spain

D. Cano-Ott Centro de Investigaciones Energéticas Medioambientales y Tecnológicas (CIEMAT), Madrid, Spain

R. Cardella European Organization for Nuclear Research (CERN), Meyrin, Switzerland;
INFN - Laboratori Nazionali del Sud, Catania, Italy

A. Casanovas Universitat Politècnica de Catalunya, Barcelona, Spain

D. M. Castelluccio Istituto Nazionale di Fisica Nucleare, Sezione di Bologna, Italy;
Agenzia nazionale per le nuove tecnologie (ENEA), Bologna, Italy

R. Catherall European Organization for Nuclear Research (CERN), Meyrin, Switzerland

F. Cerutti European Organization for Nuclear Research (CERN), Meyrin, Switzerland

Gabriele Cescutti INAF, Osservatorio Astronomico di Trieste, Trieste, Italy

S. M. Cha Sungkyunkwan University, Suwon, Republic of Korea

M. Chabot Institut Physique Nucléaire dOrsay, UMR8608, CNRS-IN2P3, Universite Paris Sud 11, Orsay, France

K. Y. Chae Sungkyunkwan University, Suwon, Republic of Korea

S. Chakraborty Florida State University, Tallahassee, FL, USA

Art Champagne Triangle Universities Nuclear Laboratory (TUNL), Durham, NC, USA;
Department of Physics and Astronomy, The University of North Carolina at Chapel Hill, Chapel Hill, NC, USA

William Chantereau Astrophysics Research Institute, Liverpool John Moores University, Liverpool, UK

A. V. Chekhovska V. N. Karazin Kharkiv National University, Kharkiv, Ukraine

A. A. Chen Department of Physics and Astronomy, McMaster University, Hamilton, Ontario, Canada

Han Chen Institute of Modern Physics, Lanzhou, China

L. H. Chen China Institute of Atomic Energy, Beijing, China

Y. H. Chen Centre National de la Recherche Scientifique/IN2P3 - IPN, Orsay, France

S. Cherubini Laboratori Nazionali del Sud, INFN, Catania, Italy;
Department of Physics and Astronomy, University of Catania, Catania, Italy;
INFN, Laboratori Nazionali del Sud, Catania, Italy;
Dipartimento di Fisica e Astronomia, Università di Catania, Catania, Italy;
Istituto Nazionale di Fisica Nucleare - Laboratori Nazionali del Sud, Catania, Italy

S. Chesneyskaya ELI-NP/IFIN-HH, Bucharest, Romania

E. Chiaveri European Organization for Nuclear Research (CERN), Meyrin, Switzerland;
University of Manchester, Manchester, UK

Thomas Chillery SUPA, School of Physics and Astronomy, University of Edinburgh, Edinburgh, UK

G. F. Ciani Gran Sasso Science Institute (GSSI), L'Aquila, Italy;
INFN, Laboratori Nazionali del Gran Sasso Via G. Acitelli, L'Aquila, Italy

Aleksandra Ćiprijanović Department of Astronomy, Faculty of Mathematics, University of Belgrade, Belgrade, Serbia

G. Clai Istituto Nazionale di Fisica Nucleare, Sezione di Bologna, Italy;
Agenzia nazionale per le nuove tecnologie (ENEA), Bologna, Italy

Ondrea Clarkson Department of Physics & Astronomy, University of Victoria, Victoria, B.C., Canada;
Joint Institute for Nuclear Astrophysics, Center for the Evolution of the Elements, Michigan State University, East Lansing, MI, USA;
NuGrid collaboration, East Lansing, USA

Tom Clegg Triangle Universities Nuclear Laboratory (TUNL), Durham, NC, USA;
Department of Physics and Astronomy, The University of North Carolina at Chapel Hill, Chapel Hill, NC, USA

Alain Coc Centre des Sciences Nucléaires et des Sciences de la Matière (CSNSM), IN2P3/CNRS-Université de Paris XI, Campus Orsay, France

M. La Cognata Istituto Nazionale di Fisica Nucleare, Laboratori Nazionali del Sud, Catania, Italy;
Laboratori Nazionali del Sud di Catania, LNS-INFN, Catania, Italy

P. J. Coleman-Smith STFC Daresbury Laboratory, Daresbury, Warrington, UK

Remo Collet Stellar Astrophysics Centre, Department of Physics and Astronomy, Aarhus University, Aarhus, Denmark

David Collins Florida State University, Tallahassee, FL, USA

N. Colonna Istituto Nazionale di Fisica Nucleare, Sezione di Bari, Italy

D. S. Connolly TRIUMF, Vancouver, British Columbia, Canada

Andrew Cooper Triangle Universities Nuclear Laboratory (TUNL), Durham, NC, USA;
Department of Physics and Astronomy, The University of North Carolina at Chapel Hill, Chapel Hill, NC, USA

G. Cortés Universitat Politècnica de Catalunya, Barcelona, Spain

M. A. Cortès-Giraldo Universidad de Sevilla, Sevilla, Spain

L. Cosentino INFN - Laboratori Nazionali del Sud, Catania, Italy

B. Côté Konkoly Observatory, Research Centre for Astronomy and Earth Sciences, Hungarian Academy of Sciences, Budapest, Hungary;
Joint Institute for Nuclear Astrophysics—Center for the Evolution of the Elements, East Lansing, USA

Manoel Couder Department of Physics, University of Notre Dame, Notre Dame, IN, USA

Sergio Cristallo Istituto Nazionale di Fisica Nucleare, Sezione di Perugia, Perugia, Italy;
Istituto Nazionale di Astrofisica - Osservatorio Astronomico di Teramo, Teramo, Italy

Andrea Cristini Department of Physics and Astronomy, University of Oklahoma, Norman, USA

L. Csedreki INFN, Laboratori Nazionali del Gran Sasso Via G. Acitelli, Assergi, L'Aquila, Italy

Borbála Cseh Konkoly Observatory, Research Centre for Astronomy and Earth Sciences, Hungarian Academy of Sciences, Budapest, Hungary

B. Q. Cui China Institute of Atomic Energy, Beijing, China

Sanjana Curtis Department of Physics, North Carolina State University, Raleigh, NC, USA

G. D'Agata INFN-Laboratori Nazionali del Sud, Via S. Sofia, Catania, Italy;
Dip. di Fisica e Astronomia, Università di Catania, Via S. Sofia, Catania, Italy;
Ústav jaderné fyziky AV ČR, v.v.i, Řež, Czech Republic

Valentina D'Orazi INAF Osservatorio Astronomico di Padova, Padova, Italy

L. A. Damone Istituto Nazionale di Fisica Nucleare, Sezione di Bari, Italy;
Dipartimento di Fisica, Università degli Studi di Bari, Bari, Italy;
INFN, Sezione di Bari, Dipartimento di Fisica, Bari, Italy;
Joint Institute of Nuclear Research, Dubna, Russia;
Institute for Materials Science and Center for Nanointegration, Duisburg-Essen (CENIDE), University of Duisburg-Essen, Essen, Germany

B. Davids TRIUMF, Vancouver, British Columbia, Canada

P. J. Davies University of Manchester, Manchester, UK

T. Davinson University of Edinburgh, Edinburgh, United Kingdom

Denise B. de Castro Department for Astrophysics, Nicolaus Copernicus Astronomical Centre of the Polish Academy of Sciences, Warsaw, Poland

Selma E. de Mink Anton Pannekoek Institute for Astronomy, University of Amsterdam, Amsterdam, The Netherlands

F. De Oliveira Grand Accélérateur National d'Ions Lourds (GANIL), CEA/DRFCNRS/IN2P3, Bvd. Henri Becquerel, Caen, France

N. de Séréville Institut de Physique Nucléaire, IN2P3/CNRS-Université de Paris XI, Orsay Cedex, France

M. Degerlier Institut Physique Nucléaire dOrsay, UMR8608, CNRS-IN2P3, Universite Paris Sud 11, Orsay, France

S. Degl'Innocenti Dipartimento di Fisica, Universitá di Pisa and INFN - Sezione di Pisa, Pisa, Italy

C. Delafosse Institut de Physique Nucléaire, IN2P3/CNRS-Université de Paris XI, Orsay Cedex, France;
Institut Physique Nucléaire dOrsay, UMR8608, CNRS-IN2P3, Universite Paris Sud 11, Orsay, France

Jacqueline den Hartogh Astrophysics group, Faculty of Natural Sciences, Keele University, Keele, UK;
Konkoly Observatory, Research Centre for Astronomy and Earth Sciences, Hungarian Academy of Sciences, Budapest, Hungary;
Key Laboratory of Optical Astronomy, National Astronomical Observatories, Chinese Academy of Sciences, Beijing, China

Rosanna Depalo INFN - Sezione di Padova, Padova, Italy;
Dipartimento di Fisica e Astronomia, Università degli Studi di Padova, Padova, Italy

Jack Dermigny Triangle Universities Nuclear Laboratory (TUNL), Durham, NC, USA;
Department of Physics and Astronomy, The University of North Carolina at Chapel Hill, Chapel Hill, NC, USA

Marcella Di Criscienzo INAF—Osservatorio Di Roma, Rome, Italy

A. di Leva Universit degli Studi di Napoli Federico II, Naples, Italy

A. Di Pietro INFN - Laboratori Nazionali del Sud, Catania, Italy

M. Diakaki National Technical University of Athens (NTUA), Athens, Greece

Tiara Diamond NASA Goddard Space Flight Center, Greenbelt, MD, USA

Alexis Diaz-Torres Department of Physics, University of Surrey, Guildford, UK

M. Dietz School of Physics and Astronomy, University of Edinburgh, Edinburgh, UK

I. Dillmann TRIUMF, Vancouver, BC, Canada

Ozan Dogan Goethe University Frankfurt, Frankfurt, Germany

C. L. Doherty Konkoly Observatory, Research Centre for Astronomy and Earth Sciences, Hungarian Academy of Sciences, Budapest, Hungary;
School of Physics and Astronomy, Monash Centre for Astrophysics, Monash University, Melbourne, Australia

C. Domingo-Pardo Instituto de Física Corpuscular, CSIC - Universidad de Valencia, Valencia, Spain

Inma Dominguez Departamento de Fisica Teorica y del Cosmos, Universidad de Granada, Granada, Spain

I. Domínguez Universidad de Granada, Granada, Spain

A. Dorsival European Organization for Nuclear Research (CERN), Meyrin, Switzerland

Lori Downen Triangle Universities Nuclear Laboratory (TUNL), Durham, NC, USA;
Department of Physics and Astronomy, The University of North Carolina at Chapel Hill, Chapel Hill, NC, USA

R. Dressler Paul Scherrer Institut (PSI), Villingen, Switzerland

Q. Ducasse Physikalisch-Technische Bundesanstalt (PTB), Braunschweig, Germany

E. Dupont CEA Irfu, Université Paris-Saclay, Gif-sur-Yvette, France;
CEA/Saclay - IRFU, Gif-sur-Yvette, France

I. Durán University of Santiago de Compostela, A Coruña, Spain

Markus Dworac Goethe University Frankfurt, Frankfurt, Germany

Kevin Ebinger GSI Helmholtzzentrum für Schwerionenforschung, Darmstadt, Germany

Z. Eleme University of Ioannina, Ioannina, Greece

Laura Elisa Marcucci Istituto Nazionale di Fisica Nucleare, Pisa, Italy;
Dipartimento di Fisica "E. Fermi", Pisa University, Pisa, Italy

Anne Endres Goethe University Frankfurt, Frankfurt, Germany

Philipp Erbacher Goethe University Frankfurt, Frankfurt, Germany

N. Esker TRIUMF, Vancouver, British Columbia, Canada

A. Estrade Central Michigan University, Mount Pleasant, MI, USA

T. Faestermann Department of Physics, Technical University Munich, Garching, Germany

Michael A. Famiano Department of Physics, Western Michigan University, Kalamazoo, MI, USA

B. Fernàndez-Dominguez Universidade de Santiago de Compostela, A Coruña, Spain

A. Ferrari European Organization for Nuclear Research (CERN), Meyrin, Switzerland

Federico Ferraro Università degli Studi di Genova and INFN, Sezione di Genova, Genova, Italy

P. Ferreira Instituto Superior Tecnco, Universidade de Lisboa, Lisbon, Portugal

Stefan Fiebiger Goethe University Frankfurt, Frankfurt, Germany

P. Figuera Istituto Nazionale di Fisica Nucleare - Laboratori Nazionali del Sud, Catania, Italy;
INFN - Laboratori Nazionali del Sud, Catania, Italy

P. Finocchiaro INFN Laboratori Nazionali del Sud, Catania, Italy

Alec Fisher Florida State University, Tallahassee, FL, USA

F. Flavigny Institut de Physique Nucléaire, IN2P3/CNRS-Université de Paris XI, Orsay Cedex, France;
Institut Physique Nucléaire dOrsay, UMR8608, CNRS-IN2P3, Universite Paris Sud 11, Orsay, France

Andreea S. Font Astrophysics Research Institute, Liverpool John Moores University, Liverpool, UK

S. P. Fox Department of Physics, University of York, Heslington, York, UK

Bryce Frentz Department of Physics, University of Notre Dame, Notre Dame, IN, USA

Carla Fröhlich Department of Physics, North Carolina State University, Raleigh, NC, USA;
North Carolina State University, Raleigh, NC, USA;
GSI Helmholtzzentrum für Schwerionenforschung, Darmstadt, Germany

C. Fry Department of Physics and Astronomy, National Superconducting Cyclotron Laboratory, Michigan State University, East Lansing, MI, USA

N. Fukuda RIKEN Nishina Center, Wako, Saitama, Japan

V. Furman Joint Institute for Nuclear Research (JINR), Dubna, Russia

W. Furman Instituto Superior Tecnco, Universidade de Lisboa, Lisbon, Portugal

F. Galtarossa Laboratori Nazionali di Legnaro, LNL-INFN, Legnaro, Italy

S. Ganesan Bhabha Atomic Research Centre (BARC), Mumbai, India

Bingshui Gao National Superconducting Cyclotron Laboratory, Michigan State University, East Lansing, MI, USA;
Department of Physics and Astronomy, Michigan State University, East Lansing, MI, USA

A. Garca-Rios Centro de Investigaciones Energeticas Medioambientales y Tecnolgicas (CIEMAT), Madrid, Spain

D. García-Senz Universitat Politècnica de Catalunya, Barcelona, Spain;
Institut d'Estudis Espacials de Catalunya, Barcelona, Spain

R. Garg Department of Physics, University of York, Heslington, York, UK

A. Gawlik Uniwersytet Ldzki, Lodz, Poland;
University of Lodz, Lodz, Poland

Z. Ge RIKEN Nishina Center, Wako, Japan

A. Georgiadou Institut de Physique Nucléaire, IN2P3/CNRS-Université de Paris XI, Orsay Cedex, France;
Institut Physique Nucléaire dOrsay, UMR8608, CNRS-IN2P3, Universite Paris Sud 11, Orsay, France

Cyril Georgy Geneva Observatory, University of Geneva, Versoix, Switzerland

Roman Gernhäuser Technical University Munich, Munich, Germany

M. Giannotti Barry University, Miami Shores, FL, USA

S. Gilardoni European Organization for Nuclear Research (CERN), Meyrin, Switzerland

G. Gilardy Department of Physics, Joint Institute for Nuclear Astrophysics, University of Notre Dame, Notre Dame, IN, USA;
Centre d'Études Nucléaires de Bordeaux Gradignan, UMR 5797 CNRS/IN2P3 - Université de Bordeaux, Gradignan, France

S. Gillespie Department of Physics, University of York, Heslington, York, UK

Matthew S. Gilmer NC State University, Raleigh, NC, USA

R. Giri Department of Physics and Astronomy, Ohio University, Athens, OH, USA

T. Glodariu Horia Hulubei National Institute for Physics and Nuclear Engineering (IFIN-HH), Bucharest-Magurele, Romania

Alex Gnech Istituto Nazionale di Fisica Nucleare, Pisa, Italy;
Gran Sasso Science Institute, L'Aquila, Italy

S. Go RIKEN Nishina Center, Wako, Saitama, Japan;
Department of Physics, University of Tennessee, Knoxville, TN, USA

Kathrin Göbel Goethe University Frankfurt, Frankfurt, Germany;
Johann-Wolfgang-Goethe Universitat, Frankfurt, Germany

Joachim Goerres Department of Physics, University of Notre Dame, Notre Dame, IN, USA

V. Z. Goldberg Department of Physics & Astronomy and Cyclotron Institute, Texas A&M University, College Station, TX, USA

I. F. Gonçalves Instituto Superior Tecnco, Universidade de Lisboa, Lisbon, Portugal

E. González-Romero Centro de Investigaciones Energéticas Medioambientales y Tecnológicas (CIEMAT), Madrid, Spain

T. D. Goodacre European Organization for Nuclear Research (CERN), Meyrin, Switzerland

A. Görgen Department of Physics, University of Oslo, Oslo, Norway

S. Goriely Institut d'Astronomie et d'Astrophysique, Université Libre de Bruxelles, Brussels, Belgium

A. Gottardo Institut de Physique Nucléaire, IN2P3/CNRS-Université de Paris XI, Orsay Cedex, France;
Institut Physique Nucléaire dOrsay, UMR8608, CNRS-IN2P3, Universite Paris Sud 11, Orsay, France

Alessandro Grassi M. Smoluchowski Institute of Physics, Jagiellonian University, Kraków, Poland

L. Grassi Institut de Physique Nucléaire, IN2P3/CNRS-Université de Paris XI, Orsay Cedex, France

Uwe Greife Department of Physics, Colorado School of Mines, Golden, CO, USA

E. Griesmayer Atominstitut der Osterreichischen Universitaten, Technische Universitat Wien, Vienna, Austria

C. J. Griffin University of Edinburgh, Edinburgh, United Kingdom

R. Grzywacz Department of Physics, University of Tennessee, Knoxville, TN, USA

G. L. Guardo ELI-NP/IFIN-HH, Bucharest, Romania;
ELI-NP/IFIN-HH, Magurele, Romania;
INFN, Laboratori Nazionali del Sud, Catania, Italy;
ELI-NP, Bucharest - Magurele, Romania;
Laboratori Nazionali del Sud di Catania, LNS-INFN, Catania, Italy;
Dipartimento di Fisica e Astronomia, Univ. di Catania, Catania, Italy

C. Guerrero Universidad de Sevilla, Sevilla, Spain

Alessandra Guglielmetti Dipartimento di Fisica, Università degli Studi di Milano, Milano, Italy;
Sezione di Milano, INFN, Milano, Italy

J. Guillot Institut de Physique Nucléaire, IN2P3/CNRS-Université de Paris XI, Orsay Cedex, France;
Institut Physique Nucléaire dOrsay, UMR8608, CNRS-IN2P3, Universite Paris Sud 11, Orsay, France

V. Guimaräes Instituto de Física, Universidade de São Paulo, São Paulo, Brazil;
Institut Physique Nucléaire dOrsay, UMR8608, CNRS-IN2P3, Universite Paris Sud 11, Orsay, France

M. Gulino Department of Physics and Astronomy, University of Catania, Catania, Italy;
Engineering and Architecture Department, University of Kore, Enna, Italy;
Facoltà di Ingegneria e Architettura, Universitá "Kore", Enna, Italy;
INFN, Laboratori Nazionali del Sud, Catania, Italy;
Facoltà di Ingegneria ed Architettura, Kore University, Enna, Italy;
Istituto Nazionale di Fisica Nucleare - Laboratori Nazionali del Sud, Catania, Italy;
Kore University of Enna, Enna, Italy;
Laboratori Nazionali del Sud di Catania, LNS-INFN, Catania, Italy;
Facolt di Ingegneria e Architettura, Universit degli Studi di Enna Kore, Enna, Italy

F. Gunsing CEA Irfu, Université Paris-Saclay, Gif-sur-Yvette, France

B. Guo China Institute of Atomic Energy, Beijing, China

M. Guttormsen Department of Physics, University of Oslo, Oslo, Norway

Gy. Gyürky Institute for Nuclear Research (MTA Atomki), Debrecen, Hungary

J. Ha Department of Physics, Seoul National University, Seoul, Republic of Korea

T. W. Hagen Department of Physics, University of Oslo, Oslo, Norway

O. Hall University of Edinburgh, Edinburgh, United Kingdom

F. Hammache Institut de Physique Nucléaire, IN2P3/CNRS-Université de Paris XI, Orsay Cedex, France;
Institut Physique Nucléaire dOrsay, UMR8608, CNRS-IN2P3, Universite Paris Sud 11, Orsay, France

M. Hampel School of Physics and Astronomy, Monash Centre for Astrophysics, Monash University, Monash, VIC, Australia

Christine V. Hampton Hampton Consulting, LLC, Okemos, MI, USA

Mark Hanhardt Department of Physics, South Dakota School of Mines & Technology, Rapid City, SD, USA

H. Harada Japan Atomic Energy Agency (JAEA), Tokai-mura, Japan

L. Harkness-Brennan University of Liverpool, Liverpool, United Kingdom

Andreas Hartmann Helmholtz-Zentrum Dresden-Rossendorf, Dresden, Germany

S. Hayakawa Center for Nuclear Study, The University of Tokyo, Wako, Saitama, Japan;
Center for Nuclear Study, RIKEN, University of Tokyo, Wako, Saitama, Japan;
INFN, Laboratori Nazionali del Sud, Catania, Italy

J. J. He Key Laboratory of High Precision Nuclear Spectroscopy, Institute of Modern Physics, Chinese Academy of Sciences, Lanzhou, China;
Key Laboratory of Optical Astronomy, National Astronomical Observatories, Chinese Academy of Sciences, Beijing, China

Fabian Hebermehl Goethe University Frankfurt, Frankfurt, Germany

Tanja Heftrich Johann-Wolfgang-Goethe Universitat, Frankfurt, Germany;
Goethe University Frankfurt, Frankfurt, Germany

S. Heinitz Paul Scherrer Institut, Villigen PSI, Villigen, Switzerland

R. Hertenberger Faculty of Physics, Ludwig-Maximilians-Universität München, Munich, Germany

Falk Herwig Department of Physics & Astronomy, University of Victoria, Victoria, B.C., Canada;
Joint Institute for Nuclear Astrophysics, Center for the Evolution of the Elements, Michigan State University, East Lansing, MI, USA;
NuGrid collaboration, East Lansing, USA

J. Heyse European Commission JRC, Institute for Reference Materials and Measurements, Geel, Belgium

Raphael Hirschi Astrophysics Group, Faculty of Natural Sciences, Keele University, Keele, UK;
Kavli IPMU (WPI), University of Tokyo, Tokyo, Japan;
Astrophysics Group, Lennard-Jones Laboratories, Keele University, Keele, UK;
WPI Kavli-IPMU, University of Tokyo, Chiba, Kashiwa, Japan;
UK Network for Bridging Disciplines of Galactic Chemical Evolution (BRIDGCE), Keele, UK

Peter Hoeflich Florida State University, Tallahassee, FL, USA

E. Holmbeck Department of Physics, University of Notre Dame, Notre Dame, IN, USA

J. Hooker Department of Physics & Astronomy and Cyclotron Institute, Texas A&M University, College Station, TX, USA

P. Hoppe Max Planck Institute for Chemistry, Mainz, Germany

S. Q. Hou Key Laboratory of High Precision Nuclear Spectroscopy, Institute of Modern Physics, Chinese Academy of Sciences, Lanzhou, China

Boyan Hristov Florida State University, Tallahassee, FL, USA

Eric Hsiao Florida State University, Tallahassee, FL, USA

J. Hu Institute of Modern Physics, Chinese Academy of Sciences, Lanzhou, China

Q. H. Huang China Institute of Atomic Energy, Beijing, China

W. Huang TRIUMF, Vancouver, BC, Canada;
Department of Physics, University of Northern British Columbia, Prince George, BC, Canada

N. Hubbard Department of Physics, The University of York, York, UK

Sean Hunt Triangle Universities Nuclear Laboratory (TUNL), Durham, NC, USA;
Department of Physics and Astronomy, The University of North Carolina at Chapel Hill, Chapel Hill, NC, USA

C. Hunt Department of Physics & Astronomy and Cyclotron Institute, Texas A&M University, College Station, TX, USA

D. A. Hutcheon TRIUMF, Vancouver, British Columbia, Canada

T. Id Barkach Institut de Physique Nucléaire, IN2P3/CNRS-Université de Paris XI, Orsay Cedex, France

Christian Iliadis Triangle Universities Nuclear Laboratory (TUNL), Durham, NC, USA;
Department of Physics and Astronomy, The University of North Carolina at Chapel Hill, Chapel Hill, NC, USA

G. Imbriani Dipartimento di Fisica "E. Pancini", Università degli Studi di Napoli "Federico II", Napoli, Italy

I. Indelicato Laboratori Nazionali del Sud, INFN, Catania, Italy

A. Inoue Research Center for Nuclear Physics, Osaka University, Suita, Japan

P. Gina Isar Institute of Space Science, Bucharest-Magurele, Romania

Koji Ishidoshiro Research Center for Neutrino Science, Tohoku University, Miyagi, Japan

T. Isobe RIKEN Nishina Center, Wako, Saitama, Japan

R. J. Ivison Institute for Astronomy, University of Edinburgh, Edinburgh, UK; ESO, Garching bei München, Germany

N. Iwasa Tohoku University, Sendai, Japan;
Department of Physics, Tohoku University, Aoba, Sendai, Miyagi, Japan

P. Jaffke Theoretical Division, Los Alamos National Laboratory, Los Alamos, NM, USA

H. Jayatissa Department of Physics & Astronomy and Cyclotron Institute, Texas A&M University, College Station, TX, USA

D. G. Jenkins University of York, York, UK

E. Jericha Atominstitut der Osterreichischen Universitaten, Technische Universitat Wien, Vienna, Austria

P. Jiménez-Bonilla Atomic, Molecular and Nuclear Physics Department, University of Seville, Seville, Spain

K. Johnston European Organization for Nuclear Research (CERN), Meyrin, Switzerland

Arnd R. Junghans Helmholtz-Zentrum Dresden-Rossendorf, Dresden, Germany; European Organization for Nuclear Research (CERN), Genéve, Switzerland

Y. Kadi European Organization for Nuclear Research (CERN), Meyrin, Switzerland

Thomas Kadlecek Department of Physics, South Dakota School of Mines & Technology, Rapid City, SD, USA

D. Kahl School of Physics and Astronomy, The University of Edinburgh, Edinburgh, UK;
RIKEN Nishina Center, Wako, Saitama, Japan

Etienne A. Kaiser Astrophysics Group, Lennard-Jones Laboratories, Keele University, Keele, UK

Toshitaka Kajino National Astronomical Observatory of Japan, Mitaka, Tokyo, Japan;
Department of Astronomy, Graduate School of Science, The University of Tokyo, Bunkyo-ku, Tokyo, Japan;
School of Physics and Nuclear Energy Engineering and International Research Center for Big-Bang Cosmology and Element Genesis, Beihang University, Beijing, China

A. Kalamara National Technical University of Athens (NTUA), Athens, Greece

A. Kanellakopoulos Department of Physics, University of Athens, Athens, Greece

Anu Kankainen Department of Physics, University of Jyväskylä, Jyväskylä, Finland

F. Käppeler Karlsruhe Institute of Technology (KIT), Institut fur Kernphysik, Karlsruhe, Germany

Amanda I. Karakas School of Physics and Astronomy, Monash Centre for Astrophysics, Monash University, Melbourne, VIC, Australia

M. Karny Faculty of Physics, University of Warsaw, Warsaw, Poland

J. Karpesky Department of Physics, Colorado School of Mines, Golden, CO, USA

H. J. Karwowski University of North Carolina at Chapel Hill, Chapel Hill, NC, USA;
Triangle Universities Nuclear Laboratory, Durham, NC, USA

V. I. Kasilov NSC "Kharkiv Institute of Physics and Technology", Kharkiv, Ukraine

T. Katabuchi Tokyo Institute of Technology, Tokyo, Japan

M. Katsuma Advanced Mathematical Institute, Osaka City University, Osaka, Japan;
Institut d'Astronomie et d'Astrophysique, Université Libre de Bruxelles, Brussels, Belgium

Tanja Kausch Goethe University Frankfurt, Frankfurt, Germany

P. Kavrigin Atominstitut der Osterreichischen Universitaten, Technische Universitat Wien, Vienna, Austria

T. Kawabata Department of Physics, Osaka University, Toyonaka, Osaka, Japan

T. Kawano Theoretical Division, Los Alamos National Laboratory, Los Alamos, NM, USA

A. Khaliel Department of Physics, University of Athens, Athens, Greece

Kafa Khasawneh Goethe University Frankfurt, Frankfurt, Germany

L. H. Khiem Institute of Physics, Vietnam Academy of Science and Technology, Hanoi, Vietnam

J. Kiener Centre de Sciences Nucléaires et de Sciences de la Matière (CSNSM), CNRS/IN2P3, Université Paris-Sud, Université ParisSaclay, Orsay, France

A. Kim Ewha Womans University, Seoul, Republic of Korea

D. H. Kim Ewha Womans University, Seoul, Republic of Korea

A. Kimura Japan Atomic Energy Agency (JAEA), Tokai-mura, Japan;
Japan Atomic Energy Agency (JAEA), Naka District, Japan

G. G. Kiss RIKEN Nishina Center, Wako, Saitama, Japan;
Institute of Nuclear Research of the Hungarian Academy of Sciences, Debrecen, Hungary

N. Kivel Paul Scherrer Institut, Villigen PSI, Villigen, Switzerland

Nadine Klapper Goethe University Frankfurt, Frankfurt, Germany

I. Knapova Charles University, Prague, Czech Republic

James P. Kneller NC State University, Raleigh, NC, USA

Chiaki Kobayashi Centre for Astrophysics Research, University of Hertfordshire, Hatfield, UK

M. Kogimtzis STFC Daresbury Laboratory, Daresbury, Warrington, UK

U. Kohester Institut Laue-Langevin (ILL), Grenoble, France

M. Kokkoris National Technical University of Athens (NTUA), Athens, Greece

Y. Kopatch Joint Institute for Nuclear Research (JINR), Dubna, Russia

Christoph Köppchen Goethe University Frankfurt, Frankfurt, Germany

E. Koshchiy Department of Physics & Astronomy and Cyclotron Institute, Texas A&M University, College Station, TX, USA

Sabina Krasilovskaja Goethe University Frankfurt, Frankfurt, Germany

M. Krtička Charles University, Prague, Czech Republic

S. Kubono RIKEN Nishina Center, Wako, Saitama, Japan;
Center for Nuclear Study, University of Tokyo, Wako, Japan;
Institute of Modern Physics, Chinese Academy of Sciences, Lanzhou, China

Deniz Kurtulgil Goethe University Frankfurt, Frankfurt, Germany;
Johann-Wolfgang-Goethe Universitat, Frankfurt, Germany

Motohiko Kusakabe School of Physics, Beihang University, Beijing, China;
School of Physics and Nuclear Energy Engineering and International Research Center for Big-Bang Cosmology and Element Genesis, Beihang University, Beijing, China

M. La Cognata INFN - Laboratori Nazionali del Sud, Catania, Italy

M. La Commara University of Naples Federico II, Naples, Italy;
Istituto Nazionale di Fisica Nucleare - Section of Naples, Naples, Italy;
Dipartimento di Scienze Fisiche, Universit di Napoli, Napoli, Italy

M. Labiche STFC Daresbury Laboratory, Daresbury, Warrington, UK

I. Ladarescu Instituto de Física Corpuscular, CSIC - Universidad de Valencia, Valencia, Spain

V. Lagaki Department of Physics, University of Athens, Athens, Greece

A. M. Laird Department of Physics, The University of York, York, UK

L. Lamia INFN - Laboratori Nazionali del Sud, Catania, Italy;
Dipartimento di Fisica e Astronomia, Università di Catania, Catania, Italy

Christoph Langer Goethe University Frankfurt, Frankfurt, Germany

A. L. Lara Instituto de Física, Universidade de São Paulo, São Paulo, Brazil

A. C. Larsen Department of Physics, University of Oslo, Oslo, Norway

D. Lattuada ELI-NP/IFIN-HH, Bucharest, Romania

M. Lattuada Dipartimento di Fisica e Astronomia, Università degli Studi di Catania, Catania, Italy;
Istituto Nazionale di Fisica Nucleare - Laboratori Nazionali del Sud, Catania, Italy;
University of Catania, Catania, Italy

Amber Lauer Triangle Universities Nuclear Laboratory (TUNL), Durham, NC, USA;
Department of Physics and Astronomy, The University of North Carolina at Chapel Hill, Chapel Hill, NC, USA

I. Lazarus STFC Daresbury Laboratory, Daresbury, Warrington, UK

E. Leal-Cidoncha Universidade de Santiago de Compostela, A Coruña, Spain

Claudia Lederer-Woods School of Physics and Astronomy, University of Edinburgh, Edinburgh, UK

E. J. Lee Sungkyunkwan University, Suwon, Republic of Korea

J. Lee Department of Physics, The University of Hong Kong, Hong Kong, China

H. Leeb Atominstitut der Osterreichischen Universitaten, Technische Universitat Wien, Vienna, Austria

A. Lefebvre-Schuhl Centre de Sciences Nucléaires et de Sciences de la Matière (CSNSM), CNRS/IN2P3, Université Paris-Sud, Université ParisSaclay, Orsay, France

A. Lennarz TRIUMF, Vancouver, British Columbia, Canada

Eric J. Lentz Department of Physics and Astronomy, University of Tennessee, Knoxville, TN, USA

J. Lerendegui-Marco Universidad de Sevilla, Sevilla, Spain

E. T. Li College of Physics and Energy, Shenzhen University, Shenzhen, China; Konkoly Observatory, Hungarian Academy of Sciences, Budapest, Hungary

Kuang Li Institute of Modern Physics, Lanzhou, China

G. Lian China Institute of Atomic Energy, Beijing, China

J. Liang Department of Physics and Astronomy, McMaster University, Hamilton, Ontario, Canada

S. N. Liddick National Superconducting Cyclotron Laboratory, Michigan State University, East Lansing, USA;
Department of Chemistry, Michigan State University, East Lansing, USA

Matthias Liebendörfer Departement für Physik, Universität Basel, Basel, Switzerland

E. Lima Department of Physics, University of Oslo, Oslo, Norway

David Little Triangle Universities Nuclear Laboratory (TUNL), Durham, NC, USA;
Department of Physics and Astronomy, The University of North Carolina at Chapel Hill, Chapel Hill, NC, USA

J. Liu Department of Physics, The University of Hong Kong, Hong Kong, China

WeiPing Liu China Institute of Atomic Energy, Beijing, China

S. Lo Meo ENEA, Bologna, Italy;
INFN, Sezione di Bologna, Bologna, Italy

Katharina Lodders Department of Earth & Planetary Sciences and McDonnell Center for the Space Sciences, Washington University, Saint Louis, MO, USA

S. J. Lonsdale School of Physics and Astronomy, University of Edinburgh, Edinburgh, UK

G. Lorusso RIKEN Nishina Center, Wako, Saitama, Japan;
National Physical Laboratory, Teddington, UK

R. Losito European Organization for Nuclear Research (CERN), Meyrin, Switzerland

M. Lovely Department of Physics, Colorado School of Mines, Golden, CO, USA

Maria Lugaro Konkoly Observatory, Research Centre for Astronomy and Earth Sciences, Hungarian Academy of Sciences, Budapest, Hungary;
School of Physics and Astronomy, Monash Centre for Astrophysics, Monash University, Melbourne, VIC, Australia

Yudong Luo National Astronomical Observatory of Japan, Mitaka, Tokyo, Japan;
Department of Astronomy, Graduate School of Science, The University of Tokyo, Bunkyo-ku, Tokyo, Japan

M. Lykiardopoulou Department of Physics, University of Athens, Athens, Greece

R. G. Ma China Institute of Atomic Energy, Beijing, China

Shaobo Ma Institute of Modern Physics, Lanzhou, China

X. Ma China Institute of Atomic Energy, Beijing, China

Y. J. Ma China Institute of Atomic Energy, Beijing, China

M. MacCormick Institut de Physique Nucléaire, IN2P3/CNRS-Université de Paris XI, Orsay Cedex, France

D. Macina European Organization for Nuclear Research (CERN), Meyrin, Switzerland

E. Malami Department of Physics, University of Athens, Athens, Greece

A. Manna Istituto Nazionale di Fisica Nucleare, Sezione di Bologna, Italy;
Dipartimento di Fisica e Astronomia, Università di Bologna, Bologna, Italy

Huaqing Mao LCSE and Department of Astronomy, University of Minnesota, Minneapolis, MN, USA;
Joint Institute for Nuclear Astrophysics, Center for the Evolution of the Elements, Michigan State University, East Lansing, MI, USA

J. Marganiec Uniwersytet Ldzki, Lodz, Poland

B. Marsh European Organization for Nuclear Research (CERN), Meyrin, Switzerland

T. Martínez Centro de Investigaciones Energéticas Medioambientales y Tecnológicas (CIEMAT), Madrid, Spain

J. G. Martins Correia European Organization for Nuclear Research (CERN), Meyrin, Switzerland;
Instituto Superior Tecnco, Universidade de Lisboa, Lisbon, Portugal

A. Masi European Organization for Nuclear Research (CERN), Meyrin, Switzerland

C. Massimi Istituto Nazionale di Fisica Nucleare, Sezione di Bologna, Italy;
Dipartimento di Fisica e Astronomia, Università di Bologna, Bologna, Italy

P. Mastinu Istituto Nazionale di Fisica Nucleare, Sezione di Legnaro, Italy;
INFN - Laboratori Nazionali di Legnaro, Legnaro, Italy

M. Mastromarco European Organization for Nuclear Research (CERN), Meyrin, Switzerland;
INFN, Sezione di Bari, Dipartimento di Fisica, Bari, Italy

I. Matea Institut de Physique Nucléaire, IN2P3/CNRS-Université de Paris XI, Orsay Cedex, France;
Institut Physique Nucléaire dOrsay, UMR8608, CNRS-IN2P3, Universite Paris Sud 11, Orsay, France

C. Matei ELI-NP/IFIN-HH, Bucharest, Romania

Grant J. Mathews National Astronomical Observatory of Japan, Mitaka, Tokyo, Japan;
Center for Astrophysics, Department of Physics, University of Notre Dame, Notre Dame, IN, USA

K. Matsui RIKEN Nishina Center, Wako, Saitama, Japan;
Department of Physics, University of Tokyo, Tokyo, Japan

F. Matteucci Istituto Nazionale di Fisica Nucleare, Sezione di Trieste, Italy;
Dipartimento di Astronomia, Università di Trieste, Trieste, Italy;
Physics Department, University of Trieste, Trieste, Italy;
INAF, Osservatorio Astronomico di Trieste, Trieste, Italy;
INFN, Sezione di Trieste, Italy

E. A. Maugeri Paul Scherrer Institut (PSI), Villingen, Switzerland

M. Mazzocco Dipartimento di Fisica e Astronomia, Università di Padova, Padova, Italy;
INFN - Padova, Padova, Italy

A. Mazzone Istituto Nazionale di Fisica Nucleare, Sezione di Bari, Italy;
Istituto Nazionale di Fisica Nucleare, Bari, Italy;
INFN, Sezione di Bari, Dipartimento di Fisica, Bari, Italy;
CNR - IC, Bari, Italy

G. C. McLaughlin Department of Physics, University of Notre Dame, Notre Dame, IN, USA;
Department of Physics, North Carolina State University, Raleigh, NC, USA

E. G. Meekins Department of Physics and Astronomy, James Madison University, Harrisonburg, VA, USA

E. Mendoza Centro de Investigaciones Energeticas Medioambientales y Tecnolgicas (CIEMAT), Madrid, Spain

Roberto Menegazzo INFN - Sezione di Padova, Padova, Italy

A. Mengoni Istituto Nazionale di Fisica Nucleare, Sezione di Bologna, Italy;
Agenzia nazionale per le nuove tecnologie (ENEA), Bologna, Italy;
ENEA, Bologna, Italy;
INFN, Sezione di Bologna, Bologna, Italy

T. J. Mertzimekis Department of Physics, University of Athens, Athens, Greece

A. Meyer Institut de Physique Nucléaire, IN2P3/CNRS-Université de Paris XI, Orsay Cedex, France

B. S. Meyer Department of Physics and Astronomy, Clemson University, Clemson, SC, USA

Anthony Mezzacappa Department of Physics and Astronomy, University of Tennessee, Knoxville, TN, USA;
Joint Institute for Computational Sciences, Oak Ridge National Laboratory, Oak Ridge, TN, USA

V. Michalopoulou European Organization for Nuclear Research (CERN), Meyrin, Switzerland;
National Technical University of Athens, Athens, Greece

J. E. Midtbø Department of Physics, University of Oslo, Oslo, Norway

K. Miernik Physics Division, Oak Ridge National Laboratory, Oak Ridge, TN, USA;
Faculty of Physics, University of Warsaw, Warsaw, Poland

P. M. Milazzo Istituto Nazionale di Fisica Nucleare, Sezione di Trieste, Trieste, Italy

M. Milin Department of Physics, University of Zagreb, Zagreb, Croatia

Federica Mingrone European Organization for Nuclear Research (CERN), Genéve, Switzerland

M. Mirea Horia Hulubei National Institute for Physics and Nuclear Engineering (IFIN-HH), Bucharest-Magurele, Romania

A. Mirizzi Universita di Bari, Bari, Italy;
INFN-Bari, Bari, Italy

P. Möller Theoretical Division, Los Alamos National Laboratory, Los Alamos, NM, USA

László Molnár Konkoly Observatory, Research Centre for Astronomy and Earth Sciences, Hungarian Academy of Sciences, Budapest, Hungary

F. Montes National Superconducting Cyclotron Laboratory, Michigan State University, East Lansing, USA

B. Moon Department of Physics, Korea University, Seoul, Republic of Korea

J. Y. Moon Institute for Basic Science, Daejeon, Republic of Korea

A. I. Morales Instituto de Fisica Corpuscular (CSIC-Univ. de Valencia), Paterna, Spain

J. Moreno-Soto CEA Irfu, Université Paris-Saclay, Gif-sur-Yvette, France

Kanji Mori National Astronomical Observatory of Japan, Mitaka, Tokyo, Japan;
Graduate School of Science, The University of Tokyo, Bunkyo-ku, Tokyo, Tokyo, Japan;
School of Physics, Beihang University, Beijing, China

Viviana Mossa INFN, sezione di Bari, Bari, Italy

J. Mrazek Ústav jaderné fyziky AV ČR, v.v.i, Řež, Czech Republic

M. R. Mumpower Theoretical Division, Los Alamos National Laboratory, Los Alamos, NM, USA

Alex St. J. Murphy SUPA, School of Physics and Astronomy, University of Edinburgh, Edinburgh, UK;
UK Network for Bridging Disciplines of Galactic Chemical Evolution (BRIDGCE), Keele, UK

A. Musumarra INFN Laboratori Nazionali del Sud, Catania, Italy;
Dipartimento di Fisica e Astronomia, Università di Catania, Catania, Italy

A. Negret Horia Hulubei National Institute for Physics and Nuclear Engineering (IFIN-HH), Bucharest-Magurele, Romania;
Horia Hulubei National Institute of Physics and Nuclear Engineering, Măgurele, Romania

N. Nepal Central Michigan University, Mount Pleasant, MI, USA

Ewa Niemczura University of Wroclaw, Wroclaw, Poland

Nobuya Nishimura Yukawa Institute for Theoretical Physics, Kyoto University, Kyoto, Japan

S. Nishimura RIKEN Nishina Center, Wako, Saitama, Japan

R. Nolte Physikalisch-Technische Bundesanstalt (PTB), Braunschweig, Germany

Birgitta Nordström Niels Bohr Institute, Copenhagen, Denmark

F. Ogállar University of Granada, Granada, Spain

L. Olivier Institut de Physique Nucléaire, IN2P3/CNRS-Université de Paris XI, Orsay Cedex, France;
Institut Physique Nucléaire dOrsay, UMR8608, CNRS-IN2P3, Universite Paris Sud 11, Orsay, France

A. Oprea Horia Hulubei National Institute for Physics and Nuclear Engineering (IFIN-HH), Bucharest-Magurele, Romania;
Horia Hulubei National Institute of Physics and Nuclear Engineering, Măgurele, Romania

Takaharu Otsuka RIKEN Nishina Center for Accelerated-Based Science, Wako-shi, Saitama, Japan;
National Superconducting Cyclotron Laboratory, Michigan State University, East Lansing, MI, USA

N. Oulebsir Laboratoire de Physique Théorique, Université Abderahmane Mira, Béjaia, Algeria

Nalan Özkan Department of Physics, Kocaeli University, Umuttepe, Kocaeli, Turkey

R. D. Page University of Liverpool, Liverpool, United Kingdom

A. Pakou Department of Physics and HINP, University of Ioannina, Ioannina, Greece

Sara Palmerini Department of Physics and Geology, University of Perugia, Perugia, Italy;
Section of Perugia, INFN, Perugia, Italy;
Dipartimento di Fisica e Geologia, Università degli Studi di Perugia, Perugia, Italy;
Istituto Nazionale di Fisica Nucleare - Section of Perugia, Perugia, Italy

S. N. Paneru Department of Physics and Astronomy, Ohio University, Athens, OH, USA

P. P. Papadopoulos Department of Physics, Section of Astrophysics, Astronomy and Mechanics, Aristotle University of Thessaloniki, Thessaloniki, Greece;
Research Center for Astronomy, Academy of Athens, Athens, Greece

Panagiota Papakonstantinou Rare Isotope Science Project, Institute for Basic Science, Daejeon, South Korea

C. Parascandolo INFN - Sezione di Napoli, Napoli, Italy;
Istituto Nazionale di Fisica Nucleare - Section of Naples, Naples, Italy

A. Parikh Departament de Física i Enginyeria Nuclear, Universitat Politècnica de Catalunya, Barcelona, Spain;
Institut d'Estudis Espacials de Catalunya, Barcelona, Spain

S. Y. Park Ewha Womans University, Seoul, Republic of Korea

N. Patronis University of Ioannina, Ioannina, Greece

A. Pavlik Faculty of Physics, University of Vienna, Vienna, Austria

Albino Perego Dipartimento di Scienze Matematiche Fisiche ed Informatiche, Università di Parma, Parma, Italy

Claudio B. Pereira Observatorio Nacional, Rua General José Cristino, Rio de Janeiro, Brazil

J. Perkowski Uniwersytet Ldzki, Lodz, Poland;
University of Lodz, Lodz, Poland

L. Perrot Institut de Physique Nucléaire, IN2P3/CNRS-Université de Paris XI, Orsay Cedex, France;
Institut Physique Nucléaire dOrsay, UMR8608, CNRS-IN2P3, Universite Paris Sud 11, Orsay, France

H. Petrascu Horia Hulubei National Institute for R&D in Physics and Nuclear Engineering, Bucharest-Maguerele, Romania

C. Petrone Horia Hulubei National Institute of Physics and Nuclear Engineering, Măgurele, Romania

T. Petruse ELI-NP/IFIN-HH, Bucharest, Romania

V. H. Phong RIKEN Nishina Center, Wako, Saitama, Japan;
Department of Nuclear Physics, Faculty of Physics, VNU University of Science, Hanoi, Vietnam

D. Piatti Università degli Studi di Padova, Padova, Italy;
INFN, Padova, Italy;
Dipartimento di Fisica e Astronomia, Univ. di Padova, Padova, Italy;
INFN-Sez. di Padova, Padova, Italy

D. Pierroutsakou INFN-Sezione di Napoli, Napoli, Italy;
Istituto Nazionale di Fisica Nucleare - Section of Naples, Naples, Italy

Luciano Piersanti INAF, Osservatorio Astronomico d'Abruzzo, Teramo, Italy;
INFN, Perugia, Italy

Marco Pignatari Department of Physics and Mathematics, E.A. Milne Centre for Astrophysics, University of Hull, Hull, UK;
NuGrid Collaboration, Hull, UK;
Konkoly Observatory, Research Centre for Astronomy and Earth Sciences, Hungarian Academy of Sciences, Budapest, Hungary;
GSI Helmholtzzentrum für Schwerionenforschung, Darmstadt, Germany;
Center for the Evolution of the Elements, Joint Institute for Nuclear Astrophysics, Michigan State University, East Lansing, MI, USA

E. Pirovano Physikalisch-Technische Bundesanstalt (PTB), Braunschweig, Germany

M. Piscopo INFN - Laboratori Nazionali del Sud, Catania, Italy

Cyril Pitrou Institut d'Astrophysique de Paris, CNRS UMR 7095, Institut Lagrange de Paris, Paris, France

Rosario Gianluca Pizzone INFN-LNS, Catania, Italy

Emese Plachy Konkoly Observatory, Research Centre for Astronomy and Earth Sciences, Hungarian Academy of Sciences, Budapest, Hungary

A. Plompen European Commission JRC, Institute for Reference Materials and Measurements, Geel, Belgium

Z. Podolyak Department of Physics, University of Surrey, Guildford GU2 7XH, United Kingdom

I. Porras University of Granada, Granada, Spain

C. Portail Institut de Physique Nucléaire, IN2P3/CNRS-Université de Paris XI, Orsay Cedex, France

P. G. Prada Moroni Dipartimento di Fisica, Universitá di Pisa and INFN - Sezione di Pisa, Pisa, Italy

J. Praena Atomic, Molecular and Nuclear Physics Department, University of Granada, Granada, Spain;
Universidad de Sevilla, Sevilla, Spain

Nikos Prantzos Institut d'Astrophysique de Paris, Sorbonne Université, Paris, France

Paolo Prati University of Genova and INFN, Genoa, Italy

Boris Pritychenko National Nuclear Data Center, Brookhaven National Laboratory, Upton, NY, USA

Tijana Prodanović University of Novi Sad, Novi Sad, Serbia

A. Psaltis Department of Physics and Astronomy, McMaster University, Hamilton, Ontario, Canada;
Department of Physics, University of Athens, Zografou Campus, 15784 Athens, Greece

I. Psyrra Department of Physics, University of Athens, Athens, Greece

V. F. E. Pucknell STFC Daresbury Laboratory, Daresbury, Warrington, UK

S. M. R. Puglia INFN, Laboratori Nazionali del Sud, Catania, Italy

J. M. Quesada Atomic, Molecular and Nuclear Physics Department, University of Seville, Seville, Spain

D. Radeck Physikalisch-Technische Bundesanstalt (PTB), Braunschweig, Germany

K. Rajeev Bhabha Atomic Research Centre (BARC), Mumbai, India

D. Ramos-Doval Institut de Physique Nucléaire, CNRS-IN2P3, Univ. Paris-Sud, Université Paris-Saclay, Orsay Cedex, France

G. La Rana INFN-Sezione di Napoli, Napoli, Italy;
Dipartimento di Scienze Fisiche, Universit di Napoli, Napoli, Italy

W. Raphael Hix Physics Division, Oak Ridge National Laboratory, Oak Ridge, TN, USA;
Department of Physics and Astronomy, University of Tennessee, Knoxville, TN, USA

G. G. Rapisarda Laboratori Nazionali del Sud, INFN, Catania, Italy;
Department of Physics and Astronomy, University of Catania, Catania, Italy

B. C. Rasco Physics Division, Oak Ridge National Laboratory, Oak Ridge, TN, USA

Thomas Rauscher Centre for Astrophysics Research, University of Hertfordshire, Hatfield, UK;
Department of Physics, University of Basel, Basel, Switzerland;
UK Network for Bridging Disciplines of Galactic Chemical Evolution (BRIDGCE), Keele, UK

P. Regan National Physical Laboratory, Teddington, UK;
Department of Physics, University of Surrey, Guildford GU2 7XH, United Kingdom

Markus Reich Goethe University Frankfurt, Frankfurt, Germany

René Reifarth Goethe University Frankfurt, Frankfurt, Germany

T. Renstrøm Department of Physics, University of Oslo, Oslo, Norway

A. Riego-Perez Universitat Politecnica de Catalunya, Barcelona, Spain

Valentino Rigato Laboratori Naizonali di Legnaro, INFN, Legnaro, Italy

J. Riley Department of Physics, University of York, Heslington, York, UK

Daniel Robertson Department of Physics, University of Notre Dame, Notre Dame, IN, USA

D. Rochman Paul Scherrer Institut (PSI), Villingen, Switzerland

B. T. Roeder Department of Physics & Astronomy and Cyclotron Institute, Texas A&M University, College Station, TX, USA

G. V. Rogachev Department of Physics & Astronomy and Cyclotron Institute, Texas A&M University, College Station, TX, USA

D. Romano INAF, Astrophysics and Space Science Observatory, Bologna, Italy

S. Romano Dipartimento di Fisica e Astronomia, Istituto Nazionale di Fisica Nucleare - Laboratori Nazionali del Sud, Catania, Italy

Stephan Rosswog Department of Astronomy, The Oskar Klein Centre, Stockholm University, Stockholm, Sweden

S. Rothe University of Manchester, Manchester, UK

P. Rout Bhabha Atomic Research Centre (BARC), Mumbai, India

C. Rubbia European Organization for Nuclear Research (CERN), Meyrin, Switzerland

B. Rubio Instituto de Fisica Corpuscular (CSIC-Univ. de Valencia), Paterna, Spain

C. Ruiz TRIUMF, Vancouver, British Columbia, Canada

J. Ryan University of Manchester, Manchester, UK

K. P. Rykaczewski Physics Division, Oak Ridge National Laboratory, Oak Ridge, TN, USA

A. Saastamoinen Department of Physics & Astronomy and Cyclotron Institute, Texas A&M University, College Station, TX, USA

M. Sabaté-Gilarte European Organization for Nuclear Research (CERN), Meyrin, Switzerland;
Universidad de Sevilla, Sevilla, Spain

Y. Saito TRIUMF, Vancouver, BC, Canada

H. Sakurai RIKEN Nishina Center, Wako, Saitama, Japan;
Department of Physics, University of Tokyo, Tokyo, Japan

A. Saxena Bhabha Atomic Research Centre (BARC), Mumbai, India

J. Schell European Organization for Nuclear Research (CERN), Meyrin, Switzerland;
University of Manchester, Manchester, UK

P. Schillebeeckx European Commission JRC, Institute for Reference Materials and Measurements, Geel, Belgium

Lothar Ph. H. Schmidt Goethe University Frankfurt, Frankfurt, Germany

S. Schmidt Johann-Wolfgang-Goethe Universitat, Frankfurt, Germany

Markus S. Schöffler Goethe University Frankfurt, Frankfurt, Germany

D. Schumann Paul Scherrer Institut (PSI), Villingen, Switzerland

Christian Schwarz Goethe University Frankfurt, Frankfurt, Germany

Laura J. A. Scott Astrophysics Group, Lennard-Jones Laboratories, Keele University, Keele, UK

P. Sedyshev Instituto Superior Tecnco, Universidade de Lisboa, Lisbon, Portugal

C. Seiffert European Organization for Nuclear Research (CERN), Meyrin, Switzerland

D. Seiler Department of Physics, Technical University Munich, Garching, Germany

A. Sekhar University of Manchester, Manchester, UK

I. L. Semisalov NSC "Kharkiv Institute of Physics and Technology", Kharkiv, Ukraine

M. L. Sergi Laboratori Nazionali del Sud di Catania, LNS-INFN, Catania, Italy

O. Sgouros Department of Physics and HINP, University of Ioannina, Ioannina, Greece

Yangping Shen Department of Nuclear Physics, China Institute of Atomic Energy, Beijing, China

Shota Shibagaki Department of Applied Physics, Fukuoka University, Fukuoka, Japan

H. Shimizu Center for Nuclear Study, The University of Tokyo, Wako, Saitama, Japan

Y. Shimizu RIKEN Nishina Center, Wako, Saitama, Japan

S. Siem Department of Physics, University of Oslo, Oslo, Norway

J. A. Silano University of North Carolina at Chapel Hill, Chapel Hill, NC, USA; Triangle Universities Nuclear Laboratory, Durham, NC, USA

S. Simone INFN Laboratori Nazionali del Sud, Catania, Italy

J. Simpson STFC Daresbury Laboratory, Daresbury, Warrington, UK

I. Sivacek ASCR-Rez, CZ-250, Rez, Czech Republic

Ye. O. Skakun NSC "Kharkiv Institute of Physics and Technology", Kharkiv, Ukraine

Zuzana Slavkovská Goethe University Frankfurt, Frankfurt, Germany

A. G. Smith University of Manchester, Manchester, UK

Manfred Sobiella Helmholtz-Zentrum Dresden-Rossendorf, Dresden, Germany

P.-A. Söderström RIKEN Nishina Center, Wako, Saitama, Japan

N. Soić Department of Physics, University of Zagreb, Zagreb, Croatia

F. Soramel Dipartimento di Fisica e Astronomia, Univ. di Padova, Padova, Italy; INFN-Sez. di Padova, Padova, Italy

N. V. Sosnin University of Manchester, Manchester, UK

V. Soukeras Department of Physics and HINP, University of Ioannina, Ioannina, Greece

R. Spartá INFN, Laboratori Nazionali del Sud, Catania, Italy

C. Spitaleri Laboratori Nazionali del Sud, INFN, Catania, Italy;
Dipartimento di Fisica e Astronomia, Università degli Studi di Catania, Catania, Italy

T. Sprouse Department of Physics, University of Notre Dame, Notre Dame, IN, USA

P. Sprung Paul Scherrer Institut (PSI), Villingen, Switzerland

Artemis Spyrou National Superconducting Cyclotron Laboratory, Michigan State University, East Lansing, USA;
Department of Physics and Astronomy, Michigan State University, East Lansing, USA;
Joint Institute for Nuclear Astrophysics, Michigan State University, East Lansing, USA

Daniel Stach Helmholtz-Zentrum Dresden-Rossendorf, Dresden, Germany

A. Stamatopoulos National Technical University of Athens (NTUA), Athens, Greece

R. J. Stancliffe Department of Physics & Mathematics, E. A. Milne Centre for Astrophysics, University of Hull, Hull, SC, UK

I. Stefan Institut de Physique Nucléaire, IN2P3/CNRS-Université de Paris XI, Orsay Cedex, France

Kurt E. Stiebing Goethe University Frankfurt, Frankfurt, Germany

Klaus Stöckel Helmholtz-Zentrum Dresden-Rossendorf, Dresden, Germany;
Institute for Nuclear and Particle Physics, TU Dresden, Dresden, Germany

T. Stora European Organization for Nuclear Research (CERN), Meyrin, Switzerland

D. W. Stracener Physics Division, Oak Ridge National Laboratory, Oak Ridge, TN, USA

Oscar Straniero INAF, Osservatorio Astronomico d'Abruzzo, Teramo, Italy;
INFN Laboratori Nazionali del Gran Sasso, Assergi, Italy

E. Strano Dipartimento di Fisica e Astronomia, Univ. di Padova, Padova, Italy;
INFN-Sez. di Padova, Padova, Italy

Frank Strieder Department of Physics, South Dakota School of Mines & Technology, Rapid City, SD, USA

Jun Su Department of Nuclear Physics, China Institute of Atomic Energy, Beijing, China

Chris Sullivan National Superconducting Cyclotron Laboratory, Michigan State University, East Lansing, MI, USA;
Joint Institute for Nuclear Astrophysics: Center for the Evolution of the Elements, Michigan State University, East Lansing, MI, USA;
Department of Physics and Astronomy, Michigan State University, East Lansing, MI, USA

T. Sumikama RIKEN Nishina Center, Wako, Saitama, Japan

L. T. Sun Institute of Modern Physics, Chinese Academy of Sciences, Lanzhou, China

R. Surman Department of Physics, University of Notre Dame, Notre Dame, IN, USA

Toshio Suzuki Department of Physics, College of Humanities and Sciences, Nihon University, Setagaya-ku, Tokyo, Japan;
National Astronomical Observatory of Japan, Mitaka, Tokyo, Japan

H. Suzuki RIKEN Nishina Center, Wako, Saitama, Japan

N. U. H. Syed Department of Physics, University of Oslo, Oslo, Norway

Róbert Szabó Konkoly Observatory, Research Centre for Astronomy and Earth Sciences, Hungarian Academy of Sciences, Budapest, Hungary

T. N. Szegedi University of Debrecen, Debrecen, Egyetem Tér 1., Hungary;
Institue for Nuclear Research (ATOMKI), Debrecen, Hungary

G. Tagliente Istituto Nazionale di Fisica Nucleare, Sezione di Bari, Italy;
INFN, Sezione di Bari, Dipartimento di Fisica, Bari, Italy

J. L. Tain Instituto de Física Corpuscular, CSIC - Universidad de Valencia, Valencia, Spain

Koh Takahashi Argelander-Institute für Astronomie, Universität Bonn, Bonn, Germany

M. Takechi Department of Physics, Niigata University, Niigata, Japan

H. Takeda RIKEN Nishina Center, Wako, Saitama, Japan

B. Tang China Institute of Atomic Energy, Beijing, China

Xiaodong Tang Institute of Modern Physics, CAS, Lanzhou, China;
Joint Department for Nuclear Physics, Lanzhou University, Lanzhou, China

A. Tarifeño-Saldivia Universitat Politècnica de Catalunya, Barcelona, Spain;
Instituto de Fsica Corpuscular, CSIC-Universidad de Valencia, Valencia, Spain

L. Tassan-Got Centre National de la Recherche Scientifique/IN2P3 - IPN, Orsay, France;
European Organization for Nuclear Research (CERN), Meyrin, Switzerland;
Institut de Physique Nucléaire, CNRS-IN2P3, Univ. Paris-Sud, Université Paris-Saclay, Orsay Cedex, France

Laurent Tassan-Got European Organization for Nuclear Research (CERN), Genéve, Switzerland

V. Tatischeff Centre de Sciences Nucléaires et de Sciences de la Matière (CSNSM), CNRS/IN2P3, Université Paris-Sud, Université ParisSaclay, Orsay, France

G. Tenkila Department of Physics and Astronomy, University of British Columbia, Vancouver, British Columbia, Canada

The n_TOF Collaboration

Friedrich-Karl Thielemann Department of Physics, University of Basel, Basel, Switzerland;
Joint Institute for Nuclear Astrophysics - Center for the Evolution of the Elements, East Lansing, USA;
GSI Helmholtz Center for Heavy Ion Research, Darmstadt, Germany

Benedikt Thomas Goethe University Frankfurt, Frankfurt, Germany

S. L. Thomas STFC Rutherford Appleton Laboratory, Didcot, Oxfordshire, UK

Rachel Titus National Superconducting Cyclotron Laboratory, Michigan State University, East Lansing, MI, USA;
Joint Institute for Nuclear Astrophysics: Center for the Evolution of the Elements, Michigan State University, East Lansing, MI, USA;
Department of Physics and Astronomy, Michigan State University, East Lansing, MI, USA

P. Tiwari Department of Physics and Astronomy, National Superconducting Cyclotron Laboratory, Michigan State University, East Lansing, MI, USA

H. K. Toft Department of Physics, University of Oslo, Oslo, Norway

E. Tognelli Dipartimento di Fisica, Universitá di Pisa and INFN - Sezione di Pisa, Pisa, Italy

A. Tolosa-Delgado Instituto de Fisica Corpuscular (CSIC-Univ. de Valencia), Paterna, Spain

D. Torresi Laboratori Nazionali del Sud di Catania, LNS-INFN, Catania, Italy

L. Trache Horia Hulubei National Institute for R&D in Physics and Nuclear Engineering, Bucharest-Maguerele, Romania

Claudia Travaglio INFN - Istituto Nazionale Fisica Nucleare, Turin, Italy;
Astrophysical Observatory Turin, INFN-Turin, Turin, Italy;
INFN, Sezione di Torino, Torino, Italy

Oscar Trippella I.N.F.N. Sezione di Perugia, Perugia, Italy

O. Trippella Department of Physics and Geology, Instituto Nazionale di Fisica Nucleare, Secion of Perugia, University of Perugia, Perugia, Italy;
Istituto Nazionale di Fisica Nucleare - Section of Perugia, Perugia, Italy

A. Tsinganis European Organization for Nuclear Research (CERN), Meyrin, Switzerland

Aurora Tumino Laboratori Nazionali del Sud, INFN, Catania, Italy;
Facoltá di Ingegneria e Architettura, Universitá Kore, Enna, Italy;
Engineering and Architecture Department, University of Kore, Enna, Italy;
Istituto Nazionale di Fisica Nucleare - Laboratori Nazionali del Sud, Catania, Italy;
Dipartimento di Ingegneria e Architettura, Universitá di Enna, Enna, Italy

E. Uberseder Department of Physics & Astronomy and Cyclotron Institute, Texas A&M University, College Station, TX, USA

J. Ulrich Paul Scherrer Institut (PSI), Villingen, Switzerland

Hideyuki Umeda Department of Astronomy, Graduate School of Science, University of Tokyo, Tokyo, Japan

S. Upadhyayula Department of Physics & Astronomy and Cyclotron Institute, Texas A&M University, College Station, TX, USA

Sebastian Urlass Technische Universität Dresden, Dresden, Germany;
Helmholtz-Zentrum Dresden-Rossendorf, Dresden, Germany;
European Organization for Nuclear Research (CERN), Genéve, Switzerland

H. Utsunomiya Department of Physics, Konan University, Higashinada, Kobe, Japan

Jean-Philippe Uzan Institut d'Astrophysique de Paris, CNRS UMR 7095, Institut Lagrange de Paris, Paris, France

S. Valenta Charles University, Prague, Czech Republic

Sophie Van Eck Institut d'Astronomie et d'Astrophysique, Université Libre de Bruxelles, Brussels, Belgium

Elisabeth Vangioni Institut d'Astrophysique de Paris, CNRS UMR 7095, Institut Lagrange de Paris, Paris, France

G. Vannini Istituto Nazionale di Fisica Nucleare, Sezione di Bologna, Italy;
Dipartimento di Fisica e Astronomia, Università di Bologna, Bologna, Italy

V. Variale Istituto Nazionale di Fisica Nucleare, Sezione di Bari, Italy;
INFN, Sezione di Bari, Dipartimento di Fisica, Bari, Italy

N. Vassh Department of Physics, University of Notre Dame, Notre Dame, IN, USA

P. Vaz Instituto Superior Técnico, Lisbon, Portugal;
Instituto Superior Tecnco, Universidade de Lisboa, Lisbon, Portugal

Aparna Venkatesan Department of Physics and Astronomy, University of San Francisco, San Francisco, CA, USA

A. Ventura Istituto Nazionale di Fisica Nucleare, Sezione di Bologna, Italy;
INFN, Sezione di Bologna, Bologna, Italy

Diego Vescovi I.N.F.N. Sezione di Perugia, Perugia, Italy;
Gran Sasso Science Institute, L'Aquila, Italy

P. Vi RIKEN Nishina Center, Wako, Japan

F. L. Villante Laboratori Nazionali del Gran Sasso LNGS-INFN, L'Aquila, Assergi, Italy;
Dipartimento di Scienze Fisiche e Chimiche, Universit dellAquila, L'Aquila, Italy

V. Vlachoudis European Organization for Nuclear Research (CERN), Meyrin, Switzerland

R. Vlastou National Technical University of Athens (NTUA), Athens, Greece

A. V. Voinov Department of Physics and Astronomy, Ohio University, Athens, OH, USA

Meiko Volknandt Goethe University Frankfurt, Frankfurt, Germany

A. Wallner Faculty of Physics, University of Vienna, Vienna, Austria;
Research School of Physics and Engineering, Australian National University, Canberra, Australia

Shuo Wang Shandong Provincial Key Laboratory of Optical Astronomy and Solar-Terrestrial Environment, Institute of Space Science, Shandong University, Weihai, China

S. Warren University of Manchester, Manchester, UK

Benjamin Wehmeyer North Carolina State University, Raleigh, NC, USA;
GSI Helmholtzzentrum für Schwerionenforschung, Darmstadt, Germany

Mario Weigand Goethe University Frankfurt, Frankfurt, Germany

David Weinberger Helmholtz-Zentrum Dresden-Rossendorf, Dresden, Germany

C. Weiß European Organization for Nuclear Research (CERN), Meyrin, Switzerland

A. Wen Department of Physics and Astronomy, University of British Columbia, Vancouver, British Columbia, Canada

Ingo Wiedenhoever Florida State University, Tallahassee, FL, USA

Michael Wiescher JINA and University of Notre Dame, Notre Dame, IN, USA; University of Notre Dame, Notre Dame, IN, USA;
Department of Physics, University of Notre Dame, Notre Dame, IN, USA

K. Wikan Department of Physics, University of Oslo, Oslo, Norway

M. Williams TRIUMF, Vancouver, British Columbia, Canada;
Department of Physics, University of York, Heslington, York, UK

H-F. Wirth Faculty of Physics, Ludwig-Maximilians-Universität München, Munich, Germany

C. Wolf Johann-Wolfgang-Goethe Universitat, Frankfurt, Germany

P. J. Woods School of Physics and Astronomy, University of Edinburgh, Edinburgh, UK

Paul Woodward LCSE and Department of Astronomy, University of Minnesota, Minneapolis, MN, USA;
Joint Institute for Nuclear Astrophysics, Center for the Evolution of the Elements, Michigan State University, East Lansing, MI, USA

C. Wrede Department of Physics and Astronomy, National Superconducting Cyclotron Laboratory, Michigan State University, East Lansing, MI, USA

T. Wright University of Manchester, Manchester, UK

Warren P. Wright NC State University, Raleigh, NC, USA

Q. Wu Institute of Modern Physics, Chinese Academy of Sciences, Lanzhou, China

Shiwei Xu Institute of Modern Physics, Lanzhou, China

X. X. Xu Department of Physics, The University of Hong Kong, Hong Kong, China

Y. Xu ELI-NP/IFIN-HH, Bucharest, Romania

H. Yamaguchi Center for Nuclear Study, The University of Tokyo, Wako, Saitama, Japan

L. Yang Center for Nuclear Study, The University of Tokyo, Wako, Saitama, Japan

Mariya Yavahchova Institute for Nuclear Research and Nuclear Energy, Bulgarian Academy of Sciences, Sofia, Bulgaria

R. Yokoyama Physics Division, Oak Ridge National Laboratory, Oak Ridge, TN, USA

Takashi Yoshida Department of Astronomy, Graduate School of Science, University of Tokyo, Tokyo, Japan;
Graduate School of Science, The University of Tokyo, Hongo, Bunkyo-ku, Tokyo, Japan

Sandra Zavatarelli Istituto Nazionale di Fisica Nucleare - Sezione di Genova, Genoa, Italy

Remco G. T. Zegers National Superconducting Cyclotron Laboratory, Michigan State University, East Lansing, MI, USA;
Joint Institute for Nuclear Astrophysics: Center for the Evolution of the Elements, Michigan State University, East Lansing, MI, USA;
Department of Physics and Astronomy, Michigan State University, East Lansing, MI, USA

G. L. Zhang Institute of Modern Physics, Chinese Academy of Sciences, Lanzhou, China

Z.-Y. Zhang Institute for Astronomy, University of Edinburgh, Edinburgh, UK; ESO, Garching bei München, Germany

N. T. Zhang Center for Nuclear Study, University of Tokyo, Wako, Japan;
Institute of Modern Physics, Chinese Academy of Sciences, Lanzhou, China

G. Zhao Key Laboratory of Optical Astronomy, National Astronomical Observatories, Chinese Academy of Sciences, Beijing, China

Y. L. Zhu Department of Physics, North Carolina State University, Raleigh, NC, USA

Patric Ziel Goethe University Frankfurt, Frankfurt, Germany

P. Žugec Department of Physics, Faculty of Science, University of Zagreb, Zagreb, Croatia

K. Zyriliou Department of Physics, University of Athens, Athens, Greece

Part I
Carbon Fusion

Chapter 1
Resonances in Stellar Carbon Fusion

Alexis Diaz-Torres and Michael Wiescher

Abstract A quantitative study of the astrophysically important sub-barrier fusion of ^{12}C+^{12}C is reported. Low-energy collisions are described in the body-fixed reference frame using wave-packet dynamics within a nuclear molecular picture. In contrast to conventional methods, such as the potential model and the coupled-channels approach, these new calculations reveal three resonant structures in the S-factor, explaining some structures observed in the data. The structures in the data that are not explained are possibly due to cluster effects in the nuclear molecule, which need to be included in the new approach.

1.1 Introduction

The ^{12}C+^{12}C fusion cross sections at very low energies are critical for modelling energy generation and nucleosynthesis during the carbon burning phase of stellar evolution of massive stars ($M \geq 8M_{\odot}$) [1]. These cross sections also determine the ignition conditions for type-Ia supernova explosions [2]. Variations of the fusion rate in its traditional range of uncertainty moderately affect nucleosynthesis in the actual type-Ia explosion event [3]. This situation would change if resonant structures in the low-energy range of the fusion cross sections existed [4]. Such structures have been observed at higher energies and are associated with molecular states. The possible existence of such states at very low energies can significantly affect nucleosynthesis in type-Ia supernovae [5] as well as superbursts on accreting neutron stars [6]. It is therefore important to go beyond conventional approaches for averaged cross-sections, to understand the nature of these molecular phenomena and their occurrence at very low energies.

In [7], a new method based on wave-packet dynamics applied to the sub-barrier fusion of ^{12}C+^{12}C is presented. In contrast to other traditional methods, such as

A. Diaz-Torres (✉)
Department of Physics, University of Surrey, Guildford GU2 7XH, UK
e-mail: a.diaztorres@surrey.ac.uk

M. Wiescher
JINA and University of Notre Dame, Notre Dame, IN 46656, USA

A. Formicola et al. (eds.), *Nuclei in the Cosmos XV*, Springer
Proceedings in Physics 219, https://doi.org/10.1007/978-3-030-13876-9_1

the potential model [8] and the conventional coupled-channel approach [9], wave-packet dynamics quantitatively explains some observed resonances in the fusion cross sections. This is because the new method [7] allows one to include the effects of molecular states on fusion. The present contribution highlights the main results of the theoretical study reported in [7].

1.2 Wave Packet Dynamics

The method of wave packet dynamics has three steps:

(i) the definition of the initial wave function $\Psi(t=0)$,
(ii) the propagation $\Psi(0) \rightarrow \Psi(t)$, dictated by the time evolution operator, $\exp(-i\hat{H}t/\hbar)$, where $\hat{H}$ is the total time-independent Hamiltonian,
(iii) after a long propagation time, the calculation of observables (cross sections, spectra, etc.) from the time-dependent wave function, $\Psi(t)$.

The wave function and the Hamiltonian are represented in a multi-dimensional lattice. These are considered a function of a few collective coordinates such as the internuclear distance and the spherical coordinate angles of the ^{12}C symmetry axis relative to the internuclear radius, thus reducing the complexity of the quantum many-body reaction problem. The present method directly solves the time-dependent Schrödinger equation, without the traditional expansion in a basis of energy eigenstates, which is used in the conventional coupled-channels model. Despite this, the numerically calculated total wave function accounts for all the coupled-channel effects. The irreversible process of fusion at small internuclear distances is described with an absorptive potential for fusion. The heavy-ion collision is described in the rotating center-of-mass frame within a nuclear molecular picture [10]. Expressions for the kinetic-energy operator, the collective potential-energy surface (PES) and the time propagator are provided in Appendices of [7].

1.3 Model Calculations

Figure 1.1 shows real ^{12}C+^{12}C total potentials for $J = 0, 2, 4$ partial waves. Figure 1.1a displays specific cuts in the PES for head-on collisions, while Fig. 1.1b shows effective total potentials after folding the PES (including the centrifugal energy) of non-axial symmetric di-nuclear configurations with the probability density of the ground-state wave-function of the two deformed, colliding ^{12}C nuclei [7]. The Equator-Equator alignment (thin solid line) facilitates the access by tunneling to the potential pockets. All the alignments coexist and compete with each other, the kinetic energy operator driving the system towards either re-separation or fusion in the potential pocket of the Pole-Pole configuration (thick solid line). A strong, imaginary Woods-Saxon potential centered at the minimum of the Pole-Pole potential pocket in

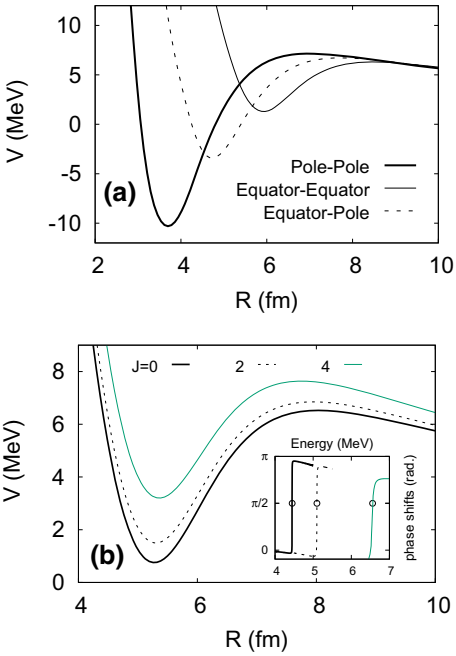

Fig. 1.1 **a** Some cuts in the real PES for ^{12}C+^{12}C as a function of the internuclear distance and three alignments. The total angular momentum is $J = 0$. **b** Effective ^{12}C+^{12}C total potentials for the $J = 0, 2, 4$ partial waves. The plot inserted shows the scattering phase shifts for specific partial waves. The occupation of these potential resonances (circles) causes the structures in the theoretical S-factor in Fig. 1.2

Fig. 1.1a (thick solid line) provides a fusion absorption, which operates very weakly at the potential pockets of the non-axial symmetric configurations (dashed and thin solid lines). The strong repulsive core of the real potentials for non-axial symmetric di-nuclear configurations hinders the effect of the imaginary fusion potential on the potential resonances formed in the corresponding real potential pockets. These potential resonances are shown in the plot inserted in Fig. 1.1b. The occupation of these resonant states (circles in plot inserted) enhances the fusion cross sections, as reflected in the theoretical S-factor in Fig. 1.2.

Figure 1.2 displays model calculations of the astrophysical S-factor (lines) compared with various data sets (symbols) [4, 11–16]. It is observed that the theoretical S-factor curves, clearly affected by uncertainties of the PES of Fig. 1.1a, are rather flat at stellar energies (<3 MeV), without resonant structures. This is because the absence of potential resonances for these energies in Fig. 1.1b. However, cluster effects in the nuclear molecule (e.g., ^{20}Ne + alpha and ^{23}Na + p) can also be very important, possibly leading to additional resonances.

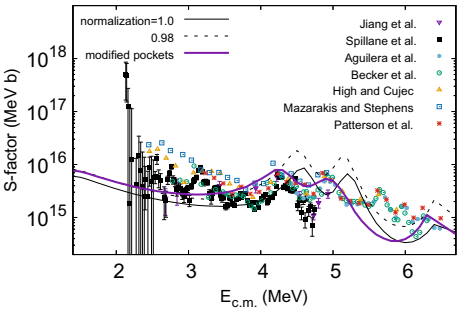

Fig. 1.2 The astrophysical S-factor for $^{12}C+^{12}C$. Measurements (symbols) are compared to model calculations (lines). The model calculations are shown for (i) two normalization factors that multiply the PES in Fig. 1.1a (thin solid and dashed lines), and (ii) a reduction by 15% of the curvature of those potential pockets (thick solid line). The latter improves the location of the predicted fusion resonances

1.4 Summary

Molecular structure and fusion are closely connected. The present calculations indicate that the fusion excitation function monotonically declines towards stellar energies. In contrast to other conventional methods, the new approach reveals three resonant structures in the theoretical S-factor, which explain some observed structures. The structures in the data that are not explained are possibly caused by cluster effects in the nuclear molecule, which need to be included in the new approach.

References

1. M. Pignatari et al., Astrophys. J. **762**, 31 (2013)
2. A. Parikh et al., Astron. Astrophys. **557**, A3 (2013)
3. E. Bravo, G. Martinez-Pinedo, Phys. Rev. C **85**, 055805 (2012)
4. T. Spillane et al., Phys. Rev. Lett. **98**, 122501 (2007)
5. E. Bravo et al., Astron. Astrophys. **535**, A114 (2011)
6. R.L. Cooper et al., Astrophys. J. **702**, 660 (2009)
7. A. Diaz-Torres, M. Wiescher, Phys. Rev. C **97**, 055802 (2018)
8. A. Diaz-Torres, L.R. Gasques, M. Wiescher, Phys. Lett. B **652**, 25 (2007)
9. M. Assuncao, P. Descouvemont, Phys. Lett. B **723**, 355 (2013)
10. W. Greiner, J.Y. Park, W. Scheid, *Nuclear Molecules* (World Scientific Publishing, Singapore, 1995)
11. C.L. Jiang et al., Phys. Rev. C **97**, 012801(R) (2018)
12. E.F. Aguilera et al., Phys. Rev. C **73**, 064601 (2006)
13. H.W. Becker et al., Z. Phys. A **303**, 305 (1981)
14. M.D. High, B. Cujec, Nucl. Phys. A **282**, 181 (1977)
15. M.G. Mazarakis, W.E. Stephens, Phys. Rev. C **7**, 1280 (1973)
16. J.R. Patterson et al., Astrophys. J. **157**, 367 (1969)

Chapter 2
On the Mass of Supernova Progenitors: The Role of the $^{12}C+^{12}C$ Reaction

Oscar Straniero, Luciano Piersanti, Inma Dominguez and Aurora Tumino

Abstract A precise knowledge of the masses of supernova progenitors is essential to answer various questions of modern astrophysics, such as those related to the dynamical and chemical evolution of Galaxies. In this paper we revise the upper bound for the mass of the progenitors of CO white dwarfs (M_{up}) and the lower bound for the mass of the progenitors of normal type II supernovae ($M^{\star}_{up}$). In particular, we present new stellar models with mass between 7 and 10 $M_{\odot}$, discussing their final destiny and the impact of recent improvements in our understanding of the low energy rate of the $^{12}C+^{12}C$ reaction.

2.1 Introduction

$M_{up}$is the minimum stellar mass that, after the core-helium burning, develops temperature and density conditions for the occurrence of a hydrostatic carbon burning. Stars whose mass is lower than this limit are the progenitors of C–O white dwarfs and, when they belong to a close binary system, may give rise to explosive phenomena, such as novae or type Ia supernovae. Stars whose mass is only slightly larger than M_{up}ignite C in a degenerate core and, in turn, experience a thermonuclear runaway. Their final destiny may be either a massive O–Ne white dwarf or an e-capture

O. Straniero (✉) · L. Piersanti
INAF, Osservatorio Astronomico d'Abruzzo, Teramo, Italy
e-mail: oscar.straniero@inaf.it

O. Straniero
INFN Laboratori Nazionali del Gran Sasso, Assergi, Italy

L. Piersanti
INFN, Perugia, Italy

I. Dominguez
Departamento de Fisica Teorica y del Cosmos, Universidad de Granada, Granada, Spain

A. Tumino
Facoltá di Ingegneria e Architettura, Universitá degli Studi di Enna Kore, Enna, Italy

INFN, Laboratori Nazionali del Sud, Catania, Italy

A. Formicola et al. (eds.), *Nuclei in the Cosmos XV*, Springer
Proceedings in Physics 219, https://doi.org/10.1007/978-3-030-13876-9_2

supernova. More massive objects ignite C in non-degenerate conditions and, after the Ne, O and Si burning, they produce a degenerate Fe core. These stars are the progenitors of various type of core-collapse supernovae among which the well known type IIp. In spite of their importance, a precise evaluation of M_{up} and $M^{\star}_{up}$ is still missing (see, e.g., [1, 2]). It relies on our knowledge of various input physics used in stellar modelling, such as the plasma neutrino rate, responsible of the cooling of the core, the equation of state of high density plasma, which affects the compressibility and the consequent heating of the core, and the $^{12}C+^{12}C$ reaction rate. In addition M_{up} and $M^{\star}_{up}$ depend on the C–O core mass, which is determined by the extension of the convective instabilities during the H and He-burning phases, such as convective overshoot, semiconvection or rotational induced mixing. In this paper, we revise the theoretical predictions of M_{up} and $M^{\star}_{up}$. New stellar models of stars whose initial mass ranges between 7 and 10 $M_{\odot}$ and nearly solar composition, i.e., Z = 0.02 and Y = 0.27, are presented. Finally we provide a quantitative evaluation of the effects of the latest $^{12}C+^{12}C$ reaction rate as revised after the new experimental studies based on the Trojan Horse Method [3].

2.2 Carbon Burning in Degenerate C–O Cores

All the models here presented have been computed with the latest version of the FUNS code (see [4, 5]). Rotation is here neglected, but its effects will be discussed in a forthcoming paper. The Kippenhahn diagram of the C burning phase of the 8.5 $M_{\odot}$ stellar model is shown in Fig. 2.1 (left). C ignites at about 0.15 $M_{\odot}$ from the center, where the temperature attains its maximum value. More inside, the cooling induced by the emission of plasma-neutrinos prevents the C burning. Suddenly, a quite extended convective shell develops, powered by the thermonuclear runaway. This episode lasts for about 4000 year. Then, for a short period of time the C burning dies down, meanwhile the contraction and the consequent heating restart, until a

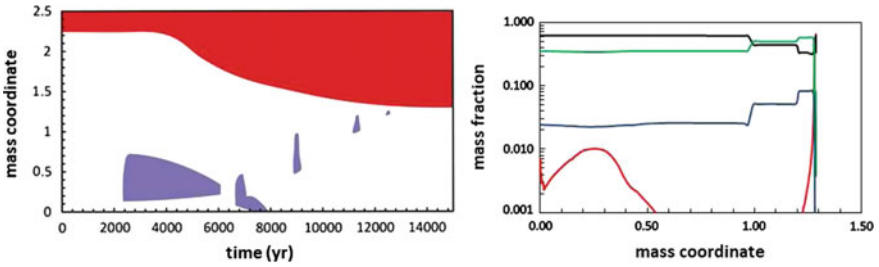

Fig. 2.1 Left: Kippenhahn diagram of the degenerate C burning in the 8.5 $M_{\odot}$stellar model. The red region corresponds to the convective envelope, while the violet regions are the convective C-burning episodes. Note that the t = 0 point is arbitrary. Right: final composition: C (red), O (black), Ne (green), Mg (blue)

new off-center C ignition follows. This time, the released thermal energy diffuses inward, so that the maximum temperature moves toward the center and a convective core develops. After about 500 year, the convective core disappears. Later on, the maximum temperature moves outside again, giving rise to 3 distinct convective C-burning episodes. The final composition of the resulting O–Ne core is shown in Fig. 2.1 (right). The main components are ^{16}O and ^{20}Ne, with a lower, but non-negligible, amount of ^{24}Mg. Note that in the innermost 0.5 $M_\odot$, the original carbon has not besn fully consumed.

2.3 M_{up} and $M^{\star}_{up}$

In order to determine the values of M_{up} and $M^{\star}_{up}$, we have computed 2 sets of models, with masses ranging between 7.0 and 10.0 $M_\odot$ (step 0.5 $M_\odot$), and different choices of the $^{12}C+^{12}C$ reaction rate, namely, the Caughlan and Fowler (CF88) [6] and the Trojan Horse (THM) [3] rates. Figure 2.2 reports the final composition of the cores

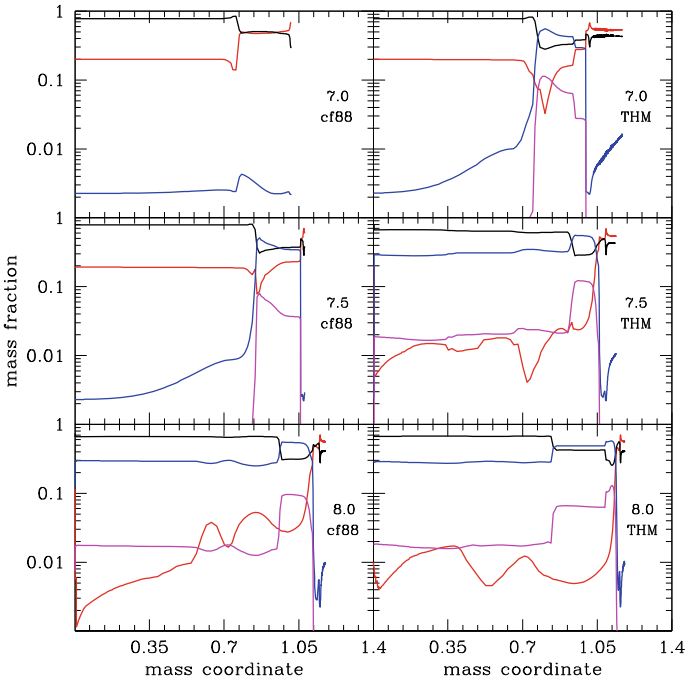

Fig. 2.2 Left: final composition within the core of the 7.0, 7.5 and 8.0 $M_\odot$ stellar model computed by adopting the CF88 rate for the $^{12}C+^{12}C$ reaction. Right: as in the left panels, but adopting the THM rate for the $^{12}C+^{12}C$ reaction. Colors represent different chemical species: C (red), O (black), Ne (blue), Mg (magenta)

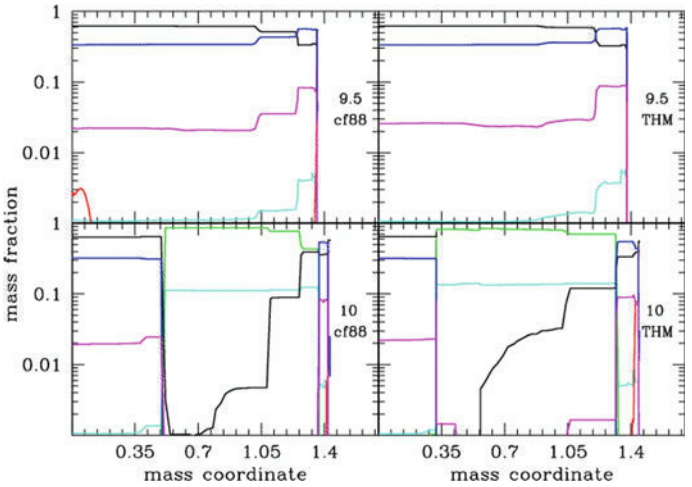

Fig. 2.3 Left panel: As in Fig. 2.2, but for M = 9.5 and 10 $M_{\odot}$. Colors represents: C (red), O (black), Ne (blue), Mg (magenta), Si (green), S (cyan)

for the models 7.0, 7.5 and 8.0 $M_{\odot}$. With the CF88 rate (left panels), the lighter model never attains the conditions for the C ignition and proceeds its evolution entering the AGB phase. Then, the 7.5 and the 8.0 $M_{\odot}$ undergo an incomplete C burning. In particular, in the 7.5 $M_{\odot}$ model, the C burning remains confined within a small shell located near the external border of the C–O core. Only for $M \geq 8.5\ M_{\odot}$, after the usual off-center ignition, the C burning propagates inward down to the center, and a complete C burning takes place, resulting in the formation of an O–Ne core. When the THM rate is adopted (right panels in Fig. 2.2), we find similar final compositions but for models $\sim$0.5 $M_{\odot}$ less massive. Concerning $M^{\star}_{up}$, Fig. 2.3 shows the final compositions of the 9.5 and 10 $M_{\odot}$ models. In this case we find little differences between the CF88 and the THM models. In both cases, the 9.5 $M_{\odot}$ model never attains the conditions for the Ne photo-dissociation. On the contrary the 10 $M_{\odot}$ models ignite C at the center. Then, they experience a complete C burning. Later on, the Ne photo-dissociation starts at about 1 $M_{\odot}$ and the evolution proceeds through the more advanced burning phases (note that we stopped the computations when the O burning was still moving inward).

References

1. C.L. Doherty, P. Gil-Pons, L. Siess, J.C. Lattanzio, H.H.B. Lau, Not. R. Astron. Soc. **446**, 2599 (2015)
2. O. Straniero, L. Piersanti, S. Cristallo, J. Phys. Conf. Ser. **665**, 012008 (2016)

3. A. Tumino et al., Nature **557**, 687 (2018)
4. O. Straniero, R. Gallino, S. Cristallo, Nucl. Phys. A **777**, 311 (2006)
5. L. Piersanti, S. Cristallo, O. Straniero, Astrophys. J. **774**, 98 (2013)
6. G.R. Caughlan, W.A. Fowler, Atomic Data Nucl. Data Tables **40**, 283 (1988)

Chapter 3
The $^{12}C+^{12}C$ Fusion Reaction at Stellar Energies

Xiaodong Tang

Abstract The carbon fusion reaction is a crucial reaction in stars. Due to its complicated reaction mechanism, there is a large uncertainty in the S* factor at stellar energies. In this talk, I will review the challenges in the study of carbon burning. An outlook for the future studies will also be presented.

The $^{12}C+^{12}C$ reaction plays an important role in a wide variety of stellar burning scenarios such as massive stars, type Ia supernovae and superbursts. The important energy range covers from few 10s keV up to around 3 MeV [1]. At sub-barrier energies, the main products of $^{12}C+^{12}C$ are n, p and α. To obtain the fusion reaction cross section at such energies, two different techniques have been used. One is the particle spectroscopy and the other is the characteristic γ-ray spectroscopy. Patterson [2], Mazarakis [3] and Becker [4] extended the measurements below 2.7 MeV by counting the protons and alphas from the fusion reaction process. As energy approaches the astrophysical region, backgrounds arising from the target impurity and other sources produce a significant background. Some proton and alpha channels could not be identified, leading to underestimation of the total fusion cross sections. Kettner [5], Aguilera [6] and Spillane [7] measured the cross sections of the characteristic γ-rays of the fusion residues, ^{23}Na, ^{20}Ne and ^{23}Mg. Since some decays of the fusion residues bypass the decay of the characteristic γ-rays, the sum of the characteristic γ-ray cross sections reflects only a fraction of the total fusion cross section. A recent direct measurement of ^{12}C(^{12}C,n)^{23}Mg has been performed at stellar energies, providing a reliable rate [8]. The results of some measurements are shown in Fig. 3.1 as the modified S factor, $S^*(E_{c.m.}) = \sigma(E_{c.m.})E_{c.m.}exp(\frac{87.21}{\sqrt{E_{c.m.}}} + 0.46E_{c.m.})$.

Mazarakis's measurement showed the S* factor had a uprising trend as the energy decreases. With the resonances at higher energies, it was found his energy needs to be shifted by +100 keV. After this correction, the uprising trend in the S* factor

X. Tang (✉)
Institute of Modern Physics, CAS, Lanzhou, People's Republic of China
e-mail: xtang@impcas.ac.cn

X. Tang
Joint Department for Nuclear Physics, Lanzhou University, Lanzhou, China

X. Tang
Institute of Modern Physics, CAS, Huairou, China

A. Formicola et al. (eds.), *Nuclei in the Cosmos XV*, Springer
Proceedings in Physics 219, https://doi.org/10.1007/978-3-030-13876-9_3

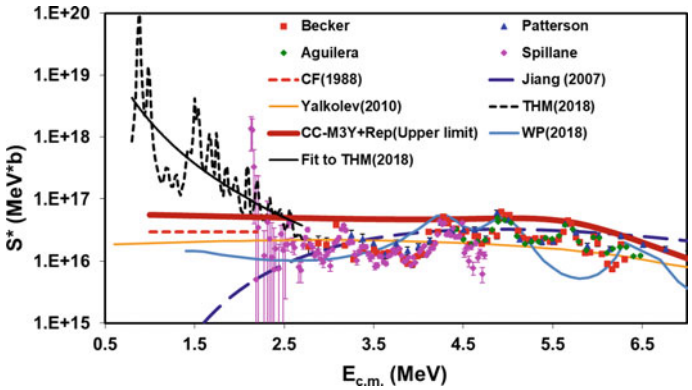

Fig. 3.1 S* factors of $^{12}C+^{12}C$. The $^{12}C+^{12}C$ data from [2, 4, 6, 7] shown as red, green, magenta and blue points, respectively. Model calculations, CC-M3Y+Rep (thick dark red), SPP (oragen), TDWP (light blue) and hindrance (blue dashed) are also shown, respectively. The recommended averaged S* factor by CF88 is shown as red dashed line. The THM result and the fit are shown as black dashed and solid lines, respectively

disappeared [9]. Barron used a smoothing method to wash out the resonances, leading to no way of checking the energy calibration [10]. Therefore, such kind of measurements should not be considered to be valid. Spillane et al. claimed a strong resonance at $E_{c.m.}$ = 2.14 MeV with a S* factor more than 2 orders of magnitude higher than any other S* factors at higher energies [7]. A measurement of $^{12}C(^{12}C,p)^{23}Na$ was carried out in the same region [11]. However, they could not confirm this strong resonance due to large error bars.

The $^{12}C+^{12}C$ has a complicated resonance feature which continues all the way from the Coulomb barrier energy down to the lowest measured energies. These resonances have a characteristic width of about 100 keV. Since there is no way to model the resonances in the unmeasured energy range, the averaged S* factor are used for extrapolation while the resonances are treated as the fluctuation. Since the width of the Gamow window is comparable or wider than the the $^{12}C+^{12}C$ resonance width, the averaged S* factor is a reasonable approach for the astrophysical application. In order to extrapolate the experimental results to the energy region of astrophysical interest, the modified S* factor was introduced to remove from the cross-section the penetrability of the Coulomb barrier, which dominates all the other effect, by taking the second-order expression for the barrier transmission of a square-well black nucleus, for l = 0, and neglecting all higher-order terms [2]. Considering the data with energies below 0.8 of the Coulomb barrier in $^{12}C+^{12}C$, Patterson recommended an averaged S* factor of 2.9×10^{16} MeV b for the lower energies [2]. The standard $^{12}C+^{12}C$ reaction rate was established by Caughlan and Fowler who revised this value to be 3×10^{16} MeV b by including more measurements [12]. This simple extrapolation agrees reasonably with some recent theoretical calculations, such as

CC-M3Y+Rep [13], TDWP [14] and barrier penetration model based on the global São Paulo potentials (SPP) [1]. Guided by the experimental S factors of the medium-heavy systems, Jiang et al. developed a phenomenological hindrance model which predicts that the $^{12}C+^{12}C$ S-factor reaches its maximum [15]. At lower energies, this model predicts a rapid drop in the S factor leading to a reduced reaction rate that is many orders of magnitude smaller than the standard rate used for astrophysical modeling. To check the predictive powers of the hindrance and other models, a measurement of the $^{12}C+^{13}C$ is being carried out at deep sub-barrier energies [16].

Recently the Trojan Horse Method (THM) has been applied to determine the $^{12}C+^{12}C$ fusion S-factor at energies below $E_{c.m.}$ = 2.7 MeV [17], resulting in a new averaged S-factor with a rising slope much faster than any models presented in Fig. 3.1. And the averaged S* factor rises fast as the energy decreases by comparing with the flat trend observed with the data obtained from the direct measurement. Why are the resonances obtained by THM so special that they change the trend of the averaged S* factor? Right now there is an ongoing debate on the applicability of the THM theory of converting the indirect measurement into the astrophysical S* factor [18, 19]. Before drawing any final conclusion from the measurement in [17] and determining the actual trend of the averaged S* factor at stellar energies, both accurate direct measurements at energies below $E_{c.m.}$ = 2.7 MeV and the validation of the THM approach at higher energies with a better overlap with the direct measurements would be urgently needed.

In contrast to the striking resonances observed in the $^{12}C+^{12}C$ fusion reaction, the other carbon systems, such as $^{12}C+^{13}C$ and $^{13}C+^{13}C$, behave more regularly. Only minor resonance features have been observed in these two systems. By comparing the cross sections for the three carbon isotope systems, $^{12}C+^{12}C$, $^{12}C+^{13}C$, and $^{13}C+^{13}C$, it is found that the cross sections for $^{12}C+^{13}C$ and $^{13}C+^{13}C$ provide an upper limit for the fusion cross section of $^{12}C+^{12}C$ over a wide energy range. After calibrating the effective nuclear potential for $^{12}C+^{12}C$ using the $^{12}C+^{13}C$ and $^{13}C+^{13}C$ fusion cross sections, it is found that a coupled-channels calculation with the ingoing wave boundary condition (CC-M3Y+Rep) predicts the major peak cross sections in $^{12}C+^{12}C$ and serves as an excellent upper bound to all the experimental $^{12}C+^{12}C$ S* factor except that the strong resonance found at 2.14 MeV exceeds this upper limit by a factor of more than 20 [20]. Another contradiction is that the indirect result obtained with THM is much higher than the upper limit.

Despite of more than half a century of studies, there are large discrepancies in how to extrapolate the averaged fusion cross section and modeling the resonances in the astrophysical energy region. Precise direct measurement at energies below 2.6 MeV is the key for resolving the problems. Such data are expected to be available by using new experiment techniques, such as particle and γ coincidence technique and underground experiment. Experimental and theoretical studies of the fusion reaction cross sections for the carbon isotope systems are useful for modeling the average trend of the $^{12}C+^{12}C$ fusion cross section.

References

1. L.R. Gasques et al., Implications of low-energy fusion hindrance on stellar burning and nucleosynthesis. Phys. Rev. C **76**, 035802 (2007). https://doi.org/10.1103/PhysRevC.76.035802
2. J.R. Patterson, H. Winkler, C.S. Zaidins, Experimental investigation of the stellar nuclear reaction ^{12}C+^{12}C at low energies. Astrophys. J. **157**, 367 (1969). https://doi.org/10.1086/150073
3. M.G. Mazarakis, W.E. Stephens, Experimental measurements of the ^{12}C+^{12}C nuclear reactions at low energies. Phys. Rev. C **7**, 1280 (1973). https://doi.org/10.1103/PhysRevC.7.1280
4. H.W. Becker, K.U. Kettner, C. Rolfs, H.P. Trautvetter, The ^{12}C+^{12}C reaction at sub-coulomb energies (II). Z. Phys. A **303**, 305 (1981). https://doi.org/10.1007/BF01421528
5. K.U. Kettner, H. Lorenz-Wirzba, C. Rolfs, The ^{12}C+^{12}C reaction at sub-coulomb energies (I). Z. Phys. A **298**, 65 (1980)
6. E.F. Aguilera et al., New γ-ray measurements for ^{12}C+^{12}C sub-coulomb fusion: toward data unification. Phys. Rev. C **73**, 064601 (2006). https://doi.org/10.1103/PhysRevC.73.064601
7. T. Spillane et al., ^{12}C+^{12}C fusion reactions near the Gamow energy. Phys. Rev. Lett. **98**, 122501 (2007). https://doi.org/10.1103/PhysRevLett.98.122501
8. B. Bucher et al., First direct measurement of ^{12}C(^{12}C, n)^{23}Mg at stellar energies. Phys. Rev. Lett. **114**, 251102 (2015). https://doi.org/10.1103/PhysRevLett.114.251102
9. C.A. Barnes, S. Trentalange, S.C. Wu, *Treatise on Heavy-Ion Science (Chap. 1)* (Plenum Press, New York, 1985), pp. 3–60
10. L. Barron-Palos et al., Absolute cross sections measurement for the ^{12}C+^{12}C system at astrophysically relevant energies. Nucl. Phys. A **779**, 318 (2006). https://doi.org/10.1016/j.nuclphysa.2006.09.004
11. J. Zickefoose et al., Measurement of the ^{12}C(^{12}C, p)^{23}Na cross section near the Gamow energy. Phys. Rev. C **97**, 065806 (2018). https://doi.org/10.1103/PhysRevC.97.065806
12. G.R. Caughlan, W.A. Fowler, Thermonuclear reaction rates V. At. Data Nucl. Data Tables **40**, 283 (1988). https://doi.org/10.1016/0092-640X(88)90009-5
13. H. Esbensen, X. Tang, C.L. Jiang, Effects of mutual excitations in the fusion of carbon isotopes. Phys. Rev. C **84**, 064613 (2011). https://doi.org/10.1103/PhysRevC.84.064613
14. A. Diaz-Torres, M. Wiescher, Characterizing the astrophysical S factor for ^{12}C+^{12}C fusion with wave-packet dynamics. Phys. Rev. C **97**, 055802 (2018). https://doi.org/10.1103/PhysRevC.97.055802
15. C.L. Jiang et al., Expectations for ^{12}C and ^{16}O induced fusion cross sections at energies of astrophysical interest. Phys. Rev. C **75**, 015803 (2007). https://doi.org/10.1103/PhysRevC.75.015803
16. D. Tudor et al., Activation measurements of ^{13}C+^{12}C fusion cross section at deep sub-barrier energies in IFIN-HH. AIP Conf. Proc. **1852** (2017). https://doi.org/10.1063/1.4984886
17. A. Tumino et al., An increase in the ^{12}C+^{12}C fusion rate from resonances at astrophysical energies. Nature **557**, 687 (2018). https://doi.org/10.1038/s41586-018-0149-4
18. A. Mukhamedzhanov, X. Tang, D. Pang, Comments on the ^{12}C+^{12}C fusion S*-factor. arXiv:1806.05921 [nucl-ex]
19. A. Mukhamedzhanov, D. Pang, Astrophysical factors of ^{12}C+^{12}C fusion from Trojan horse method arXiv:1806.08828 [nucl-th]
20. M. Notani et al., Correlation between the ^{12}C+^{12}C, ^{12}C+^{13}C, ^{13}C+^{13}C fusion cross sections. Phys. Rev. C **85**, 014607 (2012). https://doi.org/10.1103/PhysRevC.85.014607

Chapter 4
The Resonant Behaviour of the $^{12}C+^{12}C$ Fusion Cross Section at Astrophysical Energies

Aurora Tumino, C. Spitaleri, M. La Cognata, S. Cherubini, G. L. Guardo, M. Gulino, S. Hayakawa, I. Indelicato, L. Lamia, H. Petrascu, Rosario Gianluca Pizzone, S. M. R. Puglia, G. G. Rapisarda, S. Romano, M. L. Sergi, R. Spartá and L. Trache

Abstract The $^{12}C(^{12}C,\alpha_{0,1})^{20}Ne$ and $^{12}C(^{12}C,p_{0,1})^{23}Na$ reactions, which determine carbon burning in stars, have been measured from $E_{c.m.} = 2.7$ MeV down to 0.8 MeV via the Trojan Horse Method off the deuteron in ^{14}N. This range of energies is relevant for several astrophysical scenarios, from superburst ignition to hydrostatic burning. The measured astrophysical S(E) factors reveal several resonances, which are responsible for a very large increase of the reaction rate at the relevant temperatures.

4.1 Introduction

The $^{12}C+^{12}C$ fusion reactions have been investigated in different scenarios of low-energy nuclear physics for more than five decades. In particular, star evolution and nucleosynthesis of intermediate mass stars (8–10 $M_{\odot}$) and up is strongly influenced by the carbon fusion process [1]. Also superburst models with neutron stars can be constrained by the carbon burning reaction rate, in particular if resonances are found to contribute in the Gamow peak [2]. Carbon burning during the hydrostatic

A. Tumino (✉) · M. Gulino
Facoltà di Ingegneria e Architettura, Universitá "Kore", Enna, Italy
e-mail: tumino@lns.infn.it

C. Spitaleri · M. La Cognata · S. Cherubini · G. L. Guardo · M. Gulino · S. Hayakawa · I. Indelicato · L. Lamia · R. G. Pizzone · S. M. R. Puglia · G. G. Rapisarda · S. Romano · M. L. Sergi · R. Spartá
INFN, Laboratori Nazionali del Sud, Catania, Italy

C. Spitaleri · S. Cherubini · L. Lamia · S. Romano
Dipartimento di Fisica e Astronomia, Università di Catania, Catania, Italy

S. Hayakawa
Center for Nuclear Studies, The University of Tokyo, Tokyo, Japan

H. Petrascu · L. Trache
Horia Hulubei National Institute for R&D in Physics and Nuclear Engineering, Bucharest-Maguerele, Romania

A. Formicola et al. (eds.), *Nuclei in the Cosmos XV*, Springer
Proceedings in Physics 219, https://doi.org/10.1007/978-3-030-13876-9_4

phase takes place from 0.8 to 1.2 GK, corresponding to center-of-mass energies from 1 to 3 MeV. In that sub-Coulomb energy region, the cross section falls rapidly below the nanobarn range. That is why the measurement of the cross section at astrophysical energies remains a difficult task. The compound nucleus ^{24}Mg is formed at an excitation energy much above the particle decay threshold. Alpha, proton and neutron are the dominant evaporation channels, leading respectively to ^{20}Ne, ^{23}Na and ^{23}Mg, which can also be produced in excited bound states. Below a center of mass energy E_{cm} of 2.5 MeV there is not enough energy to feed ^{23}Mg even in its ground state and α and p channel are the only relevant ones at low energies. Several attempts were made to measure the ^{12}C + ^{12}C cross section at astrophysical energies, involving both, charged particle [3–5] and gamma ray spectroscopy [6–11] but, it has only been measured down to E_{cm} = 2.5 MeV, still at the beginning of the region of astrophysical interest. In a more recent study [12], the astrophysical S(E) factor exhibits new resonances at $E_{cm} \leq 3.0$ MeV, with a strong increase at E_{cm} = 2.14 MeV. This behaviour, if confirmed, would enhance the present nonresonant reaction rate of the alpha channel by a factor of 5 near T = 0.8 GK. This would contradict the proposed hypothesis that a sub-barrier fusion hindrance effect [13] might drastically reduce the reaction rate at astrophysical energies. Anyway, until now the only way to reach the astrophysical region has relied on the extrapolation procedure from higher energy data. However, extrapolation is complicated by the presence of possible resonant structures even in the low-energy part of the excitation function. Thus, further measurements extending down to at least 1 MeV would be extremely important. In this paper, we are going to discuss the indirect study of the ^{12}C(^{12}C,α)^{20}Ne and ^{12}C(^{12}C,p)^{23}Na reactions via the Trojan Horse Method (THM) [14–16] applied to the ^{12}C(^{14}N,α^{20}Ne)^{2}H and ^{12}C(^{14}N,p^{23}Na)^{2}H three-body processes in the quasi-free (QF) kinematics regime, where ^{2}H from the ^{14}N TH nucleus is spectator to the ^{12}C + ^{12}C two-body processes. Several experimental works provide evidence of direct ^{12}C transfer in the ^{12}C(^{14}N,d)^{24}Mg* reaction at 30 MeV of beam energy and up [17, 18].

The Trojan Horse Method (THM) was developed as alternative approach to determine the bare nucleus S(E) factor for rearrangement reactions. It has already been applied several times to reactions of astrophysical relevance involving light particles as spectators, such as d, ^{3}He, ^{6}Li ([19–29] and references therein). This is the first application of the THM to heavy ion reactions.

4.2 The Experiment

The experiment was performed at the Laboratori Nazionali del Sud - INFN, using a ^{14}N beam at 30 MeV accelerated by the SMP TANDEM and delivered onto a 100 μg/cm^2 C target with a beam spot on the target smaller than 1.5 mm. The experimental setups consisted of two telescopes (38 μm silicon detector as ΔE- and 1000 μm position sensitive detector (PSD) as E-detector) placed on both sides with respect to the beam direction in symmetric configuration (two on each side), covering angles

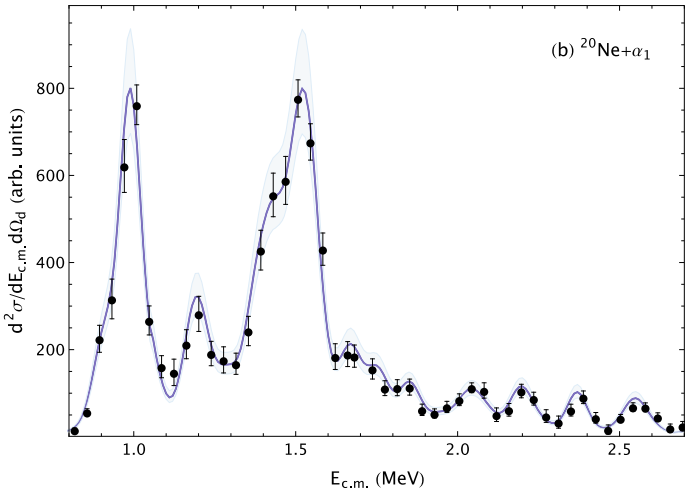

Fig. 4.1 Quasi-free two-body cross section for the $^{20}Ne+\alpha_1$ channel (black filled dots). Solid blue line with light blue band are the result of R-matrix calculations

from 7° to 30°. The ejectile of the two-body reactions (either α or p) was detected in coincidence with the spectator d particle. In order to fulfill the QF requirement for the spectator d particle to be essentially part of the beam, this particle was detected at forward angles. The trigger for the event acquisition was given by the coincidences between the two telescopes. The angular regions covered by the detectors were optimized for measuring the break-up process of interest in QF kinematics, and the investigated range of deuteron momentum values was feasible to check the existence of the QF mechanism.

4.3 Results

After completion of the several steps involved in the data analysis, the half-of-shell two-body cross section of astrophysical relevance was extracted for four channels: $^{20}Ne+\alpha_0$, $^{20}Ne+\alpha_1$, $^{23}Na+p_0$ and $^{23}Na+p_1$. The yield for the $^{20}Ne+\alpha_1$ channel is shown in Fig. 4.1 (black solid dots) as a function of the $^{12}C+^{12}C$ relative energy variable, E_{cm}.

A modified one-level (interference not included, see Methods in [30] for details) many-channel R-matrix analysis was carried out including the ^{24}Mg states reported in [30]. If one considers the α_1 and p_1 fractions of the total fusion yield observed at $E_{c.m.}$ below 2.8 MeV [5, 12] and reported in [12], the lower limits of the $\alpha_0+\alpha_1$ and p_0+p_1 contributions to the total cross sections from the present experiment at the highest energies are 0.85 ± 0.07 and 0.68 ± 0.06, respectively. However, the number of accessible excited states for both ^{20}Ne and ^{23}Na already reduces to half

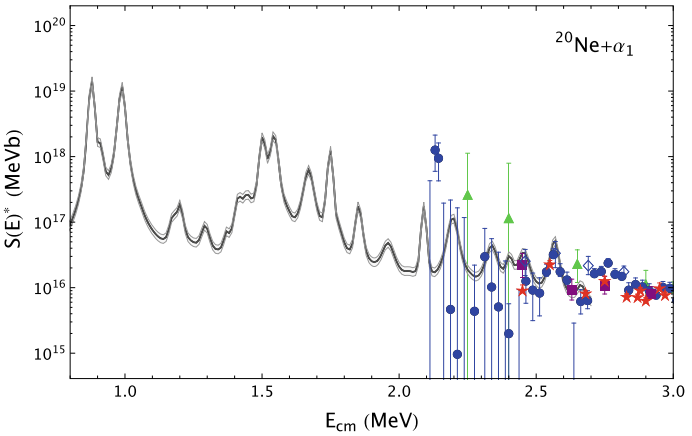

Fig. 4.2 S(E)* astrophysical factor for the ^{20}Ne+α_1 channel (black solid line and shading). Available direct data in the investigated $E_{c.m.}$ range are reported as purple filled squares [3], blue empty diamonds [6], red filled stars [7], blue filled circles [12] and green filled triangles [9]

while moving from $E_{c.m.}$ = 2.8 to 1.5 MeV and the cross sections for ^{20}Ne and ^{23}Na excited states are expected to drop steeper than those for ground states, due to the sharper decrease of the corresponding penetration factors. Monitoring the decrease of the penetration factors for the relevant states, and according to the results of [5] at $E_{c.m.} \leq 3$ MeV, the fraction of the total fusion yield from α and p channels other than $\alpha_{0,1}$ and $p_{0,1}$ was neglected in the modified R-matrix analysis with estimated errors at $E_{c.m.}$ below 2 MeV lower than 1% and 2% for the α and p channels, respectively. The result for the ^{20}Ne+α_1 channel is shown in Fig. 4.1 as middle solid blue line with light blue band arising from the uncertainties on the resonance parameters, including correlations. The resonance structure observed in the excitation functions is consistent with ^{24}Mg level energies reported in the literature. The tendency for the even J states to be clustered at about 1.5 MeV might be a sign of intermediate structure of ^{24}Mg associated with a ^{12}C+^{12}C molecular configuration. The THM reduced widths thus entered a standard R-matrix code and the S(E) factors for the four reaction channels were determined.

The results are shown in Fig. 4.2 for the ^{20}Ne+α_1 in terms of modified S(E) factor, S(E)*, as defined in [11, 12]. The black middle line and the grey band represent the best fit curve and the range defined by the total uncertainties, respectively. The grey band is the result of R-matrix calculations with lower and upper values of the resonance parameters provided by their errors.

The resonant structures are superimposed onto a flat nonresonant background taken from [12] for all channels and quoted as 0.4×10^{16} MeVb. Unitarity of the S-matrix is guaranteed within the experimental uncertainties. Normalization to direct data was done in the $E_{c.m.}$ window 2.5–2.63 MeV of the ^{20}Ne+α_1 channel where a sharp resonance corresponding to the level of ^{24}Mg at 16.5 MeV shows up and available data [3, 6, 7, 12] in this region are the most accurate among those available

in the full overlapping region with THM data. Scaling to the resonance by means of a weighted normalization, the resulting normalization error is 5% that enters the definition of the grey band of Fig. 4.2, combined in quadrature with errors on the resonance parameters.

All the existing direct data below $E_{c.m.}$ = 3 MeV are shown as blue filled circles [12], purple filled squares [3], blue empty diamonds [6], red filled stars [7] and green filled triangles [9]. Except for the data from [12], their low energy limit is fixed by background due to hydrogen contamination in the targets. Agreement between THM and direct data is apparent within the experimental errors except for the direct low-energy limit around 2.14 MeV, where THM data do not confirm the claim of a strong resonance, rather a nearby one at 2.095 MeV about one order of magnitude less intense in the $^{20}Ne+\alpha_1$ channel (see Fig. 4.2) and with similar intensity in the $^{23}Na+p_1$ one. The present result is in agreement with spectroscopy studies of [31, 32] with a deep at 2.14 MeV and no particularly strong α state around 2.1 MeV. Further agreement is found with the unpublished experimental data down to $E_{c.m.}$ = 2.15 MeV from [33] for the $^{12}C(^{12}C,p_{0,1})^{23}N$ reactions. Our result is also consistent with the total S(E)* from a recent experiment at higher energies [34] calculated at the overlapping $E_{c.m.}$ value of 2.68 ± 0.08 MeV.

The reaction rates for the four processes were calculated from the THM S(E)* factors using the standard formula reported in [35]. Since the total $^{12}C+^{12}C$ fusion yield at $E_{c.m.}$ below 2.8 MeV is likely to be exhausted by the $\alpha_{0,1}$ and $p_{0,1}$ channels (see Methods), we assume that the sum of their reaction rates in the $E_{c.m.}$ range here investigated is representative of the total one.

The reaction rate experiences a variation below 2 GK with an increase from a factor of 1.18 at 1.2 GK to a factor of more that 25 at 0.5 GK with respect to the reference rate reported in [36]. The latter increase, due mainly to the resonant structure around $E_{c.m.}$ = 1.5 MeV, endorses the fiducial value conjectured in [2] to reduce down to a factor of 2 the theoretical superburst ignition depths in accreting neutron stars for a realistic range of crust thermal conductivities and core Urca neutrino emissivities. This change is compatible with the observationally inferred superburst ignition depths. In other words, carbon burning can trigger superbursts. As for the hydrostatic carbon burning regime, the present rate change will lower temperatures and densities at which ^{12}C ignites in massive post-main-sequence stars. Taking advantage of the stellar modeling reported in [37], for core C-burning of a star of $25M_{\odot}$, the ignition temperature and density would undergo a decrease of down to 10% and 30% respectively. Additional work is needed to investigate the impact that the new $^{12}C+^{12}C$ reaction rate has in the various astrophysical contexts.

References

1. E. Garcia-Berro et al., Astrophys. J. **286**, 765 (1997)
2. R.L. Cooper et al., Astrophys. J. **702**, 660 (2009)
3. M.G. Mazarakis, W.E. Stephens, Phys. Rev. C **7**, 1280 (1973)

4. J.R. Patterson, H. Winkler, C.S. Zaidins, Astrophys. J. **157**, 367 (1969)
5. H.W. Becker, K.U. Kettner, C. Rolfs, H.P. Trautvetter, Z. Phys, A **303**, 305 (1981)
6. M.D. High, B. Cujec, Nucl. Phys. A **282**, 181 (1977)
7. K.U. Kettner, H. Lorenz-Wirzba, C. Rolfs, Z. Phys, A **298**, 65 (1980)
8. P. Rosales et al., Rev. Mex. Phys. **49**(S4), 88 (2003)
9. L. Barrón-Palos et al., Nucl. Phys. A **779**, 318 (2006)
10. L. Barrón-Palos et al., Eur. Phys. J. A Direct (2005). https://doi.org/10.1140/epjad/i2005-06-008-2
11. E.F. Aguilera et al., Phys. Rev. C **73**, 064501 (2006)
12. T. Spillane et al., Phys. Rev. Lett. **98**, 122501 (2007)
13. C.L. Jiang et al., Phys. Rev. C **75**, 015803 (2007)
14. C. Spitaleri et al., Phys. At. Nucl. **74**, 1763 (2011)
15. A. Tumino et al., Few Body Syst. **54**(5–6), 745 (2013)
16. R. Tribble et al., Rep. Prog. Phys. **77**(10), 106901 (2014)
17. K.P. Artemov et al., Phys. Lett. **149 B**, 325 (1984)
18. R.W. Zurmuehle et al., Phys. Rev. C **49**, 2549 (1994)
19. A. Rinollo et al., Nucl. Phys. A **758**, 146 (2005)
20. R.G. Pizzone et al., A & A **438**, 779 (2005)
21. S. Romano et al., Eur. Phys. J. A **27**, 221 (2006)
22. M. La Cognata et al., Phys. Rev. Lett. **101**, 152501 (2008)
23. A. Tumino et al., Phys. Rev. Lett. **98**, 252502 (2007)
24. A. Tumino et al., Phys. Rev. C **78**, 064001 (2008)
25. A. Tumino et al., Phys. Lett. B **700**, 111 (2011)
26. A. Tumino et al., Phys. Lett. B **705**, 546 (2011)
27. L. Lamia et al., Astrophys. J. **768**, 65 (2013)
28. A. Tumino et al., Astrophys. J. **785**, 96 (2014)
29. Li Chengbo et al., Phys. Rev. C **92**, 025805 (2015)
30. A. Tumino et al., Nature **557**, 687 (2018)
31. R. Abegg, C.A. Davis, Phys. Rev. C **43**, 6 (1991)
32. A. Caciolli et al., NIM B **266**, 1932 (2008)
33. J. Zickefoose, Phys. Rev. C **97**, 065806 (2018)
34. C.L. Jiang et al., Phys. Rev. C **97**, 012801(R) (2018)
35. C. Iliadis, *Nuclear Physics, of Stars* (WILEY- VCH Verlag GmbH & Co., KGaA, Weinheim, 2007)
36. G.R. Caughlan, W.A. Fowler, At. Data Nucl. Data Tables **40**, 283 (1988)
37. M. Pignatari et al., Astrophys. J. **762**, 31 (2013)

Part II
Cosmology and Big Bang Nucleosynthesis

Chapter 5
^{7}Be(n,p)^{7}Li Cross Section Measurement for the Cosmological Lithium Problem at the n_TOF Facility at CERN

L. A. Damone, M. Barbagallo, M. Mastromarco, A. Mengoni, N. Colonna, L. Cosentino, E. A. Maugeri, S. Heinitz, D. Schumann, R. Dressler, F. Käppeler, P. Finocchiaro, J. Andrzejewski, J. Perkowski, A. Gawlik, O. Aberle, S. Altstadt, M. Ayranov, L. Audouin, M. Bacak, J. Balibrea-Correa, J. Ballof, V. Bcares, F. Bečvař, C. Beinrucker, G. Bellia, A. P. Bernardes, E. Berthoumieux, J. Billowes, M. J. G. Borge, D. Bosnar, A. Brown, M. Brugger, Maurizio Busso, M. Caamaño, F. Calviño, M. Calviani, D. Cano-Ott, R. Cardella, A. Casanovas, D. M. Castelluccio, R. Catherall, F. Cerutti, Y. H. Chen, E. Chiaveri, G. Cortès, M. A. Cortès-Giraldo, Sergio Cristallo, M. Diakaki, M. Dietz, C. Domingo-Pardo, A. Dorsival, E. Dupont, I. Durán, B. Fernàndez-Dominguez, A. Ferrari, P. Ferreira, W. Furman, S. Ganesan, A. Garca-Rios, S. Gilardoni, T. Glodariu, Kathrin Göbel, I. F. Gonçalves, E. Gonzalez-Romero, T. D. Goodacre, E. Griesmayer, C. Guerrero, F. Gunsing, H. Harada, Tanja Heftrich, J. Heyse, D. G. Jenkins, E. Jericha, K. Johnston, Y. Kadi, A. Kalamara, T. Katabuchi, P. Kavrigin, A. Kimura, N. Kivel, U. Kohester, M. Kokkoris, M. Krtička, Deniz Kurtulgil, E. Leal-Cidoncha, Claudia Lederer-Woods, H. Leeb, J. Lerendegui-Marco, S. Lo Meo, S. J. Lonsdale, R. Losito, D. Macina, J. Marganiec, B. Marsh, T. Martínez, J. G. Martins Correia, A. Masi, C. Massimi, P. Mastinu, F. Matteucci, A. Mazzone, E. Mendoza, P. M. Milazzo, Federica Mingrone, M. Mirea, A. Musumarra, A. Negret, R. Nolte, A. Oprea, N. Patronis, A. Pavlik, Luciano Piersanti, M. Piscopo, A. Plompen, I. Porras, J. Praena, J. M. Quesada, D. Radeck, K. Rajeev, Thomas Rauscher, René Reifarth, A. Riego-Perez, S. Rothe, P. Rout, C. Rubbia, J. Ryan, M. Sabaté-Gilarte, A. Saxena, J. Schell, P. Schillebeeckx, S. Schmidt, P. Sedyshev, C. Seiffert, A. G. Smith, N. V. Sosnin, A. Stamatopoulos, T. Stora, G. Tagliente, J. L. Tain, A. Tarifeño-Saldivia, L. Tassan-Got, A. Tsinganis, S. Valenta, G. Vannini, V. Variale, P. Vaz, A. Ventura, V. Vlachoudis, R. Vlastou, A. Wallner, S. Warren, Mario Weigand, C. Weiß, C. Wolf, P. J. Woods, T. Wright, P. Žugec and The n_TOF Collaboration

L. A. Damone (✉) · M. Barbagallo · M. Mastromarco · N. Colonna · A. Mazzone · G. Tagliente · V. Variale
INFN, Sezione di Bari, Dipartimento di Fisica, Bari, Italy
e-mail: lucia.anna.damone@cern.ch

L. A. Damone
Universit degli Studi di Bari, Bari, Italy

A. Formicola et al. (eds.), *Nuclei in the Cosmos XV*, Springer
Proceedings in Physics 219, https://doi.org/10.1007/978-3-030-13876-9_5

M. Barbagallo · M. Mastromarco · O. Aberle · M. Bacak · J. Ballof · A. P. Bernardes · M. J. G. Borge · M. Brugger · M. Calviani · R. Cardella · R. Catherall · F. Cerutti · E. Chiaveri · A. Dorsival · A. Ferrari · S. Gilardoni · T. D. Goodacre · K. Johnston · Y. Kadi · R. Losito · D. Macina · B. Marsh · J. G. Martins Correia · A. Masi · F. Mingrone · C. Rubbia · M. Sabat-Gilarte · J. Schell · C. Seiffert · T. Stora · A. Tsinganis · V. Vlachoudis · C. Weiß
European Organization for Nuclear Research (CERN), Meyrin, Switzerland

A. Mengoni · D. M. Castelluccio · S. Lo Meo
ENEA, Bologna, Italy

A. Mengoni · S. Lo Meo · C. Massimi · G. Vannini · A. Ventura
INFN, Sezione di Bologna, Bologna, Italy

L. Cosentino · P. Finocchiaro · G. Bellia · R. Cardella · A. Musumarra · M. Piscopo
INFN - Laboratori Nazionali del Sud, Catania, Italy

E. A. Maugeri · S. Heinitz · D. Schumann · R. Dressler · N. Kivel
Paul Scherrer Institut, Villigen PSI, Villigen, Switzerland

F. Käppeler
Karlsruhe Institute of Technology (KIT), Institut fur Kernphysik, Karlsruhe, Germany

J. Andrzejewski · J. Perkowski · A. Gawlik · J. Marganiec
Uniwersytet Ldzki, Lodz, Poland

S. Altstadt · C. Beinrucker · K. Göbel · T. Heftrich · D. Kurtulgil · R. Reifarth · S. Schmidt · M. Weigand · C. Wolf
Johann-Wolfgang-Goethe Universitat, Frankfurt, Germany

M. Ayranov
European Commission, DG-Energy, Luxembourg, Belgium

L. Audouin · Y. H. Chen · L. Tassan-Got
Centre National de la Recherche Scientifique/IN2P3 - IPN, Orsay, France

M. Bacak · E. Griesmayer · E. Jericha · P. Kavrigin · H. Leeb
Atominstitut der Osterreichischen Universitaten, Technische Universitat Wien, Vienna, Austria

J. Balibrea-Correa · V. Bcares · D. Cano-Ott · A. Garca-Rios · E. Gonzalez-Romero · T. Martnez · E. Mendoza
Centro de Investigaciones Energeticas Medioambientales y Tecnolgicas (CIEMAT), Madrid, Spain

F. Bečvař · M. Krtička · S. Valenta
Charles University, Prague, Czech Republic

G. Bellia · A. Musumarra
Dipartimento di Fisica e Astronomia, Universit di Catania, Catania, Italy

E. Berthoumieux · E. Dupont · F. Gunsing
CEA/Saclay - IRFU, Gif-sur-Yvette, France

J. Billowes · J. Ryan · A. G. Smith · S. Warren · T. Wright · N. V. Sosnin · S. Rothe · J. Schell
University of Manchester, Oxford Road, Manchester, UK

D. Bosnar · P. Žugec
Department of Physics, Faculty of Science, University of Zagreb, Zagreb, Croatia

A. Brown · D. G. Jenkins
University of York, Heslington, York, UK

M. Busso · S. Cristallo · L. Piersanti
Istituto Nazionale di Fisica Nucleare, Sezione di Perugia, Perugia, Italy

M. Busso
Dipartimento di Fisica e Geologia, Universit di Perugia, Perugia, Italy

M. Caamaño · I. Duran · B. Fernandez-Dominguez · E. Leal-Cidoncha
Universidade de Santiago de Compostela, A Coruña, Spain

F. Calviño · A. Casanovas · G. Corts · A. Riego-Perez · A. Tarifeño-Saldivia
Universitat Politecnica de Catalunya, Barcelona, Spain

M. A. Corts-Giraldo · C. Guerrero · J. Lerendegui-Marco · J. Praena · J. M. Quesada · M. Sabat-Gilarte
Universidad de Sevilla, Sevilla, Spain

S. Cristallo · L. Piersanti
Istituto Nazionale di Astrofsica - Osservatorio Astronomico d'Abruzzo, Teramo, Italy

M. Diakaki · A. Kalamara · M. Kokkoris · A. Stamatopoulos · R. Vlastou
National Technical University of Athens (NTUA), Athens, Greece

M. Dietz · C. Lederer-Woods · S. J. Lonsdale · P. J. Woods
School of Physics and Astronomy, University of Edinburgh, Edinburgh, UK

C. Domingo-Pardo · J. L. Tain · A. Tarifeño-Saldivia
Instituto de Fsica Corpuscular, CSIC-Universidad de Valencia, Valencia, Spain

P. Ferreira · W. Furman · I. F. Gonçalves · J. G. Martins Correia · P. Sedyshev · P. Vaz
Instituto Superior Tecnco, Universidade de Lisboa, Lisbon, Portugal

L. A. Damone
Joint Institute of Nuclear Research, Dubna, Russia

S. Ganesan · K. Rajeev · P. Rout · A. Saxena
Bhabha Atomic Research Centre (BARC), Mumbai, India

T. Glodariu · M. Mirea · A. Negret · A. Oprea
Horia Hulubei National Institute for Physics and Nuclear Engineering (IFIN-HH), Bucharest-Magurele, Romania

H. Harada · A. Kimura
Japan Atomic Energy Agency (JAEA), Tokai-mura, Japan

J. Heyse · A. Plompen · P. Schillebeeckx
European Commission JRC, Institute for Reference Materials and Measurements, Geel, Belgium

T. Katabuchi
Tokyo Institute of Technology, Tokyo, Japan

U. Kohester
Institut Laue-Langevin (ILL), Grenoble, France

C. Massimi · G. Vannini
Dipartimento di Fisica e Astronomia, Universit di Bologna, Bologna, Italy

P. Mastinu
INFN - Laboratori Nazionali di Legnaro, Legnaro, Italy

F. Matteucci · P. M. Milazzo
Istituto Nazionale di Fisica Nucleare, Sezione di Trieste, Trieste, Italy

F. Matteucci
Dipartimento di Astronomia, Universit di Trieste, Trieste, Italy

Abstract One of the most puzzling problems in Nuclear Astrophysics is the "Cosmological Lithium Problem", i.e the discrepancy between the primordial abundance of ^{7}Li observed in metal poor halo stars (Asplund et al. in Astrophys J 644:229–259, 2006, [1]), and the one predicted by Big Bang Nucleosynthesis (BBN). One of the reactions that could have an impact on the problem is ^{7}Be(n,p)^{7}Li. Despite of the importance of this reaction in BBN, the cross-section has never been directly measured at the energies of interest for BBN. Taking advantage of the innovative features of the second experimental area at the n_TOF facility at CERN (Sabate-Gilarte et al. in Eur Phys J A 53:210, 2017, [2]; Weiss et al. in NIMA 799:90, 2015, [3]), an accurate measurement of ^{7}Be(n,p) cross section has been recently performed at n_TOF, with a pure ^{7}Be target produced by implantation of a ^{7}Be beam at ISOLDE. The mesurement started in April 2016 and lasted for two months. The experimental procedure, the setup used in the measurement and the results obtained so far will be here presented.

5.1 Introduction

Theoretical models of the Big Bang Nucleosynthesis (BBN) correctly predict the abundance of the stable isotopes of hydrogen and helium, but not for ^{7}Li that is overestimated by a factor of 3–5. This significant discrepancy between observation and predictions is known as the Cosmological Lithium Problem (CLiP) [1]. Since 95% of the primordial ^{7}Li is the product of the electron capture decay of ^{7}Be, a higher

A. Mazzone
CNR - IC, Bari, Italy

R. Nolte · D. Radeck
Physikalisch-Technische Bundesanstalt (PTB), Braunschweig, Germany

N. Patronis
University of Ioannina, Ioannina, Greece

A. Pavlik · A. Wallner
Faculty of Physics, University of Vienna, Vienna, Austria

I. Porras · J. Praena
Universidad de Granada, Granada, Spain

T. Rauscher
Centre for Astrophysics Research, School of Physics, Astronomy and Mathematics, University of Hertfordshire, Hatfield, UK

L. A. Damone
Institute for Materials Science and Center for Nanointegration, Duisburg-Essen (CENIDE), University of Duisburg-Essen, Essen, Germany

A. Wallner
Research School of Physics and Engineering, Australian National University, Canberra, Australia
https://www.cern.ch/ntof

destruction rate of ^{7}Be could, potentially, solve or at least partially explain the CLiP. In this scenario, reactions induced by neutrons on ^{7}Be, in particular the ^{7}Be(n,α)^{4}He and the ^{7}Be(n,p)^{7}Li reactions, could play an important role. However, data on these reactions have been so far scarce or completely missing. The recent construction of a second experimental area (EAR2) at n_TOF (Neutron Time of Flight) characterized by an extremely high instantaneous neutron flux (10^{8} n/cm^{2}/pulse), a good energy resolution and a low repetition rate, offered the unique opportunity to perform time-of-flight measurements of ^{7}Be(n,p)^{7}Li and ^{7}Be(n,α)^{4}He cross sections over a wide energy range, covering the one of interest for the Big Bang Nucleosynthesis. Results on the latter reaction have already been published [4]. The results on the (n,p) reaction are reported here.

5.2 Experimental Setup

The measurement of the ^{7}Be(n,p)^{7}Li reaction was performed using a telescope made of two Silicon strip detectors mounted at an angle of 90 degrees relative to the beam direction (see Fig. 5.1) [5]. To minimize the energy straggling of emitted protons inside the ^{7}Be deposit, the sample was tilted relative to the neutron beam direction by 45°.

A high-purity ^{7}Be samples of 1.1 GBq was prepared starting from 200 GBq ^{7}Be solution collected at Paul Scherrer Institute (PSI). The samples were produced at ISOLDE by implantation of a beam of ^{7}Be at 35 keV on an Aluminum backing and later installed in the vertical neutron beam of EAR2 [6].

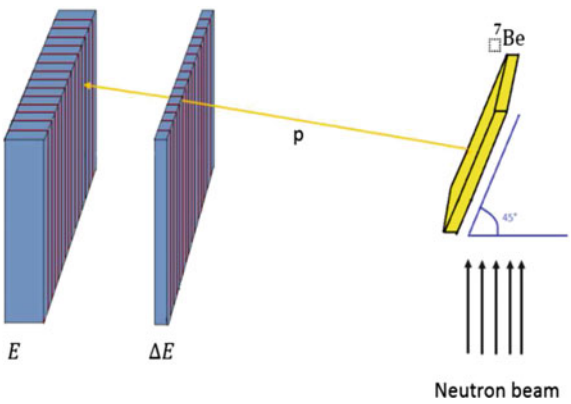

Fig. 5.1 Schematic view of the experimental setup. In yellow the support for ^{7}Be. The Silicon strip detectors are in blue. The ΔE detector is 20 μm thick, while the stopping detector is 300 μm thick

5.3 Data Analysis and Results

In order to calibrate the detector and be used as a reference, the ^{6}Li(n,t)^{4}He reaction, whose cross section is standard from thermal energy up to 1 MeV, was measured. The results compared with the evaluation from ENDF/B-VII.1 [7], are shown in Fig. 5.2, left panel. A good agreement, within 5%, from thermal neutron energy up to 1 MeV can be observed.

The protons emitted from the ^{7}Be(n,p)^{7}Li reaction were detected in coincidence and identified in the telescope. In Fig. 5.2, right panel, the ΔE vs E plot is shown and the red circle indicates the region of protons detected.

The ^{7}Be(n,p)^{7}Li cross section was extracted relative to that of the ^{6}Li(n,t) reaction (σ_{LiF}), from the ratio of the number of counts (C_{Be} and C_{LiF}), normalized to the respective total neutron fluence and taking into account the ratios of the efficiencies (ϵ_{Be} and ϵ_{LiF}), beam-sample convolution factors ($f_{C_{Be}}$ and $f_{C_{LiF}}$) and the total number of atoms in the ^{7}Be and in the ^{7}Li sample (N_{Be} and N_{Li}).

$$\sigma_{n,p}(E_n) = \frac{C_{Be}(E_n)}{C_{LiF}(E_n)} \cdot \frac{\epsilon_{LiF}}{\epsilon_{Be}} \cdot \frac{f_{C_{LiF}}}{f_{C_{Be}}} \cdot \sigma_{LiF}(E_n) \cdot \frac{N_{Li}}{N_{Be}} \tag{5.1}$$

f_C represents the convolution of the normalized neutron beam spatial profile and target nuclei distribution and has a dimension of b^{-1} [8].

Figure 5.3, left panel, shows the background-subtracted reduced cross section of the ^{7}Be(n,p)^{7}Li reaction, as a function of neutron energy, compared with the two previous direct measurements and with the ENDF/B-VII.1 evaluation. The high purity of the sample, the use of a telescope for particle identification, and the very high instantaneous neutron flux of EAR2 resulted in a practically negligible background, in particular the one associated with the natural γ-ray activity of ^{7}Be. The only source of background affecting the measurement is related to the ^{14}N(n,p) reactions in the sample backing. This contribution was found important only for neutron energies above ~500 keV. The right panel shows instead a comparison of the present reaction

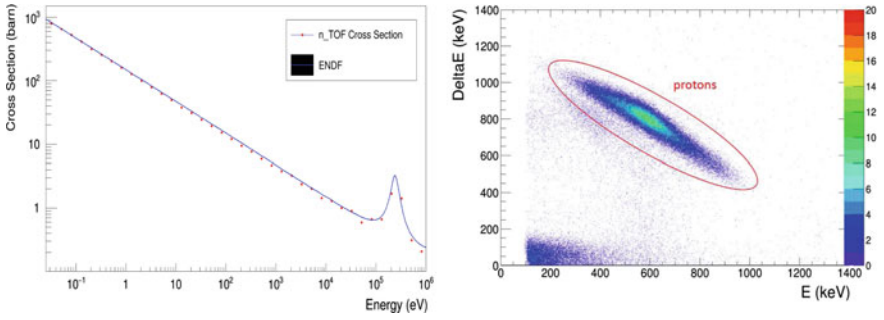

Fig. 5.2 Left panel: comparison between the ^{6}Li(n,t)^{4}He cross section measured at n_TOF and the evaluated one from ENDF/B-VII.1 data library. Right panel: E vs ΔE plot for the ^{7}Be sample

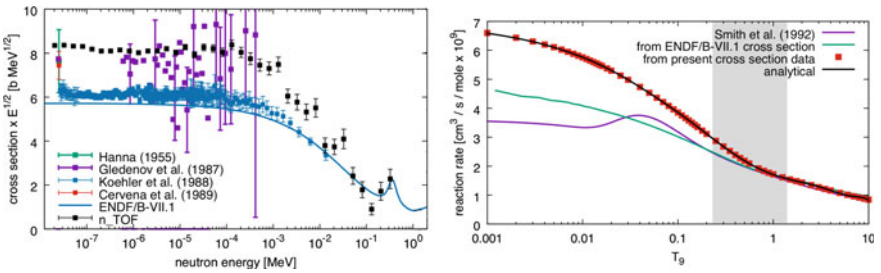

Fig. 5.3 On the left the ^{7}Be(n,p)^{7}Li reduced cross section measured at n_TOF compared with the results of previous measurements and with the ENDF/B-VII.1 library. On the right comparison of the reaction rates for the ^{7}Be(n,p)^{7}Li reaction of the present work with the commonly adopted rates and that derived from the evaluated cross section of ENDF/B-VII.1 library. The temperature range of interest for BBN is indicated by the grey band

rate with two other rates commonly adopted in BBN calculations. It can be seen that the present rate is significantly higher in a wide range up to $T_9 \sim 1$.

5.4 Conclusions

The ^{7}Be(n,p)^{7}Li cross section has been measured at n_TOF, covering for the first time the energy range of interest for the Cosmological Lithium Problem (20–200 keV) in the second experimental area (EAR2) at n_TOF, using 1.1 GBq pure ^{7}Be sample implanted at ISOLDE facility, starting from a 200 GBq ^{7}Be solution collected at PSI.

At thermal neutron energy the cross section measured at n_TOF sets a value of 52.3 ± 5.2 kb and is higher than previous results, while it is by ~40% consistent with current evaluations above 50 keV. As is shown in Fig. 5.4, the new ^{7}Be destruction

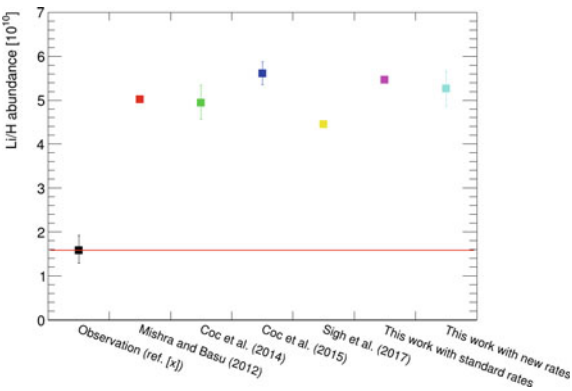

Fig. 5.4 Comparison of ^{7}Li abundance (relative to H) in units of 10^{-10} calculated over the recent years, compared with the observation of the Spite-plateau in low-metallicity stars

rate yields a decrease of the predicted cosmological Lithium abundance of 10%, insufficient to provide a viable solution to the Cosmological Lithium Problem. More details are now available in [8].

References

1. M. Asplund et al., Astrophys. J. **644**, 229–259 (2006)
2. M. Sabate-Gilarte et al., Eur. Phys. J. A **53**, 210 (2017)
3. C. Weiss et al., NIMA **799**, 90 (2015)
4. M. Barbagallo et al., Phys. Rev. Lett. **117**, 152701 (2016)
5. M. Barbagallo et al., Nucl. Instr. Meth. A **887**, 27–33 (2018)
6. E.A. Maugeri et al., Nucl. Inst. Methods Phys. Res. A **889**, 138–144 (2018)
7. M.B. Chadwick et al., Nucl. Data Sheets **112**, 2887–2996 (2011)
8. L. Damone et al., PRL **121**, 042701 (2018)

Chapter 6
Cross Section Measurements of the ^{7}Be(n,p)^{7}Li and the ^{7}Be(n,α)^{4}He Reactions Covering the Big-Bang Nucleosynthesis Energy Range by the Trojan Horse Method at CRIB

S. Hayakawa, K. Abe, O. Beliuskina, S. M. Cha, K. Y. Chae, S. Cherubini, P. Figuera, Z. Ge, M. Gulino, J. Hu, A. Inoue, N. Iwasa, D. Kahl, A. Kim, D. H. Kim, G. G. Kiss, S. Kubono, M. La Cognata, M. La Commara, L. Lamia, M. Lattuada, E. J. Lee, J. Y. Moon, Sara Palmerini, C. Parascandolo, S. Y. Park, D. Pierroutsakou, Rosario Gianluca Pizzone, G. G. Rapisarda, S. Romano, H. Shimizu, C. Spitaleri, Xiaodong Tang, O. Trippella, Aurora Tumino, P. Vi, H. Yamaguchi, L. Yang and N. T. Zhang

Abstract We performed indirect measurements of the neutron-induced reactions ^{7}Be(n,p)^{7}Li and ^{7}Be(n,α)^{4}He simultaneously by the Trojan Horse method relevant to the cosmological ^{7}Li problem. Preliminary excitation functions for (n, p_0) and (n, α) are basically consistent with the previous studies, and new information about the (n, p_1) contribution suggests possible enhancement of the total reaction rate.

S. Hayakawa (✉) · K. Abe · O. Beliuskina · S. Kubono · H. Shimizu · H. Yamaguchi · L. Yang · N. T. Zhang
Center for Nuclear Study, University of Tokyo, Wako, Japan
e-mail: hayakawa@cns.s.u-tokyo.ac.jp

S. M. Cha · K. Y. Chae · E. J. Lee
Sungkyunkwan University, Suwon, Republic of Korea

S. Cherubini · P. Figuera · M. Gulino · M. La Cognata · L. Lamia · M. Lattuada · R. G. Pizzone · G. G. Rapisarda · S. Romano · C. Spitaleri · A. Tumino
Istituto Nazionale di Fisica Nucleare - Laboratori Nazionali del Sud, Catania, Italy

S. Cherubini · L. Lamia · M. Lattuada · S. Romano · C. Spitaleri
University of Catania, Catania, Italy

Z. Ge · G. Kiss · S. Kubono · P. Vi
RIKEN Nishina Center, Wako, Japan

M. Gulino
Kore University of Enna, Enna, Italy

J. Hu · S. Kubono · X. Tang · N. T. Zhang
Institute of Modern Physics, Chinese Academy of Sciences, Lanzhou, China

A. Inoue
Research Center for Nuclear Physics, Osaka University, Suita, Japan

A. Formicola et al. (eds.), *Nuclei in the Cosmos XV*, Springer
Proceedings in Physics 219, https://doi.org/10.1007/978-3-030-13876-9_6

6.1 Introduction

It is still an open question that the prediction of the primordial ^{7}Li abundance by the standard Big-Bang Nucleosynthesis (BBN) model [1] is about 3 times larger than the observation [2], the so-called cosmological ^{7}Li problem. Although several ideas have been proposed to solve the cosmological ^{7}Li problem [3], no definitive solution has been found so far. As the basis, nuclear reaction rates involved in the BBN should be accurately reevaluated, as there are still lack or incompletion of data near the BBN energies. Especially, neutron-induced reactions on ^{7}Be are important since the radiogenic ^{7}Li abundance by the BBN strongly depends on the ^{7}Be production and destruction rates, yet less well studied owing to the fact that both species are radioactive.

The ^{7}Be(n,p)^{7}Li reaction is considered as the main process to destroy ^{7}Be. Recently, a direct measurement was performed [4], revising the cross sections upward from the precious direct data [5] below the BBN energies. However, the contribution of the transition to the first excited state of ^{7}Li at the BBN energies has never been discussed. Another important neutron-induced reaction channel ^{7}Be(n,α)^{4}He has not been investigated until recently [6–9], still lacking in direct data at the BBN energies. Thus both studies still lack the information on the total ^{7}Be(n,α)^{4}He cross section in the BBN energy region.

N. Iwasa
Tohoku University, Sendai, Japan

D. Kahl
University of Edinburgh, Edinburgh, UK

A. Kim · D. H. Kim · S. Y. Park
Ewha Womans University, Seoul, Republic of Korea

M. La Commara
University of Naples Federico II, Naples, Italy

M. La Commara · C. Parascandolo · D. Pierroutsakou
Istituto Nazionale di Fisica Nucleare - Section of Naples, Naples, Italy

J. Y. Moon
Institute for Basic Science, Daejeon, Republic of Korea

S. Palmerini · O. Trippella
Istituto Nazionale di Fisica Nucleare - Section of Perugia, Perugia, Italy

S. Palmerini
University of Perugia, Perugia, Italy

6.2 Experimental Method

We measured the ^{7}Be(n,p)^{7}Li and ^{7}Be(n,α)^{4}He reactions simultaneously by the Trojan Horse Method (THM) [10] at Center-for-Nuclear-Study Radioactive Isotope Beam (CRIB) separator [11]. The THM has been developed mainly for charged-particle induced reactions at astrophysical energies based on the plane wave impulse approximation. Recently, applicability of the THM for neutron-induced reactions has been also investigated [12], and the first application of THM to RI+n reaction has been done [13] aiming at the ^{7}Be(n,α)^{4}He reaction measurement. We developed this method so as to measure both the ^{7}Be(n,p)^{7}Li and ^{7}Be(n,α)^{4}He reactions simultaneously by introducing forward-angle telescopes for heavy-ion detection, i.e. ^{7}Li. We produced a ^{7}Be beam at 22.1 $\pm$ 0.14 MeV with an intensity of 1×10^{6} pps on target. The experimental setup consisted of two Parallel-Plate Avalanche Counters (PPACs), a CD_2 target, and six ΔE-E position-sensitive silicon-detector telescopes as shown in Fig. 6.1. The beam ions were tracked and identified event by event with the PPACs. The thickness of the CD_2 target was 64 μg/cm^2. A use of such a thin target enables to reduce the energy spread of the Q-value to 200 keV. This helps with separation of the first excited state of ^{7}Li (478 keV) in the reconstructed Q-value spectrum.

6.3 Data Analysis

The ΔE-E particle identification was successful to select the particles of interest such as ^{7}Li, α and protons. By selecting coincidence pairs of ^{7}Li-p or α-α, we confirmed that the reconstructed Q-value spectra were consistent with the known Q values of the ^{7}Be(d,^{7}Lip$_0$)^{1}H ($-$0.580 MeV) and the ^{7}Be(d,^{7}Li*p$_1$)^{1}H ($-$1.058 MeV) reactions, and the ^{7}Be(d,$\alpha\alpha$)^{1}H (16.766 MeV) reactions, respectively. Figure. 6.2 shows the Q-value spectra observed in the coincidence pairs of ^{7}Li-p (left) and α-α (right) with the corresponding Q values indicated by arrows. We also confirmed that the momentum distributions of the spectator proton in the exit three-body channels are consistent with that of the well-known p-n intercluster motion inside the deuteron nucleus

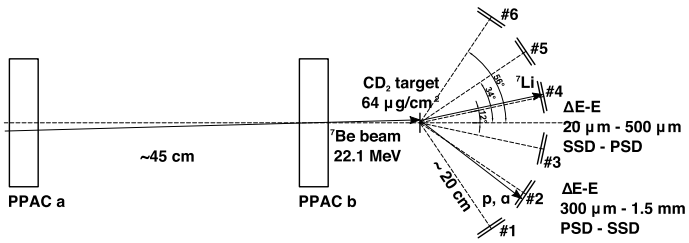

Fig. 6.1 Schematic view of the experimental setup

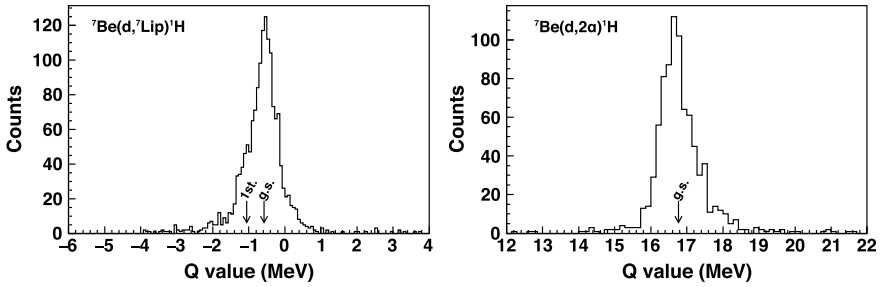

Fig. 6.2 Q-value spectra of the coincidence pairs of ^{7}Li-p (left) and α-α (right). The arrows indicate the known Q values of the ^{7}Be(d,^{7}Lip)^{1}H reaction for the ground state and the first excited state of ^{7}Li, and the ^{7}Be(d,$\alpha\alpha$)^{1}H reaction, respectively

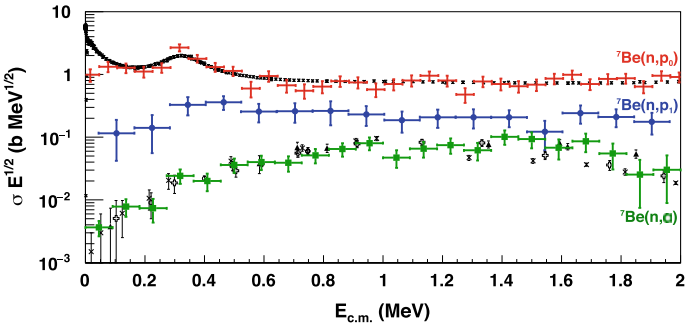

Fig. 6.3 Preliminary cross sections of the ^{7}Be(n,p$_0$)^{7}Li (red), the ^{7}Be(n,p$_1$)^{7}Li* (blue) and the ^{7}Be(n,α)^{4}He (green) reactions for $|p_s| < 60$ MeV/c. Black dots are previous experimental data [5–9, 14–17]

expressed by the Hulthén function in momentum space, both for the ^{7}Be(d,^{7}Lip)^{1}H and the ^{7}Be(d,$\alpha\alpha$)^{1}H data, which guarantees the quasifree mechanism is dominant through the reaction process.

We successfully extracted the p_0 and the p_1 yield separately as functions of the excitation energy by fitting Gaussian functions to the Q-value spectra. Preliminary cross sections of the ^{7}Be(n,p$_0$)^{7}Li, ^{7}Be(n,p$_1$)^{7}Li* and the ^{7}Be(n,α)^{4}He reactions for $|p_s| < 60$ MeV/c are shown in Fig. 6.3. Tentatively, we assume isotropy, and s-wave penetrability correction for the (n, p_0) and the (n, p_1) channels, and p-wave correction for the (n, α) channel. The (n, p_0) and the (n, α) cross sections are normalized to the previous data [5–9, 14–17], and the (n, p_1) is to the (n, p_0). The prominence in the (n, p_0) excitation function around 300 keV corresponds to the previously reported resonance by 3^+ state at $E_x = 19.24$ MeV of ^{8}Be [18]. The shape of the excitation function of the (n, α) is also roughly consistent with the previous studies [6–9]. A multi-channel R-matrix analysis is desired to confirm the penetrability correction and the normalization of the present THM data more strictly from the point of

view of the resonance structure. At present, we could reproduce the basic feature of these excitation functions simultaneously, with consistent resonance parameters not to violet the known total width nor the Wigner limits. A further analysis is ongoing.

6.4 Summary

We performed indirect measurements of the BBN reactions ^{7}Be(n,p)^{7}Li and ^{7}Be(n,α)^{4}He simultaneously by the THM via the ^{7}Be(d,^{7}Lip)^{1}H and the ^{7}Be(d,$\alpha\alpha$)^{1}H reactions at CRIB. Preliminary excitation functions for the (n, p_0) and the (n, α) channels are roughly consistent with the previous studies. In addition, we showed that the BBN energy region is accessible with our measurement and there is possible contribution of ^{7}Be(n,p$_1$)^{7}Li*. We are currently aiming to confirm and better normalize the present data by performing a multi-channel R-matrix analysis.

Acknowledgements This experiment was performed at RI Beam Factory operated by RIKEN Nishina Center and CNS, University of Tokyo, and supported by JSPS KAKENHI (Grant No. 15K17631).

References

1. A. Coc et al., J. Cosmol. Astropart. Phys. **40**, 050 (2014)
2. R.H. Cyburt et al., Rev. Mod. Phys. **88**, 015004 (2016)
3. B.D. Fields, Annu. Rev. Nucl. Part. Sci. **61**, 47 (2011)
4. L.A. Damone, arXiv:1803.05701 (2018)
5. P. Koehler et al., Phys. Rev. C **37**, 917 (1988)
6. S.Q. Hou et al., Phys. Rev. C **91**, 055802 (2015)
7. M. Barbagallo et al., Phys. Rev. Lett. **117**, 152701 (2016)
8. T. Kawabata et al., Phys. Rev. Lett. **118**, 052701 (2017)
9. L. Lmia et al., Astrophys. J. **850**, 175 (2017)
10. C. Spitaleri et al., Phys. Atom. Nucl. **74**, 1725 (2011)
11. Y. Yanagisawa et al., Nucl. Instrum. Methods A **539**, 74 (2005)
12. M. Gulino et al., Phys. Rev. C **87**, 012801 (2013)
13. L. Lamia et al., *Proceedings of 14th International Symposium on Nuclei in the Cosmos*, JPS Conference Proceedings (in publication)
14. R.L. Macklin, J.H. Gibbons, Phys. Rev. **109**, 105 (1958)
15. R.R. Borchers, C.H. Poppe, Phys. Rev. **129**, 2679 (1963)
16. C.H. Poppe et al., Phys. Rev. C **14**, 438 (1976)
17. K. Sekharan et al., Nucl. Instrum. Methods **133**, 253 (1976)
18. A. Adahchour, P. Descouvemont, J. Phys. G **29**, 395 (2003)

Chapter 7
Non-extensive Solution to Cosmological Lithium Problem

S. Q. Hou, J. J. He, A. Parikh, D. Kahl, C. A. Bertulani, Toshitaka Kajino, Grant J. Mathews and G. Zhao

Abstract The standard Big-Bang model predicts the primordial abundances of ^{2}H(D), ^{3}He, ^{4}He in excellent agreement with observations, except for ^{7}Li that is overpredicted by a factor of about three. Despite many attempted solutions to this discrepancy using conventional nuclear physics over the past decades, the lithium enigma persists. Here we present an investigation of Big Bang nucleosynthesis (BBN)

S. Q. Hou (✉) · J. J. He
Key Laboratory of High Precision Nuclear Spectroscopy, Institute of Modern Physics, Chinese Academy of Sciences, Lanzhou 730000, China
e-mail: sqhou@impcas.ac.cn

J. J. He · G. Zhao
Key Laboratory of Optical Astronomy, National Astronomical Observatories, Chinese Academy of Sciences, Beijing 100012, China

A. Parikh
Departament de Física i Enginyeria Nuclear, EUETIB, Universitat Politècnica de Catalunya, 08036 Barcelona, Spain

Institut d'Estudis Espacials de Catalunya, Barcelona 08034, Spain

D. Kahl
School of Physics & Astronomy, University of Edinburgh, Edinburgh EH9 3FD, UK

C. A. Bertulani
Texas A&M University-Commerce, Commerce, TX 75429-3011, USA

T. Kajino
Department of Astronomy, School of Science, The Univesity of Tokyo, 7-3-1 Hongo, Bunkyo-ku, Tokyo 113-0033, Japan

T. Kajino · G. J. Mathews
National Astronomical Observatory of Japan, 2-21-1 Osawa, Mitaka, Tokyo 181-8588, Japan

T. Kajino
International Research Center for Big-Bang Cosmology and Element Genesis, School of Physics and Nuclear Energy Engineering, Beihang University, Beijing 100191, China

G. J. Mathews
Center for Astrophysics, Department of Physics, University of Notre Dame, Notre Dame, IN 46556, USA

A. Formicola et al. (eds.), *Nuclei in the Cosmos XV*, Springer Proceedings in Physics 219, https://doi.org/10.1007/978-3-030-13876-9_7

predictions when we adopt a non-extensive distribution to describe the velocity profile of the nuclides in the primordial plasma. We find excellent agreement between predicted and observed primordial abundances of D, ^{4}He, ^{7}Li for the case of $1.069 \leq q \leq 1.082$, which indicates a possible new solution to the cosmological lithium problem.

7.1 Introduction

Big Bang theory is regarded as one of the most successful explanation for the origin of our Universe. However, the Big Bang theory still face what has turned out to be an intractable issue: Big Bang nucleosynthesis (BBN) predictions and their corresponding astronomical observables are consistent only for abundances of D,^{3}He,^{4}He, while the abundance of ^{7}Li is anamalously overpredicted by most present theories by a factor of about three [1, 2]. Attempts to resolve this discrepancy from the perspective of conventional nuclear physics have been unsuccessful for several decades [3, 4].

In this work we propose a solution to the lithium problem that arises naturally from a simple modification of the velocity distributions of nuclei during the BBN epoch [5]. In the BBN model, the predominant nuclear-physics inputs are thermonuclear reaction rates (derived from cross sections). A key assumption in all thermonuclear rate determinations is that the velocities of nuclei may be described by the classical Maxwell-Boltzmann (MB) distribution [6]. However, this assumption might be violated as non-thermal BBN processes may plausibly take place, for example, as a result of dark matter or stochastic primordial magnetic field (PDF) [7, 8].

As derived from non-extensive statistics [9], the Tsallis distribution can be used to describe particle velocity profile as a deviation from classical MB distribution by introducing a real parameter q and reduces to the nominal MB distribution when non-extensive parameter $q = 1$. In the following sections, we will introduce the derivation of an expression of thermonuclear reaction rates using the Tsallis distribution, and we subsequently investigate the impact of this new distribution on primordial nucleosynthesis.

7.2 Non-extensive Reaction Rate

It is well-known that thermonuclear rate for a typical $1 + 2 \rightarrow 3 + 4$ reaction is usually calculated by folding the cross section $\sigma(E)_{12}$ with a MB distribution [6]

$$\langle \sigma v \rangle_{12} = \sqrt{\frac{8}{\pi \mu_{12} (kT)^3}} \int_0^\infty \sigma(E)_{12} E \exp\left(-\frac{E}{kT}\right) dE, \tag{7.1}$$

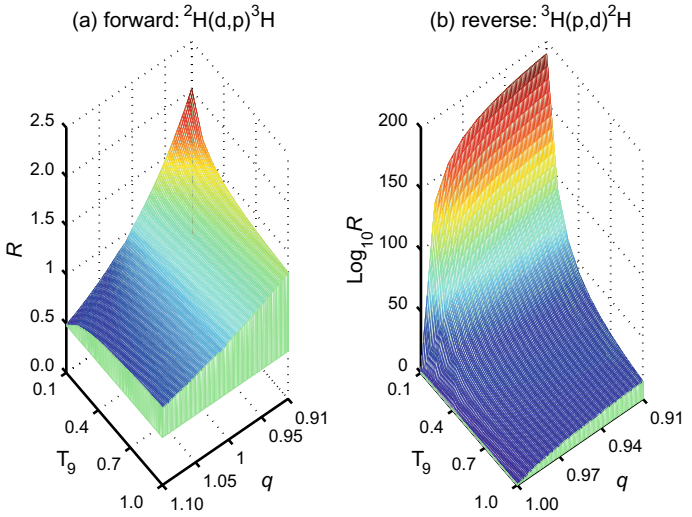

Fig. 7.1 Ratio between rates calculated using Tsallis and MB distributions for the ^{2}H(d,p)^{3}H reaction as functions of temperature T_9 and q values, **a** for forward reaction (in linear scale), and **b** for reverse reaction (in logarithmic scale)

with k the Boltzmann constant, μ_{12} the reduced mass of particles 1 and 2. In Tsallis statistics, the q-Gaussian velocity distribution can be expressed by Silva et al. [10]

$$f_q(\mathbf{v}) = B_q \left(\frac{m}{2\pi kT}\right)^{3/2} \left[1 - (q-1)\frac{m\mathbf{v}^2}{2kT}\right]^{\frac{1}{q-1}}, \tag{7.2}$$

where B_q denotes the q-dependent normalization constant. Thus, the non-extensive reaction rate becomes

$$\langle \sigma v \rangle_{12} = B_q \sqrt{\frac{8}{\pi \mu_{12}}} \times \frac{1}{(kT)^{3/2}} \times \int_0^{E_{\max}} \sigma_{12}(E) E \left[1 - (q-1)\frac{E}{kT}\right]^{\frac{1}{q-1}} dE, \tag{7.3}$$

with $E_{\max} = \frac{kT}{q-1}$ for $q > 1$, and $+\infty$ for $0 < q < 1$. The corresponding reverse rate is expressed as the following equation:

$$\langle \sigma v \rangle_{34} = c \times B_q \sqrt{\frac{8}{\pi \mu_{12}}} \times \frac{1}{(kT)^{3/2}} \times \int_0^{E_{\max}-Q} \sigma_{12}(E) E \left[1 - (q-1)\frac{E+Q}{kT}\right]^{\frac{1}{q-1}} dE. \tag{7.4}$$

As an example, Fig. 7.1 shows the impact of q values on the forward and reverse rates as functions of temperature for ^{2}H(d,p)^{3}H, one of the most important reactions involved in the BBN. In the region of $0.1 \leq T_9 \leq 1.0$ and $0.91 \leq q \leq 1.1$, the forward rate calculated with the Tsallis-distribution deviates from the MB rates by relatively modest factor of 2 at most. However, the reverse rate is *super*sensitive to deviations of q from unity. For $0.91 \leq q \leq 1$ (i.e., $q < 1$), the corresponding Tsallis reverse rate deviates tremendously from the MB rates by about 200 *orders of magnitude*. For instance, even with a very small deviation ($q = 0.999$), the Tsallis reverse rate of ^{2}H(d,p)^{3}H is about 10^{10} times larger than the MB reverse rate at 0.2 GK. As for the $q > 1$ case, the Tsallis reverse rate is negligible small in comparison to the MB rates.

7.3 BBN Calculation

We have for the first time used a non-extensive velocity distribution to determine thermonuclear reaction rates of primary importance to BBN in a consistent manner, details seen in [5]. Figure 7.2 shows predicted abundances as a function of the non-extensive parameter q along with observed primordial abundances of D, ^{4}He and ^{7}Li, which can be found in [5]. For these species, agreement at the 1σ level is found

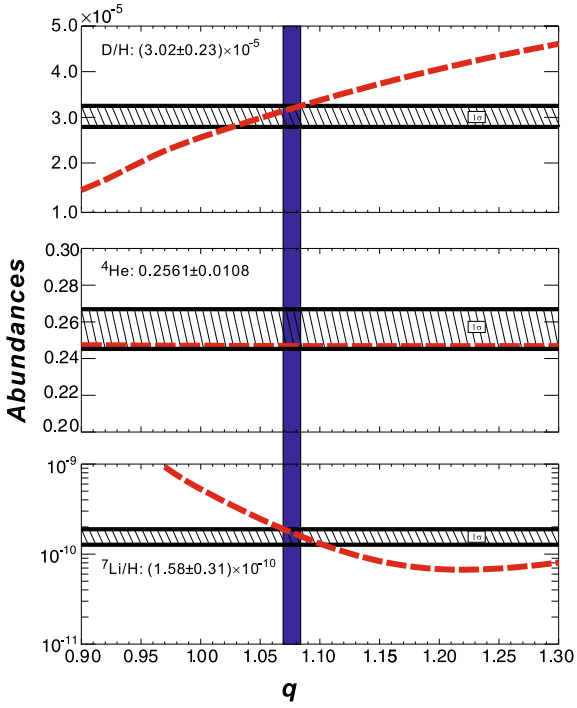

Fig. 7.2 Predicted primordial abundances versus the non-extensive parameter q (in red dashed lines). The observed primordial abundances with 1σ uncertainty for D, ^{4}He, and ^{7}Li are drawn. The vertical (dark blue) band constrains the range of q parameter, i.e., $1.069 \leq q \leq 1.082$, which reconcile the predicted D, ^{4}He, and ^{7}Li abundances with the observed ones

for $1.069 < q < 1.082$ as shown in dark blue band. Thus, we find that deviations from the MB distribution of baryon velocities during BBN offer a new solution to the cosmological lithium problem. This solution might be suited for scenario where stochastic PMF fluctuations is taken into account [8]. We encourage extensions of the present study to astrophysical sites of higher density to further interrogate and test the usual assumptions of classical statistics.

Acknowledgements This work was financially supported by the Major State Basic Research Development Program of China (2016YFA0400503) and the the National Natural Science Foundation of China (Nos. 11705244, 11490562, 11135005, 11321064).

References

1. R.H. Cyburt et al., Primordial nucleosynthesis in light of WMAP. Phys. Lett. B **567**, 227 (2003). https://doi.org/10.1016/j.physletb.2003.06.026
2. A. Coc et al., Updated Big Bang nucleosynthesis confronted to WMAP observations and to the abundance of light elements. Astrophys. J. **600**, 544 (2004). https://doi.org/10.1086/380121
3. S.Q. Hou et al., Revised thermonuclear rate of ^{7}Be(n, α)^{4}He relevant to Big-Bang nucleosynthesis. Phys. Rev. C **91**, 055802 (2015). https://doi.org/10.1103/PhysRevC.91.055802
4. R.H. Cyburt et al., Big bang nucleosynthesis: present status. Rev. Mod. phys **88**, 015004 (2016). https://doi.org/10.1103/RevModPhys.88.015004
5. S.Q. Hou et al., Non-extensive statistics to the cosmological lithium problem. Astrophys. J. **834**, 165 (2017). https://doi.org/10.3847/1538-4357/834/2/165
6. C.E. Rolfs, W.S. Rodney, *Cauldrons in the Cosmos* (University of Chicago Press, Chicago, 1988)
7. K. Jedamzik, M. Pospelov, Big Bang nucleosynthesis and particle dark matter. New J. Phys. **11**, 105028 (2009). https://doi.org/10.1088/1367-2630/11/10/105028
8. Y. Luo, T. Kajino et al., Fluctuating Cosmic Magnetic Field, Non-Maxwellian distribution, and Impact on Big-Bang Nucleosynthesis. Master Thesis, The University of Tokyo, Tokyo (2018)
9. C. Tsallis, Possible generalization of Boltzmann-Gibbs statistics. J. Stat. Phys. **52**, 479 (1988). https://doi.org/10.1007/BF01016429
10. R. Silva Jr. et al., A Maxwellian path to the q-nonextensive velocity distribution function. Phys. Lett. A **249**, 401 (1998). https://doi.org/10.1016/S0375-9601(98)00710-5

Chapter 8
Experimental Challenge to the Cosmological Li Problem

S. Kubono, T. Kawabata, N. Iwasa, J. J. He and S. Q. Hou

Abstract The cosmological Li problem, the overproduction of ^{7}Li in the big bang nucleosynthesis (BBN), still is one of the serious remaining problems for the big bang model. Several experiments were performed for the problem in recent years, especially, on the reaction channel of ^{7}Be+n. These efforts were summarized including our works by indirect methods. The ^{7}Be(n,α)^{4}He reaction was found to have a major component of the p-wave contribution, not s-wave as thought previously. The contribution of this reaction for destruction of ^{7}Be can be concluded to be less effective than assumed before, and thus this reaction does not help to solve the Li problem. A new measurement of the ^{7}Be(n,p)^{7}Li reaction was reported to be larger than before at low energies, and the ^{7}Be(n,p$_1$)^{7}Li* reaction is also shown to be significant for the Li problem by our new study at JAEA, suggesting a need of further work on this reaction for the Li problem. Other possibilities for ^{7}Be destruction was also discussed, especially by the ^{7}Be+d channel.

S. Kubono (✉)
RIKEN Nishina Center, 2-1 Hirosawa, Wako, Saitama 351-0198, Japan
e-mail: kubono@riken.jp

Center for Nuclear Study, University of Tokyo, Wako, Saitama 351-0198, Japan

T. Kawabata
Department of Physics, Osaka University, Toyonaka, Osaka 560-0043, Japan

N. Iwasa
Department of Physics, Tohoku University, Aoba, Sendai, Miyagi 980-8578, Japan

J. J. He
National Astronomical Observatories, CAS, Beijing 100012, China

S. Q. Hou
Institute of Modern Physics, Chinese Academy of Sciences, Lanzhou 730000, China

A. Formicola et al. (eds.), *Nuclei in the Cosmos XV*, Springer
Proceedings in Physics 219, https://doi.org/10.1007/978-3-030-13876-9_8

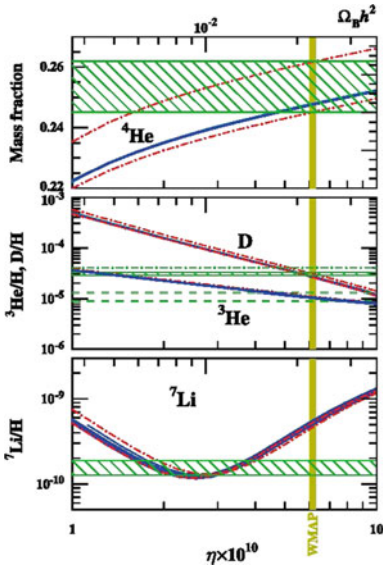

Fig. 8.1 Light elemental observation and the BBN prediction as a function of baryon to photon ratio, shown by curves [6]

8.1 The Cosmological ^{7}Li Problem

Nucleosynthesis is one of the keys for studying the evolution of the universe as well as various stellar phenomena. Almost all the elements were produced by nuclear reactions along the evolution of the universe. Thus, studying nucleosynthesis is a powerful way to look back the history of the universe, and investigate the mechanism of the evolution [1].

The primordial nucleosynthesis (BBN) just after the big bang is one of the key elements that basically support the big bang model [2]. The nuclear reactions there took place in an environment of rich protons and neutrons under high temperature conditions for the first ten minutes just after the big bang, and produced primarily the very light nuclides, ^{1}H, ^{2}H, ^{3,4}He, and ^{6,7}Li. The ^{7}Li abundance in halo stars together with other light nuclides is considered to be of primordial origin, having a plateau toward very early epoch of our universe [3]. However, the BBN calculation using the recently well determined baryon-to-photon ratio(η) by the cosmic microwave background measurements by WMAP [4] and the ESA Plank Mission [5] has revealed an overestimate roughly by a factor of three [6] (see Fig. 8.1). This discrepancy is called the cosmological Li problem. There is a possibility that this problem comes from unstudied, or not well studied nuclear reactions in BBN, although so much efforts have been made for many years in nuclear astrophysics. Primarily, there are three possibilities of solution for the cosmological Li problem; some uncertainties in nuclear reaction rates, astronomical observation, or some unknown physics. Thus, this problem for nuclear physics side should be worked out by checking all possible nuclear reactions relevant thoroughly.

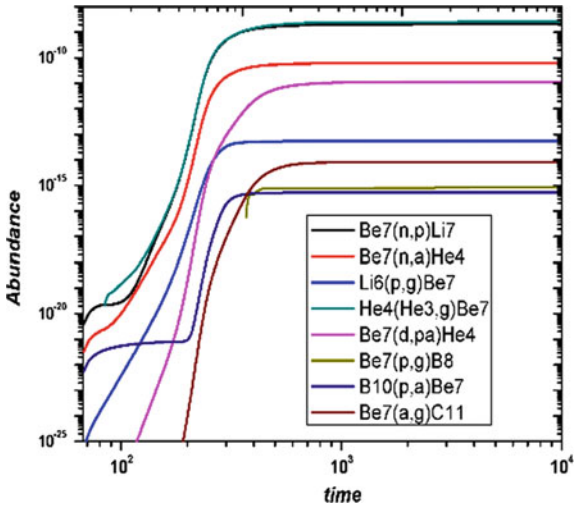

Fig. 8.2 The nuclear reactions relevant to ^{7}Be production and destruction in the standard BBN model. Here, the Wagoner rate [2] was adopted for the ^{7}Be(n,α)^{4}He reaction

^{7}Li of BBN origin is considered to have been produced primarily through the electron capture of ^{7}Be which was produced by the ^{3}He(α,γ)^{7}Be reaction and survived the BBN epoch. Figure 8.1 shows a typical BBN calculation we made. The ^{7}Be is considered to be destroyed during BBN by the (n,p), (n,α) and (d,pα) reactions, as shown in Fig. 8.2. The ^{7}Be(n,p) reaction was considered to be well investigated, and there was no experiment until recently on ^{7}Be (n,α). Recently, there are significant progresses on these reaction studies, which I will mainly discuss in the following sections. The next possible destruction channel ^{7}Be+d will be also touched.

8.2 The ^{7}Be(n,α)^{4}He Reaction for ^{7}Be Destruction

In 2014, since there was no reliable data on the reaction cross section of ^{7}Be(n,α)^{4}He at the BBN temperature region, it was evaluated using the mirror reaction data. Hou collected most available data on the ^{7}Li(p,α)^{4}He reaction, and evaluated the ^{7}Be(n,α) cross section by correcting for the Coulomb and centrifugal potential penetrabilities [7]. The result, shown by the open triangles in Fig. 8.3, clearly indicated an important role of resonances at around 20 MeV of ^{8}Be in the BBN temperature region, shown by the shaded band in the figure, as they have large resonance widths.

The cross sections of the ^{7}Be(n,α)^{4}He reaction was directly measured at the n-ToF facility using a ^{7}Be target [8]. They measured the s-wave component of the reaction, which is considered to be dominant at very low energies. The measurement was made for a small fraction (~5%) of the s-wave component, and the total s-wave component was estimated using a theoretical calculation for the decay paths unmeasured. The total s-wave cross sections follow the 1/*v* rule as can be seen by the dotted line in

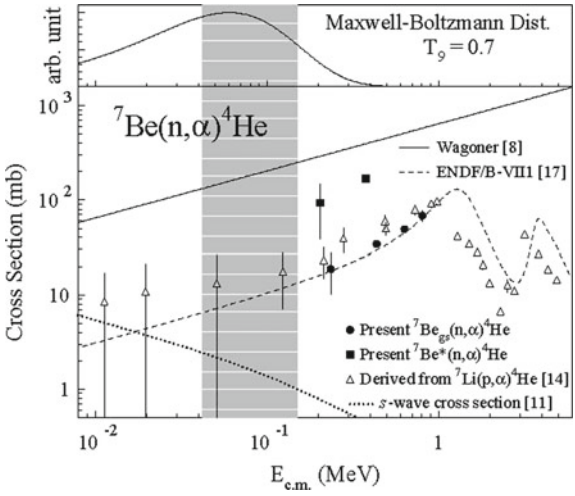

Fig. 8.3 The ^{7}Be(n,α)^{4}He cross sections obtained by estimating from the ^{7}Li(p,α)^{4}He reaction data (open triangle) [7], the time reverse measurement (closed circles) [9], and the estimated cross sections from the direct ^{7}Be(n,α)^{4}He measurement and theory (dotted line) [8]

Fig. 8.3. The experiment covered up to around 10 keV, and should see a large p-wave contribution, but they did not, which needs to be clarified why.

The p-wave components were measured at RCNP, Osaka using the time-reverse reaction ^{4}He(α,n)^{7}Be at the long TOF facility for precision neutron measurements [9]. Since the neutron detector sees only the target-neutron interaction in this facility, almost background free spectra were obtained for all the measurements. The total cross sections of the transitions to the ground state and the first excited state in ^{7}Be were obtained by integrating the angular distributions measured at four incident energies. The ^{7}Be(n,α)^{4}He cross sections were obtained by converting the cross sections of ^{4}He(α,n)^{7}Be using the detailed balance. The results are very much consistent with the theoretical estimates made by Hou et al. [7], confirming the p-wave dominace.

The cross sections of ^{7}Be(n,α)^{4}He at the BBN temperature, the shaded area in Fig. 8.3, were investigated recently by two experimental efforts using the Trojan Horse Method at the LNL, Italy [10] and the CRIB facility of the University of Tokyo in RIBF of RIKEN [11]. As were presented in this symposium, the two experimental results are consistent with the time reverse measurement [9].

The new results obtained above can be compared with the presently adopted reaction rate by Wagoner, the solid line in Fig. 8.3. The sum of the experimentally obtained s-wave and p-wave contributions is roughly an order of magnitude smaller than the Wagoner's. In order to solve the Li problem, we needed to have an order of magnitude larger rate of ^{7}Be(n,α)^{4}He than the Wagoner's. Thus, the conclusion is that the ^{7}Be(n,α)^{4}He reaction channel has a minor effect for the cosmological Li problem.

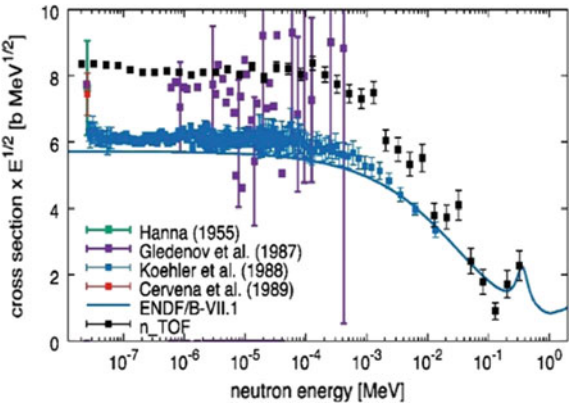

Fig. 8.4 The ^{7}Be(n,p)^{7}Li reaction cross sections. The closed black squires indicate the new data reported from [15]. They seem to agree with the previous data [12, 13] at low energies

8.3 The ^{7}Be(n,p)^{7}Li Reaction for ^{7}Be Destruction

As can be seen in Fig. 8.2, the ^{7}Be(n,p)^{7}Li reaction channel is considered to play the major role for destruction of ^{7}Be [12–14]. Recently, this reaction was revisited by three experiments, although it was believed to be well understood [6]. One was reported in this session by Damone [15] from the n-TOF group who studied the ^{7}Be(n,p)^{7}Li reaction cross sections by the direct measurement. They reported about 35% larger cross sections at low energies than the Koehler data [14], and consequently the new result gives 10% reduction of ^{7}Be in BBN, as can be seen in Fig. 8.4. This new data seems to agree with the data group of [12, 13]. It is not so obvious yet which group is correct.

The large contribution for the ^{7}Be(n,p)^{7}Li reaction in BBN seems to come from the 3^{+} resonance in ^{8}Be, which can be excited by p-wave, not s-wave. Thus, the angular distribution measurement is important to derive exact cross sections. Unfortunately, the n-TOF experiment assumed s-wave for all the resonances in the analysis. To be precise for the Li problem, it is recommended to measure the angular distributions at all energies, as this channel has the largest contribution for ^{7}Be destruction.

There is another important point to note for this reaction study. The reaction channel of ^{7}Be(n,p_1)^{7}Li* (0.487, $1/2^{-}$) was neglected in most studies [6]. At the thermal energy, it was estimated to be about 1% or less [14], although the transition of p_1 was not separated from p_0. At very low energy there is a 2^{-} resonance which favors the p_0 decay by s-wave, but not p_1. However, there are natural parity states with large width just above the 3^{+} resonance. The p_1 decay from these resonances can have the same angular momentum as to the p_0 decay. Thus, the ^{7}Be(n,p_1)^{7}Li* reaction would also influence to ^{7}Be destruction in BBN.

Very recently, we successfully measured at JAEA tandem facility the decay properties of the resonances relevant in ^{8}Be [16]. The data is still in preliminary stage in

analysis, but the result indicates significant p_1 transitions from the resonances except for the 2^- and 3^+ states. Thus, the p_1 contribution would not be so large, but cannot be neglected. Similar results were obtained for p_1 using THM at the CRIB facility, which was presented by Hayakawa in this meeting [11].

8.4 ^{7}Be Destruction by Other Particles

As can be seen in Fig. 8.2, ^{7}Be can be destroyed not only by neutrons but also by other particles, especially by deuterons. The ^{7}Be(d,p)^{8}Be reaction was studied experimentally before [17, 18], and it seems to have only a minor effect for the Li Problem. However, as was reported by Wiedenhoever [19] in this meeting, the ^{7}Be(d,α)^{5}Li reaction may have a considerable effect for destruction of ^{7}Be. See this proceedings for detail.

The remaining possible channels relevant to the Li Problem would be ^{7}Be+^{3}He, and ^{7}Be+t. They were studied previously by an indirect method [20], but the contributions are not well understood yet. These channels need to be further investigated. Another possibility is the nuclear reactions in the BBN network that are not directly relevant to destruction of ^{7}Be, which also need to be revisited carefully.

8.5 Summary

I briefly overviewed the recent efforts in nuclear physics for the cosmological Li problem, especially for destruction of ^{7}Be during the BBN epoch. Now, we may conclude that the ^{7}Be(n,α)^{4}He reaction cross sections has been confirmed to be roughly one order of magnitude smaller than the Wagoner prediction. Thus, this reaction has a minor effect for destruction of ^{7}Be, and does not solve the Li problem.

The ^{7}Be(n,p)^{7}Li reaction, which is considered to be the dominant destruction channel of ^{7}Be, also was revisited by direct and indirect methods. There are still some insufficiency in determining the cross sections, i.e., the angular distribution effect for the total cross section deduction, and the contribution of the p_1 transition. This would be the subject of the coming years.

The ^{7}Be+d channels, now being actively investigated, may have a certain effect for ^{7}Be destruction. It should be thoroughly investigated. The channels of ^{7}Be+^{3}He, t, and α are less extensively investigated, and need to be investigated seriously.

Although I discussed primarily the efforts from the nuclear reaction rate study for the cosmological Li problem, it should be very interesting to have various approaches like astronomical observations as well as a new possibility in other physics for BBN.

References

1. S. Kubono et al. (ed.) *Proceedings of the 14th International Symposium on Nuclei in the Cosmos (NIC2016)*. Japanese Phys. Soc. Conf. Proc. No. **14**
2. R.V. Wagoner, Astrophys. J. Suppl. Ser. **18**, 247 (1969)
3. F. Spite, M. Spite, Astron. Astrophys. **115**, 357 (1982); S.G. Ryan et al., Astrophys. J. **600**, L57 (2000); L. Sbordone et al., Astron. Astrophys. **522**, A26 (2010)
4. J. Dunkley et al., Astrophys. J., Suppl. Ser. **180**, 306 (2009)
5. P.A.R. Ade et al., (Plank Collaboration), Astron. Astrophys. **571**, A15 (2014)
6. M. Smith et al., Astophys. J. Suppl. **85**, 219 (1993); A. Adahchour, P. Discouvemont, J. Phys. G. Nucl. Par. Phys. **29**, 395 (2003); A. Coc et al., Phys. Rev. D **87**, 123530 (2013); R.H. Cyburt et al., Rev. Mod. Phys. **88**, 015004 (2016)
7. S.Q. Hou, J.J. He, S. Kubono, Y.S. Chen, Phys. Rev. C **91**, 055802 (2015)
8. M. Barbagallo et al., Phys. Rev. Lett. **117**, 152701 (2016)
9. T. Kawabata et al., Phys. Rev. Lett. **118**, 052701 (2017)
10. L. Lamia, Astrophys. J. **850**, 175 (2017), and contribution to this proceedings
11. S. Hayakawa, contribution to this proceedings
12. R.C. Hanna, The London, Edinburgh, and Dublin Ph. Mag. J. Science **46**, 381 (1955)
13. Y.M. Gledenov et al., Int. Conf. Neutron Phys. Kiev **2**, 232 (1987)
14. P.E. Koehler et al., Phys. Rev. C **37**, 917 (1988)
15. L. Damone et al., Phys. Rev. Lett. **121**, 042701 (2018)
16. N. Iwasa, S. Kubono, private communication
17. C. Angulo et al., Astrophys. J. **630**, L105 (2005)
18. P.D. O'Malley et al., Phys. Rev. C **84**, 042801(R) (2011)
19. I. Wiedenhoever, private communication, contribution to this proceedings
20. F. Hammache et al., Phys. Rev. C **88**, 062803(R) (2013)

Chapter 9
The Cosmologically Relevant $^{7}Be(n,\alpha)^{4}He$ Reaction in View of the Recent THM Investigations

L. Lamia, C. Spitaleri, M. Mazzocco, S. Hayakawa, C. A. Bertulani, A. Boiano, C. Boiano, Carlo Broggini, Antonio Caciolli, Rosanna Depalo, F. Galtarossa, G. L. Guardo, M. Gulino, S. Kubono, M. La Cognata, M. La Commara, G. La Rana, M. Lattuada, Roberto Menegazzo, A. Pakou, C. Parascandolo, D. Piatti, D. Pierroutsakou, Rosario Gianluca Pizzone, S. Romano, G. G. Rapisarda, M. L. Sergi, O. Sgouros, F. Soramel, V. Soukeras, E. Strano, D. Torresi, Aurora Tumino, H. Yamaguchi, F. L. Villante and G. L. Zhang

L. Lamia (✉) · C. Spitaleri · G. L. Guardo · M. Gulino · M. La Cognata · M. Lattuada · R. G. Pizzone · S. Romano · G. G. Rapisarda · M. L. Sergi · D. Torresi · A. Tumino
Laboratori Nazionali del Sud di Catania, LNS-INFN, Catania, Italy
e-mail: llamia@lns.infn.it

L. Lamia · C. Spitaleri · G. L. Guardo · M. Lattuada · S. Romano
Dipartimento di Fisica e Astronomia, Univ. di Catania, Catania, Italy

M. Mazzocco · A. Caciolli · R. Depalo · D. Piatti · F. Soramel · E. Strano
Dipartimento di Fisica e Astronomia, Univ. di Padova, Padova, Italy

M. Mazzocco · C. Broggini · A. Caciolli · R. Depalo · R. Menegazzo · D. Piatti · F. Soramel · E. Strano
INFN-Sez. di Padova, Padova, Italy

A. Pakou · O. Sgouros · V. Soukeras
Department of Physics and HINP, University of Ioannina, Ioannina, Greece

A. Boiano · M. La Commara · G. La Rana · C. Parascandolo · D. Pierroutsakou
INFN-Sezione di Napoli, Napoli, Italy

S. Hayakawa · C. Boiano · H. Yamaguchi
Center for Nuclear Study, University of Tokyo, Tokyo, Japan

S. Kubono
Riken Nishina Center, Wako, Saitama, Japan

M. La Commara · G. La Rana
Dipartimento di Scienze Fisiche, Universit di Napoli, Napoli, Italy

M. Gulino · A. Tumino
Facolt di Ingegneria e Architettura, Universit degli Studi di Enna Kore, Enna, Italy

F. L. Villante
Laboratori Nazionali del Gran Sasso LNGS-INFN, L'Aquila, Assergi, Italy

Dipartimento di Scienze Fisiche e Chimiche, Universit dellAquila, L'Aquila, Italy

S. Kubono · G. L. Zhang
Institute of Modern Physics, Chinese Academy of Sciences, Lanzhou, China

A. Formicola et al. (eds.), *Nuclei in the Cosmos XV*, Springer
Proceedings in Physics 219, https://doi.org/10.1007/978-3-030-13876-9_9

Abstract The cosmologically relevant ^{7}Be(n,α)^{4}He has been matter of recent studies aimed at contributing to the long-standing Li-problem. Here a brief description of the twin THM investigations will be shown and the main results discussed.

9.1 Introduction

Lithium puzzle is one the most intriguing unsolved problem at our days. Its predicted abundance by CMB evaluations is generally accepted to be a factor ∼3 higher than the one deduced by halo stars observations (see [1] for a general review). However, recent observations and stellar models for Pop.II stars seem to alleviate such a discrepancy. These models tend to predict a higher value of primordial lithium [2], starting from which possible stellar depletion mechanism could have left the lithium value at the currently observed value. In this charming scenario, nuclear physics solutions have been largely investigated in the past [3, 4] and reaction rate determination for both the producing and the destruction channels involving lithium are really necessary in order to reduce the corresponding uncertainties. In particular, the role of the unstable ^{7}Be ($t_{1/2}$ = 53.22 ± 0.06 d) during BBN era is currently matter reflecting in a boost of devoted experimental investigations [5–7]. Recently, the Trojan Horse Method (THM) [8–16] have been applied for measuring the cross section of the (n,α) reaction channel on ^{7}Be by means of charge-symmetry hypothesis applied to the previous ^{7}Li(p,α)^{4}He THM data corrected for Coulomb effects. The deduced ^{7}Be(n,α)^{4}He data overlap with the Big Bang nucleosynthesis energies and the deduced reaction rate allows us to evaluate the corresponding cosmological implications [17]. In addition, the BELICOS (BEryllium and LIthium in the COSmos) experiment has been also performed at INFN-LNL via THM application to the ^{7}Be+^{2}H quasi-free reaction reaction ignited at a beam energy of 20 MeV. A parallel experiment has been also discussed in [18].

9.2 The THM Experiments

Recently, the ^{7}Be(n,α)^{4}He cross section has been derived by applying the charge-symmetry hypothesis to previous ^{7}Li(p,α)^{4}He THM data, as discussed in [17]. Charge-symmetry hypothesis (CSH) is still a largely debated topic in nuclear physics particularly for low-energy induced reactions. However, the agreement between the cross section values derived in [6] by means of the detailed balance principle and the ones derived in [19] represents a test for the goodness of CSH for this system.

C. A. Bertulani
Department of Physics, Tohoku University, Sendai, Japan

F. Galtarossa
Laboratori Nazionali di Legnaro, LNL-INFN, Legnaro, Italy

For the purpose of our work, two data sets have been considered for applying CSH to the already existing THM ^{7}Li(p,α)^{4}He data. In particular, we adopted the data discussed in [11, 20]. These data allowed for the extraction of the ^{7}Li(p,α)^{4}He via a deuteron and ^{3}He breakup THM experiments, separately. In addition, because we are interested in using the experimental data useful for the ^{7}Be(n,α)^{4}He investigation, only part of available data have been considered. In particular, because of the difference in mass of the two entrance channels ^{7}Li+p and ^{7}Be+n, a difference of 1.644 MeV is present between the center-of-mass energies covered in the two cases. For such a reason, only ^{7}Li(p,α)^{4}He THM data covering a center-of-mass energy $E_{Li-p} > 1.644$ MeV have been taken into account. These data have been then correct for Coulomb effects and threshold energies, as discussed in [17]. The result of such investigation show a marked agreement with the trend of the cross section data of [6, 19], with the advantage of producing a cross section measurement right in the energy region of BBN. The good agreement once again showed the goodness of our assumption as previously done in [19]. From the deduced reaction rate, we found a very small decrease within 10% of the corresponding reaction rate. Although this results improve the production of lithium, its impact is far to solve completely the lithium-problem thus suggesting, once again, other solutions rather than the nuclear ones [4, 17].

Besides the previous investigation, the ^{7}Be(n,α)^{4}He reaction (Q = 18.99 MeV) has been studied by means of the THM applied to the quasi-free reaction ^{2}H(^{7}Be, α^{4}He)p (Q = 16.765 MeV), by using a 20.4 MeV ^{7}Be beam impinging on a 400 μg/cm^{2} thick CD_2 target. By using deuteron as TH-nucleus, the two emerging alpha particles have been detected while the kinematical quantities of the undetected proton have been reconstructed by means of momentum-energy conservation laws. The experiment has been performed at the EXOTIC facility [21]. A ^{7}Be beam has been produced by means of a 33 MeV ^{7}Li beam interacting with a 1 bar H_2 cryogenic gas target. At the end of the beam line, an intensity of 5–8 $\times 10^{5}$ pps and a purity of about 99% were measured. The adopted experimental setup for the present ^{7}Be+^{2}H has been described in [22]. It is part of the EXPADES array described in [23]. The detectors have been located around the so-called QF angular pairs, i.e. the angular pairs at which alpha particles are emitted in correspondence of low-momenta of the undetected proton, thus completely covering the kinematic region at which the contribution of the QF reaction mechanism is expected to be dominant. A symmetrical configuration of the detection system has been chosen to double statistics. The alpha particles emitted in the angular range 27° ± 8° have been detected by means of a ΔE-E telescope made up of an ionization chamber (IC), (ΔE stage), and two 300 μm silicon detectors acting as E stage. The IC's have had an active depth of 61.5 mm and have been filled with 100 mbar isobutane gas. Entrance and exit windows were made up by 1.5 μm thick mylar foils with an effective area of 60 × 60 mm^{2} to match the E silicon-stage. The further stage of the analysis foresees the selection of the events corresponding to the three-body reaction channel ^{2}H(^{7}Be, α^{4}He)p. By using the standard ΔE-E technique to select the Z = 2 loci in the telescopes, the alpha-alpha events of interest have been reconstructed once the energy loss in the CD_2 target as well as in the IC has been properly evaluated. To assess the proper selection of the exit channel the

experimental Q-value spectrum has been deduced for the selected events, leading to an experimental value of about 16.76 MeV, in agreement with the theoretical one of 16.765 MeV. A Gaussian fit of such a peak leads to a FWHM of about 2 MeV, reflecting the experimental FWHM of the ^{7}Be beam (FWHM$\approx$1 MeV), energy loss effects in the CD_2 target ($\approx$0.7 MeV) and angular resolution ($\pm 0.4^{\circ}$) effects. In order to select the QF-reaction mechanism, on which the full THM data analysis is based, the trend of the momentum distribution for the p-n intercluster motion inside deuteron has been studied, showing a good agreement with the theoretical Hulthen wave function in momentum space. This agreement marks unambiguously the QF-reaction mechanism thus allowing us to further proceed in the extraction of the ^{7}Be(n,α)^{4}He cross section. Thus, the two body reaction cross section needs to be properly evaluated taking into account HOES (half-off energy shell effects) as well as normalization to the available direct data of [5, 6, 19].

References

1. C. Bertulani, T. Kajino, Prog. Part. Nucl. Phys. **89**, 56 (2016)
2. T. Nordlander et al., Astrophys. J. **753**, 48 (2012)
3. C. Broggini, L. Canton, G. Fiorentini et al., J. Cosmol. Astropart. Phys. **6**, 30 (2012)
4. R.G. Pizzone, R. Spartà, C.A. Bertulani et al., Astrophys. J. **786**, 112 (2014)
5. M. Barbagallo, A. Musumarra, L. Cosentino et al., Phys. Rev. Lett. **117**, 152701 (2016)
6. T. Kawabata, Y. Fujikawa, T. Furuno et al., Phys. Rev. Lett. **118**, 052701 (2017)
7. I. Wiedenhoever in *Contribution to this Conference*
8. C. Spitaleri, L. Lamia, A. Tumino et al., Phys. Rev. C **69**, 055806 (2004)
9. C. Spitaleri, M. La Cognata, L. Lamia et al., Eur. Phys. J. A **52**, 77 (2016)
10. L. Lamia, C. Spitaleri, E. Tognelli et al., Astrophys. J. **811**, 99 (2015)
11. R.G. Pizzone, C. Spitaleri, L. Lamia et al., Phys. Rev. C **83**, 045801 (2011)
12. M. Gulino, C. Spitaleri, X.D. Tang et al., Phys. Rev. C **87**, 012801 (2013)
13. M.L. Sergi, C. Spitaleri, M. La Cognata et al., Phys. Rev. C **91**, 065803 (2015)
14. J. Grineviciute, L. Lamia, A. Mukhamedzhanov et al., Phys. Rev. C **91**, 014601 (2015)
15. A. Tumino, C. Spitaleri, M. La Cognata et al., Nature **557**, 687 (2018)
16. R.G. Pizzone, C. Spitaleri, C.A. Bertulani et al., Phys. Rev. C **87**, 025805 (2013)
17. L. Lamia et al., Astrophys. J. **850**, 175 (2017)
18. S. Hayakawa et al., AIP **1947**, 020011 (2018)
19. S.Q. Hou et al., Phys. Rev. C **91**, 055802 (2015)
20. A. Tumino et al., Euro. Phys. J. A **27**, 243 (2006)
21. F. Farinon, T. Glodariu, M. Mazzocco et al., Nucl. Instr. Meth. B **266**, 4097 (2008)
22. L. Lamia et al., EPJWC **165**, 01032 (2017)
23. D. Pierroutsakou, A. Boiano, C. Boiano et al., Nucl. Instr. Meth. A **834**, 46 (2016)

Chapter 10
Few-Nucleon Reactions of Astrophysical Interest: A Review

Laura Elisa Marcucci, Alex Gnech and Alessandro Grassi

Abstract We review the theoretical studies of the proton-deuteron and α-deuteron radiative captures. The two theoretical frameworks used, the *ab-initio* and the cluster approach, respectively, are also briefly discussed.

10.1 Introduction

In this brief review of theoretical studies for few-nucleon reactions of astrophysical interest, we consider two different approaches, which we refer to as "*ab-initio* method" and "cluster method". In the first one, the nucleus is seen as a system of A nucleons interacting among themselves and with external electroweak probes. The main ingredients of the calculation are a realistic description of the nuclear interaction and currents, and an "exact" method to solve the quantum-mechanical problem, both for bound and scattering states. We will review in Sect. 10.2 such an approach at work for the proton-deuteron radiative capture ($p + d \rightarrow {}^3\mathrm{He} + \gamma$), following the recent work of [1] (see also [2], and references therein).

Within the so-called cluster method, the nucleus is seen as a system of clusters, whose choice depends on the considered system and reaction. The essential ingredient of this method is the inter-cluster potential model. We will see in Sect. 10.3 the cluster method at work for the α-deuteron radiative capture ($\alpha + d \rightarrow {}^6\mathrm{Li} + \gamma$), following the recent work of [3].

L. E. Marcucci (✉)
Dipartimento di Fisica "E. Fermi", Pisa University, 56127 Pisa, Italy
e-mail: laura.elisa.marcucci@unipi.it

L. E. Marcucci · A. Gnech
Istituto Nazionale di Fisica Nucleare, Sezione di Pisa, 56127 Pisa, Italy

A. Gnech
Gran Sasso Science Institute, 67100 L'Aquila, Italy

A. Grassi
M. Smoluchowski Institute of Physics, Jagiellonian University, 30348 Kraków, Poland

A. Formicola et al. (eds.), *Nuclei in the Cosmos XV*, Springer
Proceedings in Physics 219, https://doi.org/10.1007/978-3-030-13876-9_10

In all these studies the observable of interest is the astrophysical S-factor, defined as $S(E) = E \exp(2\pi\eta)\,\sigma(E)$, where η is the Sommerfeld parameter and $\sigma(E)$ is the capture cross section.

10.2 The *ab-initio* Method Applied to the *pd* Reaction

The pd radiative capture S-factor has been recently calculated in [1], within an *ab-initio* approach, based on phenomenological realistic models for the nuclear interaction and currents. Here we consider the results in the energy range 30–300 keV, of interest for Big Bang Nucleosynthesis (BBN). The nuclear interaction includes both two- and three-nucleon potentials, the Argonne v_{18} (AV18) [4] and the Urbana IX (UIX) [5] model, respectively. The Hyperspherical Harmonics (HH) method is used to solve the $A = 3$ bound and scattering problem (see [6, 7] and references therein). To be remarked that the HH method is at present the only one able to calculate the pd scattering state at low relative energies, including Coulomb interaction between the charged initial particles. The nuclear electromagnetic current operator is written as a sum of one- and many-body terms, the latter constructed so as to satisfy the current conservation relation exactly with the adopted Hamiltonian as in [8]. For a review see also [9]. The one-body term is obtained performing a $1/m$ expansion (m is the nucleon mass) of the single-nucleon covariant current up to order $\mathcal{O}(1/m^3)$. The term $\mathcal{O}(1/m^3)$ has been found important in the study of the nd radiative capture at thermal energies [10].

The calculated S-factor in the BBN energy range is shown in the left panel of Fig. 10.1, where it is compared with the previous *ab-initio* calculation of [8], with the best fit of [2], and with the available experimental data [11–14]. By inspection of the figure we can conclude that the results of [1] are systematically larger than those of [8] as well as the polynomial fit of [2]. The origin of this difference can be traced back in part to the one-body $\mathcal{O}(1/m^3)$ term, responsible for an increase of 1–3 % over the whole energy range, but mostly to the more accurate new solutions for the $A = 3$ scattering problem. The difference with the available experimental data in the BBN region [13], however, is even larger.

The consequences of this new S-factor determination for BBN has been discussed in [1], where it has been shown that the predicted deuterium primordial abundance is in nice agreement with experiment [15].

10.3 The Cluster Method Applied to the αd Reaction

The αd radiative capture S-factor has been recently studied within the cluster method in [3, 16]. In [16], the initial state is calculated solving a two-body $\alpha + d$ problem, while the ^{6}Li nucleus is seen as a $\alpha + n + p$ three-body system. In [3] both the initial and final nuclear states are studied within a two-body framework. In this

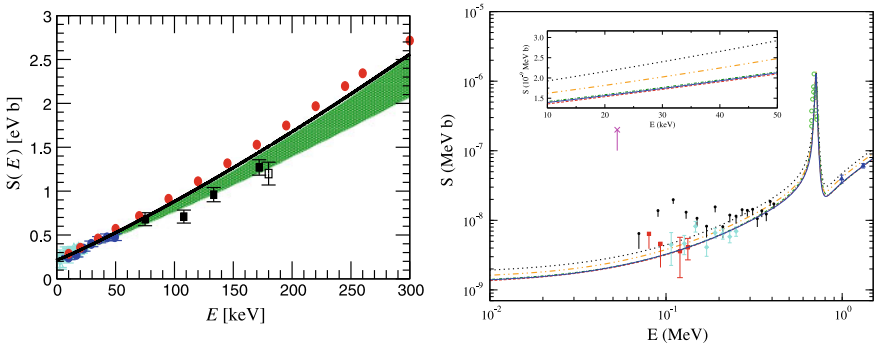

Fig. 10.1 Left panel: The *pd* S-factor in the 0–300 keV energy range, as calculated in [1] (red filled circles), is plotted together with the available experimental data of [11–14], the calculation of [8] (solid black line), and the best fit to data of [2] (green band). Right panel: The αd S-factor in the 0–1.5 MeV energy range, as calculated in [3], plotted together with the available experimental data of [21–27]. In the insert, the tail of the S-factor in the 10–50 keV energy range. The black dotted, red dashed, green dot-dashed, orange dot-dot-dashed and blue solid lines correspond to the results obtained with the potential models of [3, 17–20], respectively

contribution we will review this last work. The main ingredient of the calculation is the $\alpha + d$ potential. Five models have been considered: four of them are taken from the literature [17–20]. The first three are central potentials, including a spin-independent and a spin-orbit interaction. Therefore, they are unable to reproduce the ^{6}Li magnetic dipole and electric quadrupole moments. Only the model of [20] retains a tensor component. However, this model, as well as the one of [17], is unable to reproduce the S-state asymptotic normalization coefficient (ANC), which turns out to be crucial at the low energy of interest for BBN. In [3] then a new model for the $\alpha + d$ potential has been constructed, which is able to reproduce, besides the ^{6}Li binding energy, magnetic dipole and electric quadrupole moments, also the ANC, and the $\alpha + d$ elastic scattering phase shifts. Therefore, this new potential model should be considered as the most accurate model within this two-body cluster approach. The long-wavelength approximation is then used in order to calculate the S-factor, and only the electric dipole (E_1) and quadrupole (E_2) operators are retained. To be noticed that the E_1 contribution is isospin suppressed at low energies [3].

The predicted S-factor is shown in the right panel of Fig. 10.1, and is compared with the available experimental data [21–27]. As we can see by inspection of the figure, the S-factor at low energies has a strong dependence with respect to the ANC value, as expected. In fact, the three potential models able to reproduce the ANC, i.e. those of [3, 18, 19], give very close results. The potential models of [17, 20], giving a larger value for the ANC, predict higher values for the S-factor. The use of a relatively large number of potential models allows us to conclude that within the two-body cluster approach, the theoretical uncertainty is of the order of 20 %, when all the potentials are considered, but becomes a few % when only the three potentials which reproduce the correct ANC value are taken into account. The available experimental

data, though, are not accurate enough in order to discriminate between the results obtained with these five potentials.

The effect of this recent S-factor prediction on the ^{6}Li and ^{7}Li+^{7}Be primordial abundances has been studied in [3], where is has been shown that no significant changes have been produced, compared with previous predictions.

10.4 Summary and Conclusions

We have presented two recent studies of few-nucleon radiative captures within the *ab-initio* and the cluster method, and the theoretical results have been compared with the available experimental data. Also, the implications for BBN primordial abundances predictions have been briefly discussed.

Both approaches can be improved. For instance, within the *ab-initio* approach, it is highly desirable to apply the so-called chiral effective field theory framework, in order to be able to provide a robust estimate for the theoretical uncertainty (see [9] and references therein). On the other hand, the cluster approach remains the only alternative for reactions where A is too large to apply *ab-initio* methods, as at present the case of the $p\,^6$Li radiative capture, also of interest for the primordial lithium abundance [28].

References

1. L.E. Marcucci, G. Mangano, A. Kievsky, M. Viviani, Implication of the proton-deuteron radiative capture for Big Bang Nucleosynthesis. Phys. Rev. Lett. **116**, 102501 (2016); Erratum: Phys. Rev. Lett. **117**, 049901 (2016). https://doi.org/10.1103/PhysRevLett.116.102501, https://doi.org/10.1103/PhysRevLett.117.049901
2. E.G. Adelberger et al., Solar fusion cross sections II: the pp chain and CNO cycles. Rev. Mod. Phys. **83**, 195 (2011). https://doi.org/10.1103/RevModPhys.83.195
3. A. Grassi, G. Mangano, L.E. Marcucci, O. Pisanti, $\alpha + d \rightarrow {}^6\mathrm{Li} + \gamma$ astrophysical S-factor and its implications for Big Bang nucleosynthesis. Phys. Rev. C **96**, 045807 (2017). https://doi.org/10.1103/PhysRevC.96.045807
4. R.B. Wiringa, V.G.J. Stoks, R. Schiavilla, Accurate nucleon-nucleon potential with charge-independence breaking. Phys. Rev. C **51**, 38 (1995). https://doi.org/10.1103/PhysRevC.51.38
5. B.S. Pudliner et al., Quantum Monte Carlo calculations of nuclei with $A<7$. Phys. Rev. C **56**, 1720 (1997). https://doi.org/10.1103/PhysRevC.56.1720
6. A. Kievsky et al., A high-precision variational approach to three- and four-nucleon bound and zero-energy scattering states. J. Phys. G **35**, 063101 (2008). https://doi.org/10.1088/0954-3899/35/6/063101
7. L.E. Marcucci et al., $N - d$ Elastic scattering using the hyperspherical harmonics approach with realistic local and non-local interactions. Phys. Rev. C **80**, 034003 (2009). https://doi.org/10.1103/PhysRevC.80.034003
8. L.E. Marcucci et al., Electromagnetic structure of $A = 2$ and 3 nuclei and the nuclear current operator. Phys. Rev. C **72**, 014001 (2005). https://doi.org/10.1103/PhysRevC.72.014001

9. L.E. Marcucci et al., Electromagnetic Structure of Few-Nucleon Ground States. J. Phys. G **43**, 023002 (2016). https://doi.org/10.1088/0954-3899/43/2/023002
10. L. Girlanda et al., Thermal neutron captures on d and ^{3}He. Phys. Rev. Lett. **105**, 232502 (2010). https://doi.org/10.1103/PhysRevLett.105.232502
11. G.M. Griffiths, M. Lal, C.D. Scarfe, The reaction $d(p,\gamma)^3$He below 50 keV. Can. J. Phys. **41**, 724 (1963). https://doi.org/10.1139/p63-077
12. G.J. Schmid et al., Effects of Non-nucleonic Degrees of Freedom in the $d(\overrightarrow{p},\gamma)^3$He and $p(\overrightarrow{d},\gamma)^3$He Reactions. Phys. Rev. Lett. **76**, 3088 (1996). https://doi.org/10.1103/PhysRevLett.76.3088
13. L. Ma et al., Measurements of ^{1}H($\overrightarrow{d}$, γ)3He and ^{2}H($\overrightarrow{p}$, γ)^{3}He at very low energies. Phys. Rev. C **55**, 588 (1997). https://doi.org/10.1103/PhysRevC.55.588
14. C. Casella et al., (LUNA Collaboration): first measurement of the $d(p,\gamma)^3$He cross section down to the solar Gamow peak. Nucl. Phys. A **706**, 203 (2002). https://doi.org/10.1016/S0375-9474(02)00749-2
15. R.J. Cooke et al., Precision measures of the primordial abundance of deuterium. Astrophys. J. **781**, 31 (2014). https://doi.org/10.1088/0004-637X/781/1/31
16. D. Baye, E.M. Tursunov, Isospin-forbidden electric dipole capture and the $\alpha(d,\gamma)^6$Li reaction. J. Phys. G **45**, 085102 (2018). http://stacks.iop.org/0954-3899/45/i=8/a=085102
17. F. Hammache et al., High-energy breakup of ^{6}Li as a tool to study the Big Bang nucleosynthesis reaction ^{2}H(α, γ)^{6}Li. Phys. Rev. C **82**, 065803 (2010). https://doi.org/10.1103/PhysRevC.82.065803
18. A.M. Mukhamedzhanov, L.D. Blokhintsev, B.F. Irgaziev, Reexamination of the astrophysical S factor for the α+$d \rightarrow {}^6$Li+ γ reaction. Phys. Rev. C **83**, 055805 (2011). https://doi.org/10.1103/PhysRevC.83.055805
19. E.M. Tursunov, S.A. Turakulov, P. Descouvemont, Theoretical analysis of the astrophysical S-factor for the capture reaction $\alpha + d \rightarrow {}^6$Li + γ in the two-body model. Phys. Atom. Nucl. **78**, 193 (2015). https://doi.org/10.1134/S1063778815010196
20. S.B. Dubovichenko, Tensor ^{2}H^{4}He interactions in the potential cluster model involving forbidden states. Phys. Atom. Nucl. **61**, 162 (1998)
21. R.G.H. Robertson et al., Observation of the capture reaction ^{2}H(α, γ)^{6}Li and its role in production of ^{6}Li in the Big Bang. Phys. Rev. Lett. **47**, 1867 (1981). https://doi.org/10.1103/PhysRevLett.47.1867
22. J. Kiener et al., Measurements of the Coulomb dissociation cross section of 156 MeV ^{6}Li projectiles at extremely low relative fragment energies of astrophysical interest. Phys. Rev. C **44**, 2195 (1991). https://doi.org/10.1103/PhysRevC.44.2195
23. P. Mohr et al., Direct capture in the 3^+ resonance of ^{2}H(α, γ)^{6}Li. Phys. Rev. C **50**, 1543 (1994). https://doi.org/10.1103/PhysRevC.50.1543
24. F.E. Cecil, J. Yan, C.S. Galovich, The reaction $d(\alpha,\gamma)^6$Li at low energies and the primordial nucleosynthesis of ^{6}Li. Phys. Rev. C **53**, 1967 (1996). https://doi.org/10.1103/PhysRevC.53.1967
25. S.B. Igamov, R. Yarmukhamedov, Triple-differential cross section of the ^{208}Pb(^{6}Li,αd)^{208}Pb Coulomb breakup and astrophysical S-factor of the $d(\alpha,\gamma)^6$Li reaction at extremely low energies. Nucl. Phys. A **673**, 509 (2000). https://doi.org/10.1016/S0375-9474(00)00132-9
26. M. Anders et al., (LUNA Collaboration): first direct measurement of the ^{2}H(α, γ)^{6}Li cross section at Big Bang energies and the primordial lithium problem. Phys. Rev. Lett. **113**, 042501 (2014). https://doi.org/10.1103/PhysRevLett.113.042501
27. D. Trezzi et al., (LUNA Collaboration): Big Bang ^{6}Li nucleosynthesis studied deep underground. Astr. Phys. **89**, 57 (2017). https://doi.org/10.1016/j.astropartphys.2017.01.007
28. A. Gnech, L.E. Marcucci, A two body description of ^{6}Li(p, γ)^{7}Be reaction, in *These proceedings*

Chapter 11
Data for the s Process from n_TOF

C. Massimi, O. Aberle, V. Alcayne, J. Andrzejewski, L. Audouin, V. Bécares, V. Babiano-Suarez, M. Bacak, M. Barbagallo, Th. Benedikt, S. Bennett, E. Berthoumieux, J. Billowes, D. Bosnar, A. Brown, Maurizio Busso, M. Caamaño, L. Caballero-Ontanaya, F. Calviño, M. Calviani, D. Cano-Ott, A. Casanovas, D. M. Castelluccio, F. Cerutti, E. Chiaveri, G. Clai, N. Colonna, G. Cortés, M. A. Cortès-Giraldo, L. Cosentino, Sergio Cristallo, L. A. Damone, P. J. Davies, M. Dietz, C. Domingo-Pardo, R. Dressler, Q. Ducasse, E. Dupont, I. Durán, Z. Eleme, B. Fernàndez-Dominguez, A. Ferrari, P. Finocchiaro, V. Furman, Kathrin Göbel, A. Gawlik, S. Gilardoni, I. F. Gonçalves, E. González-Romero, C. Guerrero, F. Gunsing, S. Heinitz, J. Heyse, D. G. Jenkins, Arnd R. Junghans, F. Käppeler, Y. Kadi, A. Kimura, I. Knapova, M. Kokkoris, Y. Kopatch, M. Krtička, Deniz Kurtulgil, I. Ladarescu, Claudia Lederer-Woods, S. J. Lonsdale, D. Macina, A. Manna, T. Martínez, A. Masi, P. Mastinu, M. Mastromarco, F. Matteucci, E. A. Maugeri, A. Mazzone, E. Mendoza, A. Mengoni, V. Michalopoulou, P. M. Milazzo, Federica Mingrone, J. Moreno-Soto, A. Musumarra, A. Negret, F. Ogállar, A. Oprea, N. Patronis, A. Pavlik, J. Perkowski, Luciano Piersanti, C. Petrone, E. Pirovano, I. Porras, J. Praena, J. M. Quesada, D. Ramos-Doval, Thomas Rauscher, René Reifarth, D. Rochman, M. Sabaté-Gilarte, A. Saxena, P. Schillebeeckx, D. Schumann, A. Sekhar, S. Simone, A. G. Smith, N. V. Sosnin, P. Sprung, A. Stamatopoulos, G. Tagliente, J. L. Tain, A. Tarifeño-Saldivia, L. Tassan-Got, A. Tsinganis, J. Ulrich, Sebastian Urlass, S. Valenta, G. Vannini, V. Variale, P. Vaz, A. Ventura, Diego Vescovi, V. Vlachoudis, R. Vlastou, A. Wallner, P. J. Woods, T. Wright, P. Žugec and The n_TOF Collaboration

C. Massimi (✉) · D. M. Castelluccio · G. Clai · A. Manna · A. Mengoni · G. Vannini · A. Ventura
Istituto Nazionale di Fisica Nucleare, Sezione di Bologna, Italy
e-mail: massimi@bo.infn.it

C. Massimi · A. Manna · G. Vannini
Dipartimento di Fisica e Astronomia, Università di Bologna, Bologna, Italy

O. Aberle · M. Bacak · M. Barbagallo · M. Calviani · F. Cerutti · E. Chiaveri · A. Ferrari · S. Gilardoni · D. Macina · A. Masi · M. Mastromarco · V. Michalopoulou · F. Mingrone · M. Sabaté-Gilarte · L. Tassan-Got · A. Tsinganis · S. Urlass · V. Vlachoudis
European Organization for Nuclear Research (CERN), Meyrin, Switzerland

V. Alcayne · V. Bécares · D. Cano-Ott · E. González-Romero · T. Martínez · E. Mendoza
Centro de Investigaciones Energéticas Medioambientales y Tecnológicas (CIEMAT), Madrid, Spain

J. Andrzejewski · A. Gawlik · J. Perkowski
University of Lodz, Lodz, Poland

A. Formicola et al. (eds.), *Nuclei in the Cosmos XV*, Springer
Proceedings in Physics 219, https://doi.org/10.1007/978-3-030-13876-9_11

L. Audouin · D. Ramos-Doval · L. Tassan-Got
Institut de Physique Nucléaire, CNRS-IN2P3, Univ. Paris-Sud, Université Paris-Saclay, 91406 Orsay Cedex, France

V. Babiano-Suarez · L. Caballero-Ontanaya · C. Domingo-Pardo · I. Ladarescu · J. L. Tain
Instituto de Física Corpuscular, CSIC - Universidad de Valencia, Valencia, Spain

M. Bacak
Technische Universität Wien, Vienna, Austria

M. Bacak · E. Berthoumieux · E. Berthoumieux · E. Dupont · F. Gunsing · J. Moreno-Soto
CEA Irfu, Université Paris-Saclay, 91191 Gif-sur-Yvette, France

M. Barbagallo · N. Colonna · L. A. Damone · A. Mazzone · G. Tagliente · V. Variale
Istituto Nazionale di Fisica Nucleare, Sezione di Bari, Italy

Th. Benedikt · K. Göbel · D. Kurtulgil · R. Reifarth
Goethe University Frankfurt, Frankfurt, Germany

S. Bennett · J. Billowes · E. Chiaveri · P. J. Davies · A. Sekhar · A. G. Smith · N. V. Sosnin · T. Wright
University of Manchester, Manchester, UK

D. Bosnar · P. Žugec
Department of Physics, Faculty of Science, University of Zagreb, Zagreb, Croatia

A. Brown · D. G. Jenkins
University of York, York, UK

M. Busso · S. Cristallo · L. Piersanti · D. Vescovi
Istituto Nazionale di Fisica Nucleare, Sezione di Perugia, Italy

M. Busso
Dipartimento di Fisica e Geologia, Università di Perugia, Perugia, Italy

M. Caamaño · I. Durán · B. Fernández-Dominguez
University of Santiago de Compostela, A Coruña, Spain

F. Calviño · A. Casanovas · G. Cortés · A. Tarifeño-Saldivia
Universitat Politècnica de Catalunya, Barcelona, Spain

M. Castelluccio · G. Clai · A. Mengoni
Agenzia nazionale per le nuove tecnologie (ENEA), Bologna, Italy

M. A. Cortés-Giraldo · C. Guerrero · J. M. Quesada · M. Sabaté-Gilarte
Universidad de Sevilla, Sevilla, Spain

L. Cosentino · P. Finocchiaro · A. Musumarra · S. Simone
INFN Laboratori Nazionali del Sud, Catania, Italy

S. Cristallo · L. Piersanti
Istituto Nazionale di Astrofisica - Osservatorio Astronomico di Teramo, Teramo, Italy

L. A. Damone
Dipartimento di Fisica, Università degli Studi di Bari, Bari, Italy

M. Dietz · C. Lederer-Woods · S. J. Lonsdale · P. J. Woods
School of Physics and Astronomy, University of Edinburgh, Edinburgh, UK

R. Dressler · S. Heinitz · D. Rochman · D. Schumann · P. Sprung · J. Ulrich · E. A. Maugeri
Paul Scherrer Institut (PSI), Villingen, Switzerland

Q. Ducasse · E. Pirovano
Physikalisch-Technische Bundesanstalt (PTB), Bundesallee 100, 38116 Braunschweig, Germany

Z. Eleme · N. Patronis
University of Ioannina, Ioannina, Greece

V. Furman · Y. Kopatch
Joint Institute for Nuclear Research (JINR), Dubna, Russia

I. F. Gonçalves · P. Vaz
Instituto Superior Técnico, Lisbon, Portugal

J. Heyse · P. Schillebeeckx
European Commission, Joint Research Centre, Geel, Retieseweg 111, 2440 Geel, Belgium

A. Junghans · S. Urlass
Helmholtz-Zentrum Dresden-Rossendorf, Dresden, Germany

F. Käppeler
Karlsruhe Institute of Technology, Campus North, IKP, 76021 Karlsruhe, Germany

A. Kimura
Japan Atomic Energy Agency (JAEA), Tokai-mura, Naka District, Japan

I. Knapova · M. Krtička · S. Valenta
Charles University, Prague, Czech Republic

M. Kokkoris · V. Michalopoulou · A. Stamatopoulos · R. Vlastou
National Technical University of Athens, Athens, Greece

P. Mastinu
Istituto Nazionale di Fisica Nucleare, Sezione di Legnaro, Italy

F. Matteucci · P. M. Milazzo
Istituto Nazionale di Fisica Nucleare, Sezione di Trieste, Italy

F. Matteucci
Dipartimento di Astronomia, Università di Trieste, Trieste, Italy

A. Mazzone
Consiglio Nazionale delle Ricerche, Bari, Italy

A. Musumarra
Dipartimento di Fisica e Astronomia, Università di Catania, Catania, Italy

A. Negret · A. Oprea · C. Petrone
Horia Hulubei National Institute of Physics and Nuclear Engineering, Măgurele, Romania

F. Ogállar · I. Porras · J. Praena
University of Granada, Granada, Spain

A. Pavlik
Faculty of Physics, University of Vienna, Vienna, Austria

T. Rauscher
Department of Physics, University of Basel, Basel, Switzerland

T. Rauscher
Centre for Astrophysics Research, University of Hertfordshire, Hertfordshire, UK

A. Saxena
Bhabha Atomic Research Centre (BARC), Mumbai, India

Abstract A considerable amount of (n,γ) reactions has been studied, so far, at the neutron time-of-flight facility n_TOF at CERN. The experimental program aims at determining and improving cross sections for a number of isotopes relevant to *s*-process nucleosynthesis. A brief summary of some physical cases related to the *s*-process nucleosyntheis is presented in this work together with ongoing experiments and challenging future programs.

11.1 Introduction

The origin of heavy elements ($A > 56$) is thought to be caused by successive neutron capture reactions and β decays. This *s*-process nucleosynthesis path extends up to lead and bismuth [1, 2]. The observed abundances are a mixture of abundance contributions from the *s* and *r* process with small contaminations from the *p* process [3, 4]. After the pioneering survey by Burbidge and collaborators [5], 6 decades of experiments and progress in stellar models have brought the *s*-process nucleosynthesis to a considerably refined level. For instance, it is now understood that the *s* process takes place in the He-burning layers of low-mass asymptotic giant branch (AGB) stars and during the He- and C-burning phases of massive stars. The nucleosynthesis of nuclides in the $A \approx 60$–90 mass region (the so-called weak component) is driven by the ^{22}Ne(α,n)^{25}Mg reaction in massive stars, which provides the required neutron intensities at temperature higher than about 3–400 million Kelvin. On the contrary, at lower temperatures typical of AGB stars, the ^{13}C(α,n)^{16}O acts as primary neutron source and drives the synthesis of nuclides in the $A \approx 90$–209 mass region (the so-called main component). In this framework, the comparison of the stellar abundance patterns with s-process calculations yields important constraints on stellar evolution modelling, provided that nuclear physics inputs are accurately known. Among all the various experimental quantities responsible for the good quality of stellar models, β-decay half-lives, capture cross sections of isotopes in the β-stability valley and reaction rates of the neutron reaction sources are the most relevant physics data.

11.2 Experimental Determination of Stellar Cross Section

The key nuclear physics quantity for *s*-process modelling are the Maxwellian-averaged capture cross sections (MACS), defined as:

D. Vescovi
Gran Sasso Science Institute, Viale Francesco Crispi 7, LAquila, Italy

A. Wallner
Australian National University, Canberra, Australia

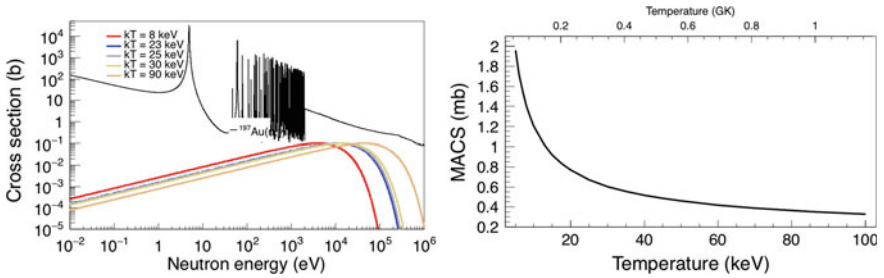

Fig. 11.1 Left panel: ^{197}Au(n,γ) cross section in the region of interest to the *s* process, the bottom curves represent the Maxwellian neutron energy distribution for different stellar burning stages. Right panel: Au MACS at stellar temperatures between 0.1 and 1 GK

$$< \sigma >= \frac{2}{\sqrt{\pi}(k_B T)^2} \int_0^\infty \sigma_\gamma(E) E e^{-\frac{E}{k_B T}} dE, \tag{11.1}$$

where T is the stellar temperature, and $\sigma_\gamma(E)$ the energy dependent capture cross section. The MACS takes into account the effect of the stellar temperature (between 0.1 and 1 GK) where the *s* process takes place. Two methods are currently adopted for the experimental determination of the MACS: activation and Time-of-flight technique. The first method is an energy-integrated measurement, where the neutron spectrum corresponds to a stellar spectrum. This method has extensively been used for measurements of MACS at $k_B T$ = 25 keV, relatively to the one of ^{197}Au, which is considered as a reference. With the second technique, adopted at n_TOF, $\sigma_\gamma(E)$ is measured and the MACS is obtained by folding with the neutron energy distribution, thus enabling the determination of the MACS as a function of the temperature. It is worth recalling the n_TOF research activities [6, 7] related to the international cooperative effort [8] to improve the ^{197}Au cross section standard, which is of primary importance for activation measurements. Figure 11.1 shows the $\sigma_\gamma(E)$ of ^{197}Au(n,γ), together with its MACS for different temperatures.

11.3 n_TOF Experimental Program

Some of the studies carried out at n_TOF (a non-exhaustive list of examples), about the role of branch-point isotopes, s-only isotopes, bottle necks in the *s* process path and neutron source reactions are hereafter briefly summarised.

11.3.1 Branch-Point Isotopes

The reaction flow path of the *s* process proceeds along the β-stability valley. When a long-lived isotope is encountered, depending on the stellar conditions, the competition between neutron capture and β decay can take place. Because of this competition, the reaction path divides into different branches and the resulting isotopic pattern can reveal the physical conditions: neutron density, temperature and pressure, of the stellar environment where the s process is taking place.

Despite their importance, some few measurements of (n,γ) cross sections on unstable isotopes are present in literature in the energy region of interest. For instance, among the 21 relevant cases [3] only 8 isotopes have been studied so far. And among them, the cross section of 5 isotopes has been measured as a function of neutron energy via time-of-flight at n_TOF. The results of ^{151}Sm(n,γ) and ^{63}Ni(n,γ) provided new information for the characterisation of the pulsed *s*-process nucleosynthesis in AGB stars and for the production of ^{63}Cu, ^{64}Ni, and ^{65}Zn in massive stars, respectively [9–11]. The preliminary results of the isotopes with half-lives of a few years, i.e. ^{147}Pm, ^{171}Tm and ^{204}Tl, indicate that their capture cross sections are smaller than theoretical predictions and therefore important consequences are expected. For the future, the n_TOF Collaboration is preparing the detector setup for the measurement campaign on the branching at ^{79}Se, which can constrain the temperature of the s-process nucleosynthesis in massive stars.

11.3.2 s-Only Isotopes: The Case of ^{154}Gd

The *s* process is known to be responsible for the production of about one half of the elemental abundances between iron and bismuth. Moreover about 40 isotopes can be produced only via the *s* process because they are shielded against the β-decay chains from the *r*-process region by stable isobars. Therefore their pure *s*-process origin allows one to check the robustness of stellar models in galactic chemical evolution models (GCE). In addition, they can be used to constrain the so-called ^{13}C pocket (i.e. the shape and the extension of the neutron source).

The n_TOF Collaboration has recently measured the ^{154}Gd(n,γ) cross section, because of a large disagreement between GCE models for this isotope. In Fig. 11.2 some examples of the capture yield determined at n_TOF are compared with the data in literature.

The preliminary new data could rule out one of the possible causes of the inconsistency, as the cross section seems sizeably lower than reported in literature (i.e. the MACS at $k_B T = 8$ keV is about 10% lower than previously thought).

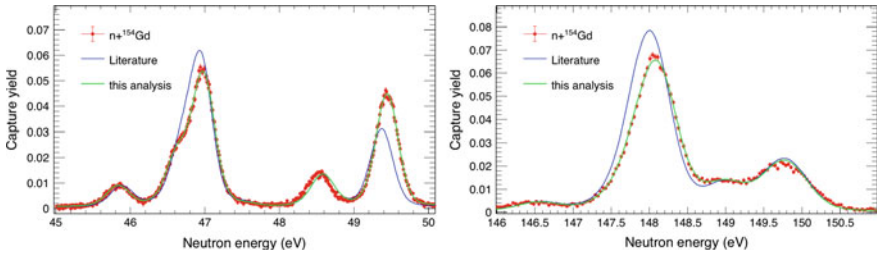

Fig. 11.2 ^{154}Gd(n,γ) capture yield measured at n_TOF compared to its evaluated cross section in nuclear data libraries

11.3.3 ^{140}Ce as Bottle Neck of s-Process Flow at N = 82

Isotopes with very small cross sections act as bottle necks in the neutron capture chain and build up large abundances. This nuclear feature can explain 3 sharp structures in the isotopic solar abundance distribution (see for instance the inset of Fig. 11.2 in [3]) related to the *s*-process. These 3 maxima correspond to nuclei with a magic number of neutrons (N = 50, 82 and 126), whose nuclear configuration makes them particularly stable. A precise and accurate knowledge of the neutron capture cross section is sometimes challenging, as the experimental signature is dominated by the background. However their MACS largely affect the efficiency for the production of heavier elements. The region at N = 82 has partially been investigated at n_TOF in the past, when the production of ^{140}Ce was studied [12], we are now measuring the ^{140}Ce(n,γ) cross section, in order to accurately model the synthesis of heavier elements and reproduce the observed abundances.

11.3.4 Constraining the ^{22}Ne(α,n) Reaction

The reaction rate of ^{22}Ne(α,n)^{25}Mg has an obvious fundamental role in the weak component. In addition, it determines the final abundance pattern of the main component, although it contributes only about 5% to the total neutron budget of AGB stars. The small size of the cross section in the energy range relevant to *s* process makes the direct measurement exceedingly difficult, and no conclusive results have been reported so far below $E_\alpha \approx 830$ keV. As a consequence, the uncertainty in the reaction rate is dominated by the poorly known properties of states in ^{26}Mg between the resonance at $E_\alpha \approx 830$ keV and the threshold. To characterise these levels, we have studied the n+^{25}Mg system and provided valuable pieces of information [13, 14] which are now being adopted in some international cooperative effort for the determination of the ^{22}Ne(α,n) reaction rate together with the one of the competing ^{22}Ne(α,γ) reaction.

11.4 Summary

In the last 2 decades, the nuclear data activity of the n_TOF Collaboration has provided relevant information for the characterisation of several aspects of the *s*-process nucleosynthesis. After two years of technical stop, foreseen in 2019–2021, the n_TOF facility will restart its operation and new data are expected from challenging experiments.

References

1. C. Domingo-Pardo et al. (n_TOF Collaboration). Phys. Rev. C **75**, 015806 (2007)
2. C. Domingo-Pardo et al. (n_TOF Collaboration). Phys. Rev. C **74**, 025807 (2006)
3. F. Käppeler, R. Gallino, S. Bisterzo, W. Aoki, Rev. Mod. Phys. **83**, 157 (2011)
4. J.J. Cowan, F.K. Thielemann, J.W. Truran, Phys. Rep. **208**, 267 (1991)
5. E.M. Burbidge, G.R. Burbidge, W.A. Fowler, F. Hoyle, Rev. Mod. Phys. **29**, 547 (1957)
6. C. Massimi et al. (n_TOF Collaboration). Phys. ReV. C **81**, 044616 (2010)
7. C. Lederer et al. (n_TOF Collaboration). Phys. Rev. C **83**, 034608 (2011)
8. C. Massimi et al., Eur. Phys. J. A **50**, 124 (2014)
9. U. Abbondanno et al. (n_TOF Collaboration). Phys. Rev. Lett. **93**, 161103 (2004)
10. C. Lederer et al. (n_TOF Collaboration). Phys. Rev. Lett. **110**, 022501 (2013)
11. C. Lederer et al. (n_TOF Collaboration). Phys. Rev. C **89**, 025810 (2014)
12. R. Terlizzi et al. (n_TOF Collaboration). Phys. Rev. C **75**, 035807 (2007)
13. C. Massimi et al. (n_TOF Collaboration). Phys. Rev. C **85**, 044615 (2012)
14. C. Massimi et al. (n_TOF Collaboration). Phys. Lett. B **768**, 1 (2017)

Chapter 12
The Study of the ^{6}Li(p,γ)^{7}Be Reaction at LUNA

D. Piatti

Abstract The ^{6}Li(p,γ)^{7}Be reaction is of interest in many different astrophysical scenarios, as for example the early stages of the star evolution. Recently a resonant structure was observed at E_{cm} = 195 keV but it is still not confirmed by both theoretical and experimental studies. In order to investigate the existence of the resonance and to constrain the ^{6}Li(p,γ)^{7}Be S-factor at low energies a direct measurement was performed at LUNA. A High Purity Germanium was used in close geometry. A Silicon detector was inserted in backward geometry in order to detect the α particles by ^{6}Li(p,α)^{3}He reaction. Five solid targets were irradiated from E_p = 80 keV up to E_p = 390 keV and the ongoing analysis suggests there are no resonances.

12.1 Astrophysical Motivation

Pre-main sequence and main sequence stars deplete ^{6}Li via ^{6}Li(p,γ)^{7}Be and ^{6}Li(p,α)^{3}He reactions, which are activated at T $\geq$ 3 MK. Because of this progressive depletion ^{6}Li detection in stars is a powerful tool to track the evolution of stars [1].

While the ^{6}Li(p,α)^{3}He reaction is well known [2], the S-factor of the ^{6}Li(p,γ)^{7}Be reaction is still uncertain at energies of astrophysical interest, E $\leq$ 400 keV. Recently it has been found a resonant structure at E_{cm} = 195 keV (E_x = 5.8 MeV) [3], which is still not confirmed by both theoretical [4] and experimental studies [5], see Fig. 12.1. The suggested excited state could explain the angular distribution of the ^{6}Li(p,α)^{3}He reaction that implies the contribution of both positive and negative levels [2]. In addition it may affect the ^{3}He(^{4}He,γ)^{7}Be cross section and the predicted abundances by the Big Bang Nucleosynthesis [3].

D. Piatti for LUNA collaboration.

D. Piatti (✉)
Università degli Studi di Padova, Padova, Italy
e-mail: denise.piatti@studenti.unipd.it

INFN, Padova, Italy
e-mail: denise.piatti@pd.infn.it

A. Formicola et al. (eds.), *Nuclei in the Cosmos XV*, Springer
Proceedings in Physics 219, https://doi.org/10.1007/978-3-030-13876-9_12

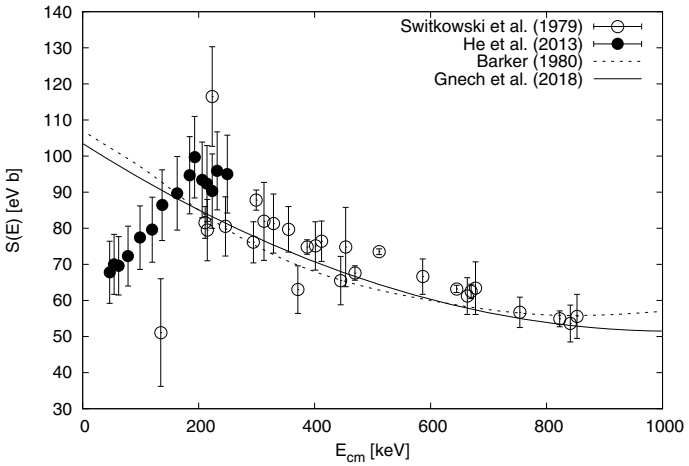

Fig. 12.1 Some of the literature data for the ^{6}Li(p,γ)^{7}Be S-factor. The experimental data with dots. The dashed line is a theoretical curve for the S-factor. The solid line is the theoretical calculation by A. Gnech, whose contribution is inserted in this volume

The necessity to a new direct measurement at low energies is evident. The present work describes the study of ^{6}Li(p,γ)^{7}Be performed at LUNA (Laboratory for Underground Nuclear Astrophysics) in order to investigate the existence of the resonance and to constrain the S-factor at low energies.

In the next sections the experimental setup is described and some preliminary results are presented.

12.2 Experimental Setup

LUNA experimental hall is located at National Laboratories of Gran Sasso (LNGS) in Italy under 1400 m of rocks, which represent a natural shield against the cosmic rays background, the muon flux is reduced of six orders of magnitude and the neutron flux of three orders of magnitude [6].

A high intensity and well collimated proton beam can be accelerated from 50 keV up to 400 keV by the LUNA400kV electrostatic accelerator [7]. The beam can be delivered either to a gas or a solid target beam line.

For the present study the solid target beam line was exploited. The beam is focused to the scattering chamber thanks to both electrical and magnetic optical elements. In addition one static aperture, diameter 3 mm, defines the final size of the beam, see Fig. 12.2. The beam focus can be monitored thanks to two Faraday Cups located along the beam line. In addition the current can be read on the target directly. Before entering the scattering chamber the beam passes through a copper tube which is in thermal contact with LN_2. This is used as suppression for the secondary electrons

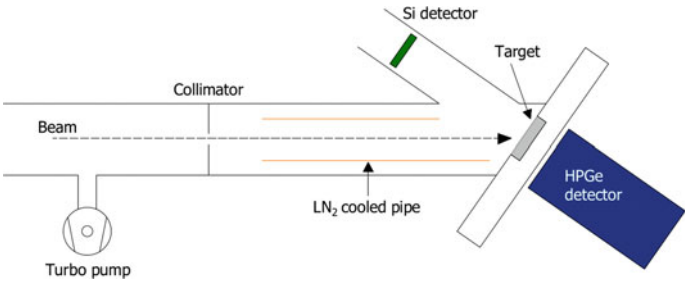

Fig. 12.2 The scattering chamber used for the present study

produced by the beam impinging on the target. In addition the cold finger prevents the carbon build up on the target surface. The target was mounted at the end of the scattering chamber at 55° with respect to the beam direction (w.r.t) on a customized CF flange. As a matter of fact a water cooling system was installed on the target holder in order to keep the target cold during the irradiation preventing the target degradation.

The γ-rays produced by the $^{6}Li(p,\gamma)^{7}Be$ reaction were detected by a coaxial High Purity Germanium (HPGe), which was positioned in close geometry and parallel to the target surface, thus at 55° w.r.t. the beam direction in order to minimize effects due to the angular distribution. The efficiency was measured at low energies using three different standard sources, ^{137}Cs, ^{60}Co and ^{88}Y. At high energies the efficiency was fixed exploiting the $E_p = 278$ keV resonance of the $^{14}N(p,\gamma)^{15}O$ reaction [8]. The efficiency was measured at different source to detector distances in order to analytically correct the experimental efficiency curve for the True Coincidence Summing (TCS), see Fig. 12.3. In addition the $^{6}Li(p,\gamma)^{7}Be$ reaction produces two primaries: γ_0 by the capture to the ground state and γ_1 by the capture to the first excited state $E_x = 429$ keV. The experimental data for γ_0 and γ_1 must be corrected for the TCS too.

In backward position, at 125° w.r.t. the beam direction, a Silicon detector was inserted in order to measure the $^{6}Li(p,\alpha)^{3}He$ reaction to perform a relative determination of the $^{6}Li(p,\gamma)^{7}Be$ S-factor. In order to reproduce the experimental conditions the efficiency of the Silicon detector was measured exploiting the $E_p = 151$ keV resonance of the $^{18}O(p,\alpha)^{15}N$ [9]. The discrepancy between the observed efficiency and the expected solid angle was explored by a Geant3 code. The measured efficiency was reproduced by simulating a circular beamspot with a diameter of 5 mm and moved of 3 mm from the center of the target, that seems to match the current case, see Fig. 12.4.

Five targets were irradiated with different composition and thickness in an energy range between 80 keV and 390 keV, see Table 12.1. The nominal enrichment in ^{6}Li is between 95% and 99% for all the targets. All the targets were evaporated on tantalum backings at ATOMKI Laboratories, Debrecen (Hungary). The target degradation was periodically checked at a reference energy. After the irradiation at LUNA the targets

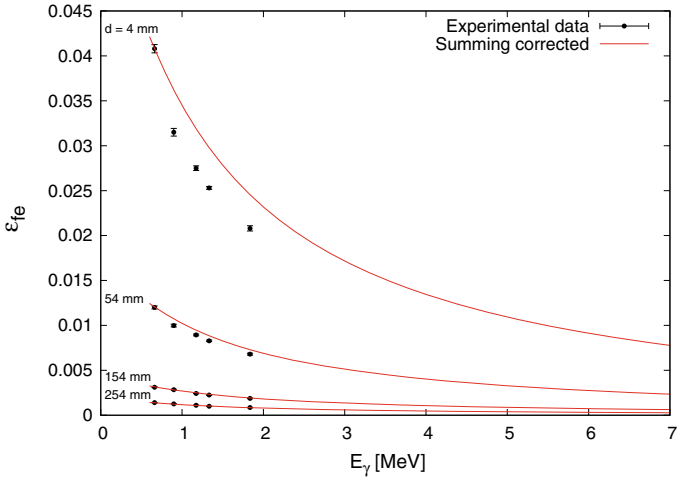

Fig. 12.3 In order to make the plot more clear only four distances were taken into account. In black the experimental (affected by the summing) efficiency data from the sources measurements. The solid lines are the corrected curves for the efficiency. The measurement of the ^{6}Li(p,γ)^{7}Be cross section was performed with the HPGe at the nominal distance of 4 mm

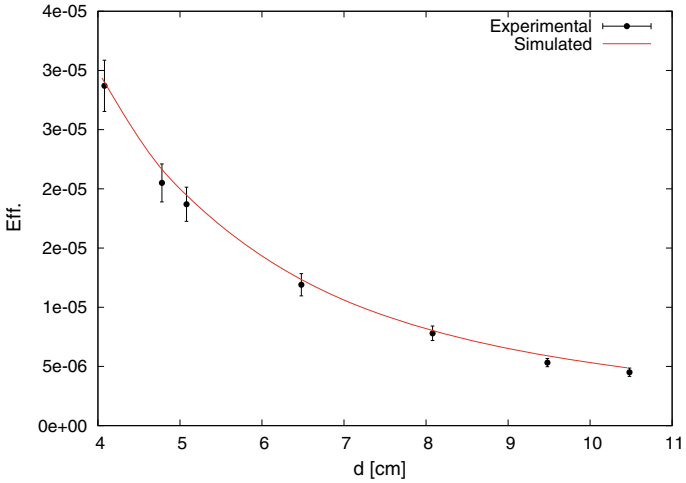

Fig. 12.4 Experimental efficiency for the Si detector compared with the simulated one with the Geant3 code

Table 12.1 Composition and thickness of the targets irradiated at LUNA

Target	Nominal thickness
Li_2O-7	40 $\mu g/cm^2$
Li_2O-9	20 $\mu g/cm^2$
Li_2WO_4-3	100 $\mu g/cm^2$
Li_2WO_4-1	130 $\mu g/cm^2$
LiCl	Infinite

were moved to the Helmholtz Zentrum Dresden Rossendorf (HZDR) laboratories in order to investigate the real thickness and composition via Nuclear Reaction Analysis and Elastic Recoil Analysis.

12.3 Preliminary Results and Conclusions

The analysis is actually ongoing for only one target, namely the Li_2WO_4-1. The areas for γ_0 and γ_1 were obtained and corrected for the TCS and the calculated branching ratio was compared with the literature values, a good agreement was found, Fig. 12.5.

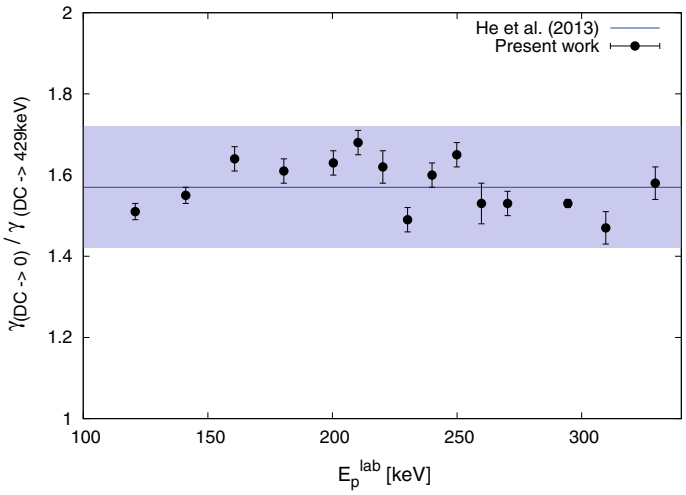

Fig. 12.5 Black points represent the experimental b.r. with only the statistical errorbars. The line is the value presented in [3] and the grey area is the uncertainty

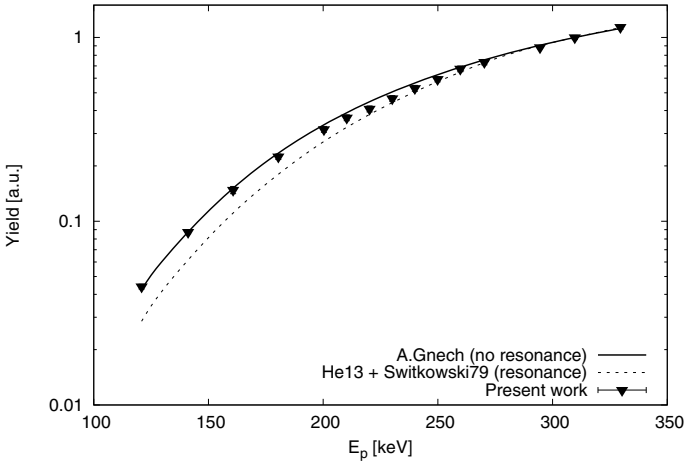

Fig. 12.6 The experimental yield, black dots, compared with the expected yield for the proton beam energies explored by the current study assuming S-factor reported in literature see Fig. 12.1

Then the total yield was compared with the expected values starting from the S-factor in literature, both with and without the resonance, see Fig. 12.6. The experimental yields at low energies are in disagreement with the expected values starting from the S-factor by He et al. [3].

References

1. D. Calyton, Handbook of Isotopes in the Cosmos: Hydrogen to Gallium, Cabridge Planetary Science (2003)
2. J. Cruz et al., Experimental study of proton-induced nuclear reactions in 6,7 Li. J. Phys. G **35**, 014004 (2008). http://stacks.iop.org/0954-3899/35/i=1/a=014004
3. J.J. He et al., A drop in the ^{6}Li(p, γ)^{7}Be reaction at low energies. Phys. Lett. B, **725**, 287–291 (2013). http://www.sciencedirect.com/science/article/pii/S0370269313006084
4. F.C. Barker, Neutron and proton capture by Li-6. Aust. J. Phys. **33**, 159–176 (1980)
5. Z.E. Switkowski et al., Cross section of the reaction ^{6}Li(p, γ)^{7}Be. Nucl. Phys. A **331**, 50–60 (1979). http://www.sciencedirect.com/science/article/pii/0375947479903002
6. C. Broggini et al., LUNA: status and prospects. Prog. Part. Nucl. Phys. **98**, 55–84 (2018)
7. A. Formicola et al., The LUNA II 400 kV accelerator. Nucl. Instrum. Methods Phys. Res. A **507**, 609–616 (2003)
8. M. Marta et al., The ^{14}N(p, γ)^{15}O reaction studied with a composite germanium detector. Phys. Rev. C **83**, 045804 (2011)
9. C. Bruno et al., Resonance strengths in the ^{17,18}O(p, α)^{14,15}N reactions and background suppression underground. Eur. Phys. J. A **51**, 94 (2005)

Chapter 13
A New Measurement of the ^{2}H(p,γ)^{3}He Cross Section in the BBN Energy Range at LUNA

Sandra Zavatarelli

Abstract Fusion reaction cross sections have an influence on the element formation in the earliest stages of the Universe and in all the stellar objects formed later on: a precise knowledge on nuclear physics input is fundamental since the abundances of the primordial elements are sensitive to the physics of the early universe and are therefore a tool to test the cosmological models. Presently the abundance of deuterium deduced from observation of Damped Lyman Alpha (DLA) absorption systems at high redshift is more accurate with respect to the predictions, mainly because the Big Bang Nucleosynthesis (BBN) calculation is affected by the paucity of data for the deuterium burning reaction $^2H(p,\gamma)^3He$ cross section at the relevant energies. Deep underground in the Gran Sasso Laboratory, Italy, the LUNA collaboration is pursuing a dedicated effort to measure the $^2H(p,\gamma)^3He$ cross section directly at BBN energies (30–300 keV). The campaign is divided into two phases based on a BGO and a high-purity germanium (HPGe) detector, respectively. The LUNA measurement is here described and the impact on cosmology and particle physics highlighted.

13.1 The Primordial Nucleosynthesis and the D/H Abundance Predictions

The Big-Bang Nucleosynthesis (BBN) models describe the production of the lightest nuclides via a dynamic interplay among the four fundamental forces during the first minutes of cosmic time, as the result of the competition between the rapidly expanding universe and the reaction rate of relevant nuclear processes [1–3]. In the standard BBN the only free parameter is the baryon density, usually normalised to the black-body photon density $\eta = n_B/n_\gamma$. Both densities change with time and temperature but their ratio remains constant from the end of BBN to the present.

Sandra Zavatarelli on behalf of the LUNA collaboration.

S. Zavatarelli (✉)
Istituto Nazionale di Fisica Nucleare - Sezione di Genova,
via Dodecaneso 33, 16146 Genoa, Italy
e-mail: zavatare@ge.infn.it

A. Formicola et al. (eds.), *Nuclei in the Cosmos XV*, Springer
Proceedings in Physics 219, https://doi.org/10.1007/978-3-030-13876-9_13

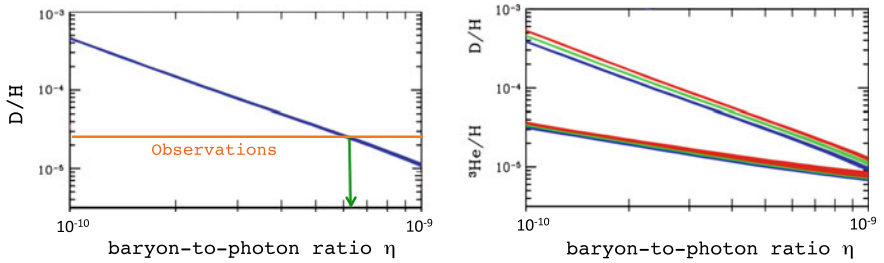

Fig. 13.1 *Left* – The BBN prediction for the D/H ratio as a function of η (in blue color) is compared with observations (in orange) [1, 3]: the crossing of the two curves settles η; *Right* – The D/H and ^{3}He/H ratio for different N_{eff} values [1] (blue = 2, green = 3, red = 4)

Because standard BBN is a one-parameter theory, the comparison between any abundance measurement with the BBN calculation determines η the baryon-to-photon ratio, or equivalently the present baryon density $\Omega_{b,0}$, through the relation: $10^{10}\eta = (273.78 \pm 0.18)\Omega_{b,0}h^2$ (Fig. 13.1, *left*) [4]. Additional measurements over-constrain the theory by providing a consistency check [5].

New observations and analysis of quasar absorption systems have dramatically improved the determination of D/H: a notable precision of 1.2% has been achieved, $10^5(D/H)_P = (2.527 \pm 0.030)$ [3].

Unluckily, the predictions for this quantity are more uncertain since they are influenced by a network of nuclear reactions [2]: according to BBN, as a consequence of temperature decrease of the Universe, the equilibrium between deuteron production through p(n, γ)^{2}H and its photo-dissociation was broken and the deuterium nuclei just created were destroyed through the ^{2}H(^{2}H,p)^{3}H, the ^{2}H(^{2}H,n)^{3}He and the ^{2}H(p,γ)^{3}He reactions. The overall primordial deuterium abundance is thus determined by the values of all these cross sections, experimentally studied in nuclear laboratories since the middle of last century. While the ^{2}H(^{2}H,p)^{3}H and the ^{2}H(^{2}H,n)^{3}He are known with a precision of 1%, the ^{2}H(p,γ)^{3}He reaction represents the main source of error for calculations because is quite uncertain: only one data set exists at the BBN energies [6], with a large error (9%). New theoretical models for this fusion reaction [7], based on an ab-initio approach, predict significantly higher values for the cross section, at the level of 20%.

If the theoretical values, provided with no error, are adopted in the BBN codes, the comparison with observational D/H abundance constrains the baryon density to $100\Omega_{b,0}h^2(BBN) = (2.166 \pm 0.015 \pm 0.011)$ [3].

On the other side, the baryon density has been independently fixed by a series of precise measurements of microwave background anisotropies, most recently by Planck, yielding to $100\Omega_{b,0}h^2(CMB) = (2.226 \pm 0.023)$ [3]. The two determinations are broadly consistent but their difference corresponds to a $\sim$1.5 σ discrepancy. If conversely, the measured value of ^{2}H(p,γ)^{3}He cross section is used as input in the BBN calculations instead of the theoretical one, the discrepancy is removed [3]. In conclusion a new measurement with a few % accuracy is very important to

reduce the BBN uncertainty on deuterium abundance to the same level of observations and to eventually constrain possible new physics effects: the D/H ratio is, in fact, very sensitive to number of relativistic degrees of freedom N_{eff} (see Fig. 13.1, *right*) and can contribute to settle tight bounds on the number of equivalent neutrino flavours [1, 8].

13.2 The LUNA Study of the ^{2}H(p,γ)^{3}He Reaction

Deep underground in the Gran Sasso laboratory, the 50 kV and later on, the 400 kV LUNA (Laboratory for Underground Nuclear Astrophysics) accelerators, have demonstrated to be suited to extend toward stellar energies the study of the proton-capture reactions [9].

The LUNA collaboration already measured the ^{2}H(p,γ)^{3}He reaction in the solar Gamow peak region (2.5 keV < E < 22 keV) [10]. Unfortunately all the old experimental points are far below the BBN energies, thus justifying a renewed experimental effort. At the energies of interest the ^{2}H(p,γ)^{3}He reaction proceeds through a not resonant mechanism directly to the ground state of ^{3}He. The incoming proton can be captured both in a *s*-wave or *p*-wave orbital angular momentum state and the emitted gamma-ray shows a not isotropic angular distribution dominated by the M1 and E1 components. Since the Q-value of the reaction is quite large (Q = 5.493 MeV) the gamma-ray energy is above the natural radioactivity endpoint, a feature that fully exploits the cosmic ray suppression at LNGS. The experimental set-up consists of a 400 kV electrostatic accelerator providing intense current of protons up to 500 μA: the beam power is measured through a constant temperature gradient calorimeter. In order to achieve the needed high precision the measurements have been repeated by exploiting two different experimental approaches.

In the former, a windowless deuterium gas target, 10 cm long at 0.3 mbar of pressure was inserted into the center of a 28 cm long, 7 cm thick BGO detector, divided into six sectors, each covering an azimuthal angle of 60° [11]. The almost 4π geometry together with the high detection efficiency for 5.5 MeV-γ's (62%) reduces the dependence of the counting rate on the angular distribution of the emitted γ rays and makes this setup particularly suitable to the lowest beam energies (E_{cm} = 30–200 keV). The latter phase was based on a 137% HpGe detector, placed at ∼4 cm distance from the beam axis and coupled to a a windowless deuterium gas target, 33 cm long. Thanks to high energy resolution of the HpGe (10 keV at 6 MeV) this configuration is less sensible to beam induced backgrounds at the higher energies (E_{cm} > 140 keV). The explored energy window (E_{cm} = 70–270 keV) was chosen to have a sizeable overlap with the BGO-based measurements. As an interesting feature, this setup offers also the possibility to measure the angular distribution of the emitted gammas because of the Doppler effect:

$$E_\gamma = \frac{m_p^2 + m_d^2 - m_{He}^2 + 2E_p m_d}{2(E_p + m_d - p_p cos(\theta_{lab}))}. \tag{13.1}$$

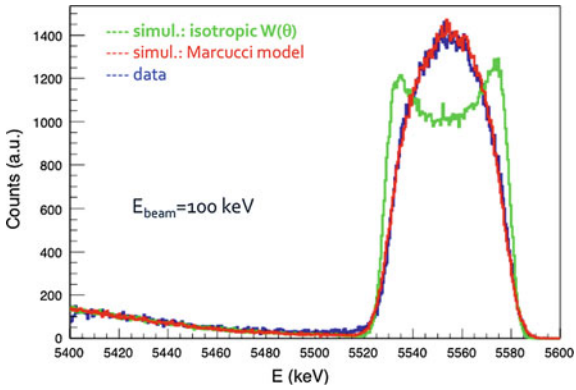

Fig. 13.2 The measured shape of the full γ absorption peak (in blue color) is compared with expectations from the theoretical ab-initio models [7] (red) and by an isotropical γ emission (green)

where m_p, m_d and m_{He} are respectively, the proton, deuteron and ^{3}He mass, E_p and p_p are the beam energy and momentum and θ_{lab} is the γ emission angle.

From the measured energy shape of the full absorption peak, the γ angular distribution can be deduced and the predictions nuclear physics models validated (see Fig. 13.2).

In both approaches, several checks have been performed to exclude possible systematical effects: detailed informations are reported in [12, 13]. The analysis of the acquired data is still on-going: in general, a smooth cross section variation with the energy has been observed, with values on average higher respect to the literature data.

In conclusion, thanks to the low cosmic background of LNGS and the expertise of the LUNA collaboration, a complete and high precision set of data points has now been acquired, covering the complete BBN energy range and offering the possibility to fully exploit the D/H primordial abundance as a probe of ΛCDM.

References

1. R.H. Cyburt et al., Rev. Mod. Phys. **88**, 015004 (2016)
2. O. Pisanti et al., Comput. Phys. Commun. **178**, 956 (2008)
3. R.J. Cooke, M. Pettini, C.C. Steidel, Astrophys. J. **855**, 102 (2018)
4. G. Steigman, JCAP **10**, 016 (2006)
5. C. Gustavino et al., Eur. Phys. J. A **52**, 74 (2016)
6. L. Ma et al., Phys. Rev. C **55**, 558 (1997)
7. L.E. Marcucci et al., Phys. Rev. Lett. **116**, 102501 (2016)
8. E. Di Valentino et al., Phys. Rev. D **90**, 023543 (2014)
9. F. Cavanna, P. Prati, Int. J. Mod. Phys. A **33**, 1843010 (2018)
10. C. Casella et al., Nucl. Phys. A **706**, 203–216 (2002)
11. F. Ferraro et al., Eur. Phys. J. A **54**, 44 (2018)
12. V. Mossa, in *Contribution to the NIC 2018 Conference Proceedings*
13. K. Stoeckel, in *Contribution to the NIC 2018 Conference Proceedings*

Part III
Galactic Chemical Evolution

Chapter 14
Galactic Chemical Evolution with Rotating Massive Star Yields

Nikos Prantzos

Abstract I present results from a recent work studying galactic chemical evolution with yields from rotating massive stars; they include, for the first time, the combined effect of metallicity, mass loss and rotation for a large grid of stellar masses and for all stages of stellar evolution. The yields of massive stars are weighted by a metallicity dependent function of the rotational velocities, constrained by observations.

14.1 Impact of Rotation on Massive Star Yields

Rotation affects the yields of massive stars both directly and indirectly.

- Directly because (a) the mixing induced by the combined effects of meridional circulation and secular shear brings in contact nuclear species that otherwise would remain well separated (this concerns mainly the H and He layers: species produced in one of the layers may move onto the other and serve as fuel or just be saved from destruction); and (b) the size of the various convective regions (core and shells) are modified, changing therefore the physical evolution of the star.
- Indirectly because the inclusion of rotation alters significantly the surface properties of most of the stellar models, especially at subsolar metallicities, pushing them towards conditions where they lose an enormous amount of mass that would not be lost in absence of rotation.

Several of the - potentially important - effects of rotating massive stars on GCE are summarized in [1]:

(i) production of large amounts of N at low metallicity, from *both* rotating AGB and massive stars, explaining the observed primary behaviour of N in the Galactic halo;
(ii) production of quasi-primary ^{13}C at very low metallicities by massive stars, helping to understand the low $^{12}C/^{13}C$ ratio observed in halo stars;

N. Prantzos (✉)
Institut d'Astrophysique de Paris, Sorbonne Université, Paris, France
e-mail: prantzos@iap.fr

A. Formicola et al. (eds.), *Nuclei in the Cosmos XV*, Springer
Proceedings in Physics 219, https://doi.org/10.1007/978-3-030-13876-9_14

(iii) production of Galactic Cosmic Rays (GCR) mainly from the accelerated winds of massive stars, explaining the observed GCR excess of ^{22}Ne and helping to understand the observed primary behavior of spallogenic Be; and
(iv) production of substantial amounts of "light s-nuclei" - resulting from the weak s-process in massive stars - which may help to understand the large dispersion of the "light/heavy" s-element ratio in halo stars.

Previous studies of the s-element evolution in the Milky Way were based on grids of yields poorly sampled in stellar masses and metallicities, obtained by post-processing nucleosynthesis calculations and/or just including either one of the possible stellar s-element sources (LIM stars or MS), and adopting an *ad hoc* contribution from the other source. Full (coupled) stellar evolutionary models and nucleosynthesis post-process calculations in LIM stars have shown the extreme sensitivity on the initial stellar metallicity of the s-process, namely to the ratio of the seed-nuclei (mainly Fe) to free neutrons. Detailed calculations in massive stars also show this trend with metallicity, with an additional important contribution from rotationally induced mixing (Fig. 14.1).

14.2 The Model

The novelty of the adopted model in [2] is threefold: the use of a complete set of isotopes from H to U, the use of a new grid of stellar yields over the whole stellar mass range and the use of a weighted average of those yields through an empirically calibrated, metallicity-dependent function of rotation velocities.

The adopted grid of LIM stars (from the FRUITY database [3]) and of massive stars (from [4]) covers a large range of masses and metallicities and, for massive stars, different initial rotational velocities: 0, 150 and 300 kms^{-1}. On the basis of recent ideas on massive star explosions, it is assumed that stars with M $>$ 25 M$_\odot$ contribute only through the stellar wind, for all values of initial metallicity and rotational velocity.

Due to our current ignorance on the dependence of the stellar rotation with metallicity, the adopted yields of rotating massive stars are weighted with a metallicity dependent function. This function is empirically determined, as to obtain both the observed primary behavior of nitrogen versus [Fe/H] (requiring a large average rotational velocity at low metallicities) and to avoid overproduction of s-elements around [Fe/H]~ -1 (requiring lower rotational velocities for disk stars).

Since most heavy elements have a mixed origin (s- and r-), fiduciary yields are adopted for the isotopes of r-process origin; namely, it is assumed that they are produced in CCSNe, their yield being solar-scaled to that of ^{16}O. This permits the study of the behavior of the other isotopes (of mixed origin), as well as the behavior of the elements (Fig. 14.2).

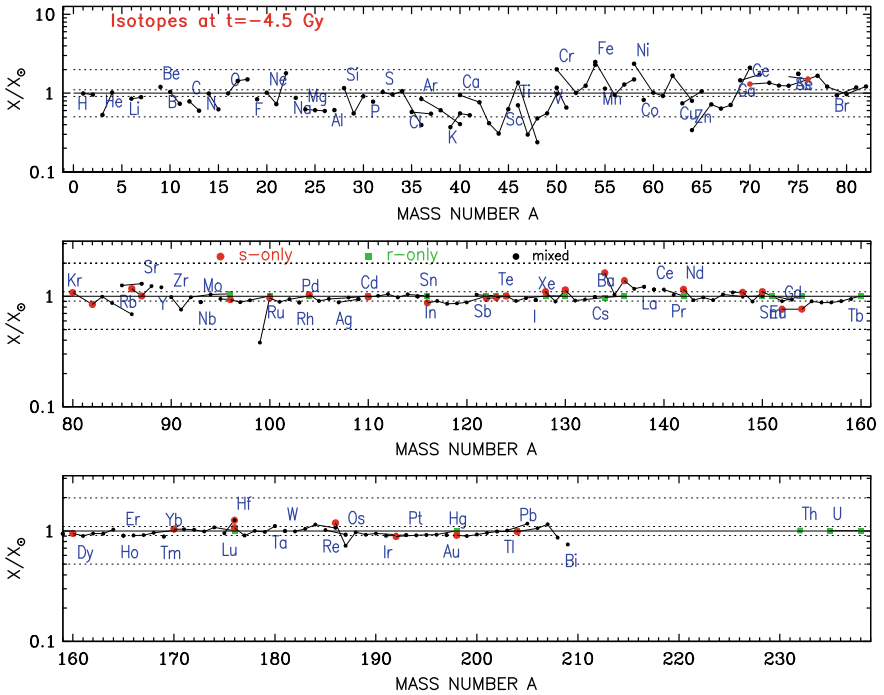

Fig. 14.1 Distribution of isotopic abundances (plotted as $X/X_{\odot}$) obtained at the time of the formation of the solar system and compared to solar system data. Yields for isotopes lighter than the Fe-peak and those on the s-process path are from stellar nucleosynthesis models. r- isotopes are assumed to originate in massive stars and their yields are fiduciary. Dotted horizontal lines bound the regions where over/underproduction factors of 2 and of 10%, respectively, are obtained. Red dots denote s-only nuclei, green squares r-only nuclei and black dots those of mixed origin. p-isotopes do not appear on the figure. Element symbols appear close to the lightest isotope of a given element

14.3 Discussion

We find that the resulting elemental and isotopic composition at the epoch of solar system formation compare remarkably well to the observed proto-solar one. Among the main findings we note:

– The abundances of all major isotopes of the multi-isotopic elements up to Fe (^{12}C, ^{14}N, ^{16}O, ^{20}Ne, ^{28}Si, ^{32}S, ^{36}Ar, ^{40}Ca, ^{54}Cr, ^{56}Fe) are well reproduced, in most cases to better than 10%.
– Proto-solar fluorine abundance is well reproduced (at the 85% level), with no need for ν-induced nucleosynthesis. About 2/3 of the proto-solar F abundance comes from rotating massive stars, the remaining 1/3 resulting from LIM stars. The isotope ^{15}N is produced along the same nucleosynthesis path that leads to ^{19}F and is also well reproduced, with no need for either nova or ν-induced nucleosynthesis.

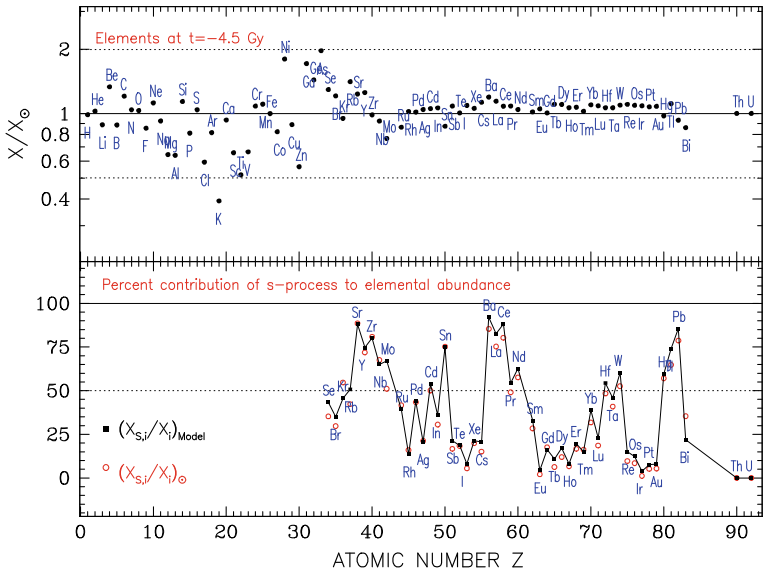

Fig. 14.2 *Top*: Model distribution of elemental abundances obtained at the time of the formation of the solar system compared to the observed solar system data. Dotted horizontal lines indicate a factor of two with respect to the solar system value. *Bottom*: Percentage contribution of the s-process to the elemental abundances at solar system formation. Model results are in black squares and measured solar system data in red open circles. The dotted horizontal line at 50% defines elements produced mostly by the s- or the r- processes (above or below it), respectively

– Rotating massive stars are found to have an important impact on the production of light s-elements (A < 90), through the increased production of the neutron source ^{22}Ne. In our model, the proto-solar abundances of s-only isotopes with A < 90 are accounted by rotating massive stars at the 50–85% level. In contrast, only a few % of the s-only isotopes with A > 90 is made in such stars. This allows us to obtain an abundance distribution for the s-only isotopes remarkably flat (to better than 10% for most of them) in the entire mass range 70 < A < 204.

We also compare our GCE predictions with a large body of observational data obtained from a number of recent large spectroscopic surveys and concerning [X/Fe] versus [Fe/H] in halo and disk stars. The main conclusions concern

– The evolution of N and F who are mostly affected by the rotational massive stars yields, their behavior turning from a secondary (without rotation) to a primary one (with rotation). Rotation has already been suggested as the explanation for primary N, but it is the first time that this effect is obtained with the use of a metallicity-dependent distribution of rotational velocities and not on the basis of a single velocity. Determinations of [F/Fe] and and [F/O] ratios in metal-poor unevolved stars are urgently needed to check our finding.

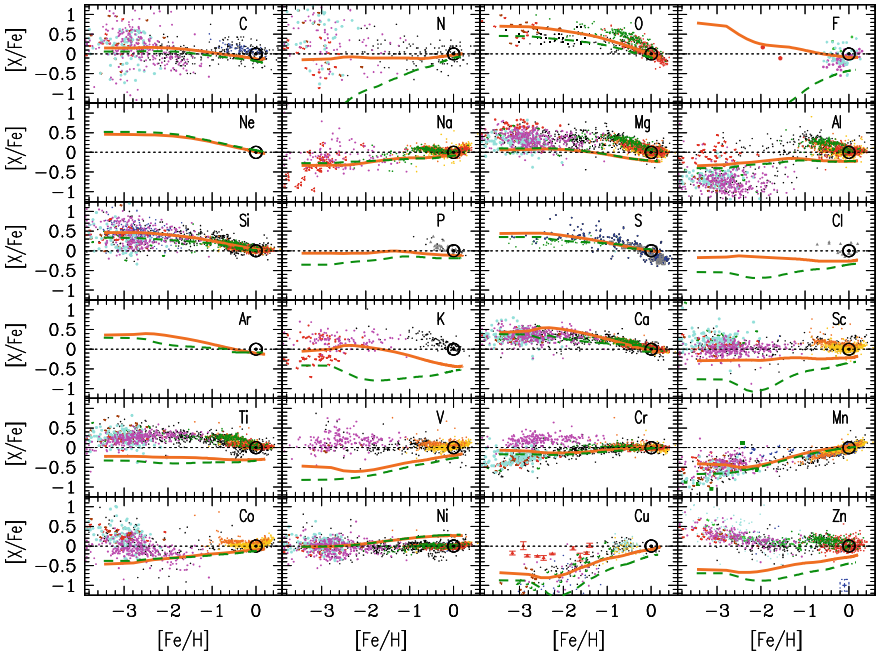

Fig. 14.3 Evolution of abundance ratios [X/Fe] as a function of [Fe/H] for elements up to the Fe-peak and comparison to observational data. Our baseline model with rotating massive star yields is in solid orange curves; the same model but with non-rotating massive star yields is in dashed green curves

– The evolution of the s-elements, in particular the lightest ones (Sr, Y, Zr) at low metallicity ([Fe/H] < -0.5). The predicted trends are in better agreement with the average observed ones although we find some deficiency for Zr and Mo. For the heavy s-elements (Ba, La etc.) the impact is lower, but still significant.

14.4 Summary

In summary, we have revisited the chemical evolution of the halo and the local disk with a consistent GCE model and metallicity-dependent yields from rotating massive stars, as well as LIM stars and SNIa. For the first time, we found that some metallicity-dependent distribution of the initial rotational velocities of massive stars has to be assumed, and we adopted such a distribution on the basis of observed abundances of key elements (nitrogen and s-elements). Under this assumption, we found that the adopted yields can help to improve our understanding of a large number of observations, particularly regarding the isotopic and elemental abundances of s-elements at the epoch of solar system formation as well as during Galactic evolution.

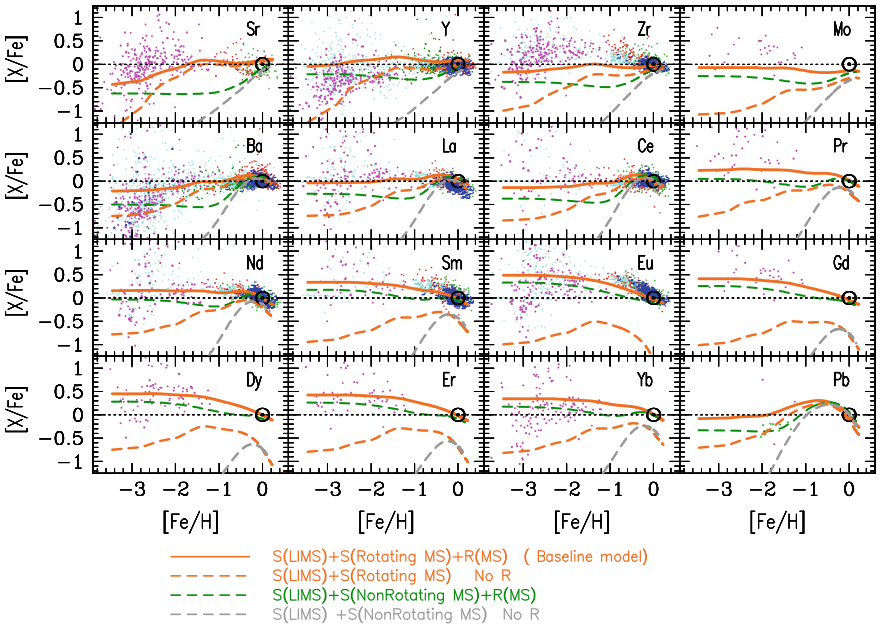

Fig. 14.4 Same as in Fig. 14.3, but for elements heavier than the Fe-peak. Two models have been added, both without the r-component, one for the rotating massive stars (*orange dashed*) and one for the non-rotating massive stars (*gray dashed*)

For some lighter elements, the inclusion of rotation in massive stellar models turns them into primaries (N, F) or improves the situation (Sc), but for others (Mg, K, V and Ti at all metallicities, and some Fe-peak elements at very low metallicities) the situation does not improve and important discrepancies with the observations remain. Finally, we find that rotating massive star yields may help to explain only partially the large dispersion observed in [X/Fe] at low metallicities for most of the heavy elements. A full explanation probably requires both inhomogeneous chemical evolution of the early ISM and formation of the early Galaxy through hierarchical merging of sub-haloes with different evolutionary histories (Fig. 14.4).

References

1. A. Maeder, G. Meynet, C. Chiappini, The first stars: CEMP-no stars and signatures of spinstars. Astron. Astrophys. **576**, id. A56, 17 (2018)
2. N. Prantzos, C. Abia, M. Limongi, A. Chieffi, S. Cristallo, Chemical evolution with rotating massive star yields—I. The solar neighbourhood and the s-process elements. Mon. Not. R. Astron. Soc. **476**, 3432–3459 (2018)

3. S. Cristallo, L. Piersanti, O. Straniero, The FRUITY database on AGB stars: past, present and future. J. Phys. Conf. Ser. **665**, article id. 012019 (2016)
4. M. Limongi, A. Chieffi, Presupernova Evolution and Explosive Nucleosynthesis of Rotating Massive Stars in the Metallicity Range $-3 \leq$ [Fe/H] ≤ 0. Astrophys. J. Suppl. Ser. **237**, article id. 13, 33 (2018)

Chapter 15
Inhomogeneous Chemical Evolution of r-Process Elements in the Galactic Halo

Benjamin Wehmeyer, Carla Fröhlich, Marco Pignatari and Friedrich-Karl Thielemann

Abstract The origin of the heaviest elements is still a matter of debate. For the rapid neutron capture process ("*r*-process"), multiple sites have been proposed, e.g., neutron star mergers and (sub-classes) of supernovae (e.g., [1–4]). *R*-process elements have been measured in a large fraction of metal-poor stars [5]. Galactic archeology studies show that the r-process abundances among these stars vary by over two orders of magnitude. On the other hand, abundances in stars in the galactic disk do not differ greatly. This leads to two major open questions: (1) What is the reason for such a huge abundance scatter of *r*-process elements in the early galaxy? (2) While the large scatter at low metallicities might point to a rare production site, why is there barely any scatter at solar-like metallicities? We use the high resolution $((20\,\mathrm{pc})^3$/cell) inhomogeneous chemical evolution tool "ICE" to study the role of the contributing source(s) of *r*-process elements. Our main findings are that in addition to neutron star mergers, a second, early acting site is necessary. We assume "magnetorotationally driven supernovae" as this additional and earlier r-process site and conclude that our simulations with an adequate combination of these two sites successfully reproduce

B. Wehmeyer (✉) · C. Fröhlich
North Carolina State University, Raleigh, NC 27695-8202, USA
e-mail: bwehmey@ncsu.edu

M. Pignatari
Department of Physics and Mathematics, E.A. Milne Centre for Astrophysics, University of Hull, Hull HU6 7RX, UK

NuGrid Collaboration, Hull, UK
URL: http://nugridstars.org

Konkoly Observatory, Research Centre for Astronomy and Earth Sciences, Hungarian Academy of Sciences, Konkoly Thege Miklos ut 15-17, Budapest 1121, Hungary

F.-K. Thielemann
Department of Physics, University of Basel, Klingelbergstr. 82, 4056 Basel, Switzerland

GSI Helmholtzzentrum für Schwerionenforschung, Planckstraße 1, Darmstadt 6422491, Germany

B. Wehmeyer · C. Fröhlich · M. Pignatari
Joint Institute for Nuclear Astrophysics - Center for the Evolution of the Elements, East Lansing, USA

A. Formicola et al. (eds.), *Nuclei in the Cosmos XV*, Springer
Proceedings in Physics 219, https://doi.org/10.1007/978-3-030-13876-9_15

the observed r-process elemental abundances in the Galactic halo. Finally, we discuss the potential role of neutron star-black hole mergers as alternative earlier r-process site.

15.1 Introduction

The cosmic life cycle depends on many ingredients, including the different stellar production sites, their variations as a function of metallicity, and their occurrence frequency during galactic chemical evolution. Gas clouds may form stars which experience different evolutionary stages according to their individual properties (like mass and metallicity, e.g., [6, 7]). The end of their life time is either characterized by strong stellar winds that eject most of the outer envelopes of the star and leaving behind a white dwarf (for lower mass stars), or in violent events like supernovae or hypernovae/gamma-ray bursts, leaving behind either a neutron star or a black hole ([8], and references therein). Eventually, such compact objects might merge, leading to neutron star mergers, neutron star - black hole mergers or black hole mergers.

The ejected yields of heavy r-process elements and the relative contributions of the proposed stellar sites like supernovae and neutron star mergers are still matter of debate (e.g., [1, 2, 9]).

We use the inhomogeneous Galactic chemical evolution tool "ICE" [3, 10, 11] to examine the influence of some of the main parameters of the cosmic life cycle. With ICE's high resolution ((20 pc)^3/cell) models, we study the impact of abundances in supernova remnants on newly born stars. This approach explains the inhomogeneities in the early Galactic evolution stages as a fundamental reason of the observed scatter of r-process elements in low metallicity stars [5].

15.2 GCE Model

We set up a simulation cube with an edge length of of 2 kpc. The resolution of the simulation is (20 pc)^3. In each time step of 10^6 years, the following calculations are performed (cf. [3, 10, 11] for details):

1. The star formation rate is calculated using Schmidt's law (power 1.5) [12].
2. The stars are distributed into the simulation cells, higher mass cells are favored.
3. The mass of a newly born star is chosen randomly, consistently with a Salpeter IMF (with an integrated slope of -1.35).
4. The newly born star inherits the chemical properties of the ISM out of which it is formed.
5. Considering its mass and metallicity, the life time of a star is calculated following the Geneva Stellar Evolution and Nucleosynthesis Group prescriptions [13].

6. When stars have reached the end of their life time, the following occurs:
   - Low and intermediate mass stars will return their mass via stellar winds leaving white dwarfs behind.
   - Massive stars explode as core collapse supernovae, leaving neutron stars behind.

   For both cases, the surrounding ISM is moved (by a Sedov blast wave with an energy deposition of 10^{51} erg), until 5×10^4 solar masses of ISM are swept-up.
7. A fraction (P_{SNIa}) of double IMS systems will undergo a supernova of type Ia once both stars have become a white dwarf.
8. A fraction (P_{NSM}) of double HMS systems will undergo a neutron star merger (NSM) event after the two stars have undergone their individual supernova events and the two remaining neutron stars have spiraled in for a delay ("coalescence") time.
9. Stars in the surrounding ISM (in the affected cells) inherit the exploding star's abundances plus the event specific yield.

15.3 Observations

We use europium (Eu) as r-process nucleosynthesis diagnostic element. The largest fraction of Eu in the Universe is made by the r-process (e.g., [14]). The abundance of Eu is also easier to measure in the spectra of stars compared to other r-process elements like Pt or Ir [15]. Observations used in the figures to compare with our simulations are taken from the SAGA database (e.g., [16], http://saga.sci.hokudai.ac.jp) where the full list of references can be found.

15.4 Results and Discussion

When neutron star mergers are the exclusive site of r-process nucleosynthesis, it is not possible to explain the observed galactic abundances. Compared to observations in the early galaxy, their contribution to the abundances of r-process elements sets in at too high metallicities (assuming standard merger probabilities), or their too frequent occurrence leads to too high abundances at higher metallicities (close to solar, high merger probability case). The influence of the in-spiral time scale of the two neutron stars ("coalescence time") only marginally affects the abundance curve, see Fig. 15.1 for illustration. Other groups' approaches find that another way to achieve low-metallicity but highly r-process abundant stars is using a hierarchical sub-halo assembling scheme. These sub-halos might have experienced lower star formation efficiencies before merging, which might help to keep the iron inventory low during the r-process abundance increase [17, 18]. Yet, this approach might have difficulties to reproduce age-metallicity relations of *observed* sub-halo (dwarf) systems. Hence,

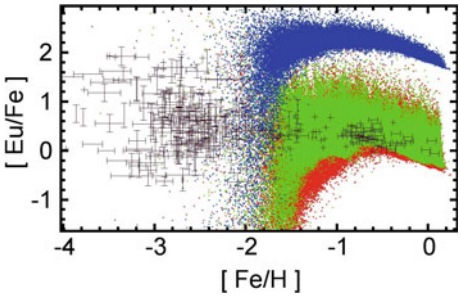

Fig. 15.1 Effect of probability and coalescence time scale of a simulation with NSM as only r-process nucleosynthesis site. Grey error bars indicate observations, whereas blue, green, and red dots represent model stars corresponding to environments with different probability or coalescence time scale for NSM events. Figure adopted from [3]

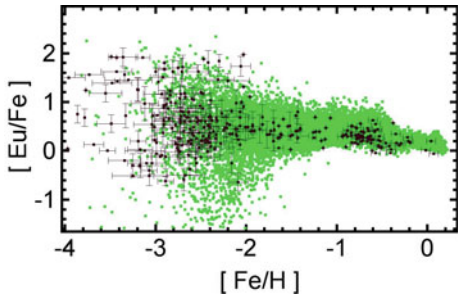

Fig. 15.2 Abundances of r-process elements in a model with both neutron star mergers and magneto-rotationally driven supernovae as r-process nucleosynthesis sites. Probability of MHD supernovae is one per 1000 regular core-collapse supernovae. Figure adopted from [3]

it remains unclear whether the approach can be applied to the bulk of these systems [18].

15.4.1 Jet-Supernovae

Recent nucleosynthesis calculations successfully reproduced an r-process in "magnetorotationally driven supernovae" (or "jet-supernovae"/"collapsars"/"magnetars", e.g., [19, 20]). If one in 1000 supernovae explodes as a Jet-SN (and acts as a second source of r-process elements), this contribution sets already in at lower metallicities. A combined environment with both mentioned nucleosynthesis sites reproduces the observed r-process element abundances. This is shown in Fig. 15.2.

15.4.2 Neutron Star—Black Hole Merger

Recent simulations of core-collapse supernovae (e.g., PUSH [21], or similar conclusions as in, e.g., [22]) suggest that some progenitors fail to explode after their core collapsed and bounced. In lieu of undergoing an explosion, these stars collapse to a black hole at the end of their life time. This implies, that no metals from the star are added back to the interstellar medium. Such an object might merge with a neutron star that was produced in a companion star's supernova, and eject r-process rich material [23, 24]. Since this event requires the presence of only one neutron star, only *one* successful supernova explosion is required before the merging of the two objects. This r-process nucleosynthesis event may occur in an environment more metal-poor compared to "classical" neutron star mergers. This neutron star - black hole merger scenario might be another additional scenario to explain the presence of highly r-process rich stars at low metallicities. We will use the results of the PUSH supernova simulation framework to find out how many stars undergo a failed SN channel, and use these results in our simulation suite to explore the r-process contribution from neutron star - black hole mergers.

Acknowledgements BW is supported by a mobility fellowship of the Swiss National Science Foundation (SNF). The work at NC State (BW, CF) was partially supported by the United States Department of Energy, Office of Science, Office of Nuclear Physics (award numbers SC0010263 and DE-FG02-02ER41216), and by the Research Corporation for Science Advancement under a Cottrell Scholar Award. BW and FKT were supported by the European Research Council (FP7) under ERC Advanced Grant Agreement No. 321263 - FISH, and the SNF. MP acknowledges the support from the SNF and the "Lendület-2014" Programme of the Hungarian Academy of Sciences (Hungary), of STFC through the University of Hull Consolidated Grant ST/R000840/1, and of ERC Consolidator Grant (Hungary) funding scheme (project RADIOSTAR, G.A. n. 724560). BW, CF, and MP acknowledge support of the National Science Foundation (USA) under grant No. PHY-1430152 (JINA Center for the Evolution of the Elements). This article is based upon work from the "ChETEC" COST Action (CA16117), supported by COST (European Cooperation in Science and Technology).

References

1. F. Matteucci, D. Romano, A. Arcones, O. Korobkin, S. Rosswog, MNRAS **438**, 2177 (2014)
2. S. Shen, R. Cooke, E. Ramirez-Ruiz, P. Madau, L. Mayer, J. Guedes, Astrophys. J. **807**, 115 (2015)
3. B. Wehmeyer, M. Pignatari, F.-K. Thielemann, MNRAS **452**, 1970 (2015)
4. F.-K. Thielemann, M. Eichler, I.V. Panov, B. Wehmeyer, ARNPS **67**, 253 (2017)
5. I. Roederer, J. Cowan, A. Karakas, K.-L. Kratz, M. Lugaro, J. Simmerer, K. Farouqi, C. Sneden, Astrophys. J. **724**, 975 (2010)
6. S.E. Woosley, A. Heger, T.A. Weaver, Rev. Mod. Phys. **74**, 1015 (2002)
7. A.I. Karakas, J.C. Lattanzio, PASA **31**, id.e030 62 (2014)
8. N. Langer, Annu. Rev. Astron. Astrophys. **50**, 107 (2012)
9. S. Shibagaki, T. Kajino, G.J. Mathews, S. Chiba, S. Nishimura, G. Lorusso, Astrophys. J. **816**, 79 (2016)
10. B. Wehmeyer, M. Pignatari, F.-K. Thielemann, AIPC **1743**, id.040009 (2016)

11. B. Wehmeyer, M. Pignatari, F.-K. Thielemann, JPSCP **14**, 020201 (2017)
12. M. Schmidt, Astrophys. J. **121**, 161 (1959)
13. G. Schaller, D. Schaerer, G. Meynet, A. Maeder, Astron. Astrophys. Suppl. Ser. **96**, 269 (1992)
14. S. Bisterzo, C. Travaglio, R. Gallino, M. Wiescher, F. Käppeler, Astrophys. J. **787**, id.10 (2014)
15. C. Sneden, J.J. Cowan, R. Gallino, Annu. Rev. Astron. Astrophys. **46**, 241 (2008)
16. T. Suda, Y. Katsuta, S. Yamada, T. Suwa, C. Ishizuka, Y. Komiya, K. Sorai, M. Aikawa, M.Y. Fujimoto, PASJ **60**, 1159 (2008)
17. Y. Ishimaru, S. Wanajo, N. Prantzos, Astrophys. J. Lett. **804**, L35 (2015)
18. T. Ojima, Y. Ishimaru, S. Wanajo, N. Prantzos, P. Francois, Arxiv: 1808.03390 (submitted)
19. C. Winteler, R. Käppeli, A. Perego, A. Arcones, N. Vasset, N. Nishimura, M. Liebendörfer, F.-K. Thielemann, Astrophys. J. **750**, L22 (2012)
20. N. Nishimura, T. Takiwaki, F.-K. Thielemann, Astrophys. J. **810**, 109N (2015)
21. K. Ebinger, S. Curtis, C. Frohlich, M. Hempel, A. Perego, M. Liebendörfer, F.-K. Thielemann, ApJ. **870**, 1 (2019)
22. T. Sukhbold, T. Ertl, S.E. Woosley, J.M. Brown, H.-T. Janka, Astrophys. J. **821**, 38 (2016)
23. N. Mennekens, D. Vanbeveren, Astron. Astrophys. **564**, A134 (2014)
24. K. Kiuchi, Y. Sekiguchi, K. Kyutoku, M. Shibata, K. Taniguchi, T. Wada, Phys. Rev. D **92**, id 064034 (2015)

Part IV
Massive Stars and CCSNe—Stellar Contribution: NS Mergers

Chapter 16
Nucleosynthesis in Core-Collapse Supernovae

Carla Fröhlich, Sanjana Curtis, Kevin Ebinger, Matthias Liebendörfer, Albino Perego and Friedrich-Karl Thielemann

Abstract Core-collapse supernovae (CCSNe) are one of the most important nucleosynthesis sites and they hold a key role in the evolution of galaxies. In the explosion, CCSNe eject freshly synthesized iron-group nuclei from explosive burning alongside of intermediate mass elements (from hydrostatic and explosive burning), and carbon and oxygen from the pre-explosion evolution. In the neutrino-driven wind, nuclei beyond the iron group can be synthesized under neutron-rich conditions (weak r-process) and proton-rich conditions (νp-process). The signature of CCSN nucleosynthesis can be observed in the atmospheres of the oldest stars. Here, we will compare the nucleosynthesis from different progenitor models exploded with the PUSH method in spherical symmetry.

16.1 Introduction

Core-collapse supernovae (CCSNe) mark the death of massive stars (more massive than about 10 $M_\odot$). For the chemical enrichment, CCSNe play an important role in synthesizing elements and ejecting these freshly synthesized elements into the interstellar medium. The CCSN problem is a complex multi-physics problem which also requires adequate pre-explosion properties of a massive star as initial conditions. Despite many advances in massive star evolution [1, 2, e.g.] and hydrodynamical modeling of CCSNe in 2D and 3D [3, 4, e.g.], the problem of the explosion mechanism is still not fully solved. This poses a challenge for nucleosyn-

C. Fröhlich (✉) · S. Curtis
Department of Physics, North Carolina State University, Raleigh, NC 27695, USA
e-mail: cfrohli@ncsu.edu

K. Ebinger · F.-K. Thielemann
GSI Helmholtzzentrum für Schwerionenforschung, 64291 Darmstadt, Germany

M. Liebendörfer · F.-K. Thielemann
Departement für Physik, Universität Basel, Basel 4056, Switzerland

A. Perego
Dipartimento di Scienze Matematiche Fisiche ed Informatiche,
Università di Parma, 43124 Parma, Italy

A. Formicola et al. (eds.), *Nuclei in the Cosmos XV*, Springer
Proceedings in Physics 219, https://doi.org/10.1007/978-3-030-13876-9_16

thesis predictions from CCSNe. For example, CCSN nucleosynthesis predictions for entire grids of models are only available from simple explosion prescriptions such as thermal/kinetic bomb or piston approaches [5, 6] which have well-known limitations especially regarding the electron fraction (Y_e) in the innermost ejecta (see e.g. [7] for a detailed discussion). At the same time, only very few nucleosynthesis predictions are available from multi-dimensional CCSN simulations [8–12]. Recently, various attempts have been made at mimicking the net effects of multi-dimensional simulations in effective 1D models [13–17]. Most of these works are aimed at investigating the progenitor-remnant connection. Nucleosynthesis yields were computed in [17] (however without including the effects of neutrino interactions on the Y_e in the nucleosynthesis) and in [18] (including neutrino interactions in the hydrodynamics and the nucleosynthesis calculations). Here, we will compare the nucleosynthesis results obtained with the PUSH method [18–20] for two different pre-explosion models.

16.2 Inputs and Method

We investigate the nucleosynthesis resulting from the explosion of two massive star, pre-explosion models suitable for SN 1987A: s18.8 (a non-rotating, solar-metallicity single-star evolution models from the WHW02 series [21]) and b15-7 (a LMC-metallicity model originating from the binary merger of a primary red supergiant and a secondary main-sequence star [22]). Both models have been exploded using the PUSH method as described in [18, 20]. For the hydrodynamic simulation of the collapse and explosion, we use the hydrodynamics code Agile [24] together with a nuclear equation of state [25] and spectral neutrino transport [26, 27]. The key features of PUSH in the context of nucleosythesis are that it enables a consistent treatment of (i) the location of the mass cut, (ii) the electron fraction, and (iii) the entropy of ejecta. In particular, charged-current reactions on free nucleons are taken into account consistently in the hydrodynamics and in the nucleosynthesis calculations. The detailed nucleosynthesis is calculated in a post-processing approach with a large nuclear reaction network [18].

To set the free parameters in the PUSH method ($k_{\rm push}$ and $t_{\rm rise}$, see [19]), we require that a pre-explosion model of suitable zero age main sequence (ZAMS) mass simultaneously reproduces the observationally derived values for explosion energy and isotopic yields from SN 1987A. Both models used here have a suitable ZAMS mass for SN 1987A (18.8 $M_\odot$ for s18.8 and 21.1 for b15-7). For a description of the calibration procedure, see [19]. For model s18.8 we use the calibration obtained in [20]. We repeated the calibration procedure for model b15-7, which was specifically developed as progenitor of SN 1987A [22], and found similar values for $k_{\rm push}$ and $t_{\rm rise}$ [23].

16.3 Results

Here, we focus on the overall nucleosynthesis results from the two SN 1987A models s18.8 and b15-7. For the detailed yields of model s18.8 see [18] and for the detailed yields of b15-7 see [23]. From the calibration procedure, both models reproduce the yields of ^{56,57,58}Ni from SN 1987A. In both cases, the ^{44}Ti yield is too low (it is well-known that spherically symmetric models have difficulties predicting Ti-yields consistent with observations [28]). In Fig. 16.1, the complete calculated abundances for both models are shown. Overall, the abundances from both models are very similar. The largest differences are found in the mass range $20 < A < 40$. These are predominantly nuclei that are synthesized during the hydrostatic evolution and are only ejected in the supernova explosion. The difference can easily be understood from the different evolutionary path of the two models: s18.8 is the evolution of a single 18 $M_\odot$ star at solar metallicity, while b15-7 is the result from a binary merger of a 15 $M_\odot$ red supergiant and a 7 $M_\odot$ main sequence star at LMC metallicity. Hence, the outer structure of these two models is quite different.

In Fig. 16.2, we show the resulting elemental iron-group yields for both models compared to the abundances of metal-poor star HD 84937. The yields are very comparable between the two models and also consistent with the observed abundances.

16.4 Discussion

We present nucleosynthesis results for two different pre-explosion models suitable to reproduce the observed properties of SN 1987A. While the pre-explosion models are quite different (s18.8 is a red supergiant, single star; b15-7 is blue supergiant from

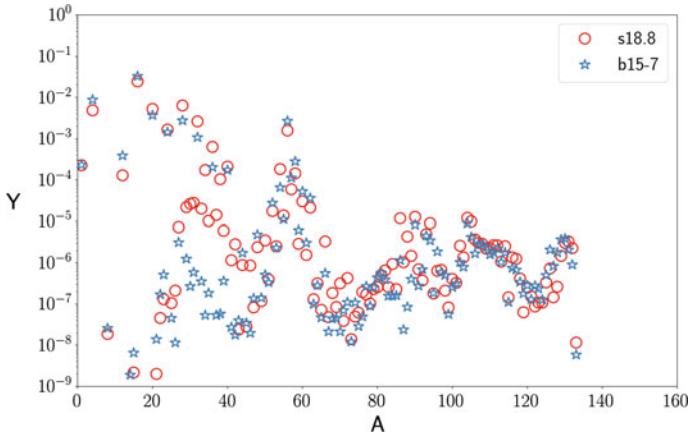

Fig. 16.1 Mass-integrated final abundances as function of the mass number A for models s18.8 (red circles) and b15-7 (blue stars)

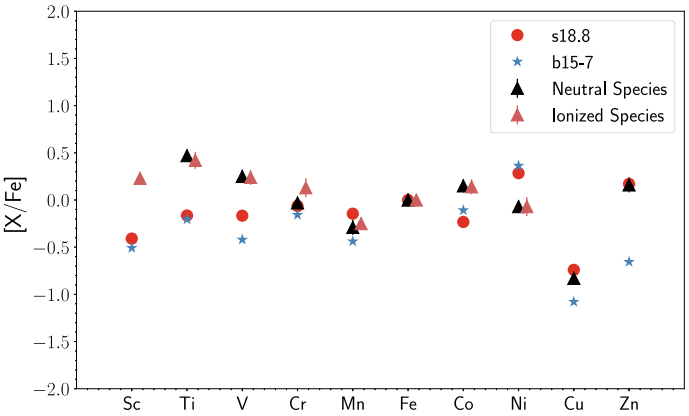

Fig. 16.2 Observed elemental iron-group abundances for HD 84937 (triangles) and our results for s18.8 (red circles) and b15-7 (blue stars)

a binary evolution), the overall nucleosynthesis yields are similar, in particular for the iron-group. The largest differences are found in the intermediate mass elements which have significant contributions from burning during the pre-explosion phase. A more in-depth analysis is the subject of Fröhlich [23].

Acknowledgements This work was supported by the US Department of Energy (award numbers SC0010263 and DE-FG02-02ER41216).

References

1. A. Chieffi, M. Limongi, Astrophys. J. **836**, 79 (2017)
2. R. Hirschi, D. Arnett et al., in *IAU Symposium* ed. by A. Marcowith, M. Renaud, G. Dubner, A. Ray, vol. 331 (2017)
3. H.-T. Janka, T. Melson, A. Summa, Ann. Rev. Nucl. Part. Sci. **66**, 341 (2016)
4. A. Burrows, D. Vartanyan et al., Space Sci. Rev. **214**, 33 (2018)
5. S.E. Woosley, T.A. Weaver, Astrophys. J. **101**, 181 (1995). https://doi.org/10.1086/192237
6. F.-K. Thielemann, K. Nomoto, M.A. Hashimoto, Astrophys. J. **460**, 408 (1996)
7. C. Fröhlich, P. Hauser et al., Astrophys. J. **637**, 415 (2006)
8. A. Harris, W.R. Hix et al., Astrophys. J. **843**, 2 (2017)
9. S. Wanajo, B. Müller et al., arXiv:1701.06786 (2017)
10. M. Eichler, K. Nakamura et al., arXiv:1708.08393 (2017)
11. T. Yoshida, Y. Suwa et al., Mon. Not. R. Astr. Soc. **471**, 4275 (2017)
12. A. Wongwathanarat, T. Janka et al., Astrophys. J. **842**, 13 (2017)
13. M. Ugliano, T. Janka et al., Astrophys. J. **757**, 69 (2012)
14. O. Pejcha, T. Thompson, Astrophys. J. **801**, 90 (2015)
15. B. Müller, A. Heger et al., Mon. Not. R. Astr. Soc. **460**, 742 (2016)
16. T. Ertl, T. Janka et al., Astrophys. J. **818**, 124 (2012)
17. T. Sukhbold, T. Ertl et al., Astrophys. J. **821**, 38 (2016)
18. S. Curtis, K. Ebinger et al., Astrophys. J. **870**, 2 (2019)

19. A. Perego, M. Hempel et al., Astrophys. J. **806**, 275 (2018)
20. K. Ebinger, S. Curtis et al., Astrophys. J. **870**, 1 (2019)
21. S.E. Woosley, A. Heger, T.A. Weaver, Rev. Mod. Phys. **74**, 1015 (2002)
22. A. Menon, A. Heger, Mon. Not. R. Astr. Soc. **469**, 4649 (2017)
23. Fröhlich, S. Curtis, K. Ebinger, et al., submitted to J. Phys. G
24. M. Liebendörfer et al., Phys. Rev. D **63**, 104003 (2001)
25. M. Hempel, J. Schaffner-Bielich, Nucl. Phys. A **837**, 210 (2010)
26. M. Liebendörfer, S.C. Whitehouse, T. Fischer, Astrophys. J. **698**, 1174 (2009)
27. A. Perego, R.M. Cabezón, R. Käppeli, Astrophys. J. Suppl. **223**, 22 (2016)
28. G. Magkotsios, F.X. Timmes, M. Wiescher, Astrophys. J. **741**, 78 (2011)

Chapter 17
Neutron Star Mergers as r-Process Sources

Stephan Rosswog

Abstract The astrophysical origin of the rapid neutron capture elements has been a puzzle since the 1950s. While evidence for a compact binary merger origin has been growing over the last two decades, the final confirmation only came from the recent multi-messenger observation of a merging neutron star binary. The slope of the bolometric electromagnetic luminosity strongly suggests the radioactive decay of freshly synthesized r-process nuclei as power source. The spectral evolution from blue to red indicates that a broad range of r-process nuclei has been produced. Both the ejecta mass and the event rate from this first event are at the upper end of the pre-detection expectations. These number suggest that neutron star mergers are the major r-process source in the cosmos, but additional sources cannot be excluded and may even be welcome from a chemical evolution perspective. With the large number of neutron star detections expected per year for LIGO/VIRGO's next science run one can be optimistic to soon get answers to questions that have plagued (nuclear) astrophysics for many years.

17.1 The Quest for the Astrophysical r-Process Site

Approximately half of the elements heavier than iron are formed via rapid neutron capture or "r-process". The distinguishing feature as compared to the slow neutron capture process is that captures are much faster than the competing $\beta-$decays. While the basic nuclear reaction mechanisms have been identified more than half a century ago [1, 2], the astrophysical production site/s has/have remained elusive until very recently. For this reason, the astrophysical origin of the r-process elements has been named as one of the "11 Science Questions for the new Century" [3].

S. Rosswog (✉)
Department of Astronomy, The Oskar Klein Centre,
Stockholm University, Stockholm, Sweden
e-mail: stephan.rosswog@astro.su.se
URL: http://compact-merger.astro.su.se

A. Formicola et al. (eds.), *Nuclei in the Cosmos XV*, Springer
Proceedings in Physics 219, https://doi.org/10.1007/978-3-030-13876-9_17

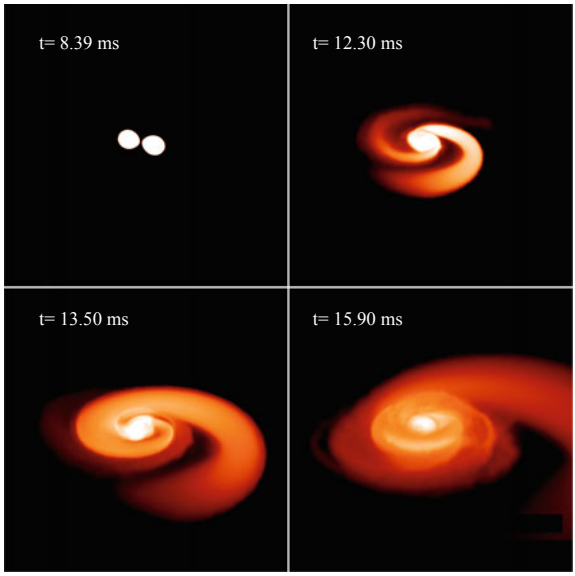

Fig. 17.1 Volume rendering of the merger of a 1.4 and a 1.5 $M_\odot$ neutron star

The traditionally favoured r-process production sites were core-collapse supernovae and in particular the neutrino-driven wind emerging after the birth of a proto-neutron star seemed like a viable nucleosynthesis environment [4–6]. As an alternative production site, Lattimer and Schramm [7, 8] suggested that neutron star matter ejected during a neutron star black hole encounter could have a high potential for heavy element nucleosynthesis and the chemical evolution of the cosmos. It remained, however, an open question whether a sufficient amount of matter could be ejected in such an event, the original estimates were "$\sim$0.05 $M_{ns} \pm 0.05$ M_{ns}" [7]. Binary neutron star mergers were also discussed as r-process sites and neutrino sources [9] and potential gamma-ray burst engines [9, 10]. The first hydrodynamics-plus-nucleosynthesis calculations [11–13] demonstrated that typical ejecta masses from a neutron star merger are, with some dependence on mass ratio, spin and equation of state, $\sim$0.01 $M_\odot$. A recent simulation of an unequal mass binary merger (1.4 and 1.5 $M_\odot$ is shown in Fig. 17.1. Folded with the estimated merger rates these numbers yield an amount of galactic r-process similar to the observed one. Most importantly, the simulations showed [12] that elements up to and beyond the 3rd r-process peak around $A = 195$ are a natural consequence of the enormous neutron richness. Nuclei in this regime had always been a serious challenge for neutrino-driven supernova winds and could only be obtained by a substantial (and unrealistic) tuning of the wind parameters.The first results [11] immediately triggered the question about observable manifestations of the radioactivity from the freshly produced r-process elements [14] (now called "macronovae" [15] or "kilonovae" [16]). These post-merger EM transients have become a subject of intense research over the last decade, see e.g. [16–25] for recent reviews.

17.2 Lessons from the First Binary Neutron Star Merger Detection

The first multi-messenger detection. The first direct detection of gravitational waves (GW) from a merging neutron star binary [26] and the subsequent detection all across the electromagnetic (EM) spectrum [27–32] brought a quantum leap in our understanding of compact object astrophysics. The advanced LIGO facilities observed the GW chirp signal for about 1 min. 1.74 s after the merger the Fermi satellite detected a burst of gamma rays [30] from the same location. This detection constrains the gravitational wave propagation speed with a fractional accuracy of $\sim 10^{-15}$ to the speed of light [33]. Moreover, the GW detection also demonstrated that it is possible to extract masses and to constrain the tidal deformability of a neutron star and therefore its equation of state. The burst was exceptionally close, but at the same time the observed emission was exceptionally weak. It was therefore initially debated whether the GRBs was a normal, but off-axis or a very peculiar burst [28]. By now there is now growing consensus that it would have appeared as a normal bright sGRB would it have been observed along the main emission axis [34–36].

Implications of the macronova emission. The observed post-merger macronova emission has provided conclusive evidence that neutron star mergers are at least *a* (likely even *the*) major source of cosmic r-process. In Fig. 17.2, left panel, we show the result of a numerical experiment where we expand a homogeneous cloud of matter with different velocities and electron fractions (black, green, blue and red lines), see [37] details. The nuclear heating rates $\dot{q}$ [erg/g s] depend only moderately on the velocity (here varied between 0.1 and 0.4 c), but substantially on the electron fraction. Trajectories with Y_e below or equal to 0.3 produce heating rates that agree well with the observed bolometric luminosity slope.[1] Such material produces substantial amounts of r-process (see Fig. 2 in [37] for the detailed abundance distributions). Matter with higher Y_e hardly produces r-process contributions and does not agree with the slope of the bolometric light curve (red lines). This provides robust evidence that really r-process elements have been synthesized. Note also, that we used a mass of $1.5 \times 10^{-2}\,\mathrm{M}_\odot$ to compare heating rates [erg/g s] with luminosities [erg/s]. This implies that –under the extreme assumption that 100% of the radioactive decay energy have been transformed into detected radiation– at the very least $1.5 \times 10^{-2}\,\mathrm{M}_\odot$ have been ejected during the merger, but more realistically a few times this number.

This heating rate experiment is, however, not conclusive concerning the question whether the 3rd r-process peak elements have been produced or not: matter with $Y_e = 0.2$ (producing the 3rd peak) and matter with $Y_e = 0.3$ (not producing r-process with $A > 130$) agree equally well with the bolometric light curve slope. The major insight concerning the 3rd r-process peak comes from the colour evolution of the observed transient. Matter below the threshold value of $Y_e^{\mathrm{crit}} \approx 0.25$ [38] reaches the 3rd r-process peak and produces in particular lanthanides ($57 \leq Z \leq 71$), while matter with $Y_e > Y_e^{\mathrm{crit}}$ does not. The complex atomic structure of lanthanides leads to

[1] Data taken from https://kilonova.space.

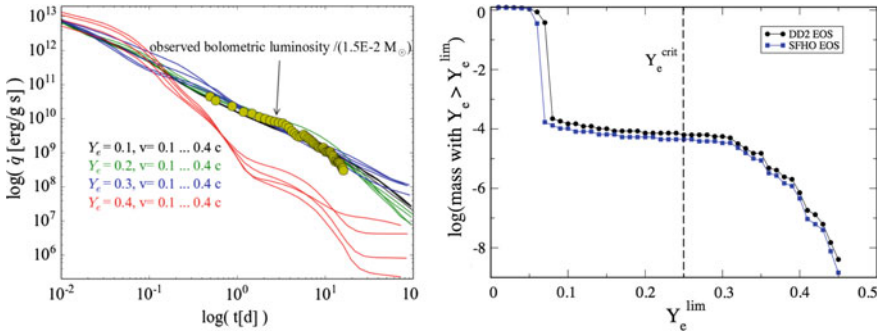

Fig. 17.2 Left: Observed, bolometric emission [erg/s] (divided by a mass scale of 1.5×10^{-2} $M_\odot$) compared to the nuclear heating rates obtained for different expansion velocities and electron fractions. Matter with Y_e below $\approx$0.3 is undergoing a substantial r-process and the corresponding heating rates agree well with the slope of the bolometric luminosity. Right: mass inside an initial 1.4 $M_\odot$ neutron star (for DD2 and SFHo equation of state) that has an electron fraction about $Y_e^{\rm lim}$. Note that for both equations of state less than 10^{-4} $M_\odot$ is initially above the critical Y_e-value of 0.25

an enormous number of possible line transitions ($\sim 10^8$ in some cases) which in turn results in very large effective opacities ($\sim$10 cm^2/g) [19, 39]. As a result, radiation is efficiently trapped inside the ejecta and once the matter becomes transparent after $\sim$1 week, the radiation escapes predominantly at red wavelengths. Material with higher Y_e, in contrast, produces only light r-process elements with substantially lower effective opacities ($\sim$1 cm^2/g), therefore the peak emission is reached earlier ($\sim$1 day) and radiation escapes predominantly in the blue part of the spectrum. The electromagnetic counterpart of GW170817 was surprisingly bright in the blue part of the spectrum after around a day [32, 40, 41] and then evolved quickly into a red transient peaking after about a week [42, 43]. The brightness of the early blue peak came to many in the community as a surprise and comparison with models suggest [44] that as much as $\sim$0.03 $M_\odot$ of matter with an electron fraction $>$0.25 has been ejected. Given that the initial neutron stars hardly contain any such matter (less than 10^{-4} $M_\odot$), see the right panel of Fig. 17.2 for the mass distribution with Y_e for two popular equations of state, it would seem entirely unnatural that *all* of the ejecta should have their electron fraction raised above the critical value of 0.25. Therefore, avoiding the production 3rd r-process peak elements seems extremely unlikely. The fact that a strong early blue peak was observed, however, implies that a substantial fraction of matter had its electron fraction changed (by positron and/or neutrino capture) and that we have witnessed weak interaction "in flagranti" during the observation of GW170817 and its electromagnetic counterparts. This also underlines the paramount importance of carefully modelling weak interactions and neutrino transport in neutron star merger simulations.

17.3 Outlook

The first multi-messenger detection of a binary neutron star merger has conclusively solved some long-standing puzzles such as the origin of short GRBs and of the r-process elements. While overall confirming most theoretical expectations, some of the numbers are uncomfortably large. For example, the total ejecta mass has been estimated as $\sim 0.07\ M_\odot$ *and* the merger rates inferred from the first event are as high as the 1540^{+3200}_{-1220} Gpc^{-3} year^{-1} [26]. This could easily overproduce the galactic r-process content. If the current rate estimates should be overly optimistic large, this would actually resolve a slight tension both with binary population synthesis and earlier expectations for the merger rates from nucleosynthesis (see e.g. Fig. 2 in [45]). Binary evolution models can under favourable conditions reach rates from 200 to 400 Gpc^{-3} year^{-1} [46–48]. A number of $\sim$300 Gpc^{-3} year^{-1} would also a "sweet spot" for other constraints (merger simulations, observed gamma ray bursts, ^{244}Pu, r-process in dwarf galaxies) [45, 49]. Another possibility, would be that GW170817 was an exceptional encounter and ejected substantially more matter than the average event. Recent studies [50] suggest that galactic elemental evolution would be easier to understand if there was another heavy r-process source besides neutron star mergers. With expected detection rates of 1–50 DNS mergers per year for the upcoming science run [51], we can be optimistic to get answers on many of our questions in the near future.

References

1. A.G.W. Cameron, Chalk River Rept. **CRL-41** (1957)
2. E.M. Burbidge et al., Rev. Mod. Phys. **29**, 547 (1957)
3. Committee On The Physics Of The Universe, D.O.E. Astronomy, *Connecting Quarks with the Cosmos: 11 Science Questions for the New Century* (2003)
4. K. Takahashi, J. Witti, H.T. Janka, Astron. Astrophys. **286**, 857 (1994)
5. Y.Z. Qian, S.E. Woosley, Astrophys. J. **471**, 331 (1996)
6. R.D. Hoffman, S.E. Woosley, Y.Z. Qian, Astrophys. J. **482**, 951 (1997)
7. J.M. Lattimer, D.N. Schramm, Astrophys. J. (Lett.) **192**, L145 (1974)
8. J.M. Lattimer, D.N. Schramm, Astrophys. J. **210**, 549 (1976)
9. D. Eichler, M. Livio, T. Piran, D.N. Schramm, Nature **340**, 126 (1989)
10. B. Paczynski, Astrophys. J. Lett. **308**, L43 (1986)
11. S. Rosswog et al., in *Nuclear Astrophysics*, ed. by W. Hillebrandt, E. Muller (1998), p. 103
12. C. Freiburghaus, S. Rosswog, F.K. Thielemann, Astrophys. J. **525**, L121 (1999)
13. S. Rosswog et al., Astron. Astrophys. **341**, 499 (1999)
14. L.X. Li, B. Paczyński, Astrophys. J. Lett. **507**, L59 (1998)
15. S.R. Kulkarni, ArXiv Astrophysics e-prints (2005)
16. B.D. Metzger et al., MNRAS **406**, 2650 (2010)
17. S. Rosswog, Astrophys. J. **634**, 1202 (2005)
18. L.F. Roberts et al., Astrophys. J. Lett. **736**, L21 (2011)
19. D. Kasen et al., Astrophys. J. **774**, 25 (2013)
20. J. Barnes, D. Kasen, Astrophys. J. **775**, 18 (2013)
21. D. Grossman et al., MNRAS **439**, 757 (2014)

22. S. Rosswog et al., MNRAS **439**, 744 (2014)
23. D. Kasen et al., MNRAS **450**, 1777 (2015)
24. R. Fernandez, B.D. Metzger, Ann. Rev. Nucl. Part. Sci. **66**, 23 (2016)
25. B.D. Metzger, Living Rev. Relativ. **20**, 3 (2017)
26. B.P. Abbott et al., Phys. Rev. Lett. **119**(16), 161101 (2017)
27. B.P. Abbott et al., Astrophys. J. Lett. **848**, L12 (2017)
28. M.M. Kasliwal, Science **358**, 1559 (2017)
29. S.J. Smartt, Nature **551**, 75 (2017)
30. A. Goldstein et al., Astrophys. J. Lett. **848**, L14 (2017)
31. G. Hallinan et al., Science **358**, 1579 (2017)
32. P.A. Evans et al., Science **358**, 1565 (2017)
33. B.P. Abbott et al., Astrophys. J. Lett. **848**, L13 (2017)
34. J.D. Lyman et al., Nat. Astron. **2**, 751 (2018)
35. K.P. Mooley et al., ArXiv e-prints (2018)
36. R. Margutti et al., Astrophys. J. Lett. **856**, L18 (2018)
37. S. Rosswog et al., Astron. Astrophys. **615**, 132 (2018)
38. O. Korobkin et al., MNRAS **426**, 1940 (2012)
39. M. Tanaka, K. Hotokezaka, Astrophys. J. **775**, 113 (2013)
40. D.A. Coulter et al., Science **358**, 1556 (2017)
41. M. Nicholl et al., Astrophys. J. Lett. **848**, L18 (2017)
42. C. McCully et al., Astrophys. J. Lett. **848**, L32 (2017)
43. N.R. Tanvir et al., Astrophys. J. Lett. **848**, L27 (2017)
44. D. Kasen et al., Nature **551**, 80 (2017)
45. S. Rosswog et al., Class. Quantum Gravity **34**(10), 104001 (2017)
46. M.U. Kruckow, T.M. Tauris, N. Langer, M. Kramer, R.G. Izzard, MNRAS (2018)
47. M. Chruslinska, K. Belczynski, J. Klencki, M. Benacquista, MNRAS **474**, 2937 (2018)
48. A. Vigna-Gómez et al., ArXiv e-prints, arXiv:1805.07974 (2018)
49. K. Hotokezaka, T. Piran, M. Paul, Nat. Phys. **11**, 1042 (2015)
50. B. Côté et al., eprint arXiv:1809.03525 (2018)
51. B.P. Abbott et al., Living Rev. Relativ. **21**, 3 (2018)

Chapter 18
Impact of Electron-Captures on N = 50 Nuclei on Core-Collapse Supernovae

Rachel Titus, Chris Sullivan, Remco G. T. Zegers, B. Alex Brown and Bingshui Gao

Abstract Sensitivity studies of the late stages of stellar core collapse with respect to electron-capture rates indicate the importance of a region of nuclei near the N = 50 shell closure, just above doubly magic ^{78}Ni. In the present work, it has been demonstrated that uncertainties in key characteristics of the evolution, such as the lepton fraction, electron fraction, entropy, stellar density, and in-fall velocity are about 50% due to uncertainties in the electron-capture rates on nuclei in this region, although thousands of nuclei are included in the simulations. The present electron-capture rate estimates used for the nuclei in this region of interest are primarily based on a simple approximation, and it is shown that the estimated rates are likely overestimated by an order of magnitude or more. More accurate microscopic theoretical models are required to obtain Gamow-Teller strength distributions, upon which electron-capture rates are based. The development of these models and the benchmarking of such calculations rely on data from charge-exchange experiments at intermediate energies. An experimental campaign to study Gamow-Teller strength distributions in nuclei at and near N = 50, including ^{86}Kr and ^{88}Sr, with the (t, ^{3}He) reaction at NSCL is underway and preliminary results indicate the electron-capture rates in the weak rate library are indeed overestimated.

Weak rates, such as electron-capture rates and β-decay rates, are important nuclear physics inputs for a variety of astrophysical simulations. In particular, simulations of the late stages of core-collapse, prior to a supernova explosion, depend heavily on the electron-capture rates included in the simulation. The weak rate library [1] includes the most accurate weak rate tables available currently, and can be used in

R. Titus (✉) · C. Sullivan · R. G. T. Zegers · B. Alex Brown · B. Gao
National Superconducting Cyclotron Laboratory, Michigan State University, East Lansing, MI 48824, USA
e-mail: taverner@nscl.msu.edu

Joint Institute for Nuclear Astrophysics: Center for the Evolution of the Elements, Michigan State University, East Lansing, MI 48824, USA

R. Titus · C. Sullivan · R. G. T. Zegers · B. Alex Brown
Department of Physics and Astronomy, Michigan State University, East Lansing, MI 48824, USA

A. Formicola et al. (eds.), *Nuclei in the Cosmos XV*, Springer Proceedings in Physics 219, https://doi.org/10.1007/978-3-030-13876-9_18

conjunction with the neutrino transport code, NuLib [2], to generate opacities for use in astrophysical simulations. The core-collapse supernova simulations discussed in this work use the spherically-symmetric, general relativistic hydrodynamics code, GR1D [3], using the SFHo equation of state [4] and a 15 solar-mass progenitor [5].

A number of weak rate tables are included in the weak-rate library, as detailed in [6]. These rate tables are based on Gamow-Teller strength distributions, which can be obtained from charge-exchange experiments, complemented with information about low-lying states from β-decay, or from theoretical calculations. Since measurements are only available for a limited set of nuclei, most of the rates contained in these tables are calculated using theoretical methods, such as shell model or Monte Carlo shell model calculations. Theoretical calculations are also necessary because the temperature of the core of a dying star is finite and transitions from excited states in the parent nucleus, which, in general, are not measurable, contribute. Experimental results are used to validate and benchmark current theoretical models [7], in order to ensure that they are providing the most accurate nuclear physics inputs to simulations.

Detailed theoretical calculations for electron-capture rates have not been performed for all nuclei that participate in astrophysical simulations. This is particularly true for the extremely exotic nuclei near the neutron and proton drip lines, and those nuclei in the higher mass regions. Theoretical models in these areas are still being refined and benchmarked using available experimental results. When neither experimental nor theoretical rates are available for a nucleus, the weak rate library uses an approximate method to calculate the electron-capture rates. Typically, an electron-capture rate is obtained by a sum over the Gamow-Teller strength distribution, weighted by the stellar density, temperature, and excitation energy of the state. The approximate method, instead, uses a single Gamow-Teller state at 2.5 MeV with a strength of 4.6, as determined from fits to middle-mass, mid-shell, stable nuclei [8]. While successful for nuclei immediately adjacent to the fitting region, this approximation breaks down when considering heavy nuclei and those near to a shell closure. For these nuclei, especially in the N = 50 region, the neutron orbitals are filled and block the low-lying Gamow-Teller strength, instead only allowing transitions to higher excitation energy. Hence, the electron-capture rate is reduced because higher-lying states contribute less strongly to the rate. Using the occupancy calculation presented by Macfarlane [9] as a test, it is expected that the approximate method, because it does not account for the Pauli-blocking effect described above, will overestimate the electron-capture rates of heavy, neutron-rich nuclei by an order of magnitude or more [6].

This potential for extreme overestimation of electron-capture rates is important to consider as there is always a need for accurate nuclear physics inputs for core-collapse supernova simulations. In particular, it is necessary to focus on the accuracy of the rates in the N = 50 region because of the results of a recent sensitivity study [1]. In this study, a region of neutron-rich nuclei, centered on the N = 50 region, was found to have the strongest effect on the change in electron fraction in the late stages of core-collapse. Further examination showed that the vast majority of these nuclei use electron-capture rates calculated from the approximate method. Because the nuclei lie on or near the neutron shell closure, the Pauli-blocking effect is expected to be

strong, causing the electron-capture rates to be smaller than the approximate method currently assumes.

To test the effect that such an overestimation would have on the simulations, a second sensitivity study was performed. A region of 74 nuclei, hereafter referred to as the high-sensitivity region, was chosen, and two sets of simulations were performed. The first scaled the electron-capture rates of all of the nuclei participating in the simulation, and the second scaled the electron-capture rates of the 74 nuclei in the high-sensitivity region. A number of quantities at core bounce, such as lepton fraction, entropy, stellar density and in-fall velocity, from the simulation were compared in order to observe the effect of the variation of the electron-capture rates. Using a scaling factor of 0.1, it was found that the high-sensitivity region nuclei were responsible for half of the change in the above quantities compared to the case in which all of the electron-capture rates were scaled [6].

From this result, it is evident that overestimated electron-capture rates in the high-sensitivity region have a significant effect on the behavior of simulations of the late stages of core collapse. Therefore, it is important to obtain more accurate rates, whether by theoretical methods, or by experimental measurements. Presently, the models for the N = 50 region are lacking and require further development. Therefore, experimental work should be focused on studying the N = 50 nuclei, and using the extracted electron-capture rates to validate and benchmark theoretical models as they are developed.

Charge-exchange reaction experiments are favored for extracting Gamow-Teller strength distributions for use in calculating electron capture rates for several reasons. First, charge-exchange reactions in the (n,p)-direction connect the same initial and final states as an electron-capture reactions, making an intuitive parallel between the two reactions. Second, while it might nice to measure such reactions directly, for example via a β-decay experiment, such reactions are limited by the Q-value window. Charge-exchange reactions are not limited by this window, yielding a complete excitation energy spectrum. Finally, there exists a well-established proportionality between the charge-exchange cross section at zero momentum transfer and the Gamow-Teller strength distribution. Because of this relationship, it is simple to extract the strength distribution and use it to calculate electron-capture rates for the nucleus being studied.

Recent experimental work at the National Superconducting Cyclotron Laboratory has been focused on examining neutron-rich nuclei in the region near the N = 50 shell closure. Experiments on ^{86}Kr and ^{88}Sr directly examine N = 50 nuclei, probing the effect of Pauli blocking on the extracted electron-capture rates. Currently, studies of more neutron-rich nuclei or those contained in the high-sensitivity region are not possible because the nuclei are unstable, and the beams for experiments in inverse kinematics lack the necessary intensity.

Although the analysis of the aforementioned experiments is ongoing, preliminary results indicate that the Gamow-Teller strength is much smaller than the B(GT) = 4.6 used by the approximate method. In the case of ^{88}Sr, the preliminary electron-capture rate extracted differs from the approximate electron-capture rate by approximately 2 orders of magnitude. Based on the conclusions from the sensitivity study described

above, if we assume all of the electron-capture rates in the high-sensitivity region show a similar level of overestimation, then this introduces extremely large uncertainties into current results from the simulations.

In order to reduce the uncertainties in the simulated results, it is necessary to improve the electron-capture rates using the simulation. First, the approximate method will need to be updated so that its results are also applicable for heavy, unstable nuclei. A first step for this has been taken, through the work of Raduta [10]; the new approximate method includes the isospin of the nuclei, yielding somewhat more accurate electron-capture rates. Additionally, experimental data will be used to develop and test new theoretical models that can be used to generate electron-capture rates for wide swaths of nuclei. As new rates become available, they will be included in the weak rate library, and the resulting improved simulations will provide a more accurate view of the late stages of core collapse.

References

1. C. Sullivan et al., Astrophys. J. **816**, 44 (2016)
2. E. O'Connor, Astrophys. J. Suppl. Ser. **219**, 24 (2015)
3. E. O'Connor, C.D. Ott, Class. Quantum Gravity **27**, 114103 (2010)
4. A.W. Steiner, M. Hempel, T. Fischer, Astrophys. J. **774**, 17 (2013)
5. S.E. Woosley, T.A. Weaver, Astrophys. J. Suppl. Ser. **101**, 181 (1995)
6. R. Titus et al., J. Phys. G Nucl. Part. Phys. **45**, 014004 (2017)
7. A.L. Cole et al., Phys. Rev. C **86**, 015809 (2012)
8. K. Langanke, G. Martínez-Pinedo, J.M. Sampaio et al., Phys. Rev. Lett. **90**, 241102 (2003)
9. M.H. Macfarlane, Phys. Lett. B **182**, 265 (1986)
10. A.R. Raduta, F. Gulminelli, M. Oertel, Phys. Rev. C **95**, 025805 (2017)

Chapter 19
Learning About Nucleosynthesis from Multi-dimensional Simulations of Core-Collapse Supernovae

W. Raphael Hix, J. Austin Harris, Eric J. Lentz, Stephen Bruenn, O. E. Bronson Messer and Anthony Mezzacappa

Abstract For more than two decades, we have understood that the development of a successful core-collapse supernova is inextricably linked to neutrino heating and three dimensional fluid flows, with large scale hydrodynamic instabilities allowing successful explosions that spherical symmetry would prevent. Unfortunately, our understanding of the nucleosynthesis that occurs in these supernovae, and therefore the impact of supernovae on galactic chemical evolution, has generally ignored much that we have learned about the central engine of these supernovae over the past two decades. Now, with two and three dimensional simulations of core-collapse supernovae run to sufficient duration, we are learning how the multi-dimensional, neutrino-driven character of the explosions directly impacts the nucleosynthesis and other observables of core-collapse supernovae. Here we focus on lessons from multi-dimensional models which implement realistic nuclear reaction networks.

19.1 Nucleosynthesis in Core-Collapse Supernova

Much of our theoretical understanding of the nucleosynthesis in core collapse supernovae (CCSNe) relies on parameterized models where the turbulent, neutrino-driven inner workings of the supernova are replaced with a kinetic energy piston or a thermal

W. Raphael Hix (✉) · O. E. Bronson Messer
Physics Division, Oak Ridge National Laboratory, Oak Ridge, TN, USA
e-mail: raph@ornl.gov

W. Raphael Hix · E. J. Lentz · A. Mezzacappa
Department of Physics and Astronomy, University of Tennessee, Knoxville, TN, USA

J. Austin Harris · O. E. Bronson Messer
National Center for Computational Sciences,
Oak Ridge National Laboratory, Oak Ridge, TN, USA

S. Bruenn
Department of Physics, Florida Atlantic University, Boca Raton, FL, USA

A. Mezzacappa
Joint Institute for Computational Sciences,
Oak Ridge National Laboratory, Oak Ridge, TN, USA

A. Formicola et al. (eds.), *Nuclei in the Cosmos XV*, Springer
Proceedings in Physics 219, https://doi.org/10.1007/978-3-030-13876-9_19

energy bomb (see, e.g., [1–3]). In such bomb or piston simulations, the explosion's energy, its delay time and the *mass cut*, which separates the ejecta from matter destined to become part of the neutron star, are externally supplied parameters. Better are models which include parameterized, but neutrino-driven, explosions (see, e.g., [4, 5]), but these still do not allow the fundamentally different behavior afforded by multi-dimensional fluid flows. Relatively few studies have considered the full impact of the turbulent, neutrino-driven central engine. Wanajo et al. [6] and Harris et al. [7, 8] did so in the context of two-dimensional models with spectral neutrino transport and sophisticated neutrino opacities. However, the nucleosynthesis in [6–8] are computed by post-processing, since these models employed only an α-network within the simulation. This is a general flaw in state of the art models of the core-collapse mechanism, with many not even reaching this level of sophistication in their tracking of the nuclear composition.

19.2 Realistic Reaction Networks in CCSN Models

Here, we present preliminary results for a set of models that include a much larger nuclear reaction network alongside sophisticated neutrino transport and multi-dimensional hydrodynamics. These models, like those of Harris et al. [7, 8], were computed with the CHIMERA supernova modeling code [9, 10]. The models presented here replace the α-network used in [7, 8] with a network containing 160 species stretching from Hydrogen to Germanium, generally including all isotopes from those with equal numbers of neutrons and protons to the most neutron-rich stable species. While insufficient for the investigation of highly neutronized matter within the proto-neutron star, the p-process or r-process, these 160 species cover the majority of the products of explosive nucleosynthesis in supernovae. Furthermore, inclusion self-consistently within the simulation allows the full impact of compositional mixing and thermonuclear energy release to be considered. Two and three dimensional simulations have been run including the 160 species network for a first generation, 9.6 solar mass star from Heger [priv. comm.] (labeled D9.6–HPC). In addition, a series of 2D simulations are being run with this larger network, covering stellar masses from 9 to 15 solar masses, using solar metallicity progenitors from [3] (labeled D#–WH07 in this manuscript), [4] (labeled D#–SEWBJ16) and [11] (labeled D#–EYF12).

The progress of the 2D models is presented in Fig. 19.1. As the explosion begins to develop, regions of space become locally *unbound* when the sum of their thermal, kinetic and gravitational energy becomes positive. The solid lines in the left panel show the evolution of the diagnostic energy, the integral of these energies over the unbound matter. The dashed lines include the energy cost of unbinding the portions of the star above the unbound matter. This corrected diagnostic energy should approach the ultimate explosion energy (the kinetic energy of the ejecta) asymptotically. The temporal evolution of the corrected diagnostic energy provides an indication of the development of the explosion, with the lightest models being nearly asymptotic by

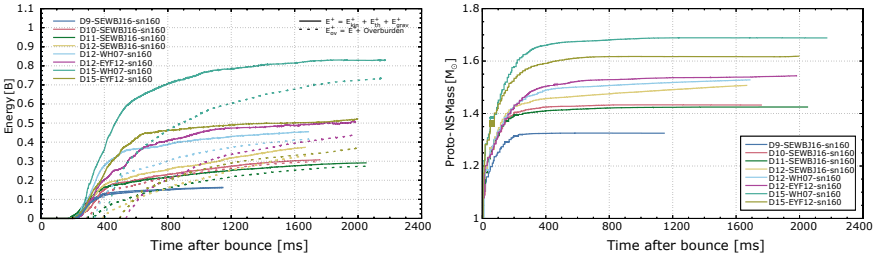

Fig. 19.1 Temporal evolution of the explosion energy (left panel; dashed lines) and neutron star mass (right panel) for a set of 2D models from a variety of progenitors

1 s after the formation of the proto-neutron star, while the explosion energies of 12 and 15 solar mass models continue to increase at 2 s. The right panel of Fig. 19.1 provides a complementary analysis of the completeness of the explosion development by showing the temporal evolution of the proto-neutron star mass. The continued growth in the PNS mass for the more massive models beyond 1 s after bounce indicates that significant accretion continues. This accretion in turn powers the neutrino luminosities that drive the growth of the explosion energy.

The temporal evolution of the isotopic composition of the ejecta can be factored into two components. The first is the production or destruction of the various isotopes in parcels of matter by explosive burning and the freezeout from nuclear statistical equilibrium. The second is the presence of those parcels in the ejecta. Like the explosion energy, defining the ejecta during the developing explosion is uncertain. For that purpose in this analysis, we define the ejecta to be all matter which is locally unbound, as discussed in the previous paragraph. Figure 19.2 shows the temporal evolution of 6 isotopes for the same set of 2D models discussed in Fig. 19.1. The ejected mass of ^{16}O is increasing in all models, as the shock unbinds matter in the oxygen layer, with the rate of change determined largely by the strength of the explosion, which generally grows with progenitor mass over this range. For ^{16}O, the impact of matter from the oxygen-rich layers of the progenitor joining the ejecta is much larger than the impact of explosive oxygen burning in the shock, except at early moments in the explosion. Note the significant difference in ^{16}O ejecta between the three 12 solar mass models (D12-SEWBJ16, D12-WH07 & D12-EYF12), reflective of differences in stellar structure and explosion energy (which is in turn dependent on stellar structure).

The behavior of ^{28}Si is more complex, since it is both created by explosive oxygen burning and destroyed by explosive silicon burning as well as joining and leaving the ejecta. Alone of the isotopes shown here, ^{28}Si shows a general decrement at late times, in the most extreme case (D12-SEWBJ16) the final ejected mass is a third of the peak value. The immediate cause of this decline is hydrodynamic rather than thermonuclear, with relatively low velocity silicon-rich matter being slowed by shear flows and work done on overlying layers until it becomes once again bound to the PNS. As this now bound matter falls toward the PNS, some accretes onto the

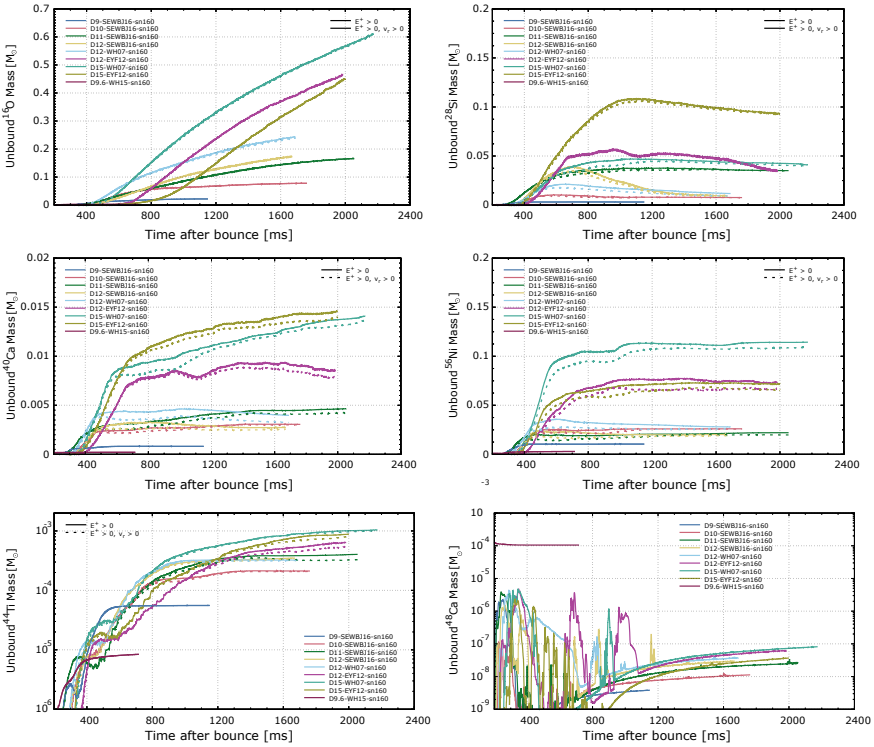

Fig. 19.2 Temporal evolution of the ejecta masses of ^{16}O, ^{28}Si, ^{40}Ca, ^{48}Ca, ^{44}Ti and ^{56}Ni for a set of 2D models from a variety of progenitors

PNS, fueling continued neutrino emission, but some is re-energized and rejoins the ejecta. The heating leads to nuclear processing, primarily α-rich freezeout, boosting the abundances of intermediate mass and iron-peak isotopes like ^{40}Ca, ^{56}Ni and especially ^{44}Ti. The impact of this late accretion and ejection is stronger for ^{44}Ti because much of the ^{40}Ca and ^{56}Ni are made in the first $\sim$0.5 s by explosive silicon burning.

A feature unique to multi-dimensional models is the ejection of neutron-rich matter. With neutrino-matter interactions in the hot bubble driving the matter proton-rich, neutron-rich matter must be drawn up from the vicinity of the neutron star by mechanical means. As discussed by [6], in the case of low mass iron cores (as well as oxygen-neon cores), convection behind the shock, launched very early in such models, dredges neutron-rich matter into the ejecta from the envelope of the PNS. For electron fractions (Y_I) $\sim$ 0.4, this matter is rich in ^{48}Ca, provided the entropy remains low. Figure 19.3 shows the spatial distribution of ^{48}Ca and ^{44}Ti from the D9.6–HPC–3D model. Note that the ^{48}Ca lies over top of the ^{44}Ti which was produced later in the hot bubble behind the shock. For more massive iron core progenitors, matter from near the PNS does not join the ejecta at early times, however it is possible

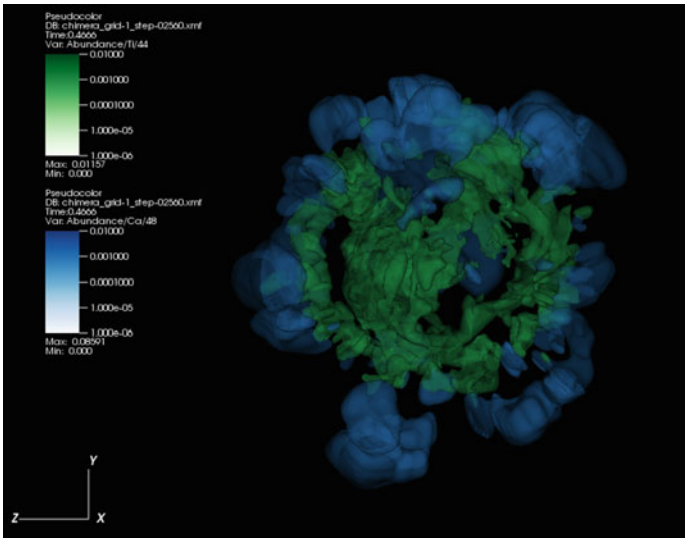

Fig. 19.3 Comparison of the distribution of ^{48}Ca and ^{44}Ti for a 3D model of the explosion of a 9.6 $M_{\odot}$ mass, zero metallicity star

for accretion streams at later times to dredge such matter into the ejecta. The spikes in the lower right panel of Fig. 19.2 shows the resulting impact on the ^{48}Ca content of the ejecta. In all of these models, the ^{48}Ca is subsequently destroyed by α capture as the entropy increases due to internal shocks and neutrino heating, however in one model of [7] significant amounts of ^{48}Ca did survive.

Supernova models including realistic nuclear reaction networks capable of following the dominant explosive burning and NSE freeze-out nucleosynthesis processes afford increased physical fidelity through inclusion of compositional mixing and more accurate thermonuclear energy release. They also afford the ability to test the reliability of post-processing studies by comparing post-processing for these models with the abundances calculated by the same network within the model.

Acknowledgements The research presented here was supported by the U.S. Department of Energy Offices of Nuclear Physics and Advanced Scientific Computing Research and the National Science Foundation Nuclear Theory Program (PHY-1516197). The computing resources were provided by the National Energy Research Scientific Computing Center, supported by the U.S. DOE Office of Science under Contract No. DE-AC02-05CH11231.

References

1. M. Limongi, A. Chieffi, Astrophys. J. Suppl. **237**, 13 (2018)
2. H. Umeda, T. Yoshida, in *Handbook of Supernovae*, ed. by A.W. Alsabti, P. Murdin (Springer International Publishing AG, 2017), p. 1753
3. S.E. Woosley, A. Heger, Phys. Rep. **442**, 269 (2007)
4. T. Sukhbold, T. Ertl, S.E. Woosley, J.M. Brown, H.T. Janka, Astrophys. J. **821**, 38 (2016)
5. A. Perego, M. Hempel, C. Fröhlich, K. Ebinger, M. Eichler, J. Casanova, M. Liebendörfer, F.K. Thielemann, Astrophys. J. **806**, 275 (2015)
6. S. Wanajo, B. Müller, H.T. Janka, A. Heger, Astrophys. J. **852**, 40 (2018)
7. J.A. Harris, W.R. Hix, M.A. Chertkow, C.T. Lee, E.J. Lentz, O.E.B. Messer, Astrophys. J. **843**, 2 (2017)
8. J.A. Harris, W.R. Hix, M.A. Chertkow, S.W. Bruenn, E.J. Lentz, O.E.B. Messer, A. Mezzacappa, J.M. Blondin, E. Endeve, E.J. Lingerfelt, Astrophys. J. (2018) (in prep.)
9. S.W. Bruenn, E.J. Lentz, W.R. Hix, A. Mezzacappa, J.A. Harris, O.E.B. Messer, E. Endeve, J.M. Blondin, M.A. Chertkow, E.J. Lingerfelt, P. Marronetti, K.N. Yakunin, Astrophys. J. **818**, 123 (2016)
10. E.J. Lentz, S.W. Bruenn, W.R. Hix, A. Mezzacappa, O.E.B. Messer, E. Endeve, J.M. Blondin, J.A. Harris, P. Marronetti, K.N. Yakunin, Astrophys. J. **807**, L31 (2015)
11. C.I. Ellinger, P.A. Young, C.L. Fryer, G. Rockefeller, Astrophys. J. **755**, 160 (2012)

Chapter 20
Fission Properties Relevant for GW170817

M. R. Mumpower, N. Vassh, T. Sprouse, P. Jaffke, T. Kawano, E. Holmbeck, Y. L. Zhu, R. Surman, G. C. McLaughlin and P. Möller

Abstract The recent observation of gravitational waves and electromagnetic counterpart to GW170817 [1] has provided fresh impetus to understand the formation of the heaviest elements on the periodic table. The merging of two neutron stars offers a potentially robust site for the neutron-rich nucleosynthesis of these elements in the rapid neutron capture process (r process). However, many challenging problems remain in both the astrophysical modeling of merger events and the nuclear physics inputs. Among the nuclear physics needs for the r process, fission properties may be particularly important. The dynamical ejecta of mergers is expected to be so neutron-rich that the resulting r process produces nuclei above the predicted $N = 184$ shell closure and terminates via fission. We focus our discourse on recent nuclear model developments in the description of fission, apart of the Fission In R-process Elements (FIRE) collaboration. We discuss new calculations of neutron-induced and β-delayed fission properties using FRDM2012. We present new microscopic fission yields predicted from FRLDM. We report on the relevance of these calculations to nucleosynthetic yields, the impact on reheating of the ejecta in addition to the influence on kilonova observables.

20.1 Introduction

The astrophysical location where the formation of the heavy elements above iron on the periodic table occurs remains a longstanding open issue in nuclear astrophysics. Neutron star mergers provide sufficiently neutron-rich environments for the formation of the heaviest elements known as the actinides. In the low-electron fraction

M. R. Mumpower (✉) · P. Jaffke · T. Kawano · P. Möller
Theoretical Division, Los Alamos National Laboratory, Los Alamos, NM 87545, USA
e-mail: mumpower@lanl.gov
URL: http://matthewmumpower.com

N. Vassh · T. Sprouse · E. Holmbeck · R. Surman · G. C. McLaughlin
Department of Physics, University of Notre Dame, Notre Dame, IN 46556, USA

Y. L. Zhu
Department of Physics, North Carolina State University, Raleigh, NC 27695, USA

A. Formicola et al. (eds.), *Nuclei in the Cosmos XV*, Springer
Proceedings in Physics 219, https://doi.org/10.1007/978-3-030-13876-9_20

outflows of these events fission may become active. We focus our contribution on the calculation of neutron-induced fission rates and fission yields. We discuss the impact of these calculations on extremely neutron-rich r-process outflows when the bulk of the nuclear flow or r-process path pushes to the actinides.

20.2 Models

We base our calculation of neutron-induced fission rates on the statistical Hauser-Feshbach formalism of [2]. This standard approach to describe reaction mechanisms relies on several model inputs including the nuclear level density, neutron optical model and γ strength function. We use the Portable Routines for Integrated nucleoSynthesis Modeling (PRISM) nucleosynthesis network to calculate the resultant abundances [3]. For this contribution we select nuclear properties based off the 2012 version of the Finite-Range Droplet Model (FRDM2012) consisting of a suite of nuclear masses, decay, reaction and fission properties [4–7] with fission yields calculated on a 5D potential energy surface of the Finite-Range Liquid Drop Model (FRLDM) as discussed in [8].

20.3 Results

Neutron-induced fission rates evaluated at $T_9 = 1$ across the chart of nuclides are shown in Fig. 20.1. The fast rates encountered by the r-process path after the $N = 184$ shell closure induce fission recycling thus preventing the nuclear flow to higher mass number. As the r-process path moves back to stability, towards the north and west

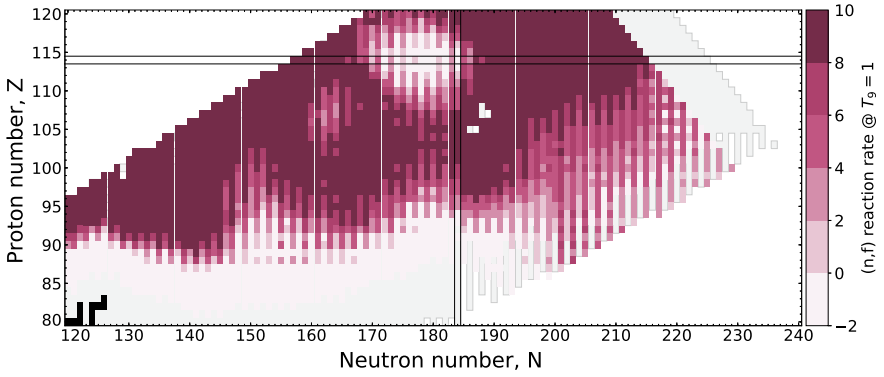

Fig. 20.1 Neutron-induced fission rates evaluated at $T_9 = 1$ across the chart of nuclides based off FRDM2012 nuclear properties

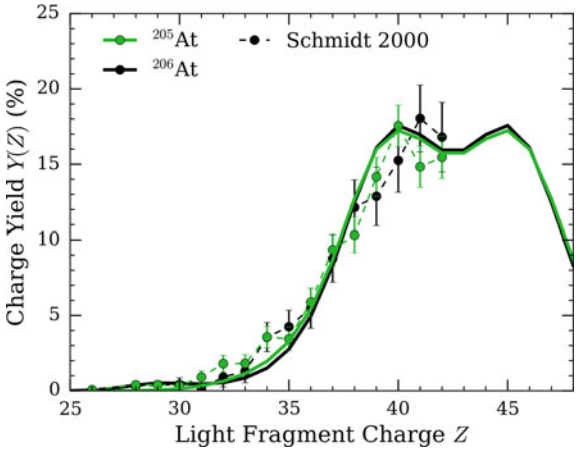

Fig. 20.2 FRLDM charge yields compared to the data of [11]

in this figure, it will encounter regions of β-delayed fission. The interplay between these two nuclear processes during this time shape lighter mass regions and set the population of more stable actinides [9].

Fission yields also play a crucial role in the r-process as they dictate where the light fragments land in the NZ-plane. We have begun investigating the predictions of FRLDM in isotopes near stability, with the comparison to data for several astatine ($Z = 85$) isotopes shown in Fig. 20.2. Further comparisons have been made to known nuclei at higher Z that are relevant to the r-process. The calculation of the fission yield of ^{254}Cf($Z = 98$) for instance was made in [10]. The spontaneous fission of this nucleus was found to have a substantial influence on the brightness of the late-time kilonova emission.

We extend the work of [10] to even more neutron-rich conditions of [12]. Figure 20.3 shows the dominance of ^{254}Cf in the radioactive heating at late times. The impact of ^{254}Cf is even larger compared to the work of [10] due to the increased

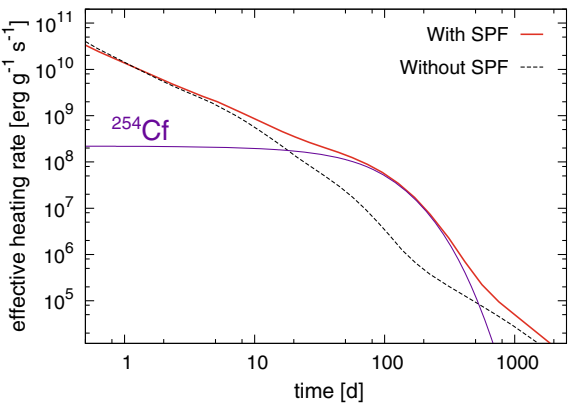

Fig. 20.3 The impact of ^{254}Cf on radioactive heating is found to be greater in more neutron-rich conditions as compared to the results of [10]

production of this isotope in lower-electron fraction material. If the electromagnetic observations are not obscured by other components, the late-time brightness of the kilonova may be used as a proxy to determine if actinide nucleosynthesis has occurred.

20.4 Conclusions

Fission properties can play an important role in determining the nucleosynthetic outcome of astrophysical ejecta with low electron fraction. Fast neutron-induced fission rates recycle r-process material down to lower mass numbers thus providing a termination point to the r-process. Fission yields from FRLDM were found to be in good agreement in isotopic chains near stability thus pointing to this model being well suited for extension into the r-process region.

References

1. B.P. Abbott et al., Gw170817: observation of gravitational waves from a binary neutron star inspiral. Phys. Rev. Lett. **119**, 161101 (2017)
2. T. Kawano, R. Capote, S. Hilaire, P. ChauHuu-Tai, Statistical hauser-feshbach theory with width-fluctuation correction including direct reaction channels for neutron-induced reactions at low energies. Phys. Rev. C **94**, 014612 (2016)
3. M.R. Mumpower, T. Kawano, J.L. Ullmann, M. Krtička, T.M. Sprouse, Estimation of M 1 scissors mode strength for deformed nuclei in the medium- to heavy-mass region by statistical Hauser-Feshbach model calculations. Phys. Rev. C **96**(2), 024612 (2017)
4. P. Möller, A.J. Sierk, T. Ichikawa, H. Sagawa, Nuclear ground-state masses and deformations: FRDM (2012). At. Data Nucl. Data Tables **109**, 1–204 (2016)
5. M.R. Mumpower, T. Kawano, P. Möller, Neutron-γ competition for β -delayed neutron emission. Phys. Rev. C **94**(6), 064317 (2016)
6. P. Möller, M.R. Mumpower, T. Kawano, W.D. Myers, Nuclear properties for astrophysical and radioactive-ion-beam applications (II). At. Data Nucl. Data Tables (2018)
7. Patrick Jaffke, Peter Möller, Patrick Talou, Arnold J. Sierk, Hauser-feshbach fission fragment de-excitation with calculated macroscopic-microscopic mass yields. Phys. Rev. C **97**, 034608 (2018)
8. P. Möller, A.J. Sierk, T. Ichikawa, A. Iwamoto, M. Mumpower, Fission barriers at the end of the chart of the nuclides. Phys. Rev. C **91**(2), 024310 (2015)
9. M.R. Mumpower, T. Kawano, T.M. Sprouse, N. Vassh, E.M. Holmbeck, R. Surman, P. Moller. β-delayed fission in r-process nucleosynthesis. *ArXiv e-prints*, Feb 2018
10. Y. Zhu, R.T. Wollaeger, N. Vassh, R. Surman, T.M. Sprouse, M.R. Mumpower, P. Moller, G.C. McLaughlin, O. Korobkin, T. Kawano, P.J. Jaffke, E.M. Holmbeck, C.L. Fryer, W.P. Even, A.J. Couture, J. Barnes, Californium-254 and kilonova light curves. Astrophys. J. Lett. **863**, L23 (2018)
11. K.-H. Schmidt, S. Steinhäuser, C. Böckstiegel, A. Grewe, A. Heinz, A.R. Junghans, J. Benlliure, H.-G. Clerc, M. de Jong, J. Müller, M. Pfützner, B. Voss, Relativistic radioactive beams: a new access to nuclear-fission studies. Nucl. Phys. A **665**, 221–267 (2000)
12. S. Goriely, A. Bauswein, H.-T. Janka, r-process nucleosynthesis in dynamically ejected matter of neutron star mergers. Astrophys. J. **738**, L32 (2011)

Chapter 21
Explosive Nucleosynthesis: What We Learned and What We Still Do Not Understand

Friedrich-Karl Thielemann

Abstract This review touches on historical aspects, going back to the early days of nuclear astrophysics, initiated by B^2FH and Cameron, discusses (i) the required nuclear input from reaction rates and decay properties up to the nuclear equation of state, continues (ii) with the tools to perform nucleosynthesis calculations and (iii) early parametrized nucleosynthesis studies, before (iv) reliable stellar models became available for the late stages of stellar evolution. It passes then through (v) explosive environments from core-collapse supernovae to explosive events in binary systems (including type Ia supernovae and compact binary mergers), and finally (vi) discusses the role of all these nucleosynthesis production sites in the evolution of galaxies. The focus is put on the comparison of early ideas and present, very recent, understanding.

21.1 Introduction

In this short text it is not possible to give an overview over more than 60 years of nuclear astrophysics, and especially explosive nucleosynthesis, but we try to address the questions how it all started, what nuclear and technical input was/is required, how initially parametrized calculations developed into full scale (magne-to-)hydrodynamic simulations, which nucleosynthesis processes take place, and how they impact ejecta compositions, which again make their way into galactic evolution and the present solar abundance composition. The solar neutrino problem is solved, the expansion of the Universe understood with the aid of type Ia superovae, the role of neutron star mergers was clarified in 2017 with GW170817. Many other open questions remain, especially how the abundance evolution from lowest metallicities to present can be understood.

F.-K. Thielemann (✉)
University of Basel, 4056 Basel, Switzerland
e-mail: f-k.thielemann@unibas.ch

GSI Helmholtz Center for Heavy Ion Research, 64291 Darmstadt, Germany

A. Formicola et al. (eds.), *Nuclei in the Cosmos XV*, Springer
Proceedings in Physics 219, https://doi.org/10.1007/978-3-030-13876-9_21

21.2 Nuclear Input and Reaction Networks

21.2.1 Nuclear Input

Over the years an enormous wealth of experimental information entered into compilations of nuclear reaction rates, initially with the lead of the Kellogg group around Willy Fowler [26, 42, 43]. Major updates were due to Angulo et al. [1, NACRE], Xu et al. [164, NACRE II], followed by Iliadis et al. [71], Longland et al. [89] I, Iliadis et al. [72–74] II, III, IV from North Carolina, which entered into Starlib [130]. Uncountable individual investigations have been undertaken by many groups, here especially the Wiescher group should be mentioned, clarifying recently the role of $^{12}C(\alpha, \gamma)^{16}O$ in stellar helium burning [33]. And the LUNA Lab at Gran Sasso plays a key role to measure minute reaction cross sections at lowest energies deep underground, important in early hydrostatic stellar burning stages (see https://luna.lngs.infn.it/index.php/scientific-output/publications). An enormous body of neutron capture reactions has been established by Bao and Käppeler [14], and Bao et al. [15], expanded more recently by the KADONIS collaboration [34]. This has been extended to unstable nuclei by the n_ToF collaboration at CERN. A constantly growing set of results, involving highly unstable nuclei, comes from radioactive ion beam facilities at MSU, GSI, RIKEN, GANIL, and Lanzhou.

Theoretical developments to predict nuclear reaction rates started with Truran et al. [145], utilizing the statistical (Hauser-Feshbach) model with ground state properties, continuing with Truran [147], Michaud and Fowler [98, 99, adding improved optical potentials], Arnould [10, the first one including excited states], Arnould and Beelen [11], and Truran [148]. Holmes et al. [64], and Woosley et al. [160] made use of level densities via a back-shifted Fermi gas. Thielemann et al. [138, 139] developed the SMOKER code, Rauscher and Thielemann [123, 124] extended it to the NoSMOKER approach. Panov et al. [118] included fission. Present efforts center around T. Rauscher, extending NoSMOKER to SMARAGD [125], and S. Goriely et al., who started out with the MOST code in 1997 [52], introducing since then many improvements with applications of the TALYS code (e.g. [53]).

Weak interaction rates, like e.g. beta-decays, electron captures, neutrino interactions are of equal importance, pioneered by Kratz et al. [81], Möller and Kratz [101] to measure/predict beta-decay half-lives; Fuller et al. [49], Langanke and Martinez-Pinedo [83], addressing electron capture rates as well as neutrino interactions with nuclei. Many others followed, like e.g. [92], focussing on neutron-rich nuclei far from stability, especially important for the r-process. All predictions of such efforts for unstable nuclei, addressing also fission, have an intimate relation to properties of nuclear mass models (see e.g. [134]). Combined information has entered Complete Reaction Libraries, e.g. presently publicly available Reaclib, Bruslib, Starlib, as well as the Equation of State database CompOSE [116].

21.2.2 Reaction Neworks

Early approaches to solve nuclear reaction networks, which are stiff systems of ordinary differential equations and not solvable with the means of explicit methods, were undertaken by Truran et al. [145, 146] and Arnett and Truran [6]. The solution via the implicit backward Euler method was obtained in a linear approach. Woosley et al. [159], Arnould [12], Thielemann et al. [137], changed this to a fully converged multi-dimensional Newton-Raphson scheme. Restricted nuclear networks have long been used in stellar evolution codes (e.g. [69]). Presently in use on a global basis are BasNet (going back to [137]), NetGen (in Bruslib), XNET [60], Timmes et al. [144], Cabezon et al. [22], NucNet [97], WinNet [158], SkyNet [88].

21.3 Stellar Models

First explosive nucleosynthesis calculations were all based on parameter studies rather than realistic stellar models, but were highly important to explore results. All explosive burning stages, from H, He, C, Ne, O, Si-burning to nuclear statistical equilibrium (NSE) have been tested by these early investigations e.g. expl. Si-burning: Fowler and Hoyle [41], Bodansky et al. [17], expl. O- and Si-burning: Woosley et al. [159], expl. Ne- and C-burning: Arnett [4], Howard et al. [67], Truran and Cameron [149], Arnett and Wefel [9], Morgan [104]. As initial stellar models examined only early burning stages, these investigations had to be done via parameter studies with assumed adiabatic expansions from initial peak temperatures and densities. First attempts to model late burning stages and provide pre-collapse models for supernova explosions were undertaken by Arnett [7], Weaver et al. [154, leading to the Kepler code], and Nomoto and Hashimoto [114]. Presently highly sophisticated input exists from Limongi and Chieffi ([87], FRANEC), Heger and Woosley [58, KEPLER], Meynet, Hirschi and collaborators (e.g. [50], GENEC), Paxton et al. [119, MESA], Umeda/Yoshida (e.g. [165]), Nakamura et al. [106]. Stellar models have been verified by the solution of the solar neutrino problem [90].

21.4 Type Ia Supernovae

Binary systems with accretion onto one compact object can lead to (depending on the accretion rate) explosive events with thermonuclear runaway (under electron-degenerate conditions). In case of accreting white dwarfs this can cause nova or type Ia supernova explosions. The explanation of type Ia supernovae goes back to Hoyle and Fowler [68]. First carbon-detonation models were developed by Arnett [5], Arnett et al. [8], and Woosley [161], later discarded as they did not fit observations. Iben and Tutukov [70] and Webbink [155] laid the theoretical groundwork for so-

called single and double degenerate systems, depending whether one white dwarf is or two white dwarfs are involved in the binary system. First 1D deflagration models were developed by Nomoto et al. [111–113] and Woosley and Weaver [162]. Müller and Arnett [105] and later Khokhlov et al. [78] started general combustion approaches. Consistent ignition modeling for degenerate condition is approached with the MAESTRO code [166]. Presently, single-degenerate systems starting with central carbon deflagration, double degenerate mergers, He-accretion caused double detonations, and even white dwarf collisions are considered (for a review see e.g. [142]). Major progress is due to observations, disentangling the possible scenarios [51, 91, 110]. Important understanding for the combination of contributing scenarios comes from their nucleosynthesis of Mn (^{55}Co-decay) and Zn in galactic evolution ([131], Hoeflich et al. [61], [85, 100, 150]).

21.5 Core-Collapse Supernovae (CCSNe)

We are on the path of solving the core-collapse supernova problem in a self-consistent way. While early approaches assumed that the bounce of the collapsing Fe-core at nuclear densities would permit a sufficiently energetic shock front and an explosion, this has been shifted to explosions driven by neutrinos [16]. There exists a growing set of 2D and 3D CCSN explosion simulations (see e.g. reviews by Janka et al. [75, 76], Burrows [20, 21], Bruenn et al. [18], Foglizzo et al. [40], Nakamura et al. [106], Cabezon et al. [23]). Active groups are based in Garching/Belfast/Monash/RIKEN (Janka, Müller, Müller, Just …), Princeton/Caltech/MSU (Burrows, Ott, Couch …), Oak Ridge (Mezzacappa, Hix, Lenz, Messer, Harris …), Tokyo/Kyushu (Takiwaki, Nakamura, Kotake), Paris (Foglizzo et al.), and Basel (Liebendörfer, Cabezon, Hempel …). Open questions relate to the stellar mass limit where core-collapse ends in black hole formation [82, 117], and when - due to rotation and magnetic fields - this leads to hypernovae [115].

To provide complete nucleosynthesis predictions from self-consistent multi-D simulations is still in its infancy. For this reason 1D approximations, based on piston or thermal bomb approaches have been undertaken for many years (e.g. [58, 87, 115, 140]). They lack self-consistent predictions of explosion energies, mass cuts between neutron star and ejecta, as well as the neutron-richness (Y_e) of the innermost ejecta. More recently improved 1D approximations have followed, attempting to mimic multi-D effects and avoiding the shortfalls mentioned above [35, 38, 120, 135, 151]. A major role in determining the composition of the innermost ejecta play neutrino interactions with outflowing matter. Opposite to early ideas that matter close to the proto-neutron star would be neutron-rich, neutrino capture on neutrons (favored by the neutron-proton mass difference) is winning against antineutrino capture on protons and turns matter (slightly) proton-rich, causing a νp-process [30, 37, 46, 47, 122, 153] . While such a νp-process is supported by present simulations, an r-process is apparently not occurring, at most a weak r-process [2, 93, 126]. For possible exceptions, in case of fast rotation and strong magnetic fields, see the next section.

21.6 Origin of the Heavy Elements

The production of a fraction of the heavy elements up to Pb and Bi has long been postulated since B^2FH [19] and Cameron [24] via the slow neutron capture (s-) process in shell He-burning during stellar evolution (see e.g. [77]). The origin of the heaviest elements up to Th, U, and Pu (and beyond) via the rapid neutron capture (r-) process remained a puzzle until very recently, despite much progress in understanding the nuclear physics impact (see e.g. [29], Kratz et al. [80], [13, 54, 121]). Regular core-collapse supernovae were champions for many years (see early ideas in [29] and neutrino-wind powered models in [136, 163] or later in [39]), but apparently they cannot provide the conditions required [44], as matter turns rather proton- than neutron-rich via neutrino interactions (see previous section). A rare fraction of magneto-rotational supernovae, dependent on initial rotation rates and magnetic fields, seems to have a chance for succeeding [25, 48, 56, 102, 103, 107–109, 158]. Neutron star mergers have been proven to support the conditions for a full r-process since GW170817. For a review before this event, from the early proposals [36, 84], over first simulations [32, 128, 129] and the first nucleosynthesis predictions [45] up to early 2017 see [141]. Numerous investigations have followed this observational break-through by e.g. Barnes, Hotokezaka, Kasen, Metzger, Rosswog, Tanaka, Wollager (for references see [65]).

21.7 Chemical Evolution and Explosive Nucleosynthesis

Since B^2FH [19] and Cameron [24] we know that essentially all elements beyond H and He are made in stars. The Big Bang produced only H, He, and some Li [31]. The production of heavier elements as a function of time/metallicity depends on occurrence frequencies and delay times for individual nucleosynthesis contributions in galaxies, scrutinized by ever improving observational facilities [86]. The observed enhanced value of [α/Fe] abundance ratios (α = O, Ne, Mg, Si, S, Ca, Ar, Ti) at low metallicities, turning down to solar values at metallicities from [Fe/H] = -1 to 0, due to the input of Ni and Fe-enhanced type Ia supernovae, is reasonably well understood since Matteucci and Greggio [94], Wheeler et al. [157], Timmes et al. [143], Kobayashi et al. [79], Matteucci [95, 96], and Nomoto et al. [115]. Recent supernova models [30] can explain the Fe-group. A more interesting question is which role Mn and Zn play in this game. The low value of [Mn/Fe] at low metallicities, rising above [Fe/H] = -1, indicates its origin as ^{55}Co from type Ia supernovae ([100]). [Zn/Fe] = 0, i.e. solar values, can be made in regular core-collapse supernovae [30, 46], but the upturn (with a sizable scatter) below [Fe/H] = -2 has to be due to hypernovae and/or a certain class of magneto-rotational supernovae [150]. The reason that [Zn/Fe] stays at 0 also beyond [Fe/H] = -1, when type Ia supernovae take over the production of Fe-group elements, indicates that there must also exist a type Ia

subclass producing Zn (as ^{64}Ge), caused probably by He-detonations, permitting a strong alpha-rich freeze-out.

The large scatter of [Eu/Fe] at low metallicities by more than two orders of magnitude [57, 127, 133] indicates a rare site for the strong r-process. This could be consistent with neutron star mergers, but also be due to (still only proposed) magneto-rotational supernovae (their existence being supported by the observations of magnetars as endpoints of such events, Greiner et al. [55]). Chemodynamical galactic evolution calculations have been performed e.g. by Argast et al. [3], Cescutti et al. [27], van de Voort et al. [152], Shen et al. [132], Wehmeyer et al. [156], Hirai et al. [59], Coté et al. [28], Hotokezaka et al. [66]. There exists sufficient supporting material that neutron star mergers are probably the main contributor for the solar r-process composition, but they occur with a delay in galactic evolution which causes problems explaining the [Eu/Fe] ratios at metallicites as low as [Fe/H] = −3. So-called actinide boost stars, i.e. objects found at such low metallicities with enhanced Th/Eu and U/Eu ratios, have probably not the typical solar r-process origin. Their features seem explainable by an interplay between the r-process path and fission properties. Conditions which are slightly less neutron-rich in magneto-rotational supernovae than in neutron star mergers possibly support such resulting final compositions [62, 63]. Similar results are found by Eichler and Wu (private communication).

Notes and Comments: I want to thank the organizers of NIC XV at Gran Sasso for asking me to present this special invited talk. It gave me challenges to cover an extended research field from its beginnings up to present. I enjoyed especially following the ongoing progress and thank M. Busso and G. Meynet for advice. I apologize that this review is probably biased and also not complete. It omits almost completely nucleosynthesis in stellar evolution and explosive events in novae, X-ray bursts and superbursts. It would not have been possible without the insight I obtained working with my collaborators and students. Thanks go to my teachers (Arnett, Arnould, Cameron, Fowler, Hilf, Hillebrandt, Schramm, Truran), my long-term collaborators outside Basel (Cowan, Kratz, Langanke, Nomoto, Panov, Wiescher), all PhD students, often supervised jointly within the extended Basel group (Brachwitz, Dillmann, Ebinger, Eichler, Fehlmann, Freiburghaus, Frensel, Fröhlich, Heinimann, Hix, Käppeli, Liebendörfer, Mocelj, Oechslin, Perego, Reichert, Rembges, Rosswog, Scheidegger, Wehmeyer), and my present/former Basel co-workers (Arcones, Cabezon, Hempel, Hirschi, Kolbe, Kuroda, Liebendörfer, Martinez-Pinedo, Nishimura, Pignatari, Pan, Rauscher), of whom many have dispersed around the world.

References

1. C. Angulo, M. Arnould, M. Rayet et al., Nucl. Phys. A **656**, 3 (1999)
2. A. Arcones, F.-K. Thielemann, J. Phys. G Nucl. Phys. **40**, 013201 (2013)
3. D. Argast, M. Samland, F.-K. Thielemann, Y.-Z. Qian, Astron. Astrophys. **416**, 997 (2004)
4. W.D. Arnett, Astrophys. J. **157**, 1369 (1969)
5. W.D. Arnett, Astrophys. Space Sci. **5**, 180 (1969)

6. W.D. Arnett, J.W. Truran, Astrophys. J. **157**, 339 (1969)
7. W.D. Arnett, Astrophys. J. Suppl. **35**, 145 (1977)
8. W.D. Arnett, J.W. Truran, S.E. Woosley, Astrophys. J. **165**, 87 (1971)
9. W.D. Arnett, J.P. Wefel, Astrophys. J. Lett. **224**, L139 (1978)
10. M. Arnould, Astron. Astrophys. **19**, 92 (1972)
11. M. Arnould, W. Beelen, Astron. Astrophys. **33**, 215 (1974)
12. M. Arnould, Astron. Astrophys. **46**, 117 (1976)
13. M. Arnould, S. Goriely, K. Takahashi, Phys. Rep. **450**, 97 (2007)
14. Z.Y. Bao, F. Käppeler, At. Data Nucl. Data Tables **36**, 411 (1987)
15. Z.Y. Bao, H. Beer, F. Käppeler et al., At. Data Nucl. Data Tables **76**, 70 (2000)
16. H.A. Bethe, Rev. Mod. Phys. **62**, 801 (1990)
17. D. Bodansky, D.D. Clayton, W.A. Fowler, Astrophys. J. Suppl. **16**, 299 (1968)
18. S.W. Bruenn, E.J. Lentz, W.R. Hix, et al., Astrophys. J. **818**, 123 (2016)
19. E.M. Burbidge, G.R. Burbidge, W.A. Fowler, F. Hoyle, Rev. Mod. Phys. **29**, 547 (1957)
20. A. Burrows, Rev. Mod. Phys. **85**, 245 (2013)
21. A. Burrows, D. Vartanyan, J.C. Dolence, M.A. Skinner, D. Radice, Space Sci. Rev. **214**, 33 (2018)
22. R.M. Cabezón, D. García-Senz, E. Bravo, Astrophys. J. Suppl. **151**, 345 (2004)
23. R.M. Cabezón, K.-C. Pan, M. Liebendörfer et al. (2018), arXiv:1806.09184
24. A.G.W. Cameron, *Chalk River Report CRL-41 (1957)* (Dover Publications, New York, 2013)
25. A.G.W. Cameron, Astrophys. J. **587**, 327 (2003)
26. G.R. Caughlan, W.A. Fowler, At. Data Nucl. Data Tables **40**, 283 (1988)
27. G. Cescutti, D. Romano, F. Matteucci, C. Chiappini, R. Hirschi, Astron. Astrophys. **577**, A139 (2015)
28. B. Côté, C.L. Fryer, K. Belczynski et al., Astrophys. J. **855**, 99 (2018)
29. J.J. Cowan, F.-K. Thielemann, J.W. Truran, Phys. Rep. **208**, 267 (1991)
30. S. Curtis, K. Ebinger, C. Fröhlich et al. (2018), arXiv:1805.00498
31. R.H. Cyburt, B.D. Fields, K.A. Olive, T.-H. Yeh, Rev. Mod. Phys. **88**, 015004 (2016)
32. M.B. Davies, W. Benz, T. Piran, F.K. Thielemann, Astrophys. J. **431**, 742 (1994)
33. R.J. deBoer, J. Görres, M. Wiescher et al., Rev. Mod. Phys. **89**, 035007 (2017)
34. I. Dillmann, T. Szücs, R. Plag et al., Nucl. Data Sheets **120**, 171 (2014)
35. K. Ebinger, S. Curtis, C. Fröhlich et al. (2018), arXiv:1804.03182
36. D. Eichler, M. Livio, T. Piran, D.N. Schramm, Nature **340**, 126 (1989)
37. M. Eichler, K. Nakamura, T. Takiwaki et al., J. Phys. G Nucl. Phys. **45**, 014001 (2018)
38. T. Ertl, H.-T. Janka, S.E. Woosley, T. Sukhbold, M. Ugliano, Astrophys. J. **818**, 124 (2016)
39. K. Farouqi, K.-L. Kratz, B. Pfeiffer et al., Astrophys. J. **712**, 1359 (2010)
40. T. Foglizzo, R. Kazeroni, J. Guilet et al., Publ. Astron. Soc. Aust. **32**, e009 (2015)
41. W.A. Fowler, F. Hoyle, Astrophys. J. Suppl. **9**, 201 (1964)
42. W.A. Fowler, G.R. Caughlan, B.A. Zimmerman, Annu. Rev. Astron. Astrophys. **5**, 525 (1967)
43. W.A. Fowler, G.R. Caughlan, B.A. Zimmerman, Annu. Rev. Astron. Astrophys. **13**, 69 (1975)
44. C. Freiburghaus, J.-F. Rembges, T. Rauscher et al., Astrophys. J. **516**, 381 (1999)
45. C. Freiburghaus, S. Rosswog, F.-K. Thielemann, Astrophys. J. Lett. **525**, L121 (1999)
46. C. Fröhlich, P. Hauser, M. Liebendörfer et al., Astrophys. J. **637**, 415 (2006)
47. C. Fröhlich, G. Martínez-Pinedo, M. Liebendörfer et al., Phys. Rev. Lett. **96**, 142502 (2006)
48. S.-I. Fujimoto, N. Nishimura, M.-A. Hashimoto, Astrophys. J. **680**, 1350 (2008)
49. G.M. Fuller, W.A. Fowler, M.J. Newman, Astrophys. J. **293**, 1 (1985)
50. C. Georgy, S. Ekström, P. Eggenberger et al., Astron. Astrophys. **558**, A103 (2013)
51. D.A. Goldstein, D. Kasen, Astrophys. J. Lett. **852**, L33 (2018)
52. S. Goriely, in G. Reffo et al. (eds.) *Nuclear Data for Science and Technology* (Italian Physical Society, 1997), p. 811
53. S. Goriely, S. Hilaire, A.J. Koning, Astron. Astrophys. **487**, 767 (2008)
54. S. Goriely, G. Martínez Pinedo, Nucl. Phys. A **944**, 158 (2015)
55. J. Greiner, P.A. Mazzali, D.A. Kann, et al., Nat. **523**, 189 (2015)
56. G. Halevi, P. Mösta, MNRAS **477**, 2366 (2018)

57. T.T. Hansen, E.M. Holmbeck, T.C. Beers et al., Astrophys. J. **858**, 92 (2018)
58. A. Heger, S.E. Woosley, Astrophys. J. **724**, 341 (2010)
59. Y. Hirai, Y. Ishimaru, T.R. Saitoh et al., MNRAS **466**, 2474 (2017)
60. W.R. Hix, F.-K. Thielemann, J. Comput. Appl. Math. **109**, 321 (1999)
61. P. Hoeflich, S. Chakraborty, W. Comaskey et al., Mem. Soc. Astron. Ital. **88**, 302 (2017)
62. E.M. Holmbeck, T.C. Beers, I.U. Roederer et al., Astrophys. J. Lett. **859**, L24 (2018)
63. E.M. Holmbeck, R. Surman, T.M. Sprouse et al. (2018b), arXiv:1807.06662
64. J.A. Holmes, S.E. Woosley, W.A. Fowler, B.A. Zimmerman, At. Data Nucl. Data Tables **18**, 305 (1976)
65. C.J. Horowitz, A. Arcones, B. Côté et al. (2018), arXiv:1805.04637
66. K. Hotokezaka, P. Beniamini, T. Piran (2018), arXiv:1801.01141
67. W.M. Howard, W.D. Arnett, D.D. Clayton, S.E. Woosley, Astrophys. J. **175**, 201 (1972)
68. F. Hoyle, W.A. Fowler, Astrophys. J. **132**, 565 (1960)
69. I. Iben Jr., Quart. J. R. Astron. Soc. **26**, 1 (1985)
70. I. Iben Jr., A.V. Tutukov, Astrophys. J. Suppl. **54**, 335 (1984)
71. C. Iliadis, J.M. D'Auria, S. Starrfield, W.J. Thompson, M. Wiescher, Astrophys. J. Suppl. **134**, 151 (2001)
72. C. Iliadis, R. Longland, A.E. Champagne, A. Coc, R. Fitzgerald, Nucl. Phys. A **841**, 31 (2010)
73. C. Iliadis, R. Longland, A.E. Champagne, A. Coc, Nucl. Phys. A **841**, 251 (2010)
74. C. Iliadis, R. Longland, A.E. Champagne, A. Coc, Nucl. Phys. A **841**, 323 (2010)
75. H.-T. Janka, Annu. Rev. Nucl. Part. Sci. **62**, 407 (2012)
76. H.-T. Janka, T. Melson, A. Summa, Annu. Rev. Nucl. Part. Sci. **66**, 341 (2016)
77. F. Käppeler, R. Gallino, S. Bisterzo, W. Aoki, Rev. Mod. Phys. **83**, 157 (2011)
78. A. Khokhlov, E. Müller, P. Hoeflich, Astron. Astrophys. **270**, 223 (1993)
79. C. Kobayashi, H. Umeda, K. Nomoto, N. Tominaga, T. Ohkubo, Astrophys. J. **653**, 1145 (2006)
80. K.-L. Kratz, J.-P. Bitouzet, F.-K. Thielemann, P. Moeller, B. Pfeiffer, Astrophys. J. **403**, 216 (1993)
81. K.-L. Kratz, H. Gabelmann, W. Hillebrandt et al., Z. Phys. A Hadrons Nuclei **325**, 489 (1986)
82. T. Kuroda, K. Kotake, T. Takiwaki, F.-K. Thielemann, MNRAS **477**, L80 (2018)
83. K. Langanke, G. Martínez-Pinedo, Rev. Mod. Phys. **75**, 819 (2003)
84. J.M. Lattimer, D.N. Schramm, Astrophys. J. Lett. **192**, L145 (1974)
85. S.-C. Leung, K. Nomoto, Astrophys. J. **861**, 143 (2018)
86. C. Li, G. Zhao, M. Zhai, Y. Jia, Astrophys. J. **860**, 53 (2018)
87. M. Limongi, A. Chieffi, Astrophys. J. Suppl. **237**, 13 (2018)
88. J. Lippuner, L.F. Roberts, Astrophys. J. Suppl. **233**, 18 (2017)
89. R. Longland, C. Iliadis, A.E. Champagne et al., Nucl. Phys. A **841**, 1 (2010)
90. A.B. McDonald, Rev. Mod. Phys. **88**, 030502 (2016)
91. D. Maoz, F. Mannucci, G. Nelemans, Annu. Rev. Astron. Astrophys. **52**, 107 (2014)
92. T. Marketin, L. Huther, G. Martínez-Pinedo, Phys. Rev. C **93**, 025805 (2016)
93. G. Martínez-Pinedo, T. Fischer, A. Lohs, L. Huther, Phys. Rev. Lett. **109**, 251104 (2012)
94. F. Matteucci, L. Greggio, Astron. Astrophys. **154**, 279 (1986)
95. F. Matteucci, *Astrophysics and Space Science Library*, vol. 253 (2001)
96. F. Matteucci, *Chemical Evolution of Galaxies: Astronomy and Astrophysics Library* (Springer, Berlin, 2012). ISBN 978-3-642-22490-4
97. B.S. Meyer, D.C. Adams, Meteorit. Planet. Sci. Suppl. **42**, 5215 (2007)
98. G. Michaud, W.A. Fowler, Phys. Rev. C **2**, 2041 (1970)
99. G. Michaud, W.A. Fowler, Astrophys. J. **173**, 157 (1972)
100. T. Mishenina, T. Gorbaneva, M. Pignatari, F.-K. Thielemann, S.A. Korotin, MNRAS **454**, 1585 (2015)
101. P. Möller, J.R. Nix, K.-L. Kratz, At. Data Nucl. Data Tables **66**, 131 (1997)
102. P. Mösta, C.D. Ott, D. Radice et al., Nature **528**, 376 (2015)
103. P. Mösta, L.F. Roberts, G. Halevi et al., Astrophys. J. **864**, 171 (2018)
104. J.A. Morgan, Astrophys. J. **238**, 674 (1980)

105. E. Müller, W.D. Arnett, Astrophys. J. **307**, 619 (1986)
106. K. Nakamura, T. Takiwaki, T. Kuroda, K. Kotake, Publ. Astron. Soc. Jpn. **67**, 107 (2015)
107. S. Nishimura, K. Kotake, M. Hashimoto et al., Astrophys. J. **642**, 410 (2006)
108. N. Nishimura, T. Takiwaki, F.-K. Thielemann, Astrophys. J. **810**, 109 (2015)
109. N. Nishimura, H. Sawai, T. Takiwaki, S. Yamada, F.-K. Thielemann, Astrophys. J. Lett. **836**, L21 (2017)
110. U.M. Noebauer, M. Kromer, S. Taubenberger et al., MNRAS **472**, 2787 (2017)
111. K. Nomoto, Astrophys. J. **253**, 798 (1982a)
112. K. Nomoto, Astrophys. J. **257**, 780 (1982b)
113. K. Nomoto, F.-K. Thielemann, K. Yokoi, Astrophys. J. **286**, 644 (1984)
114. K. Nomoto, M. Hashimoto, Phys. Rep. **163**, 13 (1988)
115. K. Nomoto, C. Kobayashi, N. Tominaga, Annu. Rev. Astron. Astrophys. **51**, 457 (2013)
116. M. Oertel, M. Hempel, T. Klähn, S. Typel, Rev. Mod. Phys. **89**, 015007 (2017)
117. K.-C. Pan, M. Liebendörfer, S.M. Couch, F.-K. Thielemann, Astrophys. J. **857**, 13 (2018)
118. I.V. Panov, I.Y. Korneev, T. Rauscher et al., Astron. Astrophys. **513**, A61 (2010)
119. B. Paxton, L. Bildsten, A. Dotter et al., Astrophys. J. Suppl. **192**, 3 (2011)
120. A. Perego, M. Hempel, C. Fröhlich et al., Astrophys. J. **806**, 275 (2015)
121. I. Petermann, K. Langanke, G. Martínez-Pinedo et al., Eur. Phys. J. A **48**, 122 (2012)
122. J. Pruet, R.D. Hoffman, S.E. Woosley, H.-T. Janka, R. Buras, Astrophys. J. **644**, 1028 (2006)
123. T. Rauscher, F.-K. Thielemann, At. Data Nucl. Data Tables **75**, 1 (2000)
124. T. Rauscher, F.-K. Thielemann, At. Data Nucl. Data Tables **88**, 1 (2004)
125. T. Rauscher, Int. J. Mod. Phys. E **20**, 1071 (2011)
126. L.F. Roberts, S. Reddy, G. Shen, Phys. Rev. C **86**, 065803 (2012)
127. I.U. Roederer, H. Schatz, J.E. Lawler et al., Astrophys. J. **791**, 32 (2014)
128. S. Rosswog, M. Liebendörfer, F.-K. Thielemann et al., Astron. Astrophys. **341**, 499 (1999)
129. M. Ruffert, H.-T. Janka, Rev. Mod. Astron. **10**, 201 (1997)
130. A.L. Sallaska, C. Iliadis, A.E. Champange et al., Astrophys. J. Suppl. **207**, 18 (2013)
131. I.R. Seitenzahl, D.M. Townsley, *Handbook of Supernovae* (Springer International Publishing AG, 2017), p. 1955. ISBN 978-3-319-21845-8
132. S. Shen, R.J. Cooke, E. Ramirez-Ruiz et al., Astrophys. J. **807**, 115 (2015)
133. C. Sneden, J.J. Cowan, R. Gallino, Annu. Rev. Astron. Astrophys. **46**, 241 (2008)
134. A. Sobiczewski, Y.A. Litvinov, M. Palczewski, At. Data Nucl. Data Tables **119**, 1 (2018)
135. T. Sukhbold, T. Ertl, S.E. Woosley, J.M. Brown, H.-T. Janka, Astrophys. J. **821**, 38 (2016)
136. K. Takahashi, J. Witti, H.-T. Janka, Astron. Astrophys. **286**, 857 (1994)
137. F.-K. Thielemann, M. Arnould, W. Hillebrandt, Astron. Astrophys. **74**, 175 (1979)
138. F.-K. Thielemann, M. Arnould, J.W. Truran, *Advances in Nuclear Astrophysics*, vol. 525 (1986)
139. F.-K. Thielemann, M. Arnould, J.W. Truran, Capture gamma-ray spectroscopy 1987 (1988), p. 730
140. F.-K. Thielemann, K. Nomoto, M.-A. Hashimoto, Astrophys. J. **460**, 408 (1996)
141. F.-K. Thielemann, M. Eichler, I.V. Panov, B. Wehmeyer, Annu. Rev. Nucl. Part. Sci. **67**, 253 (2017)
142. F.-K. Thielemann, J. Isern, A. Perego, P. von Ballmoos, Space Sci. Rev. **214**, 62 (2018)
143. F.X. Timmes, S.E. Woosley, T.A. Weaver, Astrophys. J. Suppl. **98**, 617 (1995)
144. F.X. Timmes, Astrophys. J. Suppl. **124**, 241 (1999)
145. J.W. Truran, C.J. Hansen, A.G.W. Cameron, A. Gilbert, Can. J. Phys. **44**, 151 (1966)
146. J.W. Truran, W.D. Arnett, A.G.W. Cameron, Can. J. Phys. **45**, 2315 (1967)
147. J.W. Truran, Astrophys. Space Sci. **2**, 384 (1968)
148. J.W. Truran, Astrophys. Space Sci. **18**, 306 (1972)
149. J.W. Truran, A.G.W. Cameron, Astrophys. J. **219**, 226 (1978)
150. T. Tsujimoto, N. Nishimura, Astrophys. J. Lett. **863**, L27 (2018)
151. M. Ugliano, H.-T. Janka, A. Marek, A. Arcones, Astrophys. J. **757**, 69 (2012)
152. F. van de Voort, E. Quataert, P.F. Hopkins, D. Kereš, C.-A. Faucher-Giguère, MNRAS **447**, 140 (2015)

153. S. Wanajo, Astrophys. J. **647**, 1323 (2006)
154. T.A. Weaver, G.B. Zimmerman, S.E. Woosley, Astrophys. J. **225**, 1021 (1978)
155. R.F. Webbink, Astrophys. J. **277**, 355 (1984)
156. B. Wehmeyer, M. Pignatari, F.-K. Thielemann, MNRAS **452**, 1970 (2015)
157. J.C. Wheeler, C. Sneden, J.W. Truran Jr., Annu. Rev. Astron. Astrophys. **27**, 279 (1989)
158. C. Winteler, R. Käppeli, A. Perego et al., Astrophys. J. Lett. **750**, L22 (2012)
159. S.E. Woosley, W.D. Arnett, D.D. Clayton, Astrophys. J. Suppl. **26**, 231 (1973)
160. S.E. Woosley, W.A. Fowler, J.A. Holmes, B.A. Zimmerman, At. Data Nucl. Data Tables **22**, 371 (1978)
161. S.E. Woosley, R.E. Taam, T.A. Weaver, Astrophys. J. **301**, 601 (1986)
162. S.E. Woosley, T.A. Weaver, Annu. Rev. Astron. Astrophys. **24**, 205 (1986)
163. S.E. Woosley, J.R. Wilson, G.J. Mathews, R.D. Hoffman, B.S. Meyer, Astrophys. J. **433**, 229 (1994)
164. Y. Xu, K. Takahashi, S. Goriely et al., Nucl. Phys. A **918**, 61 (2013)
165. T. Yoshida, K. Takahashi, H. Umeda, K. Ishidoshiro, Phys. Rev. D **93**, 123012 (2016)
166. M. Zingale, A. Nonaka, A.S. Almgren et al., Astrophys. J. **740**, 8 (2011)

Part V
Nuclear Data and Astrophysics

Chapter 22
The Beta-Oslo Method: Experimentally Constrained (n, γ) Reaction Rates Relevant to the r-Process

A. C. Larsen, S. N. Liddick, Artemis Spyrou, M. Guttormsen, F. L. Bello Garrote, J. E. Midtbø and T. Renstrøm

Abstract Unknown neutron-capture reaction rates remain a significant source of uncertainty in state-of-the-art r-process nucleosynthesis reaction network calculations. As the r-process involves highly neutron-rich nuclei for which direct (n, γ) cross-section measurements are virtually impossible, indirect methods are called for to constrain (n, γ) cross sections used as input for the r-process nuclear network. Here we discuss the newly developed beta-Oslo method, which is capable of provding experimental input for calculating (n, γ) rates of neutron-rich nuclei. The beta-Oslo method represents a first step towards constraining neutron-capture rates of importance to the r-process.

22.1 Introduction

On August 17, 2017, the LIGO and Virgo gravitational-wave detectors measured, for the first time, a direct signal from two colliding neutron stars [1]. Follow-up measurements with telescopes sensitive to electromagnetic radiation confirmed that the rapid neutron-capture process (r-process) [2, 3] had indeed taken place in the collision (e.g., [4]). Hence, a long-standing question in nuclear astrophysics was at least partly solved; one astrophysical r-process site is now confirmed.

A. C. Larsen (✉) · M. Guttormsen · F. L. Bello Garrote · J. E. Midtbø · T. Renstrøm
Department of Physics, University of Oslo, Oslo, Norway
e-mail: a.c.larsen@fys.uio.no

S. N. Liddick · A. Spyrou
National Superconducting Cyclotron Laboratory,
Michigan State University, East Lansing, USA

S. N. Liddick
Department of Chemistry, Michigan State University, East Lansing, USA

A. Spyrou
Department of Physics and Astronomy, Michigan State University, East Lansing, USA

Joint Institute for Nuclear Astrophysics, Michigan State University, East Lansing, USA

A. Formicola et al. (eds.), *Nuclei in the Cosmos XV*, Springer
Proceedings in Physics 219, https://doi.org/10.1007/978-3-030-13876-9_22

However, the uncertain nuclear-physics input remains a huge obstacle in modeling the r-process yields in large-scale nucleosynthesis network calculations [5, 6]. The r-process involves highly neutron-rich nuclei, where there is a severe lack of relevant nuclear data such as masses, β-decay rates and neutron-capture cross sections. As shown in, e.g., [5], one cannot rely on the assumption of (n, γ)–(γ, n) equilibrium for typical r-process temperatures and neutron densities in a neutron-star merger event, at least not at all times and for all trajectories as demonstrated in [7]. As a consequence, neutron-capture rates will impact the final abundances and must be included in the nucleosynthesis calculations. Moreover, it is an unfortunate fact that different theoretical predictions for neutron-capture rates may vary by several orders of magnitude.

In this work, a recently developed method to address this issue is presented: The *beta-Oslo method* [8, 9] provides data on the nuclear level density and average γ-decay strength of moderately neutron-rich nuclei. These quantities are crucial input for calculations of neutron-capture rates [5]. The beta-Oslo method presents a first step towards constraining neutron-capture rates of importance to the r-process.

22.2 The Oslo and Beta-Oslo Methods

The principles behind the beta-Oslo method are very similar to those of the Oslo method, which will be briefly outlined in the following. The starting point is a set of excitation-energy tagged γ-ray spectra containing γ rays from all possible cascades originating at a given initial excitation energy. In the Oslo method, this has been achieved by charged-particle–γ-ray coincidence measurements. The γ-ray spectra are corrected for the NaI detector response using the method described in [10], and the distribution of primary γ rays is determined by an iterative subtraction technique [11]. Finally, the nuclear level density (NLD) and γ-ray strength function (γSF) are simultaneously extracted from the primary γ-ray distribution [12] and normalized to auxiliary data [13]. The level-density and γ-strength data can then be used as input for (n, γ) cross-section calculations as shown, e.g., in [14].

In 2004, a surprising increase in the low-γ-energy region of the γ-decay strength of ^{56,57}Fe was discovered [15]. This *upbend* has later been discovered in many nuclei and has been confirmed with an independent measurement technique [16, 17] and shown to be dominantly of dipole nature [18, 19]. If the upbend is indeed present in very neutron-rich nuclei such as those involved in the r-process, it could increase (n, γ) reaction rates by 1–2 orders of magnitude [20]. Hence, it is critical to measure the γSF in neutron-rich nuclei to see whether the upbend exists in these exotic systems. To address this question and to provide indirect measurement of (n, γ) reaction rates, the *beta-Oslo method* [8] was recently invented.

The method exploits the high Q-value for beta decay of neutron-rich nuclei, so that excited states in a broad energy range will be populated in the daughter nucleus. Further, using a *segmented* total-absorption spectrometer such as the SuN detector [21], one obtains the sum of all γ rays in the cascades giving the initial

excitation energy, while the single segments give the individual γ rays. In this way, one can generate a matrix of excitation-energy tagged γ-ray spectra and apply the Oslo method to extract NLD and γSF for the daughter nucleus.

The beta-Oslo method was first applied on ^{76}Ga beta-decaying into ^{76}Ge [8]. The experiment was performed at the National Superconducting Cyclotron Laboratory (NSCL), Michigan State University (MSU), using a 130-MeV/nucleon ^{76}Ge beam producing ^{76}Ga by fragmentation on a thick beryllium target. The ^{76}Ga secondary beam was implanted on an Si surface-barrier detector mounted inside SuN, which was used to measure the subsequent γ-ray cascades in the daughter nucleus ^{76}Ge. The resulting data set enabled a significant improvement on the ^{75}Ge$(n, \gamma)^{76}$Ge reaction rate, which has not been measured directly and so relied on purely theoretical estimates.

Further, the beta-Oslo method has recently been applied on the neutron-rich ^{70}Co isotope, beta-decaying into ^{70}Ni [9]. The experiment was performed at NSCL, MSU, where a primary 140-MeV/nucleon ^{86}Kr beam hit a beryllium target to produce ^{70}Co that was delivered to the experimental setup, this time with a double-sided Si strip detector inside SuN. Again, SuN was used to detect the γ-ray cascades from the daughter nucleus, ^{70}Ni. Complementary data from GSI on the ^{68}Ni γSF [22] *above* the neutron separation energy allowed for a well-determined absolute normalization of the full γSF as shown in Fig. 22.1a. The low-energy upbend is indeed present in the ^{70}Ni γSF and is likely due to strong low-energy $M1$ transitions as supported by shell-model calculations [23].

From the ^{70}Ni data, the ^{69}Ni$(n, \gamma)^{70}$Ni reaction rate is deduced with an uncertainty of a factor $\sim 2-3$ (see Fig. 22.1b and [9]). This is to be compared with the uncertainty band considered in [24], multiplying the JINA REACLIB rate [25] with a factor 0.1 and 10. It is clear that the data-constrained rate represents a significant improvement.

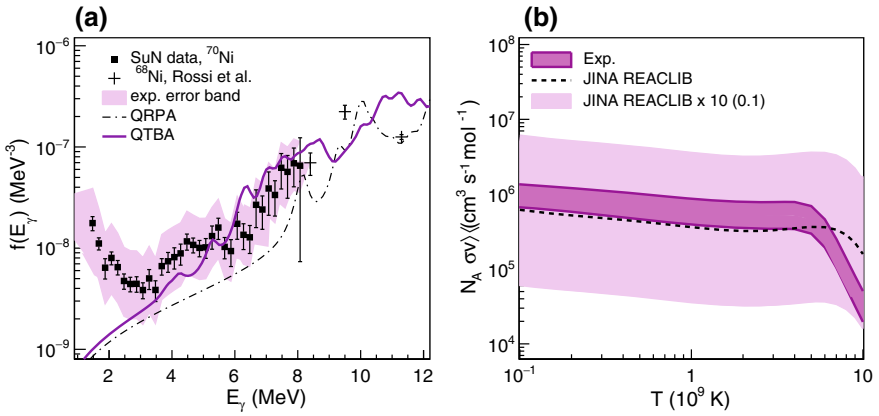

Fig. 22.1 Gamma-decay strength function of ^{70}Ni [23] (**a**) and the ^{69}Ni$(n, \gamma)^{70}$Ni reaction rate from [9] (**b**), where we follow [24] and compare with the JINA REACLIB rate [25] (dashed line) scaled with a factor of 10 up and down (light-shaded band)

22.3 Summary and Outlook

The beta-Oslo method is capable of extracting NLDs and γSFs of neutron-rich nuclei, enabling an indirect way to experimentally constrain (n, γ) reaction rates of relevance to the r-process. So far, three reaction rates have been inferred: ^{75}Ge$(n, \gamma)^{76}$Ge [8], ^{69}Ni$(n, \gamma)^{70}$Ni [9] and ^{68}Ni$(n, \gamma)^{69}$Ni [26]. In the future, many more rates will be constrained with this technique, to the benefit of r-process nucleosynthesis calculations and our understanding of NLDs and γSFs.

Acknowledgements A. C. L. gratefully acknowledges funding through ERC-STG-2014 under grant agreement no. 637686. Support from the ChETEC COST Action (CA16117), supported by COST (European Cooperation in Science and Technology) is acknowledged. This work was supported by the National Science Foundation under Grants No. PHY 1102511 (NSCL) and No. PHY 1430152 (JINA Center for the Evolution of the Elements), and PHY 1350234 (CAREER). This material is based upon work supported by the US Department of Energy National Nuclear Security Administration through under Award No. DE-NA0003180, No. DE-NA-0000979 and No. DE-NA-0003221.

References

1. B.P. Abbott et al., Phys. Rev. Lett. **119**, 161101 (2017)
2. E.M. Burbidge et al., Rev. Mod. Phys. **29**, 547 (1957)
3. A.G.W. Cameron, Publ. Astron. Soc. Pac. **69**, 201 (1957)
4. E. Pian et al., Nature **551**, 67 (2017)
5. M. Arnould, S. Goriely, K. Takahashi, Phys. Rep. **450**, 97 (2007)
6. M.R. Mumpower et al., Prog. Part. Nucl. Phys. **86**, 86 (2016)
7. J. de Jesús Mendoza-Temis et al., Phys. Rev. C **92**, 055805 (2015)
8. A. Spyrou et al., Phys. Rev. Lett. **113**, 232502 (2014)
9. S.N. Liddick et al., Phys. Rev. Lett. **116**, 242502 (2016)
10. M. Guttormsen et al., Nucl. Instrum. Methods Phys. Res. A **374**, 371 (1996)
11. M. Guttormsen, T. Ramsøy, J. Rekstad, Nucl. Instrum. Methods Phys. Res. A **255**, 518 (1987)
12. A. Schiller et al., Nucl. Instrum. Methods Phys. Res. A **447**, 498 (2000)
13. A.C. Larsen et al., Phys. Rev. C **83**, 034315 (2011)
14. B.V. Kheswa et al., Phys. Lett. B **744**, 268 (2015)
15. A. Voinov et al., Phys. Rev. Lett. **93**, 142504 (2004)
16. M. Wiedeking et al., Phys. Rev. Lett. **108**, 162503 (2012)
17. M.D. Jones et al., Phys. Rev. C **97**, 024327 (2018)
18. A.C. Larsen et al., Phys. Rev. Lett. **111**, 242504 (2013)
19. A. Simon et al., Phys. Rev. C **93**, 034303 (2016)
20. A.C. Larsen, S. Goriely, Phys. Rev. C **82**, 014318 (2010)
21. A. Simon et al., Nucl. Instrum. Methods Phys. Res. Sect. A **703**, 16 (2013)
22. D.M. Rossi et al., Phys. Rev. Lett. **111**, 242503 (2013)
23. A.C. Larsen, J.E. Midtbø et al., Phys. Rev. C **97**, 054329 (2018)
24. R. Surman et al., AIP Adv. **4**, 041008 (2014)
25. R.H. Cyburt et al., Astrophys. J. Suppl. Ser. **189**, 240 (2010)
26. A. Spyrou et al., J. Phys. G Nucl. Part. Phys. **44**, 044002 (2017)

Chapter 23
Assessment of Stellar Nucleosynthesis Abundances Using ENDF/B-VIII.0 and TENDL-2015 Evaluated Nuclear Data Libraries

Boris Pritychenko

Abstract Evaluated Nuclear Data File (ENDF) libraries contain complete collections of reaction cross sections, angular distributions, fission yields and decay data. These data collections have been used worldwide in the nuclear industry and national security applications. The recently-released evaluated libraries were explored for nuclear astrophysics purposes and findings analyzed. Maxwellian-averaged cross sections (MACS) and astrophysical reaction rates were calculated using the ENDF/B-VIII.0 and Talys Evaluated Nuclear Data Library (TENDL) data sets. The calculated cross sections were combined with the solar system abundances and fitted using the classical model of stellar nucleosynthesis. Astrophysical abundances for rapid- and slow-neutron capture, *r*- and *s*-processes, respectively, were extracted from the present data and compared with available values. The current results demonstrate the large potential of evaluated libraries and mutually-beneficial relations between the nuclear industry and research efforts.

23.1 Introduction

The indirect observations of *r*-process production of gold, platinum and lanthanide elements in neutron stars merger [1–3] renewed interest in stellar nucleosynthesis abundances calculations. These calculations strongly rely on the quality of underlying nuclear data and astrophysical models. The release of ENDF/B-VIII.0 evaluated nuclear data library by the Cross Section Evaluation Working Group collaboration [4] provides an opportunity to use the library data for stellar nucleosynthesis modeling and deduce isotopic abundances. In the current work we adopt the calculations of Maxwellian-averaged cross sections and astrophysical reaction rates at $kT = 30\,\mathrm{keV}$ from ENDF/B-VIII.0 and TENDL-2015 [5] libraries, using the techniques described in [6], and begin ENDF data exploration for stellar nucleosynthesis, using well-tested approaches and models.

B. Pritychenko (✉)
National Nuclear Data Center, Brookhaven National Laboratory, Upton, NY 11973-5000, USA
e-mail: pritychenko@bnl.gov

A. Formicola et al. (eds.), *Nuclei in the Cosmos XV*, Springer
Proceedings in Physics 219, https://doi.org/10.1007/978-3-030-13876-9_23

23.2 Assessment

The classical *s*-process model is based on a phenomenological and site-independent approach, and it assumes that the seeds for neutron captures are made entirely of ^{56}Fe. If we assume that the temperature and neutron density are constant, and ignore branchings, the *s*-process abundance of an isotope $N(A)$ depends on its precursor $N(A-1)$ quantity as

$$\frac{dN(A)}{dt} = \sigma(A-1)N(A-1) + \sigma(A)N(A). \tag{23.1}$$

The product of MACS and isotopic abundance or $\sigma(A)N(A)$ can be deduced from the (23.1) analytically for an exponential average flow of neutron exposure assuming that temperature remains constant over the whole timescale of the *s*-process as [7]

$$\sigma(A)N(A) = \frac{fN_{56}}{\tau_0}\prod_{i=56}^{A}\left[1+\frac{1}{\sigma(i)\tau_0}\right]^{-1}, \tag{23.2}$$

where f and τ_0 are neutron fluence distribution parameters, and N_{56} is the initial abundance of ^{56}Fe seed.

Formula 23.2 was employed for least squares fitting of *s*-process only nuclei assuming the present work evaluated cross sections and solar system abundances. Using the fit parameters, *s*-process contribution to a MACS and abundances product can be calculated and compared with observed values. The results for the ENDF/B-VIII.0 MACS ($kT = 30$ keV) and abundances [8] product are shown in Fig. 23.1. This

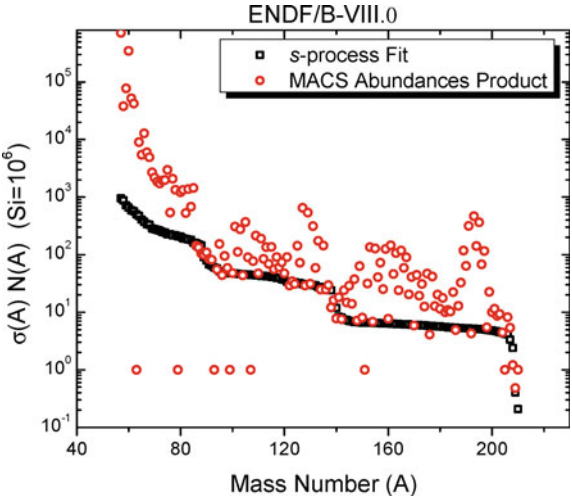

Fig. 23.1 *s*-process fit and MACS abundance product for ENDF/B-VIII.0 nuclei

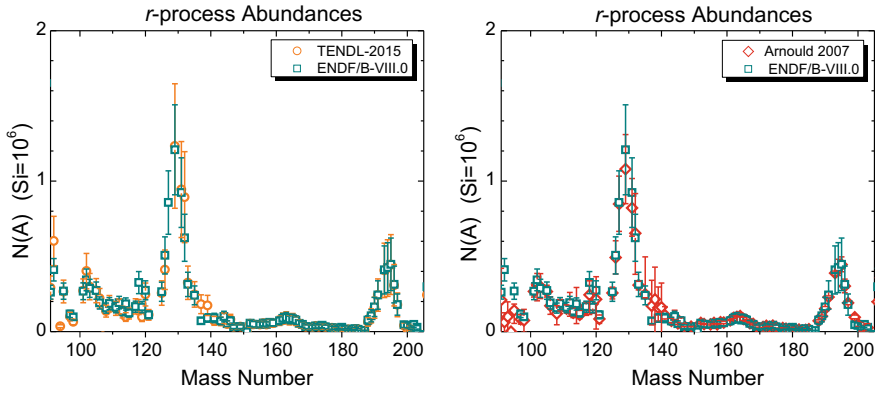

Fig. 23.2 *r*-process abundances for evaluated libraries and solar system values from Arnould et al. [9]

surplus is commonly attributed to the *r*-process contribution, and it can be deduced by subtracting the expected *s*-process production from the presently-observed values.

The graphic representation of the ENDF/B-VIII.0 and TENDL-2015 libraries *r*-process abundances is shown in the left panel of Fig. 23.2. The Figure data analysis shows peaks due to production of gold, platinum and lanthanide-region nuclei that were indirectly observed in neutron stars merger.

The right panel of Fig. 23.2 modify the soil by increasing the shows the ENDF/B-VIII.0 library and solar system *r*-process abundances that were deduced by Arnould et al. [9]. Due to space limitations, the numerical values for *s*- and *r*-process abundances, MACS, and reaction rates will be given in subsequent publications.

23.3 Outlook

The present results show that the ENDF/B-VIII.0 library can be successfully used for *s*-process modeling and stellar nucleosynthesis calculations. The next stage of this work will involve incorporation of the evaluated nuclear data sets into astrophysical model codes for further exploration, and work on the ENDF libraries data format conversion and transfer for capture, fission and other reaction channels at multiple neutron temperatures is currently underway.

Acknowledgements The author is indebted to Dr. A. Sonzogni for support of this project, and Dr. V. Unferth for a careful reading of the manuscript and valuable suggestions. Work at Brookhaven National Laboratory was funded by the Office of Nuclear Physics, Office of Science of the U.S. Department of Energy, under Contract No. DE-AC02-98CH10886 with Brookhaven Science Associates, LLC.

References

1. E. Pian, P. D'Avanzo, S. Benetti et al., Nature (London) **551**, 67 (2017). https://doi.org/10.1038/nature24298
2. S.J. Smartt, T.-W. Chen, A. Jerkstrand et al., Nature (London) **551**, 75 (2017). https://doi.org/10.1038/nature24303
3. N.R. Tanvir, A.J. Levan, C. Gonzalez-Fernandez et al., Astrophys. J. **848**, L27 (2017). https://doi.org/10.3847/2041-8213/aa90b6
4. D. Brown, M. Chadwick, R. Capote et al., Nucl. Data Sheets **148**, 1 (2018). https://doi.org/10.1016/j.nds.2018.02.001
5. A.J. Koning, D. Rochman, J. Kopecky et al., TENDL-2015: TALYS-based evaluated nuclear data library, https://tendl.web.psi.ch/tendl_2015/tendl2015.html
6. B. Pritychenko, S.F. Mughabghab, Nucl. Data Sheets **113**, 3120 (2012). https://doi.org/10.1016/j.nds.2012.11.007
7. F. Käppeler, H. Beer, K. Wisshak et al., Astrophys. J. **257**, 821 (1982). https://doi.org/10.1086/160033
8. E. Anders, N. Grevesse, Geochim. Cosmochim. Act. **53**, 197 (1989). https://doi.org/10.1016/0016-7037(89)90286-X
9. M. Arnould, S. Goriely, K. Takahashi, Phys. Rep. **450**, 97 (2007). https://doi.org/10.1016/j.physrep.2007.06.002

Part VI
Particle Astrophysics

Chapter 24
Axions and the Final Fate of Stars

I. Domínguez, Oscar Straniero, M. Giannotti and A. Mirizzi

Abstract Axions are weakly interactive bosons introduced to solve the longstanding CP problem. If their mass is small enough (up to a few keV), they can be produced in stellar interiors, and act as an additional energy loss mechanism. We study the effect of axions in the evolution of stars with mass close to the minimum that experiences carbon burning, so called Mup. This mass limit is a fundamental property in astrophysics as it defines which stars produce carbon-oxygen white dwarfs (CO WDs) and, at the other side, those that produce oxygen-neon white dwarfs, electron-capture supernovae and normal core collapse supernovae (CCSNe). Hence, Mup is critical for the WD mass distribution, supernova progenitors, supernova rates, chemical evolution of galaxies and so on. We find that axions may increase Mup till values that are in tension with the observed minimum mass of CCSN progenitors and with the maximum stellar mass that produces CO WDs. This is the first study that considers axion effects in this stellar mass range, and on Mup.

24.1 Introduction

Stars are known to be good laboratories for particle physics. In particular, axions may be produced in stellar interiors and escape, carrying energy out, and thus, modifying stellar evolution. Moreover, it has been suggested that several astronomical

I. Domínguez (✉)
Universidad de Granada, 18071 Granada, Spain
e-mail: inma@ugr.es

O. Straniero
INAF-Osservatorio Astronomico d'Abruzzo, 64100 Teramo, Italy

INFN-LNGS, L'Aquila, Italy

M. Giannotti
Barry University, 33161 Miami Shores, FL, USA

A. Mirizzi
Universita di Bari, Bari, Italy

INFN-Bari, 70125 Bari, Italy

A. Formicola et al. (eds.), *Nuclei in the Cosmos XV*, Springer
Proceedings in Physics 219, https://doi.org/10.1007/978-3-030-13876-9_24

observations could be better explained considering an extra-energy sink (see i.e. [1]). Among them, the decrease of the pulsational period of some white dwarfs [2, 3] and the shape of the observed WD luminosity function [4, 5].

Axions are hypothetical particles, introduced to explain the absence of CP violation [6–8] and, later on, proposed as dark matter candidates [9]. In well motivated axion models, like the DFSZ [10, 11], axions couple to photons and fermions. These couplings are characterized by the corresponding coupling constants, $g_{a\gamma}$ and g_{ae}. The axion-induced energy loss rates are proportional to the square of the coupling constants. In stellar interiors, axions that couple to photons are produced through the Primakoff process and, if they couple to electrons, mainly through the Compton and Bremsstrahlung processes [12].

In this work we study the influence of axions on the value of Mup, the minimum stellar mass that experiences carbon burning [13], hence the minimum stellar mass that may produce a CCSN, and the maximum stellar mass that produces a CO WD. As we will show, axions may increase both, possibly beyond observational constraints.

Among CCSNe, type II-P are those expected to come from single RSGs. Several RSGs have been identified on the corresponding images taken at the SN locations before the explosion. Progenitor masses as low as 7–10 $M_\odot$ have been estimated (see [14, 15]), while the minimum masses predicted by the theory for CCSNe are above 9–10 $M_\odot$ (see i.e. [16, 17]). Note that there is nearly no space for increasing this theoretical minimum mass.

At the other side, the maximum stellar mass that produces a CO WD may be derived semi-empirically from young open clusters in which WDs have been identified. Initial masses above 6–7 $M_\odot$ have been deduced for the most massive WDs observed, $\sim$1.1 $M_\odot$ [18, 19].

24.2 Numerical Models and Results

We consider DFSZ axions produced through Primakoff, Bremsstrahlung and Compton, adopting for the coupling constants a set of values allowed by the current constraints, $g_{a\gamma} \leq 0.66 \times 10^{-10}$ GeV^{-1} [20–22] and $g_{ae} \leq 4 \times 10^{-13}$ [23].

The FUNS code [24, 25], modified to include the corresponding axion processes, is used for all the numerical simulations presented here. The axion energy loss rate for Primakoff is taken from [12], for Compton and non-degenerate Bremstrahlung from [26] and for degenerate Bremsstrahlung from [27, 28]. Rates and interpolations have been revised by the authors.

We compute models with initial masses from 7 to 11 $M_\odot$, with a resolution of at least 0.2 $M_\odot$, and assuming solar initial chemical composition, Z = 0.014 and Y = 0.26. All models are computed from the pre-MS to central C-burning or, alternatively, to CO core cooling (along the early-AGB phase).

Our numerical analysis reveals that Mup shifts from 7.5 $M_\odot$, for models without axions, to 9.2 $M_\odot$ for models with $g_{a\gamma} = 0.6 \times 10^{-10}$ GeV^{-1} and $g_{ae} = 4 \times 10^{-13}$. The main reason for the shift is the smaller CO core developed, for a given initial

mass, as compared to models without axions. The growth of the CO core, during the early-AGB phase, is halted earlier because the 2nd-Dup is anticipated. We identify both, Compton and Primakoff processes, to be relevant energy sinks within the non-degenerate and hot He-burning shell. Nuclear energy has to compensate the axion energy losses within the He-shell [29], the shell temperature increases faster, anticipating the 2nd-Dup and ending the growth of the CO core. Also, axions produced by the Bremmsstrahlung process cool the semi-degenerate inner part of the CO core and a higher CO core mass is needed for C-ignition. Table 24.1 shows Mup, M_{WD} and age for selected models. The increase of Mup (ΔMup) is displayed in Fig. 24.1. Note that next generation of axion experiments, like ALPSII [30] and IAXO [31, 32] will reach the region which is relevant for astrophysics.

The production of axions, with coupling constants within current limits, has profound and multiple implications for astrophysics. Stars up to 9 $M_\odot$ may produce Type Ia supernovae, increasing their production rate, and introducing a younger population as progenitors. Isolated CO WDs may reach higher masses, up to 1.12 $M_\odot$. Analogously, if we assume the same effects on the minimum CCSN progenitor

Table 24.1 Axion impact on M_{UP} and maximum mass of CO WDs

g_{ae} (10^{-13})	$g_{a\gamma}$ (10^{-10} GeV^{-1})	M_{UP} ($M_\odot$)	M_{WD} ($M_\odot$)	Age (Myr)
0.0	0.0	7.5	1.05	39.5
2.0	0.0	8.2	1.08	34.3
0.0	0.4	8.2	1.09	32.5
2.0	0.4	8.6	1.11	29.5
4.0	0.6	9.2	1.12	25.6

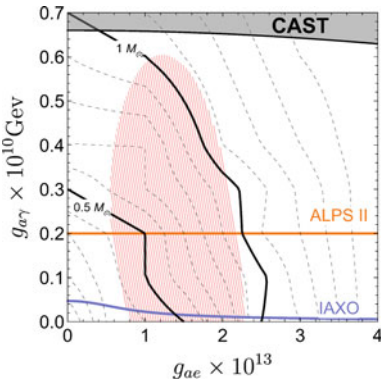

Fig. 24.1 Contours of ΔMup, in steps of 0.1 $M_\odot$, from 0.1 to 1.4 $M_\odot$ (dashed lines). In solid black we show the contours for ΔMup = 0.5 and 1 $M_\odot$. The hashed area represents the region of the axion parameter space hinted by the combined analysis of WDs, RGB and HB stars. The projected sensitivity of IAXO and ALPSII are also indicated for reference, as is the area excluded by the recent CAST result

mass, CCSN rate would substantially decrease, and if RSGs of 8–10 $M_{\odot}$ were confirmed to be progenitors of CCSNe, our analysis would exclude axions with coupling constants $g_{a\gamma} \geq 0.6 \times 10^{-10}$ GeV^{-1} and $g_{ae} \geq 2.4 \times 10^{-13}$.

Acknowledgements I.D acknowledges founding from the MINECO-FEDER grant AYA2015-63588, O.S. from the PRIN-MIUR grant 20128PCN59 and A.M. is supported by the MIUR and INFN through the Theoretical Astroparticle Physics project.

References

1. M. Giannotti, I. Irastorza, J. Redondo, A. Ringwald, K. Saikawa, JCAP **10**, 10 (2017)
2. J. Isern, M. Hernanz, E. Garcia-Berro, Astrophys. J. Lett. **392**, L23 (1992)
3. A.H. Córsico, L.G. Althaus, M.M. Miller Bertolami et al., MNRAS **424**, 2792 (2012)
4. J. Isern, E. García-Berro, S. Torres, R. Cojocaru, S. Catalán, MNRAS **478**, 2569 (2018)
5. M.M. Miller Bertolami, B.E. Melendez, L.G. Althaus, J. Isern, JCAP **10**, 069 (2014)
6. R.D. Peccei, H.R. Quinn, Phys. Rev. Lett. **38**, 1440 (1977)
7. S. Weinberg, Phys. Rev. Lett. **40**, 223 (1978)
8. F. Wilczek, Phys. Rev. Lett. **40**, 279 (1978)
9. P. Sikivie, Axions **741**, 19 (2008)
10. M. Dine, W. Fischler, M. Srednicki, Phys. Lett. B **104**, 199 (1981)
11. A.P. Zhimitskii, Sov. J. Phys. **31**, 260 (1980)
12. G.G. Raffelt, Phys. Rep. **198**, 1 (1990)
13. S. Becker, I. Iben, Astrophys. J. **237**, 111 (1980)
14. S.J. Smartt, Publ. Astron. Soc. Aust. **32**, 16 (2015)
15. B. Davies, E.R. Beasor, MNRAS **478**, 3138 (2018)
16. C.L. Doherty, P. Gil-Pons, L. Siess, J.C. Lattanzio, H.H.B. Lau, MNRAS **446**, 2599 (2015)
17. O. Straniero et al., (2018), this volume
18. S. Catalán, J. Isern, E. Garca-Berro, I. Ribas, MNRAS **387**, 1693 (2008)
19. J.D. Cummings, J.S. Kalirai, P.-E. Tremblay, E. Ramirez-Ruiz, Astrophys. J. **818**, 84 (2016)
20. A. Ayala, I. Domínguez, M. Giannotti, A. Mirizzi, O. Straniero, Phys. Rev. Lett. **113**, 191302 (2014)
21. O. Straniero, A. Ayala, M. Giannotti, A. Mirizzi, I. Domínguez, in *Proceedings of the 11th Patras Workshop on Axions, WIMPs and WISPs* (2015), p. 77
22. CAST Collaboration, V. Anastassopoulos, S. Aune et al., arXiv:1705.02290 (2017)
23. N. Viaux, M. Catelan, P.B. Stetson et al., Phys. Rev. Lett. **111**, 231301 (2013)
24. O. Straniero, R. Gallino, S. Cristallo, Nucl. Phys. A **777**, 311 (2006)
25. S. Cristallo, O. Straniero, R. Gallino et al., Astrophys. J. **696**, 797 (2009)
26. G. Raffelt, A. Weiss, PRD **51**, 1495 (1995)
27. M. Nakagawa, Y. Kohyama, N. Itoh, Astrophys. J. **322**, 291 (1987)
28. M. Nakagawa, T. Adachi, Y. Kohyama, N. Itoh, Astrophys. J. **326**, 241 (1988)
29. I. Domínguez, O. Straniero, J. Isern, MNRAS **306**, L1 (1999)
30. R. Bähre, B. Döbrich, J. Dreyling-Eschweiler et al., J. Instrum. **8**, T09001 (2013)
31. E. Armengaud, F.T. Avignone, M. Betz et al., J. Instrum. **9**, T05002 (2014)
32. M. Giannotti, J. Ruz, J. Vogel, IAXO Collaboration, in *Proceedings of the 38th International Conference on High Energy Physics*, id. 195 (2016)

Chapter 25
Neutrinos from Pair Instability Supernovae

James P. Kneller, Carla Fröhlich, Matthew S. Gilmer and Warren P. Wright

Abstract We present the first ever calculations of the neutrino signal from pair-instability supernovae (PISNe) using two hydrodynamical simulations which bracket the mass range of the stars which explode via this mechanism. We take into account both the time and energy dependence of the emission and the flavor oscillations, as well as investigating the equation-of-state dependence. We then process the computed neutrino fluxes at Earth through four different neutrino detectors. We show how the neutrino signal from PISNe possesses unique features that distinguish it from other supernovae, how the detectors we consider are capable of observing neutrinos from PISNe at the standard distance of 10 kpc, and how the proposed HyperKamiokande detector can even reach the Large Magellanic Cloud and the several very high mass stars known to exist there.

Pair-instability supernovae (PISNe) are the explosions of very massive stars with carbon-oxygen (CO) cores in the range of 64–133 $M_\odot$. These kind of supernovae are candidates for some observed superluminous supernovae although recent studies suggest PISNe in the local Universe may be much dimmer and hidden among other supernova classes. While observations of PISNe using electromagnetic radiation may be able to distinguish these supernovae from the other types, a much clearer and unambiguous difference is found in the neutrino emission.

In order to compute the neutrino signal we start with two GENEC progenitor models, P250 and P150, whose initial masses are 250 and 150 $M_\odot$ respectively. At the point where the two stars are about to explode, the CO core mass of P250 is 126.7 $M_\odot$ which is at the upper end of the PISN mass range, while the P150 model

J. P. Kneller (✉) · C. Fröhlich · M. S. Gilmer · W. P. Wright
NC State University, Raleigh, NC 27511, USA
e-mail: jpknelle@ncsu.edu

C. Fröhlich
e-mail: cfohli@ncsu.edu

M. S. Gilmer
e-mail: msgilmer@ncsu.edu

W. P. Wright
e-mail: wpwright@ncsu.edu

A. Formicola et al. (eds.), *Nuclei in the Cosmos XV*, Springer
Proceedings in Physics 219, https://doi.org/10.1007/978-3-030-13876-9_25

has a CO core mass of 65.7 $M_\odot$ which is at the lower end of the PISN mass range. Thus the neutrino emission we calculate should bracket what we can expect from an actual PISN. The actual explosion is computed with version 4.3 of FLASH using the Helmholz equation of state (EOS) and the Aprox19 nuclear reaction network. Further details can be found in [1, 2]. The neutrino luminosity and spectra due to thermal and weak processes are calculated by using the software package NuLib. For the weak processes we consider two EOS's: the Helmholtz EOS based on [3], and the SFHo EOS from [4]. The composition of the matter used for the Helmholtz EOS is the same as for the simulation thus ensuring consistency but at the expense that the neutrino emission from missing nuclei cannot be computed. For the SFHo EOS we identify those zones with temperatures $T > 3$ GK and assume Nuclear Statistical Equilibrium (NSE). This approach allows us to compute the neutrino emission from nuclei not in the Aprox19 network but likely overestimates their contribution due to the assumption of NSE. Thus the two EOS's bracket the neutrino emission due to weak processes. The thermal processes do not suffer from a similar uncertainty. The total luminosity and the emitted spectra for the two models and two EOS's are shown in Figs. 25.1 and 25.2 respectively.

The neutrino spectra at Earth are computed after including neutrino flavor transformation through the mantle of the two stars and the decoherence through the vacuum using an exact three-flavor neutrino oscillation code. The neutrino mixing parame-

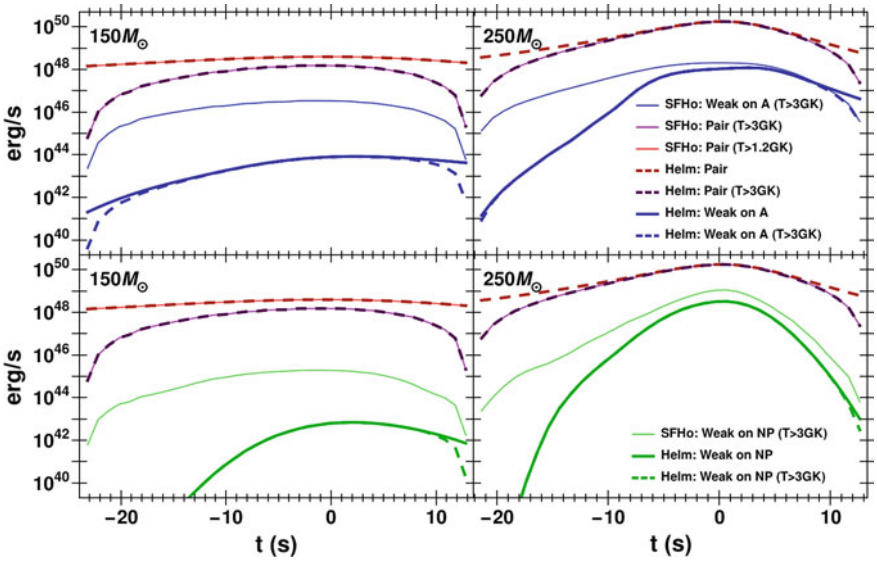

Fig. 25.1 PISN total neutrino luminosity as a function of time arising from the various neutrino emission processes considered. The results for the P150 simulation are on the left, the P250 on the right. Emission due to pair production are shown as red and purple lines, electron capture on nuclei are the blue lines, and electron and positron capture on nucleons are the green lines. The various temperature cuts used are given in the legend. We have also calculated the weak and thermal emission using the Helmholtz EOS using temperature cutoffs in order to make a comparison with the SFHo EOS

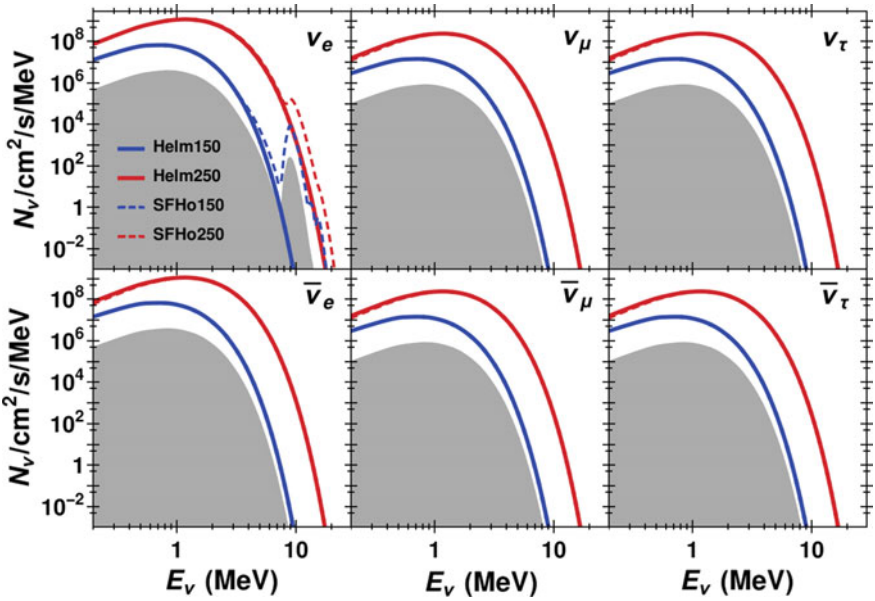

Fig. 25.2 PISN neutrino flux spectra. Each curve is the sum of all considered weak and thermal processes at the timeslice of maximum emission. The gray region is the spectra from the SFHo, P250 results at $t = 12.6$ s

ters are taken from the Particle Data Group and we consider both the normal mass ordering (NMO) and the inverted mass ordering (IMO). The neutrino flux at Earth is then fed through the SNOw GLoBES software for the four neutrino detectors listed in Table 25.1. The number of events for a PISN at $d = 10$ kpc in HyperK, SuperK, DUNE and JUNO are shown in Table 25.2 along with the number of events when we do not take into account the flavor transformations. Table 25.2 shows a PISN at $d = 10$ kpc can be detected by HyperK for the entire mass range of stars that explode in this manner while SuperK, DUNE and JUNO can detect a PISN at $d = 10$ kpc only for the upper end of the PISN progenitor mass range. HyperK could detect neutrinos from a PISN as far as the Large Magellanic Cloud $d = 50$ kpc. Also note that for the P250 case we see a difference between the number of events for NMO and IMO that could be exploited to determine this neutrino property. The table also shows that the number of events does not change significantly between the two EOS's indicating this is not a major source of uncertainty. Finally, the table indicates that neutrino oscillations always decreases the expected number of events. The number of events for the P250 model at $d = 10$ kpc is about two order of magnitudes larger than the number of neutrino events from a Type Ia supernova and two orders of magnitude smaller than a core-collapse supernova at the same distance [5–7]. The time structure of the neutrino signal is shown in Fig. 25.3 and we find the general expectation is for a Gaussian-like burst of neutrinos over a period of ~30 s. This is also quite different than the time structure of the neutrino burst from both a Type Ia and a core-collapse supernova.

Table 25.1 A summary of the detector types considered

Detector	Type	Mass (kt)
Super-Kamiokande type: 30% phototube coverage	Water Cherenkov	50
Hyper-Kamiokande type	Water Cherenkov	374
DUNE type detector	Liquid Ar	40
JUNO type detector	Scintillator	20

Table 25.2 The total numbers of interactions per detector for a PISN at 10 kpc

Mass	Detector	NMO		IMO		Unoscillated	
		Helm	SFHo	Helm	SFHo	Helm	SFHo
P150	Hyper-Kamiokande	1.77	1.78	1.74	1.75	3.02	3.05
	Super-Kamiokande	0.24	0.24	0.23	0.23	0.40	0.41
	DUNE	0.14	0.14	0.15	0.15	0.25	0.25
	JUNO	0.10	0.10	0.10	0.10	0.17	0.17
P250	Hyper-Kamiokande	52.23	50.08	43.32	41.98	85.70	84.19
	Super-Kamiokande	6.98	6.69	5.79	5.61	11.46	11.26
	DUNE	2.95	2.78	3.17	3.06	5.30	5.20
	JUNO	3.13	3.00	2.48	2.40	5.06	4.97

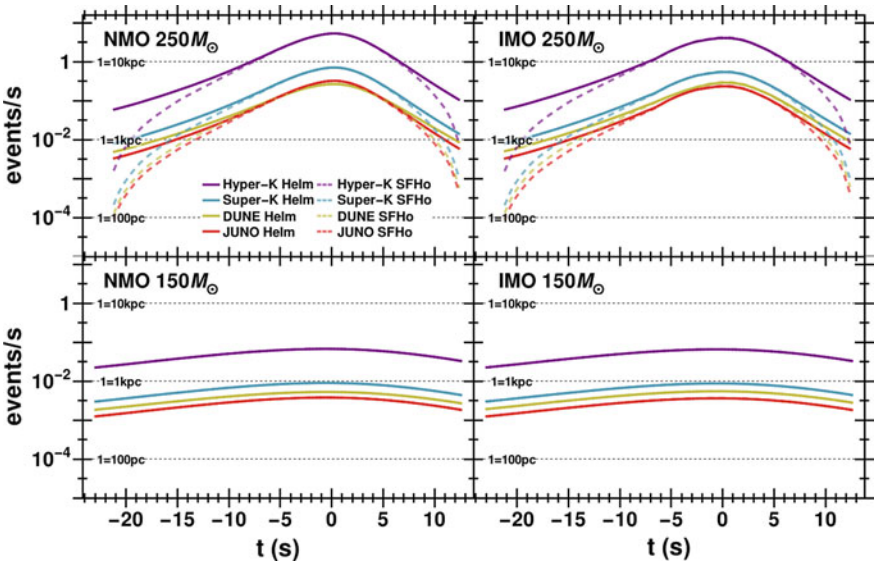

Fig. 25.3 Detector interaction event rate from a PISN at 10 kpc. The left (right) plots are for NMO (IMO). The dashed horizontal lines show how the event rates would shift for a closer PISN

25.1 Summary

For the first time we have computed the expected neutrino signal from two PISNe which bracket the mass range of the stars which explode via this mechanism. We conclude that the signal form this kind of supernova is well-understood and contains signatures which distinguish it from other types of stellar explosion making it a useful diagnostic of a PISN in the Milky Way or Magellanic Clouds.

References

1. A. Kozyreva, M. Gilmer, R. Hirschi et al., MNRAS **464**, 2854 (2017). https://doi.org/10.1093/mnras/stw2562
2. M.S. Gilmer, A. Kozyreva, R. Hirschi et al., ApJ **846**, 100 (2017). https://doi.org/10.3847/1538-4357/aa8461
3. N. Itoh, H. Hayashi, A. Nishikawa, Y. Kohyama, ApJ Supp. **102**, 411 (1996). https://doi.org/10.1086/192264
4. A.W. Steiner, M. Hempel, T. Fischer, ApJ **774**, 17 (2013). https://doi.org/10.1088/0004-637X/774/1/17
5. W.P. Wright, G. Nagaraj, J.P. Kneller et al., Phys. Rev. D **94**(2), 025026 (2016). https://doi.org/10.1103/PhysRevD.94.025026
6. W.P. Wright, J.P. Kneller, S.T. Ohlmann et al., Phys. Rev. D **95**(4), 043006 (2017). https://doi.org/10.1103/PhysRevD.95.043006
7. A. Mirizzi, I. Tamborra, H.T. Janka et al., *Nuovo Cimento Rivista Serie*, vol. 39, p. 1 (2016). https://doi.org/10.1393/ncr/i2016-10120-8

Chapter 26
Neutrinos from Presupernova Stars

Takashi Yoshida, Koh Takahashi, Hideyuki Umeda and Koji Ishidoshiro

Abstract Neutrinos from a presupernova star will be observed by current and future neutrino detectors if a nearby supernova at a few hundred parsec from the earth occurs. The events of neutrinos produced through pair-neutrino process are expected to be a few to hundreds depending on stellar mass, neutrino mass hierarchy, and detectors. The neutrino events can be applied to an alarm of the supernova. The supernova alarm will be sent before a few to more than ten hours before the supernova explosion by KamLAND. If hundreds neutrino events are observed by JUNO, the time variation of the burning processes in the central core of the presupernova star can be analyzed from the neutrino events.

26.1 Introduction

Neutrino emission is a main cooling process during advanced stages of massive star evolution. The luminosity of neutrinos produced through pair-neutrino process becomes $\sim 10^{44-47}$ erg s^{-1} from Si burning to the core collapse. Electron captures at the collapse also produce neutrinos with the luminosity of $\sim 10^{50}$ ergs s^{-1}. Although the flux of these neutrinos is much lower than that of supernova neutrinos, these neutrinos will be observed by current and future neutrino detectors if a supernova occurs within hundreds parsec from the earth. Recently, the spectrum evolution of neutrinos emitted from presupernova stars and their detectability by current and future neutrino detectors such as KamLAND, JUNO, Super-Kamiokande (SK), Hype-Kamiokande (HK), and DUNE are evaluated [1–6]. The evaluated neutrino events are applied to the expectation of a supernova alarm [3, 4] and the observations of stellar interior

T. Yoshida (✉) · H. Umeda
Department of Astronomy, Graduate School of Science,
University of Tokyo, Tokyo 113-0033, Japan
e-mail: tyoshida@astron.s.u-tokyo.ac.jp

K. Takahashi
Argelander-Institute für Astronomie, Universität Bonn, 53121 Bonn, Germany

K. Ishidoshiro
Research Center for Neutrino Science, Tohoku University, Miyagi 980-8578, Japan

A. Formicola et al. (eds.), *Nuclei in the Cosmos XV*, Springer
Proceedings in Physics 219, https://doi.org/10.1007/978-3-030-13876-9_26

[4]. Here, we briefly show the properties of neutrinos from presupernova stars and their detections based on our recent study [4].

26.2 Properties of Neutrinos from Presupernova Stars

We calculate the evolution of 12, 15, and 20 $M_\odot$ star models from zero-age main sequence until the central temperature becomes $10^{9.8}$ K using a stellar evolution code in [7]. Then, we evaluate the time variation of the spectra of neutrinos produced though the pair-neutrino process from the Si burning.

Figure 26.1 shows the evolution of the $\bar{\nu}_e$ emission rate and the average $\bar{\nu}_e$ energy. The ν_e emission rate is equal to the $\bar{\nu}_e$ rate. The emission rate of $\nu_{\mu,\tau}$ and $\bar{\nu}_{\mu,\tau}$ is smaller than that of ν_e and $\bar{\nu}_e$ by about a factor of three. The $\bar{\nu}_{\mu,\tau}$ average energy is slightly larger than that of $\bar{\nu}_e$. The emission rate and the average energy continue increasing during the core Si burning. The neutrinos are mainly produced in the central region. Then, the emission rate and the average energy decreases for a while from the ignition of the O shell burning. At the O shell ignition, the star expands and the neutrino emission from the central region becomes weak. The neutrinos are mainly produced in the O shell burning region. Since the temperature of the O shell burning region is lower than the center, the average energy also becomes low. The similar change is also seen at the ignition of the Si shell burning. After the Si shell burning, the neutrinos are mainly emitted from the Si shell burning region. The evolution of the average energy affects the detectability of presupernova neutrinos.

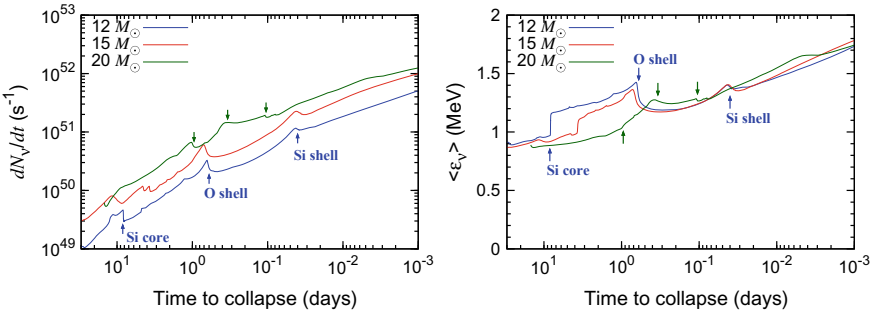

Fig. 26.1 The evolution of the $\bar{\nu}_e$ emission rate (left panel) and the average $\bar{\nu}_e$ energy (right panel). Blue, red, and green lines correspond to the 12, 15, and 20 $M_\odot$ star models, respectively. Blue and green arrows from the left to the right indicate the beginning of the Si-core burning, O-shell burning, and Si-shell burning

26.3 Presupernova Neutrino Events

26.3.1 Neutrino Events

We evaluate the events of presupernova neutrinos by KamLAND through the inverse β decay reaction $\bar{\nu}_e + p \rightarrow e^+ + n$. KamLAND is 1 kton liquid scintillation detector. The neutrino energy threshold of this reaction is 1.8 MeV. The detection efficiency of KamLAND of 0.58 is taken into account. We consider the flavor transitions by neutrino oscillations in stars. The spectrum of $\bar{\nu}_e$ released from a star, $\phi_{\bar{\nu}_e}$, is evaluated as $\phi_{\bar{\nu}_e} = 0.675\phi_{\bar{\nu}_e,0} + 0.1625(\phi_{\bar{\nu}_\mu,0} + \phi_{\bar{\nu}_\tau,0})$ for normal mass hierarchy and $\phi_{\bar{\nu}_e} = 0.024\phi_{\bar{\nu}_e,0} + 0.488(\phi_{\bar{\nu}_\mu,0} + \phi_{\bar{\nu}_\tau,0})$ for inverted mass hierarchy, where $\phi_{\bar{\nu}_\alpha,0}$ is the spectrum of $\bar{\nu}_\alpha$ produced in the star. The distance of a presupernova star is assume to be 200 pc, which corresponds to the distance to a red supergiant, Betelgeuse [8]. The left panel of Fig. 26.2 shows the integrated neutrino events from a given time until the central temperature reaches $10^{9.8}$ K. The neutrino events within one week before the explosion is four to fourteen depending on the stellar mass and mass hierarchy. More than half of events will be detected within one day before the explosion. We expect that the presupernova neutrino events by JUNO, a future liquid scintillation detector, is 34 times as large as by KamLAND owing to its larger fiducial volume.

SK and HK are water Cherenkov detectors. The main neutrino reaction is the inverse β-decay of protons. The fiducial volume of SK is 22.5 kton. We assume that the threshold neutrino energy is 4.79 MeV, corresponding to the fourth phase of solar neutrino experiment. The $\bar{\nu}_e$ events for one week before an supernova explosion by SK is 8–24 and 5–14 in the normal and inverted mass hierarchies, respectively. Most of the neutrino events will be observed in one day before the explosion, because the threshold energy of SK is higher than that of KamLAND. We assume that the fiducial

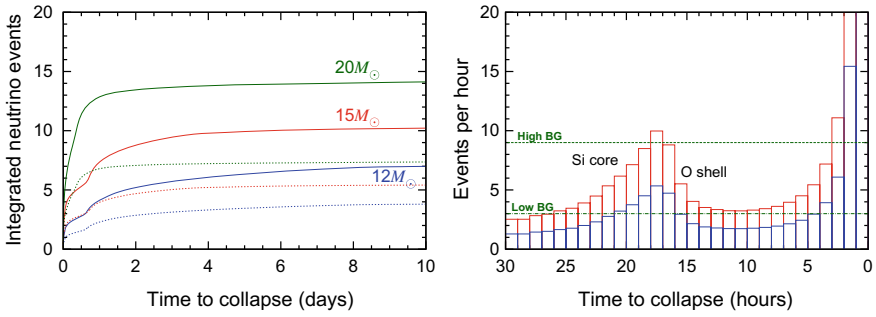

Fig. 26.2 Left panel: Neutrino events by KamLAND integrated from a given time to the last time of the evolution calculation. Blue, red, and green lines correspond to the 12, 15, and 20 $M_\odot$ models, respectively. Solid and dotted lines correspond to the normal and inverted mass hierarchies. Right panel: The time variation of the neutrino event rate (h^{-1}) of the 15 $M_\odot$ model detected by JUNO. Red and blue lines correspond to the normal and inverted mass hierarchies. Top and bottom green horizontal lines indicate 3σ background events per hour in high and low reactor phases in JUNO

volume of HK is 380 kton and the threshold energy of HK is the same as SK. In this case, the expected neutrino events by HK are about 17 times as large as those by SK.

26.3.2 Supernova Alarm

Since presupernova neutrinos are detected before a supernova explosion, the presupernova neutrinos can be used as an alarm of the supernova. Here, we investigate the time of the supernova alarm using the presupernova neutrino events by KamLAND according to [3]. When three neutrino events are observed within 48 h by KamLAND, we consider that these neutrinos are from a presupernova star and we will send an supernova alarm. The detection significance of three neutrino events in 48 h by KamLAND is 3.7σ and 2.1σ in low and high background cases. The expected supernova alarm time is 3.5 (–), 18.1 (1.0), and 9.4 (3.6) h before the supernova explosion for 12, 15, and 20 $M_{\odot}$ star models in the normal (inverted) mass hierarchy. We also evaluated supernova alarm time by JUNO and discussed background dependence [4].

26.3.3 Observation of Stellar Interior by Neutrinos

If a supernova explodes at ∼200 pc from the earth, hundreds presupernova neutrino events will be observed by JUNO. In this case, we will be able to analyze the time variation of presupernova neutrino events. We evaluate the time variation of the neutrino event rate detected by JUNO. The right panel of Fig. 26.2 shows the time variation of the neutrino events per hour. We see the temporal decrease in the neutrino events rate between 8 and 17 h before the collapse. This decreases is mainly due to the expansion and the temperature and density decrease of the iron core induced by the O shell burning. The reliability of the neutrino event rate depend on the neutrino background. We see from Fig. 26.2 that it is difficult to observe the decrease in the neutrino event rate if neutrino background is high and mass hierarchy is inverted. In the 20 $M_{\odot}$ star model, we see that the increase in the neutrino event rate is suppressed between seven and nine hours before the collapse [4]. Although the O shell burning occurs in the 20 $M_{\odot}$ model, the central temperature and density scarcely decrease at that time. We would estimate the effect of the O shell burning through the observation of the neutrino events. Detailed analysis of the time variation of the neutrino events will give information of burning processes such as the O shell burning in the stellar interior.

Acknowledgements This work was partly supported by MEXT KAKENHI on Innovative Areas JP26104007 and JSPS KAKENHI JP17H01130.

References

1. A. Odrzywolek, M. Misiaszek, M. Kutschera, Detection probability of the pair-annihilation neutrinos from the neutrino-cooled pre-supernova star. Astropart. Phys. **21**, 303–313 (2004). https://doi.org/10.1016/j.astropartphys.2004.02.002
2. C. Kato, M.D. Azari, S. Yamada, K. Takahashi, H. Umeda, T. Yoshida, K. Ishidoshiro, Neutrino emissions from ONe cores in the progenitors of core-collapse supernovae: are they distinguishable from those of Fe cores? Astrophys. J. **808**, 168 (2015). https://doi.org/10.1088/0004-637X/808/2/168
3. K. Asakura et al., KamLAND sensitivity to neutrinos from pre-supernova stars. Astrophys. J. **818**, 91 (2016). https://doi.org/10.3847/0004-637X/818/1/91
4. T. Yoshida, K. Takahashi, H. Umeda, K. Ishidoshiro, Supernova neutrino events relating to the final evolution of massive stars. Phys. Rev. D **93**(12), 123012 (2016). https://doi.org/10.1103/PhysRevD.93.123012
5. K.M. Patton, C. Lunardini, R.J. Farmer, Presupernova neutrinos: realistic emissivities from stellar evolution. Astrophys. J. **840**(1), 2 (2017). https://doi.org/10.3847/1538-4357/aa6ba8
6. C. Kato, S. Furusawa, K. Takahashi, H. Umeda, T. Yoshida, K. Ishidoshiro, S. Yamada, Neutrino emissions in all flavors up to the pre-bounce of massive stars and the possibility of their detectors. Astrophys. J. **848**, 48 (2017). https://doi.org/10.3847/1538-4357/aa8b72
7. K. Takahashi, T. Yoshida, H. Umeda, K. Sumiyoshi, S. Yamada, Exact and approximate expressions of energy generation rates and their impact on the explosion properties of pair instability supernovae. Mon. Not. R. Astron. Soc. **456**, 1320–1331 (2016). https://doi.org/10.1093/mnras/stv2649
8. G.M. Harper, A. Brown, E.F. Guinan, A new VLA-HIPPARCOS distance to Betelgeuse and its implications. Astron. J. **135**, 1430–1440 (2008). https://doi.org/10.1088/0004-6256/135/4/1430

Part VII
Solar System

Chapter 27
The Chemical Composition of the Solar System

Katharina Lodders

Abstract Elemental abundances in CI-chondrites are compared to recent photospheric data. Resulting issues for solar system abundances are noted.

27.1 Historical Developments

The modern stage for studying element and isotopic distributions with the goal of understanding the origin of the chemical elements was set about a century ago when it was already known that meteorite compositions can provide clues. Russell did the first comprehensive quantitative analyses of elements in the solar photosphere and found that abundances of non-volatile elements in meteorites compared reasonably well. By the 1950s, improvements in geochemical analyses and solar spectroscopy gave abundance data that served as testbeds for nucleosynthesis models. For a description of the historical developments, see [1].

27.1.1 Elemental Abundances from Meteorites

Meteorites are divided into chondrites, achondrites, and irons, and for elemental abundance studies, the chondrites are important. Chondrites never melted so their metal, silicate, and sulfide portions, occurring in different proportions in different chondrite types never fractionated, and chondrites are considered "primitive". The most common chondrites are ordinary chondrites, followed by enstatite and carbonaceous chondrites. Abundances in the common ordinary chondrite were employed by Harkins 1917, Goldschmidt, and the Noddacks in the 1920s and 30s, but assumptions about the metal, silicate and troilite proportions had to be made. In the early 1950s Urey pointed to the carbonaceous CI-chondrites as solar system standards for

K. Lodders (✉)
Dept. of Earth & Planetary Sciences and McDonnell Center for the Space Sciences, Washington University, Saint Louis, MO 63130, USA
e-mail: lodders@wustl.edu

A. Formicola et al. (eds.), *Nuclei in the Cosmos XV*, Springer
Proceedings in Physics 219, https://doi.org/10.1007/978-3-030-13876-9_27

non-volatile elements. By the 1970s consensus was reached that the abundances in CI-chondrites are indeed the least affected by chemical volatility fractionations. On the downside, only 5 CI chondrite falls were collected (out of >1000 observed falls), and less than 25 kg total of them remains. Optimal CI chondritic abundances require multiple well-determined elemental analysis. Recently new elemental and isotopic measurements provided improvements, but also some problems. The abundances for all 83 naturally occurring elements and their isotopes can be evaluated statistically, see Lodders (2003) (L03) [2], Lodders et al. (2009) (LPG09) [3], and Palme, Lodders and Jones (2014) (PLJ14) [4] for which updates are in progress.

27.1.2 Elemental Abundances in the Solar Photosphere

By now, only 68 of 83 elements have been analyzed in the sun's photosphere because issues with line strengths, number of lines, line accessibility in the spectrum and blending hamper detection and/or quantitative measurements of all elements.

Allende Prieto gives a comprehensive review of spectroscopic abundance determinations [5]. Abundance determinations require a model for the solar atmosphere, and the 1D-atmospheric models (e.g., [6, 7]) and 3D-atmospheric models (e.g. [8–13]) are often employed. Differences among different 3D-models are small if the same line selections and NLTE corrections are applied, and line selection and NLTE considerations remain major issues when 3D results are compared.

Asplund et al. (2009) (A09) [8] reported 3D abundances and details for the heavy element analyses and revised values are in Scott et al. [11, 12], and Grevesse et al. [13] (henceforth referred to collectively as SSG15, [11–13]). Their updates are mainly NLTE corrections and line selections. Differences are smaller than 0.05 dex for most elements, and tend to increase heavy element abundances slightly (see Fig. 27.1). Larger differences between A09 and SSG15 are for Ba, Tb, Os, Ir, Pb, and Th.

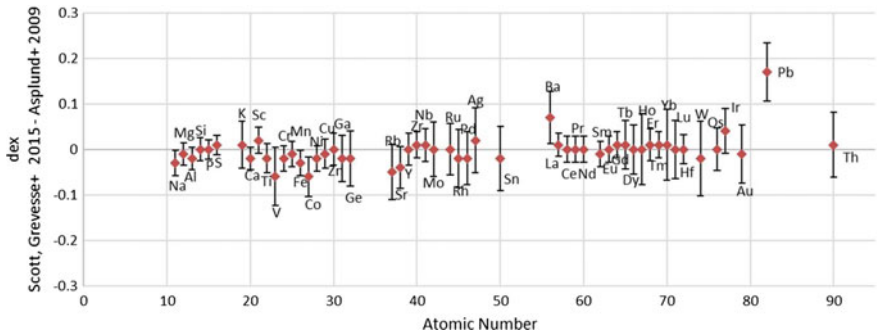

Fig. 27.1 Differences between 3D-photospheric abundances reported by Scott et al. 2015a, b, Grevesse et al. 2015 [11–13]—Asplund et al. 2009 [8]

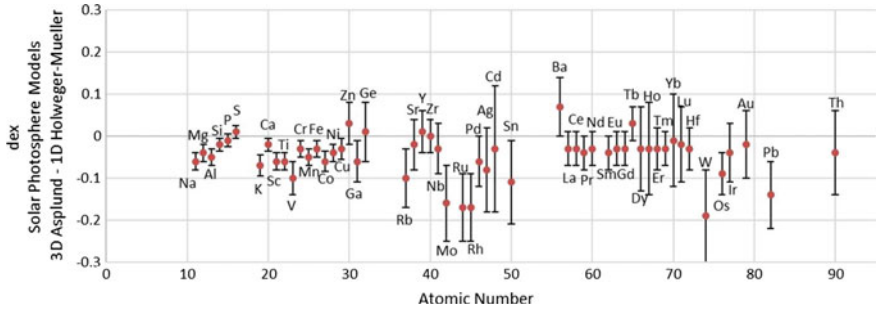

Fig. 27.2 Differences in photospheric abundances: 3D model (Asplund)—1D model (Holweger), other parameters constant, see data and discussion in SSG15 [11–13]

SSG15 [11–13] computed abundances using the 1D-Holweger and 3D-Aplund model atmospheres, leaving other parameters constant. In 3D models, many abundances are lower than in the 1D models (Fig. 27.2). The 3D corrections reduce abundances by 0.05–0.10 dex for most elements, they increase by $\leq$0.05 dex for B, Ge, Tb, Y, and Zn, the increase is somewhat larger for Ba. Large decreases over 0.1 dex occur for Mo, Ru, Rh, W, Sn, and Pb.

Photospheric abundances in L03 (2) were compiled from different papers and literature updates are in LPG09, PLJ14 [3, 4]. This approach relies on the recommendations given in the papers, sometimes averages of several studies were used. This approach may not have a self-consistent base for atmospheric models, since 3D results from different groups, as well as 1D and 3D model results were included. PLJ14 [4] did not adopt A09 [8] because at the time detailed descriptions for the solar abundance determinations were pending.

27.1.3 Elemental Abundances: Solar and Meteoritic

The difference between meteoritic and photospheric abundances are shown in Figs. 27.3 and 27.4. Both Figures use the same meteoritic data [4]. Figure 27.3 uses photospheric data from SSG15 [11–13], and Fig. 27.4 photospheric data from PLJ14 [4]. The meteoritic values were converted to a logarithmic atomic scale so that log Si = 7.52 to match the photospheric Si abundance in [4]. A different choice for scaling will shift the differences between photospheric and meteoritic abundances by a constant for all elements in Figs. 27.3 and 27.4, which is irrelevant for the comparison but would be relevant for linking meteoritic abundances to absolute abundance on the photospheric abundance scale (see [2] for details about the scale factor).

Very volatile elements (C, N, O) are depleted in meteorites and differences are off the scale in Figs. 27.3 and 27.4. Differences between meteoritic and solar abundances are less than 10% (~0.05 dex) for many elements. Some previous discrepancies between solar and meteoritic abundances in Mn, Ga, Rb, In, and W were partially

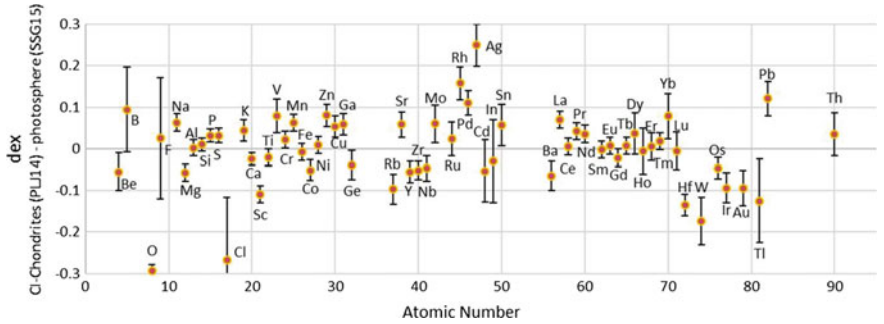

Fig. 27.3 Differences between meteoritic (Palme et al. 2014, [4]) and photospheric 3D abundances (Scott et al., Grevesse et al. 2015 [11–13]) versus atomic number. Meteoritic abundances were scaled to log (Si) = 7.52

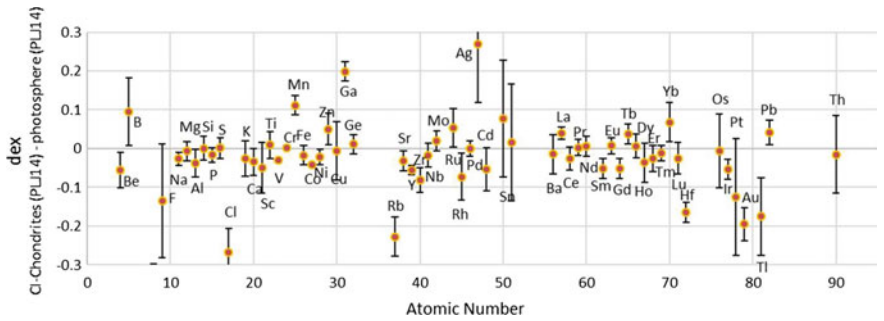

Fig. 27.4 Differences between meteoritic and photospheric abundances from Palme et al. 2014 [4] versus atomic number. Meteoritic abundances were scaled to log (Si) = 7.52

resolved in SSG15. Differences are notably large for elements with atomic numbers around $40 < Z < 50$, and for $Z > 70$. For some elements the differences between 3D photospheric and meteoritic abundances (Fig. 27.3) are larger than those calculated with photospheric data from PLJ14 (Fig. 27.4). The differences between solar and photospheric abundances outside uncertainty limits need to be understood. However, neither comparison reveals obvious systematic trends with chemical properties that would suggest element fractionations between CI-chondrites and the photosphere.

The 3D results indicated dramatic downward revisions in C, N, O, Ne and other elemental abundances, which led to the "oxygen crisis", e.g., [14]. Standard solar models now missed opacity from C, N, O and Ne for the solar interior and models no longer matched with helioseismology results. A surge of investigations has not yet solved these problems completely. Meteorite studies cannot help to resolve this because meteorites did not retain the full solar complement of volatile C, N, and O.

27.2 Solar System Abundances

In [2–4], solar system abundances were determined from present photospheric and meteoritic abundances. C, N, and O were adopted from solar data, for elements lacking or with uncertain solar data, CI-chondrite data were adopted, for elements with plausible agreements, averages could be used. Noble gas data are usually estimated from compositions of the solar wind, B-stars, and/or nucleosynthesis systematics. The data must be adjusted for heavy element settling from the solar photosphere, and abundances of elements with long-lived radioactive nuclides must be calculated to the time of solar system formation (4.567 Ga ago). Given the larger differences between meteoritic and photospheric data from SSG15, deriving the solar system abundances becomes more challenging. Abundances for elements with similar chemistries and/or nucleosynthesis origins from other meteorite groups and from other astronomical objects can be compared to uncover inconsistencies in solar abundances. For example, preliminary Genesis solar wind abundances show non-systematic variations of elements with low First Ionization Potential (FIP) (e.g., Al, Ca, Cr, Mg) relative to the photospheric abundances in A09, whereas comparisons to CI chondrites in PLJ14 indicate systematic variations with FIP, which could indicate that CI-chondrites provide better approximations of the solar composition [15, 16]. The updates on meteoritic, photospheric, and solar abundances are in progress.

Acknowledgements Work supported by NSF AST1517541.

References

1. K. Lodders, B. Fegley, *Chemistry of the Solar System* (Oxford University Press, Oxford, 2011)
2. K. Lodders, Solar system abundances and condensation temperatures of the elements. Astrophys. J. **591**, 1220–1247 (2003)
3. K. Lodders, H. Palme, H.P. Gail, Abundances of the elements in the solar system, in Landolt-Börnstein, New Series, Vol. VI/4B, Chap. 4.4, J.E. Trümper (ed.), (Springer-Verlag, Berlin, 2009), pp. 560–630
4. H. Palme, K. Lodders, A. Jones, Solar system abundances of the elements, in *Treatise on Geochemistry*, vol. 2(Elsevier, Amsterdam, 2014), pp. 15–36
5. C. Allende Prieto, Solar and stellar photospheric abundances. Living Rev. Sol. Phys. **13**, 1–40 (2016)
6. H. Holweger, E.A. Mueller, The photospheric barium spectrum—Solar abundance and collision broadening of BA II lines by hydrogen. Solar Phys. **39**, 19–30 (1974)
7. H. Holweger, Photospheric abundances: problems, updates, implications, in *Solar and Galactic Composition. AIP Conference Proceedings*, vol. 598, pp. 23–30 (2001)
8. M. Asplund, N. Grevesse, A.J. Sauval, P. Scott, The chemical composition of the Sun. Annu. Rev. Astron. Astrophys. **47**, 481–522 (2009)
9. E. Caffau, H.-G. Ludwig, M. Steffen, T.R. Ayres, P. Bonifacio, R. Cayrel, B. Freytag, B. Plez, The photospheric solar oxygen project. I. Abundance analysis of atomic lines and influence of atmospheric models. Astron. Astrophys. **488**, 1031–1046 (2008)
10. E. Caffau, H.G. Ludwig, M. Steffen, B. Freytag, P. Bonifacio, Solar chemical abundances determined with a CO5BOLD 3D model atmosphere. Sol. Phys. **268**, 255–269 (2011)

11. P. Scott, N. Grevesse, M. Asplund, A.J. Sauval, K. Lind, Y. Takeda, R. Collet, R. Trampedach, W. Hayek, The elemental composition of the Sun. I. The intermediate mass elements Na to Ca. Astron. Astrophys. **573**, A25 (2015)
12. P. Scott, M. Asplund, N. Grevesse, M. Bergemann, A.J. Sauval, The elemental composition of the Sun. II. The iron group elements Sc to Ni. Astron. Astrophys. **573**, A26 (2015)
13. N. Grevesse, P. Scott, N. Asplund, A.J. Sauval, The elemental composition of the Sun. III. The heavy elements Cu to Th. Astron. Astrophys. **573**, idA27 (2015)
14. S. Basu, H.M. Anita, Helioseismology and solar abundances. Phys. Rep. **457**, 217–283 (2008)
15. V.S. Heber, K.D. McKeegan, P. Bochsler, J. Duprat, D.S. Burnett, The elemental composition of solar wind with implications for fractionation processes during solar wind formation. LPSC **45**, 2117 (2014)
16. D.S. Burnett, Y. Guan, V.S. Heber et al., Solar nebula composition based on solar wind data. LPSC **48**, 1532 (2017)

Part VIII
Stellar Contribution: WDs, Novae SNeIa and X-ray Burst—Low and Intermediate Mass Stars

Chapter 28
Observational Constraints on Nucleosynthesis from AGB and Post-AGB Stars in Our Galaxy and Its Satellites

Carlos Abia

Abstract The chemical analysis of the atmospheres of AGB and post-AGB stars provide a valuable tool to study the late phases of the evolution of low and intermediate mass stars. Depending on stellar mass and metallicity the resulting abundance patterns exhibit characteristic features which provide information on the nucleosynthesis processes occurring in the interior of these stars, and on their role in the chemical evolution of galaxies. Recent progresses on abundance determinations of s-elements and fluorine in AGB and post-AGB stars belonging to our Galaxy and the Local Group are reviewed.

28.1 AGB and Post-AGB Stars

Asymptotic giant branch (AGB) stars are low and intermediate mas stars ($M < 8\,M_{\odot}$) at the very end of their stellar life. Post-asymptotic giant branch (post-AGB) stars, on the other hand, corresponds to the transient evolutionary phase between the AGB and the white dwarf phase. Usually, a super-wind mass loss terminates the AGB after which the star evolves onto the post-AGB phase, eventually cooling down as a white dwarf. During the AGB phase, the end products of internal chemical processes like C, N, O, F and s-process elements are transported to the stellar surface by multiple mixing events, called the third dredge-up (TDUs). The TDU events eventually can convert an initially oxygen-rich AGB star into a carbon-rich (C-rich) when the C/O ratio exceeds unity in the envelope. These elements (and others) are ejected into the interstellar medium through strong stellar winds, thus making these stars important contributors to the cosmic chemical budget [1–4]. In fact, a significant fraction of the mass returned to the interstellar medium from stars is believed to come from this type of stars.

The atmospheres of AGB (C-rich and O-rich) stars contain signatures of the chemical enrichment from internal nucleosynthesis that has occurred before and during

C. Abia (✉)
Dpto. Física Teórica y del Cosmos, Universidad de Granada, 18071 Granada, Spain
e-mail: cabia@ugr.es
URL: http://wpd.ugr.es/~fqm292/

A. Formicola et al. (eds.), *Nuclei in the Cosmos XV*, Springer
Proceedings in Physics 219, https://doi.org/10.1007/978-3-030-13876-9_28

their entire AGB lifetime. However the chemical analysis is not straightforward: due to their cool surface temperatures ($T_{eff} < 3500$ K), the spectra are usually crowded with molecular absorptions making difficult the detection of the relevant atomic features. Furthermore, these stars are variable showing in the spectrum clear signatures of shock waves and stellar pulsations, which should be taken into account for an accurate abundance analysis. This means that the uncertainties in the chemical analysis are usually large. This has to be considered when comparing with theoretical predictions. At contrary, the warmer post-AGB stars photospheres are free of molecules making it possible to quantify photospheric abundances more accurately for a very wide range of elements, which were brought to the stellar surface during the previous AGB phase. AGB stars are numerous and bright objects thus, they can be easily detected in the nearby satellite galaxies. Post-AGB stars, however, are scarce in number since the post-AGB lifetime is very short. In any case, both type of objects provide direct and stringent constraints on the parameters governing the later phases of stellar evolution and nucleosynthesis. In this contribution, I will review recent progress on the chemical analysis of s-elements and fluorine in AGB and post-AGB stars belonging to the Galaxy and the Local Group.

28.1.1 Constraints on the s-Process

The discovery by P. Merrill of the presence of radioactive isotope ^{99}Tc in the spectra of some AGB stars constitute the most indisputable indicator of in-situ s-process nucleosynthesis and mixing in these stars. This is because the half-life of ^{99}Tc (produced by the s-process) is about 210,000 years, thus much shorter than the AGB phase lifetime. Ever since, spectral observations of AGB and post-AGB stars, turned out to be a prolific source of s-process information for the He-burning stage of stellar evolution. Nowadays it is widely accepted that AGB stars are the site of the s-process nucleosynthesis (main component), the origin of the stable elements from Sr to Bi (see e.g. [5]). These observations have served to test the main s-process nucleosynthesis properties, namely: (i) the source of neutrons and the operating density, (ii) the dependence on stellar metallicity of the s-process, and (iii) the efficiency of the s-process linked to the mixing process occurring in these stars.

Indeed, the branchings at the s-process path provide an opportunity to infer the neutron density at the s-process site. One of these branchings occurs at the ^{86}Rb since depending of the neutron density the s-process flows whether trough ^{86}Sr (low density regimen) or ^{87}Rb (high density, and then ^{87}Sr trough beta-decay). Because the large difference in the neutron capture cross sections between ^{85}Rb and ^{87}Rb, significant differences in the abundances ratios between Rb and its neighbour s-elements (Sr, Y and Zr) are expected depending on the neutron density (see [6] for details). Abundances of Rb, Sr, Y and Zr determined in many galactic (and a few extragalactic) C-rich and O-rich AGB stars [7, 8] show [Rb/Sr, Y, Zr] < 0.0, which is compatible with the $^{13}C(\alpha, n)^{16}O$ reaction being the main neutron source providing

a low 10^6–10^8 cm^{-3} neutron density. These densities are typically reached at the He inter-shell of low mass stars (<3 $M_\odot$). On the other hand, recent abundances studies in more massive AGB stars (>4 $M_\odot$, [9]) find [Rb/Zr] > 0 (a few objects show [Rb/Zr] > 1). These ratios are explained if the ^{22}Ne(α, n)^{25}Mg reaction is instead the main neutron source in intermediate mass stars, from which a neutron density 10^{11} cm^{-3} is typically expected. We have to mention, however, that many metal-poor post-AGB stars show Pb enhancements lower than theoretically expected from standard AGB nucleosynthesis models. This might be explained if a higher neutron density ($\sim 10^{15}$ cm^{-3}, [10]) operates at the s-process site. However, it is not clear yet which mechanism can provide this high density and in what kind of objects may it operate.

On the other hand, the neutron exposure at the s-process can be tested from the abundance ratio between the heavy-mass (hs: Ba, La, Ce) and the low-mass (ls: Sr, Y, Zr) s-elements [hs/ls]. Observations in galactic and extragalactic AGB stars show an increase of [hs/ls] ratio with decreasing metallicity [12, 13], also observed in Ba-stars (see this proceeding), which is in nice agreement wih theoretical predictions. This correlation naturally appears from the dependence of the s-process on the metallicity: the lower the metallicity the heavier s-elements are produced preferentially. All these observations confirm also the relation between the neutron exposure [hs/ls], and third dredge-up efficiency, [s/Fe]. Nevertheless, again post-AGB stars in an ample range of metallicities seem to deviate from the former correlation (e.g. [14]): they show no correlation between [hs/ls] versus [Fe/H]. Currently there is not a clear explanation for this behavior.

28.1.2 The Puzzle of Fluorine

Fluorine is also a useful tracer of the physical conditions prevailing in stellar interiors but its origin is still not well known. Recent observations in unevolved stars of near solar metallicity seem to show a correlation with metallicity (and the oxygen abundance), which points out for a secondary origin of this element, at least for this metallicity range [15]. The production of fluorine in AGB stars has (mainly) a secondary nature [16] thus, these objects have been proposed to be one of the main sources. However, despite abundance analysis in AGB stars show clear enhancements in their envelopes [11], the actual F enhancements found are not fully understood nor the corresponding theoretical yields seem to be enough to account for the observations in unevolved stars [17] from chemical evolution model basis. Figure 28.1 shows the [F/Fe] ratios so far determined in galactic and extragalactic AGB C-rich stars compared with theoretical predictions for a representative 2 $M_\odot$ AGB stellar model. The increase of the [F/Fe] ratio for decreasing metallicity predicted nicely agrees with observations, however, AGB stars of SC-type[1] (green symbols) show larger F enhancements than expected. This finding is not well understood as these stars

[1] These stars have a C/O very close to unity within a few hundredth.

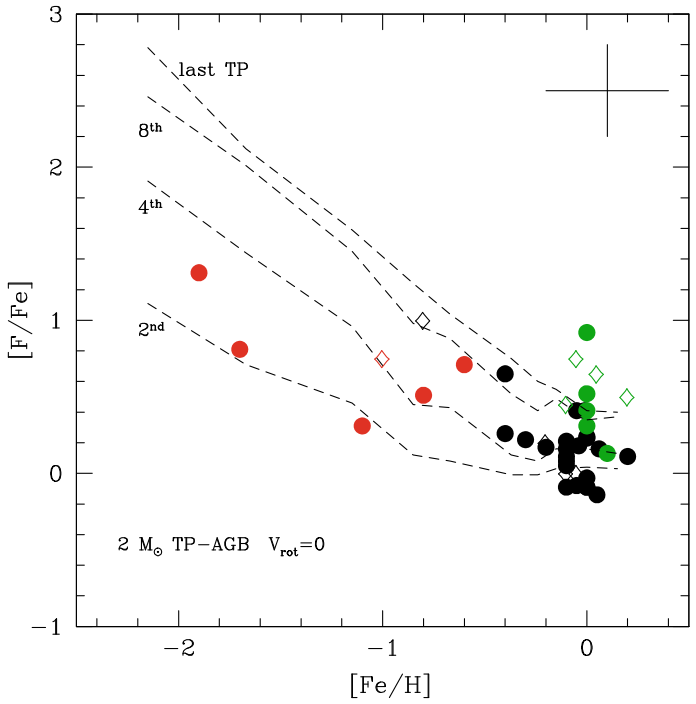

Fig. 28.1 [F/Fe] ratios derived in AGB carbon stars in the Galaxy and in some satellite galaxies (red coloured) belonging to the Local Group (see [11]). Black symbols refer to normal carbon stars while the green ones to SC-type carbon stars. Open diamonds are newly analysed stars (Abia et al. in preparation). Dashed lines are theoretical predictions for a 2 $M_{\odot}$ AGB stellar model with no rotation (see [12]) at different thermal pulses (TP)

should be in an early stage in the AGB phase compared with normal AGB carbon stars (black symbols) and thus, lower [F/Fe] ratios would be expected. Furthermore, since neutrons are needed to produce ^{19}F [16], a correlation between fluorine and the s-element enhancements is also expected in AGB stars. This correlation is, however, marginally observed as many AGB carbon stars (mainly of the SC-type) show large F enhancements without the corresponding s-element one and vice versa [11]. More observational and theoretical effort is needed to understand the mechanism(s) for the production of this element in AGB stars.

Acknowledgements This work has been partially supported by the Spanish grant AYA2015-63588-P within the European Founds for Regional Development (FEDER). The author acknowledges to K. Cunha, O. Straniero and S. Cristallo for fruitful discussions on the subject.

References

1. M. Busso, R. Gallino, G.J. Wasserburg, Nucleosynthesis in asymptotic giant branch stars: relevance for galactic enrichment and solar system formation. Ann. Rev. Astron. Astrophys. **37**, 239B (1999). https://doi.org/10.1146/annurev.astro.37.1.239
2. H. van Winckel, Why Galaxies Care about Post-AGB stars, in *Why Galaxies Care about AGB Stars II: Shining Examples and Common Inhabitants*, vol. 455 (Astronomical Society of the Pacific, 2011), pp.133–141
3. A. Karakas, J. Lattanzio, The dawes review 2: nucleosynthesis and stellar yields of low- and intermediate-mass single stars. Publ. Astron. Soc. Aust. **31**, 62 (2014). https://doi.org/10.1017/pasa.2014.21
4. O. Straniero, R. Gallino, S. Cristallo, s-process in low-mass asymptotic giant branch stars. Nucl. Phys. A **777**, 311 (2006). https://doi.org/10.1016/j.nuclphysa.2005.01.011
5. F. Käppeler et al., The s process: nuclear physics, stellar models, and observations. Rev. Mod. Phys. **83**, 157 (2011). https://doi.org/10.1103/RevModPhys.83.157
6. H. Beer, R.L. Macklin, Measurement of the Rb-85 and Rb-87 capture cross sections for s-process studies. Astrophys. J. **339**, 962–977 (1989). https://doi.org/10.1086/167351
7. C. Abia et al., The 85Kr s-process branching and the mass of carbon stars. Astrophys. J. **599**, 1117–1134 (2001). https://doi.org/10.1086/322383
8. D.L. Lambert et al., The chemical composition of Red Giants. IV. The neutron density at the s-process site. Astrophys. J. **450**, 302 (1995). https://doi.org/10.1086/176141
9. V. Pérez-Mesa et al., Rubidium and zirconium abundances in massive Galactic asymptotic giant branch stars revisited. Astron. Astrophys. **606**, A20 (2017). https://doi.org/10.1051/0004-6361/201731245
10. M. Lugaro et al., Post-AGB stars in the Magellanic Clouds and neutron-capture processes in AGB stars. Astron. Astrophys. **583**, A77 (2015). https://doi.org/10.1051/0004-6361/201526690
11. C. Abia et al., The origin of flourine: abundances in AGB stars revisited. Astron. Astrophys. **584C**, 1A (2015). https://doi.org/10.1051/0004-6361/201526586e
12. S. Cristallo et al., Evolution, nucleosynthesis, and yields of AGB stars at different metallicities. III. Intermediate-mass models, revised low-mass models, and the ph-FRUITY interface. Astrophys J. Suppl. Ser. **219**, 40C (2015). https://doi.org/10.1088/0067-0049/219/2/40
13. C. Abia et al., Chemical analysis of carbon stars in the local group. II. The Carina dwarf spheroidal galaxy. Astron. Astrophys. **481**, 161 (2008). https://doi.org/10.1051/0004-6361:20079114
14. K. De Smedt et al., Detailed homogeneous abundance studies of 14 Galactic s-process enriched post-AGB stars: in search of lead (Pb). Astron. Astrophys. **587A**, 6D (2016). https://doi.org/10.1051/0004-6361/201527430
15. H. Jönsson et al., Fluorine in the solar neighborhood: no evidence for the neutrino process. Astrophys. J. **835**, 50 (2017). https://doi.org/10.3847/1538-4357/835/1/50
16. S. Cristallo et al., Effects of nuclear cross sections on 19F nucleosynthesis at low metallicities. Astron. Astrophys. **570**, A46 (2014). https://doi.org/10.1051/0004-6361/201424370
17. N. Prantzos et al., Chemical evolution with rotating massive star yields–I. The solar neighbourhood and the s-process elements. Mon. Not. R. Astron. Soc. **473**, 3432 (2018). https://doi.org/10.1093/mnras/sty316

Chapter 29
Heavy Elements Nucleosynthesis on Accreting White Dwarfs Surface: Seeding the p-Process

Umberto Battino, Claudia Travaglio, Marco Pignatari and Claudia Lederer-Woods

Abstract The production of the proton-rich isotopes beyond iron that we observe today in the solar system is still uncertain. Thermonuclear supernovae (SNe Ia) exploding within the single-degenerate scenario have been proposed to be a potential source for these isotopes. We calculate accretion models and the nucleosynthesis for four WD with different initial mass 0.85, 1.26, 1.32 and 1.38 solar masses models), calculating the full abundance distribution. The abundance distribution peaks between Fe and Zr for the model at 1 $M_{\odot}$, while for larger WDs much higher production efficiency is obtained beyond iron, with a strong production up to the Pb region. Using these results, we compute the nucleosynthesis of proton rich heavy isotopes using a multi-D SNe Ia model, and discuss the uncertainties affecting our results.

29.1 Introduction: Type Ia Supernovae Progenitors

SNe Ia are luminous stellar explosions which marks the fatal destruction of accreting white dwarfs (WD) in binary systems. The two scenarios to make SNIa explosions are Single-Degenerate (SD) and Double Degenerate (DD; [6]). SNe Ia are fundamental sources for galactical chemical evolution. They produce iron group elements in the ejecta exposed to the most extreme SN conditions [7]. In the ejecta exposed to less extreme conditions, intermediate mass elements like Si and Ca are made, as also confirmed from optical spectra of recent SNIa remnants [5]. Travaglio et al. [12] showed how SNIa could be a relevant source for the *p*-process isotopes made by photo-disintegrations reactions on assumed pre-existing heavy-element seeds distri-

U. Battino (✉) · C. Lederer-Woods
University of Edinburgh, Edinburgh EH9 3FD, UK
e-mail: ubattino@ed.ac.uk

C. Travaglio
INFN - Istituto Nazionale Fisica Nucleare, Turin, Italy

M. Pignatari
E.A. Milne Centre for Astrophysics, University of Hull, Hull HU6 7RX, UK

Center for the Evolution of the Elements, Joint Institute for Nuclear Astrophysics, Michigan State University, 640 South Shaw Lane, East Lansing, MI 48824, USA

A. Formicola et al. (eds.), *Nuclei in the Cosmos XV*, Springer
Proceedings in Physics 219, https://doi.org/10.1007/978-3-030-13876-9_29

bution formed from the neutrons released during the He-flashes occurring all along the accretion. In this work, we want to verify the assumption [12] made about pre-existing heavy-element seeds distribution on the WD surface, self-consistently computing stellar models and the nucleosynthesis taking place along the mass accretion phase.

Present stellar evolution theory predicts that the maximum CO-core mass in non-rotating AGB stars cannot exceed 1.1 $M_{\odot}$. This fact and the lack of He II lines detection (expected from stably accreting WDs in this mass range) from elliptical galaxies seems to indicate that the SD-channel for SNe is highly unlikely [2, 14]. Similarly as done in [2], we computed the mass retention-efficiency (defined as the difference between the accreted and ejected mass after each He-flash instability along the mass accretion) of our rapidly accreting white dwarf models (RAWD): we obtained low retention-coefficient values of few percent for $M_{wd} < 1\ M_{\odot}$, which are in agreement with [2], confirming how difficult reaching the Chandrasekhar limit is when starting from this WD mass. The retention efficiency grows anyway with the WD mass, ranging between 60 and 80% for WD masses higher than $1.3M_{\odot}$ (for a similar work considering He-accreting see also [9]). On the other hand, [3] showed that in rotating massive AGB stars the final CO-core mass is markedly increased, obtaining final CO-core masses in the range between 1.1 and 1.4 $M_{\odot}$. Rotating stars modelled with MESA [8], GENEC [4] and STAREVOL [11] stellar codes are under analysis: preliminary results seems to confirm results by [3] (den Hartogh, Battino, Ekstrom, Charbonnel et al. 2019 in prep.).

29.2 Stellar Models and Nucleosynthesis Calculations

The stellar models presented in this section are computed using the stellar code MESA revision 4219. Mass loss is only considered when Super-Eddington wind conditions are met. In this work, we adopted different constant mass-accretion rates (always around $10^{-7}\ M_{\odot}$) in order to achieve steady H-burning regime, occasionally triggering H-flashes in particular during the first phases of the accretion. Table 29.1 lists the initial WD mass and metallicity of the RAWD models calculated. Full nucleosynthesis calculations were performed using the post-processing code *mppnp*, which is described in detail in [10].

Table 29.1 Accreting WD models and their initial mass and metallicity

Name	Mass ($M_{\odot}$)	Metallicity
M1p025.Z1m2	1.025	0.01
M1p250.Z1m2	1.250	0.01
M1p316.Z1m2	1.316	0.01
M1p376.Z1m2	1.376	0.01

The production factors tend to increase with the increase of the WD mass, due to the most efficient production of neutrons. This can be seen in Fig. 29.1 top panel, where the abundance distribution calculated for different WD masses is shown. The distributions obtained for the M1p025.Z1m2 and M1p259.Z1m2 model show

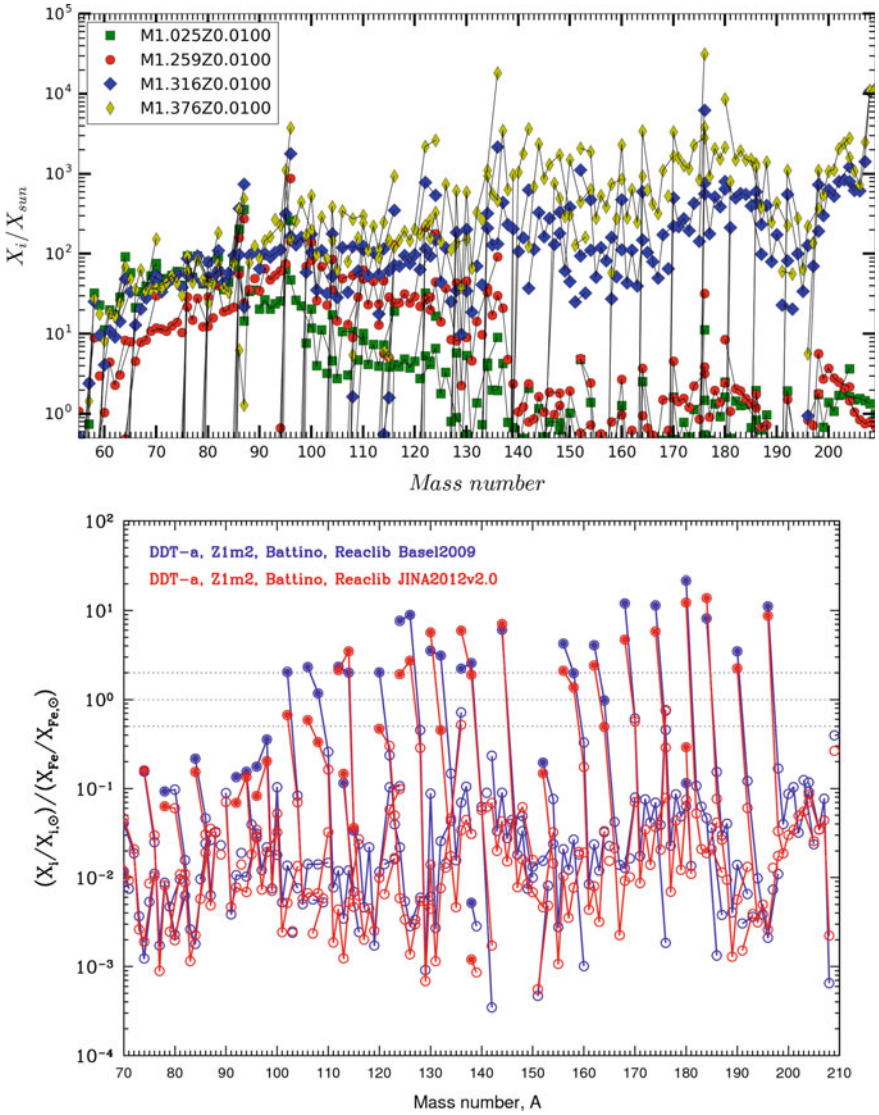

Fig. 29.1 Top panel: Final abundance distribution calculated for models M1p025.Z1m2, M1p259.Z1m2, M1p316.Z1m2 and M1p376.Z1m2. Bottom panel: Final abundance distribution from explosive nucleosynthesis calculations obtained when the abundances showed in the top panel are used as a starting abundance distribution

a significant production up to ^{136}Xe, while the one obtained in M1.376.Z1m2 and M1.316.Z1m2 continues with large efficiency up to the Pb region. In the figure, the larger neutron exposure is obtained by numerous H-flashes which trigger proton captures onto the abundant ^{12}C producing ^{13}C, which is then completely burned via ^{13}C(α,n)^{16}O in a region of the order of 10^{-7} $M_{\odot}$ at very high temperature (T $\sim$ 0.3 GK) resulting in *i*-process conditions [1] and a nuclear production reaching the Pb region. Notice that this happens during the time interval before the onset of the TP. These abundances, produced on the surface of WDs of different masses, have been then translated into initial abundances at different mass coordinates to compute explosive nucleosynthesis. These results are shown in the bottom panel: (see [12] for a description of the multi-D SNe Ia model here adopted), p-nuclei are significantly produced to and above the Solar-System level in the mass range $96 < A < 196$. Notice that the lightest p-nuclei, underproduced in these simulations, receive anyway a significant contribution from Type II Sne (see [13]).

Notes and Comments We presented for the first time a heavy-element distribution calculated from realistic simulations of WD-accretion phase in the single degenerate scenario channel to SNIa. The final abundance distribution presents large quantities of Rb, Kr, Zr, Ba-peak isotopes, including Pb for our M1p316.Z1m2 and M1p376.Z1m2 models. Is therefore globally very similar to the one adopted in [12]. When used as a starting abundance distribution, p-nuclei are significantly produced in the mass range $96 < A < 196$. This research was enabled in part by support provided by WestGrid (www.westgrid.ca) and Compute Canada Calcul Canada (www.computecanada.ca). NuGrid data is served by Canfar CADC. UB and CLW acknowledge support from the Science and Technology Facilities Council UK (ST/M006085/1), and the European Research Council ERC-2015-STG Nr. 677497.

References

1. J. Cowan et al., Astrophys. J. **212**, 149–158 (1977)
2. P.A. Denissenkov et al., Astrophys. J. Lett. **834**, L10 (2017)
3. I. Dominguez et al., Astrophys. J. **472**, 783–788 (1996)
4. P. Eggenberger et al., Astrophys. Space Sci. **316**, 43 (2008)
5. A.V. Filippenko et al., Annu. Rev. Astron. Astrophys. **35**, 309–355 (1997)
6. I. Iben Jr. et al., Astrophys. J. **277**, 333 (1984)
7. K. Iwamoto et al., Astrophys. J. Suppl. **125**, 439–462 (1999)
8. B. Paxton et al., Astrophys. J. Suppl. **192**, 3 (2011)
9. L. Piersanti et al., Mon. Not. R. Astron. Soc. **445**, 3239–3262 (2014)
10. M. Pignatari et al., Astrophys. J. Suppl. **225**, 24 (2016)
11. L. Siess et al., Astron. Astrophys. **358**, 593–599 (2000)
12. C. Travaglio et al., Astrophys. J. **739**, 93 (2011)
13. C. Travaglio et al., Astrophys. J. **854**, 18 (2018)
14. T.E. Woods et al., Mon. Not. R. Astron. Soc. **432**, 1640–1650 (2013)

Chapter 30
The Importance of the $^{13}C(\alpha,n)^{16}O$ Reaction in Asymptotic Giant Branch Stars

Sergio Cristallo

Abstract I will present a theoretical sensitivity study, carried out with the FUNS evolutionary stellar code, to evaluate the effects induced on the s-process nucleosynthesis by variations of the $^{13}C(\alpha,n)^{16}O$ cross section. Some peculiar evolutionary phases, particularly sensitive to this rate, will be discussed in detail.

30.1 The Importance of the s-Process for Multi-messenger Astrophysics

In the epoch of multi-messenger astrophysics, a detailed knowledge of the nucleosynthesis occurring in stellar objects (from low mass stars, ending their lives as white dwarf, to highly compact interacting objects) is mandatory. The recent kilonova event, following the detection of gravity waves in GW170817, proved that the rapid neutron capture process (the r process) is at work during these events (see e.g., [1, 2]). This nucleosynthesis process is characterized by extremely large neutron densities ($n_n > 10^{23}$ cm^{-3}). However, to date the theoretical knowledge of the r-process is not accurate enough to provide a comprehensive and independent picture of the nucleosynthesis occurring in those mergers. As a consequence, the r-process contribution to the solar inventory is commonly calculated as a residual from its slow neutron capture process counterpart (the s-process), i.e. r% = 1 − s%. The latter is characterized by rather low neutron densities ($n_n \sim 10^7$ cm^{-3}). In Fig. 30.1 (left panel), two solar r-process residual distributions are reported: the first is calculated with the classical theory (i.e. ignoring stellar models; [3]), while the second is the result of a Galactic Chemical Evolution model, which takes into account yields from low and massive stars ($1 \leq M/M_\odot \leq 120$) at various epochs [4]. A detailed knowledge of s-process nucleosynthesis is therefore an essential condition to attain a full understanding of the pollution history of our Galaxy, including its r-process

S. Cristallo (✉)
INAF - Osservatorio d'Abruzzo, via Maggini snc Teramo, 64100 Teramo, Italy
e-mail: sergio.cristallo@inaf.it

INFN - Sezione di Perugia, via Pascoli snc Perugia 06123, Perugia, Italy

A. Formicola et al. (eds.), *Nuclei in the Cosmos XV*, Springer
Proceedings in Physics 219, https://doi.org/10.1007/978-3-030-13876-9_30

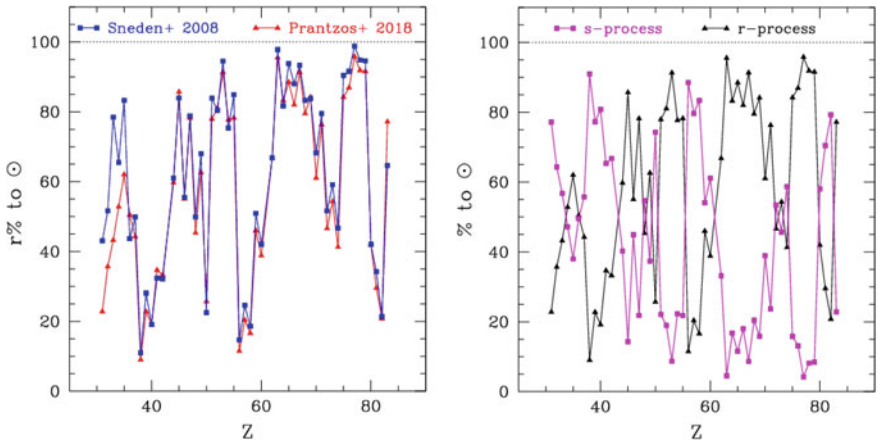

Fig. 30.1 Left panel: r-process residuals distributions from [3] and [4]. Right panel: s-process and r-process contributions to the solar heavy elements inventory (data from [4])

component. In the right panel of Fig. 30.1, I report the s- and r- contributions to the solar heavy elements distributions provided by Prantzos et al. [4].

The s-process consists of two components: a weak component (from the iron peak to the first s-process peak, close to the Sr-Y-Zr region), which is produced by massive stars during their core He- and C-shell burnings (see, e.g., [5]) and a main component, synthesized by low and intermediate mass stars ($1 \leq M/M_{\odot} \leq 8$) during their Asymptotic Giant Branch (AGB) phase (for reviews see [6, 7]). As a matter of fact, AGB stars are among the most important polluters of the Milky Way, because the isotopes freshly synthesized in their interiors are recurrently mixed up to the surface and ejected in the interstellar medium via strong stellar winds. From the modelling point of view, the major uncertainties affecting AGB stars are the treament of convection and the mass-loss law (for details see [8]). From the nuclear point of view, there are few reactions able to influence the whole s-process distribution. Among them, there are the two main neutron sources: the $^{13}C(\alpha,n)^{16}O$ and the $^{22}Ne(\alpha,n)^{25}Mg$ reactions. The latter, which plays a minor role in low mass AGB stars, has been recently studied by Massimi [9]. On the other side, owing to its astrophysical importance, the $^{13}C(\alpha,n)^{16}O$ has been the subject of many studies (see for instance [10]). From the experimental point of view, there are ongoing experiments aiming at the direct determination of its cross section (LUNA, see A. Best contribution, this volume) or focusing on specific ^{17}O states (n_TOF, see S. Urlass contribution, this volume). From the theoretical point of view, latest results have been published by Cristallo et al. [11] and will be presented in next sections.

30.2 The Importance of the $^{13}C(\alpha,n)^{16}O$ Reaction in AGB Stars

The standard paradigm of the s-process adfirms that the $^{13}C(\alpha,n)^{16}O$ reaction fully burns in radiative conditions between two Thermal Pulses (TPs), at a temperature around 90 MK [12]. However, [13] found that some ^{13}C may not be fully consumed during the interpulse in some low-mass AGB models at solar-like metallicities. If this occurs, the residual ^{13}C burns at higher temperature in the convective shell triggered by a TP, modifying the isotopic composition close to s-process branching points. The $^{13}C(\alpha,n)^{16}O$ reaction may also influence the physical and chemical evolution of the early TP-AGB evolution of low mass low metallicity models. In particular, those stars may suffer peculiar events in which protons are engulfed in the convective shell triggered by the first fully developed TP. As a consequence, hydrogen burns on-flight, and the energy provided by the $^{13}C(\alpha,n)^{16}O$ reaction (plus the additional contribution from the relative neutron capture) plays a key role (see e.g. [14]).

30.3 Results

Recently, [11] performed a sensitivity study to evaluate the effects of a variation of the $^{13}C(\alpha,n)^{16}O$ cross section on the s-process nucleosynthesis occurring in AGB stars. The rate has been varied by a factor 1.5 and 2 (upward and downward) with respect to the value proposed by Heil et al. [15], assumed as a reference case. As expected, it has been found that s-process distributions for masses above 3 $M_\odot$

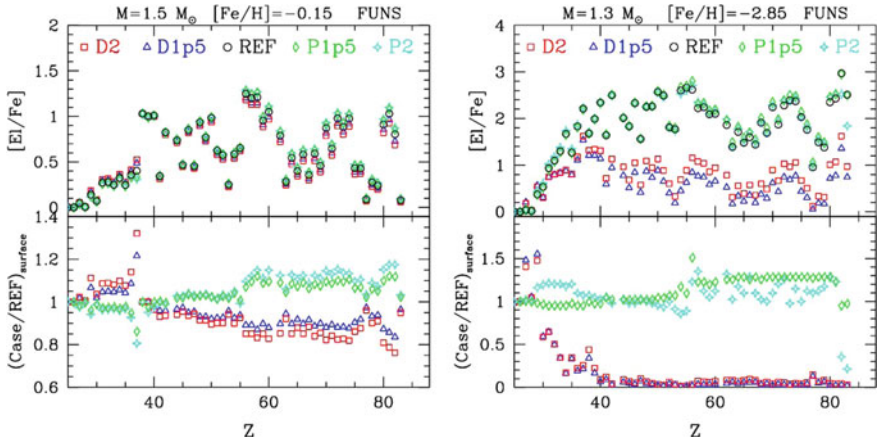

Fig. 30.2 Left panel: elemental distributions obtained with different values of the $^{13}C(\alpha,n)^{16}O$ cross section in a low mass model at solar-like metallicity. Right panel: as in the left panel, but for a low metallicity model

at any metallicity are not sensitive to any change of the rate, thus confirming the robustness of s-process theory. However, low mass models ($M < 3\ M_{\odot}$) at close-to-solar metallicities show appreciable variations (on average 10% with peaks up to 30%) in the elemental composition, when the rate of the $^{13}C(\alpha,n)^{16}O$ is changed (see left panel of Fig. 30.2). For what concerns single isotopes, variations up to a factor 20 are found (for example ^{60}Fe). The most interesting results, however, come from low-mass low-metallicity models. When protons are engulfed in the convective shell, the He-burning energy budget receives an important contribution from the $^{13}C(\alpha,n)^{16}O$ reaction (and from the following neutron captures). The resulting surface distributions strongly depend on the adopted rate (see right panel of Fig. 30.2), with the heavier elements abundances changing by almost two orders of magnitude.

References

1. B. Metzger, Kilonova counterparts of binary neutron star mergers. AAS, 2312901 (2018)
2. D. Kasen, J. Barnes, *Radioactive Heating and Late Time Kilonova Light Curves*. arXiv:1807.03319 (2018)
3. C. Sneden, J.J. Cowan, R. Gallino, Neutron-capture elements in the early galaxy. Annu. Rev. Astron. Astrophys. **46**, 241 (2008). https://doi.org/10.1146/annurev.astro.46.060407.145207
4. N. Prantzos, C. Abia, M. Limongi, A. Chieffi, S. Cristallo, Chemical evolution with rotating massive star yields - I. The solar neighbourhood and the s-process elements. Mon. Not. R. Astron. Soc. **476**, 3432 (2018). https://doi.org/10.1093/mnras/sty316
5. M. Pignatari et al., The weak s-process in massive stars and its dependence on the neutron capture cross sections. Astrophys. J. **710**, 155 (2010). https://doi.org/10.1088/0004-637X/710/2/1557
6. F. Herwig, Evolution of asymptotic giant branch stars. Astron. Astrophys. **43**, 435 (2005). https://doi.org/10.1146/annurev.astro.43.072103.150600
7. O. Straniero, R. Gallino, S. Cristallo, s process in low-mass asymptotic giant branch stars. Nucl. Phys. A **777**, 311 (2006). https://doi.org/10.1016/j.nuclphysa.2005.01.011
8. S. Cristallo, s-Process nucleosynthesis in low-mass AGB stars at different metallicities. Publ. Astron. Soc. Pac. **118**, 1360 (2006). https://doi.org/10.1086/507774
9. C. Massimi, The n_TOF collaboration, Neutron spectroscopy of ^{26}Mg states: constraining the stellar neutron source $^{22}Ne(\alpha,n)^{25}Mg$. Phys. Lett. B. **768**, 1 (2017). https://doi.org/10.1016/j.physletb.2017.02.025
10. O. Trippella, M. La Cognata, Concurrent Application of ANC and THM to assess the $^{13}C(\alpha, n)^{16}O$ absolute cross section at astrophysical energies and possible consequences for neutron production in low-mass AGB stars. Astrophys. J. **837**, 41 (2017). https://doi.org/10.3847/1538-4357/aa5eb5
11. S. Cristallo et al., The Importance of the $^{13}C(\alpha, n)^{16}O$ reaction in asymptotic giant branch stars. Astrophys. J. **859**, 105 (2018). https://doi.org/10.3847/1538-4357/aac177
12. O. Straniero et al., Radiative C-13 burning in asymptotic giant branch stars and s-processing. Astrophys. J. **440L**, 85 (1995). https://doi.org/10.1086/187767
13. S. Cristallo et al., Evolution, nucleosynthesis, and yields of low-mass asymptotic giant branch stars at different metallicities. Astrophys. J. **696**, 797 (2009). https://doi.org/10.1088/0004-637X/696/1/797
14. S. Cristallo et al., Constraints of the physics of low-mass AGB stars from CH and CEMP stars. Astrophys. J. **833**, 181 (2016). https://doi.org/10.3847/1538-4357/833/2/181
15. M. Heil et al., The $^{13}C(\alpha, n)$ reaction and its role as a neutron source for the s process. Phys. Rev. C **78**, 5803 (2008). https://doi.org/10.1103/PhysRevC.78.025803

Chapter 31
Thermonuclear Supernovae: Prospecting in the Age of Time-Domain and Multi-wavelength Astronomy

Peter Hoeflich, Chris Ashall, Alec Fisher, Boyan Hristov, David Collins, Eric Hsiao, Ingo Wiedenhoever, S. Chakraborty and Tiara Diamond

Abstract We show how new and upcoming advances in the age of time-domain and multi-wavelength astronomy will open up a new venue to probe the diversity of SN Ia. We discuss this in the context of the ELT (ESO), as well as space based instrument such as James Webb Space Telescope (JWST). As examples we demonstrate how the power of very early observations, within hours to days after the explosion, and very late-time observations, such as light curves and mid-infrared spectra beyond 3 years, can be used to probe the link to progenitors and explosion scenarios. We identify the electron-capture cross sections of Cr, Mn, and Ni/Co as one of the limiting factors we will face in the future.

31.1 Introduction

Thermonuclear Supernovae, stellar explosions of White Dwarf Stars (WD)/the degenerate C/O cores of low mass stars are important for understanding the Universe. As well as being one of the building blocks and drivers of modern cosmology, they are also important for understanding the origin of elements, and are laboratories for the explosion physics of WDs in close binary systems. Here, we focus on new developments. For a general discussion from our perspective, see [1–3]. Recently advances in observations and theory have caused new problems to emerge. One of these is the discrepancy in the Hubble constant H_o obtained using the Microwave background (66.93 ± 0.62 km/s/Mpc, [4]) and that obtained using the empirical SNe Ia-based methods (73.24 ± 1.74, [5]). This discrepancy may have direct consequences for: the

P. Hoeflich (✉) · C. Ashall · A. Fisher · B. Hristov · D. Collins · E. Hsiao · I. Wiedenhoever · S. Chakraborty
Florida State University, Tallahassee, FL 32309, USA
e-mail: phoeflich@fsu.edu

T. Diamond
NASA Goddard Space Flight Center, Greenbelt, MD 20771, USA

A. Formicola et al. (eds.), *Nuclei in the Cosmos XV*, Springer
Proceedings in Physics 219, https://doi.org/10.1007/978-3-030-13876-9_31

interpretation of the Big-bang nucleosynthesis (Li-problem), high precision cosmology, early Black Hole formation, and new physics beyond the high-energy standard model.

The majority of Type Ia supernovae appear to be rather homogeneous with a well defined luminosity decline relation of light curves Δm_{15} [18] and similar spectra. However, there is in fact some diversity in their observations which has been hypothesized to be due to various progenitor channels and explosion scenarios. Potential progenitor systems may either consist of two WDs, called a double degenerate (D-D) system, or a single WD with a donor which may be main sequence, red giant, or Helium (He) star, called a single degenerate (SD) system [19]. The various explosion scenarios can be distinguished by three possible triggering mechanisms: (a) Compressional heat in a slow accretion triggers the explosion when the WD approaches (!) the Chandrasekhar mass M_{Ch} in either SD or DD systems. The flame propagates as a detonation (Det.), a deflagration (Defl.) or, more likely, starts as deflagration and transitions to a detonation with or without a pulsation phase (DDT, PDDT); (b) Heat released on dynamical time scales triggers a detonation of a DD-system (dynamical mergers); (c) in Helium detonations (HeDs,) a surface He-detonation triggers a detonation in a C/O core of a sub-M_{Ch} WD with a He-star companion. Core-degenerates (CD) are explosions within a Red-Supergiant by (a) or (b).

From theory, the empirical SNe Ia relations dm_{15} and *CMAGIC* (Fig. 31.2) for cosmology are stable because basic nuclear physics determines: the structure of the progenitor WD, the explosion physics, and the average expansion velocities. This 'Stellar amnesia' leads to similar light curve shapes and spectral evolution. All sce-

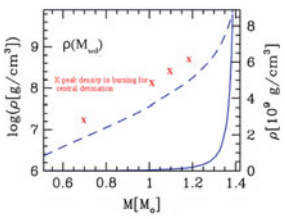

Scenario	Initial mass	Defl.	Det.	M_{56Ni}	$A\rho$	$A(X_i)$	C & O	stable Ni
Det.	1.3 – 1.37	-	x	0.83-1.3	<<	no	no	x
Defl.	1.25 – 1.38	x		0.05: ... 0.6	<<	small scale	< 0.1	x
DDT	1.25 – 1.38	x	x	0.05-0.0.8	<< (axial)	some	$\approx 10^{-4...-2}$ *	x
PDDT	1.25 – 1.38	x	x	0.1-0.8	<<	some	typical ≈ 0.3 *(s)	x
HeD	0.6-1.2	-	x	0.-1.07	<	some	no →some for M(1.1...1.2)	no
CD	> 1.37	x:	x:	up to 1.4:	<:	x:	large (s)	no (:)
Mergers	0.6 – 2.7	no	x	0.-1.7:	large(:)	x	x (s)	no

Fig. 31.1 *Right*: Characteristics of explosion scenarios including the range of total mass M_{WD} in $M_\odot$, modes of burning, $M_{56\mathrm{Ni}}$ production in $M_\odot$, asymmetries in density $A\rho$ and abundances $A(X_i)$, presence of unburned C/O and stable Ni. x denotes the presence of the feature. The production of electron capture isotopes depends on the nuclear physics, which is dominated by the density of burning, versus hydrodynamical time scales (≈1 s). The exact production depends on the nuclear rates and recent revisions [6, 7]. The production of electron capture isotopes becomes important beyond 10^8 g/cm^3. *Left*: The central density of the WD is shown as a function of M_{WD}. For M_{Ch} explosions this indicates the highest density of burning. In contrast, for HeDs, the detonation waves compress the material and increases the density. Therefore the corresponding relation for HeDs is indicated by red dots. E.g. to first order and as an upper limit, we may expect similar electron capture isotopes in HeD and DDTs at 1.2 and 1.3 $M_\odot$, respectively. Note, however, that the duration of compression by a detonation is shorter than the WD expansion time scale resulting in about 1/2 the shift in abundance with respect to EC isotopes [2, 8]

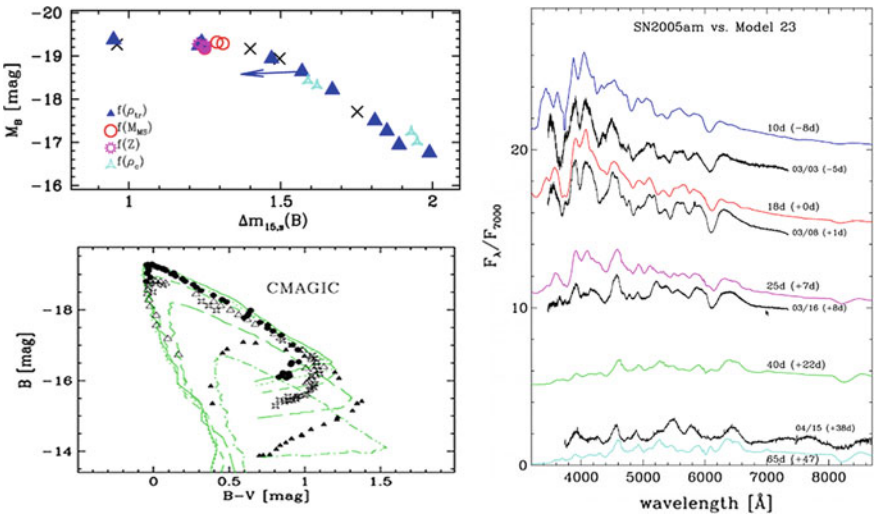

Fig. 31.2 Comparison of observable properties of 'classical', spherical delayed-detonation models with observations [9]. We show the width-luminosity $\Delta m_{15,s}(B)$ (*upper left*) and the brightness-color relation of the normal bright SN2005M, SN2004eo, SN2005am and the subluminous SN2005ke (black X) and models (blue) with transition densities of $27, 23, 16, 8 \times 10^6$ g cm^{-3} originating from a WD with a main sequence mass of $M_{MS} = 5\,M_\odot$, an initial central density $\rho_c = 2^9$ g/cm^3 and solar metallicity Z unless denoted. As example, the comparison between the normal bright SN2005am and model spectra is shown on the right panel

narios may contribute to the SNe Ia population but there is observational evidence that one scenario dominates (Figs. 31.1 and 31.2) [9, 20]. However which one dominates is heavily discussed in the community. Dynamical mergers are not likely as they predict high continuum polarization and aspherical explosions, this is not seen in the data [21, 22]. The DDT (M_{Ch}) seems to explain most of the observed properties of SNe Ia (Fig. 31.2), and DDT model-based, $\delta - Ceph.$-independent distances give an $H_o = 68 \pm 4$ km/Mpc/s [8, 9]. However, HeDs have recently become a serious contender because their main-flaw, the need for a large He-layers on the surface of the WD, can be migrated by a mixing of the He and C, as long as the $M_{WD} > 1.1\,M_\odot$ [23]. In this scenario the optical spectra and LCs become similar to DDTs. However, these HeDs result in systematically larger H_o when analyzing observations.

31.2 New Early Time Observations

They [11] provide a new tool to probe the outermost $10^{-4\ldots-5}\,M_\odot$ layers of the ejecta (Fig. 31.3). Within the M_{Ch} scenarios like DDTs these outermost layers consist of H- and He for main-sequence/red-giant and He-star donors, respectively. When the detonation burning passes through the 'surface'-layers the burning time scales

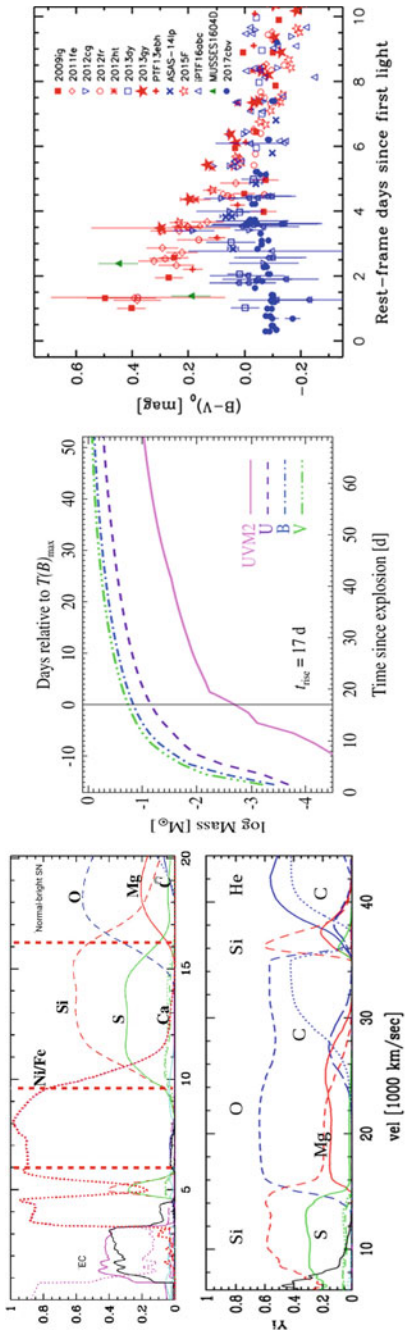

Fig. 31.3 Nuclear signatures are a possible probe of the donor star for SD systems and M_{Ch} mass explosions. *Upper left*: The overall abundance structure as a function of velocity [*in* 1000 km/s] of our reference model. *Lower left*: Same but the very outer layers for a DDT model with a He-star as donor. *Middle*: The mass exposed in the UV, U, B and V bands [10] as a function of time. *Right*: Observations right after the explosion, where the very outer layers are probed, indicate a bifurcation among objects with similar subsequent LC and spectra [11]

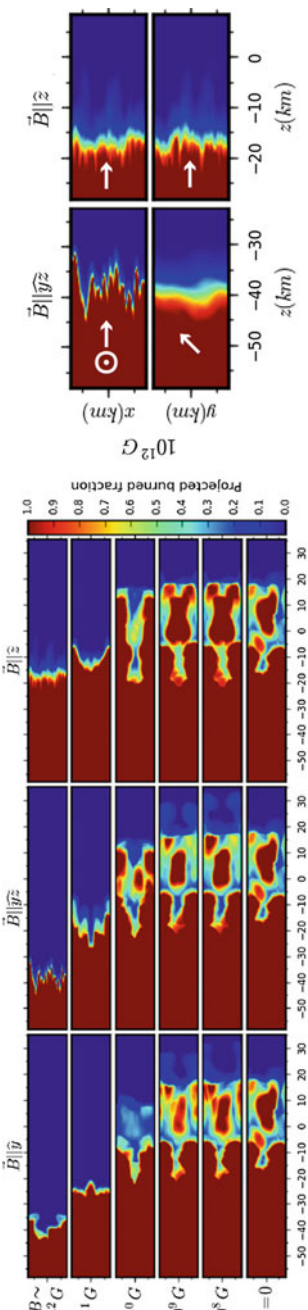

Fig. 31.4 Possible consequence of multi-dimensional effects on the production of EC isotopes. We show the influence of B fields on the normalized burned fraction nuclear burning front in a flux tube with properties corresponding to the regime of non-distributed burning (based on Enzo). The axis are in km. The initial B-field is parallel (*left*), at 45° (*middle*), and orthogonal to the flux tube (*right*). For B close to the saturation field (*right plot*), comb-like structures occur which increase the surface and, thus, the burning reate by factors of 4–5. B emerge as important component with $B > 10^{4...6} G$ both from late-time NIR spectra and LCs [12–14], and may suppress excessive strong Rayleigh-Taylor mixing which would degrade a tight Δm_{15} relation

for hydrogen burning are too long [24] but a He/C mixture would ignite leaving a nuclear signature at high velocity and during the first 2–5 days as observed (Fig. 31.3, lower left and middle). Alternative explanations may be high mass HeDs, PDDTs or ongoing interaction pending further analysis.

31.3 Late and Ultra-time Observations in the Mid-infrared

They are a novel tool to probe for the distribution electron capture isotopes and, with it, the underlying physics of flames Fig. 31.4. The detection of stable Ni at late times can distinguish between M_{Ch} explosions or high mass ($M \approx 1.2 M_{\odot}$ HeDs from mergers or low mass HeDs (Fig. 31.5). Unfortunately, the ^{57}Ni/Co production, which is analyzed in very late time light curves of SNe Ia, is rather insensitive to density of burning for M_{WD} larger than $1.1 M_{\odot}$. This does not allow us to distinguish massive HeD from M_{Ch} models. However, as the density of burning increases the Cr, Mn and stable Ni abundances becomes more prominent, see the table in Fig. 31.6. These lines are predominantly located in the the mid-IR and will be observable with JWST in the near future. By doppler shifts, line profiles will provide the spatial location and test for mixing versus nuclear effects. JWST and ELT will open up the parameter space for many SNe Ia and allow to use the spectra during the ^{57}Co regime (Fig. 31.6) emphasizing the need for high-precision, electron capture nuclear data for Mn, Cr, Ni isotopes on the 20–40 % level based on our tests.

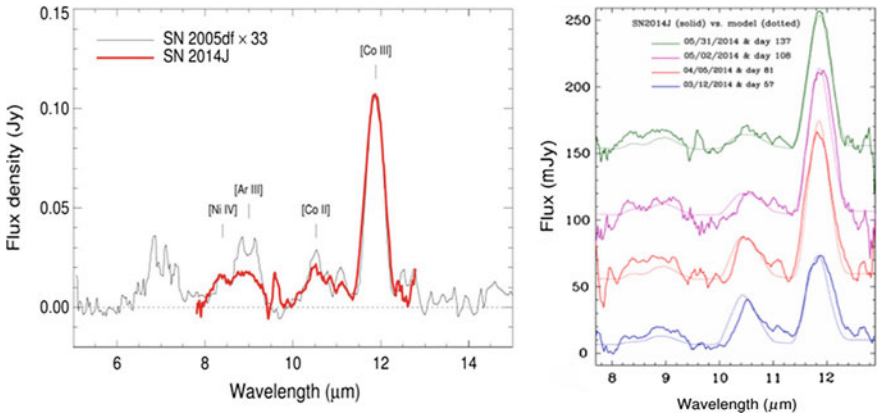

Fig. 31.5 *Left*: The MIR spectra at day 135 of SN 2005df the Spitzer Space Telescope (red, [15]) and SN 2014J (black). *Right*: The time series for SN2014J obtained at the Grand Canari Telescope (right) [16]. The dotted lines give the synthetic spectra of our reference DDT model with the wavelength in μm

rhoc	cr52	mn55	fe52 # mn52 cr52	fe53 # mn53 cr53	fe54	fe55 * fe55 mn55	fe56	t=0d t=100d t->inf
d02	1.9E-06	1.9E-07	1.2E-02	6.0E-04	6.9E-03	1.5E-05	1.5E-04	
d05	1.2E-06	3.0E-08	1.9E-02	1.3E-03	3.4E-02	2.1E-05	1.0E-04	
d10	1.3E-06	2.7E-08	2.0E-02	1.6E-03	1.0E-01	1.6E-04	1.2E-04	
d20	5.5E-03	1.4E-05	3.4E-02	2.6E-03	2.2E-01	1.1E-02	1.1E-01	
d35	5.0E-02	2.4E-03	3.7E-02	2.7E-03	2.0E-01	8.0E-03	2.3E-01	

rhoc	fe58	co55 # mn55 mn55	co57 # co57 fe57	ni56 # ni56 fe56	ni57 # ni57 fe57	ni58	zn60 # ni60 ni60	t=0d t=100d t->inf
d02	1.5E-05	2.5E-03	2.3E-05	1.0E+00	1.9E-02	1.5E-02	8.0E-03	
d05	2.5E-05	8.8E-03	1.3E-05	1.0E+00	1.7E-02	1.6E-02	5.2E-03	
d10	2.7E-05	1.3E-02	6.3E-05	1.0E+00	1.8E-02	4.4E-02	3.8E-03	
d20	5.3E-05	2.1E-02	3.7E-03	1.0E+00	1.6E-02	6.5E-02	1.8E-05	
d35	4.5E-03	2.0E-02	2.4E-03	1.0E+00	1.5E-02	6.3E-02	1.8E-04	

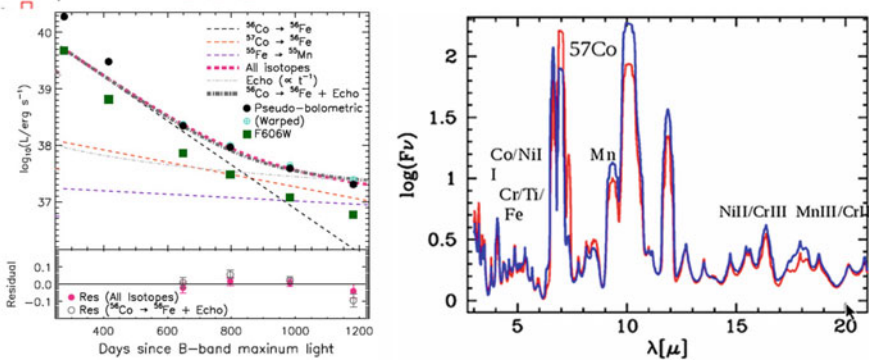

Fig. 31.6 Ultra-late time observations are a probe for high density burning. *Top*: EC isotopes at 0, 100 days and infinity for DDT models with ρ_c between $2 \ldots 35 \times 10^8$ g/cm^3 (d02…d35) for a delayed-detonation model with ρ_c between $2...35 \times 10^8$ g/cm^3 (d02...d35) for various times t. *Lower left*: The bolometric and monochomatic LCs, obtained by the Hubble Space telescope, become dominated by rare, short lived isotopes rather than the positron decay channel of ^{56}Co (from [17]), and require proton trapping which requires initial B fields larger than $10^6 G$. *Lower right*: Predicted spectra at day 3000 are shown for $0B$ (red) and $10^6 G$ (blue). The precence of the electron capture isotopes Cr, Mn, and Ni/Co should be noted

Acknowledgements We thank the FSU Foundation for funds which allowed to attend the meeting. The work has been supported by the NSF grant 1715133.

References

1. P. Hoeflich, *Explosion Physics of Thermonuclear Supernovae and Their Signatures*, page 1151 (2017)
2. P. Hoeflich, Physics of type Ia supernovae. Nucl. Phys. A **777**, 579–600 (2006)
3. P. Hoeflich, P. Dragulin, J. Mitchell, B. Penney, B. Sadler, T. Diamond, C. Gerardy, Properties of SN Ia progenitors from light curves and spectra. Front. Phys. **8**, 144–167 (2013)
4. Planck Collaboration, R. Adam, P.A.R. Ade, N. Aghanim et.al., Planck 2015 results. I. Overview of products and scientific results. Astron. Astrophys. **594**, A1 (2016)
5. A.G. Riess, L.M. Macri, S.L. Hoffmann et al., A 2.4% determination of the local value of the hubble constant. Astrophys. J. **826**, 56 (2016)
6. F. Brachwitz, D. Dean, W.R. Hix, K. Iwamoto, K. Langanke, G. Martinez-Pinedo, K. Nomoto, M. Strayer, F.-K. Thielemann, H. Umeda, The role of electron captures in chandrasekhar mass models for type ia supernovae. Astrophys. J. **536**, 934 (2000)
7. F.-K. Thielemann, J. Isern, A. Perego, P. von Ballmoos, Nucleosynthesis in supernovae. Space Sci. Rev. **214**, 62 (2018)
8. P. Hoeflich, A. Khokhlov, Explosion models for type IA supernovae: a comparison with observed light curves, distances, H 0, and Q 0. Astrophys. J. **457**, 500 (1996)
9. P. Hoeflich, E. Y. Hsiao, C. R. Ashall, and the CSP collaboration, Light and color curve properties of type Ia supernovae: theory versus observations. Astron. J. **846**, 58 (2017)
10. C. Gall, M.D. Stritzinger, C. Ashall, E. Baron, C.R. Burns, P. Hoeflich et al., Two transitional type Ia supernovae located in the Fornax cluster member NGC 1404: SN 2007on and SN 2011iv. Astron. Astrophys. **611**, A58 (2018)
11. M.D. Stritzinger, B.J. Shappee, A.L. Piro, et. al., Red vs Blue: early observations of thermonuclear supernovae reveal two distinct populations? ArXiv e-prints, July 2018
12. P. Hoeflich, C.L. Gerardy, K. Nomoto, K. Motohara, R.A. Fesen, K. Maeda, T. Ohkubo, N. Tominaga, Signature of electron capture in iron-rich ejecta of SN 2003du. Astron. J. **617**, 1258–1266 (2004)
13. R. Penney, P. Hoeflich, Thermonuclear supernovae: probing magnetic fields by positrons and late-time IR line profiles. Astron. J. **795**, 84 (2014)
14. T.R. Diamond, P. Hoeflich, C.L. Gerardy, Late-time near-infrared observations of SN 2005df. Astron. J. **806**, 107 (2015)
15. C.L. Gerardy, P. Hoeflich, R.A. Fesen et al., SN 2003du: signatures of the circumstellar environment in a normal SNe Ia? Astron. J. **607**, 391–405 (2004)
16. C.M. Telesco, P. Hoeflich, D. Li et al., Mid-IR spectra of type Ia SN 2014J in M82 spanning the first 4 months. Astron. J. **798**, 93 (2015)
17. Y. Yang, L. Wang, D. Baade, P.J. Brown, A. Cikota, M. Cracraft, P.A. Höflich, J.R. Maund, F. Patat, W.B. Sparks, J. Spyromilio, H.F. Stevance, X. Wang, J.C. Wheeler, Late-time flattening of type ia supernova light curves: constraints from SN 2014J in M82. Astron. J. **852**, 89 (2018)
18. M.M. Phillips, The absolute magnitudes of Type IA supernovae. Astron. J. Lett. **413**, L105–L108 (1993)
19. R. Di Stefano, R. Voss, J.S.W. Claeys, Single-and double-degenerate models of type Ia Sne, nuclear-burning white dwarfs, spin, and supersoft X-ray sources, in *AAS/High Energy Astrophysics Division*, vol. 12 (2011), page 33.04
20. C. Contreras, M. Hamuy, M.M. Phillips et al., The Carnegie supernova project: first photometry data release. Astron. J. **139**, 519–539 (2010)
21. F. Patat, P. Hoeflich, D. Baade et al., VLT Spectropolarimetry of the Type Ia SN 2005ke. A step towards understanding subluminous events. Astron. Astrophys. **545**, A7 (2012)
22. A. Rest, N.B. Suntzeff, K. Olsen et al., Light echoes from ancient supernovae in the Large Magellanic Cloud. Nature **438**, 1132–1134 (2005)
23. K.J. Shen, K. Moore, The initiation and propagation of helium detonations in white dwarf envelopes. Astron. J. **797**, 46 (2014)
24. P. Höflich, B.E. Schaefer, X-ray and gamma-ray flashes from type ia supernovae? Astron. J. **705**, 483–495 (2009)

Chapter 32
Experimental Study of the $^{30}P(p,\gamma)^{31}S$ Reaction in Classical Novae

A. Meyer, N. de Séréville, F. Hammache, P. Adsley, A. Parikh, M. Assié, M. Assunção, B. Bastin, D. Beaumel, K. Béroff, Alain Coc, G. D'Agata, C. Delafosse, F. De Oliveira, F. Flavigny, S. P. Fox, A. Georgiadou, A. Gottardo, L. Grassi, J. Guillot, V. Guimaräes, N. Hubbard, T. Id Barkach, J. Kiener, A. M. Laird, A. L. Lara, M. MacCormick, I. Matea, L. Olivier, N. Oulebsir, L. Perrot, C. Portail, J. Riley, Á. M. Sánchez Benítez, I. Stefan and V. Tatischeff

A. Meyer (✉) · N. de Séréville · F. Hammache · P. Adsley · M. Assié · D. Beaumel · C. Delafosse · F. Flavigny · A. Georgiadou · A. Gottardo · L. Grassi · J. Guillot · T. Id Barkach · M. MacCormick · I. Matea · L. Olivier · L. Perrot · C. Portail · I. Stefan
Institut de Physique Nucléaire, IN2P3/CNRS-Université de Paris XI, 91406 Orsay Cedex, France
e-mail: meyer@ipno.in2p3.fr

A. Parikh
Departament de Física i Enginyeria Nuclear, Universitat Politècnica de Catalunya, 08036 Barcelona, Spain

M. Assunção · V. Guimaräes · A. L. Lara
Instituto de Física, Universidade de São Paulo, Rua do Matão 1371, São Paulo 05508-090, Brazil

B. Bastin · F. De Oliveira · Á. M. Sánchez Benítez
Grand Accélérateur National d'Ions Lourds (GANIL), CEA/DRFCNRS/IN2P3, Bvd. Henri Becquerel, 14076 Caen, France

K. Béroff
Institut des Sciences Moléculaires d'Orsay (ISMO), UMR 8214, CNRS, Université Paris Sud, Orsay, France

A. Coc · J. Kiener · V. Tatischeff
Centre des Sciences Nucléaires et des Sciences de la Matière (CSNSM), IN2P3/CNRS-Université de Paris XI, 91405 Campus Orsay, France

G. D'Agata
INFN-Laboratori Nazionali del Sud, Via S. Sofia, 95125 Catania, Italy

G. D'Agata
Dip. di Fisica e Astronomia, Università di Catania, Via S. Sofia, 95125 Catania, Italy

S. P. Fox · N. Hubbard · A. M. Laird · J. Riley
Department of Physics, The University of York, York YO10 5DD, UK

N. Oulebsir
Laboratoire de Physique Théorique, Université Abderahmane Mira, 06000 Béjaia, Algeria

Á. M. Sánchez Benítez
Departamento de Ciencias Integradas, University of Huelva, 21071 Huelva, Spain

A. Formicola et al. (eds.), *Nuclei in the Cosmos XV*, Springer Proceedings in Physics 219, https://doi.org/10.1007/978-3-030-13876-9_32

Abstract The $^{30}P(p,\gamma)^{31}S$ reaction is one of the few remaining reactions whose rate uncertainty has a strong impact on classical novae model predictions. To reduce the nuclear uncertainties associated to this reaction, we measured the $^{31}P(^{3}He,t)^{31}S$ reaction at the ALTO facility. Simultaneous detection of the triton and proton decays from the populated resonances will provide the proton branching ratios. The astrophysical context of this work, the current situation of the $^{30}P(p,\gamma)^{31}S$ reaction rate, the experimental set-up and the analysis of the single and coincidence events will be presented.

32.1 Introduction

Classical novae occur in binary systems consisting of a white dwarf accreting hydrogen-rich material from a companion main-sequence star. The outer layers of the underlying white dwarf are mixed with the accreted material. The pressure and the temperature in the accumulated envelope increase until a thermonuclear runaway occurs, ejecting part of the envelope into the circumstellar medium. Although theoretical models are successful in reproducing the overall characteristics of classical novae, several key issues remain unexplained, such as the mixing mechanism and the degree of mixing between the outer layers of the white dwarf and the accreted matter, and the observed ejecta masses.

Sensitivity studies using one-dimensional hydrodynamical models [1] and post-processing calculations [2] have shown that the $^{30}P(p,\gamma)^{31}S$ reaction is one of the few remaining reactions whose rate uncertainty has a strong impact on classical novae model predictions. Indeed, this reaction is a bottleneck for nucleosynthesis of nuclei up to Ca, the heaviest species that can be produced in ONe novae. In particular, the rate of the $^{30}P(p,\gamma)^{31}S$ reaction strongly influences the $^{30}Si/^{28}Si$ isotopic ratio, which is an important signature that helps to identify presolar meteoritic grains that may originate from a nova [3]. Furthermore, studies identified that elemental abundance ratios of Si/H, O/S, S/Al, O/P and P/Al can be used to constrain the degree of mixing [4] and the peak temperature during the explosion [5]. The predicted ratios of these elemental abundances are greatly affected by the $^{30}P(p,\gamma)^{31}S$ reaction rate uncertainty.

32.2 $^{30}P(p,\gamma)^{31}S$ Current Status

Resonances involved in the $^{30}P(p,\gamma)^{31}S$ reaction correspond to excited states in the ^{31}S compound nucleus located above the proton threshold (S_p = 6.131 MeV). The relevant energy range, known as the Gamow window, goes up to 600 keV above this threshold for temperatures achieved in classical novae (0.1–0.4 GK). A direct measurement of the $^{30}P(p,\gamma)^{31}S$ cross section is not currently feasible due to the low available intensities of ^{30}P radioactive ion beams. So far, various indirect methods

have been used to populate the states in the Gamow window. More recent experimental works have concentrated on determining the energies, spins and parities of these states [6–12].

In order to calculate the reaction rate, which is expected to be dominated by the sum of contributions from narrow, isolated resonances, the resonance strengths ($\omega\gamma$) are necessary:

$$\omega\gamma = \frac{(2J_R + 1)}{(2J_p + 1)(2J_{^{30}P} + 1)} \frac{\Gamma_p \Gamma_\gamma}{\Gamma}, \tag{32.1}$$

where J_R, J_p and $J_{^{30}P}$ are the spins of the resonance in ^{31}S, the proton and ^{30}P (ground state), respectively. The total width of the resonance Γ is the sum of the proton partial width Γ_p and the γ-ray partial widths Γ_γ (other decay channels are energetically forbidden at the excitation energies of interest). Strengths of key low energy resonances close to the proton threshold have recently been constrained experimentally [10]. So far, the proton branching ratios were measured once for states above 6.7 MeV at Yale University's Wright Nuclear Structure Laboratory [13].

We performed a new measurement of proton branching ratios to extend the existing data to states at lower excitation energy and to reduce the current uncertainties. For this purpose, the same charge-exchange reaction ^{31}P(^{3}He,t)^{31}S used at Yale was used to populate the states of interest in ^{31}S.

32.3 Experiment

The choice of the charge-exchange reaction was motivated by its low selectivity, thus most known states above the proton threshold are populated [14, 15].

A 25-MeV ^{3}He beam from the tandem accelerator at the ALTO facility (Accélérateur Linéaire et Tandem d'Orsay) was used to bombard a ^{31}P target of 53 μg/cm^2-thickness deposited onto a 104 μg/cm^2-thick carbon backing. An Enge split-pole magnetic spectrometer [16] at 10° in the laboratory was used to momentum analyze the emitted particles (*p, d, t,* α) which were detected at the focal plane of the spectrometer by a position-sensitive gas chamber, a proportional gas-counter (energy loss measurement) and a plastic scintillator (residual energy measurement). Six Double-Sided Silicon Strip Detectors (DSSSDs) were mounted at backward angles in the reaction chamber to detect the protons from the decay of the populated states of ^{31}S emitted in coincidence with the tritons. A schematic of the experiment set-up can be found in [17].

A Faraday cup was positioned at 0° to stop the beam and measure the accumulated charge. A thick shield was set up across the center of the reaction chamber to protect the silicon detectors from radiation coming from beam-induced radioactivity in the Faraday cup and beam scattering (see Fig. 32.1). Mounts with two vertically stacked DSSSDs were used such as three angular ranges were covered from θ_{lab} = 103° to 171.5°. Since the split-pole was set at 10° in the laboratory, corresponding to

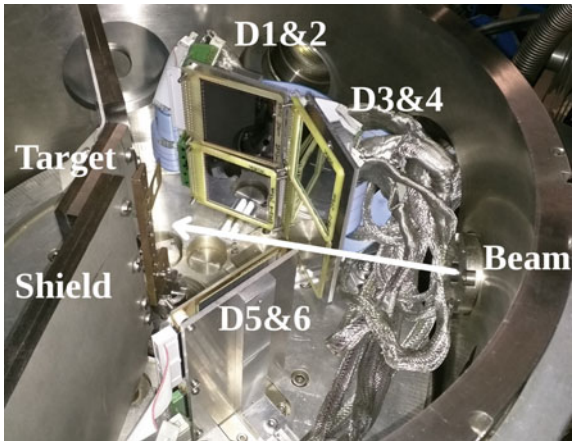

Fig. 32.1 Photograph of the DSSSD array inside the split-pole reaction chamber. A Faraday cup is placed at 0° behind the target ladder and is shielded from the DSSSDs

$\theta_{c.m.} \simeq 28°$ for the recoiling ^{31}S nuclei, the center-of-mass of the recoil angular coverage of the DSSSD array was between 75° and 177.5°, leading to a better center-of-mass angular coverage compared to the Yale setup for which the split-pole angle was 1.5° [13]. In this experiment, the discriminator threshold was lowered in order to detect the low-energy protons, having energies of a few hundred keV, associated with the resonances of interest.

32.4 ^{31}P(^{3}He,t)^{31}S*(p)^{30}P Single and Coincidence Events

The focal-plane magnetic rigidity (Bρ) spectrum at energies of astrophysical interest (indicated by black arrows in Fig. 32.2) was obtained after triton particle identification (as described in [17]).

To extract the t-p coincidence events, the DSSSDs were first calibrated in energy using a pulse generator to obtain the electronic offset and a triple nuclide alpha-particle source to measure the gain factor. A similar energy deposited, within 3 times the resolution, was required in the front and back strips within a same silicon detector. The time difference between the DSSSDs and the split-pole events, gated on the tritons, showed that the t-p coincidence events formed a peak above the random coincidence background, with a time resolution of about 25 ns which agrees with the kinematics of the reaction. After applying a cut on the timing peak, the proton kinematic locus could be seen on the DSSSD energy versus split-pole magnetic rigidity spectrum (see Fig. 32.3). The most prominent diagonal band corresponds to proton decays of resonances in ^{31}S to the ground state of ^{30}P.

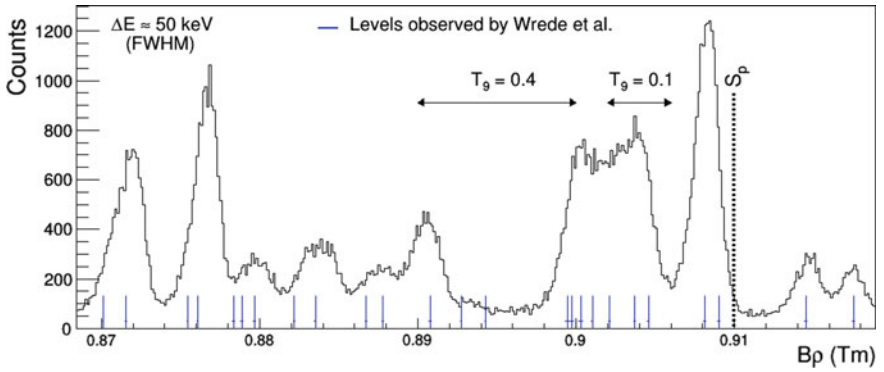

Fig. 32.2 Focal-plane triton spectrum from the $^{31}P(^{3}He,t)^{31}S$ reaction at 25 MeV and $\theta_{lab} = 10°$. Black arrows indicate the energy range of the Gamow window for the two extreme temperatures of interest. The comparison with the levels observed by Wrede et al. [13], in blue, shows a satisfying agreement

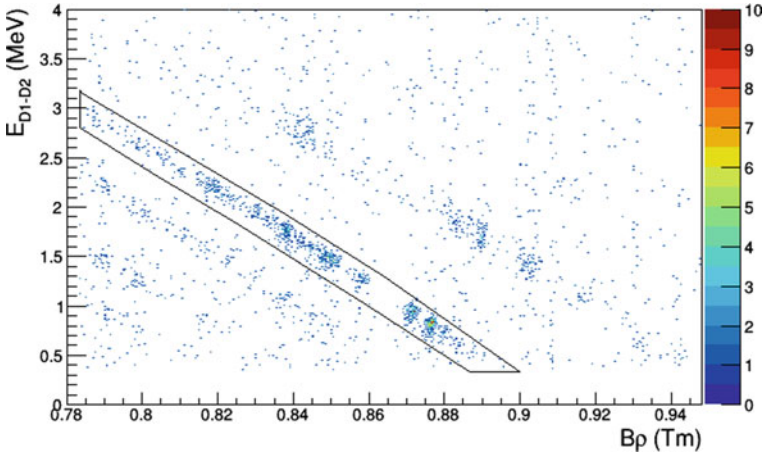

Fig. 32.3 Energy in the DSSSDs 1 and 2 (see Fig. 32.1) versus split-pole magnetic rigidity ($B\rho$) spectrum of canditate t-p coincidence events from the $^{31}P(^{3}He,t)^{31}S^{*}(p)^{30}P$ reaction. The most prominent diagonal band, indicated by the black selection, corresponds to proton decays of resonant states in $^{31}S^{*}$ to the ground state of ^{30}P

32.5 Summary and Perspectives

The $^{30}P(p,\gamma)^{31}S$ reaction is important for classical novae nucleosynthesis. We performed a coincidence measurement using the non selective $^{31}P(^{3}He,t)^{31}S$ reaction to indirectly populate ^{31}S unbound states and extract the proton branching ratios. The triton-singles events spectrum has been obtained and the t-p coincidence events have

been identified. Analysis is in progress to extract the final coincidence spectrum and the angular correlations. The proton branching ratios which will be finally obtained will be used to calculate an updated ^{30}P(p,γ)^{31}S reaction rate.

References

1. J. José et al., Synthesis of intermediate-mass elements in classical novae: from Si to Ca. Astrophys. J. **560**, 897 (2001)
2. C. Iliadis et al., The effects of thermonuclear reaction-rate variations on nova nucleosynthesis: a sensitivity study. Astrophys. J. Suppl. **142**, 105 (2002)
3. S. Amari et al., Presolar grains from novae. Astrophys. J. **551**, 1065 (2001)
4. K.J. Kelly et al., Nuclear mixing meters for classical novae. Astrophys. J. **777**, 130 (2013)
5. L.N. Downen et al., Nuclear thermometers for classical novae. Astrophys. J. **762**, 105 (2013)
6. A. Parikh et al., Improving the ^{30}P(p,γ)^{31}S rate in oxygen-neon novae: constraints on J$^{\pi}$ values for proton-threshold states in ^{31}S. Phys. Rev. C **83**(4), 045806 (2011)
7. D. Irvine et al., Evidence for the existence of the astrophysically important 6.40-MeV state of ^{31}S. Phys. Rev. C **88**(5), 055803 (2013)
8. D.T. Doherty et al., Level structure of ^{31}S: From low excitation energies to the region of interest for hydrogen burning in novae through the ^{30}P(p,γ)^{31}S reaction. Phys. Rev. C **89**, 045804 (2014)
9. B.A. Brown et al., Shell-model studies of the astrophysical rapid-proton-capture reaction ^{30}P(p,γ)^{31}S. Phys. Rev. C **89**, 062801 (2014)
10. A. Kankainen et al., Measurement of key resonance states for the ^{30}P(p,γ)^{31}S reaction rate, and the production of intermediate-mass elements in nova explosions. Phys. Lett. B **769**, 549 (2017)
11. M.B. Bennett et al., Isospin mixing reveals ^{30}P(p,γ)^{31}S resonance influencing nova nucleosynthesis. Phys. Rev. Lett. **116**, 102502 (2016)
12. M.B. Bennett et al., Detailed study of the decay ^{31}Cl(β,γ)^{31}S. Phys. Rev. C **97**, 065803 (2018)
13. C. Wrede et al., Measurement of ^{31}S energy levels and reevaluation of the thermonuclear resonant ^{30}P(p,γ)^{31}S reaction rate. Phys. Rev. C **79**(4), 045803 (2009)
14. C. Wrede et al., New ^{30}P(p,γ)^{31}S resonances and oxygen-neon nova nucleosynthesis. Phys. Rev. C **76**(5), 052802(R) (2007)
15. A. Parikh et al., Spectroscopy of the ^{19}Ne for the thermonuclear ^{15}O(α,γ)^{19}Ne and ^{18}F(p,α)^{15}O reaction rates. Phys. Rev. C **92**, 055806 (2015)
16. J.E. Spencer, H.A. Enge, Split-pole magnetic spectrograph for precision nuclear spectroscopy. Nucl. Instrum. Methods **49**, 181 (1967)
17. A. Meyer et al., Study of key resonances in the ^{30}P(p,γ)^{31}S reaction in classical novae. EPJ Web Conf. **184**, 02010 (2018)

Chapter 33
s-Processing from MHD-Induced Mixing and Isotopic Abundances in Presolar SiC Grains

Sara Palmerini, Maurizio Busso, Oscar Trippella and Diego Vescovi

Abstract It has been known for decades that s-process elements from Sr to Pb are produced by Asymptotic Giant Branch stars. However only recently, physically-based mixing mechanisms for the formation of ^{13}C have been proposed. Among them, we aim to verify the robustness of the model of a MHD induced ^{13}C-pocket formation. In doing that we present results of nucleosynthesis models for low mass AGB stars, developed from the MHD scenario, compared with the isotopic abundance ratios of s-elements from presolar Mainstream SiC grains.

The slow neutron capture nucleosynthesis process (s-process) is responsible for the production of about 50% of nuclei heavier than Fe in the Galaxy. Several observational evidences demonstrate that low mass stars are the main site for s-process nucleosynthesis when ascending the so-called Asymptotic Giant Branch (or AGB). At present AGB nucleosynthesis models do provide a very nice fit to the observational constrains and, in particular, to those coming from the isotopic composition of presolar grains, which provide perhaps the strongest benchmark to the models. Indeed these tiny particles of dust are litteraly pieces of the stars in which they form and their isotopic composition can be determined in terrestrial laboratories with high precision (up to per mil). Results achieved by AGB nucleosynthesis models in reproducing the record of isotopic abundance ratios of s-elements in presolar Mainstream

S. Palmerini (✉) · M. Busso
Dipartimento di Fisica e Geologia, Università degli Studi di Perugia,
via A. Pascoli, 06125 Perugia, Italy
e-mail: sara.palmerini@pg.infn.it

S. Palmerini · M. Busso · O. Trippella · D. Vescovi
I.N.F.N. Sezione di Perugia, via A. Pascoli, 06125 Perugia, Italy

D. Vescovi
Gran Sasso Science Institute, viale F. Crispi, 7, 67100 L'Aquila, Italy

A. Formicola et al. (eds.), *Nuclei in the Cosmos XV*, Springer
Proceedings in Physics 219, https://doi.org/10.1007/978-3-030-13876-9_33

SiC grains[1] have been reported, among several authors involved in the field, in the recent papers by Liu et al. [1–4]. In low mass AGBs ($M \leq 3M_{\odot}$) the $^{13}C(\alpha,n)^{16}O$ reaction, burning in the He-intershell, is the main source of neutrons for the s-process and the crucial point is to determine the "size" and the profile of the ^{13}C reservoir that better accounts for the observations. This is the parametric approach adopted in the years by researchers forced to extensive parameterisations by the lack of knowledge about the physical mechanisms responsible for the injection of protons from the stellar envelope into the He-rich layers, which yields to the formation of the ^{13}C pocket. Only recently, attempts to solve this problem started to consider quantitatively physically-based mixing mechanisms. Among them, MHD[2] processes in the plasma were suggested to yield mass transport thanks to magnetic buoyancy [5].

The MHD-mixing has been already proven to account for the composition of oxide grains of AGB origin, when applied to the H-shell of AGB stars with $M \leq 2M_{\odot}$ [6]. We aim to verify if the same mechanism might also drive the formation of a ^{13}C pocket suitable to reproduce the signature of the s-process recorded in the composition of SiC grains (which form in the envelope of C-rich AGB stars). For this reason we have not undertaken a fine tunning of the parameters defining the "pocket", but we compare with grain abundances the output of our nucleosynthesis models, in which the ^{13}C reservoir is shaped by the stellar MHD coupled with physical conditions of the stellar layers below the convection at the moment of the third dredge-up (namely the plasma diffusivity, kinematic viscosity, and the magnetic Prandtl number, see [7] and [8] for details).

Examples of the comparisons between our predictions for isotopic and elemental ratios, pulse after pulse, and the measured data are included in Figs. 33.1, 33.2 and 33.3. For brevity, we show here comparisons between model predictions and measurements just for a few isotopic ratios of Zr and Ba, which we choose as the most rappresentative ones belonging to the light (*ls*) and heavy (*hs*) s-elements group, respectively. Moreover, we show the comparison of the trends displayed by Zr isotopes with respect to those of Ba (Fig. 33.3), being the correlation between *ls* and *hs* a crucial constraint on the ^{13}C pocket (see e.g. [3]). In the right-hand panels of the figures, we present the model curves pertaining to the G-component of calculations for $3M_{\odot}$ stars, which represent the maximum nucleosynthesis effects possible for each model free from any isotopic shifts induced by the mass loss choices adopted in the stellar models. Even if error bars of grain data are large and not all the points are reproduced, Figs. 33.1, 33.2 and 33.3 present a satisfactory agreement between models and measurements. Indeed the quality of the fit that models adopting the magnetic ^{13}C pocket offer to grain data is comparable with that of other "parametric" attempts to reproduce the SiC isotopic abundances, available in the literature. An extended discussion and more details on the comparison between our model predictions and grain data can be found in the paper by Palmerini et al. 2018 [10].

[1] Among Silicon Carbide (SiC) grains those belonging to the Mainstream group are the most numerous and have carbon and nitrogen isotopic compositions that, together with traces of s-elements, hint to AGB origins.

[2] Magnetic Hydro Dynamic.

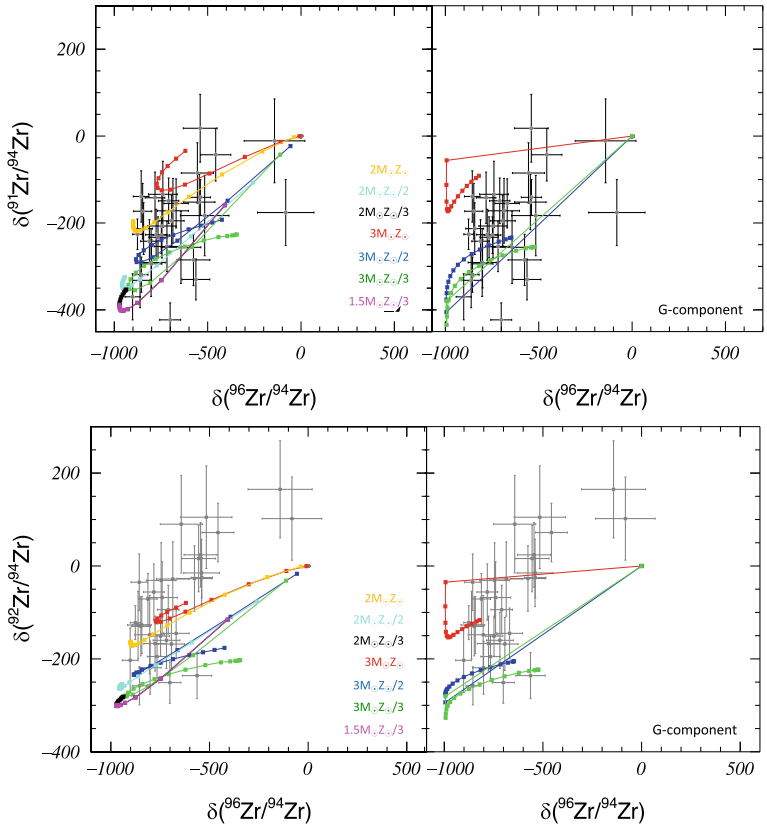

Fig. 33.1 Comparison between our model predictions and presolar grain abundances in two three-isotope plots for Zr. The measurements of $^{91}Zr/^{94}Zr$, $^{92}Zr/^{94}Zr$, and $^{96}Zr/^{94}Zr$ in SiC grains are from [3] and [9]. The curves show the evolution in time of the abundances in the stellar envelopes; the dots along the lines represent the various thermal pulses. Model calculations are for AGB stars with mass from 1.5 to $3M_{\odot}$ and metallicity from 1/3 solar to solar, as indicated by the labels. The G-component, namely the pure s-process composition of the He-intershell material, is included in the right panel for the $3M_{\odot}$ models to show the maximum effect achievable by nucleosynthesis processes

Very recently, Liu et al. [4] confirmed that Sr-Ba isotopic abundances in SiC grain can be well reproduced by the MHD induced ^{13}C-pocket [8], which, at the state of the art, is the sole model able to consistently explain also the Ni isotopic distribution recorded in these grains [11]. After reproducing the s-element distribution in the Sun [7] and in post-AGB stars [8], addressing the precise constraints offered by the record of isotopic abundance ratios in presolar SiC grains is the third test successfully passed by the MHD-induced mixing in the field of the s-process. This fact suggests that, among all the physical models proposed for the formation of the ^{13}C-pocket, this mechanisms is perhaps the most promising one being able to account for

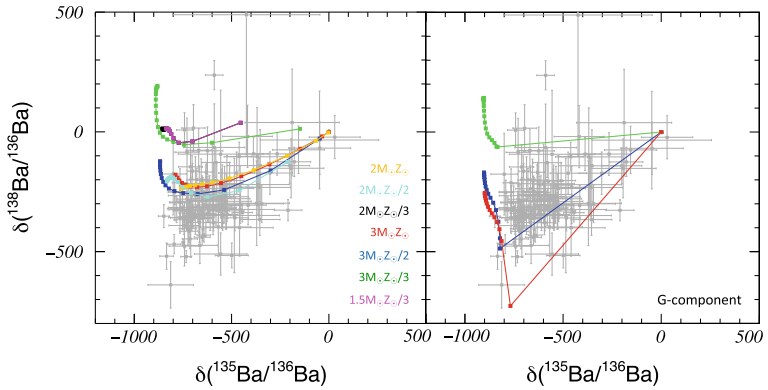

Fig. 33.2 Comparison between our model predictions and presolar grain abundances in a three-isotope plots for Ba. The nucleosynthesis models and the notation used are the same as in Fig. 33.1. The measurements of $^{138}Ba/^{136}Ba$ and $^{135}Ba/^{136}Ba$ in Mainstream SiC grains are from [3] and [9]

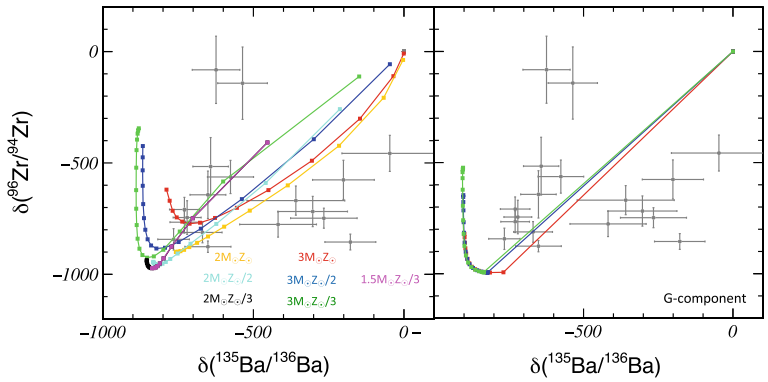

Fig. 33.3 Comparisons between our model predictions and values for some Ba and Zr isotopes, using $^{135}Ba/^{136}Ba$ as abscissa. The nucleosynthesis models and the notation used are the same as in Fig. 33.1. Measurements in presolar SiC grains are from [9]

observational and experimental constraints coming from heterogeneous sources. However a big challenge remains: understanding the origins of short-lived radioactivities in the early Solar System. Indeed so far none of the suggested models has been really able to reproduce the abundances of all the now extinct radioactivities, which were alive in the solar nebula [12].

References

1. N. Liu, R. Gallino, S. Bisterzo et al., Astron. J. **786**, 66 (2014)
2. N. Liu, R. Gallino, S. Bisterzo et al., Astron. J. **788**, 163 (2014)

3. N. Liu, M.R. Savina, R. Gallino, S. Bisterzo et al., Astron. J. **803**, 12 (2015)
4. N. Liu, R. Gallino, S. Cristallo et al., arXiv:1808.03614
5. M.C. Nucci, M. Busso, Astron. J. **787**, 141 (2014)
6. S. Palmerini, O. Trippella, M. Busso, Mon. Not. R. Astron. Soc. **467**, 1193 (2017)
7. O. Trippella, M. Busso, E. Maiorca et al., Astrophys. J. **787**, 41 (2014)
8. O. Trippella, M. Busso, S. Palmerini et al., Astrophys. J. **818**, 125 (2016)
9. K.M. Hynes, F. Gyngard, LPSC XL. Abstract **1198** (2009)
10. S. Palmerini, O. Trippella, M. Busso, Geochim. Cosmochim. Acta **221**, 21 (2018)
11. R. Trappitsch, T. Stephan, M.R. Savina et al., Geochim. Cosmochim. Acta **221**, 87 (2018)
12. D. Vescovi, M. Busso, S. Palmerini et al., Astron. J. **863**, 115 (2018)

Chapter 34
The Evolution of CNO Isotope Ratios: A Litmus Test for Stellar IMF Variations in Galaxies Across Cosmic Time

D. Romano, Z.-Y. Zhang, F. Matteucci, R. J. Ivison and P. P. Papadopoulos

Abstract Determining the shape of the stellar initial mass function (IMF) and whether it is constant or varies in space and time is the Holy Grail of modern astrophysics, with profound implications for all theories of star and galaxy formation. On a theoretical ground, the extreme conditions for star formation (SF) encountered in the most powerful starbursts in the Universe are expected to favour the formation of massive stars. Direct methods of IMF determination, however, cannot probe such systems, because of the severe dust obscuration affecting their starlight. The next best option is to observe CNO bearing molecules in the interstellar medium at millimetre/submillimetre wavelengths, which, in principle, provides the best indirect evidence for IMF variations. In this contribution, we present our recent findings on this issue. First, we reassess the roles of different types of stars in the production of CNO isotopes. Then, we calibrate a proprietary chemical evolution code using Milky Way data from the literature, and extend it to discuss extragalactic data. We show that, though significant uncertainties still hamper our knowledge of the evolution of CNO isotopes in galaxies, compelling evidence for an IMF skewed towards high-mass stars can be found for galaxy-wide starbursts. In particular, we analyse

D. Romano (✉)
INAF, Astrophysics and Space Science Observatory,
via Gobetti 93/3, 40129 Bologna, Italy
e-mail: donatella.romano@oabo.inaf.it

Z.-Y. Zhang · R. J. Ivison
Institute for Astronomy, University of Edinburgh, Royal Observatory,
Blackford Hill, Edinburgh EH9 3HJ, UK

ESO, Karl-Schwarzschild-Str. 2, 85748 Garching bei München, Germany

F. Matteucci
Physics Department, University of Trieste, via Tiepolo 11, 34131 Trieste, Italy

INAF, Osservatorio Astronomico di Trieste, via Tiepolo 11, 34131 Trieste, Italy

INFN, Sezione di Trieste, via Valerio 2, 34127 Trieste, Italy

P. P. Papadopoulos
Department of Physics, Section of Astrophysics, Astronomy and Mechanics,
Aristotle University of Thessaloniki, 54124 Thessaloniki, Greece

Research Center for Astronomy, Academy of Athens, Athens, Greece

A. Formicola et al. (eds.), *Nuclei in the Cosmos XV*, Springer
Proceedings in Physics 219, https://doi.org/10.1007/978-3-030-13876-9_34

a sample of submillimetre galaxies observed by us with the Atacama Large Millimetre Array at the peak of the SF activity of the Universe, for which we measure $^{13}C/^{18}O \simeq 1$. This isotope ratio is especially sensitive to IMF variations, and is little affected by observational uncertainties. At the end, ongoing and future developments of our work are briefly outlined.

34.1 The Stellar IMF and Its Chemical Imprints

First introduced by Salpeter [1], the stellar initial mass function (IMF) parameterizes the relative numbers of stars that fall in different mass ranges. Since a star's initial mass is the main driver of its evolution, it goes without saying how crucial the IMF is to studies of star and galaxy formation and evolution.

Stars of different initial masses inject in the interstellar medium (ISM) various chemical elements, on different timescales. The net yields[1] are a strong function of the adopted IMF (the stellar metallicity plays a secondary role, except at extremely low metallicities). The IMF shape can thus be recovered, in principle, from its chemical imprints [3]. This is particularly attractive for environments where direct observations are unfeasible. Indeed, direct observations (either star counts or integrated stellar properties) are limited to optical, ultra-violet and near-infrared wavelengths. They have generally led to the notion of a universal IMF in the local Universe ([4], but see [5, 6]), but provided hints for variations in early-type galaxies [7, 8]. In this contribution we deal with high-redshift submillimetre galaxies (SMGs), that undergo vigorous star formation (SF) with rates of conversion of gas into stars of 100–1000 $M_\odot$ yr^{-1} [9], and have their stellar light heavily obscured by dust [10]. We focus on these systems because it is exactly in their high-density, cosmic-ray dominated ISM where fundamentally altered conditions for SF are met [11], possibly resulting in an IMF sensibly biased towards high-mass stars [12]. The question is then, are there any practical, indirect methods to probe the IMF in these dust-shrouded systems?

34.2 Carbon, Nitrogen, and Oxygen: Stellar Production and Galactic Evolution

It has been pointed out [13, 14] that CNO-bearing molecules observed at millimetre/submillimetre wavelengths might provide the best evidence for IMF variations in dust-obscured galaxies, straight after direct determinations. We have demonstrated [15, 16] that, in particular, the $^{13}C/^{18}O$ ratio is most sensible to IMF variations and

[1] The net yield of a given element is defined as the matter restored to the ISM in the form of the newly created element, normalized to the total mass locked up into low mass stars and stellar remnants, per stellar generation [2].

little biased by differential astro-chemical and lensing effects for the bulk of the molecular gas in galaxies; this permits its use as a functional IMF tracer in high-redshift starbursts. Our assertion is based on current instrumental and theoretical advancements; in the following we discuss the latter.

The main isotope of carbon, ^{12}C, is forged as a primary element (i.e., starting from hydrogen and helium) in stars of all masses. The other stable carbon isotope, ^{13}C, is produced (similarly to ^{14}N) mostly in intermediate-mass stars, partly as a primary and partly as a secondary element (when starting from ^{12}C seeds already present at star's birth). Massive stars may provide significant amounts of primary ^{13}C and ^{14}N at very low metallicities, but only if they rotate fast [17]. Regarding oxygen, ^{16}O and ^{18}O are synthesised in high-mass stars, the first as a genuine primary element and the second mainly as a secondary one. Intermediate-mass stars and novae both produce interesting amounts of ^{17}O. Novae are also responsible for the synthesis of ^{15}N (see J. José, these proceedings). Overall, both ^{12}C/^{13}C and ^{16}O/^{18}O in galaxies are expected to decrease with time (metallicity). In Fig. 34.1, the predictions of our best-fit chemical evolution model for the Milky Way are compared with the relevant ^{12}C/^{13}C (upper panels) and ^{16}O/^{18}O data (lower panels; see [15] for details). As [15] remarked, given the paucity of data for the solar neighbourhood (left panels), in order to select the best-fitting yield set it is mandatory to analyse the Galactic gradient (right panels). We find a good match between model predictions and observations when using the yields from [18] for low- and intermediate-mass stars and [19] for massive stars. We stress that this choice is not unique; in particular, we need to test new

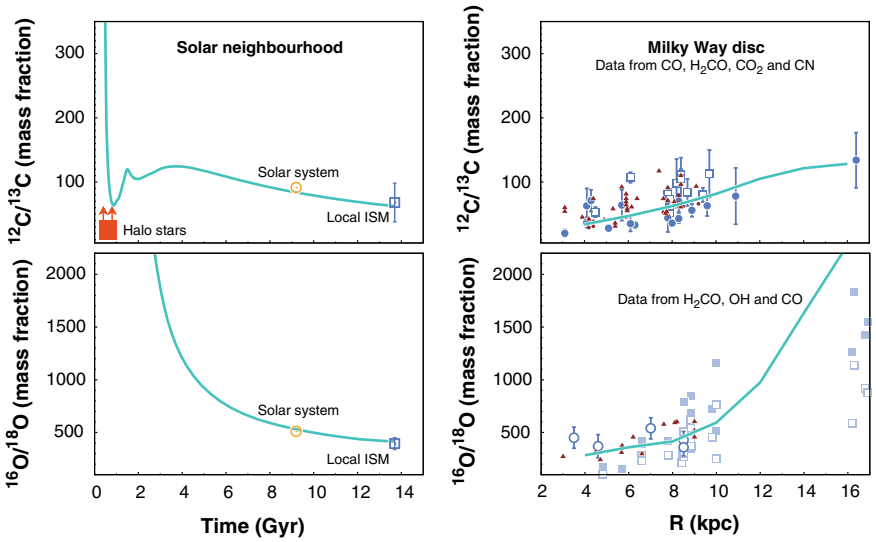

Fig. 34.1 *Upper panels*: evolution of ^{12}C/^{13}C in the solar neighbourhood (on the left) and present-day gradient across the Galactic disc (on the right). The predictions of the best-fitting model of [15] are shown together with the data from different sources (see [15] for references). *Lower panels*: same for ^{16}O/^{18}O

stellar yields that have recently –or will soon– become available for use in chemical evolution models (see A. Chieffi and R. Hix, these proceedings).

Once the stellar yields are calibrated against the Milky Way data, we can build up models for other galaxies. In particular, we want to explain the ratio of $^{13}C/^{18}O \simeq 1$ measured by us [16] from simultaneous observations of ^{13}CO and $C^{18}O$ emission lines using the Atacama Large Millimetre Array for a sample of four strong CO emitters. Our targets are caught at redshift 3–2, namely, two to three billion years after the big bang. They are expected to have SF histories cleaner than local starbursts (that emerge after ∼13 Gyr of evolution) and, hence, ISM abundances more closely related to the current SF episode. We first assume a Kroupa IMF (the same adopted for the Milky Way), and change the strength and duration of the SF episode until a value of $^{13}C/^{18}O \simeq 1$ is obtained. The final stellar mass is 2×10^{11} $M_\odot$ in all cases, typical of SMGs. With the Kroupa IMF, only short bursts (lasting less than 100 Myr) with unrealistically high SF rates (up to 15,000 $M_\odot$ yr^{-1}) can match ISM values of $^{13}C/^{18}O$ around unity (see Fig. 34.2, right-hand panels). The ratio, moreover, suddenly increases to standard galactic disc values as soon as the SF activity ceases, owing to the delayed release of substantial amounts of ^{13}C from intermediate-mass stars. The only way to recover a stable, low $^{13}C/^{18}O$ value is to assume an IMF skewed towards high-mass stars (see Fig. 34.2, left-hand panels).

Conclusions and Outlook. Our result that the IMF must be top-heavy in high-redshift starbursts is based on a novel approach –we measure the $^{13}C/^{18}O$ ratio in these systems in a regime free from the pernicious effects of dust and use detailed chemical evolution models to disentangle the effects of changes in the IMF or in the

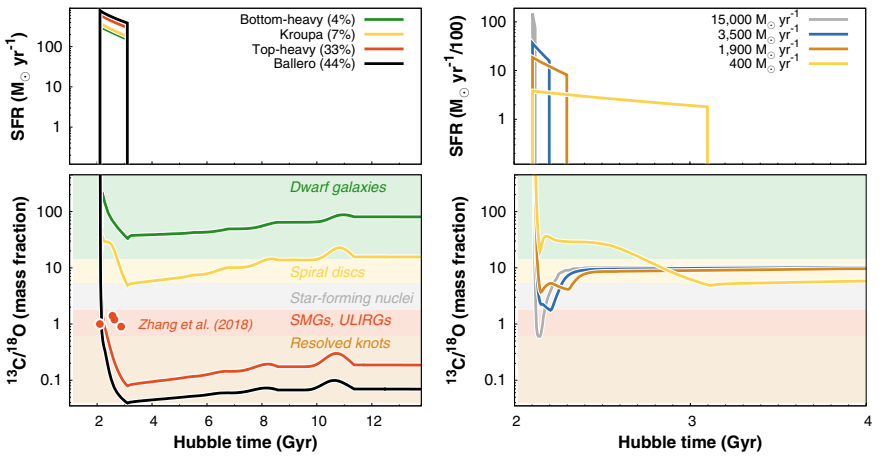

Fig. 34.2 SF rates *(upper panels)* and evolution of $^{13}C/^{18}O$ *(lower panels)* for seven representative SMG models. We modify either the IMF (left-hand panels) or the SF strength and duration (right-hand panels), but always end up with $2 \times 10^{11} M_\odot$ of stars. The fraction of high-mass stars ($m > 8 M_\odot$) is reported, for each IMF, in the top-right corner of the top-left panel. See [16], their Table 1, for details about the adopted IMFs

SF history on the predicted evolution– and is consistent with recent, independent claims of IMF variations in galaxies [6, 7, 12]. We are currently ploughing on with the extension of the analysis to other types of galaxies and to other abundance ratios. As discussed in [16], it is likely that most fundamental parameters in the field of galaxy formation and evolution will have to be re-addressed, following the increasing evidence for a non-universal IMF in galaxies.

References

1. E.E. Salpeter, Astrophys. J. **121**, 161 (1955)
2. A. Maeder, Astron. Astrophys. **264**, 105 (1992)
3. F. Matteucci, *Chemical Evolution of Galaxies* (Springer-Verlag, Berlin, 2012)
4. N. Bastian, K.R. Covey, M.R. Meyer, Ann. Rev. Astron. Astrophy. **48**, 339 (2010)
5. M. Geha et al., Astrophys. J. **771**, 29 (2013)
6. F.R.N. Schneider et al., Science **359**, 69 (2018)
7. M. Cappellari et al., Nature **484**, 485 (2012)
8. M. Sarzi et al., Mon. Not. R. Astron. Soc. **478**, 4084 (2018)
9. R.J. Ivison et al., Mon. Not. R. Astron. Soc. **298**, 583 (1998)
10. J.M. Simpson et al., Astrophys. J. **844**, L10 (2017)
11. P.P. Papadopoulos, Astrophys. J. **720**, 226 (2010)
12. Z. Yan, T. Jerabkova, P. Kroupa, Astron. Astrophys. **607**, A126 (2017)
13. C. Henkel, R. Mauersberger, Astron. Astrophys. **274**, 730 (1993)
14. P.P. Papadopoulos et al., Astrophys. J. **788**, 153 (2014)
15. D. Romano et al., Mon. Not. R. Astron. Soc. **470**, 401 (2017)
16. Z.-Y. Zhang, D. Romano et al., Nature **558**, 260 (2018)
17. G. Meynet, A. Maeder, Astron. Astrophys. **390**, 561 (2002)
18. A.I. Karakas, Mon. Not. R. Astron. Soc. **403**, 1413 (2010)
19. K. Nomoto, C. Kobayashi, N. Tominaga, Ann. Rev. Astron. Astrophys. **51**, 457 (2013)

Part IX
Techniques, Tools and Facilities for Nuclear Astrophysics

Chapter 35
Direct $^{13}C(\alpha,n)^{16}O$ Cross Section Measurement at Low Energies

A. Best, G. F. Ciani, J. Balibrea-Correa and L. Csedreki

Abstract The reaction $^{13}C(\alpha,n)^{16}O$ is the main neutron source in the "s process", which is responsible for the production of about half of the heavy elements in the universe. It operates in thermally pulsing low mass AGB stars at temperatures of about 90 MK. This translates to a Gamow window between 140 and 230 keV, far below the Coulomb barrier. Various measurements of the low energy cross section of $^{13}C(\alpha,n)^{16}O$ have been performed in the past, and while remarkable results have been achieved, ultimately the environmental background on the surface of the earth has been a limiting factor. The LUNA collaboration is currently performing a measurement of $^{13}C(\alpha,n)^{16}O$ in the low-background environment of the LNGS, where the environmental neutron flux is reduced by over three magnitudes with respect to the surface. This unique location, together with a high-efficiency low background detector and state of the art electronics that allow suppression of the intrinsic background, has already enabled us to push the low-energy cross section limit beyond what has been reached before. Here we present the current status of the experiment, the plans for an upcoming next measurement campaign and preliminary results.

The reaction $^{13}C(\alpha,n)^{16}O$ has been established as the main neutron source for the slow neutron capture ("s") process, which is responsible for the production of ∼50% of the elements heavier than iron in the universe (see [1] and references therein). The s process occurs in thermal pulsing asymptotic giant branch stars, at temperatures of around 90 MK. The corresponding effective energy range in which the reaction cross section needs to be known lies between about 140 and 230 keV. The cross section in this range is very low ($<10^{-12}$ b), making direct measurements very challenging.

A. Best, G. F. Ciani, J. Balibrea-Correa and L. Csedreki for the LUNA collaboration.

A. Best (✉) · J. Balibrea-Correa
Università di Napoli "Federico II", and INFN, Sezione di Napoli, 80126 Napoli, Italy
e-mail: andreas.best@unina.it

G. F. Ciani
Gran Sasso Science Institute, Viale F. Crispi 7, 67100 L'Aquila, Italy

L. Csedreki
INFN, Laboratori Nazionali del Gran Sasso (LNGS), 67100 Assergi, Italy

A. Formicola et al. (eds.), *Nuclei in the Cosmos XV*, Springer
Proceedings in Physics 219, https://doi.org/10.1007/978-3-030-13876-9_35

The extrapolation from higher-energy data into the astrophysically relevant region is complicated by the existence of a near threshold state in ^{17}O, whose influence on the cross section can only be inferred indirectly. Although in the recent years impressive progress has been made in both direct and indirect measurements (see [2] and references therein) further direct studies are desirable, providing cross section data very close to or inside of the Gamow window.

The measurements that have pushed the low-energy limits the most so far were limited by the natural background on the Earth's surface [3, 4]. In order to overcome the problem of the natural background and to allow measurements of the ^{13}C(α,n)^{16}O reaction at lower energies the LUNA (Laboratory for Underground Nuclear Astrophysics) collaboration is currently carrying out an experimental campaign in the deep underground Gran Sasso National Laboratory (LNGS). The $>$1 km rock overburden provides an efficient shielding from cosmic rays, basically eliminating the cosmic-ray induced component of the neutron background. The remaining neutron flux at the LNGS is due to fission and alpha-capture induced reactions in the surrounding rocks and the concrete walls of the laboratory. The thermal component, which is the dominant one, is reduced by a factor of $\approx 10^3$ with respect to the surface [5].

The setup used for the measurement consists of ^{3}He counters embedded in a thermalising polyethylene matrix and is described in detail in the articles by L. Csedreki and G. F. Ciani in the present volume. In order to suppress the internal background of the counters themselves the signals are digitised and a pulse shape discrimination method can be applied to identify neutron- and alpha-induced signals. This is discussed in the article by J. Balibrea-Correa in this volume and in [6]. In short, the detection efficiency of the setup is $>$30%, and the total background rate is about 4 counts/h (this background is approximately equally due to outside neutrons and intrinsic alphas). Targets are produced by evaporating enriched ^{13}C on Ta backings, and the stability as a function of deposited charge is regularly controlled by changing to a proton beam and performing an analysis of the shape of a primary gamma-ray from the ^{13}C(p,γ)^{14}N reaction.

The maximum beam energy at LUNA is 400 keV, allowing for some overlap with the previous direct data - although it needs to be said that the literature data at these low energies have very large uncertainties. In the near future this issue will be addressed by connecting the low-energy region to the better known higher-energy data using the to be installed 3.5 MV accelerator "LUNA MV". The goal of the present campaign is the measurement of the low energy cross section. Preliminary results are shown in Table 35.1 and Fig. 35.1. So far a total charge of about 80 C has been deposited on various targets, covering the energy range between 360 and 400 keV ($\sim$ 275 to 310 keV c.m.). The statistical uncertainty is about 10% even at the lowest energy, which is also the lowest energy ^{13}C(α,n)^{16}O data point ever directly measured.

The current experimental campaign foresees at least two more beam times and we are expecting to reach statistics of about 10% at 250 keV (c.m.). Also foreseen to be included in those beam times are dedicated measurements of the beam-induced background.

Table 35.1 Deposited charges and raw counts for the energies covered so far at LUNA

E_α (keV)	Charge (C)	Raw counts
400	11	1375
390	16.7	1408
380	17	1177
370	13.7	569
360	20.4	474

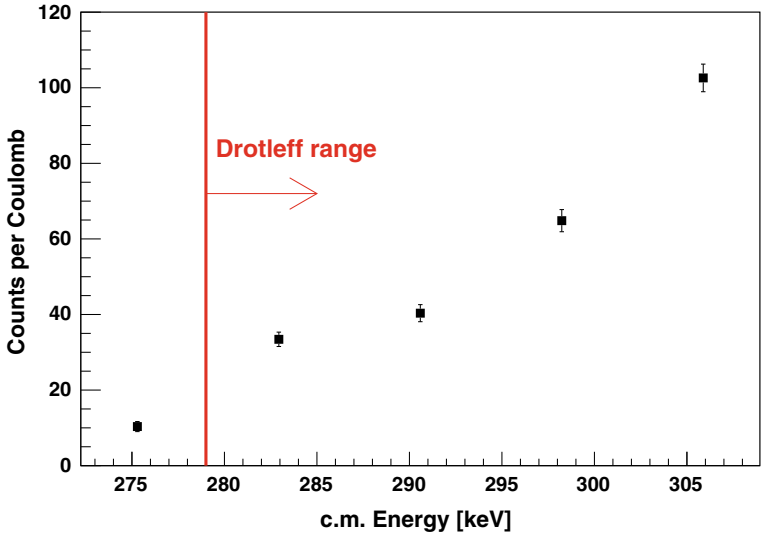

Fig. 35.1 Background-subtracted yield of the $^{13}C(\alpha,n)^{16}O$ reaction as a function of c.m. energy. The vertical line marks the lowest energy data point that has been directly measured previous to the experiment described here [3]

In summary, the low-energy cross section of the main s process neutron source, the reaction $^{13}C(\alpha,n)^{16}O$, is currently being measured at the LNGS using a low-background array of moderated ^{3}He counters. We already have extended the energy range of direct cross section measurements beyond what has previously been achieved, and have greatly improved upon the precision of the low energy data. In the near future LUNA will continue with measurements at even lower energies, and in order to control systematic effects will create a connection to the higher-energy region using the soon-to-be installed LUNA MV accelerator.

References

1. F. Käppeler, R. Gallino, S. Bisterzo, W. Aoki, Rev. Mod. Phys. **83**, 157 (2011)
2. S. Cristallo, M.L. Cognata, C. Massimi, A. Best, S. Palmerini, O. Straniero, O. Trippella, M. Busso, G.F. Ciani, F. Mingrone, L. Piersanti, D. Vescovi, Astrophys. J. **859**(2), 105 (2018). http://stacks.iop.org/0004-637X/859/i=2/a=105
3. H.W. Drotleff, A. Denker, H. Knee, M. Soine, G. Wolf, J.W. Hammer, U. Greife, C. Rolfs, H.P. Trautvetter, Astrophys. J. **414**, 735 (1993). https://doi.org/10.1086/173119
4. M. Heil, R. Detwiler, R.E. Azuma, A. Couture, J. Daly, J. Görres, F. Käppeler, R. Reifarth, P. Tischhauser, C. Ugalde, M. Wiescher, Phys. Rev. C **78**, 025803 (2008). https://doi.org/10.1103/PhysRevC.78.025803
5. A. Best, J. Görres, M. Junker, K.L. Kratz, M. Laubenstein, A. Long, S. Nisi, K. Smith, M. Wiescher, Nuclear instruments and methods in physics research section A: Accelerators. Spectrometers, detectors and associated equipment. **812**, 1 (2016). https://doi.org/10.1016/j.nima.2015.12.034
6. J. Balibrea-Correa, G. Ciani, R. Buompane, F. Cavanna, L. Csedreki, R. Depalo, F. Ferraro, A. Best, Nuclear instruments and methods in physics research section A: Accelerators, spectrometers, detectors and associated equipment (2018). https://doi.org/10.1016/j.nima.2018.07.086. http://www.sciencedirect.com/science/article/pii/S0168900218309318

Chapter 36
Nuclear AstroPhysics at ELI-NP: Preliminary Experiments with ELISSA Detector

G. L. Guardo, D. Balabanski, S. Chesneyskaya, M. La Cognata, D. Lattuada, C. Matei, T. Petruse, Rosario Gianluca Pizzone, G. G. Rapisarda, S. Romano, C. Spitaleri, Aurora Tumino and Y. Xu

Abstract The Extreme Light Infrastructure-Nuclear Physics (ELI-NP) facility, under construction in Magurele near Bucharest in Romania, will provide high-intensity and high-resolution gamma ray beams that can be used to address hotly debated problems in nuclear astrophysics. For this purpose, a silicon strip detector array (named ELISSA) will be realized in a common effort by ELI-NP and Laboratori Nazionali del Sud (INFN-LNS), in order to measure excitation functions and angular distributions over a wide energy and angular range. An experimental campaign is ongoing in order to test the feasibility of the future study at ELI-NP. With this aim, an experiment has been approved at INFN-LNS in order to measure the $^{19}F(p,\alpha_\pi)^{16}O$ reaction at astrophysical energies using a prototype of the ELISSA array. Moreover, an exploratory experiment to measure the $^{7}Li(\gamma,^{3}H)^{4}He$ reaction has been performed at High Intensity Gamma Source (HIγS). The good preliminary results of our tests and simulations allows us to conclude that the ELISSA detector will be very suitable for nuclear astrophysics experiments with the upcoming gamma ray beam at the ELI-NP facility.

36.1 The ELISSA Detector

The upcoming ELI-NP facility will provide, for the first time, pencil size gamma beams in the range between 200 keV and 19.5 MeV with a bandwidth better than 0.5%, spectral density of about 10^4 photons/s/eV and linear polarization higher than 95% [1, 2].

G. L. Guardo (✉) · D. Balabanski · S. Chesneyskaya · D. Lattuada · C. Matei · T. Petruse · Y. Xu
ELI-NP/IFIN-HH, Magurele, Bucharest, Romania
e-mail: luca.guardo@eli-np.ro

M. La Cognata · R. G. Pizzone · G. G. Rapisarda · S. Romano · C. Spitaleri · A. Tumino
Laboratori Nazionali del Sud, INFN, Catania, Italy

S. Romano · C. Spitaleri
Dipartimento di Fisica e Astronomia, Universitá degli Studi di Catania, Catania, Italy

A. Tumino
Facoltá di Ingegneria e Architettura, Universitá Kore, Enna, Italy

A. Formicola et al. (eds.), *Nuclei in the Cosmos XV*, Springer
Proceedings in Physics 219, https://doi.org/10.1007/978-3-030-13876-9_36

Such a facility will open new experimental perspectives for studies in the field of photonuclear physics. Moreover, thanks to these excellent features, this Gamma Beam System will provides unique opportunities to perform accurate measurements of small cross sections (order of μb or even less) of nuclear reactions of astrophysical interest and hence of the astrophysical S-factors that are essential for stellar evolution modeling.

Resistive strip silicon detector arrays have been successfully designed and commissioned for studies of nuclear reactions, e.g. ORRUBA (Oak Ridge Rutgers University Barrel Array) or ANASEN (Array for Nuclear Astrophysics Studies with Exotic Nuclei) [3, 4].

In the case of photonuclear reactions of astrophysical relevance, since photodissociations are induced at photon energies slightly larger than particle emission thresholds owing to the typical temperatures in stars, the emitted fragments have low energies, ranging from few hundreds keV to few MeV. Therefore, low-threshold detectors are necessary. Thus, the Extreme Light Infrastructure Silicon Strip Array (ELISSA) is under construction [5]. Monte Carlo simulation using a code based on GEANT4 tracking libraries and the n-body event generator of ROOT, as described in [6], proved that the barrel configuration is particularly suited as it guarantees a very good resolution and granularity, ensuring also a compact detection system (useful as it would allow a simple integration with ancillary detectors, such as neutron arrays) and a limited number of electronics channels [7]. The final setup of the ELISSA array will consist of X3 silicon-strip detectors (manufactured by Micron Semiconductor Ltd.) arranged into a barrel configuration that could be made up of 3 rings of 12 position sensitive detectors, for a total angular coverage of 100° in the laboratory system. The angular coverage is extended by using end cap detectors such as the assembly of four QQQ3 segmented detectors by Micron Semiconductor [8]. A sketch of the final expected setup is shown in Fig. 36.1.

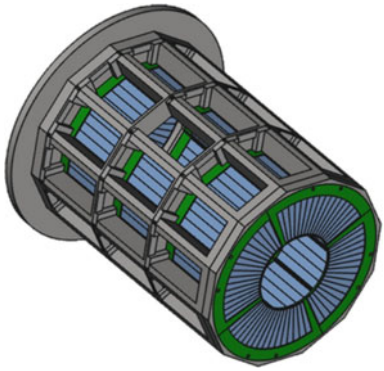

Fig. 36.1 Final design of the ELISSA detector. It will be made of three rows of PSD detectors to form a barrel plus eight end cap detectors to extend the angular coverage

36.2 The $^{19}F(p,\alpha_\pi)^{16}O$ Reaction

After an exhaustive test campaign during which a batch of forty X3 detectors have been characterized with particular emphasis on energy and position resolution, ballistic deficit, leakage currents and depletion voltage [9, 10], a prototype of ELISSA is going to be used for an already approved experiment. The aim of the experiment is to measure the $^{19}F(p,\alpha_\pi)^{16}O$ reaction cross section at astrophysical energies. Indeed, ^{19}F synthesis is believed to take place in the H-He intershell region of AGB stars but current models fail to explain the high F abundances found in the low-mass AGB stars [11]. Although the $^{19}F(p,\alpha)^{16}O$ is the main destruction channel and its reaction rate is determined by the sum over the rate for the (p,α_0), (p,α_π) and the (p,α_γ) channels, most of the existing measurements refer only to the $^{19}F(p,\alpha_0)^{16}O$ channel, while very little experimental info is available for the (p,α_π) and (p,α_γ) rates at very low energies. Here we refer to α_0 as the ground state of the emerging ^{16}O while α_π is the pair-emitting first exited state ($E_x = 6.05$ MeV). Finally, the combination of the transitions of $\gamma 2$, $\gamma 3$ and $\gamma 4$, is referred to as the (p,α_γ) channel [12].

For this purpose, a small prototype of the ELISSA detector will be used. We plan to use one rings made of 12 X3 detectors, covering the angular range 40°–80°. In order to increase the investigated angular range we plan to use also an end cap on the forward direction made up of 4 QQQ3 detectors covering the 15°–35° range (as shown in left panel of 36.2). Our simulations show that ELISSA will ensure the energy separation between the different channels and the kinematical identification of the outgoing reactions (right panel of 36.2) for which a good resolution is a crucial parameter aiming to investigate the cross section and angular distribution of the $^{19}F(p,\alpha)^{16}O$ reaction in the energy range between ≈450 keV and ≈1000 keV, where up to now no definite conclusions are drawn with direct measurements.

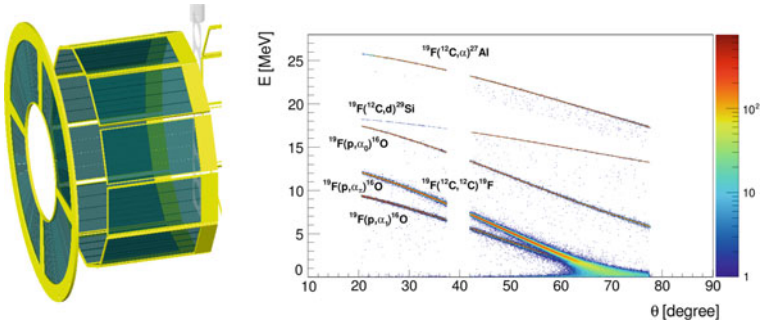

Fig. 36.2 Left panel: Final design of the prototype that will be used for the experiment. Right panel: Monte Carlo simulation for the expected reaction channels involved in the experiment

36.3 The ^{7}Li(γ,^{3}H)^{4}He Reaction

One of the unresolved problems in nuclear astrophysics is the so-called "cosmological Li problem". Big-Bang Nucleosynthesis (BBN) predicts the abundances of light elements ^{4}He, D, ^{3}He and ^{7}Li that are produced shortly after the Big Bang. There is good agreement between calculated and observed abundances for all these light nuclei except for ^{7}Li [13]. Moreover, the mirror alpha capture reactions ^{3}H(α,γ)^{7}Li and ^{3}He(α,γ)^{7}Be are receiving a lot of theoretical attention recently as theoretical models could provide the capture cross section at solar energies where experimental measurements are not possible [14]. For those reasons the measurement would be an ideal first day experiment with ELISSA at ELI-NP. Moreover, an exploratory experiment to measure the ^{7}Li(γ,^{3}H)^{4}He reaction has been performed at High Intensity Gamma Source (HIγS) in order to test the feasibility of such a kind of detectors with gamma beam systems.

The experiment was performed using a large area silicon detector array (SIDAR) in a lampshade configuration [15] devoted to the detections of tritons and alpha particles in coincidence. The energy and position resolutions of SIDAR are comparable to ELISSA since it is made of 12 YY1 segmented silicon detectors of different thickness [8]. The SIDAR vacuum chamber was coupled with a lead shielding system (mandatory since the gamma beam travels through air) and some beam monitoring instruments: copper scattering foil, HPGe detector at 0°, D_2O cell and neutron detectors. The promising preliminary results clearly show that the use of a silicon detector array with gamma beams allows one to measure cross sections and angular distributions of nuclear reaction of astrophysical relevance.

In conclusion, the good preliminary results of our tests and simulations allows us to say that the ELISSA detector will be very suitable for nuclear astrophysics experiment with the upcoming gamma ray beam at the ELI-NP facility.

Acknowledgements This work is supported in part by the Extreme Light Infrastructure Nuclear Physics (ELI-NP) Phase II, a project cofinanced by the Romanian Government and the European Union through the European Regional Development Fund - the Competitiveness Operational Programme (1/07.07.2016, COP, ID 1334).

References

1. N.V. Zamfir, EPJ Web of Conf. **66**, 11043 (2014)
2. D.L. Balabanski et al., EPL **117**, 28001 (2017)
3. S.D. Pain et al., Nucl. Instr. Meth. Phys. Res. B **261**, 1122 (2007)
4. M. Matos et al., PoS NIC XI **226** (2010)
5. M. La Cognata et al., JINST **12**, C03079 (2017)
6. D. Lattuada et al., EPJ Web of Conf. **165**, 01034 (2017)
7. O. Tesileanu et al., Rom. Rep. Phys. **68**, S699 (2016)
8. Micron Semiconductor, General catalogue, http://www.micronsemiconductor.co.uk/pdf/cat.pdf
9. S. Chesnevskaya et al., JINST **13**, T05006 (2018)

10. G.L. Guardo et al., EPJ Web of Conf. **165**, 01026 (2017)
11. C. Abia et al., Astron. Astrophys. **A88**, 581 (2015)
12. I. Indelicato et al., Astrophys. J. **845**, 19 (2017)
13. B.D. Fields, Annu. Rev. Nucl. Part. Sci. **61**, 47 (2011)
14. T. Neff, Phys. Rev. Lett. **106**, 042502 (2011)
15. K.A. Chipps et al., Phys. Rev. C **86**, 014329 (2012)

Chapter 37
Direct Charged-Particle Measurements Using Stable Beams Above Ground

Christian Iliadis, Art Champagne, Tom Clegg, Andrew Cooper, Jack Dermigny, Lori Downen, Sean Hunt, Amber Lauer and David Little

Abstract Many stellar burning phases are dominated by thermonuclear reactions involving stable nuclei. Prominent examples include hydrostatic hydrogen and helium burning in low-mass stars, massive stars, and thermally pulsing asymptotic giant branch stars. The nuclear reaction cross sections involved are very small and thus successful measurements require sophisticated equipment and data analysis techniques. We will provide an overview of recent experimental improvements at the Laboratory for Experimental Nuclear Astrophysics (LENA).

37.1 Astrophysical Motivation

Direct charged-particle measurements using stable beams are of continued interest for a number of astrophysical environments, including big bang nucleosynthesis, hydrostatic stellar burning phases, and stellar explosions. Prominent examples for astrophysically important nuclear reactions are $^{12}C(\alpha,\gamma)^{16}O$, $^{14}N(p,\gamma)^{15}O$, and $^{12}C + ^{12}C$. Many laboratories have additional nuclear reactions on their wish list of planned experiments. Below we will briefly discuss two scenarios involving reactions whose key importance has only recently been identified.

The first one relates to the mysteries surrounding the nature of globular clusters. They are of paramount importance for stellar evolution and early galaxy formation, and we should pay close attention to any unsolved fundamental questions related to these fascinating objects. Recently, stunning observations of red giant stars in the globular cluster NGC 2419 revealed a negative correlation between the measured Mg and K abundances [1, 2]. Since these stars all have the same metallicity ([Fe/H]

C. Iliadis (✉) · A. Champagne · T. Clegg · A. Cooper · J. Dermigny · L. Downen · S. Hunt · A. Lauer · D. Little
Triangle Universities Nuclear Laboratory (TUNL), Durham, NC 27708, USA
e-mail: iliadis@physics.unc.edu

C. Iliadis · A. Champagne · T. Clegg · A. Cooper · J. Dermigny · L. Downen · S. Hunt · A. Lauer · D. Little
Department of Physics and Astronomy, The University of North Carolina at Chapel Hill, Chapel Hill, NC 27599, USA

A. Formicola et al. (eds.), *Nuclei in the Cosmos XV*, Springer
Proceedings in Physics 219, https://doi.org/10.1007/978-3-030-13876-9_37

≈ -2), supernovae of a previous generation cannot account for the observations. Neither could these signatures be produced in the stars we observe, since they never reach temperatures high enough to impact the Mg or K abundances. The observations tell us that about 40% of all stars in that cluster consist of matter that underwent some unknown process before the stars we currently observe were born. But what is the nature of these "polluter" stars? Several different scenarios have been suggested in the past, but recent nucleosynthesis simulations indicate that neither massive stars nor AGB stars can likely explain the observations [3]. Super-AGB stars or accreting white dwarfs, on the other hand, may be more promising polluter candidates. Very recently, the impact of thermonuclear reaction rate variations on the derived abundances of elements between Mg and Sc in NGC 2419 was studied [4]. It was found that uncertain contributions of low-energy resonances in the ^{30}Si(p,γ)^{31}P reaction have a significant impact on the observations. The measurement of this reaction is discussed in these proceedings in the contribution by Dermigny and collaborators.

The second example relates to presolar stardust grains, which we observe in certain primitive meteorites. Their isotopic ratios of C, N, O, Si, etc., are vastly different than those of any other material found in the solar system. The only viable explanation for their existence is that each grain formed in a single star, survived the travel through the interstellar medium to the location of the presolar cloud, and was incorporated into primitive meteorites with their original isotopic signatures untouched (for a review, see [5]). Most presolar stardust grains are believed to originate in AGB stars and supernovae. Many classical novae are also prolific dust producers. But for reasons not clear, no presolar grains with a nova paternity have been unambiguously identified yet. Over the years, about 30 presolar grains have been put forward as nova candidate grains, although their observed isotopic ratios can only match the simulated values if the latter are mixed with ten times the amount of solar-like matter. However, the source of the pristine matter and the mixing mechanism remain elusive. Clearly, it is highly desirable to identify grains that formed directly from nova ejecta, which do not invoke any unknown mixing process. Recently, nucleosynthesis simulations strongly hinted at the nova paternity of 18 presolar grains, all of the SiC variety, without requiring any dilution of the nova ejecta [6]. Simulations also demonstrated the impact of low-energy resonances in the ^{29}Si(p,γ)^{30}P reaction on the issue of presolar grains from classical novae. This topic is discussed in these proceedings in the contribution by Downen and collaborators.

37.2 Experimental Techniques and Procedures

The previous sections identified two direct charged-particle measurements requiring stable ion beams. The important resonances are located at low energies, below 500 keV, where the cross section is very small because of a small probability for tunneling through the Coulomb and centripetal barriers. The small cross section translates directly into a tiny reaction yield. Before discussing experimental techniques in more detail, it is worthwile to pause and consider a well-known, but

sometimes overlooked, piece of information: the sensitivity of a measurement, i.e., the signal-to-noise ratio, is directly proportional to the signal count rate, but inversely proportional to the *square root* of the background count rate [7]. This implies that if the beam intensity is increased by a factor of, say, 100, and beam-induced background is negligible, the sensitivity improves by the same factor. If, on the other hand, the environmental background is reduced by a factor of 100, the sensitivity is just improved by one order of magnitude. Below we will discuss our efforts at the Laboratory for Experimental Nuclear Astrophysics (LENA) to improve the measurement sensitivity for low-yield experiments.

LENA houses two ion accelerators: a modified 1 MV Van de Graaff machine, and an electron cyclotron resonance ion source (ECRIS) with a 230 kV acceleration system. Details about the facility can be found in [8]. The Van de Graaff is mostly, although not exclusively, used for cross section calibrations, while the low-energy measurements are performed with the high-intensity 230 kV accelerator. The latter system provided proton beams of about 2 mA on target in the measurements of the ^{17}O(p,γ)^{18}F [9] and ^{22}Ne(p,γ)^{23}Na [10] reactions, which are important for understanding the nucleosynthesis in classical novae and globular clusters, respectively. Interestingly, the former reaction was also measured underground at the LUNA facility. The lowest energy measured at LUNA, where all relevant primary γ-ray decays could be observed, was 202 keV in the center of mass [11]. This can be compared to the lowest measured energy of 160 keV in the LENA study [9]. The crucial parameter enabling the measurement at much lower beam energies in the latter work was the significantly higher proton beam intensity on target (a factor of 10 larger than in the LUNA study).

All published LENA measurements to date were performed with the system described above, which operated for 9 years. However, our laboratory has recently experienced significant upgrades. A major problem was the ionization of background gas and the resulting secondary electrons were accelerated and struck interior surfaces causing intense bremstrahlung radiation and substantial column heating. This caused vacuum leaks, electrical discharges, and permanent damage to glass insulators. As a result, the acceleration tube had to be replaced with a new design. The new tube was installed in March of 2015. The system also underwent a number of other upgrades, and we are at the time of writing still in the commissioning phase. So far, we have achieved a proton beam intensity of 3.5 mA on target, and we are hopeful that the beam intensity can be increased to 10 mA. Details regarding the new LENA system can be found in [12].

A 4.5-mA proton beam of 100 keV energy implies a beam power of 450 W, which represents a severe challenge to the stability of any target. Interestingly, one of the upgrades at LENA involved a new microwave system with pulsing capability and a maximum power output of 1.2 kW. Using this system, the plasma is fully extinguished between beam pulses and subsequently reignited during each pulse. We typically operate the low-energy accelerator with a 10% duty cycle, with beam on for a period of 100 ms, and beam off for 900 ms. An example is provided on the left side in Fig. 37.1, showing pulse height spectra measured for the $E_r^{lab} = 151$ keV resonance in ^{18}O(p,γ)^{19}F. This reaction is important for interpreting oxygen isotopic ratios in

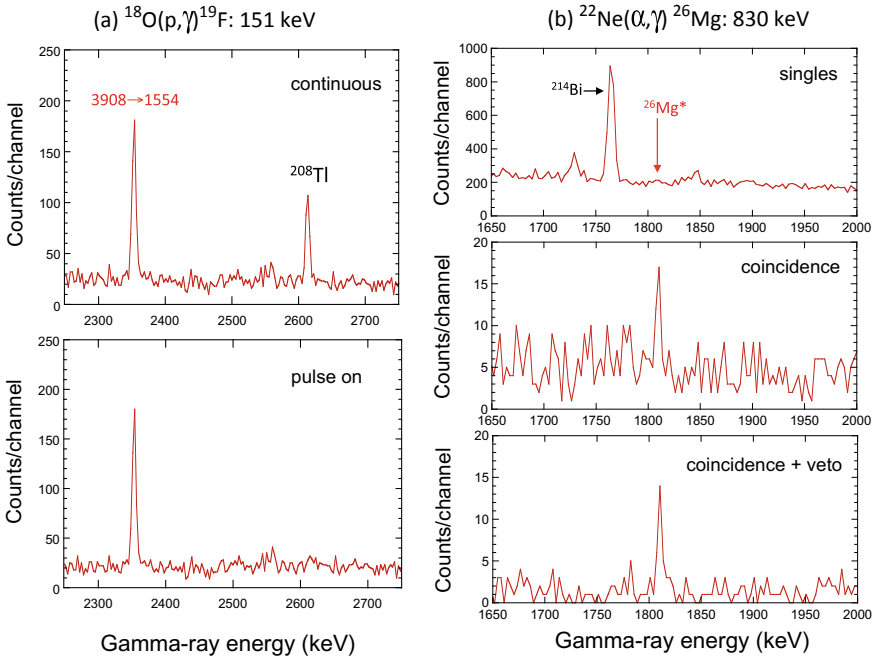

Fig. 37.1 (Left) Pulse height spectra for the $E_r^{lab} = 151$ keV resonance in ^{18}O(p,γ)^{19}F. The top panel, obtained with continuous beam, shows a secondary transition in ^{19}F (3908 keV $\rightarrow$ 1554 keV) and a room background line (^{208}Tl). The bottom panel was obtained with a pulsed beam of 10% duty cycle. Notice the disappearance of the room background line. The accumulated charges were the same for both panels. (Right) Pulse height spectra for the $E_r^{lab} = 830$ keV resonance in ^{22}Ne(α,γ)^{26}Mg. The top panel shows the singles HPGe spectrum; no peak is observed at the location of the expected transition from the first excited state to the ground state in ^{26}Mg (1808 keV). The middle panel displays the coincidence-gated spectrum, where the background peak (from ^{214}Bi) is absent, and the 1808-keV peak is clearly visible. The bottom spectrum shows the coincidence spectrum with the veto imposed, resulting in a significant reduction in cosmic-ray muon events. The accumulated charges and running times are the same in all three panels. The data were accumulated using a continuous beam on target

presolar grains from AGB stars [13]. The top panel, obtained with continuous beam, shows a secondary transition in ^{19}F (3908 keV $\rightarrow$ 1554 keV) and a room background line (^{208}Tl). The bottom panel was obtained with a pulsed beam of 10% duty cycle, implying a factor of 10 higher peak intensity, but the same average beam intensity on target compared to the top panel. Notice how the room background line disappears in the bottom panel, while the peak intensity of the beam-induced transition in ^{19}F remains unchanged.

Apart from taking advantage of a pulsed ion beam, it is of utmost importance to further reduce the background by additional means. At LENA, we employ a "coincidence-anticoincidence" detection apparatus [14]. It consists of a large-volume HPGe detector, located as close as possible to the target, and a 16-segment NaI (Tl) annulus, which surrounds both the HPGe detector and the target. Most excited nuclear

levels of astrophysical interest de-excite via emission of more than one photon. Using this apparatus, coincidence timing, and energy conditions can be imposed on events, so that the signals of interest can be discriminated from unwanted background events. In addition, the apparatus is surrounded by 5-cm-thick plastic scintillators, which act as a cosmic-ray muon veto shield. Using this system, the background can be reduced by several orders of magnitude.

An example is provided on the right side in Fig. 37.1, showing pulse height spectra measured for the $E_r^{lab} = 830$ keV resonance in ^{22}Ne(α,γ)^{26}Mg. This reaction competes for α-particles with the ^{22}Ne(α,n)^{25}Mg neutron source that operates in massive stars and AGB stars [15]. The top panel shows the singles HPGe spectrum, where no peak is observed at the location of the expected secondary transition in ^{26}Mg (at 1808 keV). The middle panel displays the coincidence-gated spectrum. The background peak, from ^{214}Bi, has disappeared, and the 1808-keV peak is clearly visible. The bottom panel shows the coincidence spectrum with the veto imposed, resulting in a significant reduction in cosmic-ray muon events.

The extraction of accurate cross section and resonance strength information from the data requires careful calibrations and corrections, e.g., for detection efficiencies, coincidence summing, angular correlations, finite beam spot sizes, etc. The most reliable way to perform these calibrations is to employ extensive Monte Carlo radiation transport codes, such as Geant4. However, this requires that the detector geometry is precisely known. For this reason, we obtained three-dimensional Computed Tomography (CT) images of our HPGe detector [16]. We used this information to build a complete Geant4 model of the apparatus, including the beam tube, target holder, passive shielding, etc. [17]. We also recently developed a method to analyze not just the net intensity of isolated peaks in the pulse height spectra, but to fit the entire measured singles and gated HPGe spectra using a binned likelihood approach based on a Bayesian method [18]. This technique has been successfully applied to the analysis of data for the ^{17}O(p,γ)^{18}F [9] and ^{22}Ne(p,γ)^{23}Na [10] reactions, which are important for understanding the nucleosynthesis in classical novae and globular clusters.

In the future, we will see many more improvements in experimental techniques and analysis methods to extract in creative ways the desired information of astrophysical interest from low-yield data.

Acknowledgements This work was supported in part by NASA under the Astrophysics Theory Program grant 14-ATP14-0007, and the U.S. DOE under contracts DE-FG02-97ER41041 (UNC) and DE-FG02-97ER41033 (TUNL).

References

1. J.G. Cohen, E.N. Kirby, The bizarre chemical inventory of NGC 2419, an extreme outer halo globular cluster. Astrophys. J. **760**, 86 (2012)
2. A. Mucciarelli, M. Bellazzini, R. Ibata, T. Merle, S.C. Chapman, E. Dalessandro, A. Sollima, News from the Galactic suburbia: the chemical composition of the remote globular cluster NGS 2419. Mon. Not. Roy. Astron. Soc. **426**, 2889 (2012)

3. C. Iliadis, A.I. Karakas, N. Prantzos, J.C. Lattanzio, C.L. Doherty, On potassium and other abundance anomalies of red giants in NGC 2419. Astrophys. J. **818**, 98 (2016)
4. J.R. Dermigny, C. Iliadis, Sensitivity to thermonuclear reaction rates in modeling the abundance anomalies of NGC 2419. Astrophys. J. **848**, 14 (2017)
5. L.R. Nittler, F. Ciesla, Astrophysics with extraterrestrial materials. Annu. Rev. Astron. Astrophys. **54**, 53 (2016)
6. C. Iliadis, L.N. Downen, J. José, L.R. Nittler, S. Starrfield, On presolar stardust grains from CO classical novae. Astrophys. J. **855**, 76 (2018)
7. G.F. Knoll, *Radiation Detection and Measurement*, 2nd edn. (Wiley, New York, 1989)
8. J.M. Cesaratto, A.E. Champagne, T.B. Clegg, M.Q. Buckner, R.C. Runkle, A. Stefan, Nuclear astrophysics studies at LENA: the accelerators. Nucl. Instr. Meth. A **623**, 888 (2010)
9. M.Q. Buckner, C. Iliadis, K.J. Kelly, L.N. Downen, A.E. Champagne, J.M. Cesaratto, C. Howard, R. Longland, High-intensity-beam study of ^{17}O(p,γ)^{18}F and thermonuclear reaction rates for $^{17}\mathrm{O} + p$. Phys. Rev. C **91**, 015812 (2015)
10. K.J. Kelly, A.E. Champagne, L.N. Downen, J.R. Dermigny, S. Hunt, C. Iliadis, A.L. Cooper, New measurements of low-energy resonances in the ^{22}Ne(p,γ)^{23}Na reaction. Phys. Rev. C **95**, 015806 (2017)
11. A. Di Leva, D.A. Scott, A. Caciolli, A. Formicola, F. Strieder, M. Aliotta, M. Anders et al., Underground study of the ^{17}O(p,γ)^{18}F reaction relevant for explosive hydrogen burning. Phys. Rev. C **89**, 015803 (2014)
12. A.L. Cooper, K.J. Kelly, E. Machado, I. Pogrebnyak, J. Surbrook, C. Tysor, P. Thompson, M. Emamian, B. Walsh, B. Carlin, A.E. Champagne, T.B. Clegg, Development of a variable energy, high-intensity, pulsed-mode ion source for low-energy nuclear astrophysics studies at LENA. Rev. Sci. Instr. **89**, 083301 (2018)
13. M.Q. Buckner, J.M. Cesaratto, C. Howard, T.B. Clegg, A.E. Champagne, S. Daigle, Thermonuclear reaction rate of ^{18}O(p,γ)^{19}F. Phys. Rev. C **86**, 065804 (2012)
14. R. Longland, C. Iliadis, A.E. Champagne, C. Fox, J.R. Newton, Nuclear astrophysics studies at the LENA facility: the γ-ray detection system. Nucl. Instr. Meth. A **566**, 452 (2006)
15. R. Longland, C. Iliadis, A.I. Karakas, Reaction rates for the s-process neutron source $^{22}\mathrm{Ne} + \alpha$. Phys. Rev. C **85**, 065809 (2012)
16. S. Carson, C. Iliadis, J. Cesaratto, A.E. Champagne, L. Downen, M. Ivanovic, J. Kelley, R. Longland, J.R. Newton, G. Rusev, A.P. Tonchev, Ratio of germanium detector peak efficiencies at photon energies of 4.4 and 11.7 MeV: experiment versus simulation. Nucl. Instr. Meth. A **618**(1–3), 190 (2010)
17. C. Howard, C. Iliadis, A.E. Champagne, Monte Carlo simulations of the LENA detector system. Nucl. Instr. Meth. **A729**, 254 (2013)
18. J.R. Dermigny, C. Iliadis, M.Q. Buckner, K.J. Kelly, γ-ray spectroscopy using a binned likelihood approach. Nucl. Instr. Meth. A **830**, 427 (2016)

Chapter 38
Neutron Induced Reactions in Astrophysics

Claudia Lederer-Woods

Abstract Neutron induced reactions play an important role in the synthesis of the chemical elements, in particular for elements heavier than iron. Methodologies for measuring stellar neutron capture cross sections and recent advances are disccussed.

38.1 Introduction

Neutron induced reactions are of key importance to nucleosynthesis in stars, in particular for the creation of the elements heavier than iron. Two neutron capture processes contribute about equally to the overall chemical element abundances, the *s* process (slow neutron capture process), and the *r* process (rapid neutron capture process). The *r* process takes place in explosive environments, such as neutron star mergers or core collapse supernovae [1]. Due to high neutron densities $n_n > 10^{20}\,\mathrm{cm}^{-3}$ generated, neutrons get rapidly captured on seed material, and the reaction path proceeds along the neutron rich side of the chart of nuclides, involving short lived, exotic species. In contrast, the *s* process happens at moderate neutron densities of about $n_n = 10^8\ \mathrm{cm}^{-3}$, and β decay typically proceeds faster than neutron capture on unstable species [2, 3]. This means that the reaction path tracks along the valley of stability and reactions involve stable and long-lived nuclei (see Fig. 38.1).

Two different stellar environments contribute to *s*-process nucleosynthesis. The main component of the *s* process occurs in low mass Asymptotic Giant Branch (AGB) stars, mainly generating elements between Zr and Bi. AGB stars of low metallicity are mainly responsible for producing Pb (strong component) [4]. The abundances ranging from Fe to Zr are dominantly produced in massive stars, which later eject material in a core collapse supernova explosion. A key difference in *s*-process conditions for the main and the weak components is the different mean neutron exposure τ, which is 0.3 mb^{-1} for the main, but only 0.07 mb^{-1} for the weak component (values quoted for $kT = 30$ keV) [5]. The high neutron exposures in AGB stars cause a reaction flow equilibrium of the form $N{<}\sigma_{n,\gamma}{>} = \mathrm{const.}$,

C. Lederer-Woods (✉)
School of Physics and Astronomy, University of Edinburgh, Edinburgh, UK
e-mail: claudia.lederer-woods@ed.ac.uk

A. Formicola et al. (eds.), *Nuclei in the Cosmos XV*, Springer
Proceedings in Physics 219, https://doi.org/10.1007/978-3-030-13876-9_38

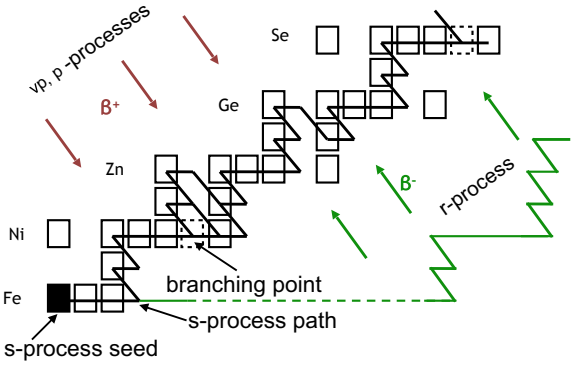

Fig. 38.1 The different nucleosynthesis processes contributing to the synthesis of elements heavier than iron. While the *s* process tracks closely to stable nuclei, the *r* process operates far on the neutron rich side, involving very short lived species. Only about 1% of abundances are created by charged particle or photon-induced reaction

with N being the abundance and $<\sigma_{n,\gamma}>$ the stellar neutron capture cross section of a particular isotope. For massive stars, neutron exposures are not large enough to reach equilibrium and consequently one neutron capture cross section impacts on abundances of several nuclei that follow along the reaction path (for an example of these propagation effects see Fig. 6 in [3]).

38.2 Experimental Techniques and Recent Results

For a reliable determination of the abundances produced in the *s* process, accurate neutron capture cross sections at stellar neutron energies are indispensable. The stellar neutron capture cross section, or Maxwellian Averaged Cross Section is defined as

$$MACS = \frac{2}{\sqrt{\pi}} \frac{1}{(kT)^2} \cdot \int_0^\infty E\sigma(E) \cdot \exp\left(-\frac{E}{kT}\right) \mathrm{d}E, \tag{38.1}$$

Neutron capture cross sections can be measured over a large energy range using the time-of-flight (tof) technique. For *s*-process studies, data should ideally cover neutron energies up to 200 keV, as this allows a reliable determination of MACSs at all temperatures relevant to the *s*-process (corresponding to kT values between 8 and 90 keV). The tof technique is based on production of a pulsed neutron beam of a wide energy spread. The sample to be measured is placed at a distance L from the neutron source, and for each reaction the neutron energy is determined via the time-of-flight between creation of the neutron and the time of detection of the reaction product (see Fig. 38.2), i.e. for the non-relativistic case:

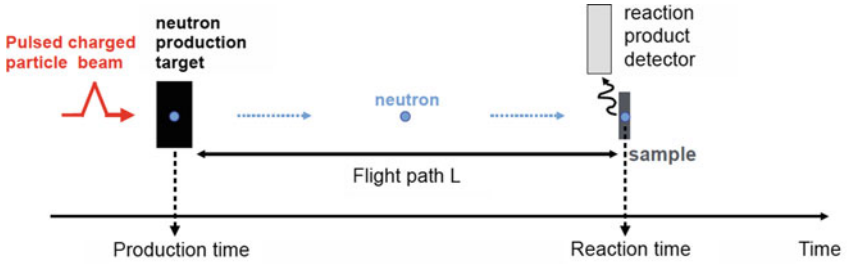

Fig. 38.2 Illustration of the neutron time-of-flight technique

$$E_n = \frac{m_n}{2}\left(\frac{L}{tof}\right)^2 \tag{38.2}$$

The direct measurement of neutron reactions on radioactive species is challenging. Neutrons are unstable, so experiments cannot be performed in inverse kinematics, which means that enough target material needs to be available, and half lives need to be long enough to allow a measurement. The *s* process branching point ^{63}Ni meets these requirements and its (n, γ) cross sections have recently been measured at n_TOF (CERN) [6] and LANSCE (Los Alamos National Laboratory) [7]. These two measurements provided the first experimental data at stellar neutron energies, and showed that the theoretical calculation of the cross section, which was used in stellar models before, is a factor of 2 too low. The new result suggest a 30% reduction in ^{64}Zn abundances produced in massive stars, as well as a 15% reduction of ^{63}Cu abundances, which thus affects the ^{63}Cu/^{65}Cu ratio [6].

There are also a number of stable isotopes where no experimental neutron capture data at stellar neutron energies are available yet, notably the two germanium isotopes ^{72,73}Ge. A campaign to measure all stable Ge isotopes has recently been completed at n_TOF [8]. First results suggest that the stellar cross section of ^{73}Ge is substantially higher than most theoretical predictions. Results on ^{73}Ge will be published in the imminent future, while data analysis for the other isotopes is still ongoing.

While neutron reactions are usually associated with the heavy elements, there are a few light isotopes for which neutron reactions are key. (n, α) and (n, p) reactions on the cosmic γ ray emitter ^{26}Al are at present the main nuclear physics uncertainty to determine ^{26}Al abundances in massive stars [9]. This is due to the fact that for each reaction channel, the two available experimental data sets exhibit large discrepancies. For ^{26}Al(n, α) reactions, cross sections obtained at the GELINA facility [10], are about a factor 2 smaller than cross section published from an experiment at LANSCE [11]. Likewise for the ^{26}Al(n, p) channel, data obtained by Trautvetter et al. [12, 13] using neutron spectra at keV energies indicate substantially smaller cross sections than measurements at LANSCE. Both reactions were recently measured at n_TOF, taking advantage of the new high flux beam line EAR-2 [14], at a distance of only 20 m from the neutron production target. A new setup for charged particle detection consisting of silicon strip detectors arranged as ΔE-E telescopes was built for that purpose at Edinburgh. The data analysis for this run is currently ongoing.

A complementary technique that allows a 'direct' measurement of the stellar cross section can be employed using activation. For reactions, where the reaction product is radioactive, the material of interest can be irradiated with a quasi-maxwellian neutron spectrum, and only small corrections are needed to extract the MACS. The most prolific method to produce such neutron spectra is using the ^{7}Li(p, n) reaction with protons of 1912 keV energy, which results in a quasi-maxwellian spectrum around $kT = 25$ keV, perfect for s-process studies [15]. As for this methodology the beam need not be pulsed, less sample material is needed for an experiment, which makes it perfectly suited for measurements on radioactive nuclei.

38.3 Outlook

The construction of new ultra high neutron flux facilities provides new exciting opportunities to measure neutron induced reactions on radioactive species, or measurements of very small cross sections. Thanks to the new high flux beam line EAR-2 at n_TOF new data on (n, p) and (n, α) reactions have been obtained on radioactive ^{7}Be [16, 17] and ^{26}Al over a wide neutron energy range using the time-of-flight technique. An ultra high flux facility providing quasi-maxwellian neutron spectra using the ^{7}Li(p, n) reaction is currently under construction at Goethe University Frankfurt (FRANZ) [18], while experiments have already started at the new LiLit at SARAF facility (Israel) [19, 20], which at present provides typically 10 times more neutron flux for activation experiments at stellar energies than previously available.

References

1. M. Arnould, S. Goriely, K. Takahashi, Phys. Rep. **450**, 97 (2007)
2. F. Käppeler et al., Rev. Mod. Phys. **83**, 157 (2011)
3. R. Reifarth, C. Lederer, F. Käppeler, J. Phys. G (2014)
4. C. Travaglio et al., Astrophys. J. **549**, 346 (2001)
5. F. Käppeler, H. Beer, K. Wisshak, Rep. Prog. Phys. **52**, 945 (1989)
6. C. Lederer, and the n_TOF Collaboration, Phys. Rev. Lett. **110**, 022501 (2013)
7. M. Weigand et al., Phys. Rev. C **92**, 045810 (2015)
8. C. Lederer, et al., Proposal to INTC (CERN), INTC-P-381 (2013)
9. C. Iliadis et al., Astrophys. J. Suppl. Ser. **193**, 16 (2011)
10. L. de Smet et al., Phys. Rev. C **76**, 045804 (2007)
11. P.E. Koehler et al., Phys. Rev. C **56**, 1138 (1997)
12. H.P. Trautvetter, F. Kaeppeler, Z. Phys. A **318**, 121 (1984)
13. H.P. Trautvetter et al., Z. Phys. A **323**, 1 (1996)
14. C. Weiss et al., NIM A **799**, 90 (2015)
15. W. Ratynski, F. Käppeler, Phys. Rev. C **37**, 595 (1988)
16. M. Barbagallo et al., Phys. Rev. Lett. **117**, 152701 (2016)
17. L.A. Damone et al., Phys. Rev. Lett. **121**, 042701 (2018)
18. R. Reifarth et al., PASA **26**, 255 (2009)
19. I. Mardor et al., Eur. Phys. J. A **54**, 91 (2018)
20. M. Tessler , et al., Stellar ^{36,38}Ar$(n, \gamma)^{37,39}$ Ar reactions and their effect on light neutron-rich nuclide synthesis, accepted by PRL (2018)

Chapter 39
Progress of Underground Nuclear Astrophysics Experiment JUNA in China

WeiPing Liu

Abstract Underground Nuclear Astrophysics Experiment in China (JUNA) will take the advantage of the ultra-low background in Jinping underground lab. A 400 kV high current accelerator with an ECR source and γ, neutron and charged particle detectors will be set up. A number of nuclear reactions important to hydrostatic stellar evolution near their Gamow window energies, such as ^{25}Mg(p,γ)^{26}Al, ^{19}F(p,α)^{16}O, ^{13}C(α,n)^{16}O and ^{12}C(α,γ)^{16}O will be directly measured.

39.1 Underground Nuclear Astrophysics

Underground nuclear astrophysics experiment is a unique approach to study directly most important reaction rates [1]. China JinPing underground Laboratory (CJPL) was established from a constructing hydro-power plants in the Jinping mountain, Sichuan, China [2]. The facility is located near the middle of traffic tunnel. The facility is shielded by 2400 m of mainly marble overburden, with radioactively quiet rock. Its ultra-low cosmic ray background, which is about 2 orders of magnitude lower than that in Gran Sasso, makes it an ideal environment for low background experiment. CJPL phase I (CJPL-I) now housing CDEX [2] and PandaX [3] dark matter experiments. CJPL phase II [2] (CJPL-II) is supported by national basic scientific facilities and will be available by the end of 2018 for much larger scale underground experiments (120,000 m^3 volume), the largest in the world. JUNA [4] will be one of its major research programs in CJPL-II, together with dark matter experiments CDEX-II and PANDA-II (Fig. 39.1).

WeiPing Liu for JUNA collaboration.

W. Liu (✉)
China Institute of Atomic Energy, P. O. Box 275(1), Beijing 102413, China
e-mail: wpliu@ciae.ac.cn

A. Formicola et al. (eds.), *Nuclei in the Cosmos XV*, Springer
Proceedings in Physics 219, https://doi.org/10.1007/978-3-030-13876-9_39

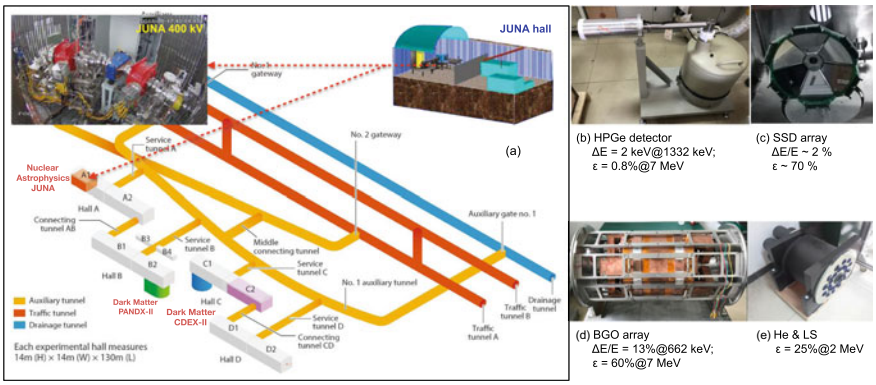

Fig. 39.1 Layout of CJPL-II and JUNA

39.2 Nuclear Reactions of Astrophysical Interest

The $^{12}C(\alpha,\gamma)^{16}O$ reaction is quoted as the holy grail in nuclear astrophysics. The uncertainty of this reaction affects not only the nucleosynthesis of elements up to iron, but also the evolution of the massive stars and their final fate (black hole, neutron star). The cross section of this reaction has to be known within an uncertainty less than 10% at helium burning temperatures ($T_9 = 0.2$), corresponding to a Gamow window around $E_{c.m.} = 300$ keV. It is extremely difficult to determine the reaction cross section at this energy. A direct measurement at $E_{c.m.} = 600$ keV near the Gamow window will be done in JUNA with high intensity ion beam of the experimental platform to provide better constrain for extrapolating models.

For total cross section and angular distribution measurement at $E_{c.m.} = 600$ keV, we will optimize the experiment condition, including: (1) optimizing the beam transmission on the basis of the beam-optics calculation, adjusting the setup of shields to suppress the background coming from the beam, (2) confirming the origin of ^{13}C and improving the implantation condition of ^{12}C implantation target to reduce the disturbance of ^{13}C, analysed by back scattering method [5]. A BGO detection array placed around the target chamber can significantly increase the detection efficiency (absolute efficiency 60% at $E_\gamma = 7$ MeV) of γ-rays. For the test measurement at $E_{c.m.} = 380$ keV, we will use $^4He^{2+}$ beam with an intensity of 2.5 emA and the high-efficiency BGO detection array.

The $^{13}C(\alpha,n)^{16}O$ reaction is the key neutron source reaction for the stellar s-process nucleosynthesis, which of importance since it is related to the big question of element synthesis heavier than iron. Due to the existence of sub-threshold resonances, there is a rather large uncertainty (30%) in this important reaction rate which limits our understanding to the nucleosynthesis of heavy elements. We plan to study directly this important reaction for the first time at energies down to $E_{c.m.} \sim 0.2$ MeV, within its relevant stellar energy range.

We are designing a fast neutron detector consisting of 24 ^{3}He proportional counters and a liquid scintillator. The scintillator has a cylindrical shape with a length of 0.4 m and a diameter of 0.4 m. The 24 ^{3}He counters are distributed in the two circles with radii of 0.1 and 0.15 m, respectively.

The energies of neutrons from the $^{13}C(\alpha,n)^{16}O$ reaction are in the range of 2–3 MeV. The produced neutrons are firstly slowed down by the liquid scintillator. After their thermalization, some neutrons enter ^{3}He counters and are detected. With the coincidence between the fast signal from fast neutron slowing down inside the liquid scintillator and the delayed signal from the thermalized neutrons captured by the ^{3}He counters, we can effectively suppress the backgrounds in liquid scintillator and ^{3}He detectors. The detection efficiency after coincidence is estimated to be 20% for neutrons from the $^{13}C(\alpha,n)^{16}O$ reaction.

The $^{25}Mg(p,\gamma)^{26}Al$ reaction is the main way to produce ^{26}Al in the galaxy and its cross section is dominated by the capture process of the isolated resonances in ^{26}Al. The temperature range of astrophysical interests is T = 0.02–2 GK, so the levels between 50 and 310 keV are more important in the study of galactic ^{26}Al.

Many experiments have been performed to study the $^{25}Mg(p,\gamma)^{26}Al$ reaction since 1970, but the experiment on the surface of earth ground can only reach to 190 keV energy level due to the small cross section and large background effects of the cosmic rays. In 2012, the laboratory of underground nuclear astrophysics (LUNA) in Italy successfully measured the resonance strength at 92 keV with the help of high shielding conditions in the underground laboratory [6]. However, the $^{25}Mg(p,\gamma)^{26}Al$ cross section of 58 keV resonant capture is inaccessible for direct measurement in the shielding conditions of LUNA experiments. Benefiting from the ultra low background and the high beam intensity, we will be able to measure the 58 keV resonance strength of $^{25}Mg(p,\gamma)^{26}Al$ with the new designed 4π BGO γ detectors array [7].

The $^{19}F(p,\alpha)^{16}O$ reaction is considered to be an important reaction in the CNO cycles. Currently, the experimental cross sections of this reaction at Gamow energies are still incomplete, and the precision of its thermonuclear reaction rate does not yet satisfy the model requirement. The proposed experiment is targeting on direct cross section measurement of the key $^{19}F(p,\alpha)^{16}O$ reaction right down to the Gamow energies (70–350 keV in the center-of-mass frame) with a precision better than 10% [8]. The charged particle array is ready for experiment. A ground based test experiment by using JUNA accelerator will be also finished in 2018.

The expected conditions and results of all four above reactions are summarized in Table 39.1.

We adopted a design of 2.45 GHz ECR which is developed to CI-ADS project. This ion source is expected to deliver 12 emA proton, 6 emA He^{+} and 2.5 emA He^{2+}. The maximum beam energy out of ion source is 50 keV/q with emittance less than 0.2 π mm mrad. The fabrication of ion source is finished. In October 2016, we achieved the first proton beam intensity of 16 mA.

For the low energy and high intensity beam, we adopted segmental voltage for the accelerating tube and we have designed an acceleration and deceleration structure for the accelerating tube electrode to reduce the space-charge effect. The fabrication

Table 39.1 Basic parameters of four reactions planned

Reaction	Ion beam	Int. (emA)	$E_{c.m.}$ (keV)	σ or $\omega\gamma$ (mb or eV)	Target (/cm^2)	eff. (%)	CNT (/day)	BKD (/day)
^{12}C(α,γ)^{16}O	^{4}He^{2+}	2	600	1×10^{-10}	10^{18} atoms	60	32	1.0
^{13}C(α,n)^{16}O	^{4}He^{1+}	10	200	4×10^{-11}	Thick target	20	7	1.0
^{25}Mg(p,γ)^{26}Al	^{1}H^{1+}	10	58	$\omega\gamma$ 2.1×10^{-13}	0.6 μg	38	1.4	1.0
^{19}F(p,α_γ)^{16}O	^{1}H^{1+}	0.1	100	7.2×10^{-9}	4 μg	60	27	1.0

of accelerator tube is finished. In 2018, we achieved the proton beam intensity of 12 mA with the beam energy of 350 keV.

The effect to background ratio of the nuclear reaction measurement will be significantly enhanced with the ultra-low background of CJPL and high current beam. All the detector and target chamber materials are tested to be satisfactory in CJPL-I for their natural background [9]. But at the same time the high current beam will bring new background, which must be shielded. We plan to construct two shielding system around the target chamber and the detectors, aiming at shielding γ-ray and neutron. We will test the design of such system by ground base experiment, Monte Carlo simulation and underground test.

39.3 Summary

In summary, a new underground nuclear astrophysics experiment JUNA planned in the space CJPL-II. Nuclear astrophysical reaction, namely ^{25}Mg(p,γ)^{26}Al, ^{19}F(p,α)^{16}O, ^{13}C(α,n)^{16}O and ^{12}C(α,γ)^{16}O, will be measured down to Gamow window. Ground test of targets and detectors is performed until 2019. The CJPL-II experimental space will be available in the year of 2019, followed by the underground installation of accelerator, shielding and detector system. The underground experiment will be started in 2020 and the first batch of experimental results will be delivered in the year of 2021.

Acknowledgements This work was supported by the National Natural Science Foundation of China (Grant Nos. 11321064 and 11490560) and the National Basic Research Program of China (Grant No. 2013CB834406 and 2016YFA0400502).

References

1. H. Costantini, A. Formicola, G. Imbriani et al., Rep. Prog. Phys. **72**, 086301 (2009)
2. J.P. Cheng, S.Y. Wu, Q. Yue, M.B. Shen, Physics **40**(3), 149 (2011)
3. J.M. Li, X.D. Ji, W. Haxton, J.S.Y. Wang, Phys. Proc. **61**, 576 (2014)
4. W.P. Liu, Z.H. Li, J.J. He, X.D. Tang et al., Sci. China-Phys. Meth. Astron. **59**, 642001 (2016)
5. P. Wang, N. Huang, Y.X. Fan et al., Nucl. Instrum. Meth. A **902**, 88 (2018)
6. F. Strieder et al., Phys. Lett. B **707**, 60 (2016)
7. Z.H. Li, J. Su, Y.J. Li et al., Sci. China-Phys. Meth. Astron. **58**, 082002 (2015)
8. J.J. He, S.W. Xu, S.B. Ma et al., Sci. China-Phys. Meth. Astron. **59**, 652001 (2016)
9. Y.P. Shen, J. Su, W.P. Liu et al., Sci. China-Phys. Meth. Astron. **60**, 102022 (2017)

Chapter 40
Trojan Horse Method: A Versatile Tool for Nuclear Astrophysics

Rosario Gianluca Pizzone

Abstract Owing the presence of the Coulomb barrier at astrophysically relevant kinetic energies, it is very difficult, or sometimes impossible to measure astrophysical reaction rates in laboratory, expecially for the presence of the electron screening effect. This is why different indirect techniques are being used along with direct measurements. The Trojan Horse Method (THM) is a unique indirect technique allowing one to measure astrophysical rearrangement reactions down to astrophysical relevant energies. The basic principle and a review of the main applications of the THM are presented.

Nuclear fusion reactions, that take place in the hot interiors of remote and long-vanished stars over billions of years, are the origin of nearly all the chemical elements in the universe [1]. The detailed understanding of the origin of the chemical elements and their isotopes has combined astrophysics and nuclear physics, and forms what is called nuclear astrophysics. In turn, nuclear reactions are the heart of nuclear astrophysics: they strongly influence the nucleosynthesis in the earliest stages of the universe and in all the objects formed thereafter, and control the associated energy generation (by processes called nuclear fusion or nuclear burning), neutrino luminosity, and evolution of stars. A good knowledge of the rates of these fusion reactions is essential for understanding this broad picture

In a stellar plasma the constituent nuclei are usually in thermal equilibrium at some local temperature T. Occasionally they collide with other nuclei, whereby two different nuclei can emerge from collision $A + x \rightarrow c + C$. The cross section $\sigma(E)$ of nuclear fusion reaction A(x,c)C is of course governed by the laws of quantum mechanics where, in most cases, the Coulomb and centrifugal barriers arising from nuclear charges and angular momenta in the entrance channel of the reaction strongly inhibit the penetration of one nucleus into another. This barrier penetration leads a steep energy dependence of the cross section. It is the challenge to the experimen-

Rosario Gianluca Pizzone for the ASFIN collaboration.

R. G. Pizzone (✉)
INFN-LNS, Catania, Italy
e-mail: rgpizzone@lns.infn.it

A. Formicola et al. (eds.), *Nuclei in the Cosmos XV*, Springer
Proceedings in Physics 219, https://doi.org/10.1007/978-3-030-13876-9_40

talist to make precise σ(E) measurements at the Gamow energy (E_G). Owing to the strong Coulomb suppression, the behavior of the cross section at E_G is usually extrapolated from the higher energies by using the definition of the smoother bare nucleus astrophysical factor S_b(E).

Although the S_b(E)-factor allows for an easier extrapolation, large uncertainties to $\sigma(E_G)$ may be introduced due to for instance the presence of unexpected resonances, or high energy tails of sub-threshold resonances. In order to avoid the extrapolation procedure, a number of experimental solutions were proposed in direct measurements for enhancing the signal-to-noise ratio at E_G.

Moreover, the measurements in laboratory at ultralow energies suffer from the complication due to the effects of electron screening [2]. This leads to an exponential increase of the laboratory measured cross section $\sigma_s(E)$ [or equivalently of the astrophysical factor $S_s(E)$] with decreasing energy relative to the case of bare nuclei. Then, although it is possible to measure cross sections in the Gamow energy range, the bare nucleus cross section σ_b is extracted by extrapolating the direct data behavior at higher energies where negligible electron screening contribution is expected. In order to decrease uncertainties in the case of charged particle induced reactions extrapolations should be avoided and therefore experimental techniques were improved (e.g. by means of underground laboratories). After improving measurements (at very low energies), electron screening effects were discovered. Finally to extract from direct (shielded) measurements the bare astrophysical S_b(E)-factor, extrapolation were performed at higher energy. In any case the extrapolation procedure is once more necessary.

40.1 The Trojan Horse Method

Alternative methods for determining bare nucleus cross sections of astrophysical interest are needed. In this context a number of indirect methods, e.g. the Coulomb dissociation (CD) [25], the Asymptotic Normalization Coefficient method (ANC) [26] and the Trojan-horse method (THM) were developed [27, 28]. For further information on the development and first principles of the method please refer to [29]. The latter has already been applied several times to reactions connected with fundamental astrophysical problems such as primordial nucleosynthesis [11, 30–32], lithium problem [4–6, 33, 34], light elements depletion [7, 35], AGB [36] and Novae nucleosynthesis [20]. It was also applied to reactions induced by radioactive ion beams [12, 13] and neutrons [21, 22]. THM selects the quasi-free (QF) contribution of an appropriate three-body reaction performed at energies well above the Coulomb barrier to extract a charged particle two-body cross section at energies of astrophysical interest. The idea of the THM [28] is to extract the cross section of an astrophysically relevant two-body reaction

$$A + x \rightarrow c + C \tag{40.1}$$

at low energies from a suitable chosen three-body quasi-free reaction

$$A + a \rightarrow c + C + S \tag{40.2}$$

In this approach S acts as a spectator to the $A + x \rightarrow c + C$ binary interaction.This is done with the help of direct processes theory assuming that the Trojan Horse nucleus a has a strong $x \oplus S$ cluster structure [37]. In many applications, this assumption is trivially fulfilled e.g. a = deuteron, x = proton, S= neutron. If the bombarding energy E_A is chosen high enough to overcome the Coulomb barrier in the entrance channel of the three-body reaction, both Coulomb barrier and electron screening effects are negligible. The polar approximation, used in the standard THM prescription has been extensively verified [38, 39] and constitutes a powerful validity test for the method which strenghten the theoretical approach. We refer to [29] for further and advanced theoretical approach to the method.

We just underline that THM allows to link the three-body cross section which is measured in the laboratory with the half-off-energy shell of the binary process of astrophysical interest. Then after inclusion of the Coulombian effects data are then compared and normalized to direct data, at the higher energies available. After that phase, reaction rate is calculated according to the standard prescriptions.

A summary of the recent results obtained by means of the THM method is summarized in Table 40.1 together with references. Table 40.1 shows success for

Table 40.1 Two-body reactions recently studied via Trojan Horse Method at the astrophysical energies

	Binary reaction	Indirect reaction	TH nucleus	References
[*a*]	^{7}Li(p,α)^{4}He	^{7}Li(d,α α)n	d = (p$\oplus$n)	[3, 4]
[*b*]	^{6}Li(d,α)^{4}He	^{6}Li(^{6}Li,α α)^{4}H	^{6}Li = ($\alpha\oplus$d)	[5]
[*c*]	^{6}Li(p,α)^{3}He	^{6}Li(d,α ^{3}He)n	d = (p$\oplus$n)	[6]
[*d*]	^{11}B(p, α)^{8}Be	^{11}B(d, ^{8}Be α)n	d = (p$\oplus$n)	[6]
[*e*]	^{10}B(p,α)^{7}Be	^{10}B(d,^{7}Be α)n	d = (p$\oplus$n)	[7]
[*f*]	^{9}Be(p,α)^{6}Li	^{9}Be(d,^{6}Li α)n	d = (p$\oplus$n)	[8, 9]
[*g*]	^{2}H(^{3}He,p)^{4}He	^{6}Li(^{3}He,p α)^{4}He	^{3}He = (p$\oplus$n)	[10]
[*h*]	^{2}H(d,p)^{3}H	^{2}H(^{6}Li,t p)^{4}He	^{6}Li = ($\alpha\oplus$d)	[11]
[*i*]	^{18}F(p,α)^{15}O	^{18}F(d,α^{15}O)n	d = (p$\oplus$n)	[12–14]
[*l*]	^{15}N(p,α)^{12}C	^{15}N(d,α^{12}C)n	d = (p$\oplus$n)	[10]
[*m*]	^{18}O(p,α)^{15}N	^{18}O(d,α^{15}N)n	d = (p$\oplus$n)	[15]
[*n*]	^{19}F(p,α)^{16}O	^{19}F(d,α^{16}O)n	d = (p$\oplus$n)	[16]
[*o*]	^{19}F(α,p)^{22}Ne	^{19}F(^{6}Li,p^{22}Ne)α	^{6}Li = ($\alpha\oplus$d)	[17, 18]
[*p*]	^{12}C(^{12}C,α)^{20}Ne	^{12}C(^{14}N,α d)^{20}Ne	^{14}N=^{12}(C$\oplus$d)	[19]
[*q*]	^{17}O(p,α)^{14}N	^{17}O(d,α^{14}N)n	d = (p$\oplus$n)	[20]
[*r*]	^{17}O(n,α)^{14}C	^{17}O(d,α^{14}C)H	d = (p$\oplus$n)	[21, 22]
[*s*]	^{13}C(α,n)^{16}O	^{13}C(^{6}Li,n d)^{16}O	^{6}Li = ($\alpha\oplus$d)	[23]
[*t*]	^{12}C(^{12}C,p)^{23}Na	^{12}C(^{14}N,p d)^{23}Na	^{14}N=^{12}(C$\oplus$d)	[19]
[*u*]	^{3}He(d,p)^{4}He	^{3}He(^{6}Li,p α)^{4}He	^{6}Li = ($\alpha\oplus$d)	[24]

(p, α), (α, p), (α, n), (p, n), (n, α), (n, p) of astrophysical interest studied with the THM method, both with stable as well unstable beams. Moreover, our study of ^{12}C(^{12}C,α)^{20}Ne and ^{12}C(^{12}C,p)^{23}Na [19] has demonstrated that we can extend the method to heavier ions [19].

The THM is complementary to direct measurements which are needed in the higher energy range where indirect data must be normalized to available data in literature. A numbers of astrophysical scenarios were thus explored helping to shed light in many cosmic problems. We underline that in many cases the THM will be a powerful aid to nuclear astrophysics knowledge especially in the investigation of the interaction of neutron-induced reactions with unstable particles.

Acknowledgements This work was supported by the Italian Ministry of the University under Grant No. RBFR082838 and "LNS Astrofisica Nucleare (fondi premiali)".

References

1. E.M. Burbidge, G.R. Burbidge, W.A. Fowler, F. Hoyle, Rev. Mod. Phys. **29**, 547 (1957)
2. H.J. Assenbaum, K. Langanke, C. Rolfs, Z. Phys, A **327**, 461 (1987)
3. M. Lattuada et al., Ap. J. **562**, 1076 (2001)
4. L. Lamia et al., Astrophys. J. **768**, 65 (2013)
5. M. Aliotta, C. Spitaleri, M. Lattuada et al., Eur. Phys. J. A **9**, 435 (2000)
6. L. Lamia et al., J. Phys. G **39**, 015106 (2012)
7. C. Spitaleri et al., Phys. Rev. C **90**, 035801 (2014)
8. S. Romano et al., Eur. Phys. J. A **27**, 221 (2006)
9. Q.-G. Wen, C.-B. Li, S.-H. Zhou et al., Phys. Rev. C **78**, 035805 (2008)
10. M. La Cognata et al., Eur. Phys. J. A **27**, 249 (2006)
11. A. Rinollo et al., Nucl. Phys. A **758**, 146c (2005)
12. S. Cherubini et al., Phys. Rev. C **92**, 015805 (2015)
13. R.G. Pizzone, B.T. Roeder, M. McCleskey et al., Eur. Phys. J. A **52**, 24 (2016)
14. M. La Cognata, R.G. Pizzone, J. José et al., Astrophys. J. **846**, 65 (2017)
15. M. La Cognata, C. Spitaleri, A. Mukhamedzhanov et al., Astrophys. J. **708**, 796 (2010)
16. I. Indelicato, M. La Cognata, C. Spitaleri et al., Astrophy. J. **845**, 19 (2017)
17. R.G. Pizzone, G. D'Agata, M. La Cognata et al., Astrophys. J. **836**, 57 (2017)
18. G. D'Agata, R.G. Pizzone et al., Astrophys. J. **860**, 61 (2018)
19. A. Tumino, C. Spitaleri, M. La Cognata, S. Cherubini, G.L. Guardo, M. Gulino, S. Hayakawa, I. Indelicato, L. Lamia, H. Petrascu, R.G. Pizzone et al., Nature **557**, 687–690 (2018)
20. M.L. Sergi, C. Spitaleri, M. La Cognata et al., Phys. Rev. C **91**, 065803 (2015)
21. G.L. Guardo, C. Spitaleri, L. Lamia et al., Phys. Rev. C **95**, 025807 (2017)
22. M. Gulino et al., Phys. Rev. C **87**, 012801 (2013)
23. M. La Cognata, C. Spitaleri, O. Trippella et al., Phys. Rev. Lett. **109**, 232701 (2012)
24. La Cognata et al., Phys. Rev. C **72**, 065802 (2005)
25. G. Baur, C.A. Bertulani, H. Rebel, Nucl. Phys. A **458**, 188 (1986)
26. A.M. Mukhamedzhanov, R.E. Tribble, Phys. Rev. C **59**, 3418 (1999)
27. G. Baur, Phys. Lett. B **178**, 135 (1986)
28. C. Spitaleri, in *Problems of Fundamental Modern Physics, II: Proceedings*, ed. by R. Cherubini, P. Dalpiaz, B. Minetti (World Science, 1991), p. 21
29. C. Spitaleri, M. La Cognata, L. Lamia, A.M. Mukhamedzhanov, R.G. Pizzone, Eur. Phys. J. A **52**, 77 (2016)
30. A. Tumino et al., Phys. Lett. B **700**, 111 (2011)

31. R.G. Pizzone et al., Astrophys. J. **786**, 112 (2014)
32. C. Li et al., Phys. Rev. C **92**, 025805 (2015)
33. R.G. Pizzone et al., Astron. Astrophys. **438**, 779 (2005)
34. L. Lamia et al., Astron. Astrophys. **541**, 158 (2012)
35. L. Lamia et al., Astrophys. J. **811**, 99 (2015)
36. S. Palmerini et al., Ap. J. **764**, 128 (2013)
37. L. Lamia, M. La Cognata, C. Spitaleri, B. Irgaziev, R.G. Pizzone, Phys. Rev. C **85**, 025805 (2012)
38. R.G. Pizzone et al., Phys. Rev. C **83**, 045801 (2011)
39. R.G. Pizzone et al., Phys. Rev. C **87**, 025805 (2013)

Chapter 41
Nuclear Reaction of Astrophysical Interest with LUNA Projects

Paolo Prati

Abstract About 25 year ago LUNA (Laboratory for Underground Nuclear Astrophysics) opened the era of underground nuclear astrophysics installing a home-made 50 kV ion accelerator under the Gran Sasso mountain. A second machine, with a terminal voltage of 400 kV, was then installed and it is still in operation. Most of the processes so far investigated were connected to the physics of solar neutrinos and hence to the hydrogen burning phase in stars. The interest to next and warmers stages of star evolution (i.e., helium and carbon burning) pushed a new project based on a ion accelerator in the MV range called LUNA-MV. Thanks to a special grant of the Italian Ministry of Research (MIUR), INFN is now building, inside one of the major hall at Gran Sasso, a new facility which will host a 3.5 MV single-ended accelerator able to deliver proton, helium and carbon beams with intensity in the mA range. The scientific program for the 1st phase of the LUNA-MV life will be described with the first experiment scheduled for June 2019.

41.1 The LUNA Approach

41.1.1 Experimental Techniques for Underground Nuclear Astrophysics

Underground nuclear astrophysics was born twenty-seven years ago in the core of Gran Sasso, with the aim of measuring cross sections in the low energy range and derive reaction rates directly at stellar temperatures. LUNA (Laboratory for Underground Nuclear Astrophysics) started its activity as a pilot project with a 50 kV accelerator [1] and it has been for about 25 years the only laboratory in the world running an accelerator deep underground, currently a 400 kV (LUNA400) accelerator with hydrogen and helium beams [2]. The extremely low laboratory background

Paolo Prati for the LUNA Collaboration.

P. Prati (✉)
University of Genova and INFN, Genova 16146, Italy
e-mail: prati@ge.infn.it

A. Formicola et al. (eds.), *Nuclei in the Cosmos XV*, Springer
Proceedings in Physics 219, https://doi.org/10.1007/978-3-030-13876-9_41

has allowed for the first time nuclear physics experiments with very small count rates, down to a couple of events per month. Only in this way, the important reactions responsible for the hydrogen burning in the Sun could be studied down to the relevant stellar energies [3, 4]. In particular, the first direct determination of the cross section of the ^{3}He(^{3}He,2p)^{4}He inside the Solar Gamow peak definitively excluded a nuclear solution to the Solar Neutrinos Problem [5] while the LUNA experiment on the bottleneck reaction of the CNO cycle, the ^{14}N(p,γ)^{15}O reduced by a factor two the value of the CNO neutrinos expected from the Sun [6]. More recently, LUNA shed light on the origin of the meteoritic stardust [7] through a low-energy study of the ^{17}O(p,α)^{14}N [8]. Full descriptions of the LUNA approach and numerous results are given in two recent review papers [9, 10].

41.1.2 Ongoing Experiments at LUNA400

The 400 kV current LUNA accelerator and the unique low-background conditions of the underground LNGS laboratory have been and still are the perfect blend for the study of most of the proton-capture reactions involved in the stellar H burning and in the Big Bang Nucleosynthesis. Actually, a scientific program based on the study of D(p,γ), ^{6}Li(p,γ), ^{13}C(α,n), ^{22}Ne(α,γ) and ^{12,13}C(p,γ) has been approved both by the LNGS-Scientific Committee and it will extend to the whole 2019. The previous study of the CNO cycle are now going to be concluded with dedicated experiments on (p,γ) reactions on carbon isotopes (^{12}C and ^{13}C).

Theoretical calculations of the products of the primordial nucleosynthesis (also Big Bang Nucleosynthesys, hereinafter BBN) provide important hints for cosmology and particle physics. The recent developments of experimental cosmology, such as, in particular, the precise determination of the CMB temperature fluctuations and the associated polarization obtained by WMAP and PLANK as well as the observation of high-redshift supernovae, revived the interest for BBN studies [11]. In practice, different observables provide spots of the Universe at different epochs. For instance, supernovae, CMB and primordial helium, deuterium and lithium show the Universe at z ~ 1, 1000 and >10^{8}, respectively. LUNA400 has contributed to improve the predictions of the BBN by significantly reducing the uncertainties of the rates of the ^{3}He(α,γ)^{7}Be and the D(α,γ)^{6}Li reactions. To complete this investigation, an accurate determination of the D(p,γ)^{3}He reaction rate is now missing and is the goal on the ongoing experiment at LUNA400. This reaction mainly affects the primordial deuterium abundance. A precise determination of its rate at BBN energies is a necessary input to constrain baryon density and effective neutrino species.

In view of the foreseen studies at the new LUNA MV facility (see Sect. 41.2), experiments on two processes that may be active in the stellar He-burning zones, when the slow neutron capture nucleosynthesis (s process) takes place are also in progress. The first, the ^{13}C(α,n)^{16}O reaction, is the most important neutron source in low-mass Asymptotic Giant Branch (AGB) stars and is responsible for the production of about half of the heavy isotopes (beyond iron) in nature. The second is the

$^{22}Ne(\alpha,\gamma)^{26}Mg$, which competes with the $^{22}Ne(\alpha,n)^{25}Mg$ reaction, another important neutron source for massive stars, and contribute to the synthesis of Mg isotopes. The on-going program is completed by the study of the $^{6}Li(p,\gamma)^{7}Be$ reaction to clarify some important nuclear physics issues and to improve the knowledge of the $^{3}He(\alpha,\gamma)^{7}Be$ process, one of the key branches of the p–p chain.

41.2 The LUNA-MV Project

A beam of higher energy is required to extend the LUNA approach to reactions between heavier isotopes, as those operating during more advanced phases of stellar evolution, namely the He and the C burnings. The LUNA MV project has been developed to overcome such a limit: the new accelerator will provide hydrogen, helium and carbon (also doubly ionized) high current beams and it will be devoted to the study of those key reactions of helium and carbon burning that determine and shape both the evolution of massive stars towards their final fate and the nucleosynthesis of most of the elements in the Universe.

In particular, the $^{12}C(\alpha,\gamma)^{16}O$ and $^{12}C+^{12}C$ reactions represent the "Holy Grail" of nuclear astrophysics and they are the most ambitious goals of this project [9, 10 and references therein]. The first of these two reactions competes with the triple-alpha during the He burning. Both release a comparable amount of energy (about 7 meV), but the He consumption of the $^{12}C(\alpha,\gamma)$ is only 1/3 of that of the 3-alpha. Therefore, a change of the $^{12}C(\alpha,\gamma)$ reaction directly affects the He burning lifetime. Furthermore, it determines the C/O ratio left at the end of the He burning. This is a fundamental quantity impacting, for instance, white dwarf cooling timescale and the outcomes of both type Ia and core-collapse supernovae. The $^{12}C+^{12}C$ fusion reaction is the trigger of C burning. The temperature at which C burning takes place depends on its rate: the larger the rate, the lower the C-burning temperature. Since the temperature controls the nucleosynthesis processes, reliable estimations of all the yields produced by C burning, for example the weak component of the s process which produce the elements between Fe and Sr, require the precise knowledge of the $^{12}C+^{12}C$ rate. The $^{12}C+^{12}C$ rate also determines the lower stellar mass limit for C ignition. This limit separates the progenitors of white dwarfs, nova and type Ia supernovae, from those of core-collapse supernovae, neutron stars, and stellar mass black holes. This mass limit also controls the estimations of the expected numbers of these objects in a given stellar population, which are required to answer crucial questions such as: how many neutrons stars are there in the Milky Way? How many double neutron stars are there in close binaries? And what is the expected merging rate? A very recent experiment carried out with the so-called Trojan Horse Method, claimed the existence of several resonances in $^{12}C+^{12}C$ in the so far un-explored region at E_{cm} 1–2.5 meV [12]. This observation would imply a significant increase in the reaction rate and a corresponding lowering of the mass limit of star for which carbon-burning can ignite. An independent verification of such result is definitively needed and LUNA-MV is the sole laboratory in the world where a low-energy direct

experiment can be performed. Actually, the $^{12}C+^{12}C$ experiment will be the main goal/task in the first years of life of the new underground facility

Among the key processes for stellar nucleosynthesis, the sources of neutrons represent a longstanding and debated open problem [13, 14]. Neutron-captures (slow or rapid, i.e., the s or r process, respectively) were early recognized as the most important mechanism to produce the elements heavier than iron. The identification of the astrophysical sites where these processes may operate requires the accurate knowledge of the efficiency of the possible neutron sources. Various reactions have been identified as promising neutron sources. Among them $^{13}C(\alpha,n)^{16}O$ and $^{22}Ne(\alpha,n)^{25}Mg$ represent the most favored candidates. This is because they operate from relatively low temperatures typical of He burning (100–300 MK) and because ^{13}C and ^{22}Ne are relatively abundant nuclei in stellar interiors. The $^{13}C(\alpha,n)^{16}O$ reaction operates in the He-burning shell of low-mass (less than 4 solar masses) AGB stars and it is the neutron source reaction that allows the creation of the bulk of the s-process elements such as Sr, Zr and the light rare earth elements in the Universe. The $^{22}Ne(\alpha,n)^{25}Mg$ reaction operates in the He-burning shell of high-mass (more than 4 solar masses) AGB stars and during the core-He burning and the shell-C burning of massive stars (more than 10 solar masses). Underground experiments with LUNA MV will allow us to gain a full understanding of these two reactions through the direct measurement of their cross sections in the energy range of astrophysical interest.

The LUNA-MV facility will be installed at the north side of Hall B of LNGS and will consist of an accelerator room with concrete walls and a further building hosting the control room and technical facilities including the cooling system, the electric power center, etc. (Fig. 41.1). The concrete walls and ceiling (thickness of 80 cm) of the accelerator room serve as neutron shielding.

The LUNA-MV accelerator is an Inline Cockcroft Walton accelerator designed and constructed by High Voltage Engineering Europe (HVEE). The machine will cover a Terminal Voltage range from 0.2 to 3.5 MV and will deliver ion beams of H^+, $^4He^+$, $^{12}C^+$ and $^{12}C^{++}$ in the energy range from 0.35 to 7 meV into two different beam lines via a 35° switching analyzing magnet (Fig. 41.1). The delivery of accelerator to LNGS is scheduled for the first months of 2019. Data taking for physics experiments is envisaged to start in late fall 2019. The scientific life of the new facility will be of 25–30 just considering the possible experiments in nuclear astrophysics and can go well beyond if including applications in other fields even outside the fundamental research frame. A proposal for the first five years of activity at LUNA-MV has been approved by the LNGS Scientific Committee. Such program includes the direct measurement of the cross section of the $^{12}C+^{12}C$, $^{13}C(\alpha,n)$ and $^{22}Ne(\alpha,n)$ reactions and a renewed study of the $^{14}N(p,\gamma)$ at energies higher than those previously explored at LUNA400. In a successive phase, the problem of $^{12}C(\alpha,\gamma)$ should also be attacked with a dedicated experiment.

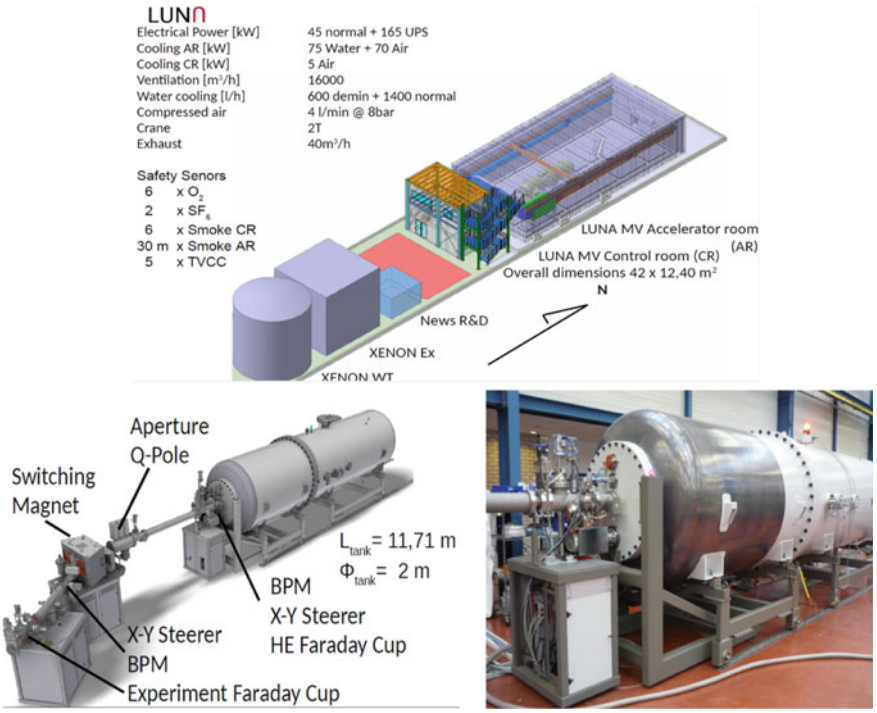

Fig. 41.1 Top panel: layout of the LUNA-MV installation with the 3.5 MV accelerator in Hall B at LNGS. Bottom panel: schematic of the LUNA-MV accelerator plus a beam line (tendered to HVEE) and a picture of LUNA-MV ready at the manufacturer factory (March 2018)

References

1. U. Greife et al., Laboratory for underground nuclear astrophysics (LUNA). Nucl. Instr. Meth. Phys. Res. A. **350**, 327–337 (1994)
2. A. Formicola et al., The LUNA 400 kV accelerator. Nucl. Instr. Meth. Phys. Res. A. **507**, 609–616 (2003)
3. H. Costantini et al., LUNA: a laboratory for underground nuclear astrophysics. Rep. Prog. Phys. **72**, 086301 (2009)
4. C. Broggini et al., LUNA: nuclear astrophysics deep underground. Annu. Rev. Nucl. Part. Sci. **60**, 53–73 (2010)
5. R. Bonetti et al., First measurement of the ^{3}He(^{3}He,2p)^{3}He cross section down to the Lower Edge of the Solar Gamow Peak. Phys. Rev. Lett. **82**, 5205 (1999)
6. A. Formicola et al., Astrophysical S factor of 14N (p, γ) 15O. Phys. Lett. B **591**, 61 (2004)
7. M. Lugaro et al., Origin of meteoritic stardust unveiled by new proton-capture rate on oxygen-17. Nat. Astron. **1**, 0027 (2017)
8. C.G. Bruno et al., Improved direct measurement of the 64.5 keV resonance in the ^{17}O(p,α)^{14}N reaction at LUNA. Phys. Rev. Lett. **117**, 142502 (2016)
9. C. Broggini et al., LUNA: status and prospects. Progr. Part. Nucl. Phys. **98**, 55 (2018)
10. F. Cavanna, P. Prati, Direct measurement of nuclear cross-section of astrophysical interest: results and perspectives. Int. J. Mod. Phys. A **33**, 1843010 (2018)

11. K.A. Olive et al., Higher D or Li: probes of physics beyond the standard model. MNRAS **426**, 1427 (2012)
12. A. Tumino et al., An increase in the $^{12}C+^{12}C$ fusion rate from resonances at astrophysical energies. Nature **557**, 687–690 (2018)
13. E.M. Burbidge et al., Synthesis of the elements in stars. Rev. Mod. Phys. **29**, 547 (1957)
14. A.G.W. Cameron, Nuclear reactions in stars and nucleogenesis. Publ. Astron. Soc. Pac. **69**, 201 (1957)

Chapter 42
Investigation of Neutron-Induced Reaction at the Goethe University Frankfurt

René Reifarth, Lukas Bott, Benjamin Brückner, Ozan Dogan, Markus Dworac, Anne Endres, Philipp Erbacher, Stefan Fiebiger, Roman Gernhäuser, Kathrin Göbel, Fabian Hebermehl, Tanja Heftrich, Christoph Langer, Tanja Kausch, Nadine Klapper, Kafa Khasawneh, Christoph Köppchen, Sabina Krasilovskaja, Deniz Kurtulgil, Markus Reich, Markus S. Schöffler, Lothar Ph. H. Schmidt, Christian Schwarz, Zuzana Slavkovská, Kurt E. Stiebing, Benedikt Thomas, Meiko Volknandt, Mario Weigand, Michael Wiescher and Patric Ziel

Abstract We present first results and plans for future neutron activation measurements at the Goethe University Frankfurt. The measurements were performed at the Van-de-Graaff accelerator employing the ^{7}Li(p,n) reaction.

42.1 Introduction

Neutron-induced reactions are relevant for many astrophysical scenarios [1]. The involved isotopes can be stable as during the s-process or radioactive as during the p-, i- or r-process. The different scenarios are characterized by different temperatures and neutron densities. Direct measurements of the relevant cross section are therefore ideally performed for many different energies. The most general method is the time-of-flight method, which typically requires large samples of isotopically enriched material, intense neutron sources and sophisticated detectors.

R. Reifarth (✉) · L. Bott · B. Brückner · O. Dogan · M. Dworac · A. Endres · P. Erbacher · S. Fiebiger · K. Göbel · F. Hebermehl · T. Heftrich · C. Langer · T. Kausch · N. Klapper · K. Khasawneh · C. Köppchen · S. Krasilovskaja · D. Kurtulgil · M. Reich · M. S. Schöffer · L. Ph. H. Schmidt · C. Schwarz · Z. Slavkovská · K. E. Stiebing · B. Thomas · M. Volknandt · M. Weigand · P. Ziel
Goethe University Frankfurt, Frankfurt, Germany
e-mail: reifarth@physik.uni-frankfurt.de

R. Gernhäuser
Technical University Munich, Munich, Germany

M. Wiescher
University of Notre Dame, Notre Dame, IN, USA

A. Formicola et al. (eds.), *Nuclei in the Cosmos XV*, Springer
Proceedings in Physics 219, https://doi.org/10.1007/978-3-030-13876-9_42

The activation method alleviates many of these costly requirements at the cost of integral measurements. The Van de Graaff accelerator at the Goethe University Frankfurt provides unpulsed proton beams of up to 20 μA in the energy regime between 1.5 and 2.5 MeV. This is ideally suited for the production of neutrons via the ^{7}Li(p,n) reaction. Many different energy spectra can be produced depending on the proton energy, the thickness of the lithium layer and the position of the irradiated sample.

42.2 Activation Technique

To obtain stellar cross sections from an activation experiment, the neutron spectrum should ideally correspond to the thermal spectrum at the respective *s*-process site [2]. The ^{7}Li(p,n)^{7}Be reaction, which represents the most prolific neutron source at low energy accelerators fulfills this requirement almost perfectly [3–5]. Adjusting the proton energy at $E_p = 1912$, 30 keV above the reaction threshold, yields a neutron spectrum with an energy dependence close to a Maxwellian distribution corresponding to $k_B T = 25$ keV almost perfectly mimicking the situation during He shell flashes in AGB stars. A typical activation setup is depicted in Fig. 42.1.

The neutron spectrum can be significantly altered, if the proton energy, the proton-energy distribution, the thickness of the lithium target, or the angular coverage of the neutron field by the sample is modified [6, 7]. The neutron flux is typically determined using a reference sample of the same shape up- and downstream of the sample.

42.3 First Measurements

The upcoming neutron facility FRANZ in Frankfurt (Germany) [8] will be based on the ^{7}Li(p,n) reaction to produce neutrons by upgrading the proton source as well as high current lithium targets. In a first step, the Van-de-Graaff accelerator at the department of physics at the Goethe University Frankfurt was used to perform measurements of neutron-induced reactions.

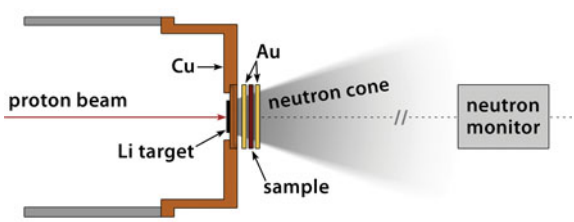

Fig. 42.1 A typical activation setup consists of a continuous neutron source, a sample positioned very close to the neutron source and a separate setup to detect to decay of freshly produced, radioactive nuclei

42.3.1 Detection of γ-Activities

We performed activations of natural samples of aluminum, potassium chloride, gallium and potassium bromide, see Figs. 42.2, 42.3 and 42.4. While recent activation measurements for the isotopes ^{27}Al [9], ^{41}K [10], and ^{79,81}Br [11] exist, no activation-based data are available for ^{37}Cl, ^{69,71}Ga as well as for the population of the isomeric state of ^{82}Br. The preliminary results shown in Figs. 42.2, 42.3 and 42.4 indicate that the activations were successful and we anticipate final results with 5–10% uncertainty.

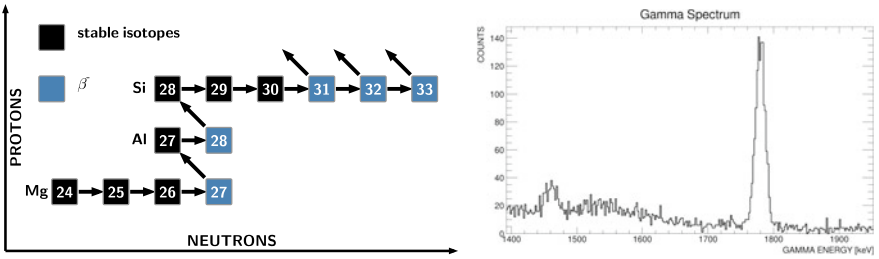

Fig. 42.2 The s-process reaction network around ^{27}Al (left) and γ-spectrum resulting from the 2.2 min decay of ^{28}Al following the activation of natural aluminum (right)

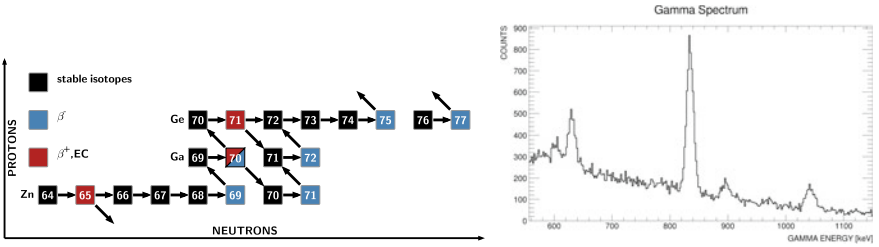

Fig. 42.3 The s-process reaction network around gallium (left) and γ-spectrum resulting from the decay of ^{70,72}Ga following the activation of natural gallium (right)

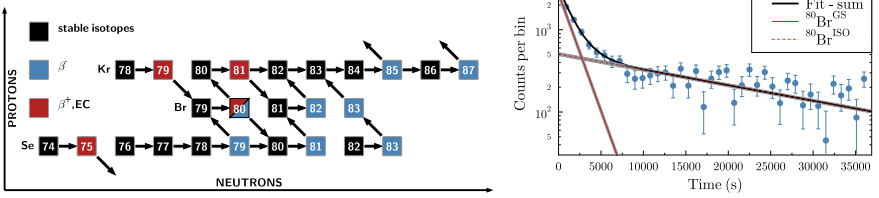

Fig. 42.4 The s-process reaction network around bromine (left) and the time dependence of the 511 keV γ-line resulting from the decay of ^{80}Br^{GS} following the activation of natural bromine (right)

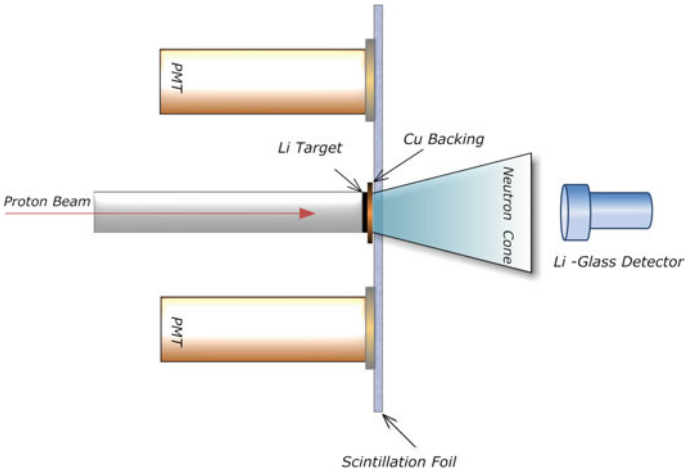

Fig. 42.5 Sketch of the NICE-setup used to measure the ^{7}Li(n,γ) cross section. The NICE-detector (Neutron-Induced Charged particle Emission) is based on a thin scintillation foil read out by photomultiplier tubes mounted on flat side of the foil

42.3.2 Detection of α-Activities

A new detection system for charged particles was successfully tested for the first time, see Fig. 42.5. This setup allows the investigation of neutron-induced reactions with charged particles in the exit channel. This includes (n,α), (n,p), and (n,fission) reactions. A first test was performed on the ^{7}Li(n,γ)^{8}Li(β^{-})^{8}Be(α)α reaction. This reaction was investigated in the past with ionization chambers [12]. For this purpose, the proton beam from the accelerator was periodically directed onto the neutron production target for 2 s and then deflected onto a beam stop for 2 s to observe the 0.8 s decay of ^{8}Li followed by the prompt α-decay of ^{8}Be.

42.4 Outlook

In the near-term future we plan to perform activation measurements with different neutron spectra to constrain the stellar reaction rates at different temperatures. As soon as the RFQ-based accelerator is operational, we will perform activation as well as time-of-flight measurements on radioactive isotopes.

Acknowledgements This research has received funding from the European Research Council under the European Unions's Seventh Framework Programme (FP/2007-2013)/ERC Grant Agreement n. 615126 and from the Deutsche Forschungsgemeinschaft RE-3461/4-1 and RE 3461/4-1.

References

1. R. Reifarth, C. Lederer, F. Käppeler, J. Phys. G Nucl. Phys. **41**(5), 053101 (2014)
2. R. Reifarth, P. Erbacher, S. Fiebiger, K. Göbel, T. Heftrich, M. Heil, F. Käppeler, N. Klapper, D. Kurtulgil, C. Langer, C. Lederer-Woods, A. Mengoni, B. Thomas, S. Schmidt, M. Weigand, M. Wiescher, Eur. Phys. J. Plus **133**, 424 (2018)
3. W. Ratynski, F. Käppeler, Phys. Rev. C **37**, 595 (1988)
4. C. Lederer, F. Käppeler, M. Mosconi, R. Nolte, M. Heil, R. Reifarth, S. Schmidt, I. Dillmann, U. Giesen, A. Mengoni, A. Wallner, Phys. Rev. C **85**(5), 055809 (2012). https://doi.org/10.1103/PhysRevC.85.055809
5. G. Feinberg, M. Friedman, A. Krása, A. Shor, Y. Eisen, D. Berkovits, D. Cohen, G. Giorginis, T. Hirsh, M. Paul, A.J.M. Plompen, E. Tsuk, Phys. Rev. C **85**(5), 055810 (2012). https://doi.org/10.1103/PhysRevC.85.055810
6. R. Reifarth, M. Heil, C. Forssén, U. Besserer, A. Couture, S. Dababneh, L. Dörr, J. Görres, R.C. Haight, F. Käppeler, A. Mengoni, S. O'Brien, N. Patronis, R. Plag, R.S. Rundberg, M. Wiescher, J.B. Wilhelmy, Phys. Rev. C **77**, 015804 (2008). https://doi.org/10.1103/PhysRevC.77.015804
7. R. Reifarth, M. Heil, F. Käppeler, R. Plag, Nucl. Inst. Methods A **608**, 139 (2009)
8. R. Reifarth, L.P. Chau, M. Heil, F. Käppeler, O. Meusel, R. Plag, U. Ratzinger, A. Schempp, K. Volk, PASA **26**, 255 (2009)
9. M. Heil, F. Käppeler, E. Uberseder, Mem. Soc. Astron. Italiana **77**, 922 (2006)
10. M. Heil, R. Plag, E. Uberseder, S. Bisterzo, F. Käppeler, A. Mengoni, M. Pignatari, Phys. Rev. C **93**(5), 055807 (2016). https://doi.org/10.1103/PhysRevC.93.055807
11. M. Heil, F. Käppeler, E. Uberseder, R. Gallino, M. Pignatari, Phys. Rev. C **77**, 015808 (2008). https://doi.org/10.1103/PhysRevC.77.015808
12. M. Heil, F. Käppeler, M. Wiescher, A. Mengoni, Ap. J. **507**, 997 (1998)

Chapter 43
Nuclear Astrophysics Underground: Status and Future

Frank Strieder, Daniel Robertson, Axel Boeltzig, Tyler Borgwardt, Manoel Couder, Bryce Frentz, Uwe Greife, Joachim Goerres, Mark Hanhardt, Thomas Kadlecek and Michael Wiescher

Abstract For more than two decades LUNA (Laboratory for Underground Nuclear Astrophysics) has been the only underground laboratory in the world. Over the years many plans have been discussed on different continents for additional laboratories dedicated to the study of nuclear reactions of astrophysical interest at very low energies under almost background free conditions. Only now some of these projects became or will soon become reality. This contribution will focus on the commissioning and features of the CASPAR (Compact Accelerator System for Performing Astrophysical Research) project, the first underground accelerator in the US located in the Sanford Underground Research Facility.

43.1 Introduction

Even more than 60 years after the groundbreaking publication [1] by Burbidge, Burbidge, Fowler, and Hoyle, Nuclear Astrophysics is still a thriving and exciting research field at the interface of nuclear physics, astrophysics, and particle physics. An important current topic is associated with the evolution of stars and its impact on the production of heavy elements. The most critical reactions are $^{12}C(\alpha, \gamma)^{16}O$, $^{13}C(\alpha,n)^{16}O$, $^{22}Ne(\alpha,n)^{25}Mg$ as well as $^{12}C+^{12}C$ fusion but other (p,γ), (α, γ), or (α,n) reactions may also play a role depending on the stellar environment. The study of these reactions at stellar energies has been a major goal by the community, in Europe, the US and increasingly also in China. However, the large cosmic ray induced background has been prohibitive for advancing these measurements into the stellar

F. Strieder (✉) · T. Borgwardt · M. Hanhardt · T. Kadlecek
Department of Physics, South Dakota School of Mines & Technology, Rapid City, SD 57701, USA
e-mail: frank.strieder@sdsmt.edu
URL: http://www.phy.sdsmt.edu/CASPAR/

D. Robertson · A. Boeltzig · M. Couder · B. Frentz · J. Goerres · M. Wiescher
Department of Physics, University of Notre Dame, Notre Dame, IN 46556, USA

U. Greife
Department of Physics, Colorado School of Mines, Golden, CO 80401, USA

A. Formicola et al. (eds.), *Nuclei in the Cosmos XV*, Springer Proceedings in Physics 219, https://doi.org/10.1007/978-3-030-13876-9_43

energy range and the present reaction rates rely on theoretical extrapolations that carry high uncertainties. Accelerator laboratories, located deep underground offer unique conditions for measuring these reactions at low energies as demonstrated by the success of the LUNA facility [2] at Gran Sasso, Italy. LUNA showed for the case of hydrogen burning reactions that many of these kinds of extrapolations can be significantly improved. Over the past years the CASPAR (Compact Accelerator System for Performing Astrophysical Research) laboratory has been constructed and commissioned at the Sanford Underground Research Facility (SURF) at former Homestake Gold mine (Lead, South Dakota, USA) to address the further need for such facilities. CASPAR operates a 1 MV accelerator that can provide beam intensities of more than hundred micro-Ampere. Furthermore, the LUNA-MV facility in Gran Sasso and as well as the JUNA project in Chinas Jinping Underground Laboratory will be operational in the near future (for details see other contributions to this volume). Successful implementation of a science program at these facilities will offer great opportunities for significant progress in the field.

43.2 CASPAR Laboratory

The implementation and operation of the CASPAR accelerator system (Fig. 43.1) is being undertaken by a small collaboration of universities: South Dakota School of Mines and Technology, University of Notre Dame and Colorado School of Mines. However, the laboratory will serve as an open access facility for the broader nuclear astrophysics community. The CASPAR laboratory is located in a dedicated, temperature controlled cavity on the Ross Campus of the 4850 ft science level of the Sanford Underground Research Facility [3] with a rock overburden of 4300 m water equivalent. The CASPAR system includes a 1 MV, high intensity Van-de-

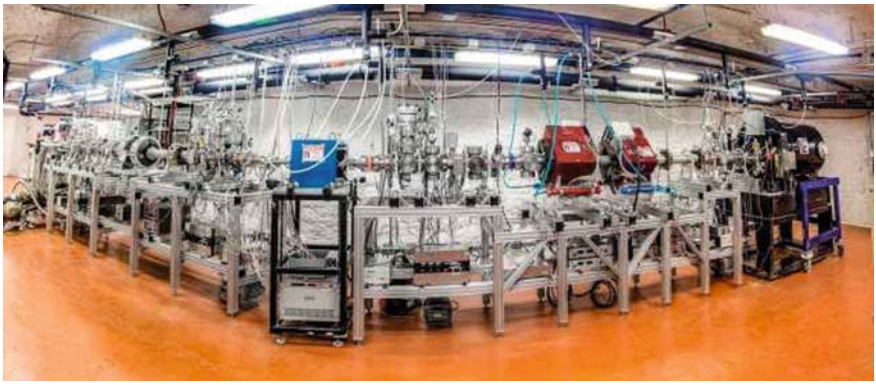

Fig. 43.1 CASPAR accelerator and beam line in the Sanford underground research facility (photo credit: Matt Kapust, SDSTA)

Graaff accelerator originally manufactured in 1958 by High Voltage Engineering. Terminal charging of the accelerator is achieved through a charge carrying belt, providing charge and 400 Hz power for the terminal components. A radio-frequency ion source at the terminal is able to provide proton and helium beams with intensities of more than hundred micro-Ampere. Prior to installation, the CASPAR accelerator has been refurbished at the University of Notre Dame. Modern fiber optic control and communication system inside the pressure vessel as well as encapsulation of vital components, will provide the level of reliability required for operation in a remote location. The ion beam energy selection and filtering is achieved through a 25° analyzing magnet (1×10^{-5} stability/h) located approximately half-way of the total ion path of 15 m between accelerator tank and target station. A solid target station and a windowless, recirculating gas target system are available for experiments at CASPAR.

Currently, the commissioning of the system is performed through a measurement of the reaction $^{14}N(p,\gamma)^{15}O$ over almost the entire energy range available from the CASPAR accelerator and utilizing a Canberra high purity germanium detector with 120% efficiency relative to a $3'' \times 3''$ NaI detector. A 5–10 cm lead shield surrounds the detector as well as the target chamber with some openings required for detector cryostat, beam line, and water-cooling lines. The detector and its lead shield are placed on a movable cart mounted on rails which allows for a variation of the distance of the detector front face to the target. Standard measurement position is in close geometry to increase the detection efficiency. However, since the close geometry results in a significant γ-ray summing effect, the influence of this effect is studied with calibrated radioactive sources and well-known resonances at different distances. Detector and target are mounted at angles of 55° and 45°, respectively, with respect to the beam axis. In order to be able to measure the cross section of the reaction $^{14}N(p,\gamma)^{15}O$ also close to the dominant low-energy resonance at $E_p = 278$ keV thin evaporated ZiN targets with a thickness of 10–20 keV at the resonance energy are used. These targets have proven to withstand beam intensities of 100 μA.

An important requirement for a successful low-energy measurement of nuclear reactions of astrophysical importance is the background suppression. Figure 43.2 shows an environmental background γ-ray spectrum obtained with the Canberra 120% HPGe detector in the CASPAR cavity. The spectrum of the shielded detector (configuration used during actual measurements) is compared to a background run taken with the same detector in the underground cavity, but without any lead shielding, as well as with a detector of similar size at the LUNA facility at Gran Sasso [2]. The suppression factors achieved in both underground laboratories are comparable. However, since the uranium and thorium content in the rocks—and as a consequence the radon contamination in air—in the Sanford Underground Research Facility is higher than in the Gran Sasso Laboratory, the low-energy background, i.e., γ-ray background below $E_\gamma = 3$ MeV, at CASPAR is increased with respect to LUNA (see Fig. 43.2). The increased low-energy background has also some effect on the background at higher γ-ray energies due to pileup and additional neutron-induced γ-ray background. Finally, the shielded HPGe detector at CASPAR has a background

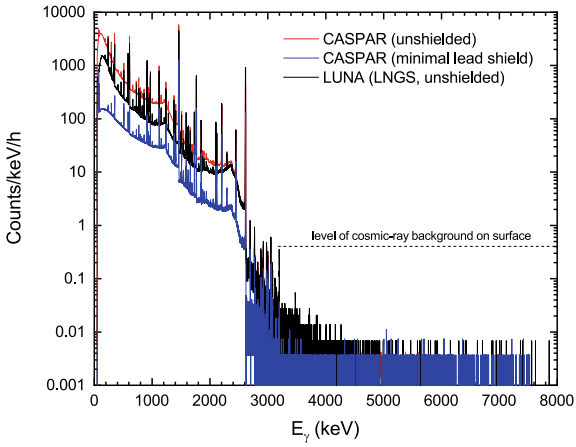

Fig. 43.2 Environmental γ-ray background in the CASPAR cavity taken with a 120% HPGe detector and compared to measurements done at Gran Sasso

rate of 3.7×10^{-4} and 2.6×10^{-4} events keV^{-1} h^{-1} in the energy range 3300–6000 and 4600–7600 keV, respectively (for quantitative comparison see also [4]).

Measurements of the reaction ^{14}N(p,γ)^{15}O are in progress in the proton energy range between lower than 200 keV and 1 MeV. The results of these measurements will be published elsewhere.

43.3 Future

The main science goal for the CASPAR project in the near term future will be a measurement of the two s-process neutron source reactions ^{13}C(α,n)^{16}O and ^{22}Ne(α,n)^{25}Mg. Apart from the r-process, the s-process provides the main path for the synthesis of heavy elements beyond iron in our universe. The s-process is characterized by slow neutron capture reactions taking place during late stellar evolution. The distribution of the heavy element products in these specific burning environments serves as a signature for the conditions in the stellar interior during these phases. Therefore, direct measurements of the two main neutron sources fueling the s-process are very important to probe our stellar models.

Recently, there have been several indirect determinations of the cross sections of these two important reactions which placed some doubts on previous direct measurements with moderated ^{3}He detectors. In particular for the reaction ^{22}Ne(α,n)^{25}Mg a recent indirect study at Texas A&M University revealed a factor of 3 smaller resonance strength for the dominating resonance at $E_\alpha = 832$ keV than in previous measurements [5]. The CASPAR accelerator covers the right energy range to remeasure this resonance with high precision and check for other, potentially important low-energy resonances. The low neutron background environment in the underground laboratory is extremely important for these studies and will lead to unprecedented precision. Studies of the ambient neutron background in the CASPAR

cavity along with improved pulse shape discrimination to distinguish different background sources in the detector are currently performed and direct measurements will start end of 2018.

Finally, one of the most important open quests in Nuclear Astrophysics with stable beams that could be answered by underground measurements is the cross section of the carbon fusion reactions. Extremely low yields and high backgrounds in γ-ray spectroscopy as well as in particle spectroscopy will make this task very challenging. A recently successful approach of measuring particle-γ-ray coincidence lacks sufficient efficiency for measurements at energies close to the Gamow window of carbon burning and also cannot access the ground state transitions in ^{12}C(^{12}C,p)^{23}Na and ^{12}C(^{12}C,α)^{20}Ne. Just a combination of a γ-ray and a particle detection setup with very high efficiency for both channels will bring significant progress. Since both channels have different experimental difficulties, the γ-ray spectroscopy approach in an underground laboratory currently seems to be the more promising path forward. However, in the next foreseeable future among the deep underground laboratories only the LUNA-MV facility can contribute to this endeavor.

Acknowledgements The authors would like to thank the invaluable technical expertise and support of the Sanford Underground Research Facility and the Nuclear Science Lab, university of Notre Dame. The project is funded by National Science Foundation (Grant No. PHY1615197), South Dakota Science and Technology Authority, and the University of Notre Dame.

References

1. E.M. Burbidge, G.R. Burbidge, W.A. Fowler, F. Hoyle, Synthesis of the elements in stars. Rev. Mod. Phys. **29**, 547 (1957). https://doi.org/10.1103/RevModPhys.29.547
2. H. Costantini, A. Formicola, G. Imbriani, M. Junker, C. Rolfs, F. Strieder, LUNA: a laboratory for underground nuclear astrophysics. Rep. Prog. Phys. **72**, 086301 (2009). https://doi.org/10.1088/0034-4885/72/8/086301
3. J. Heise, The Sanford underground research facility at homestake. J. Phys. Conf. Ser. **606**, 012015 (2015). https://doi.org/10.1088/1742-6596/606/1/012015
4. A. Boeltzig et al., Improved background suppression for radiative capture reactions at LUNA with HPGe and BGO detectors. J. Phys. G Nucl. Part. Phys. **45**, 025203 (2018). https://doi.org/10.1088/1361-6471/aaa163
5. M. Jaeger, R. Kunz, J.W. Hammer, G. Staudt, K.L. Kratz, B. Pfeiffer, ^{22}Ne(α, n)^{25}Mg the key neutron source in massive stars. Phys. Rev. Lett. **87**, 202501 (2001). https://doi.org/10.1103/PhysRevLett.87.202501

Chapter 44
Study on Explosive Nucleosynthesis with Low-Energy RI Beams at CRIB

H. Yamaguchi, S. Hayakawa, L. Yang, H. Shimizu, D. Kahl and CRIB Collaboration

Abstract Studies on nuclear astrophysics and nuclear structure have been performed using the radioactive-isotope (RI) beams at the low-energy RI beam separator CRIB of the University of Tokyo. Recent studies on astrophysical reactions in high-temperature stellar environments at CRIB are discussed. We conducted a series of α resonant scattering measurements with RI beams and the thick-target method, mainly to evaluate astrophysical reaction rates of α-induced reactions. Experimental projects based on other experimental techniques, such as the Trojan horse method or RI-implanted target, are also ongoing.

44.1 Introduction

CRIB [1, 2] is a radioactive-isotope (RI) beam separator operated by Center for Nuclear Study (CNS), the University of Tokyo, installed at the RIBF facility of RIKEN Nishina Center. CRIB can produce low-energy (<10 MeV/u) RI beams by the in-flight technique, from primary heavy-ion beams accelerated at the AVF cyclotron of RIKEN (K = 70). Most of the RI beams are produced via 2-body reactions such as (p, n), (d, p) and $(^3\mathrm{He}, n)$, taking place at an 8-cm-long gas target with a maximum pressure of 760 Torr. A cryogenic target system, in which the target gas can be cooled down to about 90 K, is currently available, and an intense ^{7}Be beam of 2×10^8 pps was produced using the system [3]. The low-energy RI beams at CRIB are particularly suitable for studies on astrophysical reactions and nuclear resonant structure.

H. Yamaguchi (✉) · S. Hayakawa · L. Yang · H. Shimizu
Center for Nuclear Study, The University of Tokyo, RIKEN Campus, 2-1 Hirosawa, Wako, Saitama 351-0198, Japan
e-mail: yamag@cns.s.u-tokyo.ac.jp

D. Kahl
School of Physics and Astronomy, The University of Edinburgh, Peter Guthrie Tait Road, Edinburgh EH9 3BF, UK

A. Formicola et al. (eds.), *Nuclei in the Cosmos XV*, Springer
Proceedings in Physics 219, https://doi.org/10.1007/978-3-030-13876-9_44

Recent nuclear astrophysics projects with low-energy RI beams at CRIB can be summarized as follows.

1. α-resonant scattering with the thick-target method in inverse kinematics (TTIK)
   The TTIK [4] is a method suitable for astrophysical reaction studies. In that method, the beam energy is degraded in a thick reaction target, and the reaction occurs at various center-of-mass energies. By detecting the position and the energy of light particles emitted after the reaction, the reaction position in the target and the reaction energy are deduced according to the kinematical relationship. This enables us to perform an efficient measurement of excitation functions even with low-intensity RI beams.
   A series of measurements of α resonant scatterings with beams of ^{7}Li [5], ^{7}Be [6], ^{30}S [7], ^{10}Be [8], ^{15}O, and ^{18}Ne have been carried out. These measurements provide resonant information to evaluate astrophysical reaction rates, and are also very suitable for investigating α cluster structure in the compound nuclei.
2. Application of Trojan horse method (THM) with RI beams
   The first measurement using the THM [9, 10] with an RI beam has been performed at CRIB [11]. The measurement was to study the ^{18}F$(p, \alpha)^{15}$O reaction, which is particularly responsible for the 511-keV γ-ray emission in nova explosions. By our experiment, the excitation function of the ^{18}F$(p, \alpha)^{15}$O reaction was obtained down to the stellar temperature, while an uncertainty on the spin and parity (J^{π}) of resonances still remained. Therefore we have performed another measurement with greater statistics in 2015, and the analysis is under way. The second THM experiment at CRIB was on the ^{7}Be$+n$ reactions, related to the cosmological lithium abundance problem in the Big-Bang nucleosynthesis [12].
3. Isomeric ^{26}Al beam and resonant scattering
   An ^{26}Al beam containing both ground states (^{26g}Al; $J^{\pi} = 5^{+}$) and isomers (^{26m}Al; $J^{\pi} = 0^{+}$) was produced at CRIB first in 2016 [13]. The ^{26}Mg(p, n) reaction was used for the beam production. The primary ^{26}Mg beam energy was at 6.7 MeV per nucleon, where the production of ^{26g}Al is fairly suppressed by the limitation of the angular momentum which can be brought into the system, and thus a high isomeric purity (number of ^{26m}Al to the total ^{26}Al) of about 50% was achieved. We applied this beam to the measurement of ^{26m}Al$+p$ resonant elastic scattering, to study ^{26m}Al(p, γ) reaction as a possible destruction reaction of ^{26m}Al in supernovae.
4. RI-implanted target
   When an RI has a lifetime sufficiently long, we can implant the RI into a host material and use it as a target. With such an implantated target, an intense and low-emittance light-ion beam can be used for measurements of light-ion + RI reactions. In 2018, a ^{7}Be-implanted gold target was produced at CRIB, transferred to JAEA Tandem facility, and then used for a ^{7}Be(d, p) reaction measurement at the energy of Big-Bang nucleosynthesis. This project was carried out in collaboration with RCNP, Osaka University and JAEA [14].

44.2 ^{10}Be + α Elastic Resonant Scattering

The study on the ^{10}Be + α system is discussed here, as a typical example of the α resonant scattering experiment. The study was performed mainly for interst in an exotic cluster structure, while ^{10}Be(α, n) or ^{10}Be(α, γ) reaction may play a role in the Big-Bang nucleosynthesis [15] or other high-temperature stellar environments.

In 1956, Morinaga [16] came up with the novel idea of a particular cluster state: the linear-chain cluster state (LCCS). Now the LCCS is commonly considered as extreme and exotic, due to its presumed propensity to exhibit bending configurations. A theoretical prediction of LCCS in ^{14}C was made by Suhara and En'yo [17, 18] with an antisymmetrized molecular dynamics (AMD) calculation, yielding a prolate band ($J^\pi = 0^+, 2^+, 4^+$) that has a configuration of an LCCS at a few MeV or more above the ^{10}Be+α threshold.

We applied the ^{10}Be+α resonant scattering method in inverse kinematics to identify the predicted LCCS band in ^{14}C [8]. The ^{10}Be beam had a typical intensity of 2×10^4 particles per second, and the beam purity was better than 95%. The ^{10}Be beam at 25.8 MeV impinged on the gas target, which was a chamber filled with helium gas at 700 Torr and covered with a 20-μm-thick Mylar film as the beam entrance window. The measured ^{10}Be beam energy at the entrance of the helium gas target, after the Mylar film, was 24.9 $\pm$ 0.3 MeV. α particles recoiling to the forward angles were detected by $\Delta E - E$ detector telescopes. We obtained an excitation function of the ^{10}Be+α resonant elastic scattering for 13.8–19.1 MeV, as shown in Fig. 44.1a.

We performed an R-matrix calculation to deduce the resonance parameters, and we identified three resonances perfectly corresponding to the predicted LCCS band; J^π are identical, and their energies and spacings are consistent with the theoretical prediction. We claimed this as the strongest indication of the LCCS ever found [8].

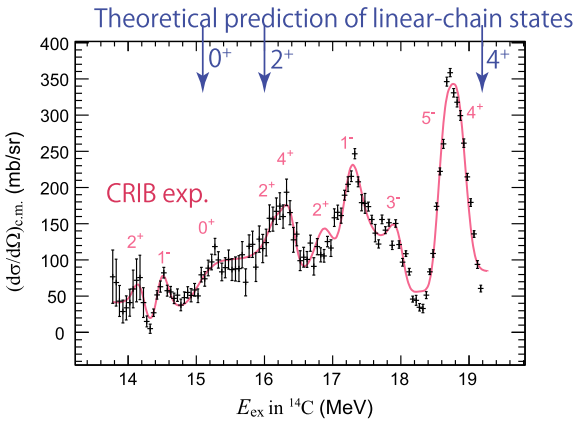

Fig. 44.1 Excitation function of the ^{10}Be + α resonant scattering for θ_{lab} = 0°–8°

Acknowledgements The experiments were performed at RI Beam Factory operated by RIKEN Nishina Center and CNS, the University of Tokyo. We are grateful to the RIKEN and CNS accelerator staff for their help. This work was partly supported by JSPS KAKENHI (Nos. 15K17662, 16K05369, and 16H03980) from the Ministry of Education, Culture, Sports, Science and Technology (MEXT) of Japan.

References

1. S. Kubono, Y. Yanagisawa, T. Teranishi, S. Kato, T. Kishida, S. Michimasa, Y. Ohshiro, S. Shimoura, K. Ue, S. Watanabe, N. Yamazaki, Eur. Phys. J. A **13**, 217 (2002)
2. Y. Yanagisawa, S. Kubono, T. Teranishi, K. Ue, S. Michimasa, M. Notani, J.J. He, Y. Ohshiro, S. Shimoura, S. Watanabe, N. Yamazaki, H. Iwasaki, S. Kato, T. Kishida, T. Morikawa, Y. Mizoi, Nucl. Instrum. Meth. Phys. Res. Sect. A **539**, 74 (2005)
3. H. Yamaguchi, Y. Wakabayashi, G. Amadio, S. Hayakawa, H. Fujikawa, S. Kubono, J. He, A. Kim, D. Binh, Nucl. Instrum. Meth. Phys. Res. Sect. A **589**, 150 (2008)
4. K.P. Artemov, O.P. Belyanin, A.L. Vetoshkin, R. Wolskj, M.S. Golovkov, V.Z. Gol'dberg, M. Madeja, V.V. Pankratov, I.N. Serikov, V.A. Timofeev, V.N. Shadrin, J. Szmider, Sov. J. Nucl. Phys. **52**, 408 (1990)
5. H. Yamaguchi, T. Hashimoto, S. Hayakawa, D.N. Binh, D. Kahl, S. Kubono, Y. Wakabayashi, T. Kawabata, T. Teranishi, Phys. Rev. C **83**(3), 034306 (2011)
6. H. Yamaguchi, D. Kahl, Y. Wakabayashi, S. Kubono, T. Hashimoto, S. Hayakawa, T. Kawabata, N. Iwasa, T. Teranishi, Y. Kwon, D.N. Binh, L. Khiem, N. Duy, Phys. Rev. C **87**, 034303 (2013)
7. D. Kahl, H. Yamaguchi, S. Kubono, A.A. Chen, A. Parikh, D.N. Binh, J. Chen, S. Cherubini, N.N. Duy, T. Hashimoto, S. Hayakawa, N. Iwasa, H.S. Jung, S. Kato, Y.K. Kwon, S. Nishimura, S. Ota, K. Setoodehnia, T. Teranishi, H. Tokieda, T. Yamada, C.C. Yun, L.Y. Zhang, Phys. Rev. C **97**, 015802 (2018)
8. H. Yamaguchi, D. Kahl, S. Hayakawa, Y. Sakaguchi, K. Abe, T. Nakao, T. Suhara, N. Iwasa, A. Kim, D. Kim, S. Cha, M. Kwag, J. Lee, E. Lee, K. Chae, Y. Wakabayashi, N. Imai, N. Kitamura, P. Lee, J. Moon, K. Lee, C. Akers, H. Jung, N. Duy, L. Khiem, C. Lee, Phys. Lett. B **766**, 11 (2017)
9. G. Baur, Phys. Lett. B **178**(2–3), 135 (1986)
10. C. Spitaleri, L. Lamia, A. Tumino, R.G. Pizzone, S. Cherubini, A. Del Zoppo, P. Figuera, M. La Cognata, A. Musumarra, M.G. Pellegriti, A. Rinollo, C. Rolfs, S. Romano, S. Tudisco, Phys. Rev. C **69**, 055806 (2004)
11. S. Cherubini, M. Gulino, C. Spitaleri, G.G. Rapisarda, M. La Cognata, L. Lamia, R.G. Pizzone, S. Romano, S. Kubono, H. Yamaguchi, S. Hayakawa, Y. Wakabayashi, N. Iwasa, S. Kato, T. Komatsubara, T. Teranishi, A. Coc, N. de Séréville, F. Hammache, G. Kiss, S. Bishop, D.N. Binh, Phys. Rev. C **92**, 015805 (2015)
12. S. Hayakawa, K. Abe, O. Beliuskina, S.M. Cha, K.Y. Chae, S. Cherubini, P. Figuera, Z. Ge et al., AIP Conf. Proc. **1947**, 020011 (2018)
13. D. Kahl, H. Shimizu, H. Yamaguchi, K. Abe, O. Beliuskina, S.M. Cha, K.Y. Chae, A.A. Chen et al., EPJ Web Conf. **165**, 01030 (2017)
14. A. Inoue, A. Tamii, H. Yamaguchi, K. Abe, S. Adachi, N. Aoi, M. Asai, M. Fukuda et al., CNS Annual Report (CNS-REP-96) p. 21 (2016)
15. A. Coc, S. Goriely, Y. Xu, M. Saimpert, E. Vangioni, Astrophys. J. **744**, 158 (2012)
16. H. Morinaga, Phys. Rev. **101**, 254 (1956)
17. T. Suhara, Y. Kanada-En'yo, Phys. Rev. C **82**, 044301 (2010)
18. T. Suhara, Y.K. En'yo, Phys. Rev. C **84**, 024328 (2011)

Part X
Poster

Chapter 45
Charged-Particle Decays of Highly Excited States in ^{19}F

P. Adsley, F. Hammache, N. de Séréville, M. Assié, D. Beaumel, M. Chabot, M. Degerlier, C. Delafosse, F. Flavigny, A. Georgiadou, J. Guillot, V. Guimaräes, A. Gottardo, I. Matea, L. Olivier, L. Perrot, I. Stefan, A. M. Laird, S. P. Fox, R. Garg, S. Gillespie, J. Riley, J. Kiener, A. Lefebvre-Schuhl, V. Tatischeff and I. Sivacek

Abstract Neutron-capture reactions on ^{18}F in the helium-burning shell play an important role in the production of ^{15}N during core-collapse supernovae. The competition between the ^{18}F$(n, p/\alpha)^{18}$O/^{15}N reactions controls the amount of ^{15}N produced. The strengths of these reactions depend on the decay branching ratios of states in ^{19}F above the neutron threshold. We report on an experiment investigating the decay branching ratios of these states in order to better constrain the strengths of the reactions.

45.1 Astrophysical Background

Spatially correlated hot-spots of ^{15}N and ^{18}O have been observed in grains which originate from core-collapse supernovae [1]. In the helium-burning shell, ^{14}N produced during the CNO cycles is converted into ^{18}F and ^{18}O by ^{14}N$(\alpha, \gamma)^{18}$F$(\beta^+)^{18}$O. During the supernovae the ^{18}O$(\alpha, n)^{21}$Ne reaction activates releasing neutrons and causing ^{18}F$(n, p/\alpha)^{18}$O/^{15}N reactions. The amounts of ^{15}N and ^{18}O produced depend sensitively on the relative strength of the ^{18}F$(n, p/\alpha)^{18}$O/^{15}N reactions [2]

P. Adsley (✉) · F. Hammache · N. de Séréville · M. Assié · D. Beaumel · M. Chabot · M. Degerlier · C. Delafosse · F. Flavigny · A. Georgiadou · J. Guillot · V. Guimaräes · A. Gottardo · I. Matea · L. Olivier · L. Perrot · I. Stefan
Institut Physique Nucléaire dOrsay, UMR8608, CNRS-IN2P3, Universite Paris Sud 11, 91406 Orsay, France
e-mail: padsley@gmail.com

A. M. Laird · S. P. Fox · R. Garg · S. Gillespie · J. Riley
Department of Physics, University of York, Heslington, York YO10 5DD, UK

J. Kiener · A. Lefebvre-Schuhl · V. Tatischeff
Centre de Sciences Nucléaires et de Sciences de la Matière (CSNSM), CNRS/IN2P3, Université Paris-Sud, Université ParisSaclay, Bâtiment 104, Orsay Campus, 91405 Orsay, France

I. Sivacek
ASCR-Rez, CZ-250 68, Rez, Czech Republic

A. Formicola et al. (eds.), *Nuclei in the Cosmos XV*, Springer Proceedings in Physics 219, https://doi.org/10.1007/978-3-030-13876-9_45

determined by ^{19}F states above the neutron threshold. At present, the astrophysical reaction rates used for astrophysical models are based on statistical-model calculations [2]; as ^{19}F is known to exhibit strong clustering behaviour [3] statistical-model calculations may be inappropriate.

Direct measurement of the pertinent cross sections is extremely challenging as neither neutrons nor ^{18}F may be easily fashioned into targets. Instead, the rates may be calculated from detailed knowledge of the properties (energies, total and partial widths, and spins and parities) of the nuclear states above the neutron threshold in ^{19}F.

We report a study of excited states by ^{19}F(p, p') to constrain the ^{18}F$(n, p)^{18}$O and ^{18}F$(n, \alpha)^{15}$N reaction rates.

45.2 Experimental Setup

A 15-MeV proton beam from the Orsay tandem was incident upon a 90-μg/cm^2 LiF foil on a carbon backing located at the target position of the 'Split-Pole' Enge magnetic spectrometer. Scattered particles were momentum analysed in the spectrometer and detected at the focal plane in a position-sensitive gas detector, a gas proportional detector and a plastic scintillator.

Charged particles decaying from the populated states in ^{19}F were detected in an array of six W1 double-sided silicon strip detectors (DSSSDs). As the beamstop was located within the scattering chamber of the spectrometer, a steel shield was placed in the chamber to reduce the background seen by the silicon detectors.

A more detailed description of the experimental setup may be found in [4].

45.3 Data Analysis and Preliminary Results

Figure 45.1 shows the coincidence spectrum where there is a hit in the focal plane and a hit in a silicon detector after imposing certain conditions on the data to check for good hits in the silicon detectors.

The focal-plane spectra gated on a particular decay channel could then be constructed by selecting those events where the 'missing' energy corresponded to the separation energy for the channel of interest. Excitation-energy spectra for the singles events, the α_0-decay-gated events and the p_0-decay-gated events are shown in Fig. 45.2.

Once the various spectra have been generated they are fitted to extract information on the state parameters e.g. the excitation energies, total widths and decay branches. We started by fitting the spectra using known state information taken from the ENSDF database [5]. However, we found that a number of states which have been observed in resonance reaction measurements particularly of ^{18}O$(p, \alpha)^{15}$N [6–8] have been omitted by the compilers of the nuclear data-sheets [9] complicating the analysis as

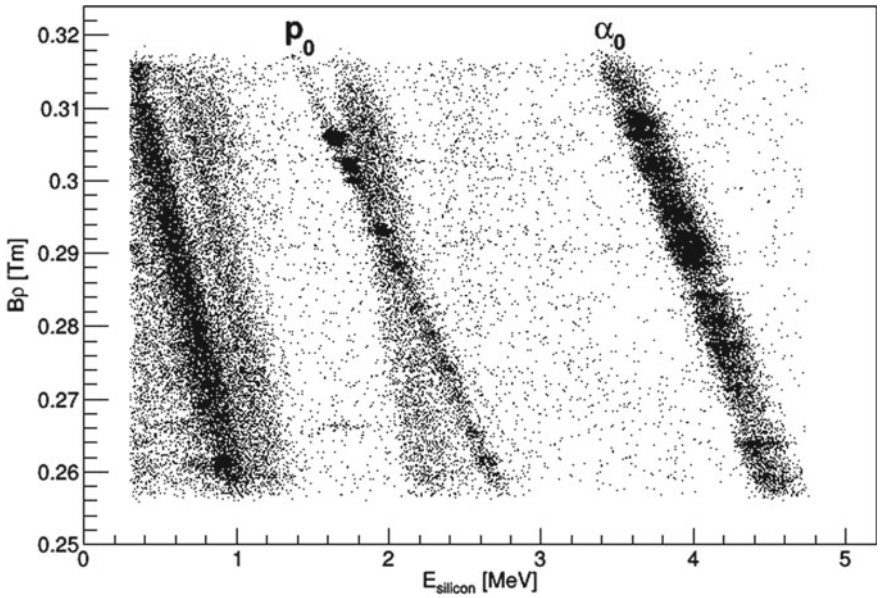

Fig. 45.1 Magnetic rigidity against the energy detected in the silicon detectors for detector number 5. The α_0 and p_0 loci are marked. The other loci are due to exited states in ^{12}C from the target backing breaking up and competing coincidence channels such as ^{19}F$(p, \alpha)^{16}$O(p) reactions

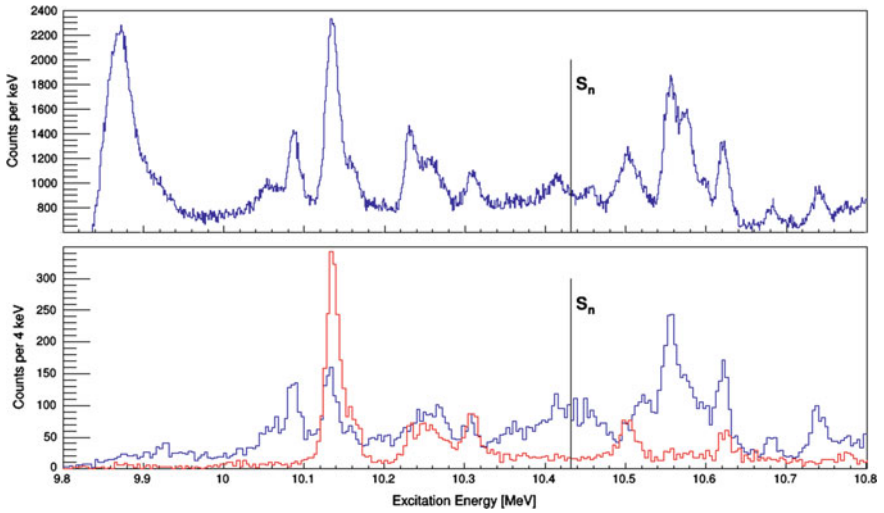

Fig. 45.2 (Top) Singles excitation-energy spectrum. (Bottom) Excitation-energy spectra gated on α_0 (blue) and p_0 (red) decays

well-defined physical parameters for these states are not available and the present experiment is unable to resolve them.

The first important observation from the present experiment is the weakness of the proton decays for many of the excited states. We can compare the ratios of the observed branching ratios to the reaction rates from statistical-model calculations [10]. The calculations predict that the ^{18}F$(n, \alpha)^{15}$N reaction rate should be around three times stronger than the ^{18}F$(n, p)^{18}$O reaction. From the results of the present experiment, we find that the ^{18}F$(n, p)^{18}$O reaction rate is much weaker relative to the ^{18}F$(n, \alpha)^{15}$N reaction rate than that predicted using TALYS with a corresponding increase in the production of ^{15}N in supernovae.

45.4 Outlook

More ^{19}F(p, p') data have been collected using the Q3D magnetic spectrometer at MLL, Garching in July 2018. The excitation-energy resolution achievable in this case is around 5 keV [11] which is around a factor of three better than the current experiment. This should allow for the states in the region of interest to be better resolved and used to guide the future progress of the coincidence analysis.

References

1. E. Groopman, T. Bernatowicz, E. Zinner, C, N, and O isotopic heterogenities in low-density supernova graphite grains from Orgueil. Astrophys. J. Lett. **754**(1), L8 (2012)
2. M.J. Bojazi, B.S. Meyer, Explosive nucleosynthesis of ^{15}N in a massive-star model. Phys. Rev. C **89**, 025807 (2014)
3. B. Buck, A.A. Pilt, Alpha-particle and triton cluster states in ^{19}F. Nucl. Phys. A **280** 133–160 (1977); Z.Q. Mao, H.T. Fortune, A.G. Lacaze, Alpha-particle spectroscopic strengths in ^{19}F and ^{20}Ne. Phys. Rev. C **53**, 1197 (1996)
4. J.E. Riley, A study of 19Ne resonances and their astrophysical implication for the detection of Novae. Ph.D. thesis, University of York (2017)
5. Evaluated Nuclear Structure Data File. http://www.nndc.bnl.gov/ensdf/
6. R.R. Carlson, C.C. Kim, J.A. Jacobs, A.C.L. Barnard, Elastic scattering and reactions of protons on O^{18}. Phys. Rev. **122**, 607 (1961)
7. S. Gorodetzky, M. Port, J. Graff, J.M. Thirion, Niveaux excités du F19 par l'étude de la réaction ^{18}O$(p, \alpha_0)^{15}$N entre 2.2 et 6 MeV (Excited levels of ^{19}F by the study of the reaction ^{18}O$(p, \alpha_0)^{15}$N between 2.2 and 6 MeV). Nucl. Phys. **42** 462–468 (1963)
8. S. Gorodetzky, M. Port, J. Graffet J.M. Thirion: Niveaux excités du ^{19}F par l'étude de la réaction ^{18}O$(p, \alpha_0)^{15}$N (Excited levels of ^{19}F by the study of the reaction ^{18}O$(p, \alpha_0)^{15}$N). J. Phys. France **24**, 978–983 (1963)
9. F. Ajzenberg-Selove, Energy levels of light nuclei A = 18–20. Nucl. Phys. A **392**, 1–184 (1983)
10. A.J. Koning, S. Hilaire, M.C. Duijvestijn, TALYS-1.0, in *Proceedings of the International Conference on Nuclear Data for Science and Technology—ND2007*, 22–27 Apr 2007 (EDP Sciences, Nice, France, 2008) pp. 211–214
11. P. Adsley, J.W. Brümmer, T. Faestermann, S.P. Fox, F. Hammache, R. Hertenberger, A. Meyer, R. Neveling, D. Seiler, N. de Séréville, H.-F. Wirth, High-resolution study of levels in the

astrophysically important nucleus ^{26}Mg and resulting updated level assignments. Phys. Rev. C **97**, 045807 (2018)
12. S. Benamara, N. de Séréville, P. Adsley et al., Study of the ^{26}Al$(n, p)^{26}$Mg and ^{26}Al$(n, \alpha)^{23}$Na reactions using the ^{27}Al$(p, p')^{27}$Al inelastic scattering reaction. J. Phys. Conf. Ser. **665**, 012018 (2016)

Chapter 46
Pulse Shape Discrimination for High Pressure ^{3}He Counters

J. Balibrea-Correa, A. Best, G. Imbriani and A. di Leva

Abstract Low counting rate experiments strongly depend on the background suppression during the measurement campaigns. In this work we present a novel Pulse Shape Discrimination methodology, based on digital filters, for high pressure ^{3}He detectors read through charge sensitive preamplifiers. In addition, the preliminary results from a semi-empirical Monte Carlo model for these detectors are exhibited.

46.1 Introduction

The success of low counting rate experiments strongly depends on the accurate knowledge and reduction of the backgrounds present during the measurement campaigns. For this reason, dark matter search and low energy nuclear astrophysics experiments are performed in underground laboratories, shielded from the cosmic rays [1, 2]. Two important examples in nuclear astrophysics are ^{13}C(α,n) and ^{22}Ne(α,n) cross-section measurements at low energies, which are considered to be the main neutron sources for the astrophysical s-process [3, 4].

The intrinsic alpha-activity contained in the walls of high pressure ^{3}He counters, used for these experiments, becomes a major source of background in low count rate scenarios. To reduce this intrinsic background, two pulse shape discrimination (PSD) methodologies were developed recently: They make use of current sensitive preamplifiers [5]; and rise-time methodology for low pressure ^{3}He counters [6]. However, most experiments are performed using charge sensitive preamplifiers and the high-pressure counters which limits the applicability of the rise-time methodology.

J. Balibrea-Correa (✉) · A. Best · A. di Leva
Universit degli Studi di Napoli Federico II, Naples, Italy
e-mail: javier.balibrea@infn.na.it

G. Imbriani
Dipartimento di Fisica “E. Pancini”,
Universitá degli Studi di Napoli “Federico II”, Napoli, Italy

A. Formicola et al. (eds.), *Nuclei in the Cosmos XV*, Springer
Proceedings in Physics 219, https://doi.org/10.1007/978-3-030-13876-9_46

In this work, the charge sensitive preamplifier signals are converted into current preamplifier, benefited of the double pulse for ^{3}He(n,p)T reactions [5], by the use of digital filters. 18 cylindrical, steel housed, 10 bar ^{3}He counters[1] read through CAEN charge sensitive preamplifiers were used. The detectors were embedded inside a polyethylene matrix and surrounded by a 2.54 cm thick 5% borated polyethylene shielding, placed underground at the Gran Sasso National Laboratory. The waveforms were digitized using CAEN 1724 cards. Two different data sets were taken: ^{3}He(n,p)T reactions labeled as "neutron" data were measured using an Am-Be calibration source and a long background data set run was acquired without the use of any neutron source labeled as "α" data. The region of interest for this work will presented as the deposited energy region where the neutron events are taken place.

46.2 Pulse Shape Analysis of the Experimental Data

The digitized waveforms were converted into current sensitive preamplifier signals by applying a first order digital high pass filter (CR) described by the following recurrence formula [7]

$$y_n = \frac{1+\xi}{2}x_n - \frac{1+\xi}{2}x_{n-1} + \xi y_{n-1} \tag{46.1}$$

where $\{x_n\}$, $\{y_n\}$ are the input and output buffers, respectively. The parameter ξ is related to the bandwidth of the filter and must be determined according to the characteristics of the input charge preamplifier signal and the digitizing sampling time.

For each converted current sensitive pulse, the fast (I_f) and slow (I_s) integrals over two different time intervals were calculated. Then the PSD parameter M, defined as $M = I_f/(I_f + I_s)$, were adjusted to maximize the differences between neutron and alpha events signatures as it displayed in Fig. 46.1. The "α" data rejection (>98%) and remaining neutron events (77%) obtained by the use of this parameter have similar performance to the literature values [5, 6].

46.3 Monte Carlo Simulations

The detector response is being investigated by developing a semi-empirical model of the ^{3}He detectors for neutron and α events, including the electronic chain used during the experiment. The simulated events were processed in the same way as the experimental data, calculating for every pulse the amplitude and the PSD parameter M.

[1] Manufactured by GE Reuter Stokes, model numbers RS-P4-0816-217 and RS-P4-0810-249.

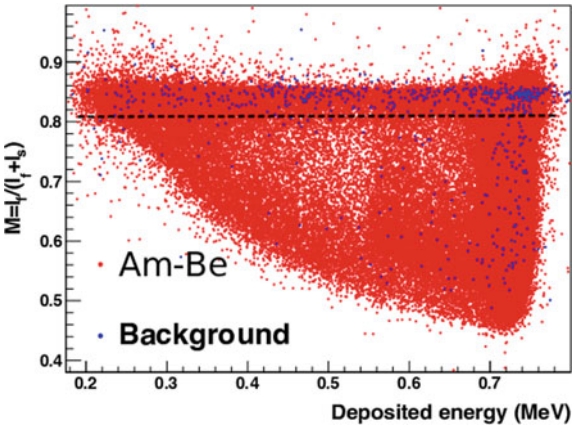

Fig. 46.1 PSD M versus deposited energy for a background (blue) and an Am-Be (red) run in the region of interest

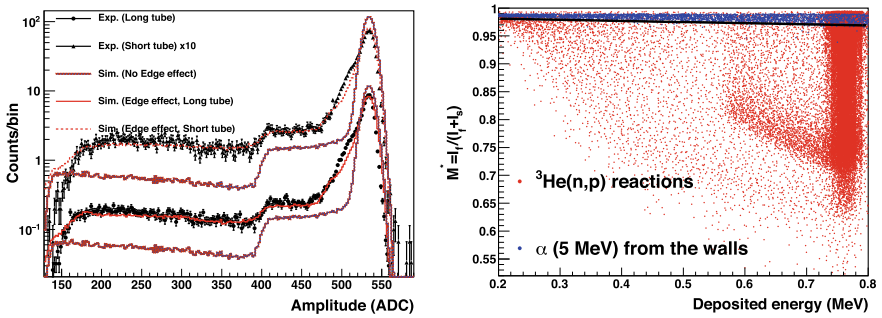

Fig. 46.2 Left: ^{3}He amplitude signature simulated compared with the experimental data used in this work. Right: PSD M—deposited energy distribution obtained from the simulation of neutron and α events

A good agreement between experimental and simulated amplitude spectra for neutron events is obtained as it displayed in left panel of Fig. 46.2. The preliminary results for the PSD simulation, displayed in right panel of Fig. 46.2, confirms the trend observed in the experimental data for neutron and "α" events. These results will be used to improve the current PSD methodologies.

46.4 Conclusions

A novel methodology based on digital techniques was developed for the PSD on high pressure ^{3}He counters read out through charge sensitive preamplifiers. The "α" events rejection, larger than 98%, and survived remaining neutron distribution, ~77%, are

similar to the PSD values for low-pressure ^{3}He counters found in the literature. In addition a semi-empirical model of the detector is being developed, which can be used to further improve PSD methods.

Acknowledgements This research has been carried out in the framework of the STAR project "UCAN", which is funded by the University of Naples "Federico II" and the Compagnia di San Paolo. The ^{3}He counters were funded by the Istituto Nazionale di Fisica Nucleare (INFN).

References

1. A. Best et al., NIM A **812**, 16 (2016)
2. D. Jordan et al., Astropart. Phys. **42**, 16 (2013)
3. F. Käppler et al., Nucl. Phys. A **777**, 219–310 (2006)
4. U. Greife et al., Astrophys. J. **414**, 735–739 (1993)
5. Z.M. Zeng et al., NIM A **866**, 242–247 (2017)
6. T.J. Langford et al., NIM A **717**, 51–57 (2013)
7. S.W. Smith, The scientist and engineer's guide to digital signal processing. http://www.dspguide.com/

Chapter 47
Photoneutron Reaction Cross Section Measurements on ^{94}Mo and ^{90}Zr Relevant to the *p*-Process Nucleosynthesis

A. Banu, E. G. Meekins, J. A. Silano, H. J. Karwowski and S. Goriely

Abstract The photodisintegration cross sections for the ^{94}Mo(γ,n) and ^{90}Zr(γ,n) reactions have been experimentally investigated with quasi-monochromatic photon beams at the High Intensity γ-ray Source (HIγS) facility of Triangle Universities Nuclear Laboratory (TUNL). Energy dependence of the photoneutron reaction cross sections was measured with high precision close to the respective neutron emission thresholds and up to 13.5 meV. These measurements contribute to a broader investigation of nuclear reactions relevant to the understanding of the *p*-process nucleosynthesis. The results are compared with the predictions of Hauser-Feshbach statistical model calculations using different models for the γ-ray strength function. The resulting ^{94}Mo(γ,n) and ^{90}Zr(γ,n) photoneutron stellar reaction rates as a function of temperature in the typical range of interest for the *p*-process nucleosynthesis show how sensitive the photoneutron reaction rate can be to the experimental data in the vicinity of the neutron threshold.

47.1 Introduction

Despite the endemic problem of reproducing the solar abundances of ^{92,94}Mo and ^{96,98}Ru most abundant *p*-nuclei [1], as well as the part of the $A < 124$ region, recent studies performed by Travaglio et al. [2] in supernova Type Ia calculations using both deflagration and delayed detonation models demonstrated that both light and heavy *p*-nuclei, including the much debated isotopes ^{92}Mo and ^{96,98}Ru, are produced

A. Banu (✉) · E. G. Meekins
Department of Physics and Astronomy, James Madison University, Harrisonburg, VA 22807, USA
e-mail: banula@jmu.edu

J. A. Silano · H. J. Karwowski
University of North Carolina at Chapel Hill, Chapel Hill, NC 27516, USA

Triangle Universities Nuclear Laboratory, Durham, NC 27708, USA

S. Goriely
Institut d'Astronomie et d'Astrophysique, Université Libre de Bruxelles, Campus de la Plaine, CP-226, 1050 Brussels, Belgium

A. Formicola et al. (eds.), *Nuclei in the Cosmos XV*, Springer
Proceedings in Physics 219, https://doi.org/10.1007/978-3-030-13876-9_47

with similar enhancement factors relative to solar abundances, provided an *s*-process enrichment of the progenitor is assumed. The model, however, predicts production of ^{94}Mo with a much lower abundance in comparison to all the other light *p*-nuclei. Another remarkable finding of [2] points out that the γ-process can make important contributions to the production of the neutron magic ^{90}Zr, previously known as genuine *s*-process nuclide.

In light of the intriguing findings of [2], we were motivated to investigate the photoneutron reactions on ^{94}Mo and ^{90}Zr. The measurements were focused on studying the energy dependence of the photoneutron reaction cross sections near the respective neutron emission thresholds and up to 13.5 MeV.

The experimental results are compared to the predictions of Hauser-Feshbach (HF) statistical model calculations using different models for the γ-ray strength function (γSF). They allow the γSF to be constrained by the present experimental data and are used to estimate the corresponding stellar photoneutron reaction rates which directly influence the *p*-process nucleosynthesis.

47.2 Experimental Setup

The measurements reported in this paper were performed using TUNL's High Intensity γ-ray Source (HIγS) facility. A schematic not-to-scale drawing of the experimental setup as it was assembled for the present experiment is shown in Fig. 47.1.

The quasi-monoenergetic γ-ray beam had an energy width in the range of 4–5% (FWHM). The γ-ray beam flux was continuously monitored and yielded values in the range of 10^7–10^8 γ/s on target. The very high γ-ray flux available at HIγS makes this

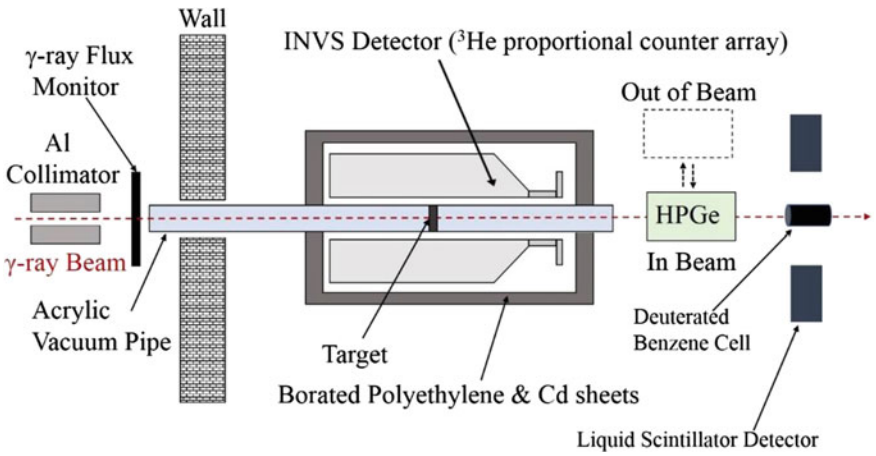

Fig. 47.1 Schematic drawing of the experimental setup in the HIγS upstream target room (not to scale). See [3] for details of the detectors sketched in the figure

facility ideal for investigation of photoneutron reaction cross sections with *p*-nuclei as targets. In-depth experimental description is provided in [3].

47.3 Results

The photoneutron reaction cross sections of the present work are compared with theoretical calculations obtained with the TALYS nuclear reaction code and two different models of the γSF, namely the Generalized Lorentzian (GLO) model and the axially-symmetric-deformed Hartree-Fock-Bogoliubov (HFB) plus QRPA model based on the D1M Gogny interaction, as illustrated in Fig. 47.2. Reference [3] provides details about these statistical models calculations.

In Fig. 47.3 are shown the resulting ^{90}Zr(γ,n)^{89}Zr and ^{94}Mo(γ,n)^{93}Mo stellar photoneutron rates as a function of the temperature in a typical range of interest for the *p*-process nucleosynthesis [1].

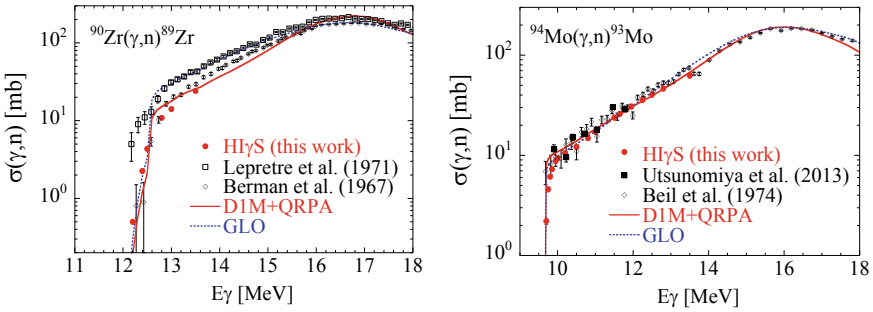

Fig. 47.2 Comparison between the present (γ,n) photoneutron reaction cross sections as a function of the γ-ray beam energy and previous data. Also included are the predictions obtained with the D1M + QRPA *E1* and *M1* strengths (solid line) and with the GLO model (dotted line)

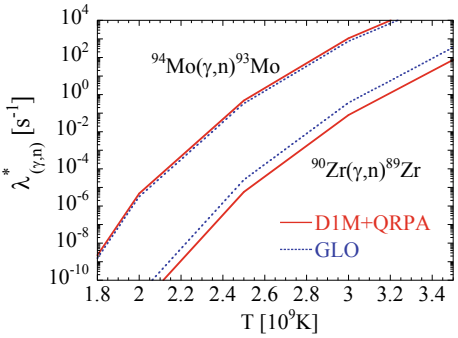

Fig. 47.3 ^{90}Zr(γ,n)^{89}Zr and ^{94}Mo(γ,n)^{93}Mo stellar reaction rates, as a function of the temperature, obtained with the D1M + QRPA (solid lines) or the GLO (dotted lines) γSF shown in Fig. 47.2

References

1. M. Arnould, S. Goriely, The *p*-process of stellar nucleosynthesis: astrophysics and nuclear physics status. Phys. Rep. **384**, 1–84 (2003)
2. C. Travaglio et al., Type Ia supernovae as sites of the *p*-process: two-dimensional models coupled to nucleosynthesis. Astrophys. J. **739**(2), 93 (2011)
3. A. Banu et al., Photoneutron reaction cross section measurements on ^{94}Mo and ^{90}Zr relevant to the *p*-process nucleosynthesis. Phys. Rev. C 99, 025802 (2019)

Chapter 48
First Time Measurement of the $^{19}F(p,\alpha_1)^{16}O$ Reaction at Astrophysical Energies: Evidence of Resonances Through the Application of the Trojan Horse Method

B. Becherini, M. La Cognata, Sara Palmerini, O. Trippella, S. Cherubini, G. L. Guardo, M. Gulino, S. Hayakawa, I. Indelicato, L. Lamia, Rosario Gianluca Pizzone, G. G. Rapisarda, C. Spitaleri and Aurora Tumino

Abstract The $^{19}F(p,\alpha)^{16}O$ reaction is an important channel of fluorine destruction in H-rich environments as the outer layers of Asymptotic Giant Branch (AGB) stars. Measurements of the $^{19}F(p,\alpha_0)^{16}O$ reaction via the Trojan Horse Method (THM) have shown the presence of resonant structures not observed before. As a consequence, the reaction rate at astrophysical temperatures (about 10^7–10^8 K) exceeds up to a factor 1.7 the one previously adopted. Here we present the result of an experiment in which THM was used to extract the Quasi-Free (QF) contribution of the $^2H(^{19}F,\alpha\ ^{16}O)n$ reaction to the $^{19}F(p,\alpha_1)^{16}O$ channel, corresponding to the population of the first excited state of the ^{16}O. Three resonances in the E_{cm} energy region below about 500 keV have been observed. This result hints to an enhancement of the $^{19}F(p,\alpha)^{16}O$ destruction rate, with respect to what presently predicted.

B. Becherini (✉) · S. Palmerini
Department of Physics and Geology, University of Perugia, Perugia, Italy
e-mail: bernardo.becherini@googlemail.com

B. Becherini · S. Palmerini · O. Trippella
Section of Perugia, INFN, Perugia, Italy

M. La Cognata · S. Cherubini · I. Indelicato · L. Lamia · R. Pizzone · G. G. Rapisarda · C. Spitaleri · A. Tumino
Laboratori Nazionali del Sud, INFN, Catania, Italy

S. Cherubini · M. Gulino · L. Lamia · G. G. Rapisarda
Department of Physics and Astronomy, University of Catania, Catania, Italy

G. L. Guardo
ELI-NP/IFIN-HH, Magurele, Romania

M. Gulino · A. Tumino
Engineering and Architecture Department, University of Kore, Enna, Italy

S. Hayakawa
Center for Nuclear Study, RIKEN, University of Tokyo, Wako Saitama, Japan

A. Formicola et al. (eds.), *Nuclei in the Cosmos XV*, Springer
Proceedings in Physics 219, https://doi.org/10.1007/978-3-030-13876-9_48

48.1 Introduction

The sole stable isotope of fluorine is ^{19}F, which can be easily destroyed in stellar interiors by several reactions. As a consequence, cosmic origins of fluorine are still uncertain. Three possible sites of fluorine nucleosynthesis have been proposed: AGB stars, Type II supernovae and Wolf-Rayet stars. The comparison between the observed fluorine abundance with those of other elements whose stellar origins are well known made by [1], foreseen the hypothesis that AGB stars were the main site of fluorine production in galaxies. However, theoretical models do not reproduce the observed aboundance of fluorine, tending to overstimate its production. To solve this problem, mechanisms of fluorine production and destruction in AGB stars have to be further investigated.

The major fluorine destruction channels are the ^{19}F(p,α)^{16}O and the ^{19}F(α,p)^{22}Ne reactions, which take place in astrophysical enviroments rich in H and He, respectively. In AGB stars affected by Cool Bottom Process (CBP) [2] or Hot Bottom Burning (HBB) [3], the F surface abundance might be reduced by those phenomena, because mixed materials undergo low temperature proton captures, and in this scenario some ^{19}F might be destroyed via the ^{19}F(p,α)^{16}O reaction. Unfortunately, no experimental data are reported by NACRE [4] for both the ^{19}F(p,α_0)^{16}O and the ^{19}F(p,α_1)^{16}O at energies below 500 keV. This lack of data forces researcher to an unsatisfactory extrapolation of the reaction rate to astrophysical energies. The first experimental study of the ^{19}F(p,α_0)^{16}O reaction at astrophysical energies was performed by [5], by using the THM to extract the quasi-free contribution to the ^{2}H(^{19}F,α ^{16}O)n and the ^{19}F(^{3}H,α ^{16}O)d reactions. The measurement shows the presence of resonant structures not observed before, which increased the reaction rate at astrophysical temperatures up to a factor of 1.7. The experiment was repeated, and updated data are reported in [6] and [7]. However, there is no data in the literature for the ^{19}F(p,α_1)^{16}O channel below 500 keV , whose contribution is not negligible at astrophysical energies (0–1 MeV) if resonances show up.

The aim of this work is to use the indirect method of THM to study the quasi-free contribution of the d(^{19}F,α_1 ^{16}O)n reaction to the ^{19}F(p,α_1)^{16}O at energies below 1 MeV.

48.2 Experiment, Data Analysis and Results

The ^{19}F(p,α_1)^{16}O reaction has been experimentaly studied via the THM experiment d(^{19}F,α ^{16}O)n, where deuteron has been chosen as TH-nucleus because of its $p-n$ structure and its radial wave function for the intercluster s-wave $p-n$ motion given by the Hulthen wave-function. Under QF conditions, the neutron emerging from the reaction represents the spectator while the proton partecipates in the two body reaction, eventually proceeding through ^{20}Ne excited levels [8]. The experiment was

performed at Laboratori Nazionali del Sud (LNS) Catania, were a ^{19}F beam of 55 MeV impinging into a CD_2 target was delivered.

The reaction of interest was identified by selecting the events in which an oxigen was detected in the telescope (PSD1 and PSD4, as shown in Fig. 48.1), in coincidence with a signal of one of the two detectors placed at higher angles, on the opposite side with respect to the beam axis. In particular, in this work we focused on the coincidence between two detectors (PSD1 and PSD5, as shown in Fig. 48.1). Following the procedure described by [5, 7], we were able to disantangle between the contributions of the different reaction channels, to isolate the α_1 channel contribution and finally to extract the three-body differential cross section in arbitrary units for this channel. The differential cross section in Fig. 48.2 shows at least three resonances below 0.5 MeV in the center of mass framework, suggesting an enhancement of the rate of the $^{19}F(p,\alpha)^{16}O$. The complete data anlysis of all the coincidences in between the telescopes, together with the normalization of the THM cross section data, will be presented in a forthcoming paper.

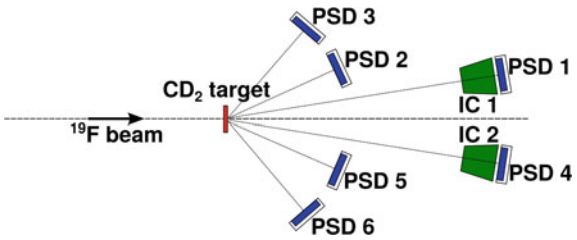

Fig. 48.1 Scheme of the experimental set-up

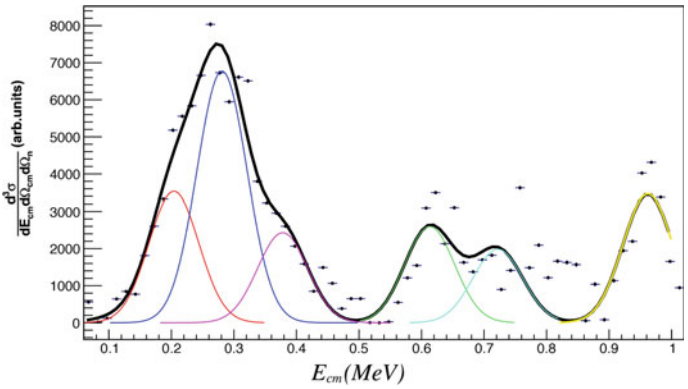

Fig. 48.2 Three-body differential cross section for the α_1 channel. Experimental data are fitted by a multi gaussian function (black curve), while colored lines show the contribution of different resonances. The energy values of the fitted resonances are the following: 0.204 MeV (red line), 0.251 MeV (blue line), 0.378 MeV (purple line), 0.663 MeV (green line), 0.742 MeV (light blue line), 1.022 MeV (yellow line)

References

1. H. Jönsson, N. Ryde, E. Spitoni et al., Astrophys. J. **835**, 50 (2017)
2. A.I. Boothroyd, I.-J. Sackmann, G.J. Wasserburg, Astrophys. J. Lett. **442**, L21 (1995)
3. J. Lattanzio, C. Frost, R. Cannon, P.R. Wood, Memorie della Società Astronomia Italiana **67**, 729 (1996)
4. C. Angulo, Am. Inst. Phys. Conf. Ser. **495**, 365 (1999)
5. M. La Cognata, A.M. Mukhamedzhanov, C. Spitaleri et al., Astrophys. J. Lett. **739**, L54 (2011)
6. M. La Cognata, S. Palmerini, C. Spitaleri et al., Astrophys. J. **805**, 128 (2015)
7. I. Indelicato, M. La Cognata, C. Spitaleri et al., Astrophys. J. **845**, 19 (2017)
8. K. Jain, N. Sarma, B. Banerjee, Nucl. Phys. A **142**, 2 (1970)

Chapter 49
Aluminium-26 from Massive Binary Stars

H. E. Brinkman, C. L. Doherty, E. T. Li, B. Côté and Maria Lugaro

Abstract Aluminium-26 is a radioactive isotope present in the early Solar System and in the current Galaxy. The most likely places for the production of this isotope are massive stars, single and binary. We simulated a single star of $20\,M_{\odot}$ with the MESA code, as well as binaries consisting of $20+18\,M_{\odot}$ stars. From these simulations, it becomes clear that binaries give higher ^{26}Al yields than single stars.

49.1 Introduction

Aluminium-26, a radioactive isotope with a half-life of 0.72 Myear, was present in the early Solar System, as inferred from ^{26}Mg excess in meteorites [1]. It is also detected in the Galaxy via γ-ray observations from COMPTEL and INTEGRAL [2]. While it is known that ^{26}Al is produced in stars, many uncertainties are left related to the production sites and the nuclear physics input. Past research has focused mostly on yields of ^{26}Al from massive single stars, both rotating and non-rotating, including their winds and supernova explosions [3–7]. However, most massive stars are found in binary systems, and this can strongly influence their yields [8]. Here we present the initial results from a project that focuses on the yields from the winds, both from single massive stars and from non-conservative mass transfer in binary massive star systems.

H. E. Brinkman (✉) · C. L. Doherty · B. Côté · M. Lugaro
Konkoly Observatory, Research Centre for Astronomy and Earth Sciences,
Hungarian Academy of Sciences, Konkoly Thege Miklos ut 15-17, Budapest 1121, Hungary
e-mail: hannah.brinkman@csfk.mta.hu; brinkmanhe@gmail.com

C. L. Doherty · M. Lugaro
School of Physics and Astronomy, Monash Centre for Astrophysics,
Monash University, Melbourne, Australia

E. T. Li
College of Physics and Energy, Shenzhen University, Shenzhen, China

B. Côté
Joint Institute for Nuclear Astrophysics—Center for the Evolution of the Elements,
East Lansing, USA

A. Formicola et al. (eds.), *Nuclei in the Cosmos XV*, Springer
Proceedings in Physics 219, https://doi.org/10.1007/978-3-030-13876-9_49

49.2 Simulations

First, we calculated a single star with an initial mass of $20\,M_\odot$ and a metallicity of Z = 0.014 using the MESA code [9]. Secondly, we calculated binary models with a primary of $20\,M_\odot$ and a secondary of $18\,M_\odot$ with different orbital periods. Further, we explored the parameter space by using semi-numerical binaries. The parameters of interest here are: the primary mass, M_1, the mass-ratio, $q = \frac{M_1}{M_2}$ and the orbital period, P. In this initial result, we did not vary the masses, this will be done in a subsequent work. With Kepler's third law (49.1) and Eggleton's approximation of the Roche lobe [10] (49.2), we calculated semi-numerical binaries, based on the numerical single star.

$$\frac{a^3}{P^2} = \frac{G(M_1 + M_2)}{4\pi^2} \tag{49.1}$$

$$\frac{R_{L1}}{a} = \frac{0.49q^{\frac{2}{3}}}{0.6q^{\frac{2}{3}} + \ln(1 + q^{\frac{1}{3}})} \tag{49.2}$$

For periods ranging from a few days to ~100 days, we calculated the size of the Roche lobe for a fixed mass-ratio of q = 20/18. At the points where the radius equals the size of the Roche lobe, we assume that the full envelope of the star is stripped away and we calculated the ^{26}Al yield by summing the amount ^{26}Al in all the cells stripped away. We chose the limits for the period in such a way that the mass-transfer will be either during hydrogen burning, case A, or after hydrogen burning, but before the envelope becomes convective during helium burning, case B. We use these limits because otherwise the ^{26}Al is already destroyed by helium burning or decayed.

49.3 Results

In Fig. 49.1 we compared the results of different studies of non-rotating single stars (the horizontal lines) to each other as well as to our results. Our single star model produced a yield of ^{26}Al of $1.5\times10^{-7}\,M_\odot$ (the solid horizontal blue line). Our binary models produced yields between 1.9×10^{-6} and $2.0 \times 10^{-7}\,M_\odot$ (blue stars). The semi-analytic binaries (blue dots) produce yields between 1.0×10^{-5} and $3.8 \times 10^{-6}\,M_\odot$.

The general trend is that the numerical binaries give a higher yield than the single stars. This is because the mass-loss is generally larger for the binaries than for the single stars. The yields from the semi-numerical binaries represent an upper limit because we have assumed that the whole envelope of the star is lost during the mass-transfer phase. In the numerical simulations this does not happen because the star reconfigures and detaches from the Roche lobe, stopping the mass-transfer, before the innermost layers are stripped.

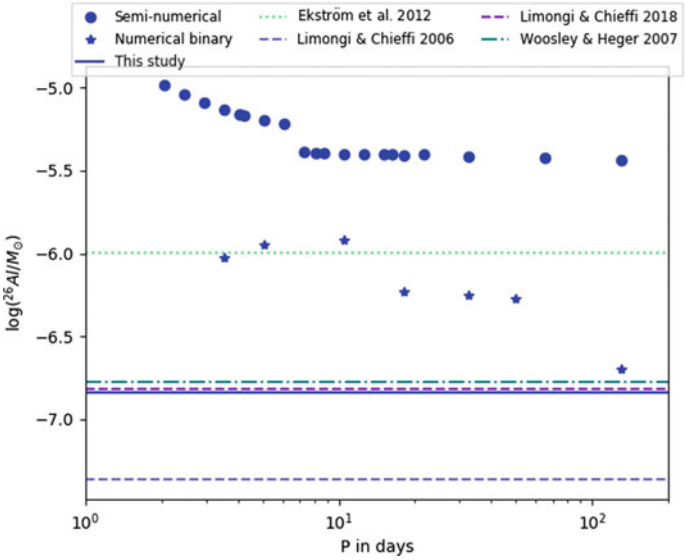

Fig. 49.1 Aluminium-26 yields in $M_\odot$ for $20\,M_\odot$ single stars (horizontal lines) and $20+18\,M_\odot$ binaries (stars (analytical) and dots (semi-analytical)) for various periods given in days

49.4 Outlook

Here we have focused on a system consisting of a $20\,M_\odot$ and a $18\,M_\odot$ star and varied the orbital periods between a few days to ∼100 days. The research will be expanded to a wider mass-range of primary stars, between 15 and $120\,M_\odot$, again with periods varying between a few days to ∼100 days. Also the mass-ratio, $q = \frac{M_2}{M_1}$, will be varied to analyse its influence on the yields.

Acknowledgements We are grateful to Moritz Pleintinger for sharing his table of the ^{26}Al yields from various studies and to George Meynet, Roland Diehl, and Moritz Pleintinger for discussion and suggestions. This work is supported by the ERC via CoG-2016 RADIOSTAR [11] (Grant Agreement 724560). H. E. Brinkman gratefully acknowledges the NIC organisers for the student support grant.

References

1. B. Jacobsen et al., Earth Planet. Sci. Lett. **272**, 353 (2008)
2. R. Diehl, Rep. Prog. Phys. **76**, 026301 (2013)
3. M. Limongi, A. Chieffi, ApJ **647**, 483 (2006)
4. A. Chieffi, M. Limongi, ApJ **764**, 21 (2013)
5. M. Limongi, A. Chieffi (2018). arXiv:1805.09640
6. S. Ekström et al., A&A **537**, 146 (2012)
7. S.E. Woosley, A. Heger, Phys. Rep. **442**, 269 (2007)

8. H. Braun, N. Langer, IAU Proc. **163**, 305 (1995)
9. B. Paxton et al., ApJS **234**, 34P (2018)
10. P. Eggleton, ApJ **268**, 368 (1983)
11. http://konkoly.hu/radiostar/

Chapter 50
Study of the E_α = 395 keV Resonance of the ^{22}Ne(α, γ)^{26}Mg Reaction at LUNA

Antonio Caciolli and D. Bemmerer

Abstract The ^{22}Ne(α,γ)^{26}Mg is the competitor of the ^{22}Ne(α,n)^{25}Mg in AGB stars, which, in turn, is an efficient source of neutrons for s-processes in medium masses AGB stars. There is a significant uncertainty in the ^{22}Ne(α,γ)^{26}Mg thermonuclear reaction rate. This has been clearly remarked the ChETEC COST Action (CA16117) considering the ^{22}Ne(α,γ)^{26}Mg among the nuclear reactions with major impact on stellar nucleosynthesis. A narrow resonance at an energy E_α = 395 keV has been claimed in the ^{22}Ne(α,γ)^{26}Mg reaction and it has been studied only with indirect methods leading to a range of possible values for its strength from 10^{-9} to 10^{-15} eV. At LUNA (Laboratory for Underground Nuclear Astrophysics) this resonance can be studied directly, thanks to a high efficiency setup, composed by a 4π-BGO detector and a windowless gas target filled with neon gas enriched in the ^{22}Ne isotope to 99.99%. This setup has been already used in a previous experiment for the study of the ^{22}Ne(p,γ)^{23}Na reaction, and in April-June 2018 a new measurement campaign will be performed. Thanks to its position inside the Laboratory of Gran Sasso, LUNA already benefits from a reduced background and in particular a factor one thousand for the neutron component. Still this remains the most important source of background in the region of interest for the ^{22}Ne(α,γ)^{26}Mg. Therefore a new borated polyethylene shielding will be employed to reduce the neutron contamination due to the environmental background by an additional order of magnitude.

A. Caciolli (✉)
Physics and Astronomy Department, University of Padua, Padua, Italy
e-mail: caciolli@pd.infn.it

INFN Section of Padua, Padua, Italy

D. Bemmerer
Helmholtz-Zentrum Dresden-Rossendorf (HZDR), Dresden, Germany

A. Formicola et al. (eds.), *Nuclei in the Cosmos XV*, Springer
Proceedings in Physics 219, https://doi.org/10.1007/978-3-030-13876-9_50

50.1 Introduction

The ^{22}Ne(α,γ)^{26}Mg competes with the ^{22}Ne(α,n)^{25}Mg reaction in AGB stars. Recently, it has been found to have a role in the uncertainty budget to calculate the abundances of ^{26}Mg and ^{31}P in intermediate-mass AGB stars. Since the ^{22}Ne(α,n)^{25}Mg has a threshold at α-beam energy of 565 keV [1], a possible resonance in the ^{22}Ne(α,γ)^{26}Mg below this threshold could affect the temperature at which the ratio of the two rates is higher than one. A direct measurement of a possible resonance at energies below the threshold is of high importance for the neutron density calculation in ABG stellar models.

The ^{22}Ne(α,γ)^{26}Mg reaction has been already studied in several of the experiments also addressing its competitor, but most of these studies rely on indirect methods (see [2] and references therein).

One of the most interesting resonances, which shows only upper limits on its resonance strength [2], is the one at $E_\alpha = 395$ keV, corresponding to the $E_X = 10{,}949$ keV excited level of the ^{26}Mg. For this resonance, a great discrepancy between different upper limits is present in literature (see [2] and reference therein). In particular, the range of possibile upper limits varies from 3.6×10^{-9} eV [3] to 8.7×10^{-15} eV [2].

Using the LUNA-400kV accelerator [4], this reaction can be studied directly. The setup planned for this study is already described in [5]. This setup is characterised by an high efficiency 4π-BGO detector surrounding the scattering chamber, which is filled with neon gas enriched in ^{22}Ne up to 99.99%. This setup was tested against results of a previous study of the ^{22}Ne(p,γ)^{23}Na reaction [6–9]. Thanks to the deep underground position [10–13] the LUNA collaboration is planning to be sensitive to a value of the resonance strength at least two orders of magnitude lower than the value in literature [3]. In order to reach this goal, an additional shielding made of 10 cm borated (5% boron included) polyethylene has been designed and mounted around the detector. This is expected to reduce the neutron flux in the region of interest (10.5–11.5 MeV) by an order of magnitude with respect to the flux already present inside the LNGS halls.

The ^{22}Ne(α,n)^{25}Mg reaction is already in the program of the future LUNA-MV [14]. Among the ChETEC network, there is an open discussion about the necessity to review other resonances of this reaction and of the ^{22}Ne(α,γ)^{26}Mg, especially at energies above the threshold of the neutron channel. Their study will be one of the goals of the new LUNA-MV accelerator that will start its activity at LNGS in 2019.

Acknowledgements Financial support by INFN, DFG (BE 4100-4/1), NAVI (HGF VH-VI-417), OTKA (K101328).

References

1. M. Jaeger, R. Kunz, A. Mayer, J.W. Hammer, G. Staudt, K.L. Kratz, B. Pfeiffer, Phys. Rev. Lett. **87**, 202501 (2001)
2. R. Longland, C. Iliadis, A.I. Karakas, Phys. Rev. C **85**, 065809 (2012)
3. C. Iliadis, R. Longland, A.E. Champagne, A. Coc, Nucl. Phys. A **841**, 251 (2010)
4. A. Best, A. Caciolli, Zs. Fülüp, Gy. Györky, M. Laubenstein, E. Napolitani, V. Rigato, V. Roca, T. Szücs, Eur. Phys. J. A **52**, 72 (2016)
5. F. Ferraro, M.P. Takács, D. Piatti, V. Mossa, M. Aliotta, D. Bemmerer, A. Best, A. Boeltzig, C. Broggini, C.G. Bruno et al., Eur. Phys. J. A **54**, 44 (2018)
6. F. Cavanna, R. Depalo, M. Aliotta, M. Anders, D. Bemmerer, A. Best, A. Boeltzig, C. Broggini, C.G. Bruno, A. Caciolli et al., Phys. Rev. Lett. **115**, 252501 (2015)
7. R. Depalo, F. Cavanna, M. Aliotta, M. Anders, D. Bemmerer, A. Best, A. Boeltzig, C. Broggini, C.G. Bruno, A. Caciolli et al., LUNA Collaboration. Phys. Rev. C **94**, 055804 (2016)
8. D. Bemmerer et al., Europhys. Lett. **122**, 52001 (2018)
9. A. Slemer, P. Marigo, D. Piatti, M. Aliotta, D. Bemmerer, A. Best, A. Boeltzig, A. Bressan, C. Broggini, C.G. Bruno et al., Mon. Not. R. Astron. Soc. **465**, 4817 (2017)
10. D. Bemmerer, F. Confortola, A. Lemut, R. Bonetti, C. Broggini, P. Corvisiero, H. Costantini, J. Cruz, A. Formicola, Z. Fülöp et al., Eur. Phys. J. A **24**, 313 (2005)
11. A. Caciolli, L. Agostino, D. Bemmerer, R. Bonetti, C. Broggini, F. Confortola, P. Corvisiero, H. Costantini, Z. Elekes, A. Formicola et al., Eur. Phys. J. A **39**, 179 (2009)
12. T. Szücs, D. Bemmerer, C. Broggini, A. Caciolli, F. Confortola, P. Corvisiero, Z. Elekes, A. Formicola, Z. Fülöp, G. Gervino et al., Eur. Phys. J. A **44**, 513 (2010)
13. C.G. Bruno, D.A. Scott, A. Formicola, M. Aliotta, T. Davinson, M. Anders, A. Best, D. Bemmerer, C. Broggini, A. Caciolli et al., Eur. Phys. J. A **51**, 94 (2015)
14. C. Broggini, D. Bemmerer, A. Caciolli, D. Trezzi, Prog. Part. Nucl. Phys. **98**, 55 (2018)

Chapter 51
The s-Process Nucleosynthesis in Low Mass Stars: Impact of the Uncertainties in the Nuclear Physics Determined by Monte Carlo Variations

Gabriele Cescutti, Raphael Hirschi, Nobuya Nishimura, Thomas Rauscher, Jacqueline den Hartogh, Alex St. J. Murphy and Sergio Cristallo

Abstract We investigated the impact of uncertainties in neutron-capture and weak reactions (on heavy elements) on the s-process nucleosynthesis in low-mass stars using a Monte-Carlo based approach. We performed extensive nuclear reaction network calculations that include newly evaluated temperature-dependent upper and lower limits for the individual reaction rates. Our sophisticated approach is able to evaluate the reactions that impact more significantly the final abundances. We found that β-decay rate uncertainties affect typically nuclides near s-process branchings, whereas most of the uncertainty in the final abundances is caused by uncertainties

G. Cescutti (✉)
INAF, Osservatorio Astronomico di Trieste, Trieste, Italy
e-mail: gabriele.cescutti@inaf.it

R. Hirschi · J. den Hartogh
Astrophysics group, Faculty of Natural Sciences, Keele University, Keele, UK

R. Hirschi
Kavli IPMU (WPI), University of Tokyo, Tokyo, Japan

N. Nishimura
Yukawa Institute for Theoretical Physics, Kyoto University, Kyoto, Japan

T. Rauscher
Department of Physics, University of Basel, Basel, Switzerland

Centre for Astrophysics Research, University of Hertfordshire, Hertfordshire, UK

J. den Hartogh
Konkoly Observatory, Budapest, Hungary

A. St. J. Murphy
SUPA, School of Physics and Astronomy, University of Edinburgh, Edinburgh, UK

S. Cristallo
Osservatorio Astronomico d'Abruzzo, Teramo, Italy

INFN—Sezione di Perugia, Perugia, Italy

A. Formicola et al. (eds.), *Nuclei in the Cosmos XV*, Springer
Proceedings in Physics 219, https://doi.org/10.1007/978-3-030-13876-9_51

in neutron capture rates, either directly producing or destroying the nuclide of interest. Combined total nuclear uncertainties due to reactions on heavy elements are approximately 50%.

51.1 Introduction

The s-process nucleosynthesis is a source of heavy elements beyond iron in the universe, taking place in stellar burning environments. There are two astronomical conditions and corresponding classes of the s-process. The s-process occurs (i) during the AGB phase of low mass stars producing heavy nuclei up to Pb and Bi, called the main s-process; (ii) in He-core and C-shell burning phases of massive stars representing the lighter components (up to $A \approx 90$), categorised as the weak s-process. Here, we investigate the main s-process production in low-mass AGB stars. There are several well known uncertainties concerning this production. In this work, we explore the nuclear reaction side, in particular the uncertainties in neutron captures and beta decays on intermediate and heavy isotopes. Our approach is to vary simultaneously all reaction rates in a Monte Carlo (MC) framework rather than one reaction at a time. We followed the same procedure as presented in detail in [1]. Furthermore, we use temperature-dependent uncertainties based both on experimental and theoretical studies as we have already done for several other processes: the s-process in massive star, γ-process in core collapse SNe and γ-process in supernovae type Ia [1–3]. On the astrophysical side, the evolution of low-mass stars is complex, especially during the TP-AGB phase [4]. It is thus not feasible to repeat such simulations 10,000 times as required by the MC procedure to complete a sensitivity study. We thus have to approximate the thermodynamic conditions inside the star with a trajectory following the key phase that we are studying (for details see [5]).

51.2 Results

As can be seen in Fig. 51.1, the overall uncertainties at the end of the trajectory approximating a ^{13}C pocket in a 3 $M_\odot$ star of solar metallicity are generally small. Indeed, most of them are smaller than 50%. This is not too surprising since the relevant temperature range ($\sim$8 keV) is accessible to experimental measurements so many of the relevant rates. There are nevertheless several nuclides, for which uncertainties are larger than a factor of two. These are generally nuclides around branching points such as ^{86}Kr. We also notice a propagation effect for nuclides more massive than ^{138}Ba. This is due to the combined effect of uncertainties in neutron capture rates above ^{138}Ba. In most cases, rates dominating the nuclear uncertainties are the neutron captures either directly producing or destroying the nuclide in question (for the full list see [5]). There are, however, three neutron-capture rates that play a significant role in the uncertainty for many nuclides during the ^{13}C-pocket conditions. These

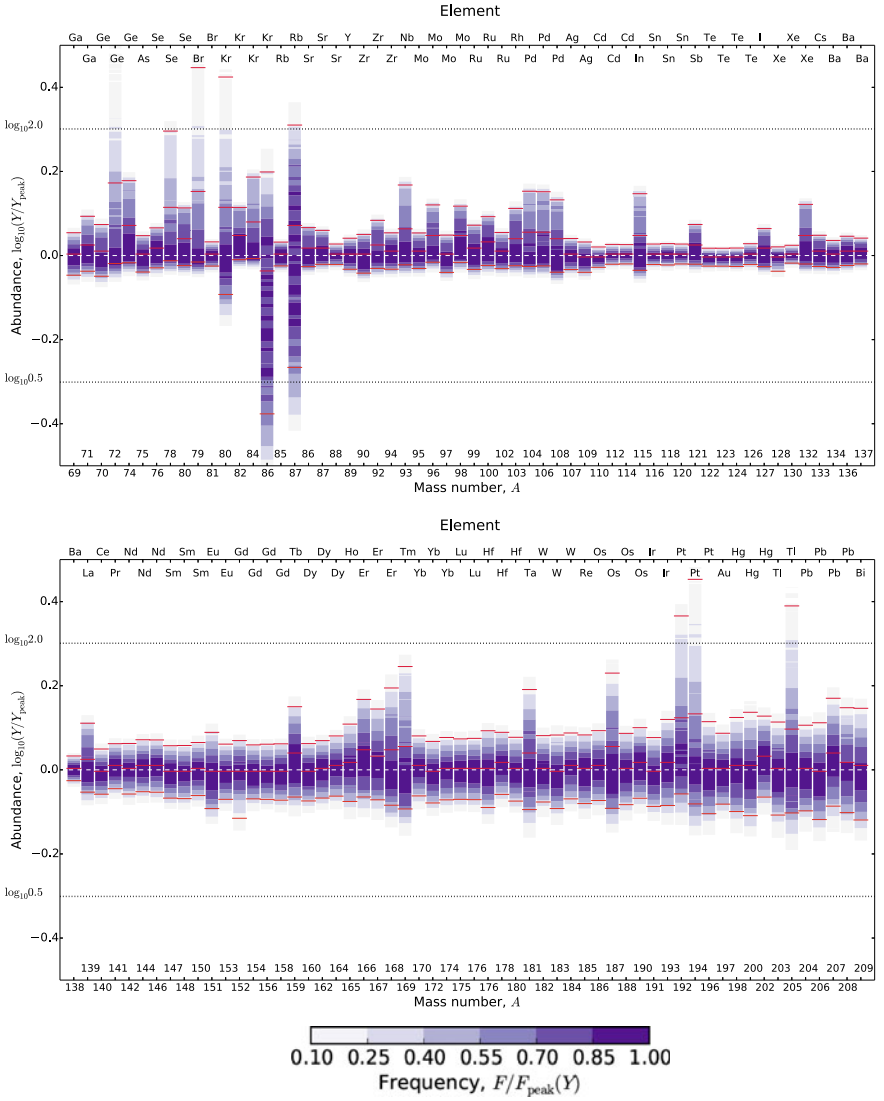

Fig. 51.1 Total production uncertainties in the s-process abundances at the end of a thermodynamic trajectory approximating a ^{13}C pocket in a 3M$_\odot$ stars of solar metallicity. The color shading denotes the probabilistic frequency and the 90% probability intervals up and down are marked for each nuclide with the red lines. The final abundances are normalised by the final abundance at the peak of the distribution. Horizontal dotted lines indicate a factor of two uncertainties

are the neutron capture rates on ^{56}Fe, ^{64}Ni, and ^{138}Ba. For a detailed analysis of the how the importance of these key rates are determined by examining the correlation between a change in a reaction rate and the change of an abundance, we refer the reader to [5].

Acknowledgements GC acknowledges financial support from the European Union Horizon 2020 research and innovation programme under the Marie Skodowska-Curie grant agreement no. 664931. This work has been partially supported by the European Research Council (EU-FP7-ERC-2012-St Grant 306901), the EU COST Action CA16117 (ChETEC), the UK STFC (ST/M000958/1), and MEXT Japan (Priority Issue on Post-K computer: Elucidation of the Fundamental Laws and Evolution of the Universe).

References

1. T. Rauscher, N. Nishimura, R. Hirschi, G. Cescutti, A.St.J. Murphy, A. Heger, Uncertainties in the production of p nuclei in massive stars obtained from Monte Carlo variations. MNRAS **463**, 4153 (2016). https://doi.org/10.1093/mnras/stw2266
2. N. Nishimura, R. Hirschi, T. Rauscher, A.St.J. Murphy, G. Cescutti, Uncertainties in s-process nucleosynthesis in massive stars determined by Monte Carlo variations. MNRAS **469**, 1752 (2017). https://doi.org/10.1093/mnras/stx696
3. N. Nishimura, T. Rauscher, R. Hirschi, A.St.J. Murphy, G. Cescutti, C. Travaglio, Uncertainties in the production of p nuclides in thermonuclear supernovae determined by Monte Carlo variations. MNRAS **474**, 3133 (2018). https://doi.org/10.1093/mnras/stx3033
4. S. Cristallo, O. Straniero, L. Piersanti, D. Gobrecht, Evolution, nucleosynthesis, and yields of AGB stars at different metallicities. III. Intermediate-mass models, revised low-mass models, and the ph-FRUITY interface. ApJS **219**, 40 (2015). https://doi.org/10.1088/0067-0049/219/2/40
5. G. Cescutti, R. Hirschi, N. Nishimura, J.W. den Hartogh, T. Rauscher, A.St.J. Murphy, S. Cristallo, Uncertainties in s-process nucleosynthesis in low-mass stars determined from Monte Carlo variations. MNRAS **478**, 4101 (2018). https://doi.org/10.1093/mnras/sty1185

Chapter 52
Stellar Nucleosynthesis: Experimental Yields of the ^{112}Sn(γ,n)^{111}Sn and ^{112}Sn(γ,p)^{111m,g}In Reactions for p-Nuclei Production Simulation

A. V. Chekhovska, I. L. Semisalov, V. I. Kasilov and Ye. O. Skakun

Abstract The bremsstrahlung yields of the photonuclear reactions ^{112}Sn(γ,n)^{111}Sn and ^{112}Sn(γ,p)^{111m,g}In on the tin-112 p-nuclide have been measured at the near and above threshold energy range. These measured yields are compared with the NON-SMOKER and TALYS code predictions.

52.1 Introduction

Whereas the overwhelming majority of naturally occurring isotopes of chemical elements of the middle and heavy masses was synthesized in stars via the reactions of slow (s) and rapid (r) capture of neutrons, a separate group of 35 weak abundant proton-rich nuclei could not be produced in these scenarios because of the ratio of their masses and the masses of the neighboring isobars ([1] and therein). To understand the stellar mechanisms of the production of these so-called p-nuclei, the low energy proton and photon induced reaction rates are required on a huge network of stable and radioactive nuclei. Theoretical calculations using the statistical model of Hauser-Feshbach [2] which in turn should be tested by comparison with the known experimental data take on special importance.

In the present study the integral yields of photonuclear reactions ^{112}Sn(γ,n)^{111}Sn and ^{112}Sn(γ,p)^{111m,g}In were measured in the near and above threshold energy range of interest for stellar nucleosynthesis. The activation technique with the high resolution γ-spectrometry based on the HPGe-detector was applied for the measurements of the (γ,n)- and (γ,p)-reaction yields on the ^{112}Sn p-nucleus.

A. V. Chekhovska (✉)
V. N. Karazin Kharkiv National University, Kharkiv 61022, Ukraine
e-mail: anastasiy101294@gmail.com

I. L. Semisalov · V. I. Kasilov · Y. O. Skakun
NSC "Kharkiv Institute of Physics and Technology", Kharkiv 61108, Ukraine

A. Formicola et al. (eds.), *Nuclei in the Cosmos XV*, Springer
Proceedings in Physics 219, https://doi.org/10.1007/978-3-030-13876-9_52

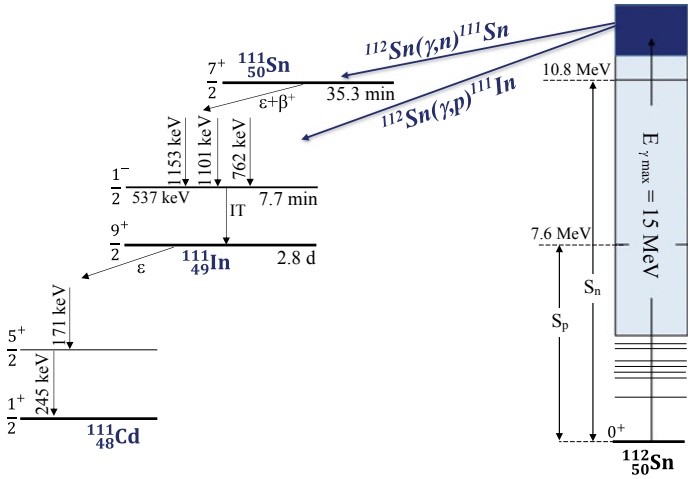

Fig. 52.1 Diagram of the photonucleon reactions on the ^{112}Sn target and decay of the residuals

Figure 52.1 shows the energy diagram of photonucleon reactions on the ^{112}Sn target nucleus and decays of the residuals. The (γ,n) reaction produces ^{111}Sn ($T_{1/2}$ = 35.3 min) nucleus, the ($\varepsilon + \beta^+$)-decay of which is followed by the emission of a large number of γ-ray groups corresponding to the transitions between levels of the ^{111}In daughter nucleus [3] populating the ^{111m,g}In long-lived isomer pair ($T^m_{1/2}$ = 7.7 min, E_γ = 538 keV; $T^g_{1/2}$ = 2.8 d, E_γ = 171, 245 keV) which in addition can be formed directly in the ^{112}Sn(γ,p)^{111m,g}In reaction.

52.2 Experiment

The intense bremsstrahlung flux was produced by the 100 μm tantalum converter at the Kharkiv electron LINAC. The tin sample weighing 77 mg enriched by ^{112}Sn isotope to 80% was positioned on the initial electron beam axis after the deflecting magnet. It was sandwiched with a gold foil of the known thickness using for the ^{197}Au(γ, n)^{196}Au reaction as the standard one [4]. The ionization chamber was monitoring the photon flux recording the X-ray dose during irradiation.

The experimental activation yield $Y_{act}(E_0)$ of the (γ,n)-reaction normalized to one target nucleus and unit bremsstrahlung flux was determined from the measured intensities N_γ of one or several strong γ-transitions followed by the ^{111}Sn decay (762, 1101, 1153 keV) via the conventional activation equation:

$$\frac{N\lambda_\gamma}{N_{targ}\varepsilon B_\gamma} = Y_{act}(E_0) \times \left(1 - e^{-\lambda t_{irr}}\right) \times e^{-\lambda t_{cool}} \times \left(1 - e^{-\lambda t_{meas}}\right) \qquad (52.1)$$

where N_{targ} is the number of the target nuclei, λ the radioactive decay constant of a residual, ε the detector efficiency, B_γ branching coefficient, t_{irr}, t_{cool}, and t_{meas} the times of irradiation, cooling and measurement of the sample activity, respectively.

The intensities of the 171 and 245 keV γ-lines in the spectra of decay gamma rays, measured over a cooling period of 40 min and more (when the ^{111m}In as the residual of the ^{112}Sn (γ,p)-reaction had decayed practically completely), obey the activation equation for a genetically related pair of radioactive nuclei:

$$\begin{aligned}\frac{N_\gamma}{N_{targ}\varepsilon B_\gamma} = Y_{act}^{(\gamma,n)}\frac{\lambda_p\lambda_d}{\lambda_d-\lambda_p}\Big[\frac{1-e^{-\lambda_p t_{irr}}}{\lambda_p^2}e^{-\lambda_p t_{cool}}\left(1-e^{-\lambda_p t_{meas}}\right)\\ -\frac{1-e^{-\lambda_d t_{irr}}}{\lambda_d^2}e^{-\lambda_d t_2}\left(1-e^{-\lambda_d t_{meas}}\right)\Big]\\ +Y_{act}^{(\gamma,p)}\frac{1-e^{-\lambda_d t_{irr}}}{\lambda_d}e^{-\lambda_d t_2}\left(1-e^{-\lambda_d t_{meas}}\right)\end{aligned} \tag{52.2}$$

in which the additional notations $Y_{act}^{(\gamma,n)}$ and $Y_{act}^{(\gamma,p)}$ are total activation yields of the ^{112}Sn(γ,n)^{111}Sn and ^{112}Sn(γ,p)$^{111m+g}$In reactions with λ_p and λ_d as the decay constants of the **p**arent and **d**aughter of the radioactive chain ^{111}Sn$\rightarrow$ ^{111g}In respectively.

52.3 Experimental Results and Theoretical Predictions

Our experimental values of the integral yields (in mbarn×MeV) for the ^{112}Sn(γ,n)^{111}Sn, ^{112}Sn(γ,p)^{111m,g}In and reactions presented as the dark circle points in Fig. 52.2 are compared with the statistical theory predictions using the computer codes NON-SMOKER [5] and TALYS 1.6 [6]. The dark points of all three panels were obtained with the genetic activation equation (52.2). The light triangle points of the ^{112}Sn(γ,n)^{111}Sn reaction (upper panel) correspond to the treatment with the conventional activation equation (52.1) and the adopted for today branching coefficient values of the ^{111}Sn nuclide decay [3]. The difference between these two value sets are explained by non-correct branching coefficient values of the ^{111}Sn nuclide decay. The experimental data for the (γ,n)-reaction (the dark points) are agreed to the NON-SMOKER prediction and the option "ld1-st2" (constant temperature model for level density-Brink-Axel model for strength function). The Varlamov values [7] (the light circle points) exceed our data by 20% and are agreed with other combination of models.

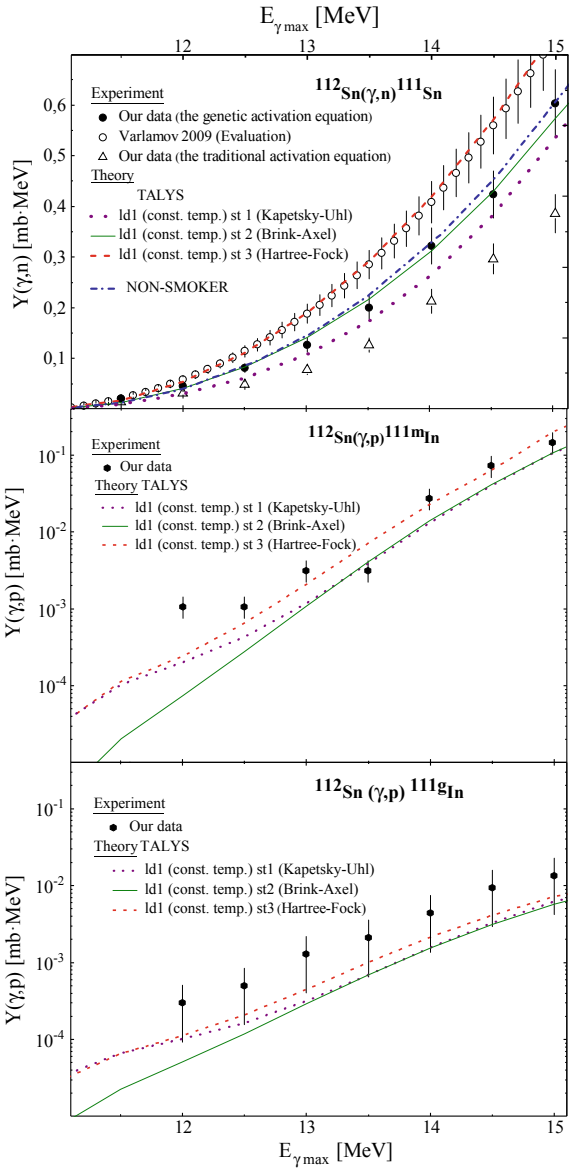

Fig. 52.2 Experimental and theoretical yields of the studied reactions

Acknowledgements This research was supported in part by the National Science Foundation under Grant No. PHY-1430152 (JINA Center for the Evolution of the Elements).

References

1. T.Rauscher, T. et al: Constraining the astrophysical origin of the p-nuclei through nuclear physics and meteoritic data. Rep. Prog. Phys. **76**(6), 066201 (2013)
2. W. Hauser, H. Feshbach, The inelastic scattering of neutrons. Phys. Rev. **87**(2), 366–373 (1952)
3. https://www.nndc.bnl.gov/nudat2/
4. O. Itoh et al., Photoneutron cross sections for Au revisited: measurements with laser Compton scattering γ-rays and data reduction by a least-squares method. Jour. of Nuclear Science and Technology **48**(2), 834–840 (2011)
5. https://nucastro.org/
6. http://www.talys.eu/
7. V.V. Varlamov et al., Analysis and evaluation of cross sctions of partial photoneutron reactions for Sn isotopes. Bull. Russian Academy of Sciences: Physics **74**(6), 833–841 (2010)

Chapter 53
The Development of 400 kV High Intensity Accelerator Facility for Jinping Underground Nuclear Astrophysics Experiments

L. H. Chen, B. Q. Cui, R. G. Ma, Y. J. Ma, Q. H. Huang, B. Tang, X. Ma, G. Lian, B. Guo, WeiPing Liu, Q. Wu and L. T. Sun

Abstract Direct measurement of the cross sections for key nuclear reactions is crucial in verifying extrapolation model, constraining theoretical calculations, and solving key scientific questions in nuclear astrophysics. However, these cross-sections are extremely small. Tiny reaction rates in laboratories at the earth's surface, the measurements are hampered by the cosmic-ray background. Experiments using high intensity beam and Measurements in ultra-low background underground labs become a promising solution of experimental nuclear astrophysics. China JinPing Underground Laboratory (CJPL) is currently deepest underground site in the word. For such experiments, a 400 kV, 10 mA accelerator specially designed for Jinping Underground Nuclear Astrophysics (JUNA) will be placed in CJPL. In this paper the recent development of the 400 kV accelerator are presented.

53.1 Introduction

The China Jinping Underground Laboratory (CJPL) is constructed at the southwest of China [1]. It's covered by over 2400 m rock depth. Jinping Underground experiments of Nuclear Astrophysics (JUNA) will take the advantage of the ultra-low background of CJPL to study a number of crucial reactions occurring at their relevant stellar energies during the evolution of hydrostatic stars [2]. For such experiments, a high intensity accelerator (400 kV with 10 emA for proton or helium beam) 400 kV high intensity accelerator has been established.

L. H. Chen (✉) · B. Q. Cui · R. G. Ma · Y. J. Ma · Q. H. Huang · B. Tang · X. Ma · G. Lian · B. Guo · W. Liu
China Institute of Atomic Energy, Beijing 102413, China
e-mail: skyrunnerchen@hotmail.com

Q. Wu · L. T. Sun
Institute of Modern Physics, Chinese Academy of Sciences, Lanzhou 730000, China

A. Formicola et al. (eds.), *Nuclei in the Cosmos XV*, Springer
Proceedings in Physics 219, https://doi.org/10.1007/978-3-030-13876-9_53

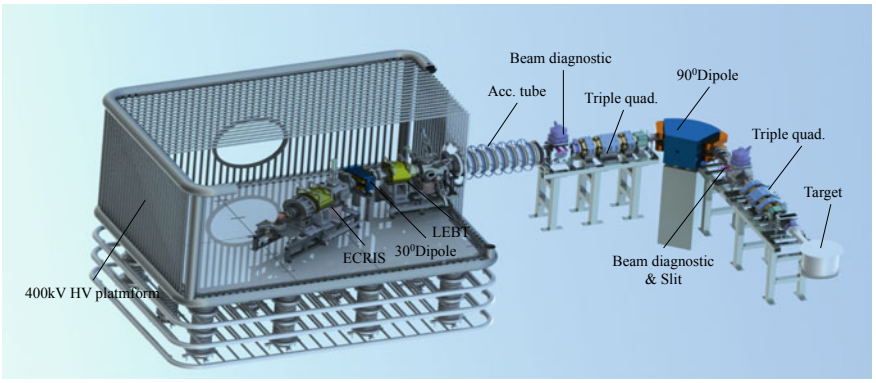

Fig. 53.1 Set-up of the 400 kV accelerator for JUNA

53.2 Overview of the 400 kV Accelerator for JUNA

The 400 kV high accelerator for JUNA experiments adopts two step acceleration and separation mode (see Fig. 53.1). The beams are extracted at 20–50 keV from a high intensity ECR ion source [3] and post-accelerated up to 400 keV by the accelerating tube. Two solenoids are set in LEBT for matching the beam into the accelerator tube. Two triple quad-poles are set after the tube for match the beam transport and satisfy the requirement of the experiments. By this method the optimum beam transport could be gotten without affected by ion source. The inhibition of beam impurities is achieved by two dipoles. One is on the 400 kV high voltage platform; the other is on the ground potential. The preliminary 30° dipole arranged in low energy beam transport line has an ability to resolute different charge-mass ratio beams (clear up the fraction of H_2^+, H_3^+ in beam etc.), and 90° dipole has a high mass resolution to resolute same charge-mass ratio (e.g., tiny D^+ in He^{2+} beam, D_2^+ in He^+ beam.) or neutral particles that would affect underground physics experiments.

53.3 The Accelerating Tube

Space charge effect is important to high intensity beam transport. Accelerating tube is used to accelerate beam from 50 to 400 keV. In accelerating tube, due to the existence of accelerating electric field, the space charge neutralization is completely destroyed. Beam quality would become worse quickly because of chare repulsion. So the accelerating tube need specially designed. An accelerating tube for few tens microampere high intensity beam has been developed in China Institute of Atomic Energy.

Uniform field acceleration structure is used in the machine. The electrode is specially designed to accommodate high intensity beam. The beam energy can be

obtained through four accelerating gaps. Each accelerating gap has a maximum load of 100 kV. Various measures of homogenization electric field are used to reduce the occurrence of sparks. The total length of the accelerating tube is 1300 mm, but the length of accelerating electric field is only 250 mm maximum that minimizes the impact of space charge effect.

53.4 The Tuning of Accelerator on the Ground

The main parts of accelerator have been installed and tuning on the ground (see Fig. 53.2). Limited by laboratory space, the triple quad-poles behind the 90° dipole are not installed. The performance of accelerating tube has been test. Over 12 mA proton beam and 5 mA helium beam have been steadily accelerated up to required energy. The beam has also been transported to Beam-stop or experimental targets. When the beam energy is below 350 keV, the operation is stable and almost no spark. As increasing the accelerating potential, the spark becomes more likely to occur (per

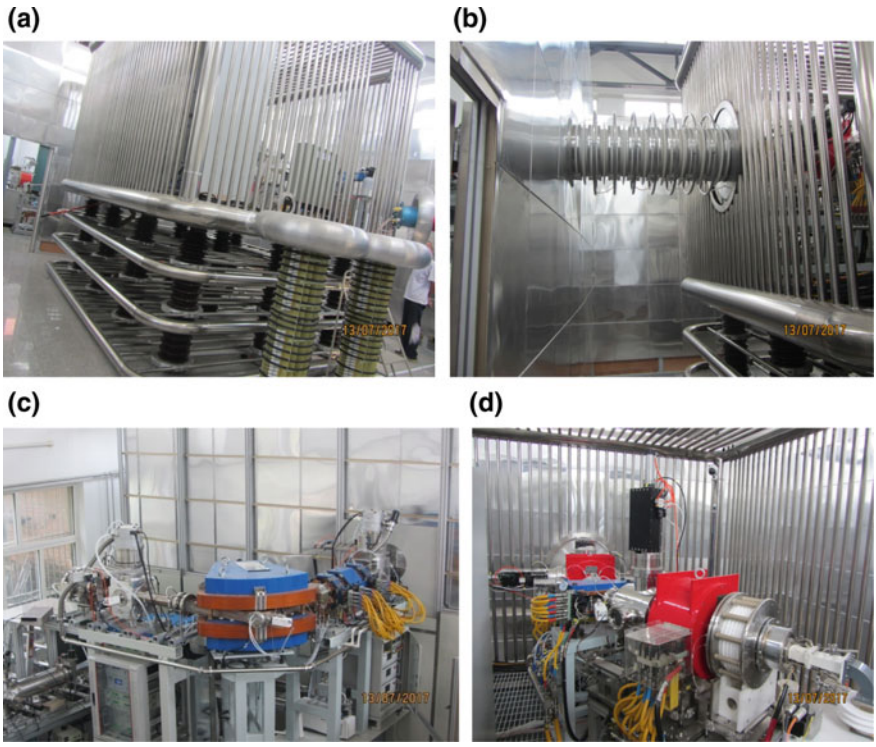

Fig. 53.2 Some photos of 400 kV accelerator for JUNA. **a** The high voltage platform; **b** the accelerating tube; **c** and **d** the ECR ion source and beam lines

few hours once). Some improvements are underway to enhance the stability of the accelerator in long-term operation.

53.5 Conclusion and Future Plan

Due to the high intensity beams have been transmitted to the terminal, validations of experimental terminal and test plans on the ground are under way. Safety protects and interlocks will be improved according to experimental results to make the machine easier to operate and more reliable. Depending on the progress of CJPL-II, the accelerator will be delivered to the underground lab before the end of 2019.

References

1. K.J. Kang, J.P. Cheng, Y.H. Chen, Y.J. Li et al., Status and prospects of a deep underground laboratory in China. J. Phys. Conf. Ser. **203**, 0120281–0120284 (2010)
2. W.P. Liu, Z.H. Li, J.J. He, X.D. Tang et al., Progress of Jinping underground laboratory for nuclear astrophysics (JUNA). Sci. China Phys. Mech. Astron. **58**(3), 1–7 (2015)
3. Q. Wu, L.T. Sun, B.Q. Cui, G. Lian et al., Design of an intensity ion source and LEBT for Jinping underground nuclear astrophysics experiments. Nucl. Instrum. Methods Phys. Res. A **830**, 214–218 (2016)

Chapter 54
^{7}Be(p,p)^{7}Be and Its Importance in Nuclear Astrophysics

Thomas Chillery

Abstract Recent Earth-bound experiments measuring solar neutrino fluxes from the Sun show discrepancies both with each other and with the standard solar model. Of the reactions involved in the production of solar neutrinos, the ^{7}Be(p,γ)^{8}B still carries the largest uncertainties. Studies have been performed of both ^{7}Be(p,γ)^{8}B [1] and ^{7}Be(p,p)^{7}Be [2]. To further constrain the (p,γ) channel S-factor at relevant energies, a precise study of the ^{7}Be(p,p)^{7}Be elastic scattering will be carried out at the Centre for Isotopic Research on Cultural and Environmental heritage in Italy [3]. Data will help to constrain the ^{7}Be(p,γ)^{8}B reaction cross section through a global R-matrix analysis. The ultimate drive of this effort in understanding the neutrino uncertainties is to use the Sun as a standard reference to better understand other stars across the Universe.

54.1 Motivation

The standard solar model (SSM) traces the Sun's evolution over the past 4.6 Gyr of main-sequence burning, predicting the present day competition between nuclear reaction chains [4]. The competition between burning paths can be used to determine the central temperature of the Sun, if the various nuclear reaction rates are precisely known. Neutrinos probe this competition, as the relative rates of the ppI, ppII, and ppIII cycles can be determined from fluxes of the pp/pep, ^{7}Be, and ^{8}B neutrinos [1]. This highlights why precise measurements of nuclear reaction cross sections are so closely connected to solar neutrino fluxes.

The solar neutrino problem was solved at the turn of the 21st century with the discovery that neutrinos oscillate between three flavours [5, 6]. As a result more

Thomas Chillery for the CIRCE Collaboration.

T. Chillery (✉)
SUPA, School of Physics and Astronomy, University of Edinburgh, Edinburgh, UK
e-mail: thomas.chillery@ed.ac.uk
URL: https://www.ph.ed.ac.uk/people/thomas-chillery; http://www.matfis.unina2.it/dipartimento/strutture-del-dipartimento/laboratori/circe-laboratory

A. Formicola et al. (eds.), *Nuclei in the Cosmos XV*, Springer
Proceedings in Physics 219, https://doi.org/10.1007/978-3-030-13876-9_54

precise measurements of relevant nucleosynthesis reactions are required to reach a finer agreement between the SSM predictions and observatory measurements.

A recent review [1] highlights that the reaction ^{7}Be(p,γ)^{8}B, a producer of ^{8}B which subsequently beta decays emitting neutrinos, currently has the highest cross section uncertainty of all reactions occurring in the Sun. The ^{7}Be(p,p)^{7}Be scattering will be studied to complement the existing (p,γ) channel data for a global R-matrix analysis.

54.2 Experimental Setup

The ^{7}Be(p,p)^{7}Be reaction will be studied at the Center for Isotopic Research on Cultural and Environmental Heritage (CIRCE) laboratory located in Italy. CIRCE utilises a caesium source and a 3 MV TTT-3 Tandem Accelerator [3] capable of accelerating radioactive ion beams. In this study ^{7}Be ions will be accelerated between E_{lab} = 1.2–6 MeV and focussed (beam spot diameter of order 5 mm) onto a 930 $\frac{\mu g}{cm^2}$ thick solid polyethylene (CH_2) target. The ^{7}Be + p reaction will thus follow inverse kinematics, whereby protons recoiled at forward angles will be detected by one of two Micron S2 silicon semiconductor detectors [7], mounted at nominal distances 25 and 120 mm from the target's center. The S2 detectors are multi-striped with 48 annular rings on the front face, allowing the recoils to be detected with angular resolution ($\Delta\theta_{lab}$ of order 0.3°). Mylar foils will be mounted in front of the detectors for protection from scattered beam projectiles that would otherwise cause radiation damage to the silicon.

Prior to measurement, the CH_2 target's upstream side was sputtered with a thin (nominal: 40 $\frac{\mu g}{cm^2}$) gold flush. This is intended to scatter incoming beam particles at backward angles, into a single channel silicon diode detector. Knowledge of the exact positioning of the diode will allow both the beam current and target degradation to be monitored during the measurement. A computer generated drawing of the experimental setup is provided in Fig. 54.1.

54.3 Initial Tests: Thick-Target Measurement with ^{7}Li Beam

Commissioning tests have been performed using ^{7}Li beam at E_{lab} = 3 and 3.5 MeV bombarding a CH_2 target. The recoil proton spectra were calibrated using a ^{241}Am and ^{239}Pu radioactive source and a pulser walkthrough. The detected proton energy takes into account the energy loss of the proton in both the target and the silicon dead layer of the S2s. Conversion from detected to centre of mass energies was performed using stopping powers provided by SRIM-2013 [8]. A sample proton spectrum (^{7}Li E_{lab} = 3 MeV) is shown in Fig. 54.2, where the trend expected from pure Rutherford scattering is overlayed in red.

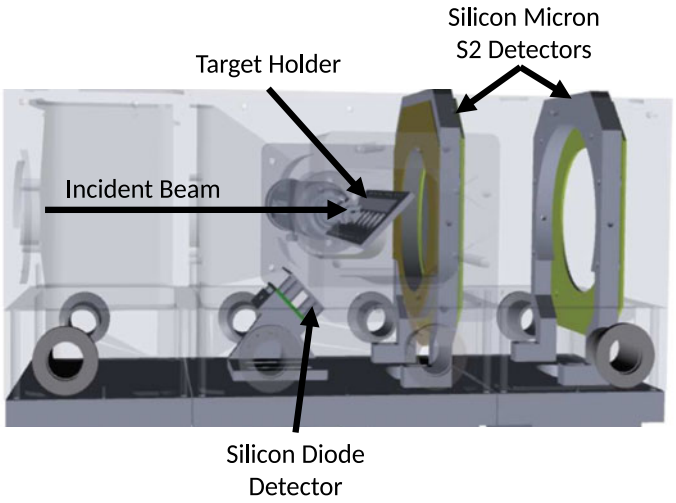

Fig. 54.1 Computer generated drawing of the target chamber

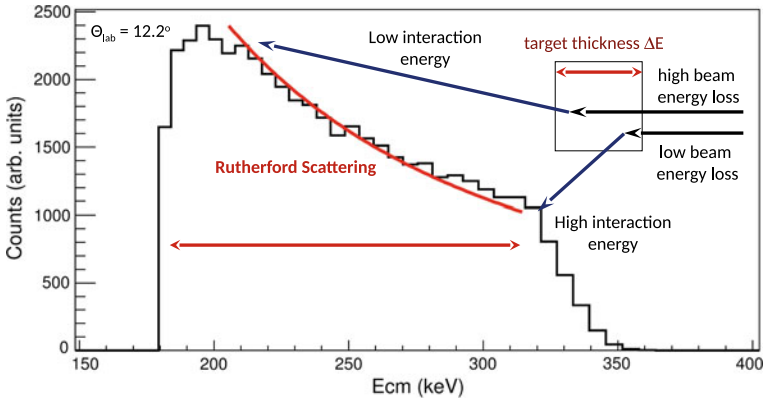

Fig. 54.2 Measured proton spectrum converted to centre of mass frame (Black). Expected Rutherford Scattering (Red) scaled to data

54.4 Future Outlook

Further commissioning of the setup is required using the ^{7}Li(p,p)^{7}Li reaction. The ^{7}Be(p,p)^{7}Be experiment is planned to run in CIRCE for Autumn/Winter 2018. The cross section/phase shifts will be extracted across the E_{lab} = 1.2–6 MeV range and a global R-matrix fit will be performed with the (p,γ) channel.

References

1. E.G. Adelberger et al., Rev. Mod. Phys. **83**, 195–245 (2011). https://doi.org/10.1103/RevModPhys.83.195
2. C. Angulo et al., Nucl. Phys. A. **716**, 211–229 (2003). https://doi.org/10.1016/S0375-9474(02)01584-1
3. B.N. Limata et al., Nucl. Inst. Meth. Phy. Res. B **266**, 2117–2121 (2008). https://doi.org/10.1016/j.nimb.2008.02.083
4. N. Vinyoles et al., Astro. J. **835**, 202, (2017). http://stacks.iop.org/0004-637X/835/i=2/a=202
5. Y. Fukuda et al., Phys. Rev. Lett. **81**, 1562–1567 (1998). https://doi.org/10.1103/PhysRevLett.81.1562
6. J.N. Bahcall et al., J. High Energy Phys. **14** (2001). http://stacks.iop.org/1126-6708/2001/i=08/a=014
7. Micron Semiconductor LTD. http://www.micronsemiconductor.co.uk
8. J.F. Ziegler, SRIM. http://www.srim.org/

Chapter 55
Direct Measurement of the $^{13}C(\alpha, n)^{16}O$ Reaction at LUNA

G. F. Ciani, L. Csedreki and A. Best

Abstract The $^{13}C(\alpha, n)^{16}O$ reaction is the main neutron source for the *s-process* in low mass AGB stars. Although several direct measurements have been performed, no dataset reaches the Gamow window (140–230 keV) due to the the nearly exponential drop of σ(E) with decreasing energy. The available dataset didn't extend to lower energies because of the strong cosmic background and some difficulties to evaluate the target degradation. To study the $^{13}C(\alpha, n)^{16}O$ cross section at low energies, ancillary measurements to characterize ^{13}C enriched evaporated targets, under an high intensity proton beam (100–200 μA), are carried out at Laboratori Nazionali del Gran Sasso (LNGS) in the framework of the LUNA experiment. The preliminary results are reported in this contribution.

55.1 State of the Art and Next LUNA Measurement

The $^{13}C(\alpha, n)^{16}O$ reaction is the major neutron source for the main component of the *s*-process in low mass ($1 - 3M_{\odot}$) Asymptotic Giant Branch (AGB) stars, whose temperature of interest is around $1-2 \times 10^8$ K. This corresponds to a Gamow window between 140 and 230 keV, below the Coulomb potential energy of the reaction. Several direct measurements have been performed by different groups [1–4]. The astrophysical S factors, S(E), are shown in Fig. 55.1. The lowest energy point has been measured by Drotleff et al. [2] with an uncertainty of 50%.

G. F. Ciani, L. Csedreki and A. Best for the LUNA collaboration.

G. F. Ciani (✉)
Gran Sasso Science Institute, Viale F. Crispi 7, L'Aquila, Italy
e-mail: giovanni.ciani@gssi.it

G. F. Ciani · L. Csedreki
INFN, Laboratori Nazionali del Gran Sasso Via G. Acitelli, 22,
67100 Assergi, L'Aquila, Italy

A. Best
Università di Napoli Federico II and INFN,
Sezione di Napoli, Strada Comunale Cinthia, 80126 Napoli, Italy

A. Formicola et al. (eds.), *Nuclei in the Cosmos XV*, Springer
Proceedings in Physics 219, https://doi.org/10.1007/978-3-030-13876-9_55

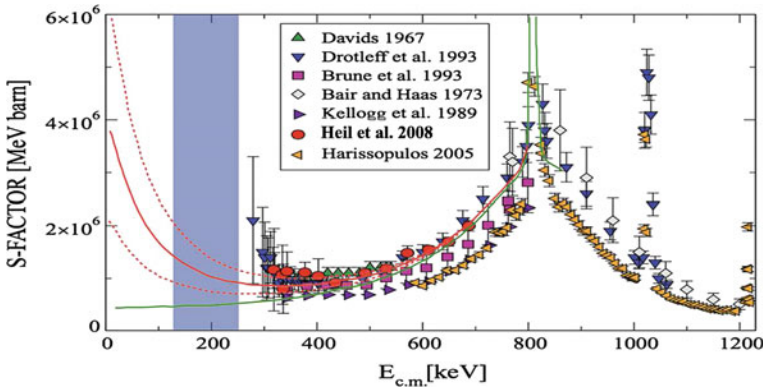

Fig. 55.1 State of the art of the direct measurement of the $^{13}C(\alpha, n)^{16}O$ reaction adapted from Heil's paper [1]. The violet band represents the Gamow window, the red solid line is the extrapolation of the astrophysical *S*-factor down to this region while its error bands are indicated by red dashed lines. The green line is an extrapolation where the presence of the threshold resonance is omitted

In addition the reaction mechanism at low energies includes also the contributions from the tail of a sub-threshold resonance at $E_R = -3\,\text{keV}$ (the resonance energy in the center-of-mass system), corresponding to $E_x = 6.356\,\text{MeV}$ state in ^{17}O.
The red and the green line indicate the R Matrix extrapolation taking and not taking in account the sub-threhsold resonance, respectively (see Fig. 55.1).
As one can see the two curves differ almost of one order of magnitude in the astrophysical energy region. In order to be reliable such an extrapolation must be more effectively constrained by as much experimental information as possible.

The LUNA collaboration proposed to measure the $^{13}C(\alpha, n)^{16}O$ cross section in the region of interest for the s process reaching an overall accuracy of 10%. The experiment has been performed at LNGS, combining the underground reduction of the neutron flux, of 3 orders of magnitude compared with the surface [5], with an intense stable alpha beam delivered by the LUNA 400 accelerator [6] in the energy range $50 < E_\alpha < 400\,\text{keV}$.

55.2 Target Preparation and Characterization

Targets used for the measurements have been produced at MTA ATOMKI (Debrecen, Hungary) evaporating 99% ^{13}C enriched powder on Tantalum backing by means of electron gun technique.

A deep target characterization has been performed focusing on the investigation of target composition, stoichiometry, and density profile as a function of cumulative charge measuring the capture process to the ground state of ^{14}N of the $^{13}C(p, \gamma)^{14}N$ reaction.
The measurements have been mainly devoted to:

- measure the presence of light element impurities in the target and in the backing which can produce, due to their relatively low Coulomb barrier, an high level of beam induced background.
- quantify the degradation and the stoichiometry modification due to the beam irradiation.

An important requirement is the quality of the solid target used: high density, high purity and high stability. All of these aspects have been studied with a complementary approach using two facilities: the 2MV Tandetron installed at MTA ATOMKI [7] and the LUNA 400 kV accelerator. The uniformity and reproducibility of the target production is performed by observing the excitation function at the narrow resonance at $E_p = 1748$ keV ($\Gamma = 120$eV) of the $^{13}C(p, \gamma)^{14}N$ reaction [8] at 2MV Tandetron. Being in the thick target Yield condition (target thickness $\Delta E \gg \Gamma$), the excitation function has the typical double arctangent function [9], so we can easily fit and extract parameters as target thickness.

A typical underground γ-spectrum acquired at $E_p = 310$ keV is shown in Fig. 55.2. The measurements were carried out using an High Purity Germanium detector in close geometry, due to the good resolution of the Ge detector (FWHM = 3 keV at E = 1460 keV corresponding to ^{40}K) possible γ-ray lines from proton capture reactions on ^{11}B, ^{12}C and ^{19}F have been investigated.

All γ-ray lines below the direct capture to the ground state transition are referable to the $^{13}C(p, \gamma)^{14}N$ reaction, with negligible observation of contaminants.
The stability test is performed by observing the reduction of the yield of the transition to the ground state in $^{13}C(p, \gamma)^{14}N$ reaction, at $E_\gamma = 7843$ keV: after 33C the yield was decreased of 17%.

55.3 Target Monitoring During $^{13}C(\alpha, n)^{16}O$ Cross Section Measurement

In Fig. 55.3 is shown a typical γ-ray transition to the ground state analysed with the γ-line shape procedure in order to study the target modification due to the degradation or to the change of the stoichiometry. The expected γ-line shape is determined by the cross section behaviour σ in the proton energy interval spanned by the incident beam during the slowing down process in the target. A detailed treatment of this procedure is beyond the aim of this contribution.

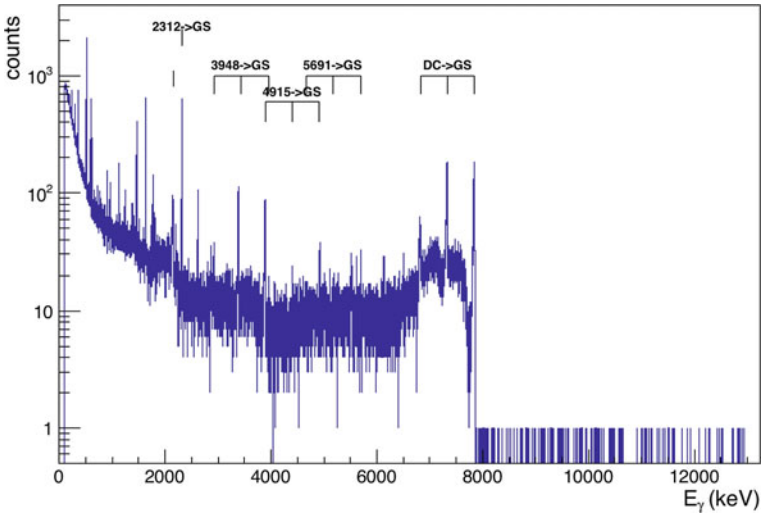

Fig. 55.2 Underground γ-spectrum of the $^{13}C(p,\gamma)^{14}N$ reaction acquired at $E_p = 310\,\text{keV}$, some of the primary γ-rays transition to the ground state are showed

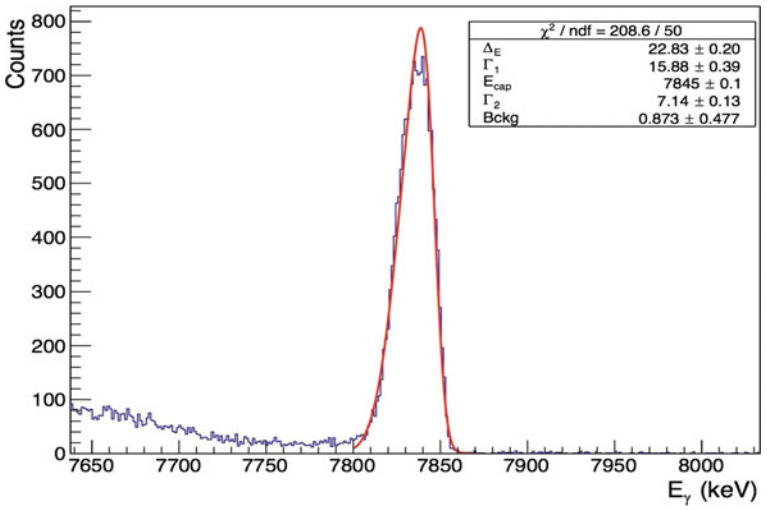

Fig. 55.3 Typical γ_0-ray line shape of the $^{13}C(\alpha,n)^{16}O$ reaction obtained at $E_p = 310\,\text{keV}$. The solid line represents the sum of the resonant and non-resonant contributions, convoluted with the simulated straggling [10]

The experimental procedure is based on an alternative proton/alpha beam irradiation. We adopt this complementary approach since from the analysis of the transition peak of DC→ GS, we are able to observe the possible presence of surface contaminations and estimate target density as function of the accumulated charge. We developed a novelty analysis approach to monitor the thickness variation as function of the active and inactive nuclei after the alpha beam bombardment (Ciani's Ph.D. in submission).

55.4 Summary

In this paper the target modification monitoring during the $^{13}C(\alpha, n)^{16}O$ cross section measurement is described.

After 1 C of alpha irradiation the beam will be switched to proton and direct capture of the $^{13}C(p, \gamma)^{14}N$ reaction is measured.

The analysis is based on the γ-line shape, which permits to extract information on the target composition and the target thickness, used in the cross section analysis. The final analysis is in progress.

References

1. Heil et al., Phys. Rev. C **78**, 025803 (2008)
2. H.W. Drotleff et al., ApJ **414**, 735–739 (1993)
3. C.R. Brune et al., Phys. Rev. C **48**, 6 (1993)
4. S. Harissopulos et al., Phys. Rev. C **72**, 062801(R) (2005)
5. Best et al., Nucl. Instr. Meth. Phys. Res A **812**, 1 (2016)
6. A. Formicola et al., Nucl. Instrum. Methods Phys. Res., Sect. A, 507, 609 (2003)
7. I. Rajta et al., NIM A **880**, 125–130 (2018)
8. G.F. Ciani et al., EPJ Conf. **165**, 01012 (2017)
9. C.E. Rolfs, W.S. Rodney, *Cauldrons in the Cosmos* (The University of Chicago Press, Chicago, 1988)
10. J.F. Ziegler, J.P. Biersack, M.D. Ziegler, *SRIM, The Stopping and Range of Ions in Matter* (SRIM Co., 2008)

Chapter 56
H-He Shell Interactions and Nucleosynthesis in Massive Population III Stars

Ondrea Clarkson, Falk Herwig, Robert Andrassy, Paul Woodward, Marco Pignatari and Huaqing Mao

Abstract We report on our ongoing investigation into the nucleosynthetic and hydrodynamic nature of mixing at the interface between the H- and He-convection zones in massive Pop III stars. Studying recent a grid of 26 1D stellar evolution simulations with different mixing assumptions, we find that H-He interactions occur in 23/26 cases. We demonstrate the nucleosynthesis expected in a H-He interaction in an $80M_{\odot}$. Finally, we describe our progress in simulating a Pop III double convection zone in the `PPM-Star` hydrodynamics code.

Pop III stars are thought to have produced and released the first elements heavier than those created in the Big Bang [1]. The most metal-poor stars we observe today may be the most direct descendants of Pop III stars and are a powerful diagnostic in our study of early cosmic chemical evolution [2].

O. Clarkson (✉) · F. Herwig
Department of Physics & Astronomy, University of Victoria,
P.O. Box 3055, Victoria, B.C. V8W 3P6, Canada
e-mail: oclark01@uvic.ca
URL: http://www.nugridstars.org

P. Woodward · H. Mao
LCSE and Department of Astronomy,
University of Minnesota, Minneapolis, MN 55455, USA

M. Pignatari
E. A. Milne Centre for Astrophysics, University of Hull, Hull HU6 7RX, UK

O. Clarkson · F. Herwig · R. Andrassy · P. Woodward · M. Pignatari · H. Mao
Joint Institute for Nuclear Astrophysics, Center for the Evolution of the Elements,
Michigan State University, 640 South Shaw Lane, East Lansing, MI 48824, USA

O. Clarkson · F. Herwig · M. Pignatari
NuGrid collaboration, East Lansing, USA

R. Andrassy
Heidelberg Institute for Theoretical Studies, Schloss-Wolfsbrunnenweg 35,
69118 Heidelberg, Germany

A. Formicola et al. (eds.), *Nuclei in the Cosmos XV*, Springer
Proceedings in Physics 219, https://doi.org/10.1007/978-3-030-13876-9_56

Interactions between H and He-convection layers have been seen in 1D stellar evolution simulations of massive Pop III stars [3, 4] but until recently, have not been investigated in detail.

Similar convective-reactive events occur in additional environments, such as He-shell flashes in low-Z low-mass stars [5–7], post-AGB stars [8], rapidly-accreting white dwarfs [9], and low-Z Super-AGB stars [10]. In these cases—just as Pop III stars—likely leading to the *i*-process with neutron densities $\approx \times 10^{13-15}$ cm^{-3}, first discussed by Cowan and Rose [11].

We have explored the possibility that the abundance patterns of the CEMP-no stars SMSS J031300, HE 1327-2326 and HE 0107-5240, among the most iron-poor stars known, could be explained by highly energetic, convective H-He shell interactions in massive Pop-III stars [12] without a strong odd-even effect. Based on a 45 $M_\odot$ stellar model that undergoes a H/He convective-reactive event during C-core burning, we ran single-zone calculations to ascertain the nucleosynthesis which may result from such an event. For these simulations we found neutron densities of $\approx 6 \times 10^{13}$ cm^{-3}, leading to striking similarities with the abundance patterns existing in some of the most metal-poor stars, particularly in abundance ratio trends seen from Na-Si and Ti-Mn.

We have run a grid of 26 models using the `MESA` stellar evolution code [13] over a mass range of $15-140 M_\odot$. For each initial mass, we use 5 different sets of mixing assumptions in order to explore the dependence of H-He interactions on marcophysical modelling choices. Our findings indicate that there are three distinct modes for the interaction: firstly, as in Clarkson et al. [12] a convective H and He-shell interaction. Secondly, a convective H-shell mixing into a convective He-core and thirdly, a convective H-shell mixing down into a radiative He-shell.

Although difficult to constrain from 1D simulations, we have preformed additional single zone calculations more, with the aim to further explore the abundances of

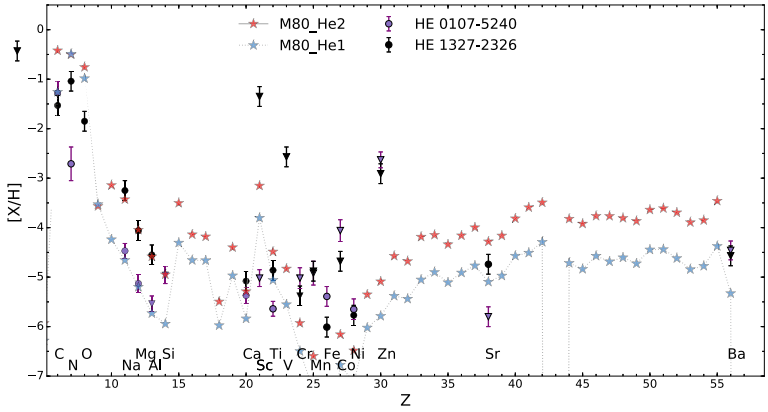

Fig. 56.1 Abundances of CEMP-no stars HE 0107-5240 and HE 2317-2326 in purple and black are shown with single zone calculations (red and blue stars) based on an 80$M_\odot$ stellar evolution simulation

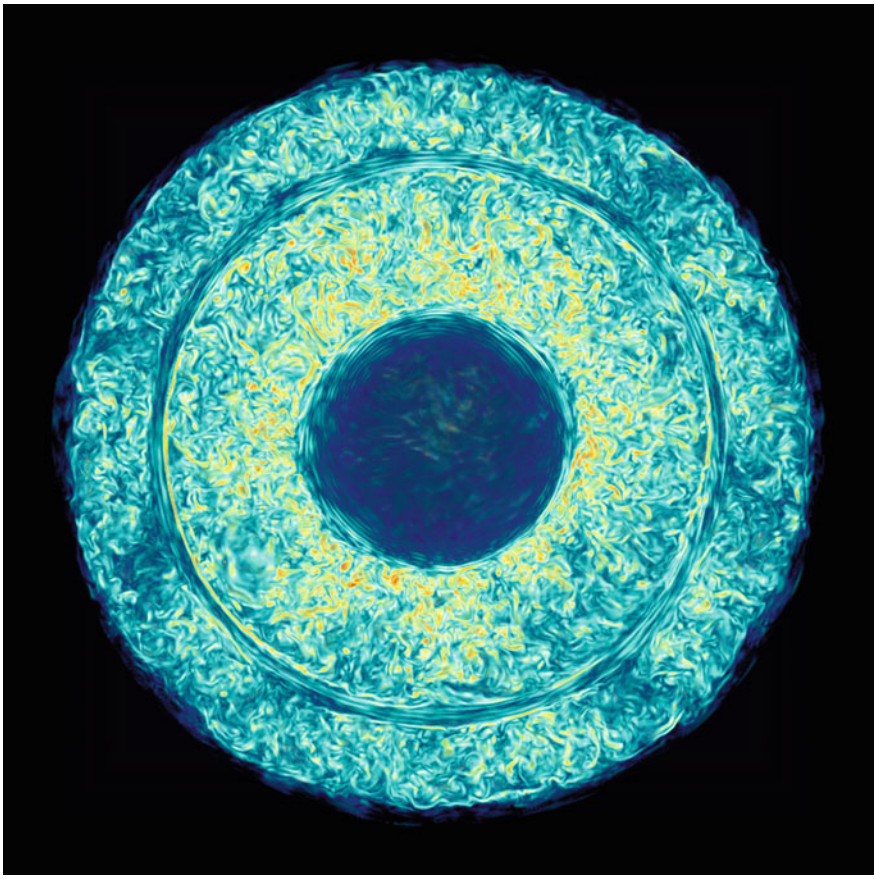

Fig. 56.2 3D simulation of convective H and He-burning shells on a 768^3 grid. Only the first 50,000 km of the H-shell is simulated in order to adequately resolve the stable layer. Colours show vorticity

HE 0107-5240 and HE 2317-2326. We ran simulations with T = 2.5×10^8 K and $\rho = 1.9 \times 10^2$ g cm^{-3} from the He-shell of an 80M$_\odot$ model from our grid of Pop III models with 1% H added, by mass. Preliminary results are shown in Fig. 56.1. We find that in order to simultaneously reproduce both light and trans-Fe elements in these stars the total neutron exposure must be a factor of ∼4 smaller than we previously reported.

We have begun using the explicit PPMstar code [14] to investigate these events. Our initial suite of simulations contain the He-shell flash convection zone and the bottom of the H-burning convection zone, separated by a radiative zone of 25,000 km (Fig. 56.2). Initially we are driving these convection zones by a constant volume heating at the bottom of the He convection zone and a corresponding cooling at the top of the H-burning convection zone. In order to realistically model this Pop III

stellar environment, several code modifications were made. In future simulations, we will be including a simplified network to model the nuclear feedback expected from the mixing of H and He-burning material. The aim of these simulations is to answer the hypothesis [12] that such an event may led to a GOSH-like instability and could potentially eject material from the star. We hope to determine whether such an event would occur, and if so, how would it unfold in a full 4π-3D environment in terms of possible asymmetries in the entrainment and how would the model respond to the nuclear feedback?

The first massive stars may have experienced violent convective-reactive interactions at the interface of the H- and He-burning regions. Three dimensional simulations with nuclear feedback are now being constructed to investigate this stellar and nuclear astrophysics environment. A light-element i process could be triggered, and may result in abundance patterns observed in CEMP-no stars without strong odd-even effect.

References

1. K. Nomoto, C. Kobayashi, N. Tominaga, Nucleosynthesis in stars and the chemical enrichment of galaxies. ARA&A **51**, 457–509 (2013)
2. A. Frebel, J.E. Norris, Near-field cosmology with extremely metal-poor stars. ARA&A **53**, 631–688 (2015)
3. M. Limongi, A. Chieffi, Presupernova evolution and explosive nucleosynthesis of zero metal massive stars. ApJS **199**, 38 (2012)
4. A. Heger, S.E. Woosley, Nucleosynthesis and evolution of massive metal-free stars. ApJ **724**, 341–373 (2010)
5. R.J. Stancliffe, D.S.P. Dearborn, J.C. Lattanzio, S.A. Heap, S.W. Campbell, 3D hydrodynamical simulations of proton ingestion, in *Galactic Archaeology: Near-Field Cosmology and the Formation of the Milky Way* ed. by W. Aoki, M. Ishigaki, T. Suda, T. Tsujimoto, N. Arimoto. Astronomical Society of the Pacific Conference Series, vol 458 (2012), p. 45
6. N. Iwamoto, T. Kajino, G.J. Mathews, M.Y. Fujimoto, W. Aoki, Flash-driven convective mixing in low-mass, metal-deficient asymptotic giant branch stars: a new paradigm for Lithium enrichment and a possible s-process. ApJ **602**, 377–388 (2004)
7. L. Dardelet, C. Ritter, P. Prado, E. Heringer, C. Higgs, S. Sandalski, S. Jones, P. Denisenkov, C. Higgs, S. Sandalski, S. Jones, P. Denisenkov, K. Venn, M. Bertolli, M. Pignatari, P. Woodward, F. Herwig, i process and CEMP-s+r stars, in *Proceedings of Science XIII Nuclei in the Cosmos (NIC XIII)* (2014)
8. F. Herwig, M. Pignatari, P.R. Woodward, D.H. Porter, G. Rockefeller, C.L. Fryer, M. Bennett, R. Hirschi, Convective-reactive Proton-^{12}C combustion in Sakurai's object (V4334 Sagittarii) and implications for the evolution and yields from the first generations of stars. ApJ **727**, 89 (2011)
9. P.A. Denissenkov, F. Herwig, U. Battino, C. Ritter, M. Pignatari, S. Jones, B. Paxton, I-process nucleosynthesis and mass retention efficiency in He-shell flash evolution of rapidly accreting White Dwarfs. ApJ **834**, L10 (2017)
10. S. Jones, C. Ritter, F. Herwig, C. Fryer, M. Pignatari, M.G. Bertolli, B. Paxton, H ingestion into He-burning convection zones in super-AGB stellar models as a potential site for intermediate neutron-density nucleosynthesis. MNRAS **455**, 3848–3863 (2016)

11. J.J. Cowan, W.K. Rose, Production of C-14 and neutrons in red giants. ApJ **212**, 149–158 (1977)
12. O. Clarkson, F. Herwig, M. Pignatari, Pop III i-process nucleosynthesis and the elemental abundances of SMSS J0313–6708 and the most iron-poor stars. MNRAS **474**, L37–L41 (2018)
13. B. Paxton, P. Marchant, J. Schwab, E.B. Bauer, L. Bildsten, M. Cantiello, L. Dessart, R. Farmer, H. Hu, N. Langer, R.H.D. Townsend, D.M. Townsley, F.X. Timmes, Modules for experiments in stellar astrophysics (MESA): binaries, pulsations, and explosions. ApJS **220**, 15 (2015)
14. F. Herwig, P.R. Woodward, P.-H. Lin, M. Knox, C. Fryer, Global non-spherical oscillations in three-dimensional 4π simulations of the H-ingestion flash. ApJ Lett. **792**, L3 (2014)

Chapter 57
A Public Code for Precision Big Bang Nucleosynthesis with Improved Helium-4 Predictions

Alain Coc, Cyril Pitrou, Jean-Philippe Uzan and Elisabeth Vangioni

Abstract A *Mathematica* code ("PRIMAT") for big bang nucleosynthesis (BBN), has been made publicly available. Its network includes more than 400 reactions with their updated thermonuclear reaction rates. In particular, it takes advantage of the recently improved weak reaction rates that include all the required theoretical corrections to reach a level of accuracy of 10^{-4} on ^{4}He. Once the uncertainties on the reaction rates and neutron lifetime are taken into account, we obtain $Y_p = 0.24709 \pm 0.00017$, D/H = $(2.459 \pm 0.036) \times 10^{-5}$ and Li/H = $(5.623 \pm 0.247) \times 10^{-10}$.

Primordial nucleosynthesis (BBN) is one of the historical observational evidences for the standard big bang model, together with the expansion of the universe and the Cosmic Microwave Background (CMB). It is very special because, within the *standard* BBN model, the thermodynamic conditions can be calculated from first principles. In addition the cross sections of most of the nuclear reactions that are of importance are measured in the laboratory, at the relevant energies. Furthermore, now that the number of neutrino families and the baryonic density have been fixed by laboratory measurements or CMB observations, the model has no free parameter. Then, it is now possible to accurately calculate the abundances of the produced "light elements": ^{4}He, D, ^{3}He and ^{7}Li.

Precision on primordial abundances, deduced from observations, have now reached the percent level for ^{4}He (1.6% [1]) and deuterium (1.2% [2]). Precision on predictions for Y_p (^{4}He mass fraction) and D/H (ratio of number of atoms) should, hence, reach the same level of accuracy. (We leave aside the *lithium problem* which is even more acute [3] with the now precise deuterium observations [2], and ^{3}He whose galactic chemical evolution is uncertain.) (Table 57.1).

A. Coc (✉)
Centre de Sciences Nucléaires et de Sciences de la Matière (CSNSM), CNRS IN2P3, Univ. Paris-Sud, Université Paris-Saclay, Bât. 104, 91405 Orsay Campus, France
e-mail: Alain.Coc@csnsm.in2p3.fr

C. Pitrou · J.-P. Uzan · E. Vangioni
Institut d'Astrophysique de Paris, CNRS UMR 7095, Institut Lagrange de Paris, 98 bis Bd Arago, 75014 Paris, France

A. Formicola et al. (eds.), *Nuclei in the Cosmos XV*, Springer Proceedings in Physics 219, https://doi.org/10.1007/978-3-030-13876-9_57

Table 57.1 Primordial abundances compared to observations. Percentages correspond to the relative uncertainties

	Observations	(%)	Predictions [4]	(%)
Y_p	0.2449 ± 0.0040 [1]	(1.6)	$\mathbf{0.24709 \pm 0.00017}$	(0.07)
D/H ($\times 10^{-5}$)	2.527 ± 0.030 [2]	(1.2)	$\mathbf{2.459 \pm 0.036}$	(1.5)
^{7}Li/H ($\times 10^{-10}$)	$1.58^{+0.35}_{-0.28}$ [9]	(20)	$\mathbf{5.623 \pm 0.247}$	(4.4)

The BBN *Mathematica* code (`PRIMAT` for PRImordial MATter), is fully described in Pitrou et al. [4], and is made publicly available at at http://www2.iap.fr/users/pitrou/primat.htm. Its network of 391 reactions and 59 β–decay processes allows to predict abundances up to the CNO region. The associated thermonuclear rates and uncertainties are identical (with only a few exceptions [4]) to the one described in Coc et al. [5]. It is inherited from our original *Fortran* code (see e.g. [6] and references therein). The reaction rates that have the strongest influence on D/H [^{2}H(p,γ)^{3}He, ^{2}H(d,p)^{3}H, and ^{3}H(d,n)^{4}He] have been re–evaluated using Bayesian methods [7, 8], and are among these exceptions. The uncertainty on the ^{4}He mass fraction came partially from the experimental neutron lifetime. However, theoretical uncertainties also affected the weak reaction rates that interconvert neutrons with protons. For these rates, the radiative, finite nucleon mass, finite temperature radiative corrections, weak-magnetism, QED plasma effects, and consequences of incomplete neutrino decoupling have all been calculated by Pitrou et al. [4] in a self-consistent manner. For all of them, detailed balance was enforced, an essential requirement as there rates govern the n/p ratio at freeze–out and, consequently, Y_p. Even if they are small, these corrections affect the predictions by 1.84% for Y_p and 1.49% for D/H larger that the observational uncertainties (Table 5 in Pitrou et al. [4]). Hence, they are essential, not only for ^{4}He abundance prediction but also for the deuterium one.

The precision on Y_p is limited by the neutron lifetime, for which we adopted the experimental value proposed by Serebrov et al. [10], namely 879.5 ± 0.8 s, keeping in mind that there is still a discrepancy between the results of "beam" and "bottle" experiments [10]. The uncertainty on D/H arise from the thermonuclar reaction rates of ^{2}H(p,γ)^{3}He, ^{2}H(d,p)^{3}H, and ^{3}H(d,n)^{4}He which need to be known at the percent level. In particular, the ^{2}H(p,γ)^{3}He reaction rate is not known with sufficient accuracy, because of the scarcity of experimental data in the region of interest and their conflicts with the more recent theoretical model [11] (see Fig. 23 in Pitrou et al. [4]). If the experimental data expected from the LUNA facillity [12] confirm this theoretical calculation [11], our deuterium prediction will decrease by 0.072×10^{-5}, i.e. D/H $\approx 2.39 \times 10^{-5}$, in tension with observations [2]. However, numerous non–standard models of BBN, initially proposed to solve the lithium problem (see e.g. [3]), can easily solve this deuterium discrepancy and very slightly reduce the lithium one. (Experimental results concerning the ^{7}Be(n,p)^{7}Li and ^{7}Be(d,p)2^{4}He reactions, presented at this conference [13, 14], reduce the ^{7}Li production, but by far less than the required amount.)

The public **PRIMAT** code allows to re-do all the calculations presented in our *Physics Report* [4] (Monte–Carlo, non-degenerate neutrinos,…). The file of tabulated reaction rates, provided with the code, can certainly be adapted to other BBN codes, and used as benchmark for comparison. The code can be developed to include new physics (e.g. our previous investigations [15, 16]) or simply to test the influence of new reaction rates. Once, the corrections to the weak rates are fully implemented in it, the *Fortran* version will also be made public. We expect to update the reaction rate library on a regular basis.

References

1. E. Aver, K.A. Olive, E.D. Skillman, The effects of He I λ 10830 on helium abundance determinations. J. Cosmol. Astropart. Phys **7**, 011 (2015)
2. R.J. Cooke, M. Pettini, C.C. Steidel, One percent determination of the primordial deuterium abundance. Astrophys. J. **855**, 102 (2018)
3. A. Coc, P. Petitjean, J.-P. Uzan et al., New reaction rates for improved primordial D/H calculation and the cosmic evolution of deuterium. Phys. Rev. D **92**, 123526 (2015)
4. C. Pitrou, A. Coc, J.-P. Uzan, E. Vangioni, Precision big bang nucleosynthesis with improved Helium-4 predictions. Phys. Rep. **754**, 1 (2018). arXiv:1801.08023 [astro-ph.CO]. https://doi.org/10.1016/j.physrep.2018.04.005
5. A. Coc, S. Goriely, Y. Xu, M. Saimpert, E. Vangioni, Standard big bang nucleosynthesis up to CNO with an improved extended nuclear network. Astrophys. J. **744**, 158 (2012)
6. A. Coc, E. Vangioni, Primordial nucleosynthesis. Int. J. Mod. Phys. E, **26**, 1741002 (2017). arXiv:1707.01004 [astro-ph.CO]
7. Á. Gómez Iñesta, C. Iliadis, A. Coc, Bayesian estimation of thermonuclear reaction rates for deuterium+deuterium reactions. Astrophys. J. **849**, 134 (2017)
8. C. Iliadis, K.S. Anderson, A. Coc, F.X. Timmes, S. Starrfield, Bayesian estimation of thermonuclear reaction rates. Astrophys. J. **831**, 107 (2016)
9. L. Sbordone, P. Bonifacio, E. Caffau et al., The metal-poor end of the Spite plateau I. Stellar parameters, metallicities, and lithium abundances. Astron. Astrophys. **522**, A26 (2010) (2016)
10. A.P. Serebrov, E.A. Kolomensky, A.K. Fomin et al., Neutron lifetime measurements with a large gravitational trap for ultracold neutrons. Phys. Rev. C **97**, 055503 (2018)
11. L.E. Marcucci, G. Mangano, A. Kievsky, Viviani, Implication of the proton-deuteron radiative capture for big bang nucleosynthesis. Phys. Rev. Lett. **116**, 102501 (2016)
12. S. Zavatarelli et al., A new measurement of the D(p,γ)^{3}He crosssection in the BBN energy range at LUNA, *these proceedings*
13. Damone, L.A. et al., ^{7}Be(n,p) cross section measurement for the cosmological lithium problem at the n_TOF facility at CERN, *these proceedings*
14. I. Wiedenhoever et al., Cross sections of ^{7}Be+d measured at low energies and implications for Big-Bang nucleosynthesis, *these proceedings*
15. A. Coc, K.A. Olive, J.-P. Uzan, E. Vangioni, Big bang nucleosynthesis constraints on scalar-tensor theories of gravity. Phys. Rev. D **73**, 083525 (2006)
16. A. Coc, N.J. Nunes, K.A. Olive, J.-P. Uzan, E. Vangioni, Coupled variations of fundamental couplings and primordial nucleosynthesis. Phys. Rev. D **76**, 023511 (2006)

Chapter 58
The LUNA Neutron Detector Array for the Direct Measurement of the $^{13}C(\alpha,n)^{16}O$ Nuclear Reaction

L. Csedreki, G. F. Ciani, A. Best, J. Balibrea-Correa and Gy. Gyürky

Abstract The direct measurement of the $^{13}C(\alpha,n)^{16}O$ nuclear reaction down to its Gamow window is essential to the complex understanding of the astrophysical *s*-process, which is responsible for the production of about half of the heavier elements above the iron group. The combination of a high efficiency experimental setup and the extremely low environmental background is required to measure cross sections of the order of picobarns. This paper presents the main features of the LUNA neutron detector array dedicated to the direct investigation of the $^{13}C(\alpha,n)^{16}O$ nuclear reaction in the Underground Laboratory of LNGS.

58.1 Introduction

The $^{13}C(\alpha,n)^{16}O$ nuclear reaction is of key importance in nuclear astrophysics. This reaction is the dominant neutron source for the synthesis of the main *s*-process component of heavy elements, a process which takes place in thermally pulsing, low-mass asymptotic giant branch stars [1]. Direct and indirect methods to investigate the behavior of the $^{13}C(\alpha,n)^{16}O$ reaction [2–5] are presented in literature. However, the extrapolation of the astrophysical S-factor of this reaction into its Gamow window ($E_{c.m.}$ = 140–230 keV, $E_{\alpha,lab}$ = 180–300 keV) is challenging due to the effect of a resonance of ^{17}O located near the threshold and high uncertainties of the experimental data in the low-energy region.

L. Csedreki et al. for the LUNA collaboration.

L. Csedreki (✉)
INFN, Laboratori Nazionali del Gran Sasso (LNGS), Assergi, Italy
e-mail: laszlo.csedreki@lngs.infn.it

G. F. Ciani
Gran Sasso Science Institute (GSSI), L'Aquila, Italy

A. Best · J. Balibrea-Correa
Università di Napoli Federico II and INFN, Sezione di Napoli, Naples, Italy

Gy. Gyürky
Institute for Nuclear Research (MTA Atomki), Debrecen, Hungary

A. Formicola et al. (eds.), *Nuclei in the Cosmos XV*, Springer
Proceedings in Physics 219, https://doi.org/10.1007/978-3-030-13876-9_58

The aim of the current LUNA campaign is the determination of the reaction cross section towards the Gamow window with an accuracy of about 10%. At these low energies ($E_{c.m.} < 250$ keV) the cross section is of the order of picobarns. Because of this the measurement takes place at the LUNA-400 kV accelerator [6] located in the LNGS Underground Laboratory where the neutron background is reduced by 3 orders of magnitude compared to the flux on the surface. The design of the experimental setup and the applied targets have already been presented in [7, 8]. The aim of this paper is to introduce the main characteristics of the experimental setup and to demonstrate its neutron background suppression.

58.2 Experimental Arrangement

The experimental setup is composed of 18 low-activity ^{3}He counters as a neutron detector array embedded in a polyethylene moderator with geometry optimized (using GEANT 4 code) for maximal detection efficiency. In order to cover the projectile energy range down to the Gamow window of the $^{13}C(\alpha,n)^{16}O$ nuclear reaction, two different implementations of the neutron array are applied. Neutron counters in vertical arrangement are dedicated to the measurement of the reaction in the $E_{\alpha,lab}$ = 360–400 keV energy regions. A multi-stage target holder is applied to minimize the possible contamination and simplify the target changing procedure during the experiment.

Below $E_{\alpha,lab} < 350$ keV projectile energy the counters are arranged in horizontal position, resulting in an increased solid angle and more moderator material between the target and the counters can be used. A single target chamber is applied in this arrangement. In both experimental conditions the moderator is composed of two parts, which can be separated allowing the mount of a HPGe detector close to the target chambers. In the energy range of the LUNA-400 accelerator, the $^{13}C(p,\gamma)^{14}N$ reaction is suitable for the monitoring of the target degradation. The schematic view of the two different implementations of the experimental setup is shown in Fig. 58.1. The left panel presents the setup with the vertical arranged counters in an open moderator position. The right panel shows the setup with horizontally arranged neutron detectors. The moderator (white) is coated with 1 inch thick borated-polyethylene for further reduction of count rates from the environmental neutron background.

58.3 Neutron Background Suppression

As it was pointed out before, the high detection efficiency and a low background rate are crucial to achieve the required sensitivity. The environmental neutron background is investigated in the LNGS Underground Laboratory and it is compared with measurements on surface. Figure 58.2. presents the comparison of the background flux

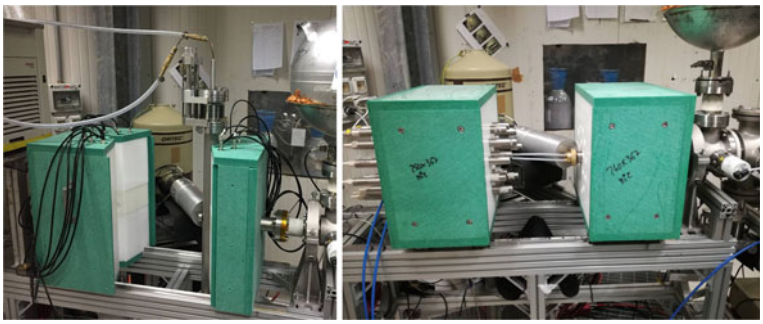

Fig. 58.1 LUNA detector array with the vertically (left part) and horizontally (right part) positioned ^{3}He counters embedded in polyethylene blocks coated with borated-polyethylene lamina

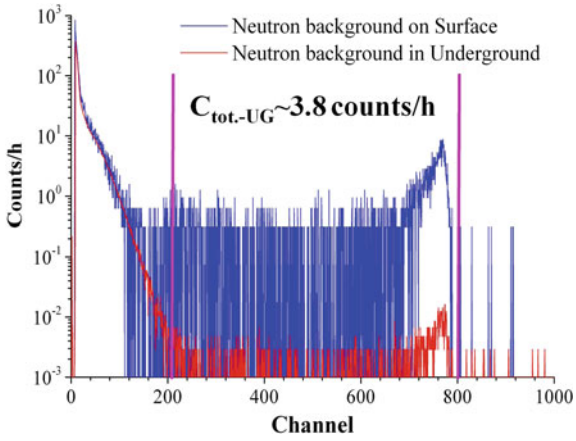

Fig. 58.2 Neutron spectrum acquired on surface (blue line) and in the underground laboratory of LNGS (red line)

in the signal region of interest. Approx. 3.7 counts/h is determined as a counting rate in the region of interest underground, which is caused by the alpha particles emitted by radioactive impurities of the detector materials and neutrons from the laboratory environment.

58.4 Summary and Outlook

In this paper the LUNA neutron detector array using ^{3}He counters is introduced. Two geometries are developed to cover the projectile energy region from $E_{\alpha,lab} = 400\,\text{keV}$ down to the Gamow window of the $^{13}\text{C}(\alpha,\text{n})^{16}\text{O}$ nuclear reaction. The experimental arrangements provide extremely low neutron background, which is mandatory to implement the cross section measurement with 10% required uncertainty. The data taking started at the beginning of 2018 and it is planned to be finished at the beginning of 2019 approaching the Gamow window of $^{13}\text{C}(\alpha,\text{n})^{16}\text{O}$.

Acknowledgements This work was partly supported by the Hungarian Scientific Research Fund NKFIH (K120666, NN128072).

References

1. R. Gallino et al., Astrophys. J. **497** (1998)
2. H. Drotleff et al., Astrophys. J. **414** (1993)
3. M. Heil et al., Phys. Rev. C **78** (2008). https://doi.org/10.1103/PhysRevC.78.025803
4. La Cognata et al., Phys. Rev. Lett. **109** (2012). https://doi.org/10.1088/0004-637X/777/2/143
5. A. M. Mukhamedzhanov, Shubhchintak and C. A. Bertulani, Phys. Rev. C 96 (2017). https://doi.org/10.1103/PhysRevC.96.024623
6. A. Formicola et al., Nucl. Instrum. Methods Phys. Res. A **507** 609–616 (2003)
7. L. Csedreki et al., EPJ Web of Conf. **165**, 01017 (2017). https://doi.org/10.1051/epjconf/201716501017
8. G.F. Ciani et al., EPJ Web of Conf. **165**, 01012 (2017). https://doi.org/10.1051/epjconf/201716501012

Chapter 59
On Barium Stars and the *s*-Process in AGB Stars

Borbála Cseh, Maria Lugaro, Valentina D'Orazi, Denise B. de Castro, Claudio B. Pereira, Amanda I. Karakas, László Molnár, Emese Plachy and Róbert Szabó

Abstract A new large set of homogeneous high resolution spectra of Barium (Ba) stars makes it now possible to compare the observational data from only one study with different AGB models. The Ba star data show an incontestable increase of the hs-type/ls-type element ratio (for example, [Ce/Y]) with decreasing metallicity. This trend in the Ba star observations is predicted by low mass, non-rotating AGB models where ^{13}C is the main neutron source.

59.1 Motivation

Barium stars are chemically peculiar giants and dwarfs with spectral classes from G to K. They show strong spectral features at the specific wavelenghts of elements heavier tha iron (e. g., Ba II at 4554 Å, Sr II at 4077 Å, [1]), which are synthesized in AGB stars through the *slow* neutron capture process. Based on radial velocity observations (e.g., [8, 9]) Ba stars belong to binary systems, in which the material formed in the interior of the primary star during the AGB phase is transferred to the companion. Since their spectra are easier to model than those of AGB stars, they are

B. Cseh (✉) · M. Lugaro · L. Molnár · E. Plachy · R. Szabó
Konkoly Observatory, Research Centre for Astronomy and Earth Sciences, Hungarian Academy of Sciences, Budapest 1121, Hungary
e-mail: cseh.borbala@csfk.mta.hu

M. Lugaro · A. I. Karakas
School of Physics and Astronomy, Monash Centre for Astrophysics, Monash University, Melbourne, VIC 3800, Australia

V. D'Orazi
INAF Osservatorio Astronomico di Padova, Vicolo dell Osservatorio 5, 35122 Padova, Italy

D. B. de Castro
Department for Astrophysics, Nicolaus Copernicus Astronomical Centre of the Polish Academy of Sciences, 00-716 Warsaw, Poland

C. B. Pereira
Observatorio Nacional, Rua General José Cristino, 77 Sao Cristovao, Rio de Janeiro, Brazil

A. Formicola et al. (eds.), *Nuclei in the Cosmos XV*, Springer Proceedings in Physics 219, https://doi.org/10.1007/978-3-030-13876-9_59

appropriate objects for testing AGB *s*-process nucleosynthesis models. Ba stars can be formed through two possible mass-transfer mechanisms: Roche-lobe overflow or wind accretion.

The efficiency of the *s* process has been measured using the abundances of the ls (light-*s*) and hs (heavy-*s*) indexes, taken as the average of different elements belonging to the first (Sr, Y, Zr) and second (Ba, La, Ce, Nd, Sm) *s*-process peaks, respectively. However, the availability and accuracy of the abundances of these elements vary in different studies. Using the largest set (182 stars) of homogeneous observational data of Ba stars published by de Castro et al. [4] we are moving forward from the use of ls and hs to directly use the available elements and to perform the first detailed error analysis [3].

59.2 Results and Conclusions

All of the available hs-type/ls-type element ratios show clear decreasing trend with increasing metallicity. This is in very good agreement with low mass AGB nucleosynthesis models and confirms that the ^{13}C is the main neutron source in AGB stars in the metallicity region $-0.8 < [Fe/H] < 0$ (Fig. 59.1). A spread of about a factor

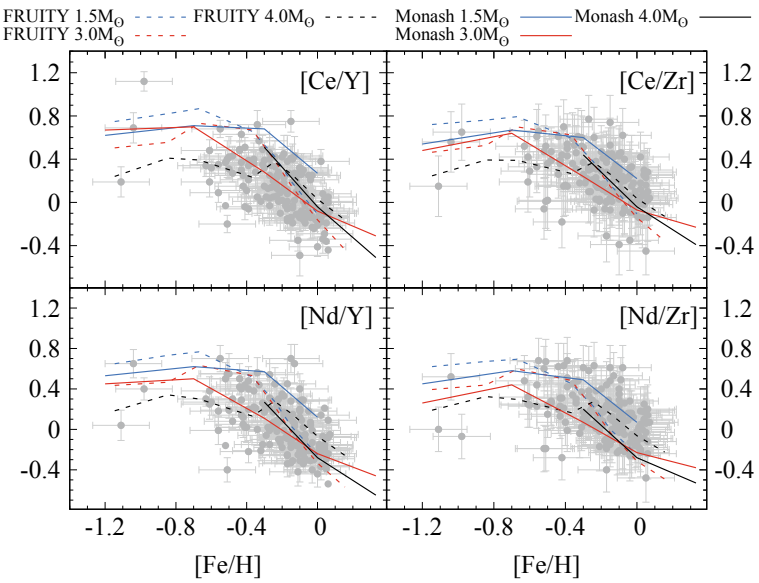

Fig. 59.1 Ba stars observations and final surface abundances of different AGB models for hs-type to ls-type element ratios as a function of metallicity. Monash label indicates the models from [5, 7], while FRUITY stands for models from [2]. The dots without error bars represent stars for which there are less than 3 lines for one of the elements

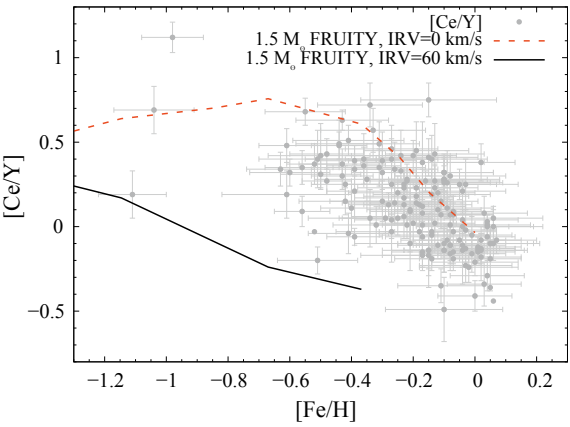

Fig. 59.2 Comparison for [Ce/Y] between the Ba stars and the 1.5 $M_{\odot}$ rotating and non-rotating (IRV = initial rotational velocity) FRUITY models [2, 10]. The dots without error bars represent stars for which there are less than 3 lines for one of the elements

of 3 is apparent in the data, indicating that other effects may be present, such as variations in the initial mass of the AGB, magnetic field or rotation.

Observations of the cores of red giant stars and of white dwarfs (the ancestors and the progeny of AGB stars, respectively) inferred via asteroseismology from Kepler observations show low core rotational velocities [6], which is in agreement with the results from the Ba star data and may derive from coupling between the core and the envelope (see Fig. 59.2).

Acknowledgements BCs, ML, LM, EP, and RSz acknowledge the support of the Hungarian Academy of Sciences (HAS) via the Lendület project LP2014-17. This project has also been supported by the Lendület Program of the HAS, project No. LP2018-7/2018 and by NKFIH grants K-115709, PD-116175, and PD-121203 and in part by the National Science Foundation under Grant No. PHY-1430152 (JINA Center for the Evolution of the Elements). LM and EP were supported by the János Bolyai Scholarship of the HAS. BCs and Vd'O acknowledge support from the ChETEC COST Action (CA16117), supported by COST (European Cooperation in Science and Technology). AIK acknowledges financial support from the Australian Research Council (DP170100521).

References

1. W.P. Bidelman, P.C. Keenan, ApJ **114**, 473 (1951)
2. S. Cristallo, O. Straniero, L. Piersanti, D. Gobrecht, ApJS **219**, 40 (2015)
3. B. Cseh et al., in preparation
4. D.B. de Castro et al., MNRAS **459**, 4299 (2016)
5. C.K. Fishlock, A.I. Karakas, M. Lugaro, D. Yong, ApJ **797**, 44 (2014)
6. J.J. Hermes et al., ApJS **232**, 23 (2017)
7. A.I. Karakas, M. Lugaro, ApJ **825**, 26 (2016)
8. R.D. McClure, ApJ **268**, 264 (1983)
9. R.D. McClure, J.M. Fletcher, J.M. Nemec, ApJ **238**, L35 (1980)
10. L. Piersanti, S. Cristallo, O. Straniero, ApJ **774**, 98 (2013)

Chapter 60
The $^{19}F(\alpha, p)^{22}Ne$ and $^{23}Na(p, \alpha)^{20}Ne$ Reactions at Energies of Astrophysical Interest via the Trojan Horse Method

G. D'Agata, Rosario Gianluca Pizzone, I. Indelicato, M. La Cognata, C. Spitaleri, V. Burjan, S. Cherubini, A. Di Pietro, P. Figuera, G. L. Guardo, M. Gulino, M. La Commara, L. Lamia, M. Lattuada, M. Mazzocco, J. Mrazek, M. Milin, Sara Palmerini, C. Parascandolo, D. Pierroutsakou, G. G. Rapisarda, S. Romano, M. L. Sergi, N. Soić, R. Spartá, O. Trippella and Aurora Tumino

G. D'Agata (✉) · V. Burjan · J. Mrazek
Ústav jaderné fyziky AV ČR, v.v.i, 250 68 Řež, Czech Republic
e-mail: g.dagata@lns.infn.it

G. D'Agata · R. G. Pizzone · I. Indelicato · M. La Cognata · C. Spitaleri · S. Cherubini · A. Di Pietro · P. Figuera · M. Gulino · L. Lamia · M. Lattuada · G. G. Rapisarda · S. Romano · M. L. Sergi · R. Spartá · A. Tumino
INFN - Laboratori Nazionali del Sud, Via Santa Sofia 62, 95123 Catania, Italy

C. Spitaleri · S. Cherubini · M. Lattuada · S. Romano
Dipartimento di Fisica e Astronomia, Università degli Studi di Catania, Via Santa Sofia 64, 95123 Catania, Italy

G. L. Guardo
ELI-NP, Str. Reactorului no. 30, P.O. BOX MG-6, Bucharest - Magurele, Romania

M. Gulino · A. Tumino
Facoltà di Ingegneria ed Architettura, Kore University, Viale delle Olimpiadi, 1, 94100 Enna, Italy

M. La Commara · C. Parascandolo · D. Pierroutsakou
INFN - Sezione di Napoli, via Cintia, 80125 Napoli, Italy

M. La Commara
Dipartimento di Scienze Fisiche, Università "Federico II", via Cintia, 80125 Napoli, Italy

M. Mazzocco
Dipartimento di Fisica e Astronomia, Università di Padova, Via Marzolo 8, 35131 Padova, Italy

INFN - Padova, Via Marzolo 8, 35131 Padova, Italy

M. Milin · N. Soić
Department of Physics, University of Zagreb, Bijenicka 32, Zagreb, Croatia

S. Palmerini · O. Trippella
Dipartimento di Fisica e Geologia, Università degli Studi di Perugia, via A. Pascoli s/n, 06123 Perugia, Italy

INFN-sezione di Perugia, via A. Pascoli s/n, 06123 Perugia, Italy

A. Formicola et al. (eds.), *Nuclei in the Cosmos XV*, Springer
Proceedings in Physics 219, https://doi.org/10.1007/978-3-030-13876-9_60

Abstract In AGB environment, Fluorine and Sodium production and destruction pathways are still not completely understood: their abundances are therefore still matter of debate. ^{19}F (only stable isotope of fluorine) abundance is strongly related to standard and extra-mixing processestype typical of the interior AGB-stars. Furthermore, the destruction channels for this element are far from being well understood. About ^{23}Na, its presence in Globular Clusters along with the well-known anticorrelation with oxygen, underline that this element has been produced in previous generations of stars: in particular, intermediate-mass AGB stars are one of the possible candidates for its production. For this reason we studied the ^{19}F(α,p)^{22}Ne and ^{23}Na(p, α)^{20}Ne reactions in the energy range of relevance for astrophysics via the Trojan Horse Method (THM), using the three-body reactions ^{6}Li(^{19}F, p^{22}Ne)d and ^{23}Na (d, pn)^{20}Ne.

60.1 Introduction

^{19}F has been clearly observed in AGB stars [1]. This element can be destroyed via ^{19}F(n,γ)^{20}F, ^{19}F(p,α)^{16}O [2, 3], and ^{19}F(α,p)^{22}Ne. Therefore in the He-intershell region, where α-particles are abundant, the ^{19}F+α reaction is expected to dominate over the competitive reaction. Looking at the destruction chains of reactions, Fluorine abundance is really sensitive to the physical condition of the stars, and can be used to clarify if stellar interior nucleosynthesis is well understood or not [4, 5]: its abundance can not be reproduced by the up-to-date models, and a possible reason of that can be found in the large uncertaities at He-burning temperatures ($0.2 \leq T_9 \leq 0.8$). Furthermore, few data about the cross-section in the energy region of astrophysical interest were present in literature before this experiment (results published in [6, 7]): The Gamow peak, in fact, lies between 0.2 and 1.2 MeV, while there are no direct measurements below 0.7 MeV. The Coulomb barrier effects strongly suppress such low energies reactions, and indirect methods such as the Trojan Horse Method (THM) [8] can be a powerful tool to overcome the difficulties related to the height of the Coulomb barrier itself.

As regard the ^{23}Na(p, α)^{20}Ne, this reaction is considered to have great importance in intermediate-mass AGB stars ($M = 4-8\ M_{\odot}$), and could be strongly related to the wide known Na/O anticorrelation in globular clusters [10]. This reaction also represents the turning point between the NeNa and MgAl cycles. ^{23}Na(p, α)^{20}Ne has not been studied at astrophysical energies with direct methods in the energy range of astrophysical interest. Here the Gamow window lies between 50 and 200 keV, while the Coulomb barrier is at 2.57 MeV. Several states of ^{24}Mg were however studied [11], via the ^{23}Na(^{3}He, d)^{24}Mg transfer reaction at 20 MeV. Two resonant states at 37 and 138 keV were found: the former had a too low cross section to be studied (but uncertainties were reduced by a factor of 515), and the latter is still the bigger source of uncertainties (approximately a factor of 12) in the temperature region near $T \sim 70 \times 10^6$ K.

Table 60.1 THM reaction rate (R_{THM}) and its ratio versus the one resulting from [9] ($\frac{R_{THM}}{R}$), for several temperatures in units of 10^9 K

Temperature (10^9K)	Rate $\left(\frac{cm^3}{mol \times s}\right)$	$\frac{R_{THM}}{R}$
0.10	2.59×10^{-22}	1.08
0.20	6.00×10^{-14}	1.81
0.30	4.67×10^{-10}	3.71
0.40	1.11×10^{-7}	3.29
0.50	5.09×10^{-6}	1.66
0.60	1.14×10^{-4}	1.12

60.2 The $^{19}F(\alpha, p)^{22}Ne$: Experimental results

To study the $^{19}F(\alpha,p)^{22}Ne$ reaction, the THM was applied by using a ^6Li beam (6 MeV energy, 5 enA intensity) impinging on a ^7LiF target (150 μm thick), using the low energy lithium beam provided by the Ruđer Bošković Institute (Zagreb, Croatia). The set-up was composed by two ΔE-E telescopes (placed at 12.3°±7° and 32.3°±7°) made up using thin silicon detectors (82 mm^2 active surface, 15 μm and 9 μm thickness respectively) as ΔE stage and thick (500 μm each) Position Sensitive Detectors (PSDs) as E stage, both meant for deuteron particles detection. On the opposite side of the beam, other 3 PSD's with the same specifics are placed at 37.7°±12°, 81°±9° and 119.9°±11° and are devoted to proton detection. Using the THM prescriptions we were able to extract the two-body cross section from the three-body process, and we found an enhancement up to a factor of four in the Gamow region (see Table 60.1 for reference) [7].

We were then able to estimate the contribution of the new cross section to low-mass AGB superficial abundance, using the NEWTON code [12] for three stellar models of 1.5, 3, and 5 $M_\odot$ and solar metallicity: The 5 $M_\odot$ AGB model appears to be most sensitive to the updated reaction rate values. In the 1.5 $M_\odot$ and the 3 $M_\odot$ models, whose He-shell burning temperatures do not exceed 2.9 and 3.2×10^8 K respectively, variations are much smaller. Once the ashes of the He-burning are brought into stellar surface by TDU, the nucleosynthesis products are diluted with envelope materials and the effects of the $^{19}F(\alpha, p)^{22}Ne$ reaction rate become negligible, and none of the studied cases shows a variation, in the ratio, larger than 5% [7].

60.3 The $^{23}Na(p, \alpha)^{20}Ne$: Preliminary Results

To study the $^{23}Na(p,\alpha)^{20}Ne$ reaction, the THM was applied using a brand new ^{23}Na beam (58 MeV energy, 0.8 enA intensity) delivered at Laboratori Nazionali del Sud. This beam impinged on a CD_2 target (deuterium acts as Trojan Horse nucleus due to its cluster structure p ⊕ n), inducing the $^{23}Na(d,pn)^{20}Ne$ three-body reaction. The

experimental setup consists in two symmetrical ΔE-E telescopes at small angles (centered at 6°) made by a PSD detector (500 μm thick) and a ionization chamber (filled with isobuthane at 50 mbar), and two symmetrical PSD at higher angles (centered at 25°, 1000 μm thick). After the selection of the heavy fragment (^{20}Ne) by means of the ΔE-E technique, the Q-value for the three-body process can be isolated and the quasi-free contribution of the ^{23}Na(p, α)^{20}Ne can be separated from the sequential decay. Once the channel is selected, an evaluation of the momentum distribution of the participant particle inside the Trojan Horse nucleus has been made. Its experimental behaviour follows a Hultén function (FWHM $\simeq$ 52 MeV/c), in agreement with literature [8]. The excitation function has also been considered, and structures consistent with the levels of the ^{24}Mg excited states in the energy region spanned by this experiment (11.5–13.5 MeV) are present. In the future, the half-of-energy-shell binary cross-section of interest will be extracted and the impact of this new measurement on the reaction rate will be evaluated.

Acknowledgements This publication was supported by OP RDE, MEYS, Czech Republic under the project SPIRAL2-CZ, CZ.02.1.01/0.0/0.0/16_013/0001679.

References

1. S. Lucatello, T. Masseron, J. Johnson et al., ApJ **729**, 40 (2011)
2. M. La Cognata, A. Mukhamezhanov, C. Spitaleri et al., ApJ L, **739**, L 54 (2011)
3. I. Indelicato, M. La Cognata, C. Spitaleri et al., ApJ **845**, 1 (2017)
4. M. Lugaro, C. Ugalde, A.I. Karakas et al., ApJ **615**, 934 (2004)
5. S. Cristallo, A. Di Leva, G. Imbriani et al., A&A **570**, 46 (2014)
6. R.G. Pizzone, G. D'Agata, M. La Cognata et al., ApJ **836**, 57 (2017)
7. G. D'Agata, R.G. Pizzone, M. La Cognata et al., ApJ **860**, 61 (2018)
8. C. Spitaleri, M. La Cognata, L. Lamia et al., Eur. Phys. J. A **52**, 77 (2016)
9. C. Ugalde, R.E. Azuma, A. Coutre et al., Phys. Rev. C **77**, 035801 (2008)
10. P. Ventura, F. D'Antona, MNRAS **410**, 2760–2766 (2011)
11. S.E. Hale, A.E. Champagne, C. Iliadis et al., Phys. Rev. C **70**, 045802 (2004)
12. O. Trippella, M. Busso, E. Maiorca et al., ApJ **787**, 41 (2014)

Chapter 61
The HEAT Project: Study of Hydrogen Desorption from Carbon Targets

Rosanna Depalo, Carlo Broggini, Antonio Caciolli, Alessandra Guglielmetti, Roberto Menegazzo and Valentino Rigato

Abstract HEAT (Hydrogen dEsorption from cArbon Targets) is a new project started in 2018 with the aim of studying the desorption of hydrogen and deuterium contaminations from carbon targets used for Nuclear Astrophysics studies, with special reference to the $^{12}C+^{12}C$ fusion reaction. $^{12}C+^{12}C$ fusion is the dominant process during stellar carbon burning and its cross section is a crucial parameter in modern astrophysics, given its strong influence on stellar evolution and nucleosynthesis. The direct measurements of the $^{12}C+^{12}C$ cross section performed so far were affected by a strong beam induced background due to the interaction of the carbon beam with hydrogen and deuterium contaminations inside the targets. The HEAT experiment aims at establishing a reproducible technique for hydrogen desorption from different types of carbon targets. The temperature of the samples will be increased uniformly up to 1200 °C through a heating device with a well defined temperature gradient. The contamination level will be measured before and after the desorption process exploiting ion beam analysis techniques.

R. Depalo (✉) · C. Broggini · A. Caciolli · R. Menegazzo
INFN - Sezione di Padova, Via Marzolo, 8 35131 Padova, Italy
e-mail: rdepalo@pd.infn.it

A. Caciolli
Dipartimento di Fisica eAstronomia, Università degli Studi di Padova,
Via Marzolo, 8 35131 Padova, Italy

A. Guglielmetti
Dipartimento di Fisica, Università degli Studi di Milano,
Via G. Celoria 16, 20133 Milano, Italy

Sezione di Milano, INFN, Via G. Celoria 16, 20133 Milano, Italy

V. Rigato
Laboratori Naizonali di Legnaro, INFN, Viale dell'Universitá 2, 35020 Legnaro, Italy

A. Formicola et al. (eds.), *Nuclei in the Cosmos XV*, Springer
Proceedings in Physics 219, https://doi.org/10.1007/978-3-030-13876-9_61

61.1 Introduction

The $^{12}C+^{12}C$ fusion reaction is a key ingredient in stellar modeling and a precise determination of is cross section is of paramount importance for a comprehensive understanding of stellar evolution and nucleosynthesis. A direct measurement of the $^{12}C+^{12}C$ cross section is especially needed at the energies of interest of hydrostatic carbon burning and type Ia supernova explosions, i.e. between 1 and 3 MeV in the center of mass [1, 2]. Literature direct measurements only extend down to 2.1 MeV [3, 4]. Moreover, a recent indirect experiment performed with the Trojan Horse Method has revealed the existence of several resonances in the Gamow window, highlighting the need for further direct measurements [5].

The main limitation found by experiments aiming at measuring the $^{12}C+^{12}C$ cross section below 2.5 MeV is the presence of a strong beam induced background due to the interaction of the carbon beam with hydrogen and deuterium contaminations inside the targets: $^{1}H(^{12}C,\gamma)^{13}N$, $^{2}H(^{12}C,p\gamma)^{13}C$ and the two-step process $^{2}H(^{12}C,{}^{2}H)^{12}C \rightarrow {}^{12}C(^{2}H,p\gamma)^{13}C$ [6]. A first quantitative study of deuterium desorption through irradiation with an intense ion beam has been recently published [7]. However, a more reproducible technique for target heating would help future experiments.

An investigation of the $^{12}C+^{12}C$ cross section will be performed at the Laboratory for Underground Nuclear Astrophysics (LUNA), in the framework of the LUNA-MV project. The Laboratory for Underground Nuclear Astrophysics is located at Gran Sasso National Laboratories (LNGS) and it is shielded against cosmic radiation by 1400 m of rock (3800 m of water equivalent) [8, 9]. This guarantees a six orders of magnitude reduction in the cosmic muon flux and a three orders of magnitude reduction in the neutron flux. As a consequence, the background in gamma ray and particle detectors is orders of magnitude lower compared to experiments at the Earth's surface [10–12].

The LUNA-MV project involves the installation of a 3.5 MV accelerator at the Gran Sasso deep underground laboratories and the $^{12}C+^{12}C$ reaction is among the first reactions that will be investigated at LUNA-MV. A deep underground measurement represents a unique opportunity to constraint the cross section of the $^{12}C+^{12}C$ reaction in the energy domain relevant for astrophysics, but in order to take full advantage of the underground location of the LUNA-MV experiment, ultra-pure carbon targets with low ^{1}H and ^{2}H contamination levels should be available.

61.2 The HEAT Project

HEAT (Hydrogen dEsorption from cArbon Targets) is a INFN-funded project started in February 2018 with the aim of establishing a reproducible technique for hydrogen desorption from different types of carbon targets.

Carbon targets will be heated up to 1200 °C through a heating device with a programmable temperature gradient. The heater and the target will be mounted on an orientable holder, allowing to perform Ion Beam Analysis in different geometries.

A water cooled target chamber has been especially designed for the HEAT project and is currently under construction. During the hydrogen desorption process, carbon samples will be heated to very high temperatures. In order to avoid overheating of the whole scattering chamber, the external surface of the chamber itself will be surrounded by a water cooling circuit.

Two arms will be installed on the scattering chamber: one at 30° and the other at 135° from the beam axis. These extensions will host the charged particle detectors for IBA (see Fig. 61.1).

The hydrogen contamination level in the samples will be measured before and after the desorption process exploiting two independent techniques:

– Elastic Recoil Detection Analysis (ERDA) will allow to measure the surface ^{1}H contamination. It will be performed delivering a ^{4}He beam to the target mounted in grazing geometry and detecting the hydrogen nuclei scattered at 30°.
– Nuclear Reaction Analysis (NRA) will be performed exploiting the intense, broad resonance at 0.6 MeV in the $^{2}H(^{3}He,p)^{4}He$ reaction and it will allow us to investigate the deuterium content of the samples to higher depths then ERDA.

Measurements will be performed at the AN2000 accelerator of Legnaro National Laboratories (Italy). The aimed sensitivity is 1 atomic ppm of hydrogen, allowing to investigate hydrogen desorption in the outmost layers of the cleanest targets studied so far (i.e. Highly Oriented Pyrolytic Graphite, which has a hydrogen contamination level of about 50 atomic ppm in the first 10 μm and 0.3 atomic ppm in the bulk [13]).

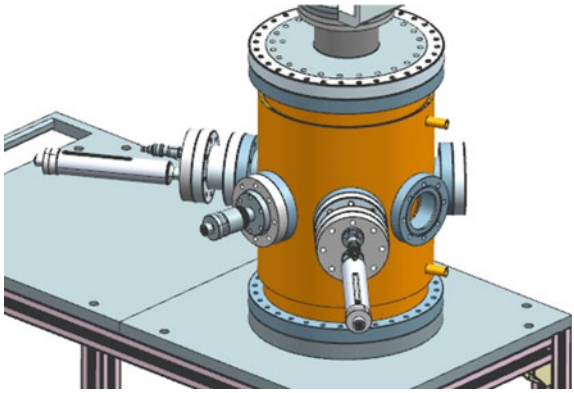

Fig. 61.1 Sketch of the scattering chamber designed for the HEAT experiment

References

1. O. Straniero et al., J. Phys.: Conf. Ser. **665**, 012008 (2016)
2. E. Bravo et al., Astr. Astrophys. **535**, A114 (2011)
3. L. Barrón-Palos et al., Nucl. Phys. A **779**, 318 (2006)
4. T. Spillane et al., Phys. Rev. Lett. **98**, 122501 (2007)
5. A. Tumino et al., Nature **557**, 687 (2018)
6. J. Zickefoose et al., Phys. Rev. C **97**, 065806 (2018)
7. L. Morales-Gallegos, Eur. Phys. J. A **54**, 132 (2018)
8. C. Broggini et al., Prog. Part. Nucl. Phys. **98**, 55 (2018)
9. F. Cavanna and P. Prati Int. J. Mod. Phys. A **33**, 1843010 (2018)
10. A. Caciolli et al., Eur. Phys. J. A **39**, 179 (2009)
11. T. Szücs et al., Eur. Phys. J. A **44**, 513 (2010)
12. C. Bruno et al., Eur. Phys. J. A **51**, 94 (2015)
13. P. Reichart et al. Nucl. Instr. Meth. Phys. Res. B **249**, 286 (2006)

Chapter 62
Explosion of Fast Spinning Sub-Chandrasekhar Mass White Dwarfs

I. Domínguez, R. M. Cabezón and D. García-Senz

Abstract We study the explosion of rotating sub-Chandrasekhar mass white dwarfs using three-dimensional hydrodynamic simulations. High rotational speeds are assumed in order to significantly distort the initial spherical geometry of the white dwarf. Unlike spherically symmetric models, when He-ignition is located far from the spinning axis the detonation wave trains arrive asynchronously to the antipodes. Models considering different masses of the He-shell, He-ignition locations and rotational velocities are analyzed. We study independently both, the detonation of the He-shell, artificially avoiding carbon-ignition, and the complete detonation of the white dwarf. Our calculations support the viability of the Double Detonation mechanism when the white dwarf is spinning fast.

62.1 Introduction

Nowadays the number of progenitor scenarios invoked to explain the Type Ia Supernova (SNe Ia) explosions is uncomfortably high [1]. In several of these scenarios the explosion of a white dwarf (WD) comes after the deposition of a large amount of energy in a small region close to the center of the WD. Such a large energy concentration raises the density and the temperature so that carbon manages to fuse with itself fast enough to induce a steady detonation wave. The supersonic detonation consumes the core of the star, giving rise to the SNe Ia display. This is the explosion mechanism behind the Gravitational Confined Detonation [2] and sub-Chandrasekhar (SubCh)-mass models of SNe Ia [3]. In the particular case of the SubCh-mass explosions,

I. Domínguez (✉)
Universidad de Granada, 18071 Granada, Spain
e-mail: inma@ugr.edu

R. M. Cabezón
sciCORE, Universität Basel, 4056 Basel, Switzerland

D. García-Senz
Universitat Politècnica de Catalunya, 08019 Barcelona, Spain

Institut d'Estudis Espacials de Catalunya, 08034 Barcelona, Spain

A. Formicola et al. (eds.), *Nuclei in the Cosmos XV*, Springer
Proceedings in Physics 219, https://doi.org/10.1007/978-3-030-13876-9_62

the concentration of energy above the core is favored by the focussing of a Helium-detonation previously formed at the base of the accreted envelope of the WD. Thus, in the SubCh-mass models of SNe Ia the explosion of the WD is the result of the combined He and C-detonations, the former acting as a trigger of the latter. In this communication we investigate the robustsness of such Double Detonation explosion mechanism in fast spinning WDs. A more detailed discussion about this subject can be found in [4].

62.2 Models and Results

The explosions, of rotating white dwarfs with masses $\simeq 1$ $M_\odot$ have been simulated using the state-of-the-art Integral Smoothed Particle Hydrodynamics (ISPH) code S-PHYNX [5]. SPHYNX implements a nuclear alpha-network of 14 nuclei completed with the heavy-ion reactions $^{12}C+^{12}C$, $^{16}O+^{16}O$, and $^{12}C+^{16}O$. An implicit coupling between the nuclear reactions and the energy equation allows to follow all the combustion stages, including the nuclear statistical equilibrium (NSE) and the freeze-out of the reactions during the expansion of the burnt material [6]. Stable white dwarfs in rigid rotation were built usind the procedure described in [4]. Fast rotation, close to the centrifugal limit, was assumed so that the WD becomes an oblated spheroid. Table 62.1 summarizes the main features of the initial models considered in this work.

It was shown in [4] that the detonation of the He-shell alone would produce, if observed, an intermediate event between a Nova explosion and a Type Ia SNe. Most likely is, however, the complete detonation of the rotating WD, and these are the models A, B, C and D presented in Table 62.1. Our simulations show that the convergence of the He-detonation at the antipodes is strong enough to detonate the core in both non-rotating (A, C) and rotating (B, D) WDs. A typical sequence of the explosion is shown in Fig. 62.1, which depicts the temperature colormap of model B (igniting at 90^0 with respect the rotation axis) in an equatorial slice. The second and third snapshots do clearly show the emergence of an off-center Carbon-detonation which volatilizes the star a few tenths of second later. The kinetic energy of the explosion and nucleosynthesis match well with a standard SNe Ia explosion.

Table 62.1 Main features of the calculated models. IME and IGE are the intermediate mass and iron group elements, respectively

Model	M_{WD}	ρ_c	ω_x	$\Delta M_{\rm He}$	E_{kin}	IME	IGE	^{56}Ni
-	$M_\odot$	(10^7 g cm^{-3})	(rad/s)	$M_\odot$	(10^{51} erg)	$M_\odot$	$M_\odot$	$M_\odot$
A	0.9590	2.60	0.00	0.1068	1.09	0.36	0.45	0.37
B	1.0815	2.57	0.50	0.1140	1.26	0.38	0.53	0.43
C	1.1052	6.82	0.00	0.0520	1.40	0.23	0.79	0.74
D	1.1872	6.87	0.65	0.0532	1.48	0.26	0.83	0.78

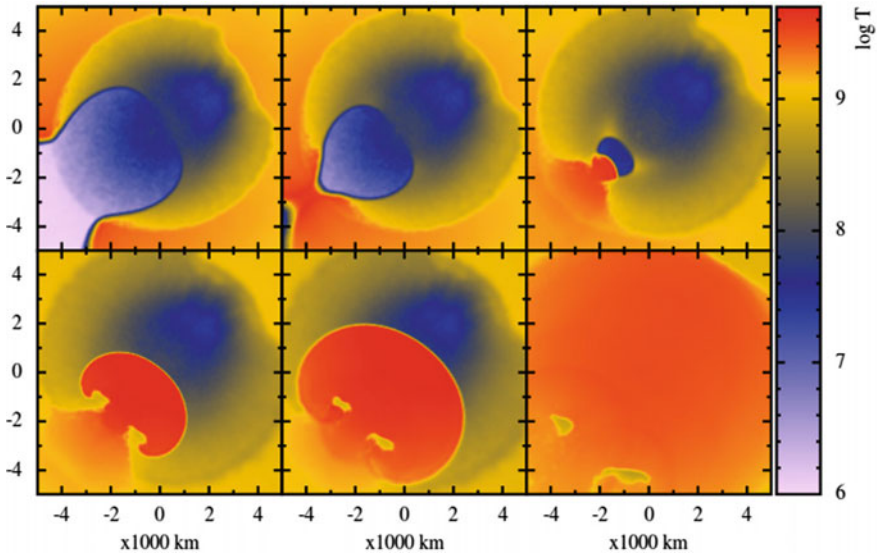

Fig. 62.1 Temperature colormap in an equatorial slice showing the core detonation of model B at t = 1.10, 1.22, 1.62, 1.72 and 2.03 s, respectively

Unlike spherically symmetric models, when helium ignition is located far from the spinning axis the detonation fronts converge asynchronically at the antipodes of the igniting point. Nevertheless, the detonation of the carbon core still remains as the most probable outcome. The detonation of the core gives rise to a strong explosion, matching most of the basic observational constraints of Type Ia Supernova. Therefore, we conclude that the Double Detonation mechanism also works when the white dwarf is spinning fast.

Acknowledgements This work has been supported by the MINECO Spanish projects AYA2017-86274-P and MINECO-FEDER AYA2015-63588-P, by the Generalitat of Catalonia SGR-661/2017 and the Swiss PASC project SPH-EXA. The authors acknowledge the support of sciCORE computing facility at University of Basel.

References

1. D. Maoz, F. Mannucci, G. Nelemans, Observational clues to the progenitors of type Ia supernovae. ARA&A **52**, 107–170 (2014). https://doi.org/10.1146/annurev-astro-082812-141031
2. T. Plewa, A.C. Calder, D.Q. Lamb, Type Ia supernova explosion: gravitationally confined detonation. ApJ **612**, L37–L40 (2004). https://doi.org/10.1086/424036
3. S.E. Woosley, T. Weaver, Sub-chandrasekhar mass models for type IA supernovae. ApJ **423**, 371–379 (1994). https://doi.org/10.1086/173813
4. García-Senz, D., Cabezón, R.M., Domínguez, I.: Surface and Core Detonation in Rotationg White Dwarfs. ApJ 862, 27 (16pp) (2018). https://doi.org/10.3847/1538-4357/aacb7d

5. R.M. Cabezón, D. García-Senz, J. Figueira, SPHYNX: an accurate density-based SPH method for astrophysical applications. A&A **606**, A78 (2017). https://doi.org/10.1051/0004-6361/201630208
6. R.M. Cabezón, D. García-Senz, E. Bravo, High-temperature combustion: approaching equilibrium using nuclear networks. ApJS **151**, 345–355 (2004). https://doi.org/10.1086/382352

Chapter 63
Low-Energy Resonances and Direct Capture Cross Section in the ^{22}Ne(p, γ)^{23}Na Reaction

Federico Ferraro

Abstract The ^{22}Ne(p, γ)^{23}Na reaction takes part in the neon-sodium (NeNa) cycle of hydrogen burning. The ^{22}Ne(p, γ)^{23}Na reaction rate was the most uncertain in the NeNa cycle because of a large number of uncertain resonances in the Gamow window. A new direct study of the ^{22}Ne(p, γ)^{23}Na reaction has been completed at the Laboratory for Underground Nuclear Astrophysics (LUNA), using a windowless gas target and two complementary setups. Three new resonances at 156.2, 189.5 and 259.7 keV have been discovered and their decay scheme has been determined both with a high-resolution setup and with a high-efficiency one. Improved upper limits have been put for the tentative resonances at 71 and 105 keV, making their contribution to the thermonuclear reaction rate almost irrelevant. The high-efficiency setup allowed the measurement of the non-resonant cross section at unprecedentedly low energies.

63.1 Introduction

In the innermost region of the convective envelope of massive asymptotic giant branch (AGB) stars, temperatures as high as $T = 0.1$ GK can be reached during the so-called hot bottom burning (HBB) process. In very massive stars, more advanced cycles of hydrogen burning are operating: the neon-sodium (NeNa) and magnesium-aluminum (MgAl) cycles [1, 2].

Galactic globular clusters are composed by hundreds of thousands of stars. While the abundance of the iron-group elements does not change among the stars in the same cluster, the abundance of lighter elements such as C, N, O, Na, Mg and Al shows large variations from star to star. In particular, an anti-correlation was observed between sodium and oxygen in stars on the red giant branch, where the ^{22}Ne(p, γ)^{23}Na

Federico Ferraro on behalf of the LUNA Collaboration.

F. Ferraro (✉)
Università degli Studi di Genova and INFN, Sezione di Genova,
Via Dodecaneso 33, 16146 Genova, Italy
e-mail: federico.ferraro@ge.infn.it

A. Formicola et al. (eds.), *Nuclei in the Cosmos XV*, Springer
Proceedings in Physics 219, https://doi.org/10.1007/978-3-030-13876-9_63

reaction plays a crucial role in the synthesis of sodium [3, 4]. The ^{22}Ne(p, γ)^{23}Na reaction rate has a sizable impact on the outcome of models seeking to reproduce such anticorrelation [1, 5]. This rate was very uncertain until recently, with a discrepancy of a factor of 1000 between the recommended rates from the NACRE [6] compilation, and the subsequent evaluations by Hale et al. [7], Iliadis et al. [8], and STARLIB [9]. The Laboratory for Underground Nuclear Astrophysics (LUNA) [10] recently studied this reaction, observing three new low-energy resonances with high-purity germanium (HPGe) detectors [11–14]. Two out of the three new ^{22}Ne(p, γ)^{23}Na resonance strengths were higher than the values or the upper limits previously obtained [6, 15] with indirect methods [7]. The existence of the two lowest out of the three new resonances at $E_p = 156.2$, 189.5, and 259.7 keV (E_p is the proton energy in the laboratory system) was recently independently confirmed in a surface-based experiment at the Triangle Universities Nuclear Laboratory (TUNL) [16]. In order to evaluate the thermonuclear reaction rate at very low temperatures, $T < 0.1$ GK, new measurements have been performed at LUNA, using a high-efficiency setup including a Bismuth Germanate (BGO) detector. In particular, the resonances at $E_p = 156.2$, 189.5, and 259.7 keV have been studied with high statistics, determining their strength and branching ratios. Two resonances at $E_p = 71$ and 105 keV, reported as tentative in an early indirect experiments [17] but not confirmed later [7, 18] have been investigated with high sensitivity. Moreover, the direct capture contribution as well as the contribution from broad resonances have been measured.

63.2 Experiment

63.2.1 Setup

A differential-pumping, extended gas target was used in combination with a $\sim 4\pi$ solid angle coverage, optically segmented BGO detector [19]. The 99.9% isotopically enriched ^{22}Ne was recycled and purified by a chemical getter which removes hydrocarbons, oxygen and nitrogen from the gas. Pressure and temperature measurements in several positions inside the chamber allowed the determination of the density profile of the target and the beam-heating effect was taken into account. The beam current was measured by a power compensation calorimeter with constant temperature gradient. Each segment of the detector is coupled to a PMT and independently digitized. Energy and time are saved for each event and offline coincidence analysis is possible.

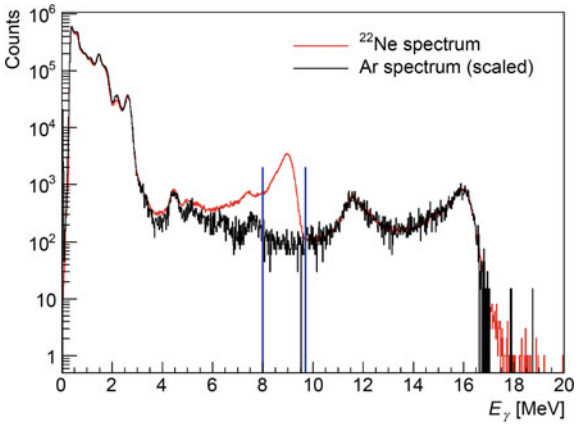

Fig. 63.1 189.5 keV resonance. Spectra obtained with ^{22}Ne (red) and Ar (black) target

63.2.2 Measurements

A yield curve was measured for each of the three previously observed resonances [11–14], varying the beam energy by 1–3 keV. Long runs were performed with a beam energy corresponding to the maximum of the yield curve, either with ^{22}Ne or argon inside the target chamber to properly subtract the beam-induced background as shown in Fig. 63.1. The singles spectra, gated on add-back counts in the region of interest were compared with GEANT4 [20] and GEANT3 [21] Monte Carlo simulations using the previously reported branching ratios [13, 19], showing good agreement. To investigate the existence of the suggested resonances at $E_p = 71$ and 105 keV, several long runs were performed at 63–78 and 95–113 keV, respectively. These resonances were not observed and upper limits were given on their strength. The off-resonance yield was measured at $E_p = 188.0$, 205.2, 250.0, and 310.0 keV, below or above the energies of known or supposed resonances, to study direct capture and the contribution by broad resonances.

63.3 Conclusion

The present strengths for the three recently observed resonances at $E_p = 156.2$, 189.5, and 259.7 keV are slightly higher than those from the LUNA-HPGe experiment [11–14] but consistent within 2 σ. Since the LUNA-HPGe experiment only measured the yield at two angles, the observed difference may be due to angular distribution effects, which do not play a significant contribution with the $\sim 4\pi$ solid angle coverage of the present LUNA-BGO experiment. The new thermonuclear reaction rate for the first time will take into account all the relevant processes at low energy. In particular, the contributions by non-resonant capture and the two suggested resonances at $E_p = 71$ and 105 keV are now based on direct experimental data [22].

References

1. A. Slemer et al., ^{22}Ne and ^{23}Na ejecta from intermediate-mass stars: the impact of the new LUNA rate for ^{22}Ne(p, γ)^{23}Na. Mon. Not. R. Astron. Soc. **465**(4), 4817–4837 (2017)
2. P.A. Denissenkov et al., The primordial and evolutionary abundance variations in globular-cluster stars: a problem with two unknowns. Mon. Not. R. Astron. Soc. **448**(4), 3314–3324 (2015)
3. E. Carretta et al., Na-O anticorrelation and HB. VII. The chemical com- position of first and second-generation stars in 15 globular clusters from GIRAFFE spectra. Astron. Astrophys. **505**, pp. 117–138 (Oct. 2009)
4. R.G. Gratton, E. Carretta, A. Bragaglia. Multiple populations in globular clusters. Lessons learned from the Milky Way globular clusters. Astron. Astrophys. Revs. **20**(50), 50 (Feb. 2012)
5. P. Ventura et al., Gas and dust from solar metallicity AGB stars. Mon. Not. R. Astron. Soc. **475**, 2282–2305 (2018)
6. C. Angulo et al., A compilation of charged-particle induced thermonuclear reaction rates. Nucl. Phys. A **656**, 3–183 (1999)
7. S.E. Hale et al., Investigation of the ^{22}Ne(p, γ)^{23}Na reaction via (^{3}He, d) spectroscopy. Phys. Rev. C **65**, 015801 (2001)
8. C. Iliadis et al., Charged-particle thermonuclear reaction rates: II. Tables and graphs of reaction rates and probability density functions. Nucl. Phys. A **841**, 31–250 (Oct. 2010)
9. A.L. Sallaska et al., STARLIB: A Next-generation Reaction-rate Library for Nuclear Astrophysics. Astrophys. J. Suppl. Ser. **207**(18), 18 (July 2013)
10. C. Broggini et al., LUNA: status and prospects. Prog. Part. Nucl. Phys. **98**, 55–84 (2018). ISSN: 0146-6410
11. F. Cavanna et al., A new study of the ^{22}Ne(p, γ)^{23}Na reaction deep underground: Feasibility, setup and first observation of the 186 keV resonance. Eur. Phys. J. A **50**(11), 179 (2014). ISSN: 1434-601X
12. F. Cavanna et al., Three New Low-Energy Resonances in the ^{22}Ne(p, γ)^{23}Na Reaction. Phys. Rev. Lett. **115**, 252501 (25 Dec. 2015)
13. R. Depalo et al., Direct measurement of low-energy^{22}Ne(p, γ)^{23}Na resonances. Phys. Rev. C **94**, 055804 (5 Nov. 2016)
14. D. Bemmerer et al., Effect of beam energy straggling on resonant yield in thin gas targets: The cases ^{22}Ne(p, γ)^{23}Na and ^{14}N(p, γ)^{15}O. EPL (Eur. Lett.) **122**(5), 52001 (2018)
15. C. Iliadis et al., Charged-particle thermonuclear reaction rates: III. Nuclear physics input. Nucl. Phys. A **841**, 251–322 (2010)
16. K. J. Kelly et al., New measurements of low-energy resonances in the ^{22}Ne(p, γ)^{23}Na reaction. Phys. Rev. C **95**, 015806 (1 Jan 2017)
17. J.R. Powers et al., Nuclear Structure of ^{23}Na: The ^{22}Ne(^{3}He, d) Reaction. Phys. Rev. C **4**, 2030–2046 (1971)
18. D.G. Jenkins et al., γ-ray spectroscopy of the A=23, T=1/2 nuclei ^{23}Na and ^{23}Mg: High-spin states, mirror symmetry, and applications to nuclear astrophysical reaction rates. Phys.Rev. C **87**(6) (2013) 064301
19. F. Ferraro et al., A high-efficiency gas target setup for underground experiments, and redetermination of the branching ratio of the 189.5 keV ^{22}Ne(p, γ)^{23}Na resonance. Eur. Phys. J. A **54**3, 44 (2018)
20. S. Agostinelli et al., GEANT 4 - a simulation toolkit. Nucl. Inst. Meth. A **506**, 250–303 (2003)
21. C. Arpesella et al., A Monte Carlo code for nuclear astrophysics experiments. Nucl. Inst. Meth. A **360**, 607–615 (1995)
22. F. Ferraro et al., Direct Capture Cross Section and the $E_p = 71$ and 105 keV Resonances in the ^{22}Ne(p, γ)^{23}Na Reaction. Phys. Rev. Lett. **121**, 172701 (17 Oct. 2018)

Chapter 64
Theoretical Calculation of the p-^{6}Li Radiative Capture

Alex Gnech and Laura Elisa Marcucci

Abstract The astrophysical S-factor for the ^{6}Li(p, γ)^{7}Be reaction is calculated in a cluster-model framework. The p-^{6}Li interaction is determined fitting elastic scattering data. Then the astrophysical S-factor is predicted, obtaining a nice agreement with the available experimental data. Moreover we try to include in our model the resonance presented in a recent experimental work.

64.1 Introduction

The ^{6}Li primordial abundance in the standard theory of Big Bang Nucleosynthesis (BBN) is in tension with results of recent measurements [1]. The ^{6}Li(p, γ)^{7}Be reaction can contribute to depletion of ^{6}Li. Therefore, the determination of astrophysical the S-factor of this reaction in the BBN energy window (50–400 keV) is fundamental in order to determine its contribution in the BBN reaction network.

In this work we treat the problem as a two-body problem, using phenomenological nuclear potentials to describe the ^{7}Be final nucleus and the initial p-^{6}Li scattering system. The parameters of the potential are fitted to p-^{6}Li elastic scattering data and to the bound states properties of ^{7}Be. Solving the two-body Schrödinger equation, we evaluate the wave functions for the scattering and the bound states, which we use to predict the S-factor of the radiative capture reaction. The final results are in nice agreement with the available experimental data at BBN energies.

A. Gnech (✉)
Gran Sasso Science Institute, 67100 L'Aquila, Italy
e-mail: alex.gnech@gssi.it

A. Gnech · L. Elisa Marcucci
Istituto Nazionale di Fisica Nucleare, sezione di Pisa, 56100 Pisa, Italy

L. Elisa Marcucci
Dipartimento di Fisica, Università di Pisa, 56100 Pisa, Italy

A. Formicola et al. (eds.), *Nuclei in the Cosmos XV*, Springer
Proceedings in Physics 219, https://doi.org/10.1007/978-3-030-13876-9_64

64.2 The Cluster Model

We consider proton and ^{6}Li as structureless particles. We build the wave functions using the prescriptions given in [2]. To describe the interactions between the clusters, we introduce an inter-cluster potential of the form,

$$V(r) = -V_0 \exp(-a_0 r^2), \tag{64.1}$$

where r is the inter-cluster distance. The parameters V_0 and a_0 are fixed in order to reproduce the binding energies of the ground state (GS) and the first excited state (FES) of the ^{7}Be separately. For the elastic scattering V_0 and a_0 are determined for each partial wave in order to reproduce the elastic scattering phase shifts reported in [2]. To take care of the electromagnetic repulsion we add a point-like Coulomb potential. The Schrödinger equation is solved using both the Numerov and the R-matrix method [3], in order to check the accuracy of the calculated wave functions.

64.3 The Astrophysical S-Factor

The main contribution to the ^{6}Li(p, γ)^{7}Be S-factor comes from the electric dipole ($E1$). The ^{7}Be has the GS with $J^\pi = 3/2^-$, and the FES with $J^\pi = 1/2^-$, both with spin 1/2. Because of the structure of the electromagnetic operator in the long wavelength approximation, the total spin in the transition is conserved. For this reason only the spin 1/2 waves in the ^{6}Li + p system will give contributions. Thus, the only waves that contribute to the $E1$ transition up to $L = 2$ are in spectroscopic notation $^2S_{1/2}$, $^2D_{3/2}$ and $^2D_{5/2}$ for the GS, and $^2S_{1/2}$ and $^2D_{3/2}$ for FES. By using these waves, we obtain for the S-factor the dashed line in Fig. 64.1. (we named it S_{bare}) As the reader can observe, even if the energy-dependence seems to agree with the Switkowski data [5], the S-factor results systematically lower compared to the data. The reason is that our model does not consider the internal structure of ^{6}Li and ^{7}Be. In order to correct for this effect, we introduce a spectroscopic factor $\mathcal{S}$ redefining the S-factor as,

$$S(E) = \mathcal{S}^2 S_{\text{bare}}(E). \tag{64.2}$$

We fitted the spectroscopic factor on the Switkowski data only [5], because the He data [4] are still under debate. The final result is the full line shown in Fig. 64.1. From the fit we obtain a $\mathcal{S} = 1.063$ with a $\chi^2/N = 1.04$. The value of the S-factor obtained at zero energy is $S(0) = 103$ eV b in line with the results of [6, 7].

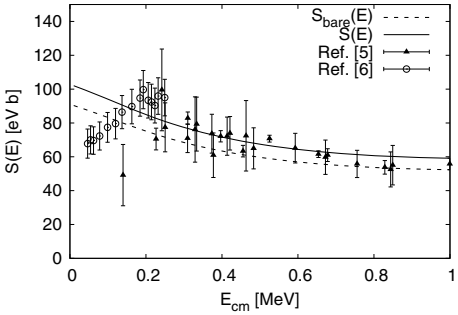

Fig. 64.1 The astrophysical S-factor for the ^{6}Li(p, γ)^{7}Be radiative capture. The dashed line is the bare calculation. The full line is the S-factor normalized with the spectroscopic factor evaluated to reproduce the data of [5]

64.4 The "He Resonance" in the Cluster Model

In [4] the authors suggest the presence of a resonance structure with $J^\pi = 1/2^+$ or $3/2^+$ with energy $E_r = 145$ MeV and width $\Gamma_r = 50$ keV. We try to introduce this contribution in our calculation. The best result is obtained supposing that the resonance is present in the $^4S_{3/2}$ wave, that couples with a tiny component of spin 3/2 in the ^{7}Be. In this way the $E1$ operator can couple the $^4S_{3/2}$ wave to the $^4P_{3/2}$ component in the GS of ^{7}Be. If we consider that the $^4P_{3/2}$ represents only the 0.01% of the total ^{7}Be GS wave function, we are able to reproduce the data of [4] quite well. The result we obtain is shown in Fig. 64.2, and it is very similar to the R-matrix fit reported in [4]. On the other hand the effect on the $^4S_{3/2}$ phase shifts is dramatic. This is shown on the right panel of Fig. 64.2, from which we can conclude the introduction of the $^4S_{3/2}$ resonance improves the description of the S-factor data of [4] but is unable to reproduce the elastic phase shift.

It is worth to note that we have tried to introduce the resonance also through the $^2S_{1/2}$ and the $^4D_{3/2}$ without obtaining any significant improvement in the description

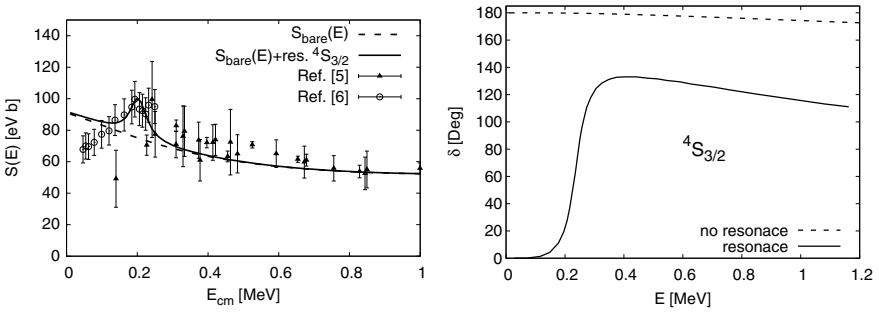

Fig. 64.2 On the left, the S-factor evaluated adding the resonance in the $^4S_{3/2}$ wave (full line) compared with the bare calculation (dashed line). On the right, the elastic phase shifts with the resonance (full line) and the elastic phase-shift evaluated fitting the data (dashed line)

of the data of [4]. Then we can conclude that, if a resonance exists, it cannot be handle by a simple two cluster-model.

References

1. M. Asplund et al., Astrophys. J. **644**, 229 (2006)
2. S.B. Dubovichenko et al., Phys. Atom. Nucl. **74**, 1013 (2011)
3. P. Descouvemont, D. Baye, Rep. Prog. Phys. **73**, 036301 (2010)
4. J.J. He et al., Phys. Lett. B **725**, 287 (2013)
5. Z.E. Switkowski et al., Nucl. Phys. A **331**, 50 (1979)
6. F.C. Barker, Aust. J. Phys. **33**, 159 (1980)
7. K. Arai, D. Baye, P. Descouvemont, Nucl. Phys. A **699**, 963 (2002)

Chapter 65
Indirect $(n, \gamma)^{91,92}$Zr Cross Section Measurements for the s-Process

M. Guttormsen, S. Goriely, A. C. Larsen, A. Görgen, T. W. Hagen, T. Renstrøm, S. Siem, N. U. H. Syed, G. Tagliente, H. K. Toft, H. Utsunomiya, A. V. Voinov and K. Wikan

Abstract Nuclear level densities (NLDs) and γ-ray strength functions (γSFs) of ^{91,92}Zr have been extracted from particle-γ coincidences using the Oslo method. The extracted γSF data, combined with photonuclear cross sections, cover the whole energy range from $E_\gamma \approx 1.5$ MeV up to the giant dipole resonance at $E_\gamma \approx 17$ MeV. The wide-range γSF data display structures at $E_\gamma \approx 9.5$ MeV, compatible with a superposition of the spin-flip $M1$ resonance and a pygmy $E1$ resonance. Furthermore, the γSF shows a minimum at $E_\gamma \approx 2$–3 MeV and an increase at lower γ-ray energies. The experimentally constrained NLDs and γSFs are shown to reproduce known (n, γ) and Maxwellian-averaged cross sections for ^{91,92}Zr using the TALYS reaction code, thus serving as a benchmark for this indirect method of estimating (n, γ) cross sections for Zr isotopes.

65.1 Introduction

The playground for the nucleosynthesis is found in the interior of stars and/or in extreme cosmic events. The major contributors to creating heavier elements are the neutron capture processes [1]. The key question for these processes is whether the

M. Guttormsen (✉) · A. C. Larsen · A. Görgen · T. W. Hagen · T. Renstrøm · S. Siem · N. U. H. Syed · H. K. Toft · K. Wikan
Department of Physics, University of Oslo, 0316 Oslo, Norway
e-mail: magne.guttormsen@fys.uio.no

S. Goriely
Institut d'Astronomie et d'Astrophysique, Université Libre de Bruxelles, Campus de la Plaine, CP-226, 1050 Brussels, Belgium

G. Tagliente
Istituto Nazionale di Fisica Nucleare, Bari, Italy

H. Utsunomiya
Department of Physics, Konan University, Okamoto 8-9-1, Higashinada, Kobe 658-8501, Japan

A. V. Voinov
Department of Physics and Astronomy, Ohio University, Athens, OH 45701, USA

A. Formicola et al. (eds.), *Nuclei in the Cosmos XV*, Springer Proceedings in Physics 219, https://doi.org/10.1007/978-3-030-13876-9_65

nuclear system after neutron absorption will keep the neutron and emitting γ rays to dissipate the energy, or will it eject the neutron or other particles/fragments and thereby producing other elements? For the *s*-process, this question is important at the so-called *branch points*, where the β^--decay rate is comparable with the (n, γ) rate.

65.2 Experiment and Methods

Nuclear level densities (NLDs) and γ-ray strength functions (γSFs) are essential quantities in estimating (n, γ) rates. At the Oslo cyclotron laboratory, we have extracted NLDs and γSFs for ^{91,92}Zr using the Oslo method [2]. The experiments [3] were performed with 17-MeV and 28-MeV proton beams for the ^{92}Zr$(p, p')^{92}$Zr and ^{92}Zr$(p, d)^{91}$Zr reactions, respectively. The target was a 2 mg/cm^2 thick metallic foil enriched to 95% in ^{92}Zr. The charged outgoing particles were measured with the SiRi system of 64 $\Delta E - E$ silicon telescopes with thicknesses of 130 and 1550 μm, respectively. The Si detectors were placed in forward direction covering $\theta = 42°$ to 54° relative to the beam. By setting 2-dimensional gates on the $(E, \Delta E)$ matrix, the outgoing charged ejectiles for the desired reaction were selected. Coincident γ rays for the residual ^{91,92}Zr were measured with the CACTUS array consisting of 28 collimated 5″ × 5″ NaI(Tl) detectors.

The energy distribution of first-generation or primary γ rays can be extracted from the unfolded total γ-ray spectra $U^E(E_\gamma)$ at an initial excitation energy E. Then the primary spectrum can be obtained by a subtraction of a weighted sum of $U^{E'}(E_\gamma)$ spectra for E' below E:

$$F^E(E_\gamma) = U^E(E_\gamma) - \sum_{E'<E} w_{E'} U^{E'}(E_\gamma). \tag{65.1}$$

The weighting coefficients $w_{E'}$ are determined by iteration [4]. The obtained primary spectra are organized into a matrix $P(E_\gamma, E)$. The next step of the Oslo method, is the factorization

$$P(E_\gamma, E) \propto \rho(E - E_\gamma)\mathcal{T}(E_\gamma), \tag{65.2}$$

where we assume that the decay probability is proportional to the NLD at the final energy $\rho(E - E_\gamma)$ according to Fermi's golden rule [5]. The decay is also proportional to the γ-ray transmission coefficient $\mathcal{T}$, which is assumed to be independent of excitation energy according to the Brink hypothesis [6].

65.3 Results and Conclusions

We have adopted the iteration procedure of Schiller et al. [2] in order to determine ρ and $\mathcal{T}$ by a least-χ^2 fit using relation (65.2). The transmission coefficient is connected to the γSF by $f(E_\gamma) = \mathcal{T}(E_\gamma)/2\pi E_\gamma^3$. The results for the NLDs and γSFs are shown in Fig. 65.1.

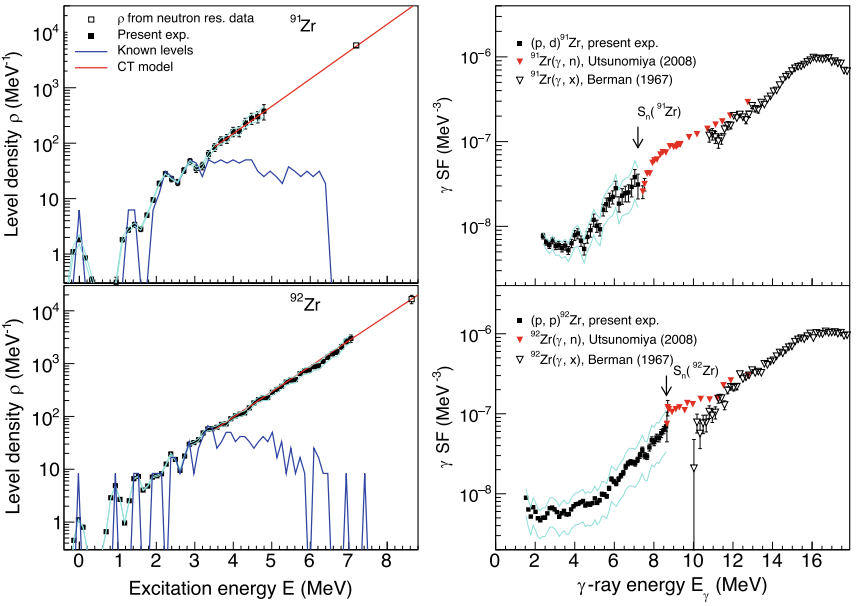

Fig. 65.1 Normalized NLDs of ^{91,92}Zr (left) and γSFs (right) extracted from the present experiment. At low excitation energies, the NLD data are normalized to known discrete levels (solid blue line). At higher excitation energies, the data are normalized to ρ at the neutron separation energy S_n using average neutron capture resonance spacing D_0. The γSFs are normalized to reproduce the average γ width $\langle \Gamma_\gamma \rangle$ for neutron capture states at S_n, and photoneutron data [7, 8]

The experimental NLDs and γSFs can now be tested on the additional experimental data relative to the radiative neutron capture cross sections ^{90}Zr$(n, \gamma)^{91}$Zr and ^{91}Zr$(n, \gamma)^{92}$Zr. A comparison of the experimentally known (n, γ) cross sections with the theoretical calculations obtained with the TALYS reaction code using the measured NLD and γSF is very gratifying. A similar comparison is made for the Maxwellian-averaged cross sections, which reveal the same agreement.

We found that our indirect method of determining the MACS is fully compatible with direct measurements, giving confidence that this approach is capable of providing reasonable cross sections for cases where direct measurements are not available.

In conclusion, the experimentally constrained NLDs and γSFs are shown to reproduce known (n, γ) and Maxwellian-averaged cross sections for ^{91,92}Zr using the TALYS reaction code, thus serving as a benchmark for this indirect method of estimating (n, γ) cross sections and MACS for the Zr isotopes.

References

1. E.M. Burbidge et al., Rev. Mod. Phys. **29**, 547 (1957)
2. A. Schiller et al., Nucl. Instrum. Methods Phys. Res. A **447**, 494 (2000)
3. M. Guttormsen et al., Phys. Rev. C **96**, 024313 (2017)
4. M. Guttormsen et al., Nucl. Instrum. Methods Phys. Res. A **255**, 518 (1987)
5. E. Fermi, *Nuclear Physics* (University of Chicago Press, 1950)
6. D. M. Brink, Doctorial Thesis (Oxford University, 1955)
7. H. Utsunomiya et al., Phys. Rev. Lett. **100**, 162502 (2008)
8. B.L. Berman et al., Phys. Rev. **162**, 1098 (1967)

Chapter 66
Heavy Puzzle Pieces: Learning About the *i* Process from Pb Abundances

M. Hampel, Amanda I. Karakas, R. J. Stancliffe, Maria Lugaro and B. S. Meyer

Abstract We examine the observed heavy-element abundances of two types of objects that show enrichments in s-process elements but whose abundance patterns are generally incompatible with *s*-process predictions: CEMP-*i* stars and Pb-poor post-AGB stars, with representative metallicities around [Fe/H] ≈ -2.5 and [Fe/H] ≈ -1.3, respectively. We can explain these abundance patterns, including the puzzlingly low Pb abundances of post-AGB stars, as results of *i*-process nucleosynthesis. To do this we use nuclear-network calculations to study heavy-element production at different constant neutron densities up to $n = 10^{15}\,\mathrm{cm}^{-3}$. The constraints posed by measured Pb abundances in these objects, allow us to characterise the neutron densities and exposures of the process responsible for creating the observed heavy-element abundances.

66.1 Introduction

Most elements heavier than iron are formed by the slow (*s*) and rapid (*r*) neutron capture processes. However, it has become clear that a neutron capture process operating at neutron densities intermediate to the *s* and *r* process (*i* process, [1]) gives rise to its own characteristic abundance pattern. This *i*-process pattern is successful at reproducing observed heavy-element abundances that could not be explained previously,

M. Hampel (✉) · A. I. Karakas · M. Lugaro
School of Physics and Astronomy, Monash Centre for Astrophysics,
Monash University, Monash, VIC 3800, Australia
e-mail: Melanie.Hampel@monash.edu

M. Lugaro
Konkoly Observatory, Research Centre for Astronomy and Earth Sciences,
Hungarian Academy of Sciences, Budapest 1121, Hungary

B. S. Meyer
Department of Physics and Astronomy, Clemson University, Clemson, SC 29634-0978, USA

R. J. Stancliffe
Department of Physics & Mathematics, E. A. Milne Centre for Astrophysics, University of Hull,
Hull, SC HU6 7RX, UK

A. Formicola et al. (eds.), *Nuclei in the Cosmos XV*, Springer
Proceedings in Physics 219, https://doi.org/10.1007/978-3-030-13876-9_66

e.g. those of carbon-enhanced metal-poor (CEMP) stars that show enrichments of s- and r-process elements (CEMP-i, also CEMP-s/r; e.g. [2, 3]). The required high neutron densities may occur in the thermal pulses of metal-poor Asymptotic Giant Branch (AGB) stars as a result of proton ingestion episodes. However, the sites of the i process are as yet unknown.

The i process has also been suggested to be the source of peculiar heavy-element abundance patterns in Pb-poor post-AGB stars in the Small and Large Magellanic Clouds. These objects with [Fe/H] ≈ -1.3 and initial masses of 1–1.5$M_{\odot}$ show particularly low Pb abundances which are inconsistent with models of s-process nucleosynthesis and AGB evolution [4–7]. This discrepancy between observed and simulated Pb abundances was also found in Galactic post-AGB stars up to a metallicity of at least [Fe/H] $\lesssim -0.7$ [8].

In this work we present our simulations of heavy-element production by i-process nucleosynthesis with a special focus on the production of Pb. The comparison with observed abundances of CEMP-i and Pb-poor post-AGB stars allows us to learn about the thermodynamic properties of possible i-process sites.

We follow the methodology used by Hampel et al. [3] to study the production of heavy elements and the evolution of their abundances when exposed to different neutron densities up to $n = 10^{15}\,\mathrm{cm}^{-3}$. In contrast to [3] we do not run the simulations to heavy-element equilibrium, but explore different total neutron exposures in order to focus on the production of Pb at the end of the neutron-capture path. For details we refer the reader to [9].

66.2 Comparison to CEMP-i and Pb-Poor Post-AGB Stars

We compare the calculated abundance patterns to 16 CEMP-i stars with $-2.8 \leq$ [Fe/H] ≤ -1.8. These are the stars from the sample studied by [3, 10] with measured Pb abundances. Figure 66.1 shows the abundances of CEMP-i star LP625-44 compared to the results of our simulation with $n = 10^{13}\,\mathrm{cm}^{-3}$, which provides the best fit amongst our models at a neutron exposure of $\tau = 2.0\,\mathrm{mbarn}^{-1}$. Overall, the majority of CEMP-i stars can be well matched by simulations with $n = 10^{13} - 10^{14}\,\mathrm{cm}^{-3}$ as expected based on the results from [3]. The required neutron exposures for all stars lie between $\tau = 2.0 - 3.4\,\mathrm{mbarn}^{-1}$, except for one star whose high Pb overabundance requires a neutron exposure as high as $\tau = 6.0\,\mathrm{mbarn}^{-1}$ to match the observed abundances.

From [4–6, 8] we study 7 post-AGB stars with [Fe/H] ≤ -0.7. These are the stars with an upper limit on their Pb abundance that is well below the expected Pb overabundance from s-process models at their measured metallicity. Figure 66.2 shows the abundances of post-AGB star J004441 which can be reproduced best by our i-process model with $n = 10^{12}\,\mathrm{cm}^{-3}$ and $\tau = 1.14\,\mathrm{mbarn}^{-1}$. For comparison, models of AGB nucleosynthesis with different ^{13}C pockets are shown, which either (i) overproduce Pb by at least 1.5 dex or (ii) fail to reproduce the overabundances of the elements past the heavy s-process peak. Our i-process models provide better fits to the abundance patterns of the post-AGB stars without either of these problems. Interestingly, all of the best fits are provided by models with $n = 10^{11} - 10^{12}\,\mathrm{cm}^{-3}$

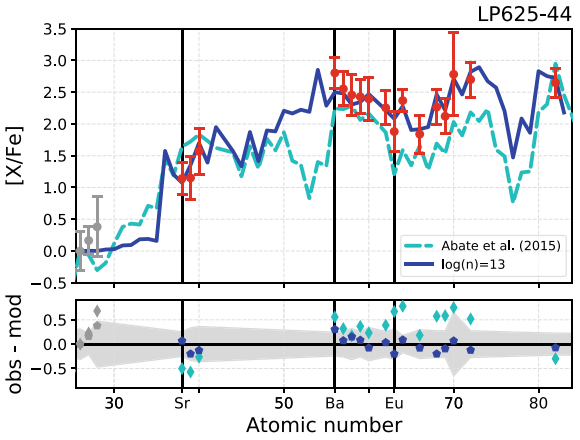

Fig. 66.1 CEMP-*i* star LP625-44 [11]: best fitting models from this work and from [10]. Figure from [9]

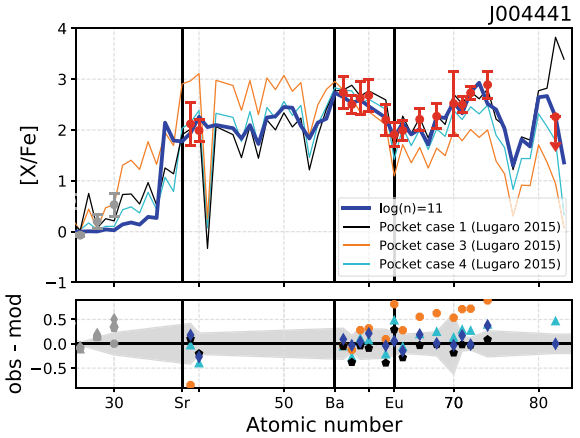

Fig. 66.2 Best fitting model for Magellanic post-AGB star J004441. For comparison, different s-process models from [7] are shown. Figure from [9]

and $\tau = 1.0 - 1.3\,\mathrm{mbarn}^{-1}$, which are considerably lower than the parameters that reproduce the CEMP-*i* abundance patterns.

66.3 Discussion and Conclusion

Our understanding of *s*-process nucleosynthesis has been challenged by the abundance patterns of CEMP stars with both Ba and Eu enhancements, as well as by the puzzlingly low Pb abundances in metal-poor post-AGB stars. *i*-process simulations provide much better fits than standard *s*-process models to these objects. However, the parameters that determine these fits, namely the neutron density n and exposure τ, cluster in different parts of the parameter space, where the fits of the post-AGB stars have lower n and τ than those of the CEMP-*i* stars. This shows that the *i*-process

which operates at different metallicities in the progenitors of these two different types of objects is not the same. While we do not have a good understanding of the progenitor responsible for the heavy-element production seen in CEMP-*i* stars (which is believed to be the companion in a binary system with the observed object) we know that the *i*-process nucleosynthesis seen in the post-AGB stars is a direct result of the low-mass star's previous evolution on the AGB.

References

1. J.J. Cowan, W.K. Rose, ApJ **212**, 149 (1977)
2. Dardelet, L., Ritter, C., Prado, P., et al. 2014, XIII Nuclei in the Cosmos (NIC XIII), 145
3. M. Hampel, R.J. Stancliffe, M. Lugaro, B.S. Meyer, ApJ **831**, 171 (2016)
4. K. De Smedt, H. Van Winckel, A.I. Karakas et al., A&A **541**, A67 (2012)
5. E. van Aarle, H. Van Winckel, K. De Smedt, D. Kamath, P.R. Wood, A&A **554**, A106 (2013)
6. K. De Smedt, H. Van Winckel, D. Kamath et al., A&A **563**, L5 (2014)
7. M. Lugaro, S.W. Campbell, H. Van Winckel et al., A&A **583**, A77 (2015)
8. K. De Smedt, H. Van Winckel, D. Kamath et al., A&A **587**, A6 (2016)
9. Hampel, M., et al., in prep (2018)
10. C. Abate, O.R. Pols, R.G. Izzard, A.I. Karakas, A&A **581**, A22 (2015)
11. W. Aoki, J.E. Norris, S.G. Ryan, T.C. Beers, H. Ando, ApJ **567**, 1166 (2002)

Chapter 67
Women Scientists Who Made Nuclear Astrophysics

Christine V. Hampton, Maria Lugaro, Panagiota Papakonstantinou, P. Gina Isar, Birgitta Nordström, Nalan Özkan, Marialuisa Aliotta, Aleksandra Ćiprijanović, Sanjana Curtis, Marcella Di Criscienzo, Jacqueline den Hartogh, Andreea S. Font, Anu Kankainen, Chiaki Kobayashi, Claudia Lederer-Woods, Ewa Niemczura, Thomas Rauscher, Artemis Spyrou, Sophie Van Eck, Mariya Yavahchova, William Chantereau, Selma E. de Mink, Etienne A. Kaiser, Friedrich-Karl Thielemann, Claudia Travaglio, Aparna Venkatesan and Remo Collet

Abstract Female role models reduce the impact on women of stereotype threat, i.e., of being at risk of conforming to a negative stereotype about one's social, gender, or racial group (Fine in Delusion of Gender. W.W. Norton & Co., NY, p. 36, 2010

C. V. Hampton (✉)
Hampton Consulting, LLC, Okemos, MI 48805, USA
e-mail: chrisvha@umich.edu

M. Lugaro · J. den Hartogh
Konkoly Observatory, Research Centre for Astronomy and Earth Sciences, Hungarian Academy of Sciences, Budapest 1121, Hungary
e-mail: maria.lugaro@csfk.mta.hu

P. Papakonstantinou
Rare Isotope Science Project, Institute for Basic Science, Daejeon 34047, South Korea

P. G. Isar
Institute of Space Science, 077125 Bucharest-Magurele, Romania

B. Nordström
Niels Bohr Institute, Blegdams vej 17, 2100 Copenhagen, Denmark

N. Özkan
Department of Physics, Kocaeli University, FI-40014 Umuttepe, Kocaeli, Turkey

M. Aliotta · C. Lederer-Woods
SUPA, School of Physics and Astronomy, University of Edinburgh, Edinburgh EH9 3FD, UK

A. Ćiprijanović
Department of Astronomy, Faculty of Mathematics, University of Belgrade, 11000 Belgrade, Serbia

S. Curtis
Department of Physics, North Carolina State University, Raleigh, NC 27606, USA

A. Formicola et al. (eds.), *Nuclei in the Cosmos XV*, Springer
Proceedings in Physics 219, https://doi.org/10.1007/978-3-030-13876-9_67

[1]; Steele and Aronson in J Pers Soc Psychol 69:797–811, 1995 [2]). This can lead women scientists to underperform or to leave their scientific career because of negative stereotypes such as, not being as talented or as interested in science as men. Sadly, history rarely provides role models for women scientists; instead, it often renders these women invisible (CafeBabel Homepage [3]). In response to this situation, we present a selection of twelve outstanding women who helped to develop nuclear astrophysics.

67.1 Introduction

Nuclear astrophysics is a melding of theoretical and experimental nuclear physics, observational astronomy, astrophysical modeling, and cosmological theory. It involves spectroscopic identifications, star classifications, prediction and discovery of stellar objects, construction of instrumentation, and chemical and physical interpretations. Women scientists have been an essential part of the development of these fields.

M. Di Criscienzo
INAF—Osservatorio Di Roma, via Frascati 33, Monteporzio Catone, 00078 Rome, Italy

A. S. Font · W. Chantereau
Astrophysics Research Institute, Liverpool John Moores University, Liverpool L3 5RF, UK

A. Kankainen
Department of Physics, University of Jyväskylä, PO Box 35 (YFL), 40014 Jyväskylä, Finland

C. Kobayashi · T. Rauscher
Centre for Astrophysics Research, University of Hertfordshire, Hatfield AL10 9AB, UK

E. Niemczura
University of Wroclaw, Kopernika 11, 51-622 Wroclaw, Poland

T. Rauscher · F.-K. Thielemann
Department of Physics, University of Basel, 4056 Basel, Switzerland

A. Spyrou
NSCL/JINA-CEE, Department of Physics and Astronomy, Michigan State University, East Lansing MI 48823, USA

S. Van Eck
Institut d'Astronomie et d'Astrophysique, Université Libre de Bruxelles, Brussels, Belgium

M. Yavahchova
Institute for Nuclear Research and Nuclear Energy, Bulgarian Academy of Sciences, Sofia, Bulgaria

67.2 Twelve Scientists

Marie Skłodowska Curie (1867–1934) chose to investigate radiation phenomena in 1896 for her Ph.D., and in doing so, explained the theoretical basis of radioactivity; developed methods for isolating radioactive isotopes; and discovered the elements Po and Ra [4]. Marie has the distinction of being the first female Nobel Laureate (Physics 1903; Chemistry 1911). Prof. Curie's outstanding achievements in Physics, Chemistry, Radiology, and Medicine; her humanitarian efforts in the throes of WWI; and her response to challenges will continue to inspire us for generations to come [5].

Lise Meitner (1878–1968) was the second woman at the University of Vienna to receive a doctorate in Physics and the first woman in Germany to become a full professor. Her most significant achievement was the theoretical explanation of nuclear fission [6]. She also discovered a number of radioactive isotopes together with Otto Hahn, with whom she collaborated for 30 years. Their discovery of Pa-231 was instrumental in establishing Protactinium as an element [7]. Prof. Meitner was nominated for the Nobel Prize 48 times (29 in Physics; 19 in Chemistry) [8].

Ștefania Mărăcineanu (1882–1944) after a teaching career in secondary schools in Romania, obtained a fellowship at the Radium Institute working with Marie Curie. In 1924, she defended her Ph.D. at the Sorbonne on the half-life of Po [9]. She also researched the interaction of Po radiation with metals. With this work she may have introduced the 'philosophical concept' of artificial radioactivity [10]. After her Ph.D., Dr. Mărăcineanu worked on developing techniques for atmospheric nucleation reactions; then returned to Romania in 1930 to install their first Radioactivity Laboratory.

Cecilia Payne Gaposchkin (1900–1979) worked as a human computer at the Harvard Observatory [11]. During her Ph.D., she made the discovery that the strength of stellar spectral lines depend not only on the stellar surface composition, but also on the degree of ionization at a given temperature. She was the first to conclude that

S. E. de Mink
Anton Pannekoek Institute for Astronomy, University of Amsterdam, Amsterdam, The Netherlands

E. A. Kaiser
Astrophysics Group, Keele University, Keele ST5 5BG, UK

F.-K. Thielemann
GSI Helmholtz Center for Heavy Ion Research, Darmstadt, Germany

C. Travaglio
Astrophysical Observatory Turin, INFN-Turin, Turin, Italy

A. Venkatesan
Department of Physics and Astronomy, University of San Francisco, San Francisco, CA 94117, USA

R. Collet
Stellar Astrophysics Centre, Department of Physics and Astronomy, Aarhus University, Aarhus, Denmark

hydrogen and helium are much more abundant in stars than all other elements [12]. Prof. Payne-Gaposchkin became the first female full-professor at Harvard's Faculty of Arts and Sciences and the first woman chair of a department at Harvard.

Maria Goeppert Mayer (1906–1972) Magic nucleon numbers, reflected in nuclear properties and in the observed solar abundances, had long puzzled physicists. In 1949, Maria devised a brilliant solution by coupling the nucleon spin with its orbital parameter [13]. She was hired for the Manhattan project, at the University of Chicago, and at Argonne National Laboratory. Prof. Mayer's work on magic numbers won her the Nobel Prize with Hans Jensen for their discoveries concerning nuclear shell structure.

Toshiko Yuasa (1909–1980) was Japan's first female nuclear physicist. She specialized in spectroscopy. In 1939 she won a French scholarship to work with Frédéric Joliot-Curie, resulting in a doctorate from the Collège de France on the continuous β-ray spectrum in artificial radioactive material. After WWII, Toshiko worked at Riken Nishina Center. She returned to France in 1949 to continue her nuclear research at CNRS. Her interests turned to reactions with synchrocyclotrons and in 1962, Prof. Yuasa earned a second doctorate from Kyoto University on the β decay of ^{6}He [14].

Georgeanne (Jan) R. Caughlan (1916–1994) studied nuclear data of reactions important for stars. Her very first efforts to provide extensive compilations of nuclear reaction rates based on current experimental information resulted in some of the most famous papers in the field [15]. Jan's career followed a very nontraditional path. After receiving a Physics degree, she dedicated herself to raising her five children. Prof. Caughlan earned her Ph.D. at the age of 48; became Professor of Physics at the age of 58; and then became Acting Dean of Graduate Studies at Montana State University.

Edith Alice Müller (1918–1995) obtained her Ph.D. in solar physics and worked on the observation and theory of the solar atmosphere. With her collaborators, L. Goldberg and L. H. Aller she published an extremely influential paper on the elements in the solar atmosphere which remained the gold standard for 20 years [16]. Edith was the first woman to be appointed General Secretary of the IAU. A named award in Prof. Müller's honor has been granted in 2018 to an outstanding Ph.D. thesis in Switzerland.

E. Margaret Peachey Burbidge (b. 1919) has played a central role in shaping nuclear astrophysics. Her early research focused on chemical abundances in stars. Her landmark 1957 paper [17] thrust the theory of stellar nucleosynthesis into the scientific spotlight. For her pioneering research, Margaret received 12 honorary degrees; was elected a Fellow of the Royal Society of London; and held many leadership positions, including becoming the first female president of the AAS. Prof. Burbidge is currently Professor Emeritus at the University of California, San Diego.

Erika Helga Ruth Böhm-Vitense (1923–2017) was the first scientist to accurately describe convective mixing in stellar interiors using a prescription that has been widely adopted for half a century now in all stellar evolutionary codes. Her 1958 paper [18] is a crucial contribution to "mixing-length" theory. She combined theory and observations in optical studies of a large variety of objects from helium stars, to super giants, to open clusters. Prof. Böhm-Vitense received the Annie Jump

Cannon Prize from AAS and the Karl Schwarzschild Medal from the Astronomische Gesellschaft.

Dilhan Ezer Eryurt (1926–2012) is regarded as the mother of Astronomy in Turkey; her life dedicated to science created a tremendous legacy. After completing her doctorate, she worked at Indiana University, NASA Goddard Space Flight Center, and the University of California. Her work revealed a striking fact about the Sun: it was much brighter and warmer in the past than it is today [19]. Prof. Eryurt received the 1969 Apollo Achievement Award; organized the first National Astronomy Congress in Turkey; founded the Astrophysics branch in Physics at the Middle East Technical University; and became Chair of the Department and Dean of the Faculty.

Beatrice Muriel Tinsley (1941–1981) was a true pioneer of the chemical evolution of galaxies. In her 1980 review article [20], we find her brilliant explanations of the modeling of galaxies and her predictions that are still pertinent today. With her Ph.D. dissertation awarded by the University of Texas in 1967, she started her journey into achieving international fame as a cosmologist. Her work was considered revolutionary with the discovery that the Universe was in a state of infinite expansion [21]. Prof. Tinsley was the first woman at Yale to advance to Professor of Astronomy.

67.3 Summary

We present role models for young scholars and encourage them to explore nuclear astrophysics as a potential career path. Our intent is also to remind the scientific community and to inform the general public about the significant role women have played and continue to play in the development of Nuclear Astrophysics. Our poster contains additional information and will be freely available for download from the ChETEC website (www.ChETEC.eu).

Acknowledgements This work is supported by ChETEC Action (CA16117) which is supported by COST (www.cost.eu). COST (European Cooperation in Science and Technology) is a funding agency for research and innovation networks. The work of PP was supported by RISP/IBS, funded by the Ministry of Science, ICT and Future Planning and the National Research Foundation of Korea (2013M7A1A1075764). The work of PGI was supported by the Romanian National Authority for Scientific Research and Innovation, CNCS/CCCDI-UEFISCDI, project numbers PN-III-P2-2.1-PED-2016-0339 and PN-III-P1-1-2-PCCDI-2017-0839 within PNCDI III.

References

1. C. Fine, *Delusion of Gender* (W.W. Norton & Co., NY, 2010), p. 36. ISBN 0-393-06838-2
2. C.M. Steele, J. Aronson, J. Pers. Soc. Psychol. **69**, 797–811 (1995). https://doi.org/10.1037/0022-3514.69.5.797
3. CafeBabel Homepage. http://www.cafebabel.co.uk/society/article/georgette-sand-when-history-makes-women-invisible.html. Last accessed 24 July 2018

4. M. Skłodowska Curie, vol 1, vol 2 (Gauthier-Villars, Paris 1910). https://doi.org/10.1038/086001a0
5. The Conversation Homepage. https://theconversation.com/us/topics/marie-curie-32867. Jorgensen, T. J., Last accessed 24 July 2018
6. L. Meitner, O.R., Frisch, Nature 143 (3615), 239 (1939). http://www.doi.org/10.1038/143239a0
7. Periodic Table of Elements: LANL. http://periodic.lanl.gov/91.shtml. Accessed 26 July 2018
8. Nobel Prize Website. https://www.nobelprize.org/nomination. Last accessed 26 July 2018
9. Ș. Mărăcineanu, Doctoral Thesis, p. 82 (Les Presses Universitaires de France, Paris, 1924)
10. M. Fontani et al., An International Journal of the History of Chemistry, Vol 1, No 1 (2017). https://riviste.fupress.net/index.php/subs/article/view/14
11. D. Sobel, *The Glass Universe* (Viking Press, NY, 2016)
12. C.H. Payne, Ph.D. Thesis (Radcliffe College, Harvard Observatory, Cambridge, MA 1925). http://adsabs.harvard.edu/abs/1925PhDT……1P
13. M. Goeppert-Mayer, Phys. Rev. **78**, 16 (1950). http://www.doi.org/10.1103/PhysRev.78.16
14. T. Yuasa, Doctoral Thesis (Kyoto University, 1962)
15. G.R. Caughlan, W.A. Fowler, At. Nucl. Data Tables **40**, 283 (1988). http://www.doi.org/10.1016/0092-640x(88)90009-5
16. L. Goldberg, E.A. Müller, L.H. Aller, ApJS **5**, 1 (1960)
17. E.M. Burbidge, G.R. Burbidge, W.A. Fowler, F. Hoyle, Rev. Mod. Phys. **29**(4), 547–650 (1957). http://www.doi.org/10.1103/RevModPhys.29.547
18. E. Böhm-Vitense, Zeitschrift für Astrophysik, **46**, 108–143 (1958). http://adsabs.harvard.edu/abs/1958ZA…..46..108B
19. D. Ezer, A.G.W. Cameron, Icarus, **1**, 422 (1963). http://www.doi.org/10.1016/0019-1035(62)90045-3
20. B.M. Tinsley, Fundam. Cosm. Phys. **5**, 287–388 (1980). http://www.doi.org/10.1086/149455
21. B.M. Tinsley, Nature **257**, 454–457 (1975). http://www.doi.org/10.1038/257454a0

Chapter 68
Presolar SiC Grains of Type AB with Isotopically Light Nitrogen: Contributions from Supernovae?

P. Hoppe, Marco Pignatari and S. Amari

Abstract Primitive solar system materials contain presolar grains that formed in the winds of evolved stars and in the ejecta of stellar explosions. Here, we report on NanoSIMS measurements of C-, N-, Al–Mg-, Si-, and S-isotopic compositions of 10 submicrometer-sized presolar SiC grains of Type AB from the Murchison meteorite. Except for one grain with the highest $^{12}C/^{13}C$ ratio we find good correlations between $^{12}C/^{13}C$, $^{14}N/^{15}N$, and $^{26}Al/^{27}Al$. The correlations are well explained by a 25 $M_{\odot}$ supernova (SN) model that considers H ingestion into the He shell. The comparison of our data with the SN model suggests that SNe might have contributed not only AB grains with heavy N, as suggested previously, but also some with light N.

68.1 Introduction

Primitive Solar System materials contain small amounts of presolar grains (e.g., SiC, graphite, oxides, silicates) which formed in the winds of evolved stars and in the ejecta of stellar explosions [1]. These pristine samples exhibit large isotope anomalies in major and minor elements, the fingerprints of nucleosynthesis and mixing processes

P. Hoppe (✉)
Max Planck Institute for Chemistry, Hahn-Meitner-Weg 1, 55128 Mainz, Germany
e-mail: peter.hoppe@mpic.de

M. Pignatari
E. A. Milne Centre for Astrophysics, University of Hull, HU6 7RX Hull, UK

S. Amari
McDonnell Center for the Space Sciences and Physics Department, Washington University, St. Louis, MO 63130, USA

M. Pignatari
NuGrid Collaboration, East Lansing, USA
URL: http://www.nugridstars.org

JINA-CEE, East Lansing, USA
URL: http://www.jinaweb.org/

Konkoly Observatory, Konkoly Thege Miklos ut 15-17, 1121 Budapest, Hungary

A. Formicola et al. (eds.), *Nuclei in the Cosmos XV*, Springer
Proceedings in Physics 219, https://doi.org/10.1007/978-3-030-13876-9_68

in their parent stars. SiC is the best studied presolar mineral. Based on C-, N-, and Si-isotopic compositions it can be divided into distinct populations. The origin of so-called SiC AB grains ($^{12}C/^{13}C \leq 10$, Si along the SiC mainstream line [1]) is still a matter of debate. Among the proposed stellar sources are supernovae (SNe) for grains with isotopically heavy N ($^{14}N/^{15}N < 440$) [2, 3], and born-again AGB stars [4] and especially J-type C stars for grains with isotopically light N ($^{14}N/^{15}N \geq 440$) [5].

Here, we report on measurements of C-, N-, Al–Mg-, Si-, and S-isotopic compositions of 10 SiC AB grains from the Murchison meteorite, conducted to explore whether H ingestion into the He shell of massive stars and SNe could have also contributed to the population of AB grains with isotopically light N.

68.2 Experimental Procedures

SiC AB grains from the Murchison separate KJD (median size 0.81 μm [6]) were identified based on their low $^{12}C/^{13}C$ ratios by C ion imaging with the NanoSIMS at MPI for Chemistry [7]. Subsequently, we acquired high-resolution (≤100 nm, Cs^+ and Hyperion O^- ion sources) ion images of C, N (measured as CN), Si, S, and Al–Mg isotopes of AB grains in multi-collection mode in three analysis sessions.

68.3 Results and Discussion

Except for one grain with the highest $^{12}C/^{13}C$ ratio we find good correlations between $^{12}C/^{13}C$, $^{14}N/^{15}N$, and $^{26}Al/^{27}Al$ for AB grains; 6 grains have isotopically heavy and 4 grains isotopically light N with $^{14}N/^{15}N$ up to 1000 (Figs. 68.1 and 68.2). An almost perfect 1:1 correlation between Al and N concentrations (Fig. 68.2) is suggestive of the presence of AlN and low levels of Al and N contamination. Magnesium is essentially monoisotopic ^{26}Mg from ^{26}Al decay (half life: 0.72 Myr). Silicon isotopes plot along the SiC mainstream line and S isotope anomalies are generally small.

We have compared our isotope data with predictions for SN models 25T-Hx by Pignatari et al. [2]. These 25 $M_\odot$ SN models consider H ingestion into the He/C zone during the pre-SN stage (H from 0.0024 to 1.2%) and artificially increased temperature and density in the He burning shell during explosion. Hydrogen ingestion and explosive nucleosynthesis leads to low $^{12}C/^{13}C$ and $^{14}N/^{15}N$, and high $^{26}Al/^{27}Al$ in the lower part of the He/C zone, called O/nova zone. The correlations between C, N, and Al are well explained by model 25T-H when matter from the O/nova zone and above (6.847–13.3 $M_\odot$) is mixed with matter from the H envelope that was partially lost during the pre-SN phase, as suggested by Liu et al. [3], and if the $^{12}C/^{13}C$ ratio

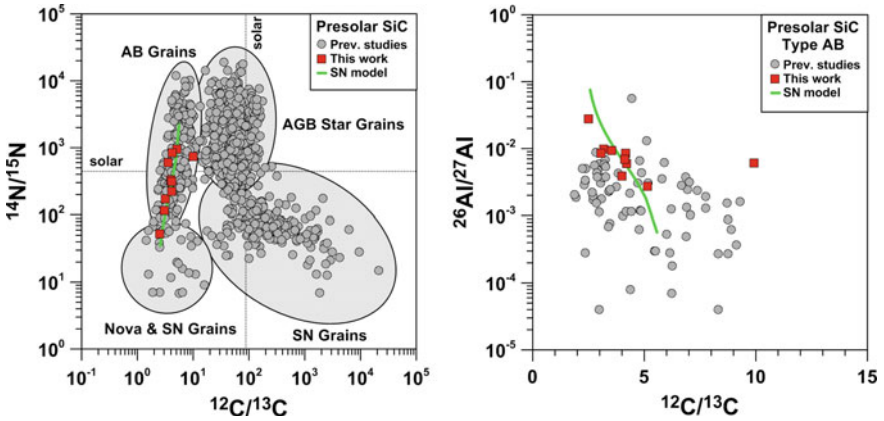

Fig. 68.1 Left: C- and N-isotopic compositions of presolar SiC grains. The AB grains of this study exhibit both light and heavy N and are well explained by the modified SN model 25T-H (green line). Right: $^{26}Al/^{27}Al$ and $^{12}C/^{13}C$ ratios of AB grains from this and previous studies and predictions from the same SN model as in the left figure. Data from previous studies are from [8]

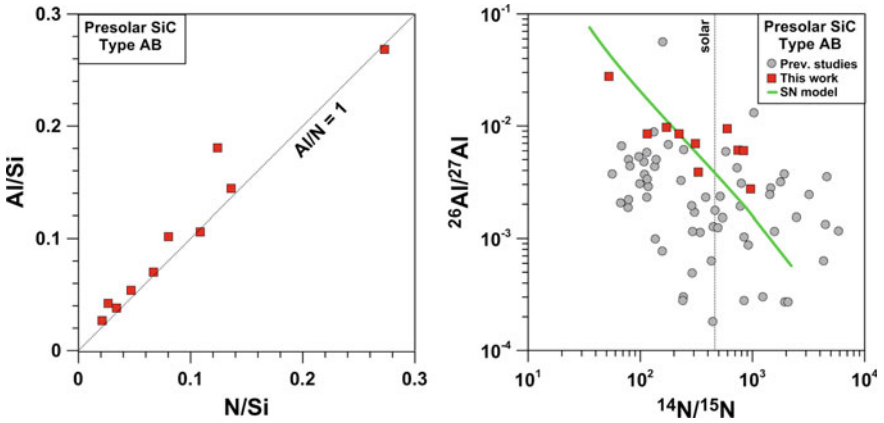

Fig. 68.2 Left: Concentrations of Al and N in SiC AB grains from this study. The data plot along the slope-1 line, suggestive of AlN and only low levels of Al and N contamination. Right: $^{26}Al/^{27}Al$ and $^{14}N/^{15}N$ ratios of SiC AB grains from this and previous studies and predictions from the same SN model as in Fig. 68.1. Data from previous studies are from [8]

in model 25T-H is decreased by a factor of 3. The comparison of our data with SN model 25T-H suggests that SNe potentially contributed both AB grains with heavy and light N.

References

1. E. Zinner, Presolar grains, in *Meteorites and Cosmochemical Processes, Treatise on Geochemistry*, vol. 1, ed. by A.M. Davis (Elsevier, Amsterdam, 2014), pp. 181–213
2. M. Pignatari, E. Zinner, P. Hoppe, C.J. Jordan, B.K. Gibson, R. Trappitsch et al., Carbon-rich presolar grains from massive stars: Subsolar $^{12}C/^{13}C$ and $^{14}N/^{15}N$ ratios and the mystery of ^{15}N. ApJ **808**, L43 (2015)
3. N. Liu, L.R. Nittler, M. Pignatari, C.M.O'D. Alexander, J. Wang, Stellar origin of ^{15}N-rich presolar SiC grains of type AB: Supernovae with explosive hydrogen burning. ApJ **842**, L1 (2017)
4. S. Amari, L.R. Nittler, E. Zinner, K. Lodders, R.S. Lewis, Presolar SiC grains of type A and B: Their isotopic compositions and stellar origins. ApJ **559**, 463–483 (2001)
5. N. Liu, T. Stephan, P. Boehnke, L.R. Nittler, C.M.O'D. Alexander, J. Wang et al.: J-type carbon stars: a dominant source of ^{14}N-rich presolar SiC grains of type AB. ApJ **844**, L12 (2017)
6. S. Amari, R.S. Lewis, E. Anders, Interstellar grains in meteorites: I. Isolation of SiC, graphite, and diamond; size distributions of SiC and graphite. GCA **58**, 459–470 (1994)
7. P. Hoppe, S. Cohen, A. Meibom, NanoSIMS: Technical aspects and applications in cosmochemistry and biological geochemistry. Geost. Geoanal. Res. **37**, 111–154 (2013)
8. K.M. Hynes, F. Gyngard, The presolar grain database: http://presolar.wustl.edu/~pgd. LPS 40, #1198 (2009)

Chapter 69
Alpha-Capture Reaction Rate for ^{22}Ne(α, n) via Sub-Coulomb α-Transfer and Its Effect on Final Abundances of s-Process Isotopes

H. Jayatissa, G. V. Rogachev, V. Z. Goldberg, E. Koshchiy, B. T. Roeder, O. Trippella, J. Hooker, S. Upadhyayula, E. Uberseder, A. Saastamoinen and C. Hunt

Abstract The ^{22}Ne(^{6}Li,d) reaction at sub-Coulomb energy was performed to measure partial α-widths of near α-threshold resonances in ^{26}Mg. New constrains on the ^{22}Ne(α,n) reaction rate have been obtained and consequences on the final abundances for some s-process isotopes are discussed.

69.1 Introduction

The ^{22}Ne(α,n) reaction is one of the two main sources of neutrons for the slow neutron capture nucleosynthesis process (s-process). The Gamow energy window for this reaction lies around $E_{c.m.} \sim 400$ to 700 keV at temperatures around 0.2–0.3 GK, which correspond to the conditions in AGB stars where this reaction is expected to be most effective. This energy window lies below the Coulomb barrier for the interacting particles. Therefore, direct measurements of this reaction cross section at these energies are challenging due to Coulomb suppression. Indirect techniques, such as α-transfer reactions, can be used instead to constrain the reaction rate. We have carried out the α-transfer ^{22}Ne(^{6}Li,d)^{26}Mg reaction, populating states at excitation energies around 10.4–11.3 MeV that dominate the ^{22}Ne(α,n) reaction rate. By using low sub-Coulomb energies in the entrance and exit channels of the α-transfer reaction the dependence of the result on the optical model potential parameters is reduced significantly.

H. Jayatissa (✉) · G. V. Rogachev · V. Z. Goldberg · E. Koshchiy · B. T. Roeder · S. Upadhyayula · J. Hooker · E. Uberseder · A. Saastamoinen · C. Hunt
Department of Physics & Astronomy and Cyclotron Institute, Texas A&M University, College Station, TX 7843, USA
e-mail: hesh@tamu.edu

O. Trippella
Department of Physics and Geology, Instituto Nazionale di Fisica Nucleare, Secion of Perugia, University of Perugia, Via A. Pascoli, 06123 Perugia, Italy

A. Formicola et al. (eds.), *Nuclei in the Cosmos XV*, Springer
Proceedings in Physics 219, https://doi.org/10.1007/978-3-030-13876-9_69

69.2 Analysis

The ^{22}Ne(^{6}Li,d) reaction has been studied previously at several beam energies above the Coulomb barrier [1–4]. This experiment, performed at the Cyclotron Institute at Texas A&M University, is the first sub-Coulomb measurement. A ^{22}Ne beam of energy 1 MeV/u was impinged on a 30 μg/cm^2 ^{6}LiF target on a 10 μg/cm^2 ^{12}C backing. This low beam energy ensured that both the entrance and exit channels of the reaction were below the Coulomb barrier. This reaction produced $\sim$ 7 MeV deuterons which were identified using the Multipole-Dipole-Multipole (MDM) spectrometer [5] placed at 5° from the beam axis. The magnetic field of the dipole was set so that the deuterons populating the states of ^{26}Mg within the Gamow window were selected. The deuterons were detected in the modified Oxford detector, located after the magnet, which consists of 4 proportional counter wires perpendicular to the path of the particles for track reconstruction, as well as a segmented MicroMegas pad and an array of 7 Cesium Iodide (CsI) detectors for dE and E signals respectively. Four distinct resonances were observed in the excitation energy spectrum of ^{26}Mg reconstructed using deuteron tracks in the Oxford detector (Fig. 69.1). These four resonances have excitation energies of 11.32, 11.10, 10.95 and 10.83 MeV. The absence of a background in this spectrum is attributed to the relatively thick entrance window of the Oxford detector which effectively stops all heavier ions with the same rigidity as the deuterons from entering the detector.

All of these four observed resonances are above the α-decay threshold of ^{26}Mg and have been observed previously. The 11.32 MeV state corresponds to the lowest resonance that was directly observed at 832 keV in the ^{22}Ne(α,n) reaction [6]. This

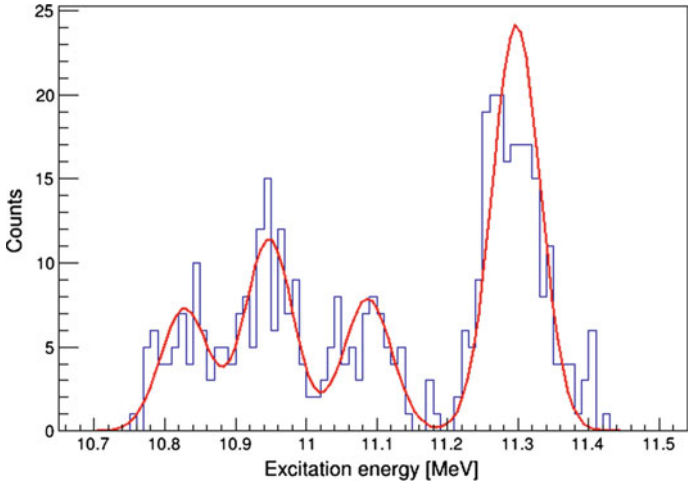

Fig. 69.1 Excitation energy spectrum of ^{26}Mg reconstructed using deuteron energies

resonance has the highest partial α width within the Gamow energy window and is the major contributor to the ^{22}Ne(α,n) reaction rate.

There have been numerous work done previously to determine the spins and parities of each of these resonances of ^{26}Mg using various techniques [1, 7–10], but there is still a significant uncertainty due to the extremely high level density of ^{26}Mg in this energy region. In the present work, due to low ^{22}Ne+^{6}Li c.m. energy, it is assumed that the transferred angular momentum for the α particle does not exceed $\ell = 2$. DWBA calculations indicate significant reduction of the α-transfer reaction cross sections for $\ell > 2$. Using 2 as an upper limit for transfered angular momentum, the partial α widths for all four observed states were calculated. In spite of sub-Coulomb energies, uncertainties for the extracted partial α-widths are still dominated by the parameters of optical model potential and correspond to about 30%. The optical model potentials were calculated for the relevant energy for deuterons and ^{6}Li using global fits [11, 12].

Assuming that the partial α-widths are small compared to the total widths of these states [13], the resonance strengths is given by $\omega\gamma \approx (2J + 1)\Gamma_\alpha$, where J is the resonance spin. It is important to note that the partial α width of the 11.3 MeV state in the present work results in a significantly smaller resonance strength (by a factor of 3) than reported in [6].

These resonance strengths were then used to calculate the rate of the ^{22}Ne(α,n) reaction in AGB stars. These were applied in NEWTON (Nucleosynthesis of Elements With Transfer Of Neutrons) code for a chosen stellar model at a temperature suitable for an AGB star to calculate the change of the abundances of isotopes created exclusively by the s-process. It was seen that the decrease of the reaction rate of the ^{22}Ne(α,n) reaction due to the smaller resonance strengths significantly effects the abundances of s-process only isotopes, in particular ^{152}Gd and ^{176}Lu. This further amplifies the importance of constraining the ^{22}Ne(α,n) reaction rate. More detailed analysis of astrophysical implications of the modified ^{22}Ne(α,n) reaction rate will be published elsewhere.

69.3 Conclusion

Sub-Coulomb α-transfer reactions provide a method to significantly reduce the dependence of the results on optical model parameters of near-threshold resonances for astrophysically important α-capture reactions. Indirect measurements performed in this work lead to smaller ^{22}Ne(α,n) reaction rate than the previously recommended [1], which in turn affects the abundances of s-process isotopes.

Acknowledgements This work was supported by the U.S. Department of Energy, Office of Science, under grant DE-FG02-93ER40773 and by the Welch Foundation (Grant No. A-1853).

References

1. R. Talwar et al., Phys. Rev. C. **93**, 055803 (2016)
2. U. Giesen et al., Nuclear Physics A **561**, 95–111 (1993)
3. C. Ugalde et al., Phys. Rev. C. **76**, 025802 (2007)
4. S. Ota et al., EPJ Web Conf. **66**, 07017 (2014)
5. D.M. Pringle et al., Nucl. Instr. Meth. Phys. Res. A **83**, 230–247 (1986)
6. M. Jaeger et al., Phys. Rev. Lett. **87**, 202501 (2001)
7. P. Adsley et al., Phys. Rev. C. **97**, 045807 (2018)
8. P. Adsley et al., Phys. Rev. C. **96**, 055802 (2017)
9. R. Longland et al., Phys. Rev. C. **80**, 055803 (2009)
10. C. Massimi et al., Phys. Lett. B **768**, 1 (2017)
11. J. Cook, Nuclear Physics A **388**, 153–172 (1982)
12. H. An et al., Phys. Rev. C. **73**, 054605 (2006)
13. K. Wolke et al., Z. Phys. A Hadrons and Nuclei **334**, 491–510 (1989)

Chapter 70
On the Activation Method for Stellar Cross-Sections Measurements: Flat Sample Correction in Measurements Relatives to Gold

P. Jiménez-Bonilla, J. Praena and J. M. Quesada

Abstract Maxwellian-averaged cross-sections (MACS) are needed for modelling s- and r-processes in stellar nucleosynthesis. In many cases MACS are experimentally obtained from measurements using the activation method with a quasi-maxwellian energy spectrum neutron flux, generated by the ^{7}Li(p,n)^{7}Be reaction at proton energy equal to 1912 keV. Due to the angular aperture of this neutron flux, neutrons experience different sample thickness, depending on its incident angle on the flat sample, so a correction is needed for absolute measurements. We propose an analytic expression for the calculation of this correction and we discuss its importance for measurements relatives to gold.

70.1 Introduction

Neutron capture reactions in r-process and s-process are responsible for the nucleosynthesis of the major part of the heavy elements beyond iron. The Maxwellian-averaged cross-section (MACS) or stellar cross-section of the involved isotopes is a key parameter for modeling s- and r-processes in these stellar sites [1, 2]. If the nucleus produced after neutron capture is unstable with a convenient half-life, an experimental spectrum-averaged cross section or SPA (that can be later corrected to a MACS) can be deduced measuring the induced gamma activity in the sample (activation technique). Usually the neutron flux is produced by the ^{7}Li(p,n)^{7}Be reaction at a proton energy E_p = 1912 keV. Then the neutron flux is kinematically collimated into a forward cone of 120 degrees opening angle, and its angle-integrated energy spectrum approximates a Maxwellian distribution at kT = 25 keV (a quasi-Maxwellian neutron spectrum or QMNS). Most measurements are carried out relatives to a reference: the sample is placed between gold foils, to obtain the neutron fluence or to cancel it in the expression of cross-sections ratio. Equations (70.1) and (70.2) show

P. Jiménez-Bonilla (✉) · J. M. Quesada
Atomic, Molecular and Nuclear Physics Department, University of Seville, Seville, Spain
e-mail: jimenezbpablo@gmail.com

J. Praena
Atomic, Molecular and Nuclear Physics Department, University of Granada, Granada, Spain

A. Formicola et al. (eds.), *Nuclei in the Cosmos XV*, Springer
Proceedings in Physics 219, https://doi.org/10.1007/978-3-030-13876-9_70

the traditional data analysis [3], where A is the total number of activated nuclei produced by the irradiation (that can be deduced from gamma activity), $\Phi = \int \phi(t)dt$ is the time integrated neutron flux, N is the number of atoms in the sample per area unit (at/b), and σ is the spectrum averaged capture cross section (SPA or SACS).

$$A_i = \sigma_i \cdot N_i \cdot \Phi \tag{70.1}$$

$$\sigma_i = \sigma_{Au} \cdot \frac{A_i \cdot N_{Au}}{A_{Au} \cdot N_i} \tag{70.2}$$

70.2 Flat Sample Correction

As seen in Fig. 70.1 left, neutrons experience different effective sample thickness depending on the emission angle. We can try to minimize this effect using a semi-spherical sample [4], otherwise we need to take into account this effect, by including a flat sample correction obtained by analytical calculation ((70.3) [5]), or by simulations [6–8]. In relative activation measurements, historically this effect has been neglected, considering that its value is practically the same for the sample and for the reference gold foils, and so it would cancel out. However, as shown in (70.3), the flat sample effect, affecting the number of activations A, is not only geometric, but its also depending on the sample cross section $\sigma(E)$. We have studied the k_f possible variation, first modelling the cross section by $\sigma(E) \sim E^{-a}$, with the exponent a ranging from 0.4 to 0.8 (valid for most isotopes). Results are shown in Table 70.1. With this modelling we observe up to 2% possible difference from the correction value for ^{197}Au ($k_{fAu} = 1.26$). However, higher differences are possible if the cross section shape is rather different from the gold one, for instance due to broad resonances (Fig. 70.1 right). We have calculated some k_f using ENDF/B-VII (E) cross sections

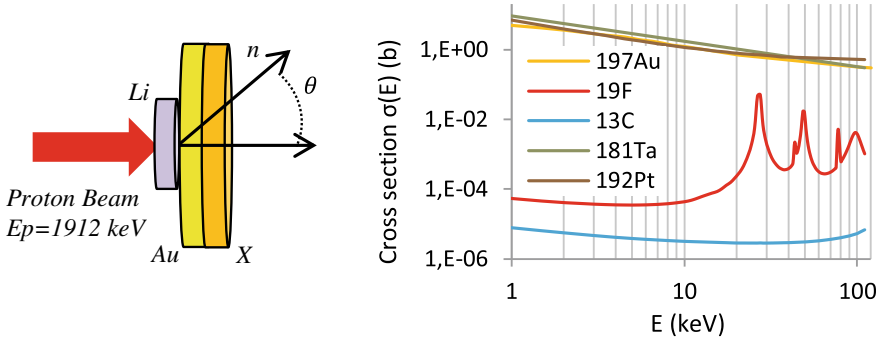

Fig. 70.1 Left: scheme of neutron different paths inside samples due to angular aperture. Right: ENDF/B-VII $\sigma(E)$ cross sections for several nuclei

Table 70.1 Values of k_f obtained with (70.3) modelling the cross section trend by $\sigma(E) \sim E^{-a}$, for exponent a ranging from 0.4 to 0.8

a	0.4	0.5	0.6	0.7	0.8
k_f	1.24	1.25	1.26	1.27	1.28

Table 70.2 k_f for several nuclei calculated with (70.3) and ENDF/B-VII cross sections

Nucl.	^{181}Ta	^{197}Au	^{176}Lu	^{192}Pt	^{19}F	^{13}C
k_f	1.27	1.26	1.26	1.24	1.21	1.11

(Table 70.2), and as an example we find differences of 4% for ^{19}F ($k_{f^{19}F} = 1.21$) and 12% for ^{13}C ($k_{f^{13}C} = 1.11$). We proposed then (70.4) as an alternative to (70.2) for data analysis:

$$k_f = \frac{A_{flat}}{A_{spheric}} = \frac{\int\int \sigma(E) \cdot \frac{1}{cos(\theta)} \cdot \phi(\theta, E) dE d\theta}{\int\int \sigma(E) \cdot \phi(\theta, E) dE d\theta} \tag{70.3}$$

$$\sigma_i = \sigma_{Au} \cdot \frac{A_i \cdot N_{Au} \cdot k_{fAu}}{A_{Au} \cdot N_i \cdot k_{fi}} \tag{70.4}$$

Neutron scattering into the materials may also increase the flat sample effect, especially if samples or backing are not thin enough. To include this effect its possible convenient to use also Montecarlo simulations [7]. When using the method proposed in [9] for a more accurate maxwellian neutron spectrum generation, as studied in [10] its possible to reduce the value and sensitivity of the k_f correction if the sample is placed further from the neutron source, covering a lower solid angle.

70.3 Conclusions

In neutron activation experiments using the quasi-maxwellian spectrum neutron flux to measure stellar cross sections, for absolute measurements a flat sample correction is needed, due to the experimental neutron flux angular aperture. We have studied its importance also for measurements relatives to gold, concluding that this correction could be relevant in some cases.

References

1. E.M. Burbidge, G.R. Burbidge, W.A. Fowler, F. Hoyle, Rev. Mod. Phys. **29**(4), 547–650 (1957)
2. I. Dillmann, R. Plag, F. Kppeler, A. Mengoni, C. Heinz, M. Pignatari, Proceedings of Science. NIC XIII **057**, (2014)

3. H. Beer, F. Kppeler, Phys. Rev. C **21**(2), 534544 (1980)
4. W. Ratynski, F. Kppeler, Phys. Rev. C **37**(2), 595604 (1988)
5. P. Jimenez-Bonilla, J. Praena, Proceedings of Science. NIC XIII **P102**, (2014)
6. G. Feinberg, M. Friedman, A. Krsa ed ad. Phys. Rev. C vol. 85, n 055810 (2012)
7. P. Jimenez-Bonilla, J. Praena and J.M. Quesada. IOP Conf. Series: J. Phys.: Conf. Series **940**, 012044 (2018)
8. R. Reifarth, M. Heil, F. Kppeler, Nucl. Instrum. Methods A **608**(1), 139–143 (2009)
9. J. Praena, P.F. Mastinu, G.Martin-Hernandez, Pub. of the Astro. Soc. of Australia **26**, 225 (2009)
10. P. Jimenez-Bonilla. Ph.D. Dissertation (University of Seville, 2018)

Chapter 71
Relative Importance of Convective Uncertainties

Etienne A. Kaiser, Raphael Hirschi, W. David Arnett, Andrea Cristini, Cyril Georgy and Laura J. A. Scott

Abstract Convection plays a key role in the evolution of stars due to energy transport and mixing of composition. Despite its importance, this process is still not well understood. One longstanding conundrum in all 1D stellar evolution codes is the treatment of convective boundaries. In this study we compare two convective uncertainties, the boundary location (Ledoux versus Schwarzschild) and the amount of extra mixing, and their impact on the early evolution of massive stars. With increasing convective boundary mixing (CBM), we find a convergence of the two different boundary locations, a decreasing blue to red super giant ratio and a reduced importance of semiconvection.

71.1 Introduction and Methodology

In the framework of the mixing-length theory (MLT) [1], the location of the convective boundary is not defined and has to be determined by either the Ledoux or the Schwarzschild criterion. In regions with a gradient in chemical composition, the two criteria differ, leading to a region mixed by semiconvection. The process responsible and the efficiency of this mixing is a matter of debate.

Another source of significant uncertainty emerges from the treatment of CBM which is not included in MLT. Several add-ons have been proposed to account for the mixing of the boundary region, however, CBM is still an open question.

E. A. Kaiser (✉) · R. Hirschi · L. J. A. Scott
Astrophysics Group, Lennard-Jones Laboratories, Keele University, Keele ST5 5BG, UK
e-mail: e.kaiser@keele.ac.uk

R. Hirschi
WPI Kavli-IPMU, University of Tokyo, Chiba, Kashiwa 277-8583, Japan

W. D. Arnett
Steward Observatory, University of Arizona, Tuscon 85721, USA

A. Cristini
Department of Physics and Astronomy, University of Oklahoma, Norman 73069, USA

C. Georgy
Geneva Observatory, University of Geneva, Ch. Maillettes 51, 1290 Versoix, Switzerland

A. Formicola et al. (eds.), *Nuclei in the Cosmos XV*, Springer
Proceedings in Physics 219, https://doi.org/10.1007/978-3-030-13876-9_71

We calculated 15 $M_\odot$, non-rotating stellar models at solar metallicity using the MESA stellar evolution code [2–5]. All stellar models are computed several times, once with the Schwarzschild and three times with the Ledoux criterion, the latter with varied semiconvective efficiency. In the Ledoux models, we use the semiconvective formalism from [6] (their (10)), with the adjustable efficiency parameter $\alpha_{\rm sc}$. In all models, we chose the exponentially decaying diffusive overshoot description ((2) from [7]) to account for CBM, with the adjustable parameter $f_{\rm CBM}$ which determines the length scale of CBM in pressure scale height.

71.2 Discussion

In general, the extra mixing, either by CBM or semiconvection, smooths out the gradients in temperature and chemical composition, stabilizing the region above the hydrogen core against dynamical and vibrational instabilities, as shown in Fig. 71.1. This reduces the differences between the two boundary criteria and they start to converge. Further distinctions are:

(i) CBM starts to appreciably change the structure already for a small value of $f_{\rm CBM}$ (>0.004).

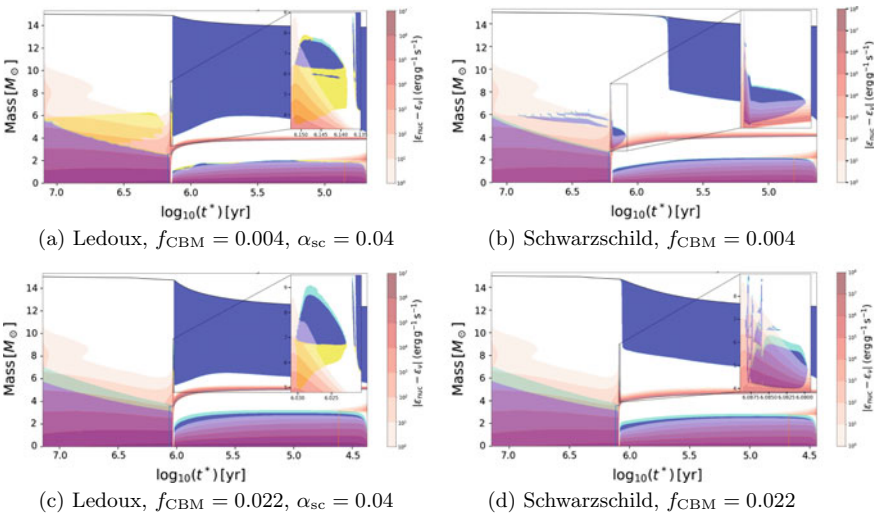

(a) Ledoux, $f_{\rm CBM} = 0.004$, $\alpha_{\rm sc} = 0.04$

(b) Schwarzschild, $f_{\rm CBM} = 0.004$

(c) Ledoux, $f_{\rm CBM} = 0.022$, $\alpha_{\rm sc} = 0.04$

(d) Schwarzschild, $f_{\rm CBM} = 0.022$

Fig. 71.1 Structure evolution diagrams, illustrating the convective and burning history until helium depletion of some of the stellar models. The x-axis shows the time left until the star begins to collapse. Blue shading indicates convective zones, turquoise shading the CBM region, yellow shading the semiconvective zones and the red gradient the nuclear energy generation rate (minus neutrino losses). The zoom shows the intermediate convective zone which is crucial to determine whether the model stays in the blue super giant (BSG) or crosses directly to the red super giant (RSG) branch

(ii) The greatest influence of semiconvection is for no or very weak CBM. 3D hydrodynamic simulation indicate a non-negligible amount of CBM [8], reducing the occurrence and thus the importance of semiconvection.
(iii) The size of the helium core, which is an indicator of the further stellar evolution, depends on the strength of the extra mixing. Generally, a higher amount of extra mixing results in larger helium cores.
(iv) The extra mixing increases the main-sequence width. Moreover, all the Ledoux models, and the Schwarzschild models with large amounts of CBM, cross the Herzsprung-Russel diagram directly towards the RSG branch whereas Schwarzschild models with no or less CBM spend time in the BSG branch.

71.3 Conclusion

This study illustrates the need to determine the amount of CBM, which might reduce the discrepancy in stellar evolution due to the different boundary locations. Moreover, the time a star spends in the BSG branch before entering the RSG branch depends strongly on the amount of extra mixing and the stability criterion. This has crucial influence on the mass loss. These uncertainties can be tackled with 3D hydrodynamic simulations and asteroseismology (e.g. [8–10]). We will investigate the impact on nucleosynthesis and the advanced burning stages in a future work.

Acknowledgements The authors acknowledge support from the ChETEC COST Action (CA16117), supported by COST (European Cooperation in Science and Technology). This research has made use of the NASA's Astrophysics Data System Bibliographic Services. RH and CG thank ISSI Bern for meeting support.

References

1. E. Böhm-Vitense, Z. Astrophys. **46**, 108 (1958)
2. B. Paxton, L. Bildsten, Dotter et al., ApJS 192, 3 (2001)
3. B. Paxton, M. Cantiello, P. Arras et al., ApJS **208**, 4 (2013). https://doi.org/10.1088/0067-0049/208/1/4
4. B. Paxton, P. Marchant, J. Schwab et al., ApJS **220**, 12 (2015). https://doi.org/10.1088/0067-0049/220/1/15
5. B. Paxton, J. Schwab, E.B. Bauer et al., ApJS **234**, 34 (2018). https://doi.org/10.3847/1538-4365/aaa5a8
6. N. Langer, K.J. Fricke, D. Sugimoto, A&A **126**, 207 (1983)
7. F. Herwig, A&A **360**, 952 (2000)
8. A. Cristini, C. Meakin, R. Hirschi et al., MNRAS **471**, 279 (2017). https://doi.org/10.1093/mnras/stx1535
9. W.D. Arnett, C. Meakin, M. Viallet et al., ApJ **809**, 30 (2015). https://doi.org/10.1088/0004-637X/809/1/30
10. W.D. Arnett, E. Moravveji, ApJ **836**, L19 (2017). https://doi.org/10.3847/2041-8213/aa5cb0

Chapter 72
Weak Interference Between the 1^- States in the Vicinity of α-Particle Threshold of ^{16}O

M. Katsuma

Abstract The subthreshold 1^-_1 state at an excitation energy $E_x = 7.12$ MeV in ^{16}O has been believed to enhance the S-factor of ^{12}C(α,γ)^{16}O. The enhancement seems to originate from strong interference between 1^-_1 and 1^-_2 ($E_x \approx 9.6$ MeV) in the vicinity of the α-particle threshold. However, weak interference between them and a resulting small $E1$ S-factor are exemplified with R-matrix theory. Including a higher-order correction of the resonance parameters, the present example appears to reproduce the experimental data consistently. It would therefore be possible that the $E1$ S-factor is reduced at low energies.

The 1^-_1 ($E_x = 7.12$ MeV) and 1^-_2($E_x \approx 9.6$ MeV) states in ^{16}O play an important role in the low-energy extrapolation of ^{12}C(α,γ)^{16}O cross sections. If complicated process of compound nuclei is assumed, strong interference between them is expected, and $E1$ transition becomes predominant. At present, this interference has been believed to describe the cross section at $E_{c.m.} = 300$ keV. However, I have predicted a small $E1$ S-factor at this energy from the potential model (PM) [1], because non-absorptive scattering results in weak coupling between shell and cluster structure in ^{16}O. Besides, I have shown that $E2$ transition is dominant because 2^+_1 ($E_x = 6.92$ MeV) has α+^{12}C structure [2, 3].

In this paper, weak interference between 1^-_1 and 1^-_2, and the resulting small $E1$ S-factor are exemplified with R-matrix theory [4]. I estimate their reduced α-particle widths from [1, 2], and use the conventional R-matrix method [5, 6]. In addition, the formal parameters are obtained from an exact expression, including a higher-order correction, because it has been reported that the parameters for 1^-_2 are not appropriately treated in the linear approximation [5]. This correction ensures that R-matrix calculations correspond to the experimental data.

Before showing an example of calculations, let me describe the R-matrix parameters. The Schrödinger equation is solved with the R-matrix,

M. Katsuma (✉)
Advanced Mathematical Institute, Osaka City University, Osaka, Japan
e-mail: mkatsuma@sci.osaka-cu.ac.jp

Institut d'Astronomie et d'Astrophysique, Université Libre de Bruxelles, Brussels, Belgium

A. Formicola et al. (eds.), *Nuclei in the Cosmos XV*, Springer
Proceedings in Physics 219, https://doi.org/10.1007/978-3-030-13876-9_72

$$R_L(E_{c.m.}) = \sum_n \frac{\tilde{\gamma}_{nL}^2}{\tilde{E}_{nL} - E_{c.m.}} + \mathcal{R}_{\alpha L}, \tag{72.1}$$

where $\mathcal{R}_{\alpha L}$ is the non-resonant component. $\tilde{E}_{nL}$ and $\tilde{\gamma}_{nL}$ are the *formal* resonance energy and *formal* reduced width, respectively. These are different from the Breit-Wigner (observed) parameters, E_{nL}, γ_{nL}. The conversion is given as

$$\tilde{E}_{nL}(E_{c.m.}) = E_{nL} + \tilde{\gamma}_{nL}^2(E_{c.m.})\Delta_L(E_{nL}, a_c)\,[\,1 + d_{nL}\,] \tag{72.2}$$

$$\tilde{\gamma}_{nL}^2(E_{c.m.}) = \frac{\gamma_{nL}^2}{1 - \gamma_{nL}^2\Delta'_L(E_{nL}, a_c)\,[\,1 + Q_{nL}(E_{c.m.}, a_c)\,]}, \tag{72.3}$$

where Q_{nL} is the higher-order correction of the resonance parameters, depending on energies. Note that $Q_{nL} = 0$ was used in most of reactions [5, 6]. Δ_L is the shift function, $\Delta'_L = d\Delta_L/dE$. d_{nL} is a parameter for multi-levels, and it is adjusted self-consistently so as to satisfy $\Delta_L(E_{nL}, a_c)R_L(E_{nL}) = 1; d_{11} = -1.0133, d_{21} = 0$. The observed parameters are 1_1^-: $E_{11} = -0.0451$ MeV, $\gamma_{11} = 0.345$ MeV$^{1/2}$; 1_2^-: $E_{21} = 2.434$ MeV, $\gamma_{21} = 0.850$ MeV$^{1/2}$. a_c is the channel radius, $a_c = 4.75$ fm. All nucleons are interacting close together in the internal region, whereas nucleons are well-separated into α and ^{12}C outside the region. Other observed parameters are taken from [7]. ANC of 1_1^- is 5.0×10^{28} fm^{-1} [1, 8].

The example of the small $E1$ S-factor is shown by the solid curve in Fig. 72.1a. The present example includes the component of the subthreshold state, and it resembles PM [1] (dashed curve). The interference between 1_1^- and 1_2^- appears to be weak. The corresponding calculations of the β-delayed α-particle spectrum of ^{16}N and the p-wave phase shift of α+^{12}C elastic scattering are consistent with the experimental results [9, 10]. (Fig. 72.1b and c) So, the small $E1$ S-factor in Fig. 72.1a is in agreement with these experimental data. The experimental α-particle width of 1_2^- ($\Gamma_\alpha^{\rm exp} = 420 \pm 20$ keV [7]) is also reproduced by the present example, $\Gamma_\alpha^{\rm th} = 432$ keV. The dotted curves are the R-matrix calculations [9] with $Q_{nL} = 0$, in which the narrow reduced widths are assumed. The derived 1_2^- width [9] does not reproduce the experimental one. Compared with the solid curves, Q_{nL} is found to reduce the $E1$ S-factor at low energies. In fact, a large energy shift for 1_2^- is expected from the large reduced width of α+^{12}C cluster structure. (Eq. 72.2) So, the resultant energy of the 1_2^- pole is found to be located in the vicinity of 1_1^-. (Fig. 72.1d) This proximity of the poles suppresses their interference, and it consequently makes the small $E1$ S-factor below the barrier.

The present example can be replaced with my previous result from PM, so I could use a hybrid model [12], $E1(R$-matrix$)$+$E2$(PM). The resulting total S-factor and reaction rates are confirmed to be concordant with [1, 13].

In summary, the weak interference between 1_1^- and 1_2^-, and the small $E1$ S-factor have been exemplified with R-matrix theory. The formal parameters are obtained from the exact expression, including the higher-order correction. The reduced α-particle widths of 1_1^- and 1_2^- are estimated from PM. The present example is consistent

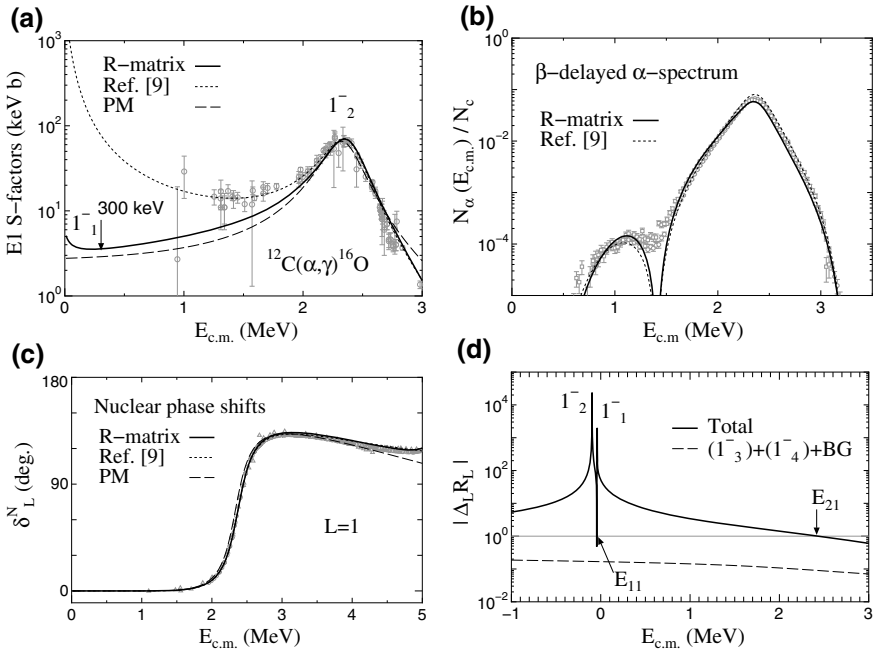

Fig. 72.1 An example of R-matrix calculations of **a** $E1$ S-factor of $^{12}C(\alpha,\gamma_0)^{16}O$, **b** β-delayed α-particle spectrum of ^{16}N, **c** p-wave phase shift of $\alpha+^{12}C$ elastic scattering. The solid, dotted, and dashed curves are the results of the present work, R-matrix method [9], and PM [1], respectively. The experimental data are taken from [9–11]. **d** The resultant R-matrix is illustrated with the solid curve. The dashed curve is the sum of 1^-_3, 1^-_4, and non-resonant components

with the experimental results of the β-delayed α-spectrum of ^{16}N, the p-wave phase shift, and the α-decay width of 1^-_2. In the example, the pole energy of 1^-_2 is located in the vicinity of 1^-_1. This proximity suppresses their interference, and it makes the small $E1$ S-factor below the barrier. It would therefore be possible in the R-matrix method that the $E1$ S-factor is reduced from the enhanced value currently expected. At the same time, the reaction rates are confirmed to be obtained from the direct-capture mechanism [1, 13].

Acknowledgements I am grateful to Prof. S. Kubono for his comments. I also thank M. Arnould, A. Jorissen, K. Takahashi, H. Utsunomiya, Y. Ohnita, and Y. Sakuragi for their hospitality at Université Libre de Bruxelles and Osaka City University.

References

1. Katsuma, M.: Phys. Rev. C **78**, 034606 (2008); ibid. **81**, 029804 (2010); ibid. **90**, 068801 (2014); Proc. of NIC XIV, JPS Conf. Proc. **14**, 021009 (2017)
2. M. Katsuma, Phys. Rev. C **81**, 067603 (2010); J. Phys. G **40**, 025107 (2013); EPJ Web of Conferences **66**, 03041 (2014)
3. Y. Fujiwara et al., Prog. Theor. Phys. Suppl. **68**, 29 (1980). and references therein
4. Katsuma, M.: arXiv:1701.02848 [nucl-th]
5. P. Descouvemont, *Theoretical Models for Nuclear Astrophysics*. Nova Science (2003)
6. I.J. Thompson, F. Nunes, *Nuclear Reactions for Astrophysics*. Cambridge Univ. Press (2009); A.M. Lane, R.G. Thomas: Rev. Mod. Phys. **30**, 257 (1958)
7. D.R. Tilley, H.R. Weller, C.M. Cheves, Nucl. Phys. A **564**, 1 (1993)
8. Oulebsir, N., *et al.*: Phys. Rev. C **85**, 035804 (2012);Brune, C.R., *et al.*: Phys. Rev. Lett. **83**, 4025 (1999);Belhout, A., *et al.*: Nucl. Phys. A **793**, 178 (2007)
9. R.E. Azuma et al., Phys. Rev. C **50**, 1194 (1994)
10. Tang, X.D., *et al.*: Phys. Rev. C **81**, 045809 (2010);Plaga, R., *et al.*: Nucl. Phys. A **465**, 291 (1987);Tischhauser, P., *et al.*: Phys. Rev. C **79**, 055803 (2009)
11. Kunz, R., *et al.*: Phys. Rev. Lett **86**, 3244 (2001);Assunção, M., *et al.*: Phys. Rev. C **73**, 055801 (2006);Plag, R., *et al.*: ibid. **86**, 015805 (2012);Ouellet, J.M.L., *et al.*: ibid. **54**, 1982 (1996);Makii, H., *et al.*: ibid. **80**, 065802 (2009)
12. Langanke, K., Koonin, S.E.: Nucl. Phys. A **439**, 384 (1985); ibid. **410**, 334 (1983)
13. Katsuma, M.: Astrophys. J. **745**, 192 (2012); PoS (NIC XIII) 106 (2015)

Chapter 73
The Effects of ^{26}Al Isomeric State on Its Ground State Production

E. T. Li, Maria Lugaro, H. E. Brinkman, C. L. Doherty and B. Côté

Abstract The ground state of unstable ^{26}Al nucleus (^{26}Al^{g}) with $T_{1/2}$ = 0.717 Myr was the first radioactive isotope detected in the galaxy, via the characteristic 1.809 MeV γ-emission of ^{26}Mg (Mahoney et al., Astrophys J 286:578, [1]). The observation is direct proof of ongoing stellar nucleosynthesis in our Galaxy and indicates that there are approximately 2–3 $M_{\odot}$ of ^{26}Al^{g} (Diehl et al., Nature 439:45, [2]). ^{26}Al has an isomeric state (^{26}Al^{m}) which is prohibited to decay into ^{26}Al^{g} due to the large spin difference. However, an equilibration between ^{26}Al^{m} and ^{26}Al^{g} could proceed via intermediate states and influence the abundance of ^{26}Al^{g}. Hence, the isomer could have an important influence on the production of ^{26}Al^{g}. A one consistent program is used to investigate the effects of ^{26}Al^{m} on ^{26}Al^{g} production by using a 20 $M_{\odot}$ stellar model in its hydrogen core burning and C/Ne shell burning.

73.1 Motivation

To understand the mechanism of the ^{26}Al^{g} production, a lot of nuclear reactions are needed to be considered. In laboratory, ^{26}Al^{m} is prohibited to decay into ^{26}Al^{g} due to the large spin difference. In hot stellar plasma, the ^{26}Al^{g} and ^{26}Al^{m} might "communicate" via γ transitions involving higher-lying ^{26}Al levels, but different theories do not agree with each other (see Fig. 73.1). Therefore, it is important to investigate the impact of the isomer on the abundances of ^{26}Al^{g}. Post-processing nucleosynthesis calculations [3] studied the effect of the communication between the ^{26}Al^{g} and ^{26}Al^{m} in massive stars [4]. Here, we present our investigations by using one consistent program.

E. T. Li (✉)
College of Physics & Energy, Shenzhen University, Shenzhen 518060, China
e-mail: let@szu.edu.cn

E. T. Li · M. Lugaro · H. E. Brinkman · C. L. Doherty · B. Côté
Konkoly Observatory, Hungarian Academy of Sciences, Budapest H-1121, Hungary

C. L. Doherty
School of Physics and Astronomy, Monash Centre for Astrophysics,
Monash University, Clayton, Australia

A. Formicola et al. (eds.), *Nuclei in the Cosmos XV*, Springer
Proceedings in Physics 219, https://doi.org/10.1007/978-3-030-13876-9_73

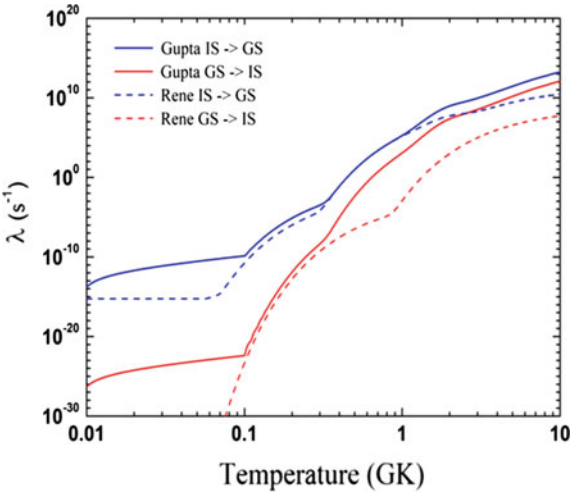

Fig. 73.1 Comparison of the effective rates between the $^{26}Al^{g}$ and $^{26}Al^{m}$. The solid lines are from Gupta and Meyer [6] and the dashed lines are from Rene et al. [7]

73.2 Simulations

A 1D stellar code MESA [5] is employed to evolve a 20 $M_{\odot}$ star. The flux of the reactions is calculated and used to investigate which reaction is important to the production of $^{26}Al^{g}$. For a 20 $M_{\odot}$ star in its hydrogen core burning, (see Fig. 73.2), $^{26}Al^{g}$ is produced by the $^{25}Mg(p, \gamma)^{26}Al^{g}$ reaction and the seed nucleus ^{25}Mg mainly come from the initial abundance. One also can see that there is almost no communication between the $^{26}Al^{g}$ and $^{26}Al^{m}$. For a 20 $M_{\odot}$ star in its hydrostatic C/Ne shell burning (see Fig. 73.3), $^{26}Al^{g}$ is mainly produced by $^{25}Mg(p, \gamma)^{26}Al^{g}$ but the seed nucleus ^{25}Mg mainly come from $^{24}Mg(n, \gamma)^{25}Mg$ and $^{22}Ne(\alpha, n)^{25}Mg$ reactions other than the initial abundance. The communication between the $^{26}Al^{g}$ and $^{26}Al^{m}$ become important and cannot be ignored. The rates of Gupta and Meyer [6] increase the net flux between the $^{26}Al^{g}$ and $^{26}Al^{m}$ by 130%.

73.3 Conclusions

For the 20 $M_{\odot}$ massive star in the hydrostatic hydrogen core burning, the communication between the $^{26}Al^{g}$ and $^{26}Al^{m}$ can be ignored. The initial abundance of ^{25}Mg influences significantly the production of $^{26}Al^{g}$. For the star in its hydrostatic C/Ne shell burning, the reaction rates between the $^{26}Al^{g}$ and $^{26}Al^{m}$ are very important, and different rates influence the $^{26}Al^{g}$, and the seed nucleus ^{25}Mg mainly come from $^{24}Mg(n, \gamma)^{25}Mg$ and $^{22}Ne(\alpha, n)^{25}Mg$ reactions.

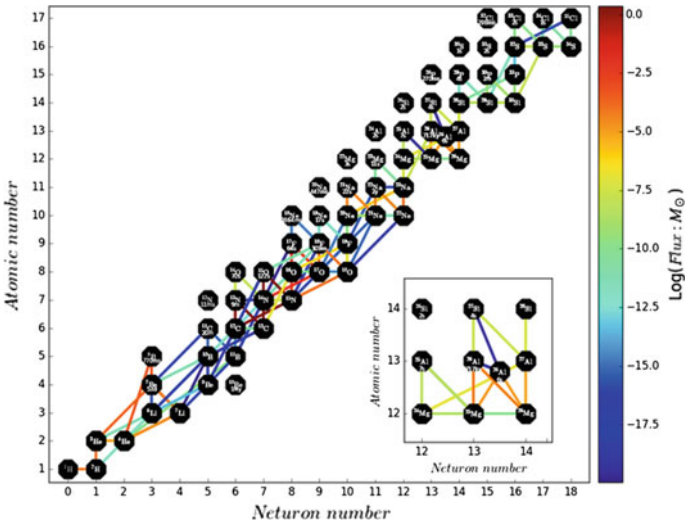

Fig. 73.2 The reaction net fluxes of a 20 $M_\odot$ star in its hydrogen core burning. The rates between the $^{26}Al^g$ and $^{26}Al^m$ are from [7]

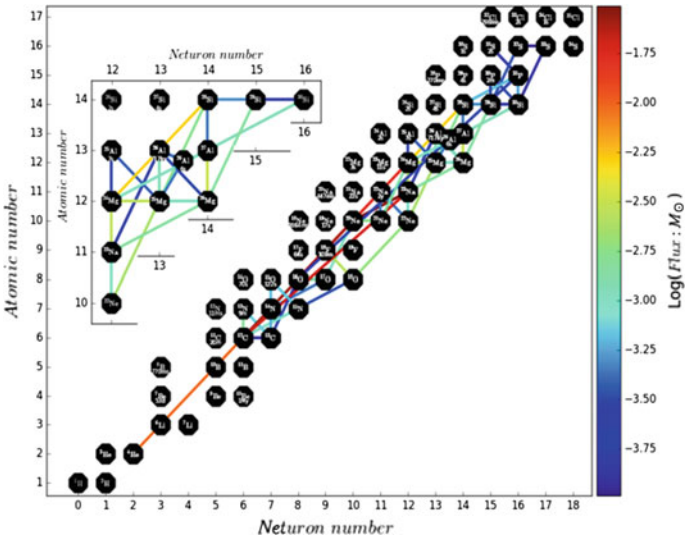

Fig. 73.3 The reaction net fluxes of a 20 $M_\odot$ star in its hydrostatic C/Ne shell burning. The rates between the $^{26}Al^g$ and $^{26}Al^m$ are from [7]

Acknowledgements This work is supported by: National Natural Science Foundation of China (11505117), Natural Science Foundation of Guangdong Province (2015A030310012) and the ERC via CoG-2016 RADIOSTAR [8] (Grant Agreement 724560). E. T. Li would like to give gratitude to the financial support of China Scholarship Council (CSC) for one year research in Konkoly Observatory, Hungarian Academy of Sciences.

References

1. W.A. Mahoney et al., Astrophys. J. **286**, 578 (1984)
2. R. Diehl et al., Nature **439**, 45 (2006)
3. C. Iliadis et al., Astrophys. J. **193**, 16 (2011)
4. M. Limongi, A. Chieffi, Astrophys. J. **647**, 483 (2006)
5. http://mesa.sourceforge.net/
6. S.S. Gupta, B.S. Meyer, Phys. Rev. C **64**, 025805 (2001)
7. R. Rene et al., Int. J Mod. Phys. A **33**, 9 (2018)
8. http://konkoly.hu/radiostar/, http://www.ncbi.nlm.nih.gov

Chapter 74
Spectroscopic Study on ^{39}Ca Using the ^{40}Ca(d,t)^{39}Ca Reaction for Classical Nova Endpoint Nucleosynthesis

J. Liang, A. A. Chen, M. Anger, S. Bishop, T. Faestermann, C. Fry, R. Hertenberger, A. Psaltis, D. Seiler, P. Tiwari, H.-F. Wirth and C. Wrede

Abstract In classical novae simulations, the uncertainty in the reaction rate of ^{38}K(p,γ) has been shown to affect the abundances of endpoint nuclides significantly. To better understand the reaction rate, we have done a spectroscopic study on ^{39}Ca. The reaction ^{40}Ca(d,t)^{39}Ca at a beam energy of 22 MeV was used to populate excited states of ^{39}Ca. Tritons were momentum analyzed using a high resolution quadrupole-dipole-dipole-dipole (Q3D) magnetic spectrograph at 4 angles. Preliminary resonance energies for ^{39}Ca within the energetic region of interest for classical novae - 6.0–6.4 MeV - were determined.

74.1 Introduction

Classical novae occur in close binary systems with a white dwarf and a main sequence/red giant companion star. In these systems, the denser white dwarf siphons hydrogen rich material from its companion star, forming a layer of nuclear fuel on the surface of the white dwarf. Thermonuclear runaway ensues, causing a dramatic increase in temperature (T = 0.1–0.4 GK) and luminosity, eventually leading to a classical nova outburst. In this process, heavier nuclei are synthesized via pro-

J. Liang (✉) · A. A. Chen · A. Psaltis
Department of Physics and Astronomy, McMaster University, Hamilton, Ontario L8S 4M1, Canada
e-mail: LiangJ27@mcmaster.ca

C. Fry · P. Tiwari · C. Wrede
Department of Physics and Astronomy, National Superconducting Cyclotron Laboratory, Michigan State University, 640 S. Shaw Ln., East Lansing, MI 48864, USA

M. Anger · S. Bishop · T. Faestermann · D. Seiler
Department of Physics, Technical University Munich, James-Franck-Str. 1, 685748 Garching, Germany

R. Hertenberger · H.-F. Wirth
Faculty of Physics, Ludwig-Maximilians-Universität München, Geschwister-Scholl-Platz 1, 80539 Munich, Germany

A. Formicola et al. (eds.), *Nuclei in the Cosmos XV*, Springer Proceedings in Physics 219, https://doi.org/10.1007/978-3-030-13876-9_74

gressive proton capture reactions and subsequent β^+ decays. The endpoint of this nucleosynthesis occurs at approximately A $\sim$ 40.

Currently, observed elemental abundances of endpoint nuclides show enhancement compared to nova models by up to an order of magnitude [1, 2]. This difference could be caused by the treatment of clumping in the ejecta [3], or due to uncertainties in nuclear reaction rates. In a sensitivity study by Iliadis et al. [4] it was shown that the ^{38}K(p,γ)^{39}Ca reaction could change abundances of the endpoint nuclides in classical novae by up to 2 orders of magnitude if the reaction rate was varied within its uncertainty.

In temperatures typical of classical novae, the total reaction rate is dominated by three $\ell = 0$ resonances within the Gamow window. These occur at excitation energies in ^{39}Ca at 6157(10), 6286(10), and 6460(10) keV. This motivated the direct measurement of the ^{39}K(p,γ)^{39}Ca reaction by Lotay et al. [5] at the DRAGON facility in TRIUMF. In [5], the resonance at 6460(10) was instead observed at 6450^{+2}_{-1}(stat.) $\pm$1 (sys.) and the resonance strength was obtained. Upper limits were determined for the resonance strengths of the others. When the reaction rate was varied within its new uncertainties it was shown that the variations in abundances of these endpoint nuclides were reduced to one order of magnitude.

High resolution spectroscopic studies of ^{39}Ca were recommended by Lotay et al. [5] to probe for additional resonances corresponding to low ℓ capture resonances in the ^{38}K+p system. To that end we performed a spectroscopic study using the reaction ^{40}Ca(d,t)^{39}Ca not only to probe for new states, but to also to improve the precision on excitation energies of existing states.

74.2 Experimental Method

The experiment was performed at the Maier-Leibnitz Laboratory (MLL), a joint facility of the Technical University of Munich and Ludwig-Maximilians-Universität. The MP Tandem Van de Graff was used to accelerate a deuteron beam to 22 MeV, which was then impinged on the following targets: natural CaF_2 on carbon backing, a calibration target of ^{32}S implanted in carbon, and a background target of natural LiF on a carbon backing.

Tritons emerging from the reaction were momentum analyzed in a quadrupole-dipole-dipole-dipole (Q3D) magnetic spectrograph. Data were taken at spectrograh angle θ_{lab} = 15, 20, 25 and 30°. Gas filled proportional counters provided energy loss signals and precise position information from charges induced on the anode strips detector along the focal plane. A scintillator provided residual energy of the tritons, and thus a unique particle identification.

Positions of the tritons were determined, corresponding to the energies of those tritons.

Table 74.1 Preliminary resonance energies of ^{39}Ca determined in the current work compared to previously evaluated values

NDS evaluated energy (keV)	This work (keV) (±) stat
6.451(2)	6.4592(6)
6.432(2)	6.431(2)
6.405(10)	6.4003(4)
6.286(10)	6.289(1)
6.157(10)	6.1507(1)
6.094(10)	6.0869(5)

74.3 Results and Discussion

The background from ^{19}F(d,t)^{18}F was well characterized by a scaled spectrum produced by a LiF target, where a polynomial, featureless background from ^{7}Li(d,t)^{6}Li was assumed.

The peaks in the background subtracted triton position spectrum, corresponding to resonance states, were fitted using exponentially modified Gaussian functions; the asymmetry accounting for the energy straggling within the target. Centroid positions and full widths at half maximum of peaks were determined for the ^{40}Ca(d,t)^{39}Ca and the ^{32}S(d,t)^{31}S calibration spectrum.

The ^{40}Ca(d,t)^{39}Ca triton spectra were calibrated by relating the positions of isolated ^{32}S(d,t)^{31}S peaks with their respective energies from [6]. Through the SPlitpole ANalysis Code (SPANC) [7], a polynomial function of the energy vs. position was determined using these calibration peaks, which was then applied to the ^{40}Ca(d,t)^{39}Ca triton spectrum to determine the energy at each centroid position.

The preliminary results of a measurement at a spectrograph angle of 20° is reported in Table 74.1. The uncertainty is purely statistical, however the addition of systematic uncertainties is unlikely to cause the total uncertainty to exceed 2–5 keV [8]. Most of the preliminary energies agree with previously tabulated values, with the exception of the 6451(2) keV state.

74.4 Conclusion

A spectroscopic study of ^{39}Ca was performed at MLL using the reaction ^{40}Ca(d,t)^{39}Ca. Preliminary data generally agrees well with previously evaluated data, and will likely reduce uncertainties in excitation energies, however a discrepancy exists between the state suggested in [5] and this preliminary work.

References

1. S. Starrfield, C. Iliadis, W.R. Hix, F.X. Timmes, W.M. Sparks, Astrophys. J. **692**, 1532 (2009)
2. J. Andrea, H. Dreschsel, S. Starrfield, Astron. Astrophys. **291**, 869 (1994)
3. C. Wendeln, L. Chomiuk, T. Finzell, J.D. Linford, J. Strader, Astrophys. J. **841**, 110 (2017)
4. C. Iliadis, A. Champagne, J. Jose, S. Starrfield, P. Tupper, Astrophys. J. Suppl. Ser. **142**, 105 (2002)
5. G. Lotay et al., Phys. Rev. Lett. **116**, 132701 (2016)
6. D. Irvine, M.Sc. thesis, McMaster University, 2012
7. D. Visser, *SPANC—Splitpole Analysis Code User Manual* (2002)
8. C. Fry et al., Phys. Rev. C **91**, 015803 (2015)

Chapter 75
Inhomogeneous Primordial Magnetic Field Strength and Its Impact on Primordial Nucleosynthesis

Yudong Luo, Toshitaka Kajino, Motohiko Kusakabe and Grant J. Mathews

Abstract We investigate the effect on the light element abundances from the presence of a primordial magnetic field (PMF) whose strength is spatially inhomogeneous. By assuming an uniform total energy density with a gaussian distribution of field strength, we find that domains of different temperatures exist in the BBN epoch due to variations in the local PMF. As a result, the effective distribution function of particle velocities averaged over domains of different temperatures deviates from the Maxwell-Boltzmann distribution. We perform BBN calculations including this effect and find that the ^{7}Li abundance is significantly reduced. We also discuss the possibility that the baryon-to-photon ratio decreased after the BBN epoch. In this case, if the ratio during BBN was larger than the cosmic microwave background constraint, all produced light elements are consistent with observational data.

75.1 Model

In the standard big bang nucleosynthesis (BBN) model, the photon energy density is homogeneous during the entire nucleosynthesis epoch. The previous study [1] introduced a constant scale invariant (SI) PMF strength within a co-moving radius 1 Mpc during the BBN epoch. However, the survival length scale for primordial magnetic

Y. Luo (✉) · T. Kajino
National Astronomical Observatory of Japan, 2-21-1 Osawa, Mitaka, Tokyo 181-8588, Japan
e-mail: ydong.luo@nao.ac.jp

Y. Luo · T. Kajino
Department of Astronomy, Graduate School of Science,
The University of Tokyo, 7-3-1 Hongo, Bunkyo-ku, Tokyo 113-0033, Japan

T. Kajino · M. Kusakabe
School of Physics and Nuclear Energy Engineering and International
Research Center for Big-Bang Cosmology and Element Genesis, Beihang University,
37, Xueyuan Rd., Haidian-qu, Beijing 100083, China

G. J. Mathews
Department of Physics, Center for Astrophysics, University of Notre Dame,
Notre Dame, IN 46556, USA

A. Formicola et al. (eds.), *Nuclei in the Cosmos XV*, Springer
Proceedings in Physics 219, https://doi.org/10.1007/978-3-030-13876-9_75

field (PMF) during the BBN epoch is constrained as $L_{sur} \sim 10^4$ cm [2], which is inside the co-moving length scale of PMF energy density. Therefore, it is possible for PMF to have a energy density fluctuations. We simply assume that the distribution function of magnetic energy density ρ_B follows $f(\rho_B)$ which is a gaussian distribution with a peak located at the mean value ρ_{Bc}, the summation of radiation energy density ρ_{rad} and ρ_B, i.e., $\rho_{tot} = \rho_{rad} + \rho_B$, is presumed to be a homogeneous quantity. Since temperature is proportional to $\rho_{rad}^{-1/4}$, it is also inhomogeneous in our model. The nuclear reactions occur locally, this means that the local velocity distribution function for baryons at a certain temperature is described by *Maxwell-Boltzmann (MB) distribution*; Globally, due to the existence of temperature inhomogeneity, it would finally lead to an effective non-MB distribution function for baryonic velocities during the BBN epoch (for detailed derivation see [3]).

75.2 Results

We encode the temperature averaged reaction rates into the BBN network calculation and compare the results with the observationally inferred abundances for D, ^{4}He and ^{7}Li. In Fig. 75.1, we plot the light element abundance as a function of baryon-to-photon ratio $\eta_{10} = \eta \times 10^{10}$. In the range of Planck constraint (light blue vertical band): $\eta_{10} = 6.10 \pm 0.04$ [4], in the grey region of the figure, the model parameters ρ_{Bc} and σ_B are ranged from $\rho_{Bc}/\rho_{tot} = 0.08$–$0.13$ and $\sigma_B = 0.04$–0.17 respectively.

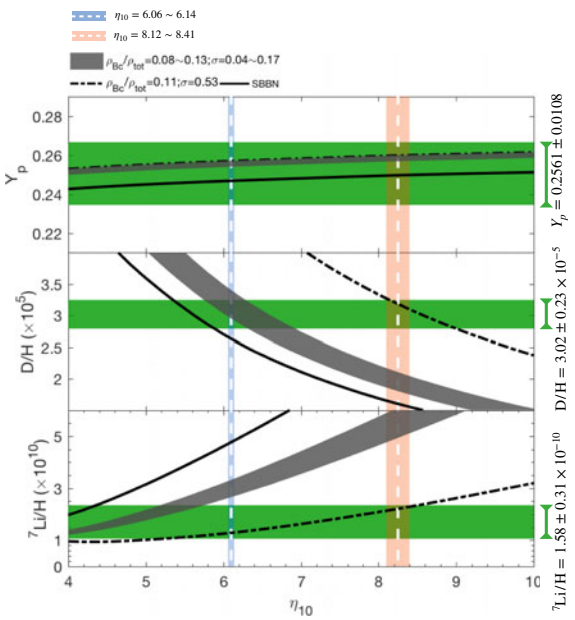

Fig. 75.1 Y_p, D/H and ^{7}Li/H prediction as a function of baryon-to-photon ratio $\eta_{10} = \eta \times 10^{10}$. The green bands show the adopted observational constraints for each elements [5–7]. The vertical blue band shows the Planck constraint on η_{10}. The light orange band shows the possible η_{10} region for which concordance is possible for all three elements

This region shows that the calculated D/H and Y_p (^{4}He mass fraction) are consistent with observations, and the ^{7}Li/H value is reduced to (3.18–3.52) $\times 10^{-10}$ compared with standard BBN (shown by solid lines). However, this is still above the constraints from metal-pool stars [5]. We also explore the possibility to find a parametric region of the baryon-to-photon ratio in which a concordance for all light element abundances can exist. As shown by dot-dashed lines, with the fraction $\rho_{\rm Bc}/\rho_{\rm tot} = 0.11$ and the fluctuation parameter $\sigma_{\rm B} = 0.53$, although there is no solution to the Li problem within the η_{10} range from Planck, at $\eta_{10} = 8.26 \pm 0.14$ (light orange vertical band), all of the elements fall into a region that is consistent with the observational constraints. It is possible to have this larger η value in BBN epoch since a dissipation of the PMF between BBN and the last scattering of the background radiation can results in an evolution of the η value, also other mechanisms such as the radiative decay of exotic particles can have the same effect.

75.3 Conclusion

In this work, we assume that the PMF energy density obeys a narrow Gaussian distribution under the presumption of a constant value of total energy density. This inhomogeneous PMF energy density eventually leads to a non-Maxwellian baryonic distribution function in our model. We encode this fluctuated PMF to the BBN calculation. By comparing our results with observational constraints on η (baryon-to-photon ratio obtained from Planck satellites), D/H and Y_p (^{4}He mass fraction), we find that a PMF whose mean energy density is $\rho_{\rm Bc}/\rho_{\rm tot} = 0.08$–$0.13$ with the fractional gaussian range $\sigma_{\rm B} = 0.04$–0.17 can reduce the predicted primordial ^{7}Li abundance to a value of ^{7}Li/H = (3.18–3.52) $\times 10^{-10}$ which is closer to the observational value. We also discussed the possibility that η is larger than the value obtained from Planck constraint, in the case that the baryon-to-photon ratio decreased after primordial nucleosynthesis. We find that with the baryon to photon ratio $\eta_{10} = 8.26 \pm 0.14$ with certain model parameters, there is a possible solution to the Li problem.

References

1. D.G. Yamazaki, M. Kusakabe, Effects of power law primordial magnetic field on big bang nucleosynthesis. Phys. Rev. D **86**(12), 123006 (2012)
2. D.G. Yamazaki et al., The search for a primordial magnetic field. Phys. Rep. **517**, 141 (2012)
3. L. Yudong et al., Big bang nucleosynthesis with an inhomogeneous primordial magnetic field strength. ApJ **72**, 172 (2019)
4. P.A.R. Ade et al., Planck 2015 results. XIII. Cosmological parameters. A&A **594**, A13 (2016)
5. L. Sbordone et al., The metal-poor end of the Spite plateau. I. Stellar parameters, metallicities, and lithium abundances. A&A **522**, 26 (2010)
6. E. Aver et al., A new approach to systematic uncertainties and self-consistency in helium abundance determinations. JCAP **05**, 003 (2010)
7. K.A. Olive et al., Higher D or Li: probes of physics beyond the standard model. MNRAS **426**, 14270 (2012)

Chapter 76
Systematic Low-Energy Enhancement of the Gamma-Ray Strength Function

J. E. Midtbø, A. C. Larsen, T. Renstrøm, F. L. Bello Garrote and E. Lima

Abstract In this work, we have studied the low-energy behaviour of the γ-ray strength function within the framework of the shell model. We have done calculations on isotopic and isotonic chains, spanning several mass regions. We find systematic trends, where the strength function exhibits a low-energy enhancement that is steeper near shell closures and flatter in the mid-shell regions. Further, we compile strength functions from discrete experimental data and find evidence for a low-energy enhancement.

Gamma-ray strength functions are an essential ingredient for s- and r-process nucleosynthesis simulations, through their role in the prediction of neutron-capture cross sections. The γ-ray strength function for all nuclei in the energy region of a few tens of MeV is qualitatively similar, dominated by the $E1$ giant dipole resonance (GDR). A growing number of nuclei have been found to exhibit an enhancement of the strength function towards $E_\gamma = 0$. This low-energy enhancement (LEE) has been shown to potentially increase neutron-capture cross sections up to about two orders of-magnitude [1, 2].

It is at present unknown how general this enhancement is – whether it is the result of peculiarities of certain nuclei, or arises from some fundamental mechanism. Considerable experimental and theoretical efforts have been put in to chart the prevalence of the LEE and to obtain a theoretical understanding of how it comes about. In this work, we study the γ-ray strength function using the nuclear shell model, employing the very efficient and versatile code KSHELL [3]. We consider nuclei in two mass regions: (*i*) the *sd* shell, using the USDA interaction [4]; and (*ii*) the $f_{5/2}pg_{9/2}$ shell atop the ^{56}Ni closure, using the JUN45 interaction [5]. In each mass region we perform a systematic survey, totaling 283 nuclei. For each nucleus, we calculate hundreds or thousands of energy levels, and all possible $M1$ transitions between the levels. See [6] for more details.

For each nucleus, we have compiled a γ-ray strength function $f_{M1}(E_\gamma)$ using the definition given in [7]. As a measure for the low-energy enhancement of the strength

J. E. Midtbø (✉) · A. C. Larsen · T. Renstrøm · F. L. Bello Garrote · E. Lima
Department of Physics, University of Oslo, N-0316 Oslo, Norway
e-mail: j.e.midtbo@fys.uio.no

A. Formicola et al. (eds.), *Nuclei in the Cosmos XV*, Springer
Proceedings in Physics 219, https://doi.org/10.1007/978-3-030-13876-9_76

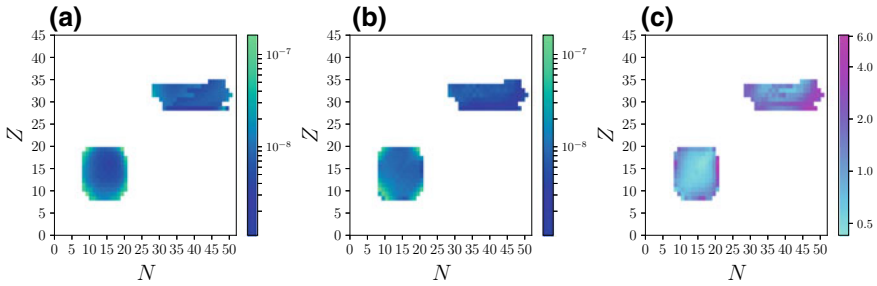

Fig. 76.1 Integrals of $M1$ γ-ray strength functions for different nuclei. Panel **a** shows the integral from 0 to 2 MeV, panel **b** shows the integral from 2 to 6 MeV, and panel **c** shows the ratio of (**a**) to (**b**)

function, we have taken the integral of $f_{M1}(E_\gamma)$ from 0 to 2 MeV and from 2 to 6 MeV, and find the ratio of the two. We are interested in how this ratio changes between nuclei. The results of this is shown in Fig. 76.1, plotted as a nuclear chart. Panels (a) and (b) show the integrals from 0 to 2 and 2 to 6 MeV, respectively, while panel (c) shows the ratio. A larger ratio indicates a stronger LEE. We do not find any cases where the ratio is lower than 1/3 – in theses cases, the strength function is flat. Trends are apparent: In both mass regions, there is LEE in regions close to either neutron or proton magic numbers, while it is diminished mid-shell, most clearly so for the *sd* shell. Furthermore, in each mass region, there is a systematic tendency for larger LEE in the bottom-right and top-left corners compared to the bottom-left and top-right ones. Intriguingly, this correlates with the regions where one expects *shears bands*, and a link between the shears band mechanism and the LEE has been suggested previously [9, 10] – but not studied in this systematic fashion.

Having all these calculations at hand, it is interesting to see how they compare to data. A source not often considered in the context of γ-ray strength functions is lifetime and branching ratio information on discrete, low-energy states. Indeed one should be cautious, as the low-energy level structure easily overshadows the statistical behaviour that enables one to speak of averages and strength functions. It is still possible to construct γ-ray strength functions, but one should expect large fluctuations. We have used the RIPL-3 library [11] to obtain state and lifetime information. Unfortunately, RIPL does not give multipolarity information about the decays. Still, the ease with which it lends itself to automatic parsing leads us to choose it over other databases. Thus, what we extract is a strength function of *presumed* $M1$ transitions, by selecting transitions between states with the same parity, and with a spin difference of $|J_i - J_f| \leq 1$.

We show results for the nuclei ^{44,45}Sc, ^{51}Ti and ^{56,57}Fe in Fig. 76.2. The shell model calculations shown use the GXPF1A interaction [12], and are not part of the systematic chart shown above. The shell-model lines marked "quasicontinuum" are compiled the same way as above, using all available states, while the ones marked "discrete" use only a discrete set, chosen to be comparable to the experimentally avail-

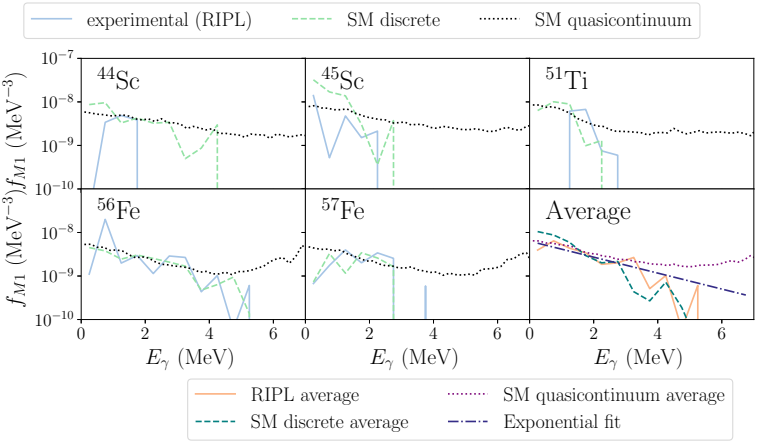

Fig. 76.2 Compiled γ-ray strength functions based on discrete data from the RIPL-3 database [11], compared to shell model calculations (see text)

able levels. The bottom right panel of Fig. 76.2 shows the average of all the strength functions, to increase statistics. The data clearly exhibit a low-energy enhancement. The exponential fit shown is the function $g(E_\gamma) = 6.3 \times 10^{-9} \exp(-E_\gamma/2.4)$.

We eagerly await new experiments that can shed light on the systematic trends of the LEE.

Acknowledgements Funding of this research from the European Research Council, ERC-STG-2014 Grant Agreement No. 637686, and from the "ChETEC" COST Action (CA16117), supported by COST (European Cooperation in Science and Technology), is gratefully acknowledged. KSHELL calculations were performed on the Stallo and Fram HPC clusters at the University of Tromsø, supported by the Norwegian Research Council.

References

1. A.C. Larsen, S. Goriely, Phys. Rev. C **82**, 014318 (2010)
2. A. Simon et al., Phys. Rev. C **93**, 034303 (2016)
3. N. Shimizu, arXiv:1310.5431 [nucl-th] (2013)
4. B.A. Brown, W.A. Richter, Phys. Rev. C **74**, 034315 (2006)
5. M. Honma et al., Phys. Rev. C **80**, 064323 (2009)
6. J. E. Midtbø et al., arXiv:1807.04036 [nucl-th] (2018)
7. G.A. Bartholomew et al., Adv. Nucl. Phys. **7**, 229–317 (1973)
8. A.C. Larsen, J.E. Midtbø et al., Phys. Rev. C **97**, 054329 (2018)
9. R. Schwengner et al., Phys. Rev. Lett. **111**, 232504 (2013)
10. R. Schwengner et al., Phys. Rev. Lett. **118**, 092502 (2017)
11. R. Capote et al., Nucl. Data Sheets **110** (2009)
12. M. Honma et al., Phys. Rev. C **69**, 034335 (2004)

Chapter 77
Impacts of the New Carbon Fusion Cross Sections on Type Ia Supernovae

Kanji Mori, Michael A. Famiano, Toshitaka Kajino, Motohiko Kusakabe and Xiaodong Tang

Abstract Recent measurement of cross sections of the carbon fusion reaction unveiled existence of low-energy resonances, which enhances reaction rates. We apply the new resonant reaction rates to the double degenerate scenario of type Ia supernovae. It is shown that merging carbon-oxygen white dwarfs are more likely to be burnt into oxygen-neon-magnesium white dwarfs by the enhanced reaction rates and collapse into neutron stars.

77.1 Introduction

The carbon fusion reactions ^{12}C(^{12}C, α)^{20}Ne and ^{12}C(^{12}C, p)^{23}Na play important roles in astrophysical phenomena including type Ia supernovae (SNe Ia[1]), massive stellar evolution, and X-ray superbursts. Because of their importance, its cross sections at astrophysical low energies have been measured for tens of years. Recently, low-energy resonances with the resonance energy of $E_{\rm R} \approx 1.5$ MeV were discov-

[1] In this paper, a type Ia supernova(e) is denoted by SN Ia (SNe Ia).

K. Mori (✉) · T. Kajino
National Astronomical Observatory of Japan,
2-21-1 Osawa, Mitaka, Tokyo 181-8588, Japan
e-mail: kanji.mori@nao.ac.jp

K. Mori · T. Kajino
Graduate School of Science, The University of Tokyo,
7-3-1 Hongo, Bunkyo-ku, Tokyo 113-0033, Japan

M. A. Famiano
Department of Physics, Western Michigan University,
Kalamazoo, MI 49008, USA

K. Mori · T. Kajino · M. Kusakabe
School of Physics, Beihang University, Beijing 100083, China

X. Tang
Institute of Modern Physics, Chinese Academy of Science,
Lanzhou, Gansu 730000, China

A. Formicola et al. (eds.), *Nuclei in the Cosmos XV*, Springer
Proceedings in Physics 219, https://doi.org/10.1007/978-3-030-13876-9_77

ered with the Trojan Horse Method using three body reactions $^{12}C(^{14}N, ^{20}Ne)^2H$ and $^{12}C(^{14}N, p^{23}Na)^2H$ [1], which enhance the reaction rates by ∼25 times at $T \approx 5 \times 10^8$ K compared with a conventional reaction rate ([2]; hereafter CF88). In this study, we explore the effect of such resonances on white dwarf (WD) binary mergers, which are a hypothetical progenitor of SNe Ia [3].

77.2 Ignition Temperature and the Fate of WD Mergers

The evolution of WD mergers is dependent on the carbon fusion reaction rates. Let us assume that the total mass of the binary is larger than the Chandrasekhar limit. In the original double degenerate scenario [4, 5], the merger forms a massive carbon-oxygen (CO) WD and carbon fusion is ignited at the center, resulting in SN explosion (accretion indiced explosion; AIE). However, it has been pointed out that off-center ignition can occur before the central ignition [6]. In this case, the CO WD is burnt into a neon-oxygen-magnesium WD, which collapses into a neutron star due to electron captures. This is often referred to as accretion induced collapse (AIC). On the other hand, if the total mass is smaller than the Chandrasekhar mass, a massive WD remains.

The ignition condition is determined by the heating rate by the fusion and cooling rate by the thermal neutrino emission. Figure 77.1 shows the ignition temperature calculated by CF88 and [1]. The hatched region shows the temperature and the density of WD mergers [7]. If the temperature of a system is higher than the ignition temperature, it becomes a NS via the AIC path, while other systems end up with a SN Ia. We can see that the enhanced reaction rate decreases the ignition temperature,

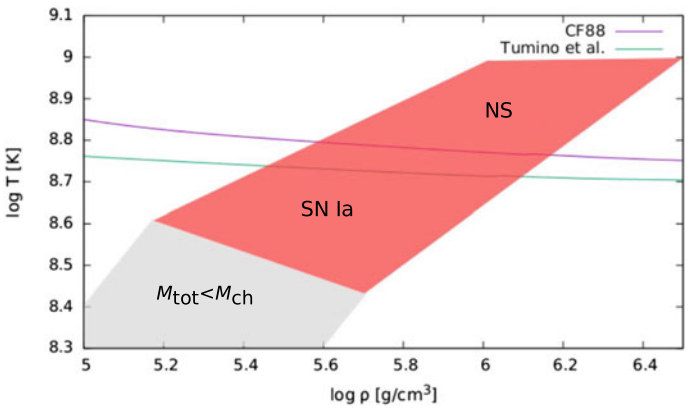

Fig. 77.1 The iginition temperature calculated with CF88 and [1]. The hatched region shows the temperature and the density of WD mergers. The labels "NS" and "SN Ia" show the fate of WD mergers above and below the ignition curves, respectively

Table 77.1 The event rates of the AIC and AIE paths in units of $10^{-14}/M_{\odot}$/year and the ratio of NSs and SNe Ia that can be explained by each scenario. Here θ^2 is the reduced width of low-energy resonance. The observational estimates of the NS birthrate and the SN Ia event rate are from [8, 9], respectively

	Theory		Theory/observation	
	AIC	AIE	AIC/NS	AIE/SN Ia
CF88	2.2 ± 0.6	6.5 ± 1.9	$0.013^{+0.018}_{-0.007}$	$0.60^{+0.37}_{-0.25}$
$\theta^2 = 0.1$	2.6 ± 0.7	6.0 ± 1.7	$0.015^{+0.021}_{-0.008}$	$0.55^{+0.34}_{-0.23}$
$\theta^2 = 1$	4.6 ± 1.3	4.2 ± 1.2	$0.027^{+0.038}_{-0.015}$	$0.38^{+0.24}_{-0.15}$

therefore the off-center carbon burning, which results in accretion induced collapse, becomes easier to occur. On the other hand, the SNe Ia become more difficult to occur.

We calculated the event rate of SNe Ia based on the double degenerate scenario as a function of the dimensional reduced width θ^2 (Table 77.1). The case of $\theta^2 = 1$ is the Wigner limit, which can be regarded as the theoretical upper limit on the strength of the resonance. The low-energy resonances found in [1] correspond to the $\theta^2 = 0.1$ case. One can see that the event rate is a decreasing function of the resonance strength, though it is still subject to large uncertainties.

77.3 Conclusion

The resent experimental results on the cross sections of the carbon fusion revealed existence of low-energy resonances, which enhance the reaction rate. The new reaction rate makes it difficult for WD mergers to evolve into SNe Ia. However, we note that the hydrodynamical model [7] does not include viscosity, which can ignite carbon burning in a longer timescale [10, 11]. In addition to that, the analysis performed in [1] is under debate [12, 13]. Extensive studies are still desirable to unveil the nature of SN Ia progenitors.

References

1. A. Tumino, C. Spitaleri, M. La Cognata et al., Nature **557**, 687 (2018). https://doi.org/10.1038/s41586-018-0149-4
2. G.R. Caughlan, W.A. Fowler, At. Data Nucl. Data Tables **40**, 283 (1988). https://doi.org/10.1016/0092-640X(88)90009-5
3. K. Mori, M.A. Famiano, T. Kajino, M. Kusakabe, X. Tang (in preparation)
4. I. Iben Jr., A.V. Tutukov, Astrophys. J. Suppl. Ser. **54**, 335 (1984). https://doi.org/10.1086/190932
5. R.F. Webbink, Astrophys. J. **277**, 355 (1984). https://doi.org/10.1086/161701
6. K. Nomoto, Y. Kondo, Astrophys. J. **367**, L19 (1991). https://doi.org/10.1086/185922

7. Y. Sato, N. Nakasato, A. Tanikawa et al., Astrophys. J. **807**, 105 (2015). https://doi.org/10.1088/0004-637X/807/1/105
8. E.F. Keane, M. Kramer, Mon. Not. Roy. Astron. Soc. **391**, 2009 (2008). https://doi.org/10.1111/j.1365-2966.2008.14045.x
9. W. Li, R. Chornock, J. Leaman et al., Mon. Not. Roy. Astron. Soc. **412**, 1473 (2011). https://doi.org/10.1111/j.1365-2966.2011.18162.x
10. J. Schwab, K.J. Shen, E. Quataert et al., Mon. Not. Roy. Astron. Soc. **427**, 190 (2012). https://doi.org/10.1111/j.1365-2966.2012.21993.x
11. K.J. Shen, L. Bildsten, D. Kasen et al., Astrophys. J. **748**, 35 (2012). https://doi.org/10.1088/0004-637X/748/1/35
12. A.M. Mukhamedzhanov, D.Y. Pang (2018). arXiv: 1806.08828
13. A. Tumino, C. Spitaleri, C., M. La Cognata et al. (2018). arXiv: 1807.06148

Chapter 78
A BGO Set-Up for the ^{2}H(p, γ)^{3}He Cross Section Measurement at the BBN Energy Range

Viviana Mossa

Abstract Deuterium is the first nucleus produced in the Universe, whose accumulation marks the beginning of the Big Bang Nucleosynthesis (BBN). Its primordial abundance is sensitive to some cosmological parameters like the baryon density and the number of the neutrino families. Presently the main obstacle to an accurate theoretical deuterium abundance evaluation is due to the poor knowledge of the ^{2}H(p, γ)^{3}He cross section at BBN energies. The aim of the present work is to describe one of the two experimental approaches proposed by the LUNA collaboration, whose goal is to measure with unprecedented precision, the reaction cross section in the energy range $30 < E_{\mathrm{c.m.}}[\mathrm{keV}] < 300$.

78.1 The BGO Set-Up

The ^{2}H(p, γ)^{3}He cross section has been measured with unprecedented accuracy by the LUNA (Laboratory for Underground Nuclear Astrophysics) collaboration thanks to the low background of the INFN underground Gran Sasso Laboratories [1]. The experimental set-up consists of a 400 kV electrostatic accelerator [2] able to provide intense current of proton up to 500 μA and a windowless deuterium gas target, 10 cm long at 0.3 mbar of pressure. The lack of a physical window prevents the beam energy loss before it enters into the chamber and limits the beam energy straggling. To confine the gas inside the interaction chamber, a strong pressure gradient between the target and the beam line is produced by three pumping stages separated by three water cooled apertures of decreasing diameter. The beam current is measured by a constant-gradient calorimeter characterized by two sides, a hot one heated to 70 °C by thermoresistors and a cold one cooled to 0 °C by a refrigerating system [3]. When the ion beam hits the hot side, it contributes to its heating and reduces correspondingly the electric power needed to keep the temperature gradient constant. The current

V. Mossa: On behalf of the LUNA collaboration.

V. Mossa (✉)
INFN, sezione di Bari, Bari, Italy
e-mail: viviana.mossa@ba.infn.it

A. Formicola et al. (eds.), *Nuclei in the Cosmos XV*, Springer
Proceedings in Physics 219, https://doi.org/10.1007/978-3-030-13876-9_78

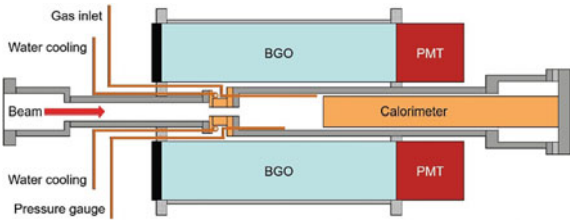

Fig. 78.1 Drawing of the target chamber inside the BGO detector

impinging on the target is thus related to the power difference between beam-on and beam-off conditions.

The γ rays emitted by the reaction are detected by a cylindrical BGO detector having a length of 28 cm with a radial thickness of 7 cm. The crystal is optically divided into six sectors, each covering an azimuthal angle of 60 degrees and the chamber and the calorimeter are hosted inside the BGO hole (Fig. 78.1), granting a configuration geometry close to 4π. With this set-up, the counting rate (full detection γ-peak) obtained is of the order of 10^4–10^5 events/hour in the considered energy range, making the measurement with the BGO detector relatively fast for reaching 10,000 events under the photopeak to ensure a low statistic uncertainty (<1%). On the other hand the large angular coverage of BGO makes the counting yield almost independent of the angular distribution of the emitted photons.

78.2 BGO-Phase Data Analysis

At first the gas target has been characterized calculating its density profile (Fig. 78.2 left side) starting from the pressure and temperature profiles directly measured along the beam axis from the pumping stages to the calorimeter. The beam heating effect, due to the beam energy loss heating the gas and thus causing a local density reduction, has been also evaluated performing measurements at constant beam energy and

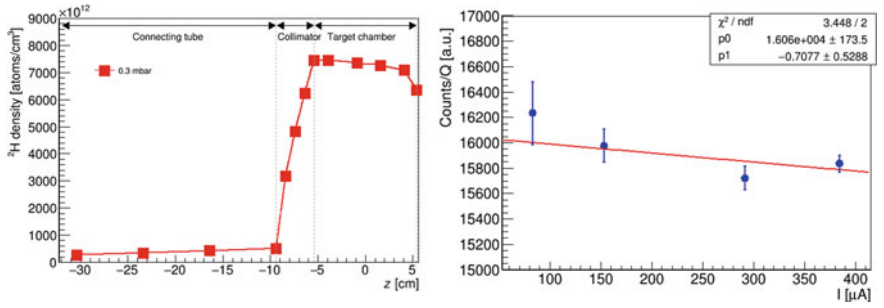

Fig. 78.2 Left side: deuterium density profile. Right side: beam heating evaluation

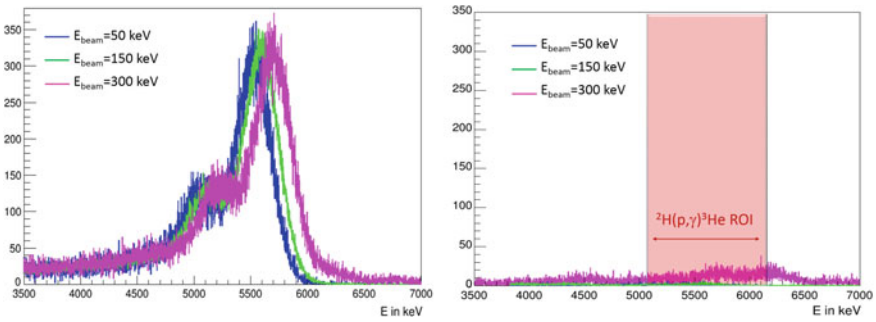

Fig. 78.3 Left side: ^{2}H(p, γ)^{3}He spectra at E_{beam} 50, 150 and 300 keV. Right side: beam induced background spectra obtained in vacuum at the same energies

different currents. In Fig. 78.2 (right side) the results obtained with a proton beam of 300 keV of energy and a current changing from about 90 to 400 μA are shown, plotting the rate of events of the ^{2}H(p, γ)^{3}He reaction ROI, normalized to the charge, as a function of the current. Since all the points lay on the same line within 2σ error, the beam heating contribution has been assumed negligible.

The detection efficiency, about 60% in the range of interest for the ^{2}H(p, γ)^{3}He reaction (5.5 MeV), has been obtained at a few per cent level using Monte Carlo simulations, tuned to match the experimental data of radioactive sources (^{137}Cs, ^{60}Co and ^{88}Y) at low energies and of the well-known resonant reaction ^{14}N(p, γ)^{15}O at $E_r = 259$ keV, emitting γ rays in the p + d energy range.

Finally the reaction cross section has been measured filling the interaction chamber with deuterium gas and changing the proton energy from 50 to 300 keV. For each investigated energy a further run in vacuum has been performed in order to evaluate the beam induced background or the eventual deuterium implantation (Fig. 78.3 right side).

The still ongoing analysis of the BGO spectra (Fig. 78.3 left side) allows the S-factor of the ^{2}H(p, γ)^{3}He reaction to be derived: currently a polynomial trend as a funtion of the center of mass energy is confirmed, with higher values than the already existing data and lower uncertainty [4].

References

1. S. Zavatarelli, A new measurement of the ^{2}H(p, γ)^{3}He cross section in the BBN energy range at LUNA, in *15th International Symposium on Nuclei in the Cosmos 2018, Springer Proceeding in Physics*
2. A. Formicola et al., The LUNA II 400 kV accelerator. Nucl. Instr. Meth. A **507**, 609 (2003). https://doi.org/10.1016/S0168-9002(03)01435-9

3. F. Ferraro, et al.: A high-efficiency gas target setup for underground experiments, and redetermination of the branching ratio of the 189.5 keV ^{22}Ne(p, γ)^{23}Na resonance. Eur. Phys. J. A **54**, 44 (2018). https://doi.org/10.1140/epja/i2018-12476-7
4. V. Mossa, Study of the ^{2}H(p, γ)^{3}He reaction in the Big Bang nucleosynthesis energy range. Ph.D. thesis, Universitá degli studi di Bari, 2018

Chapter 79
Cosmic-Ray Nucleosynthesis in Galactic Interactions

Tijana Prodanović and Aleksandra Ćiprijanović

Abstract It has been shown that galactic interactions and mergers can result in large-scale tidal shocks that propagate through interstellar gas. As a result, this can give rise to a new population of cosmic rays, additional to standard galactic cosmic rays present in star-forming galaxies. We investigate the impact of this tidal cosmic-ray population on the nucleosynthesis of light elements. We especially focus on extragalactic systems where lithium has been measured in gas phase but which have been disturbed by galactic interactions, namely the Small Magellanic Cloud and the M82. Moreover, we demonstrate that the presence of these tidal shock-waves may also have far reaching consequences on star-formation rate estimates and our general understanding of galactic evolution through affecting the far-infrared radio correlation.

79.1 Introduction

Galactic interactions result in large-scale tidal shock waves that impact interstellar medium (ISM), affect evolution of galaxies and trigger star-formation [1]. A new cosmic-ray (CR) population can be accelerated in galactic tidal shocks - tidal cosmic rays (TCRs) [2]. Presence of tidal cosmic-ray population in a galaxy would [3]: increase light element abundance with delayed and different increase in metallicity, enhance non-thermal radio emission of the galaxy, enhance dust temperature, affect far-infrared radio correlation, affect estimates of star-formation rate (SFR). Though both Li isotopes are made in CR interactions in the ratio varying between $^{7}\mathrm{Li}/^{6}\mathrm{Li} = 1.3{-}2$ depending on the CR spectrum, cosmic-ray dosimeters like ^{6}Li that are made only through CR nucleosynthesis would be affected the most. Consequently, observations of lithium abundance in the ISM of interacting systems could

T. Prodanović (✉)
University of Novi Sad, 21000 Novi Sad, Serbia
e-mail: prodanvc@df.uns.ac.rs
URL: https://personal.pmf.uns.ac.rs/tijana.prodanovic/

A. Ćiprijanović
University of Belgrade, 11000 Belgrade, Serbia

A. Formicola et al. (eds.), *Nuclei in the Cosmos XV*, Springer
Proceedings in Physics 219, https://doi.org/10.1007/978-3-030-13876-9_79

potentially reveal and quantify the TCR presence. Here we present cases of two systems that have experienced recent galactic interactions and where lithium has been measured in the gas phase – Small Magellanic Cloud (SMC) and M82, and present some estimates about whether their observed lithium abundances are consistent with their star-formation histories.

79.2 Small Magellanic Cloud and M82

Small Magellanic Cloud is a neighboring dwarf irregular galaxy, with metallicity 20% of Solar, which has suffered galaxy harassment by the Milky Way (MW) and the Large Magellanic Cloud. Furthermore, lithium was measured in the SMC in the interstellar medium to be $(^7\mathrm{Li/H})_{\mathrm{SMC}} = 4.8 \times 10^{-10}$ with isotopic ratio of $^6\mathrm{Li}/^7\mathrm{Li} = 0.13 \pm 0.05$ [4]. The observed isotopic ratio is higher than in the Milky Way at solar metallicity $^6\mathrm{Li}/^7\mathrm{Li} = 0.08$. Ćiprijanović has argued that this observed ^{6}Li abundance is inconsistent with gamma-ray observations of the SMC [5]. Prodanovic et al. [2] argued that it would be sufficient to shock the entire SMC gas twice, with tidal shocks, to account for the entire Li abundance and explain high observed isotopic ratio with production through TCR nucleosynthesis. However, galactic interactions are also known to result in episodes of intense star-formation and star-burst phases, thus one might argue that enhanced abundances of "cosmic-ray dosimeters" are the result of galactic cosmic-ray (GCR) nucleosynthesis. Here we estimate what would the mean SFR of the SMC need to be in order to account for the observed isotopic ratio with GCRs.

$$(^7\mathrm{Li}/^6\mathrm{Li})_{\mathrm{obs}} = \frac{^7\mathrm{Li}_{\mathrm{ps}} + {}^7\mathrm{Li}_{\mathrm{CR}}}{^6\mathrm{Li}_{\mathrm{CR}}} = \frac{^7\mathrm{Li}_{\mathrm{ps}}}{^6\mathrm{Li}_{\mathrm{CR}}} + 1.3 \tag{79.1}$$

where $^7\mathrm{Li}_{\mathrm{ps}}$ denotes primordial and stellar sources, while $^{6,7}\mathrm{Li}_{\mathrm{CR}}$ is lithium produced in cosmic-ray nucleosynthesis. Isotopic ratio produced in GCR interactions is taken to be $(^7\mathrm{Li}/^6\mathrm{Li})_{\mathrm{GCR}} = 1.3$, which corresponds to the same CR spectra as in the MW but can go up to $\sim$2 for calorimeters. Yields of light elements accumulated through CR nucleosynthesis are proportional to CR fluxes ϕ_{CR} and accumulation timescales τ. Thus, assuming that fusion channel dominates, we have $^{6,7}\mathrm{Li}_{\mathrm{CR}} \sim \tau\sigma_{\alpha\alpha}y_\alpha\phi_{\alpha,\mathrm{CR}}$, where $\sigma_{\alpha\alpha}$ is the interaction cross section and $y_\alpha \equiv n_\alpha/n_{\mathrm{H}}$ helium abundance. If supernovae are the only source of CRs then fluxes are proportional to star-formation rates $\phi_{\mathrm{CR}} \propto \psi$ thus we have

$$\frac{\langle\phi_{\mathrm{CR}}\rangle_{\mathrm{SMC}}}{\langle\phi_{\mathrm{CR}}\rangle_{\mathrm{MW}}} = f_{\mathrm{ps}}\frac{(^7\mathrm{Li}/^6\mathrm{Li})_{\mathrm{MW,obs}} - 1.3}{(^7\mathrm{Li}/^6\mathrm{Li})_{\mathrm{SMC,obs}} - 1.3} = \frac{\langle\psi_{\mathrm{CR}}\rangle_{\mathrm{SMC}}}{\langle\psi_{\mathrm{CR}}\rangle_{\mathrm{MW}}} \tag{79.2}$$

where f_{ps} is the ratio between SMC and MW joint primordial and stellar sources of Li. Taking the mean MW SFR to be equal to present $\psi_{\mathrm{MW}} = 1\,\mathrm{M}_\odot/\mathrm{year}$, and $f_{\mathrm{ps}} = 1$, from observed isotopic ratios we can estimate that $\langle\psi_{\mathrm{SMC}}\rangle/\langle\psi_{\mathrm{MW}}\rangle = 1.6$. If observed

SFR of the SMC $\psi_{\rm SMC} = 0.1\,{\rm M}_\odot/{\rm year} \approx 0.1\psi_{\rm MW}$ corresponds to its "quiescent" phase, and if SMC had 3 recent bursts of star-formation lasting in total ∼2 Gyr [6], we can estimate what the mean burst phase SFR had to be $\langle\psi_{\rm SMC}\rangle_* \sim 7\,{\rm M}_\odot/{\rm year}$. This is about ∼35× higher than the most intense estimated SFR in the SMC which was $0.2\,{\rm M}_\odot/{\rm year}$ [6].

M82 is a dwarf, starburst galaxy that has experienced interaction with M81 [7]. At metallicity of ∼1/2 of solar, ISM lithium abundance was inferred to be $({\rm Li/H})_{\rm M82} = 3.98 \times 10^{-9}$ [8], which is ∼2× higher abundance than solar. As post-BBN Li abundance should scale with metallicity, this observation can be explained by dilution of metals due to intense gas inflow which can accompany starburst phase. However, we can check if Li consistent with observed supernova rates. Writing the ratio of CR produced Li abundances in M82 and MW as ${\rm Li}_{\rm M82,GCR}/{\rm Li}_{\rm MW,GCR} = ({\rm Li}_{\rm M82,obs} - {\rm Li}_{\rm ps})/2.3{}^6{\rm Li}_\odot \approx 8$ where we have assumed that primordial and stellar-produced Li abundance of M82 is same as in the MW at M82 metallicity, and assuming M82 to be a calorimeter, we can estimate that ${}^7{\rm Li}_{\rm M82,CR}/{}^7{\rm Li}_{\rm MW,CR} \sim 10$. From this it follows that the ratio of mean supernova rates is ${}^7{\rm Li}_{\rm M82,CR}/{}^7{\rm Li}_{\rm MW,CR} = \langle R_{\rm SN,M82}\rangle/\langle R_{\rm SN,MW}\rangle \sim 10$. However, taking that current starburst phase lasts for ∼0.3 Gyr with current $\langle R_{\rm SN,M82}\rangle_* \sim 10 R_{\rm SN,MW}$ while quiescent phase had $\langle R_{\rm SN,M82}\rangle_q \sim 0.3 R_{\rm SN,MW}$ [7], we estimate mean supernova rate of M82 to be $\langle R_{\rm SN,M82}\rangle \sim R_{\rm SN,MW}$.

79.3 Discussion and Comments

Close fly-bys between galaxies can result in large scale tidal shocks in the galactic gas which could accelerate tidal cosmic rays and affect abundances of light elements such as lithium. SMC and M82 are systems that have experienced galactic interactions and are also the only extragalactic systems where Li abundance has been measured in gas phase. We find that high observed isotopic Li ratio of SMC and lithium abundance of M82 are inconsistent with their star-forming histories. We point out that observed inconsistencies and Li abundances could indicate that additional CR population was present in these interacting systems.

Acknowledgements The works of TP and AC are supported by the Ministry of Science of the Republic of Serbia under project number 176005, and in part by 171002 (TP).

References

1. D.B. Sanders, I.F. Mirabel, **34**, 749 (1996). https://doi.org/10.1146/annurev.astro.34.1.749
2. T. Prodanović, T. Bogdanović, D. Urošević, Galactic fly-bys: New source of lithium production. Phys. Rev. D **87**, 103014 (2013). https://doi.org/10.1103/PhysRevD.87.103014
3. D. Donevski, T. Prodanović, Possible breaking of the FIR-radio correlation in tidally interacting galaxies. MNRAS **453**, 638–644 (2015). https://doi.org/10.1093/mnras/stv1653

4. J.C. Howk, N. Lehner, B.D. Fields, G. Mathews, J: Observation of interstellar lithium in the low-metallicity Small Magellanic Cloud. Nature **489**, 121–123 (2012). https://doi.org/10.1038/nature11407
5. A. Ćiprijanović, Galactic cosmic-ray induced production of lithium in the Small Magellanic Cloud. Astropart. Phys. **85**, 24–28 (2016). https://doi.org/10.1016/j.astropartphys.2016.09.004
6. J. Harris, D. Zaritsky, The Star Formation History of the Small Magellanic Cloud. AJ **127**, 1531–1544 (2004). https://doi.org/10.1086/381953
7. Y.D. Mayya, A. Bressan, L. Carrasco, L. Hernandez-Martinez, The Star Formation History of the Disk of the Starburst Galaxy M82. ApJ **649**, 172–180 (2006). https://doi.org/10.1086/506270
8. A.M. Ritchey, D.E. Welty, J.A. Dahlstrom, D. York, G: Diffuse Atomic and Molecular Gas in the Interstellar Medium of M82 toward SN 2014J. ApJ **799**, 197–213 (2015). https://doi.org/10.1088/0004-637X/799/2/197

Chapter 80
First Radiative Proton-Capture Cross-Section Measurements in Mid-Weight Nuclei Relevant to the *p*-Process

A. Psaltis, A. Khaliel, E.-M. Assimakopoulou, A. Babounis, A. Kanellakopoulos, V. Lagaki, M. Lykiardopoulou, E. Malami, I. Psyrra, K. Zyriliou and T. J. Mertzimekis

Abstract One of the important, but still unsettled topics in Nuclear Astrophysics is the production of the *p*-nuclei. The *p*-process relies on an extended reaction network, which can be described theoretically by the Hauser–Feshbach statistical model, which in turn relies strongly on experimental data. To provide reliable data for *p*-nuclei, an experimental campaign at the Tandem Accelerator Laboratory of NCSR "Demokritos", focusing on ^{107,109}Ag$(p,\gamma)^{108,110}$Cd and ^{112}Cd $(p,\gamma)^{113}$In reaction cross-sections measurements was carried out. Both reactions were studied using a set of four HPGe detectors via the in-beam γ-ray spectroscopy, while for the latter the activation method was additionally employed to account for the population of a low-lying isomeric state. Total cross sections for proton beam energies lying inside the Gamow window for energies relevant to *p*-process nucleosynthesis were obtained for the first time. Experimental results are compared to Hauser–Feshbach calculations performed with the latest version of the `TALYS` code (v1.9). An overall good agreement has been achieved. These results provide important new input for the theoretical description of the *p*-process, but additionally for the origin of the cross-point *p*-nucleus ^{113}In.

A. Psaltis (✉) · A. Khaliel · E.-M. Assimakopoulou · A. Babounis · A. Kanellakopoulos · V. Lagaki · M. Lykiardopoulou · E. Malami · I. Psyrra · K. Zyriliou · T. J. Mertzimekis
Department of Physics, University of Athens,
Zografou Campus, 15784 Athens, Greece
e-mail: psaltisa@mcmaster.ca

A. Psaltis
Present address: Department of Physics and Astronomy,
McMaster University, Hamilton, ON L8S 4M1, Canada

A. Formicola et al. (eds.), *Nuclei in the Cosmos XV*, Springer
Proceedings in Physics 219, https://doi.org/10.1007/978-3-030-13876-9_80

80.1 Introduction

Explaining the solar abundances of the *p*-nuclei remains an open question for nuclear astrophysics. Their production site is not well settled yet, but the most promising scenario for the *p*-process to-date is the photodisintergation of s- and r-seed nuclei in the O/Ne layer of core-collapse supernovae.

As far as it concerns nucleosynthesis, the *p*-process reaction network involves thousands of nuclei, and rates are estimated in the framework of the Hauser–Feshbach statistical model. Its efficiency relies strongly on experimental input of proton-, alpha- and neutron-induced reaction cross sections, which can adjust parameters and thus improve the theoretical predictions for unmeasured reactions rates [1, 2]. To that end, a campaign of measurements at the Tandem Accelerator Laboratory of NCSR "Demokritos" focusing on radiative proton capture measurements on ^{107,109}Ag [3] and ^{112}Cd [4] in the energy range of *p*-process nucleosynthesis was undertaken.

80.2 Experimental Details

Both reactions involve *p*-nuclei never studied before. In this work, radiative proton-capture reactions were studied by means of in-beam γ-ray spectroscopy. For the case of ^{112}Cd$(p,\gamma)^{113}$In the activation method was additionally used to account for a low-lying isomeric state in ^{113}In (E = 391.7 keV, $t_{1/2}$ = 99.5 min).

The detection apparatus comprised four 100% HPGe detectors, mounted on a turntable (Fig. 80.1), so as to obtain angular distributions of the transitions of interest. In the case of ^{107,109}Ag$(p,\gamma)^{108,110}$Cd reaction, no significant angular dependence was observed in contrast with ^{112}Cd$(p,\gamma)^{113}$In (see Fig. 80.3). For each reaction the total cross section was deduced by measuring photopeak intensities of all the transitions feeding the ground state of the produced nucleus.

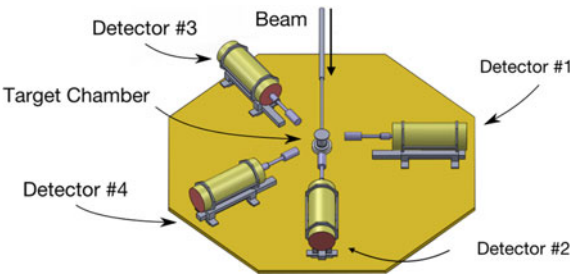

Fig. 80.1 A sketch of the experimental setup

80.3 Results and Conclusion

Measured cross sections for the ^{107}Ag$(p, \gamma)^{108}$Cd reaction are shown in Fig. 80.2, while preliminary results for the ^{112}Cd$(p, \gamma)^{113}$In are shown in Fig. 80.3. The experimental results are compared to Hauser–Feshbach calculations employing the latest version of the TALYS code (v1.9) [5]. A total of 96 different model combinations of the three main ingredients of the TALYS code, i.e. the Optical Model Potential (OMP), the Nuclear Level Density (NLD), and the γ-ray Strength Function (γSF) (See Table 80.1), resulted in the shaded areas shown.

It is worth mentioning that compared to [3], the experimental points are the same, however the Hauser–Feshbach calculations have been performed with the newest version of TALYS (v1.9) and a finer energy step ($\approx$8 keV). In addition, the effect of the γSF was exclusively studied by keeping the OMP and NLD unchanged. The combination of OMP and NLD used (See Table 80.1) seems to well reproduce the experimental data both in trend and magnitude.

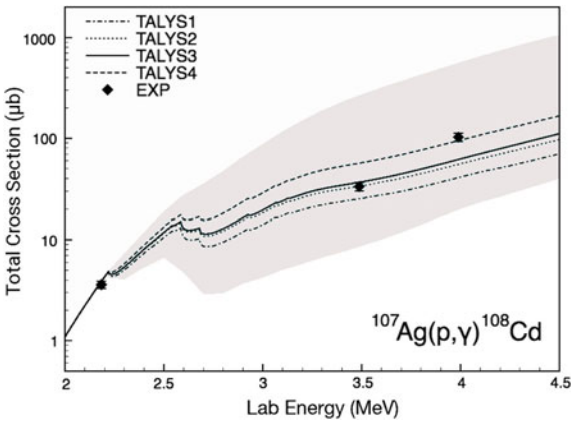

Fig. 80.2 ^{107}Ag(p, γ) reaction cross sections

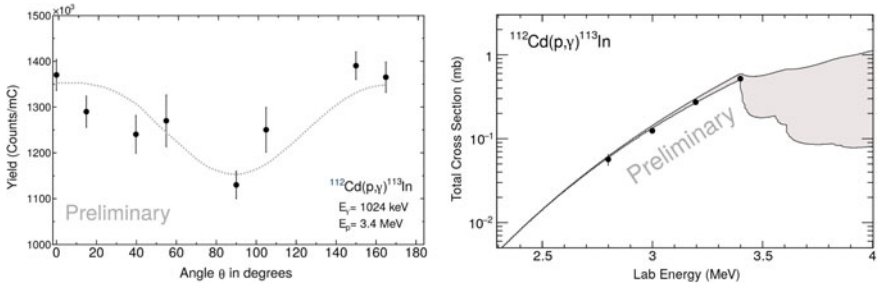

Fig. 80.3 (Left) A typical γ angular distribution (1024 keV, $E_p = 3.4$ MeV) (Right) Total reaction cross sections for the ^{112}Cd$(p, \gamma)^{113}$In reaction

Table 80.1 Combinations of models used in TALYS for the ^{107}Ag$(p, \gamma)^{108}$Cd reaction

Model	OMP	NLD	γSF
TALYS1	BDG[a]	THBFBG[b]	Kopecky-Uhl
TALYS2	BDG	THBFBG	HFB tables
TALYS3	BDG	THBFBG	HFB-BCS tables
TALYS4	BDG	THBFBG	Gogny D1M
			HFB + QRPA

[a]BDG Bauge-Delaroche-Girod
[b]THFBG T-dependent HFB, Gogny force

Note that for the ^{112}Cd$(p, \gamma)^{113}$In reaction, at E = 3.4 MeV, the respective (p, n) channel threshold is reached, hence the wide spread of model predictions thereafter (shaded region in the left panel of Fig. 80.3).

The reported (partially preliminary) results show an overall good agreement with the theoretical predictions of the TALYS code. The present study provides valuable new input for the theoretical modeling of the p-process, but undoubtedly, more experimental studies in the mass region are needed to shed light on the complex nucleosynthesis network in this mass regime.

Acknowledgements Support from EΛΙΔΕΚ (No 2017/694) is acknowledged.

References

1. M. Arnould, S. Goriely, https://doi.org/10.1016/S0370-1573(03)00242-4
2. T. Rauscher et al., https://doi.org/10.1088/0034-4885/76/6/066201
3. A. Khaliel et al., https://doi.org/10.1103/PhysRevC.96.035806
4. A. Psaltis et al., (2018) (in preparation)
5. A. Koning et al., TALYS-1.9 (2017). http://talys.eu

Chapter 81
Radiative Alpha Capture on ^{7}Be with DRAGON at Energies Relevant to the νp-Process

A. Psaltis, A. A. Chen, D. S. Connolly, B. Davids, N. Esker, G. Gilardy, Uwe Greife, W. Huang, D. A. Hutcheon, J. Karpesky, A. Lennarz, J. Liang, M. Lovely, S. N. Paneru, R. Giri, C. Ruiz, G. Tenkila, A. Wen and M. Williams

Abstract The origin of the *p*-nuclei, has been a long-standing puzzle in nuclear astrophysics. The νp-process is a candidate for the production of the light *p*-nuclei, but it presents high sensitivity to both supernova dynamics and nuclear physics. It has been recently shown that the breakout from *pp*-chains through the ^{7}Be$(\alpha, \gamma)^{11}$C reaction, which occurs prior to νp-process, can significantly influence the reaction flow, and subsequently the production of *p*-nuclei in the $90 < A < 110$ region.

A. Psaltis (✉) · A. A. Chen · J. Liang
Department of Physics and Astronomy, McMaster University, Hamilton, Ontario L8S 4M1, Canada
e-mail: psaltisa@mcmaster.ca

D. S. Connolly · B. Davids · N. Esker · W. Huang · D. A. Hutcheon · A. Lennarz · C. Ruiz · M. Williams
TRIUMF, 4004 Wesbrook Mall, Vancouver, British Columbia V6T 2A3, Canada

G. Gilardy
Department of Physics, Joint Institute for Nuclear Astrophysics, University of Notre Dame, Notre Dame, IN 46556, USA

Centre d'Études Nucléaires de Bordeaux Gradignan, UMR 5797 CNRS/IN2P3 - Université de Bordeaux, 19 Chemin du Solarium, CS 10120, Gradignan 33175, France

U. Greife · J. Karpesky · M. Lovely
Department of Physics, Colorado School of Mines, Golden, CO 80401, USA

W. Huang
Department of Physics, University of Northern British Columbia, Prince George, BC V2N 4Z9, Canada

G. Tenkila · A. Wen
Department of Physics and Astronomy, University of British Columbia, Vancouver, British Columbia V6T 1Z4, Canada

S. N. Paneru · R. Giri
Department of Physics and Astronomy, Ohio University, Athens, OH 45701, USA

M. Williams
Department of Physics, University of York, Heslington, York YO10 5DD, UK

A. Formicola et al. (eds.), *Nuclei in the Cosmos XV*, Springer Proceedings in Physics 219, https://doi.org/10.1007/978-3-030-13876-9_81

Nevertheless, this reaction has not been studied well yet in the relevant temperature range - T = 1.5–3 GK. To that end, the first direct study of important resonances of the ^{7}Be$(\alpha, \gamma)^{11}$C reaction with unknown strengths using DRAGON was recently performed at TRIUMF. The reaction was studied in inverse kinematics using a radioactive ^{7}Be ($t_{1/2}$ = 53.24 d) beam provided by ISAC-I and two resonances above the ^{11}C α-separation energy - $Q_\alpha = 7543.62$ keV - were measured. The experimental details, in particular how the recoil transmission and BGO efficiencies were accounted for considering the large cone angle for this reaction, will be presented and discussed alongside some preliminary results.

81.1 Introduction

The nucleosynthesis of heavy elements in the neutrino-driven wind of core-collapse supernovae has gained a lot of attention in recent years. Assuming that the ejecta of the supernova are proton-rich, as has been shown in simulations [1], the νp-process operates synthesizing the nuclei with $A > 64$ [2].

However, the particular scenario appears to be very sensitive to both supernova dynamics and nuclear physics input. In a recent study of the uncertainties of the aforementioned factors, Wanajo et al. [3] found that the breakout from the hot *pp*-chains through the ^{7}Be$(\alpha, \gamma)^{11}$C, which occurs prior to the onset of the νp-process, influences the reaction flow and eventually the final abundances of nuclei in the $90 < A < 110$ region.

Nevertheless, most of the reactions related to breakout processes have not yet been studied well, since they involve unstable nuclei. More specifically, for ^{7}Be$(\alpha, \gamma)^{11}$C, there are five known resonances in the relevant energy window for T = 1.5–3 GK that regulate the astrophysical reaction rate but only two of them have known strengths [4–6]. In order to improve the reaction rate at energies relevant to the νp-process, a new direct measurement of ^{7}Be$(\alpha, \gamma)^{11}$C, focusing on resonances with unknown strengths was recently performed at TRIUMF using the DRAGON recoil separator.

81.2 Experimental Details

The DRAGON recoil separator [7] has four main components: (a) the windowless, differentially pumped, recirculated gas target, (b) the γ-ray detector array consisting of 30 BGO detectors, (c) the electromagnetic separator and (d) the recoil detection system.

The ^{7}Be$(\alpha, \gamma)^{11}$C reaction also poses a great challenge for DRAGON as far as its acceptance in the light mass regime is concerned. The maximum momentum cone of the recoils far exceeds its acceptance and for this reason, simulations using `GEANT3` were performed to investigate the transmission of the recoils as well as the BGO

array efficiency. Since DRAGON measures reaction yields, resonance strengths are extracted by:

$$\omega\gamma = \frac{2Y\epsilon}{\lambda_{cm}^2}\frac{m_{^4\mathrm{He}}}{m_{^4\mathrm{He}}+m_{^7\mathrm{Be}}} \& \; Y = \frac{N_{recoils}}{N_{beam}\times\eta_{BGO}\times\eta_{sep}\times\eta_{DSSSD}\times f_q} \tag{81.1}$$

Where ϵ is the target stopping power and f_q is the charge state distribution of the recoils The aforementioned simulations provide the efficiencies of the separator and the BGO array (η_{sep} & η_{BGO}).

The reaction was studied in inverse kinematics using a radioactive ^{7}Be beam ($t_{1/2}$ = 53.24 d) provided by ISAC impinging on the ^{4}He filled gas target. The most intense charge state of ^{11}C (q = 2^+) was tuned through the separator and the recoils were detected using a double-sided silicon strip detector (DSSSD). To further increase the beam suppression, identification of real events was carried out using the BGO array signals in coincidence with the DSSSD.

81.3 Preliminary Results

Two resonances corresponding to states of ^{11}C were studied (E_x = 8.654 MeV & E_x = 8.699 MeV). Unfortunately, the radioactive ion beam was contaminated by the isobar ^{7}Li, nevertheless some encouraging results were obtained. Figure 81.1 Left shows a clean separator time-of-fight spectrum, which however suffers from low statistics. The ^{7}Be content in the beam was extracted using TRIUMF's Resonant Ionization Laser Ion Source (TRILIS) [8] and was around 10^7 pps during the experiment.

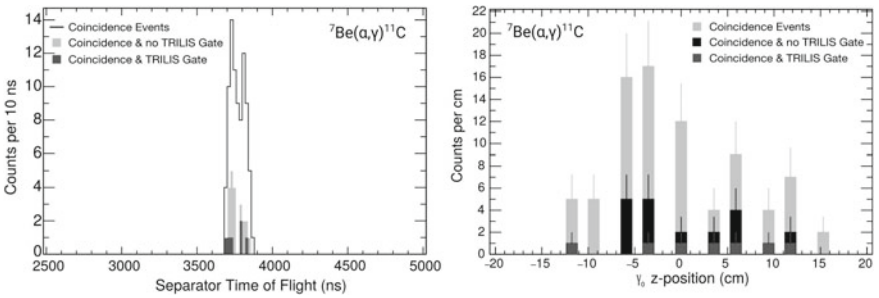

Fig. 81.1 Preliminary results from the resonance at E_x = 8.699 MeV. (Left) Separator time-of-flight, time a recoil takes to travel through DRAGON which starts by a γ-ray signal in the BGO array and stops by a hit in the DSSSD & (Right) BGO γ-ray hit pattern, γ-ray signals in the BGO array versus their position along the beam axis with respect to the target center. Coincidence events are gated only on the Separator time-of-flight and include all DSSSD triggers, while the other two include DSSSD, BGO energy and TRILIS signal cuts

81.4 Conclusion and Future Goals

A first attempt to study the astrophysically important $^{7}\mathrm{Be}(\alpha,\gamma)^{11}\mathrm{C}$ reaction was recently performed using the DRAGON recoil separator. Given the challenging nature of the reaction, detailed simulations are necessary to obtain reliable resonance strengths and this first measurement can be used as a benchmark to further improve them. A new measurement of the reaction with a more intense and pure radioactive ^{7}Be beam is expected in the near future.

References

1. S. Wanajo et al., Astrophys. J. **852**, 40 (2018). http://iopscience.iop.org/article/10.3847/1538-4357/aa9d97/meta
2. C. Fröhlich et al., Phys. Rev. Lett. **96**, 142502 (2006). https://journals.aps.org/prl/abstract/10.1103/PhysRevLett.96.142502
3. S. Wanajo, H.-T. Janka, S. Kubono, Astrophys. J. **729**, 46 (2011). http://iopscience.iop.org/article/10.1088/0004-637X/729/1/46/meta
4. G. Hardie et al., Phys. Rev. C **29**, 1199 (1984). https://journals.aps.org/prc/abstract/10.1103/PhysRevC.29.1199
5. M. Wiescher et al., Phys. Rev. C **28**, 1431 (1983). https://journals.aps.org/prc/abstract/10.1103/PhysRevC.28.1431
6. H. Yamaguchi et al., Phys. Rev. C **87**, 034303 (2013). https://journals.aps.org/prc/abstract/10.1103/PhysRevC.87.034303
7. D.A. Hutcheon et al., Nucl. Instrum. Meth. Phys. Res. A **498**, 190 (2003). https://www.sciencedirect.com/science/article/pii/S0168900202019903
8. J. Lassen et al., Hyperfine Interactions **162**, 69 (2005). https://link.springer.com/article/10.1007/s10751-005-9212-2

Chapter 82
Uncertainties in the Production of *p* Nuclides in SN Ia Determined by Monte Carlo Variations

Thomas Rauscher, Nobuya Nishimura, Raphael Hirschi, Alex St. J. Murphy, Gabriele Cescutti and Claudia Travaglio

Abstract Several thousand tracers from a 2D model of a thermonuclear supernova were used in a Monte Carlo post-processing approach to determine *p*-nuclide abundance uncertainties originating from nuclear physics uncertainties in the reaction rates.

82.1 Introduction

Type Ia supernovae (SN Ia) originating from the explosion of a white dwarf accreting mass from a companion star have been suggested as a site for the production of *p* nuclides [1]. The recently developed Monte Carlo (MC) code PizBuin [2] was applied to the post-processing of temperature and density profiles obtained with tracer particles extracted from a 2D model of a thermonuclear supernova explosion. This code

T. Rauscher (✉)
Department of Physics, University of Basel, Basel, Switzerland
e-mail: thomas.rauscher@unibas.ch

Centre for Astrophysics Research, University of Hertfordshire, Hatfield AL10 9AB, UK

N. Nishimura
Yukawa Institute for Theoretical Physics, Kyoto University, Kyoto, Japan

R. Hirschi
Astrophysics Group, Faculty of Natural Sciences, Keele University, Keele, UK

Kavli IPMU (WPI), University of Tokyo, Tokyo, Japan

A. S. J. Murphy
School of Physics and Astronomy, University of Edinburgh, Edinburgh, UK

G. Cescutti
INAF, Osservatorio Astronomico di Trieste, Trieste, Italy

C. Travaglio
INFN, Sezione di Torino, Torino, Italy

T. Rauscher · R. Hirschi · A. S. J. Murphy
UK Network for Bridging Disciplines of Galactic Chemical Evolution (BRIDGCE), Keele, UK
URL: https://www.bridgce.ac.uk

A. Formicola et al. (eds.), *Nuclei in the Cosmos XV*, Springer
Proceedings in Physics 219, https://doi.org/10.1007/978-3-030-13876-9_82

already has been applied to several other nucleosynthesis environments [3, 4] to tackle the question of how uncertainties in the nuclear reaction rates propagate into the final abundance yields. Realistic, temperature-dependent reaction rate uncertainties are used, combining experimental and theoretical uncertainties. Bespoke uncertainties are assigned to each individual rate and all rates are varied simultaneously within their uncertainty limits. This approach allows to probe the combined action of all uncertainties and proved superior to manual variation of a few rates or coupled variation of rate subsets.

In this study, 51,200 tracers were extracted from the DDT-a explosion model as described in [1]. Among these, 4624 tracers experienced conditions supporting the production of p nuclides and their temperature and density profiles were used in the MC post-processing. The reaction network included 1342 nuclides (around stability and towards the proton-rich side). To complete the study it had to be run more than 40 million times. This necessitated the use of HPC facilities.

82.2 Results

Figure 82.1 shows the total production uncertainties (all tracers combined) for each p nuclide. With the exception of ^{180}Ta, which is known to receive major contributions from other nucleosynthesis processes, the uncertainties are well below a factor of

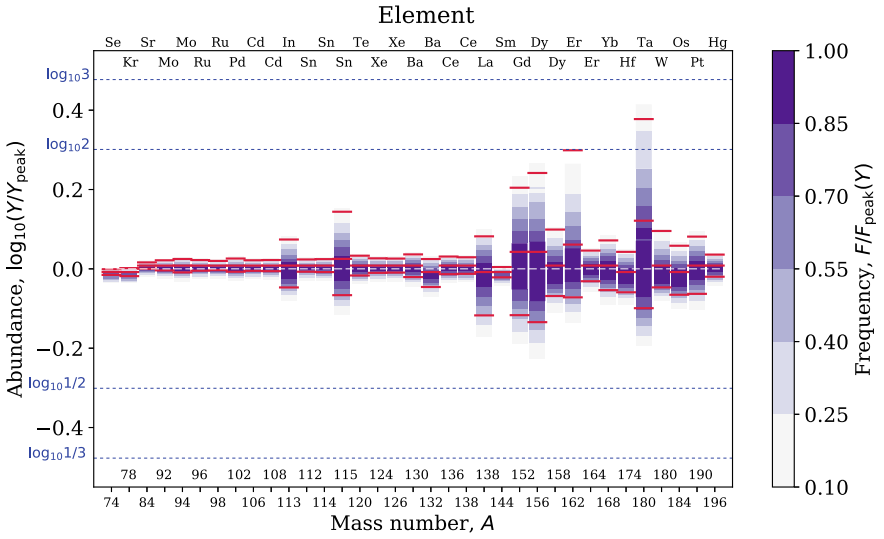

Fig. 82.1 Total production uncertainties of p nuclide due to rate uncertainties. The color shade gives the relative probabilistic frequency and the horizontal red lines enclose a 90% probability interval for each nuclide. Uncertainty factors of two and three are marked by dotted lines. Note that the uncertainties are asymmetric and that the abundance scale is logarithmic. Figure taken from [5], with permission

two, despite the fact that photodisintegration, electron capture, and β^+-decay rates of unstable nuclides bear much larger uncertainties. The uncertainties are also considerably smaller than those found for the production of p nuclides in the γ-process in explosions of massive stars (core-collapse supernovae, ccSN) [2]. This can be explained by the larger number of temperature-density combinations encountered in SN Ia, which allow alternative reaction flows bypassing suppressed reactions.

Due to the challenging demand on CPU time, only one SN Ia explosion model was studied. To be able to draw more general conclusions, uncertainty contributions from high and low density regions in the white dwarf were also scrutinised separately. The high density regions gave rise to larger uncertainties in the final abundances [5]. Based on the ratio of high- to low-density regions in other models, our results can be used to estimate the resulting uncertainties also in those other models.

As in our previous investigations [2–4], key rates were identified by correlations between rate and abundance variations. Only one reaction was found to dominate the total production uncertainty: The uncertainty in $^{145}\mathrm{Eu} + \mathrm{p} \leftrightarrow \gamma + ^{146}\mathrm{Gd}$ significantly affects the abundance uncertainty of ^{146}Sm. Again, this is due to the range of conditions found in SN Ia. Considering high- and low-density regions separately, a few other key reactions were identified. For the low-density group, five key rates were found: $^{129}\mathrm{Ba} + \mathrm{n} \leftrightarrow \gamma + ^{130}\mathrm{Ba}$ for ^{130}Ba, $^{137}\mathrm{Ce} + \mathrm{n} \leftrightarrow \gamma + ^{138}\mathrm{Ce}$ for ^{138}Ce, $^{144}\mathrm{Sm} + \alpha \leftrightarrow \gamma + ^{148}\mathrm{Gd}$ for ^{146}Sm, $^{164}\mathrm{Yb} + \alpha \leftrightarrow \gamma + ^{168}\mathrm{Hf}$ for ^{168}Yb, and $^{186}\mathrm{Pt} + \alpha \leftrightarrow \gamma + ^{190}\mathrm{Hg}$ for ^{190}Pt. For the high-density group, seven key rates were identified: $^{83}\mathrm{Rb} + \mathrm{p} \leftrightarrow \gamma + ^{84}\mathrm{Sr}$ for ^{84}Sr, $^{105}\mathrm{Cd} + \mathrm{n} \leftrightarrow \gamma + ^{106}\mathrm{Cd}$ for ^{106}Cd, $^{111}\mathrm{Sn} + \mathrm{n} \leftrightarrow \gamma + ^{112}\mathrm{Sn}$ for ^{112}Sn, $^{129}\mathrm{Ba} + \mathrm{n} \leftrightarrow \gamma + ^{130}\mathrm{Ba}$ for ^{130}Ba, $^{137}\mathrm{Ce} + \mathrm{n} \leftrightarrow \gamma + ^{138}\mathrm{Ce}$ for ^{138}Ce, $^{176}\mathrm{W} + \alpha \leftrightarrow \gamma + ^{180}\mathrm{Os}$ for ^{180}W, and $^{186}\mathrm{Pt} + \alpha \leftrightarrow \gamma + ^{190}\mathrm{Hg}$ for ^{190}Pt.

For further details on calculation and results, see [5].

Acknowledgements This work has been partially supported by the European Research Council (EU-FP7-ERC-2012-St Grant 306901), the EU COST Action CA16117 (ChETEC), the UK STFC (ST/M000958/1), and MEXT Japan (Priority Issue on Post-K computer: Elucidation of the Fundamental Laws and Evolution of the Universe). Parts of the computations were carried out on COSMOS (STFC DiRAC Facility) at the University of Cambridge. Further computations were carried out at CfCA, NAO Japan, and at YITP, Kyoto University.

References

1. C. Travaglio, F.K. Röpke, R. Gallino, W. Hillebrandt, Type Ia supernovae as sites of the p-process: two-dimensional models coupled to nucleosynthesis. Ap. J. **739**, 93 (2011). https://doi.org/10.1088/0004-637X/739/2/93
2. T. Rauscher, N. Nishimura, R. Hirschi, G. Cescutti, A.St.J. Murphy, A. Heger, Uncertainties in the production of p nuclei in massive stars obtained from Monte Carlo variations. MNRAS **463**, 4153 (2016). https://doi.org/10.1093/mnras/stw2266
3. N. Nishimura, R. Hirschi, T. Rauscher, A.St.J. Murphy, G. Cescutti, Uncertainties in s-process nucleosynthesis in massive stars determined by Monte Carlo variations. MNRAS **469**, 1752 (2017). https://doi.org/10.1093/mnras/stx696

4. G. Cescutti, R. Hirschi, N. Nishimura, J.W. den Hartogh, T. Rauscher, A.St.J. Murphy, S. Cristallo, S.Uncertainties in s-process nucleosynthesis in low-mass stars determined from Monte Carlo variations. MNRAS **478**, 4101 (2018). https://doi.org/10.1093/mnras/sty1185
5. N. Nishimura, T. Rauscher, R. Hirschi, A.St.J. Murphy, G. Cescutti, G., C. Travaglio, Uncertainties in the production of p nuclides in thermonuclear supernovae determined by Monte Carlo variations. MNRAS **474**, 3133 (2018). https://doi.org/10.1093/mnras/stx3033

Chapter 83
Germanium Detector Based Study of the ^{2}H(p,γ)^{3}He Cross Section at LUNA

Klaus Stöckel

Abstract The Big Bang Nucleosynthesis theory for a given baryon density provides the abundance of the primordial elements. Deuterium is the only isotope which, in the precision era of cosmology, is better observed than predicted, with accuracy of about 1 and 2%, respectively. This is mainly due to the uncertainty on the ^{2}H(p,γ)^{3}He cross section, known only at the 9% level in the BBN energy range (30–300 keV). The aim of the present work is to introduce one of the experimental approaches adopted by the LUNA (Laboratory for Underground Nuclear Astrophysics) collaboration, whose goal is to measure the ^{2}H(p,γ)^{3}He reaction cross section in the energy range $30 < E_{c.m.}$ [keV] < 300 with $\sim$5% accuracy.

83.1 The High Purity Germanium (HPGe) Setup

The cross section of the ^{2}H(p,γ)^{3}He reaction has been measured in the energy range 2.5–22 keV by the LUNA collaboration in the INFN underground Gran Sasso Laboratories in Italy [1–3].

A new measurement with two phases is under analysis. The LUNA 400 kV ion accelerator was used to deliver a proton beam on target [4]. In the first phase a Bismuth Germanium Oxide (BGO) detector was used [5] and the second phase was dedicated to a measurement with a HPGe setup.

Klaus Stöckel: For the LUNA Collaboration.

K. Stöckel (✉)
Helmholtz-Zentrum Dresden-Rossendorf, Dresden, Germany
e-mail: k.stoeckel@hzdr.de

Institute for Nuclear and Particle Physics, TU Dresden, Dresden, Germany

A. Formicola et al. (eds.), *Nuclei in the Cosmos XV*, Springer
Proceedings in Physics 219, https://doi.org/10.1007/978-3-030-13876-9_83

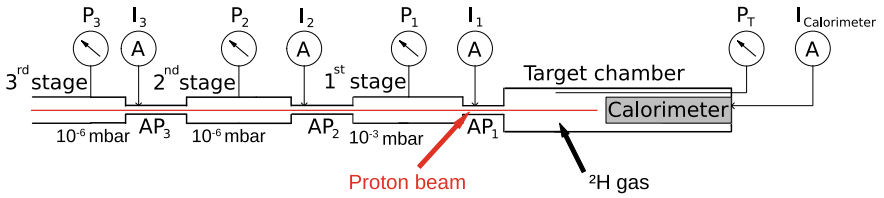

Fig. 83.1 Drawing of the three pumping stages and the target chamber with the calorimeter inside

The experimental setup for the HPGe-phase includes a differentially pumped 33 cm long windowless gas target chamber. The target gas is a 99% isotropically enriched deuterium gas at a pressure of 0.3 mbar. In order to provide a constant pressure inside the target chamber and a strong pressure gradient between the beam line and the target chamber the differential pumping system consists of three pumping stages connected with water cooled apertures of decreasing diameter (Fig. 83.1).

A constant temperature gradient calorimeter is placed inside the target chamber. It serves as a beam stop and beam current measuring device. The beam impinges on the hot side of the calorimeter which is heated up by thermoresistors to a constant temperature of 70 °C. The cold side is cooled down to 0 °C by a feedback controlled chiller [6]. The difference between the calorimeter power with and without beam is used to determine the beam current.

83.2 Analysis of the HPGe-Phase

The experimental setup consists of a 137% HPGe detector (labeled as Fixed HPGe in Fig. 83.2) in close geometry of 0.7 cm distance to the target chamber with the interaction chamber and a collimated and movable 120% HPGe detector (labeled as Movable HPGe in Fig. 83.2). With this setup the angular distribution can be inferred by exploiting the high energy resolution of the detector and the Doppler effect responsible for the broad energy distribution of the detected gamma rays coming from different directions inside the extended gas target. The ^{2}H(p,γ)^{3}He photons have an energy of about 5.5 MeV, far away from the energy of the commonly used radioactive sources. Thus, for determining the setup efficiency a different technique based on the well-known resonant reactions ^{14}N(p,γ)^{15}O and on ^{60}Co radioactive decay has been used. For this measurement the collimated 120% HPGe detector was moved along the target chamber in 3 cm steps, to measure the emitted γ-rays in coincidence mode with the fixed 137% HPGe detector. The results of the efficiency measurements were used to confirm Monte Carlo simulations for the HPGe-setup.

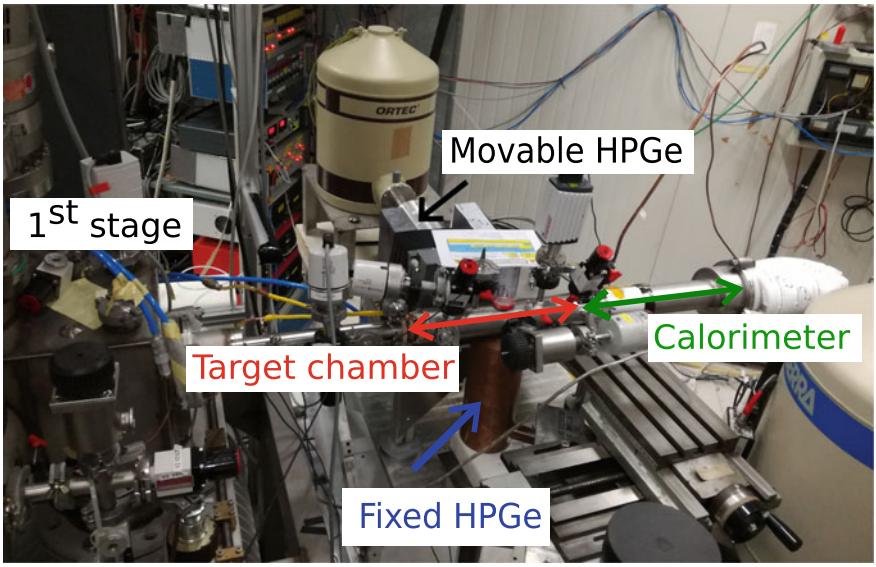

Fig. 83.2 Setup of the HPGe-phase with target chamber, HPGe-detectors and first pumping stage

In order to reduce the systematic error due to the summing correction, the setup efficiency has been measured exploiting the coincidence between two γ-rays emitted in cascade (from source as well as from reaction) and detected by two different germanium detectors, the main detector (Ge1) and a second one used as the acquisition trigger (Ge2). Whenever Ge2 detects an event 1, it enables Ge1 that can thus detect photon 2 emitted in cascade: the ratio of the observed photons with respect to the number of triggers provides the Ge1 efficiency. In case of ^{60}Co, for each radioactive decay process, two photons, γ_1 = 1.17 MeV and γ_2 = 1.33 MeV, are produced. In the case of the resonant capture, several decay branches are able to provide two photons in cascade of energies up to 6.7 MeV, even higher than the ^{2}H(p,γ)^{3}He reaction.

This method allows fixing precisely the detector energy response. To measure the cross section we did a scan in the energy range of interest (30 keV $< E_{c.m.} <$ 300 keV) with 30–50 keV steps; two runs were performed for each energy: one with deuterium gas inside the scattering chamber, the other with ^{4}He in order to evaluate the beam induced background contribution and the eventual deuterium implantation.

For proton energies below 250 keV, the beam induced background is negligible. At higher energies the resonance at 340 keV of ^{19}F(p,$\alpha\gamma$)^{16}O reaction produce some beam induced background in the region of interest, but it does not limit the precision (Fig. 83.3).

The data taking has been completed, the analysis is ongoing.

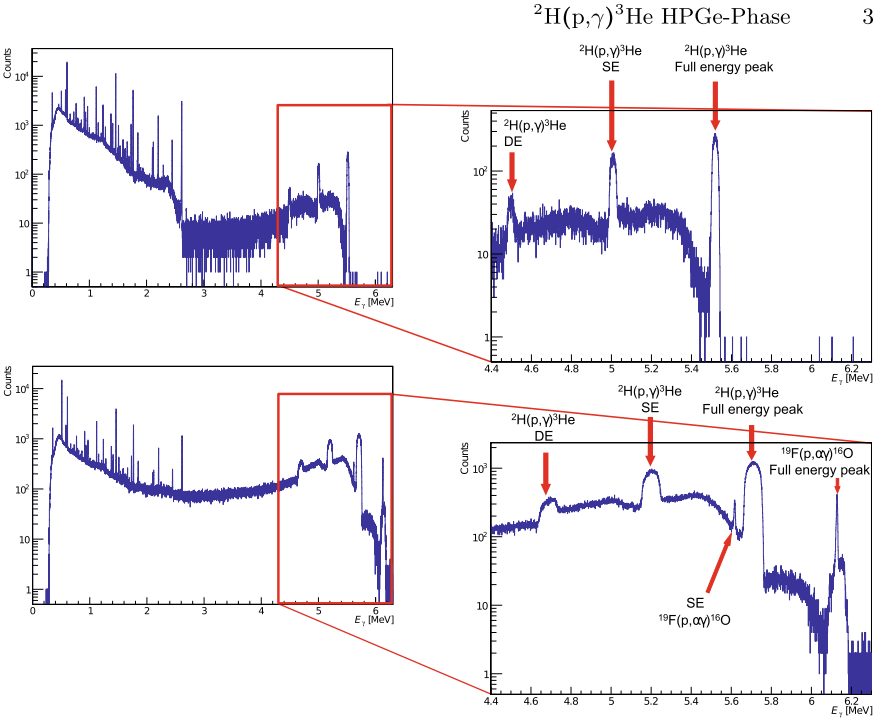

Fig. 83.3 Top picture: ^{2}H(p,γ)^{3}He spectrum of the 137%-detector at 50 keV beam energy with zoom in p + d energy region. Bottom picture: ^{2}H(p,γ)^{3}He spectrum of the 130%-detector at 335 keV beam energy with zoom in p + d energy region

Acknowledgements Supported in part by DFG (BE4 100/4-1).

References

1. C. Casella et al., Nucl. Inst. Meth. A **489**, 160–169 (2002). https://doi.org/10.1016/S0168-9002(02)00577-6
2. C. Broggini et al., Prog. Nucl. Part. Phys. **98**, 55–84 (2018). https://doi.org/10.1016/j.ppnp.2017.09.002
3. S. Zavatarelli, *Contribution to the NIC 2018 Conference Proceeding*
4. A. Formicola et al., Nucl. Inst. Meth. A **507**, 609 (2003). https://doi.org/10.1016/S0168-9002(03)01435-9
5. V. Mossa, *Contribution to the NIC 2018 Conference Proceeding*
6. F. Ferraro et al., Eur. Phys. J. A **54**, 44 (2018). https://doi.org/10.1140/epja/i2018-12476-7

Chapter 84
R-Process Nucleosynthesis in Core-Collapse Supernova Explosions and Binary Neutron Star Mergers

Toshio Suzuki, Shota Shibagaki, Takashi Yoshida, Toshitaka Kajino and Takaharu Otsuka

Abstract Beta decay rates for exotic nuclei with neutron magic number of $N = 126$ relevant to r-process nucleosynthesis are studied up to $Z = 78$ by shell model calculations. The half-lives for the waiting-point nuclei, which are found to be short compared to a standard finite-range-droplet model (FRDM), are used to study r-process nucleosynthesis in core-collapse supernova explosions and binary neutron star mergers. The element abundances are obtained up to third peak as well as beyond the peak region up to thorium and uranium. We find that thorium and uranium elements are produced more with the shorter shell-model half-lives and their abundances come close to the observed values in core-collapse supernova explosions. In case of binary neutron star mergers, thorium and uranium are produced as much as consistent with the observed values independent of the half-lives.

T. Suzuki (✉)
Department of Physics, College of Humanities and Sciences, Nihon University, Sakurajosui 3-25-40, Setagaya-ku, Tokyo 156-8550, Japan
e-mail: suzuki@phys.chs.nihon-u.ac.jp

T. Suzuki · T. Kajino
National Astronomical Observatory of Japan, Mitaka, Tokyo 181-8588, Japan

S. Shibagaki
Department of Applied Physics, Fukuoka University, Jonan, Nanakuma, Fukuoka 814-0180, Japan

T. Yoshida · T. Kajino
Graduate School of Science, The University of Tokyo, Hongo, Bunkyo-ku, Tokyo 113-0033, Japan

T. Kajino
School of Physics and Nuclear Energy Engineering, International Research Center for Big-Bang Cosmology and Element Genesis, Beihang University, Beijing 100083, People's Republic of China

T. Otsuka
RIKEN Nishina Center for Accelerated-Based Science, Hirosawa, Wako-shi, Saitama 351-0198, Japan

National Superconducting Cyclotron Laboratory, Michigan State University, East Lansing, MI 48824, USA

A. Formicola et al. (eds.), *Nuclei in the Cosmos XV*, Springer Proceedings in Physics 219, https://doi.org/10.1007/978-3-030-13876-9_84

84.1 β-Decay Half-Lives of the $N = 126$ Isotones

Beta-decay rates for exotic waiting point nuclei relevant to r-process nucleosynthesis are studied by shell-model calculations including both Gamow-Teller (GT) and first-forbidden (FF) transitions. We extend our previous work for the isotones with $Z = 64$–73 [1] to a wider range of $Z = 64$–78. The extension of the region to higher Z is important to discuss the element synthesis far beyond the third peak up to thorium and uranium. The modified G-matrix [2, 3] is adopted with configuration spaces including up to $2\hbar\omega$ excitations from the filling approximations for proton holes up to $Z = 74$, while for $Z = 75$–78 wider configuration spaces are taken. A quenching factor of $g^A_{eff}/g_A = 0.70$ (0.50) is adopted for the GT transitions for $Z \geq 76$ ($Z = 64$–75), and those for FF transitions with 1^- and 2^- are taken to be $g^A_{eff}/g_A = 0.34$ and $g^V_{eff}/g_V = 0.67$, respectively [2]. As for 0^-, the M^T_0 ($\boldsymbol{\sigma} \cdot \mathbf{p}$ term from γ_5) [1] is enhanced due to the meson exchange current effects by twice [4]. The mass formulae of FRDM [5, 6] are used except for the isotones with $N = 126$ and their daughters of the beta-decays, where the Q-values obtained by the shell-model calculations are taken.

The half-lives obtained in the present shell-model calculations [7] are found to be short compared with the standard values by FRDM [5, 6], while they are close to another shell-model evaluation [8]. See Fig. 1 and Table 1 of [7] for more details. The contributions from the FF transitions become more important for larger Z and dominant at $Z > 72$. The odd-even staggering effects in the half-lives found in the FRDM are not seen in the shell-model calculations. Calculated half-life for $Z = 78$ (^{204}Pt), $\tau_{1/2} = 38.3$ s, is found to be fairly consistent with the recent experimental data; $16+6/-5$ s [9].

84.2 R-Process Nucleosynthesis

The half-lives obtained by the present shell-model calculations are applied to investigate the r-process nucleosynthesis in three different models of core-collapse supernovae (CCSNe) and binary neutron-star mergers (NSMs). The CCSN models adopted here are the neutrino-driven wind (νDW) model in supernova explosions and the magnetohydrodynamic jet (MHDJ) supernova explosion model. We use the dynamical ejecta model for the binary NSM. It has been argued that all these three mechanisms are necessary for the r-process nucleosynthesis [10]. For nucleosynthesis calculations, β-decay half-lives of FRDM [5, 6] are used for the "standard" case while for the "modified" case β-decay half lives of the $N = 126$ isotones are changed to new ones obtained by our shell model calculation.

For the νDW model, an analytic model for the single flow of neutrino-driven winds [11] is used for the time evolution of thermal profiles. The neutrino energy spectra are assumed to obey Fermi distributions with zero chemical potentials with the temperatures, (T_{ν_e}, $T_{\bar{\nu}_e}$, T_{ν_x}) = (3.2, 5, 6 MeV), where ν_x is $\nu_{\mu,\tau}$ and $\bar{\nu}_{\mu,\tau}$. The

temperatures are determined to avoid an overproduction of the ^{11}B abundance during Galactic chemical evolution [12]. The luminosity of each flavor of neutrinos is equipartitioned and is taken to be $L_\nu = 1.0 \times 10^{51}$ erg/s [1, 7], which is a typical one during the νDW stage, that is, after a few seconds from the core bounce. The time scale of the expansion is artificially shortened by a constant factor $f_t = 0.08$ The final temperature of the wind is set to be $T_f = 8 \times 10^8$ and 1×10^8 K for the hot and cold r-process nucleosynthesis, respectively. The initial electron to baryon ratio is taken to be $Y_e = 0.40$.

The MHDJ supernova is an alternative and natural model for the CCSNe associated with jet or asymmetry. We use a jet-like supernova explosion model based upon a two-dimensional magnetohydrodynamic simulation [13] where the ejecta consist of 23 tracers to describe the thermodynamic evolution of each outflow.

In the present NSM model, we use 30 trajectories of the NSM ejecta in the hydrodynamic simulations [14–16] based on the smoothed-particle-hydrodynamic (SPH) method in Newtonian gravity where the neutrino transport is taken into account in the neutrino leakage scheme [17]. The hydrodynamic evolution of the flow trajectories is continued as a free adiabatic expansion [18].

84.3 Conclusion

In all the three models above, the third peak of the r-process abundances is shifted toward higher mass region. In the νDW model, the abundances of thorium and uranium obtained with shorter half-lives are enhanced about by three times compared to those of FRDM, and they come closer to the solar abundances [7]. In the MHDJ model, general feature of the calculated abundances is similar to the results obtained in the νDW models, though the effects of the shorter β half-lives are smaller compared with the νDW model. In the NSM model, where $Y_e \approx 0.01$–0.1, the calculated abundances of Pb-Bi and Th-U elements are found to be close to the solar abundances independent of the β-decay half-lives at $N = 126$. This suggests that NSMs are promising robust r-process sites for producing very heavy elements such as thorium and uranium. Further extensive knowledge on the nuclear input properties on and near the r-process flow path might help identify both the r-process site and the nucleosynthesis mechanism.

References

1. T. Suzuki, T. Yoshida, T. Kajino, T. Otsuka, Phys. Rev. C **85**, 015802 (2012). https://doi.org/10.1103/PhysRevC.85.015802
2. L. Rydstrom et al., Nucl. Phys. A **512**, 217 (1980). https://doi.org/10.1016/0375-9474(90)93152-V
3. S.J. Steer et al., Phys. Rev. C **78**, 061302 (2008). https://doi.org/10.1103/PhysRevC.78.061302
4. E.K. Warburton, Phys. Rev. C **44**, 233 (1991). https://doi.org/10.1103/PhysRevC.44.233

5. P. Möller, J.R. Nix, K.-L. Kratz, At. Data Nucl. Data Tables **66**, 131 (1997). https://doi.org/10.1006/adnd.1997.0746
6. P. Möller, B. Pfeiffer, K.-L. Kratz, Phys. Rev. C **67**, 055802 (2003). https://doi.org/10.1103/PhysRevC.67.055802
7. T. Suzuki, S. Shibagaki, T. Yoshida, T. Kajino, T. Otsuka, ApJ. **859**, 133 (2018). https://doi.org/10.3847/1538-4357/aabfde
8. Q. Zhi et al., Phys. Rev. C **87**, 025803 (2013). https://doi.org/10.1103/PhysRevC.87.025803
9. A.I. Morales et al., Phys. Rev. Lett. **113**, 022702 (2014). https://doi.org/10.1103/PhysRevLett.113.022702
10. S. Shibagaki et al., ApJ. **816**, 79 (2016). https://doi.org/10.3847/0004-637X/816/2/79
11. K. Takahashi, H.-T. Janka, in *Origin of Matter and Evolution of Galaxies*, ed. by T. Kajino, S. Kubono, Y. Yoshii (World Scientific, Singapore, 1997), p. 213
12. T. Yoshida, T. Kajino, D.H. Hartmann, Phys. Rev. Lett. **94**, 231101 (2005). https://doi.org/10.1103/PhysRevLett.94.231101
13. S. Nishimura et al., ApJ. **642**, 410 (2006). https://doi.org/10.1086/500786
14. O. Korobkin, S. Rosswog, A. Arcones, D. Winteler, MNRAS **426**, 1940 (2012). https://doi.org/10.1111/j.1365-2966.2012.21859.x
15. T. Piran, E. Nakar, S. Rosswog, MNRAS **430**, 2121 (2013). https://doi.org/10.1093/mnras/stt037
16. S. Rosswog, T. Piran, E. Nakar, MNRAS **430**, 2585 (2013). https://doi.org/10.1093/mnras/sts708
17. S. Rosswog, M. Liebendörfer, MNRAS **342**, 673 (2003). https://doi.org/10.1046/j.1365-8711.2003.06579.x
18. S. Rosswog et al., MNRAS **439**, 744 (2014). https://doi.org/10.1093/mnras/stt2502

Chapter 85
Precise Measurement of the ^{95}Ru and ^{95}Tc Half-Lives

T. N. Szegedi

Abstract In order to evaluate the global alpha-nucleus optical potentials used in the simulation of the astrophysical γ-process, the cross section measurement of the ^{92}Mo(α,n)^{95}Ru and ^{92}Mo(α,p)^{95}Tc reactions is in progress at MTA Atomki using the activation technique. Precise information on the half-lives of the reaction products are essential for such a measurement. The half-lives of the produced ^{95}Ru and its daughter ^{95}Tc are published in previous works, however with large uncertainties and ambiguous values, therefore, these values have been re-measured with high precision using γ-spectroscopy. Details on the experimental approach and the half-life determination are presented in this article.

85.1 Introduction

The bulk of the elements heavier than Iron are synthesized via neutron capture reactions in the astrophysical s- [1] and r- processes [2]. However, at the proton-rich side of the valley of stability there are about 30–35 neutron-deficient isotopes, the so-called p-isotopes, which cannot be synthesized via neutron capture reactions. Most probably, the main stellar mechanism building up these species, the so - called γ-process—which takes place either in the O/Ne-rich layer of type II supernovae during core collapse or during the thermonuclear explosion of a white dwarf [3]—involves photodisingtegration reactions on already produced s and r seed nuclei. The modeling of this nucleosynthesis scenario and the calculation of the p-isotope abundances require the use of large nuclear reaction networks. In such a calculation about 22,000 reactions on approximately 2000, mostly unstable, isotopes are taken into account and the necessary cross sections are provided by the Hauser - Feshbach (H-F) statistical model. Nuclear physics inputs – e.g. optical potentials, nuclear level densities, γ-ray strength functions, etc. – are needed for the statistical model and the

T. N. Szegedi (✉)
University of Debrecen, Debrecen, Egyetem Tér 1. 4032, Hungary
e-mail: tn.szegedi@atomki.mta.hu

Institue for Nuclear Research (ATOMKI), Debrecen POB.51, 4001, Hungary

A. Formicola et al. (eds.), *Nuclei in the Cosmos XV*, Springer
Proceedings in Physics 219, https://doi.org/10.1007/978-3-030-13876-9_85

ambiguities of the input parameters introduce considerable uncertainties to the cross section predictions.

The reliability of the cross section predictions and the input parameters of the H-F model can be studied by measuring charged particle capture reaction cross sections [4]. Although, several charged particle induced cross section measurements were already performed [5–9], the available experimental database is still scarce [10]. To evaluate the different open-access global alpha-nucleus optical potentials the cross section measurement of the ^{92}Mo(α,n)^{95}Ru and ^{92}Mo(α,p)^{95}Tc reactions is in progress at Atomki using the activation technique. In this method, the cross section is deduced from the off-line activity measurement of the reaction products. The activity is strongly correlated to the half-life, thus the cross section is affected by the uncertainty of the half-life value.

85.2 Precise Half-Life Measurement

The literature values of the ^{95}Ru and the ^{95}Tc half-lives are $t_{1/2} = 1.643 \pm 0.013$ h and $t_{1/2} = 20.0 \pm 0.1$ h, respectively [11]. All of these values [12–14] were measured several decades ago, in the 60s and 70s and in the publications very little experimental details are presented and therefore the cross-check of the results is essential.

For this purpose four high purity, 0.5 mm thick molybdenum plates were irradiated with alpha beams of $E_\alpha = 13$; 12; 11 and 10.5 MeV, provided by the K = 20 cyclotron accelerator of Atomki. The duration of the irradiation varied between 5 and 12 h, the typical beam intensity was 2 μA. After the irradiation the activity of the samples were measured with a 50% relative efficiency HPGe detector, the distance between the targets and the endcap of the detector was set to be 21 cm. The γ-counting started

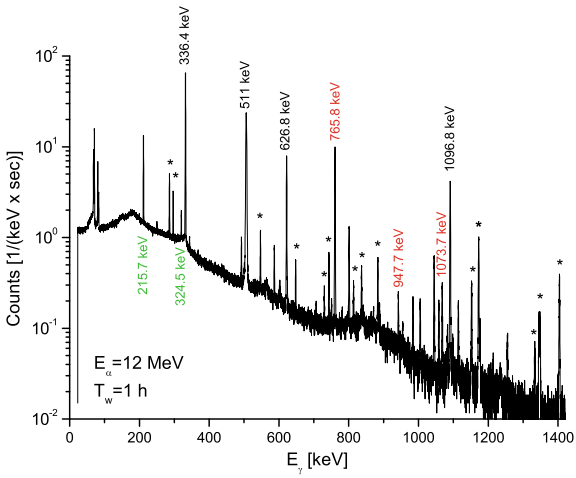

Fig. 85.1 Offline γ-ray spectrum, taken one hour after irradiating a molybdenum target with E_α= 12.0 MeV beam. Transitions belonging to the decay of ^{95}Ru, ^{95}Tc and ^{97}Ru are indicated by black, red and green letters, respectively (the stars represents the weaker transitions belonging to the decay of ^{95}Ru)

typically about 30 min after the end of the irradiation and lasted for 4–5 days, which is approximately six half-lives of the longer-lived isotope (^{95}Tc). In the first 8–10 h the spectra were stored in every 10 min to follow the decay of ^{95}Ru, after that, the spectra were recorded hourly. A typical γ-spectrum measured one hour after the end of the irradiation can be seen in Fig. 85.1.

85.3 Results

The half-life determination has been made by fitting linear function on the semi-logarithmic plot of the γ-yields as the function of time. Only those transitions were used in the analysis where the relative intensities were higher than 1%. For fitting the decay curve the least squares method was used [15].

The $t_{1/2}$ values for the ^{95}Ru and ^{95}Tc isotopes and their statistical uncertainties were calculated as the weighted average of the measured samples. The following systematical uncertainties were taken into account: selecting different background regions and using different methods for the net peak area determination (Gaussian fit and numerical integration) led to 0.09% difference in the derived $t_{1/2}$ results. Furthermore, there is a small—0.10% for ^{95}Ru and 0.18% for ^{95}Tc—difference between the half-lives based on the measurement of different γ-transitions. Finally, the stability of the γ-counting setup and the reliability of the deadtime determination was investigated by using the ^{97}Ru isotope—which has a very well known half-life ($t_{1/2}$ = 2.8370 $\pm$ 0.0014 d [16])—as standard. In each measurement the $t_{1/2}$ of the ^{97}Ru isotope was derived also and was found always to be within 0.19% to the literature value.

The data analysis is in progress, the resulted half-life values will be proclaimed elsewhere.

Acknowledgements This work was supported by NKFIH (K120666, NN128072). G. G. Kiss acknowledges support from János Bolyai research scholarship of MTA Atomki. This work was supported by the ÚNKP-18-4-DE-449 New National Excellence Program of the Ministry of Human Capacities of Hungary.

References

1. F. Käppeler et al., Rev. Mod. Phys. **83**, 157 (2011)
2. F.K. Thielemann et al., Annu. Rev. Nucl. Part. Sci. **67**, 253 (2017)
3. T. Rauscher et al., Rep. Prog. Phys. **76**, 066201 (2013)
4. G.G. Kiss et al., Phys. Rev. Lett. **101**, 191101 (2008)
5. G. Gyürky, et al., Phys. Rev. C **74**, 025805 (2006)
6. G.G. Kiss et al., Phys. Lett. B **695**, 419 (2011)
7. L. Netterdon et al., Nucl. Phys. A **916**, 149 (2013)
8. G.G. Kiss et al., Phys. Lett. B **735**, 40 (2014)
9. T. Szücs et al., Phys. Lett. B **776**, 396 (2018)

10. T. Szücs et al., Nucl. Data Sheets **120**, 191 (2014)
11. S.K. Basu, et al., Nucl. Data, Sheet **111**, 2555 (2010)
12. J.A. Pinston et al., J. Phys. **29**, 257 (1968)
13. M. Bormann et al., Nucl. Phys. A **157**, 2 (1970)
14. G.B. Vingiani et al., Nuovo Cimento **23**, 729 (1962)
15. W.R. Leo, in *Techniques for Nuclear and Particle Physics Experiments* (Springer, 1992)
16. J.R. Goodwin et al., Phys. Rev. C **80**, 045501 (2009)

Chapter 86
Stellar Yields of Rotating Pair Instability Supernovae and Comparison with Observations

Koh Takahashi

Abstract A very-massive star forming a massive CO core of ∼60–120 $M_{\odot}$ is considered to explode as a pair-instability supernova (PISN). We have calculated the PISN nucleosynthesis taking both rotating and non-rotating progenitors for the first time to conduct a systematic comparison between theoretical yields and a large sample of metal-poor star abundances. We have found that the predicted low [Na/Mg] ∼ -1.5 and high [Ca/Mg] ∼ 0.5–1.3 abundance ratios are the most important to discriminate PISN signatures from normal metal-poor star abundances, and have confirmed that no currently observed metal-poor star matches with the PISN abundance. The confirmation of the non-detection may indicate that something important is missing from current understanding of stellar physics. Finally, we discuss that qualitatively different stellar evolution, which is against the PISN explosion, results from a CO core with a higher C fraction than canonical models.

86.1 The Pair Instability Supernova

If a star is massive enough to form a CO core of ∼60–120 $M_{\odot}$, the star collapses owing to the electron-positron-pair-creation instability, in which the reaction of the electron-positron pair creation converts a part of the thermal energy into the rest mass energy so that the pressure is effectively reduced. In the collapsing core, rapid nuclear reactions of carbon and oxygen burnings take place. When the released binding energy is large enough to explode the whole star, it leads to a thermonuclear explosion called a pair-instability supernova (PISN). Because the theoretical picture is based on fundamental physics, the prediction to be exploded as the PISN has been considered to be highly robust.

K. Takahashi (✉)
Argelander Institute for Astronomy, Bonn, Germany
e-mail: ktakahashi@astro.uni-bonn.de

A. Formicola et al. (eds.), *Nuclei in the Cosmos XV*, Springer
Proceedings in Physics 219, https://doi.org/10.1007/978-3-030-13876-9_86

86.2 PISN Nucleosynthesis

We have calculated the evolution and explosion of zero-metallicity stars with the initial masses of 100–300 $M_\odot$ [1]. For the exploding models, the explosive nucleosynthesis is calculated by a postprocessing manner, considering extended 300 isotopes in the reaction network. In order to investigate the effect of the rotation induced mixing on the PISN nucleosynthesis, two sequences of rotating models, with and without the effect of magnetic angular momentum transport, are set in addition to the other sequence of nonrotating models. The main feature of the PISN nucleosynthesis is the pronounced contrast between odd-Z and even-Z elemental yields. Besides, we show that the rotation induced mixing results in the enhanced production of the primary nitrogen. However, the stellar rotation does not affect the characteristic odd-even variation in the explosive yields.

86.3 Comparison with Metal Poor Star Abundances

The expectation to have a PISN in the early universe would be much higher than in a present universe, because the typical initial mass of the zero-metallicity stars is considered to be as large as $\sim$100 $M_\odot$. If a PISN takes place in the early universe, the characteristic abundance pattern can be preserved in a metal-poor (MP) star that is formed from a primordial gas cloud enriched by the PISN (a PISN-MP star). To test the hypothesis that some MP stars in our galaxy may possess the characteristic abundance patterns of PISNe, we have compared our theoretical yields with the surface abundance patterns of more than 2000 MP stars compiled in the SAGA database [2]. The main comparison utilizes the ratio among Na, Mg, and Ca, since they are the most accessible elements for the observations and moreover the low [Na/Mg] and high [Ca/Mg] ratios are useful indicators of the large odd-even variation of the PISN nuclearsynthetic signature. The results are shown in Fig. 86.1. No candidates for the PISN-MP star has been discovered from the current sample.

86.4 Evolution of Carbon-Enhanced Very Massive Stars

The non-detection of a PISN-MP star might indicate that the actual event rate of PISNe is lower than the current prediction. Recently, we have found that a VMS with a high core C fraction evolves qualitatively different from the canonical model [3]. A multiplication factor of $f_{\rm cag} \in [0.1, 1.2]$ is introduced to decrease the reaction rate of the $^{12}C(\alpha,\gamma)^{16}O$, such that the core C fraction is increased from the canonical value of $\sim$10% in mass. With the high core C fraction, lower mass very-massive-star models come to develop shell convections by C shell burnings, and massive very-massive-star models become easier to expand. Consequently, the upper and lower

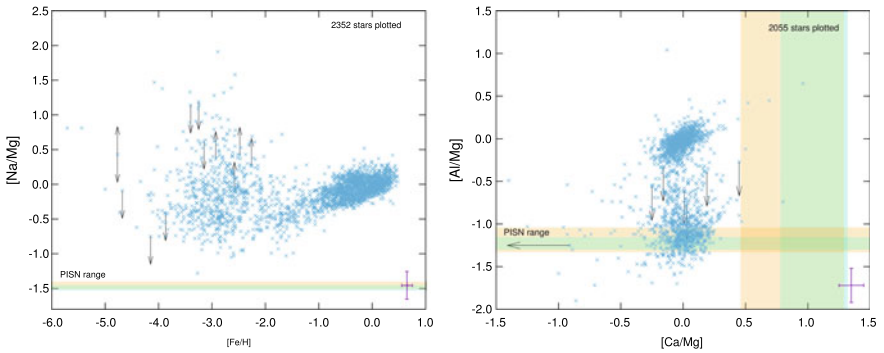

Fig. 86.1 Comparisons between theoretical expectations and surface abundances of MP stars for [Na/Mg] versus [Fe/H] (left panel) and [Al/Mg] versus [Ca/Mg] (right panel). For the observation, stellar data are plotted by blue crosses and typical errors of ±0.2 dex for [Na, Al/Mg] and ±0.1 dex for [Fe/H] and [Ca/Mg] are shown by purple crosses. The ranges of the theoretical yields by changing the initial mass are shown by the cyan and orange bands for the nonrotating and nonmagnetic rotating results, respectively

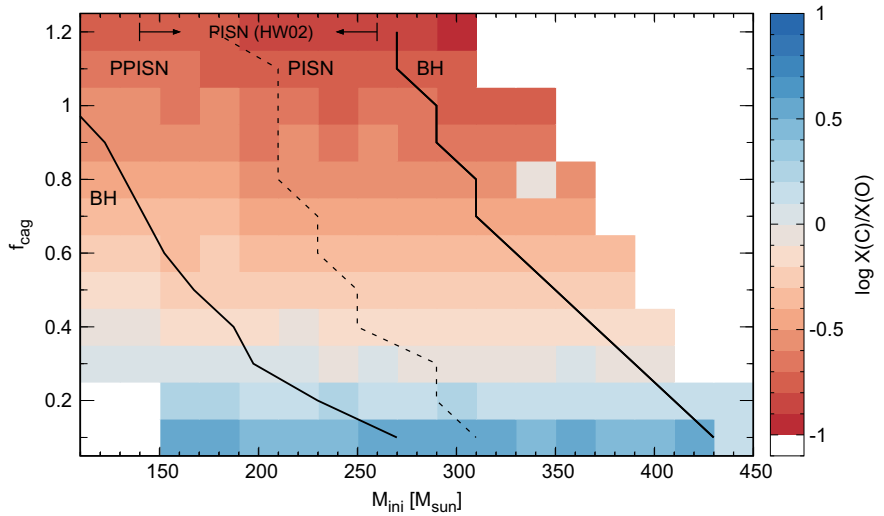

Fig. 86.2 The phase diagram showing the fate: PISN to models that explode as a PISN, PPISN to models that are affected by the pair instability but experience incomplete mass ejection, and BH to models that avoid mass ejection due to the pair instability and finally form a stellar mass BH. The boundary between PISN and PPISN is shown by the dashed line because of the relatively large uncertainty in the initial mass. The color shows the central X(C)/X(O) ratio of the CO cores

ends of not only the initial mass range but also the CO core mass range to become a PISN can be significantly shift upward (Fig. 86.2), suggesting that the event rate of PISNe can also be significantly affected. Increasing the core C fraction provides the very first idea to affect the PISN event rate by directly changing the CO core mass range for PISNe.

References

1. K. Takahashi, T. Yoshida, H. Umeda, Astrophys. J. **857**, 111 (2018)
2. T. Suda, Y. Katsuta, S. Yamada et al., Publ. Astron. Soc. Jpn. **60**, 1159 (2008)
3. K. Takahashi, Astrophys. J. **863**, 2 (2018)

Chapter 87
Stellar Surface Abundance of Light Elements and Updated (p,α) Reaction Rates

E. Tognelli, L. Lamia, Rosario Gianluca Pizzone, S. Degl'Innocenti, P. G. Prada Moroni, S. Romano, C. Spitaleri, Aurora Tumino and M. La Cognata

Abstract We present the progress in the measurements of the nuclear reaction rates for ^{6,7}Li, ^{9}Be and ^{10}B (p,α) burning channels derived using the Trojan Horse Method (THM). The effects on the predicted stellar surface abundances of such elements in pre-main sequence stars are evaluated using the Pisa up-to-date stellar evolutionary code. The present analysis is restricted to the pre-MS evolution of low-mass stars.

87.1 Introduction

The understanding of the surface stellar abundance evolution of lithium, beryllium and boron represents one of the most interesting open problems in astrophysics. These elements are burned at relatively low temperatures ($T \approx 2 - 5 \times 10^6$ K) and thus in pre-main sequence (PMS) they are gradually destroyed at different depths of stellar interior mainly by (p,α) burning reactions, in dependence on the stellar mass. Their abundances in PMS stellar surface are thus strongly influenced by the nuclear burnings as well as by the extension toward the interior of the convective envelope and by the temperature at its bottom. These elements are thus good tracers of the efficiency of mixing processes active in stellar envelopes.

E. Tognelli · S. Degl'Innocenti (✉) · P. G. Prada Moroni
Dipartimento di Fisica, Universitá di Pisa and INFN - Sezione di Pisa, Pisa, Italy
e-mail: scilla.deglinnocenti@unipi.it

E. Tognelli
e-mail: emanuele.tognelli@for.unipi.it

L. Lamia · S. Romano · C. Spitaleri
Dipartimento di Fisica e Astronomia, Universitá di Catania, Catania, Italy

L. Lamia · R. G. Pizzone · S. Romano · C. Spitaleri · A. Tumino · M. La Cognata
INFN - Laboratori Nazionali del Sud, Catania, Italy

A. Tumino
Dipartimento di Ingegneria e Architettura, Universitá di Enna, Enna, Italy

A. Formicola et al. (eds.), *Nuclei in the Cosmos XV*, Springer
Proceedings in Physics 219, https://doi.org/10.1007/978-3-030-13876-9_87

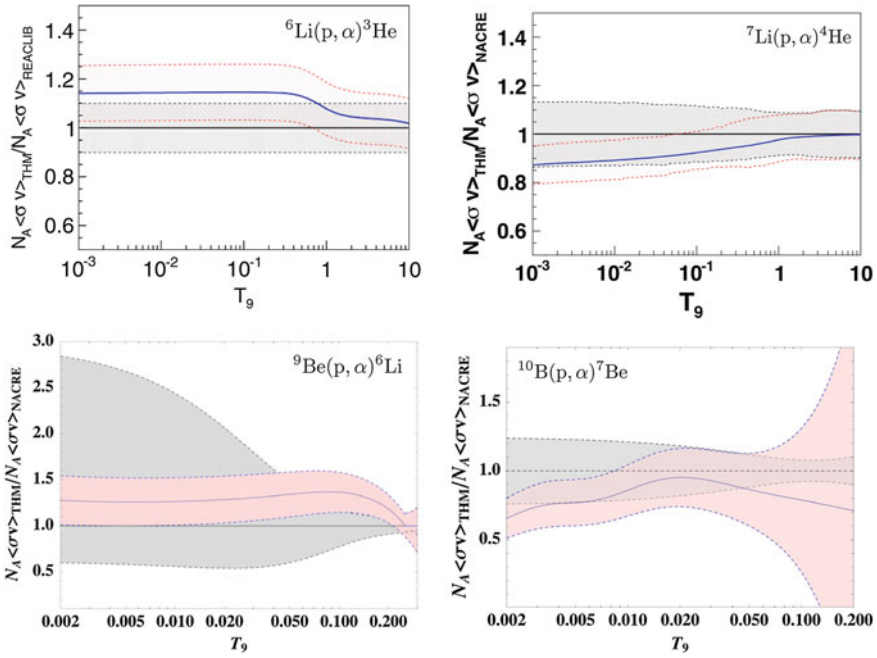

Fig. 87.1 Comparison between the recent THM and other largely used reaction rates, for the Li, Be and B (p,α) burning channels versus temperature (T9 = T/10^9 K). *Top left*: ratio between the THM [4] and JINA REACLIB ^{6}Li(p,α)^{3}He reaction rate (solid blue line), with upper and lower limits of the THM (red dashed line) and JINA (black dashed) rate. *Top right*: the same as in top left panel but for the THM [3] and NACRE ^{7}Li(p,α)^{4}He reaction rate. *Bottom left*: the same as in top left panels, but for the THM [5] and NACRE ^{9}Be(p,α)^{6}Li reaction rates. Red and grey filled area mark the THM and the NACRE reaction rate uncertainty. *Bottom right*: the same as in bottom left panel but for the THM [5] and NACRE ^{10}B(p,α)^{7}Be reaction

87.2 Updated Light Element (p,α) Reaction Rates and Surface Abundances in Pre-main Sequence

Figure 87.1 shows the recent nuclear reaction rates for ^{6,7}Li, ^{9}Be and ^{10}B(p,α) burning channels as derived using the Trojan Horse Method (THM) (see e.g. [6]) compared with those available in the NACRE [1] and JINA REACLIB [2] compilations. THM allows to measure the astrophysically relevant cross sections in correspondence, or very close, to the so-called Gamow peak without experiencing the lowering of the signal-to-noise ratio due to the presence of the Coulomb barrier between the interacting particles. The first release of the NACRE compilation is still widely adopted in the literature, even if for the ^{9}Be(p,α)^{6}Li and ^{10}B(p,α)^{7}Be reactions the rates by the more recent NACRE II compilation [9] are also available. The differences between the corresponding reaction rates are particularly evident in the low-energy regime, where light elements are destroyed in stars. The differences can reach about

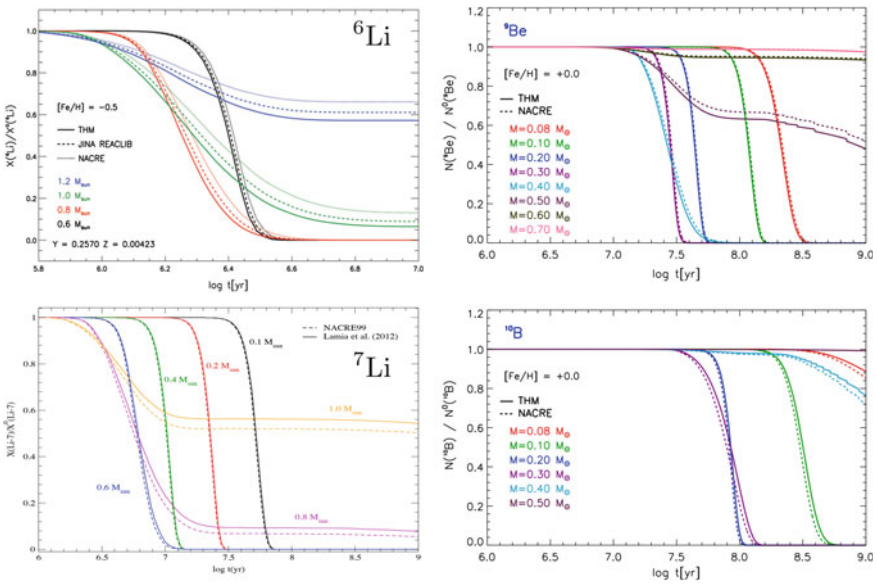

Fig. 87.2 Temporal evolution of the surface Li, Be and B isotopes for several masses and different reaction rates. *Top left*: surface ^{6}Li abundance, for models computed with the THM, NACRE and JINA ^{6}Li reaction rates. *Bottom left*: surface ^{7}Li abundance for models computed with THM, and NACRE reaction rates. *Top right*: the same as in bottom left panel but for surface ^{9}Be abundances. *Bottom right*: the same as in bottom left panel but for surface ^{10}B abundances

15% (^{6,7}Li) and about 25% (^{9}Be and ^{10}B) especially when the NACRE reaction rates are considered. However, if the more recent NACRE II rates are adopted the differences are reduced [5]. To be noted that in all cases, the uncertainty of the recent THM determinations is smaller than that estimated in NACRE/JINA compilations.

Figure 87.2 illustrates the impact of the new reaction rates on the surface light element abundances predicted using the Pisa stellar evolutionary code [7]. Regarding ^{6}Li the maximum difference is achieved between the calculations with NACRE and THM, ranging from about 13% (1.2 $M_{\odot}$) to about 60% (1.0 $M_{\odot}$). For ^{7}Li the differences between the surface abundances calculated with THM and NACRE reaction rates range from about 7% (1 $M_{\odot}$) to about 25% (0.6 $M_{\odot}$). However one has to notice that the effect of adopting different ^{6}Li /^{7}Li burning rates is less important than the effects due to errors in present chemical composition determinations and to the uncertainties in some other physical inputs adopted in the calculations (e.g. radiative opacity) [8].

The THM rate for the ^{9}Be(p,α)^{6}Li reaction is about 25% larger than the NACRE one, thus leading to a faster ^{9}Be destruction in the THM models. The differences in the predicted surface abundances are significant if surface ^{9}Be is efficiently destroyed (i.e. for $M < 0.5\ M_{\odot}$). The THM burning rate for the ^{10}B(p,α)^{7}Be reaction is smaller by about 25% with respect to the NACRE one, leading to a larger surface ^{10}B abundance at a fixed age. Because of the larger ^{10}B burning temperature

with respect to the ^{9}Be one, the effect of changing the reaction rate is relevant only for masses M $<$ 0.4 M$_{\odot}$. Although observational ^{9}Be and ^{10}B abundances are still not available for the low temperature/mass regimes typical of efficient ^{9}Be and ^{10}B burnings, it is worth to estimate the role of the improvements in nuclear physics in surface abundance predictions.

87.3 Conclusions

Thanks to the recent improvements in the evaluation of light element nuclear cross sections at astrophysical energies, the uncertainties on the predictions of surface light elements abundances have been largely reduced. In particular, the recent THM reaction rates uncertainties have an impact on the final abundance calculations smaller than that caused by the other indeterminations on input physics/chemical composition adopted in stellar models.

Acknowledgements ET, SD and PGPM acknowledge INFN (*iniziativa specifica TAsP*).

References

1. C. Angulo, M. Arnould, M. Rayet et al., A compilation of charged-particle induced thermonuclear reaction rates. Nucl. Phys. A **656**, 3 (1999). https://doi.org/10.1016/S0375-9474(99)00030-5
2. R.H. Cyburt, A.M. Amthor, R. Ferguson et al., The jina reaclib database: its recent updates and impact on type-I X-ray bursts. Astrop. J. Suppl. Ser. **189**, 240 (2010). https://doi.org/10.1088/0067-0049/189/1/240
3. L. Lamia, C. Spitaleri, M. La Cognata et al., Recent evaluation of the ^{7}Li(p,α)^{4}He reaction rate at astrophysical energies via the Trojan Horse method. Astron. Astrophy. **541**, A158 (2012). https://doi.org/10.1051/0004-6361/201219014
4. L. Lamia, C. Spitaleri, R.G. Pizzone et al., An updated ^{6}Li(p,α)^{3}He reaction rate at astrophysical energies with the Trojan Horse method. Astrophy. J. **768**, 65 (2013). https://doi.org/10.1088/0004-637X/768/1/65
5. L. Lamia, C. Spitaleri, E. Tognelli et al., Astrophysical impact of the updated ^{9}Be(p,α)^{6}Li and ^{10}B(p,α)^{7}Be reaction rates as deduced by THM. Astrophy. J. **811**, 99 (2015). https://doi.org/10.1088/0004-637X/811/2/99
6. C. Spitaleri, A.M. Mukhamedzhanov, L.D. Blokhintsev et al., The Trojan Horse Method in nuclear astrophysics. Phys. At. Nuclei **74**, 1725 (2011). https://doi.org/10.1134/S1063778811110184
7. E. Tognelli, P.G. Prada Moroni, S. Degl'Innocenti, The Pisa pre-main sequence tracks and isochrones. A database covering a wide range of Z, Y, mass, and age values. A & A, **533A**, 109 (2011). https://doi.org/10.1051/0004-6361/200913913
8. E. Tognelli, P.G. Prada Moroni, S. Degl'Innocenti, Cumulative theoretical uncertainties in lithium depletion boundary age. MNRAS **449**, 3741 (2015). https://doi.org/10.1093/mnras/stv577
9. Y. Xu, K. Takahashi, S. Goriely, M. Arnould, M. Ohta, H. Utsunomiya, NACRE II: an update of the NACRE compilation of charged-particle-induced thermonuclear reaction rates for nuclei with mass number A $<$ 16. NuPhA **918**, 61 (2013). https://doi.org/10.1016/j.nuclphysa.2013.09.007

Chapter 88
Improving Nuclear Data Input for r-Process Calculations Around A ∼ 80

A. Tolosa-Delgado, J. Agramunt, D. S. Ahn, A. Algora, H. Baba, S. Bae, N. T. Brewer, C. Bruno, R. Caballero Folch, F. Calviño, P. J. Coleman-Smith, G. Cortés, T. Davinson, I. Dillmann, C. Domingo-Pardo, A. Estrade, N. Fukuda, S. Go, C. J. Griffin, R. Grzywacz, J. Ha, O. Hall, L. Harkness-Brennan, T. Isobe, D. Kahl, M. Karny, L. H. Khiem, G. G. Kiss, M. Kogimtzis, S. Kubono, M. Labiche, I. Lazarus, J. Lee, J. Liang, J. Liu, G. Lorusso, K. Matsui, K. Miernik, F. Montes, B. Moon, A. I. Morales, N. Nepal, S. Nishimura, R. D. Page, V. H. Phong, Z. Podolyak, V. F. E. Pucknell, B. C. Rasco, P. Regan, A. Riego, B. Rubio, K. P. Rykaczewski, Y. Saito, H. Sakurai, Y. Shimizu, J. Simpson, P.-A. Söderström, D. W. Stracener, T. Sumikama, H. Suzuki, J. L. Tain, M. Takechi, H. Takeda, A. Tarifeño-Saldivia, S. L. Thomas, P. J. Woods, X. X. Xu and R. Yokoyama

A. Tolosa-Delgado (✉) · J. Agramunt · A. Algora · C. Domingo-Pardo · A. I. Morales · B. Rubio · J. L. Tain
Instituto de Fisica Corpuscular (CSIC-Univ. de Valencia), 46980 Paterna, Spain
e-mail: Alvaro.Tolosa@ific.uv.es

D. S. Ahn · H. Baba · N. Fukuda · S. Go · T. Isobe · D. Kahl · G. G. Kiss · S. Kubono · G. Lorusso · K. Matsui · S. Nishimura · V. H. Phong · H. Sakurai · Y. Shimizu · P.-A. Söderström · T. Sumikama · H. Suzuki · H. Takeda
RIKEN Nishina Center, Wako, Saitama 351-0198, Japan

S. Bae · J. Ha
Department of Physics, Seoul National University, Seoul 08826, Republic of Korea

N. T. Brewer · K. Miernik · B. C. Rasco · K.P. Rykaczewski · D. W. Stracener · R. Yokoyama
Physics Division, Oak Ridge National Laboratory, Oak Ridge, TN 37831, USA

R. Caballero Folch · I. Dillmann · Y. Saito
TRIUMF, 4004 Wesbrook Mall, Vancouver, BC V6T 2A3, Canada

F. Calviño · G. Cortés · A. Riego · A. Tarifeño-Saldivia
Universitat Politecnica de Catalunya (UPC), Barcelona, Spain

P. J. Coleman-Smith · M. Kogimtzis · M. Labiche · I. Lazarus · V. F. E. Pucknell · J. Simpson
STFC Daresbury Laboratory, Daresbury, Warrington WA4 4AD, UK

L. Harkness-Brennan · R. D. Page
University of Liverpool, Liverpool L69 7ZE, United Kingdom

C. Bruno · T. Davinson · C. J. Griffin · O. Hall · P. Woods
University of Edinburgh, Edinburgh EH9 3JZ, United Kingdom

A. Estrade · N. Nepal
Central Michigan University, Mount Pleasant, MI 48859, USA

A. Formicola et al. (eds.), *Nuclei in the Cosmos XV*, Springer
Proceedings in Physics 219, https://doi.org/10.1007/978-3-030-13876-9_88

Abstract We made an experiment to measure half-lives $T_{1/2}$ and neutron emission probabilities P_{xn} of nuclei around mass 80, aiming to improve r-process abundance calculations around the first abundance peak with a new dedicated experimental setup at RIKEN. Details of the experiment and a few preliminary results are presented.

88.1 Introduction

β-delayed neutron emission (βn) is a form of β-decay, in which one or more neutrons are emitted. This form of decay plays a key role during the synthesis of heavy elements through the r-process [1], where highly neutron-rich nuclei are produced. The half-lives of the nuclei along the r-process path determine the initial abundances. The final abundance distribution of the synthesized elements is affected by the βn decay mode in a complex way, shifting the decay path to lower masses on the one hand, while providing additional neutrons for further late captures with the opposite effect [2].

S. Go · R. Grzywacz
Department of Physics, University of Tennessee, Knoxville, TN 37996-1200, USA

A. Algora · G. G. Kiss
Institute of Nuclear Research of the Hungarian Academy of Sciences, Debrecen 4001, Hungary

J. Lee · J. Liu · X. X. Xu
Department of Physics, The University of Hong Kong, Hong Kong, China

G. Lorusso · P. Regan
National Physical Laboratory, Teddington TW11 0LW, UK

K. Matsui · H. Sakurai
Department of Physics, University of Tokyo, Tokyo 113-0033, Japan

M. Karny · K. Miernik
Faculty of Physics, University of Warsaw, 02-093 Warsaw, Poland

F. Montes
National Superconducting Cyclotron Laboratory, Michigan State University, East Lansing, USA

B. Moon
Department of Physics, Korea University, Seoul 136-701, Republic of Korea

Z. Podolyak · P. Regan
Department of Physics, University of Surrey, Guildford GU2 7XH, United Kingdom

S. L. Thomas
STFC Rutherford Appleton Laboratory, Didcot, Oxfordshire OX11 0QX, UK

M. Takechi
Department of Physics, Niigata University, Niigata 950-2102, Japan

88.2 Experimental Setup and Measurements

The BRIKEN (Beta-delayed neutron measurements at RIKEN) collaboration [3] had installed a new dedicated setup for $T_{1/2}$ and P_{xn} measurements at the Radioactive Isotope Beam Factory (RIBF) in RIKEN, which currently provides the highest intensities of the most neutron-rich nuclei produced by in-flight fission. The detection system is composed of the Advanced Implantation Detector Array (AIDA) [4], and a 4π neutron counter. It is placed at the F11 focal plane of BigRIPS spectrometer [5].

AIDA consists of a stack of six Si DSSDs. The setup registers ion implantations and the subsequently emitted β particles. The highly segmented DSSDs grant a high detection efficiency and reduce accidental implant-beta correlations.

The neutron counter, which surrounds AIDA, is made of an array of 140 ^{3}He tubes embedded in a hydrogenous matrix (PE). A parametrized Monte Carlo optimization algorithm was developed in order to determine the best position of the tubes [6]. Neutron energies are moderated by elastic scattering with the matrix and the neutrons are absorbed by the ^{3}He in an exothermic reaction. The energy deposited in the tube produces a signal that is recorded by the eventless DAQ system *Gasific* developed at IFIC, Valencia [7]. The setup includes also two HPGe detectors for high resolution γ-ray spectroscopy.

The data from BigRIPS, AIDA and BRIKEN, which run independently and synchronized, is merged and sorted by time stamp using dedicated software. The output can be used directly in the analysis procedure where complex correlations can be applied.

The first radioactive beam was delivered to the setup on November 2016 for commissioning. Two experimental campaigns were carried out in Spring and Fall of 2017, including the $A \sim 80$ run.

88.3 Analysis and Results

The P_{xn} value, the half-life and the number of parent decays are obtained from a simultaneous fit of the implant-decay curves. The example of ^{86}Ge is shown in Fig. 88.1. Most of the detected neutrons come from the beam-induced background, and a method for correcting the accidental correlations was implemented.

V. H. Phong
Department of Nuclear Physics, Faculty of Physics, VNU University of Science, Hanoi, Vietnam

L. H. Khiem
Institute of Physics, Vietnam Academy of Science and Technology, Hanoi, Vietnam

J. Liang
Department of Physics and Astronomy, McMaster University, Hamilton L8S 4M1, Canada

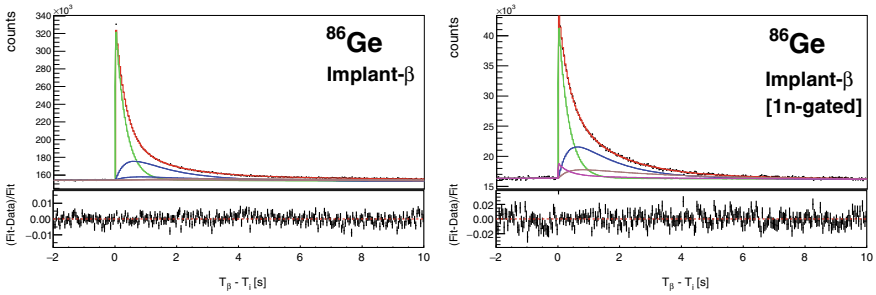

Fig. 88.1 Preliminary fits of time correlation histograms for ^{86}Ge decay. Left: implant-β. Right: implant-β (n-gated). By colors: black, data; red, total activity; green, parent activity; rest of colors, additional contributions

The energy threshold applied to the β-events causes the β-efficiency to be somewhat dependent on the energy window of the decay and beta intensity distribution, and thus on each isotope [7]. This can be taken into account introducing selected efficiencies as adjustable parameters during the fit. We are currently working on the minimization of thresholds for β-signals to further reduce the systematic uncertainties.

88.4 Impact on r-Process

Previous studies have shown the relatively large sensitivity of the abundance pattern of the r-process to $T_{1/2}$ and P_{xn} of selected isotopes [8, 9], like ^{86}Ge. We are currently working to evaluate the impact of our new $T_{1/2}$ and P_{xn} values in this region on the result of network calculations of r-process abundances.

References

1. E.M. Burbidge, G.R. Burbidge, W.A. Fowler, F. Hoyle, Rev. Mod. Phys. **29**, 547 (1957)
2. A. Arcones, G. Martinez-Pinedo, Phys. Rev. C **83**, 045809 (2011)
3. www.wiki.ed.ac.uk/display/BRIKEN/Home
4. T. Davinson et al., www2.ph.ed.ac.uk/~td/AIDA/
5. T. Kubo et al., Prog. Theor. Exp. Phys. **2012**, 03C003 (2012)
6. A. Tarifeno-Saldivia et al., J. Instrum. **12**, 04006 (2017)
7. J. Agramunt et al., Nucl. Instrum. Methods Phys. Res. A **807**, 69 (2016)
8. R. Surman, priv. comm
9. T. Shafer et al., Phys. Rev. C **94**, 055802 (2016)

Chapter 89
Development of an Ionization Chamber for the Measurement of the $^{16}O(n, \alpha)^{13}C$ Cross-Section at the CERN n_TOF Facility

Sebastian Urlass, Arnd R. Junghans, Andreas Hartmann, Federica Mingrone, Manfred Sobiella, Daniel Stach, Laurent Tassan-Got, David Weinberger and The n_TOF Collaboration

Abstract The $^{16}O(n, \alpha)^{13}C$ reaction, as the inverse reaction of the astrophysically important $^{13}C(\alpha, n)^{16}O$ reaction, is proposed to be measured at the neutron time-of-flight (n_TOF) facility of CERN. To this purpose, a Double Frisch Grid Ionization Chamber (DFGIC) containing the oxygen atoms as a component in the counting gas has been developed and a prototype was constructed at Helmholtz-Zentrum Dresden-Rossendorf(HZDR), in Germany. The first in-beam tests of the detector have been performed in November 2017 in the first (EAR1) and in April 2018 in the second (EAR2) experimental areas of the n_TOF at facility.

89.1 Introduction

The fundamental role played by the $^{13}C(\alpha, n)^{16}O$ reaction rate in the understanding of stellar nucleosynthesis processes is widely recognized. Heavy elements ($90 < A < 204$) are produced in light Asymptotic Giant Branch (AGB) stars-with masses $\frac{M}{M_\odot} < 3$ -by the slow neutron capture process (s-process), whose main source of neutrons is precisely the $^{13}C(\alpha, n)^{16}O$ reaction. Therefore, an accurate and precise knowledge of this reaction rate is crucial to correctly model the nucleosynthesis process and to predict the abundances of elements along the s-process chain [1].

The n_TOF Collaboration: https://www.cern.ch/ntof

S. Urlass (✉)
Technische Universität Dresden, 01062 Dresden, Germany
e-mail: sebastian.urlass@cern.ch

S. Urlass · A. R. Junghans · A. Hartmann · M. Sobiella · D. Stach · D. Weinberger
Helmholtz-Zentrum Dresden-Rossendorf, Bautzener Landstraße 400, 01328 Dresden, Germany

S. Urlass · A. R. Junghans · F. Mingrone · L. Tassan-Got
European Organization for Nuclear Research (CERN), Route de Meyrin 1211, Genéve, Switzerland

A. Formicola et al. (eds.), *Nuclei in the Cosmos XV*, Springer
Proceedings in Physics 219, https://doi.org/10.1007/978-3-030-13876-9_89

Direct measurements are experimentally challenging to perform because the Coulomb barrier surppresses the $^{13}C(\alpha, n)^{16}O$ reaction cross-section [2]. For this reason we propose an indirect method to obtain the neutron source reaction rate to measure the inverse $^{16}O(n, \alpha)^{13}C$ reaction cross-section at the n_TOF facility, applying the time-reversal invariance theorem. The main purpose of the n_TOF facility at CERN is to improve nuclear data by measuring neutron induced cross sections exploiting the time-of-flight technique [3]. The n_TOF facility has two vacuum beam lines to the experimental areas: the first (EAR1) with a 185 m flight path is characterized by a very high energy resolution, while the second (EAR2) with a 20 m flight path can count on an approximately 40 times higher flux intensity. Thanks to the characteristics of the facility, like the high intensity-and high energy neutron flux [3], a high precision measurement will give access to very important information as the cross section and the level parameters of the compound nucleus ^{17}O.

89.2 Development of the DFGIC and the Switch Technology

The detector developed for the measurement is a double Frisch-grid ionization chamber (DFGIC). The working principle of the DFGIC is similar as described in [4]. A photo with schematics of the DFGIC are shown in Fig. 89.1.

In November 2017 the first test of the DFGIC has been performed in EAR1. The test clearly underlined the effect of the γ-flash which is produced from spallation reactions, as all the preamplifiers were saturated. The idea to solve this problem is to put a wideband switch between the detector and the preamplifier, in order to prevent the charge collection while the γ-flash passes through the DFGIC. The main component of this circuit is an ADG902 chip consisting of CMOS transistors [5]. The switch circuit developed for the second detector test, performed in EAR2, and the reduced γ-Flash from a charge sensitive preamplifier of the DFGIC are shown in Fig. 89.2.

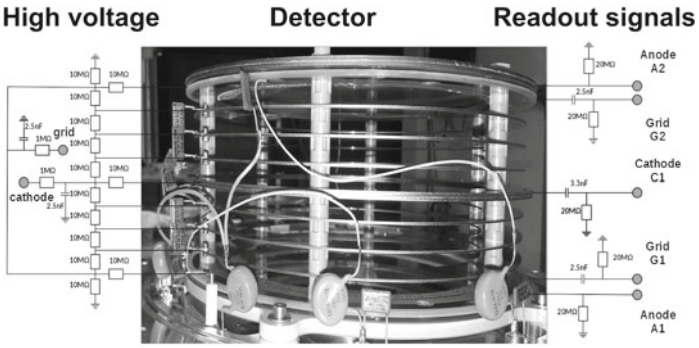

Fig. 89.1 Photo of the DFGIC detector including electrodes and guard rings. On the left the voltage divider scheme is explicited, providing the cathode and grid biases. The right part shows the readout signals (two anodes, two grids and one cathode)

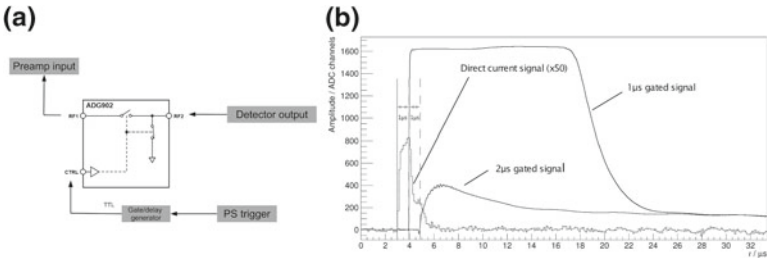

Fig. 89.2 **a** Schematics of the the switch circuit. A gate signal is applied to open the switch after a certain delay in respect to a trigger which arrives before the γ-flash. **b** Averaged signals from the detector test in EAR2 in the region of the γ-Flash. The direct measured current (without a preamplifier) is depicted as dashed line. The preamplifier signals are shown as solid lines where delays of 1 µs and 2 µs in respect to the γ-flash, for gating the signals by the switch, are applied. The latter one (2 µs) shows no saturation anymore

89.3 Summary and Outlook

In order to perform the measurement of the ^{16}O(n, α)^{13}C reaction cross-section, as the inverse reaction the ^{13}C(α, n)^{16}O reaction at the n_TOF facility at CERN, a DFGIC has been constructed at HZDR. From the first dector test in November 2017 in EAR1 the properties of the γ-flash effecting the preamplifier could be characterized. The results of that test lead to the development of a switch device for gating the preamplifier electronics. The subsequent second detecor test in EAR2 with the new wideband switch technology showed for the first time at n_TOF that it is possible to perform a measurement with a DFGIC containing a gaseous target. Before the main experiment in October 2018 the switch circuit parameters will be optimized to allow a maximum neutron energy and a sufficient γ-Flash suppression.

Acknowledgements This work has been sponsored by the Wolfgang Gentner Programme of the German Federal Ministry of Education and Research (grant no. 05E15CHA).

References

1. F. Käppeler et al., The *s* process: nuclear physics, stellar models, and observations. Rev. Mod. Phys. **83**, 157 (2011). https://doi.org/10.1103/RevModPhys.83.157
2. S. Cristallo et al., The importance of the ^{13}C(α, n)^{16}O reaction in asymptotic giant branch stars. Astrophy. J. **859**, 105 (2018). https://doi.org/10.3847/1538-4357/aac177
3. C. Guerrero et al., Performance of the neutron time-of-flight facility n_TOF at CERN. Eur. Phys. J. A **49**, 27 (2013). https://doi.org/10.1140/epja/i2013-13027-6
4. G. Giorginis et al., The cross section of the ^{16}O(n, α)^{13}C reaction in the MeV energy range, in *International Conference on Nuclear Data for Science and Technology* (2007) 140. https://doi.org/10.1051/ndata:07481

5. Data Sheet ADG901/ADG902. http://www.analog.com/media/en/technical-documentation/data-sheets/ADG901_902.pdf

Chapter 90
The Effects of a Late Single-Star Contamination of the Solar Nebula on the Early Solar System Radioactivities

Diego Vescovi and Maurizio Busso

Abstract We re-examine the origin of now-extinct radioactivities, which were alive in the early solar nebula. The Galactic inheritance broadly explains most of the isotopes involved with lifetime $\tau \gtrsim 5$ Myr. Instead, shorter-lived isotopes like ^{26}Al, ^{41}Ca and ^{135}Cs require nucleosynthesis events close in time to the solar formation. Models of final stages of Intermediate-Mass Stars (IMSs) now predict the ubiquitous formation of a ^{13}C-pocket, which always implies large excesses in ^{107}Pd with respect to ^{26}Al. Even a late contamination by a Massive Star (MS) meets serious problems, because the inhomogeneous addition of Supernova debris yields excesses on stable isotopes that disagree with measurements.

90.1 Introduction

Mass spectrometry techniques applied to pristine meteorite samples (which formed in the first few million years of the nebula lifetime), revealed the presence of radioactive species with lifetimes lower than 100 Myr in the Early Solar System (ESS) [1]. The proto-sun was previously isolated from Galactic nucleosynthesis for a time Δ around 10 Myr. In such conditions, nuclei with $\tau \gtrsim 5$–10 Myr might be explained by Galactic evolution. This is so for nuclei like ^{53}Mn, ^{107}Pd, ^{146}Sm, ^{182}Hf, ^{205}Pb, ^{247}Cm and probably also for ^{129}I [2] if it was synthesized in a peculiar neutron star merging (NSM) *r*-process site, like the one described in [3]. Even ^{60}Fe might be explained in this way [2], if we accept the recent low estimate of its abundances [4]. The presence of other *short-lived radioactivities* (SLRs) with $\tau < 5$ Myr would instead require an in situ production [1, 2]: indeed, their lifetime is so short that the isolation time Δ

D. Vescovi (✉)
Gran Sasso Science Institute, Viale Francesco Crispi, 7, 67100 L'Aquila, Italy
e-mail: diego.vescovi@gssi.it

D. Vescovi · M. Busso
INFN, Section of Perugia, Via A. Pascoli snc, 06123 Perugia, Italy

M. Busso
Department of Physics and Geology, University of Perugia,
Via A. Pascoli snc, 06123 Perugia, Italy

A. Formicola et al. (eds.), *Nuclei in the Cosmos XV*, Springer
Proceedings in Physics 219, https://doi.org/10.1007/978-3-030-13876-9_90

would be sufficient to deplete them completely [1, 2]. In particular, this is true for nuclei like ^{26}Al, ^{41}Ca and ^{135}Cs; they must therefore be explained at the local level, by a nearby nucleosynthesis event. Moreover the complementary process of solid bombardment by fast solar-wind particles was also shown to be inadequate [2, 5].

90.2 Effects of a Late AGB Star and a Late CCSN

In the context outlined above, we investigated the possibility that an Asymptotic Giant Branch (AGB) star could have contamined the solar nebula. We did this by means of two different Deep Mixing models for the ^{13}C-pocket formation: one is based on MHD (magnetohydrodynamics)-induced circulations [6, 7], the second on an opacity-driven mixing mechanism [8, 9]. In order to take into account the effects of this contamination, we followed the prescriptions described in [1, 2] and fixed the dilution factor and the time separating CAI (calcium-aluminium-rich inclusion) formation from the stellar nucleosynthesis event by imposing that the ESS abundance ratios ^{26}Al/^{27}Al and ^{41}Ca/^{40}Ca fit the measured values. We notice that a clear correlation of these ratios was early shown by Sahijpal et al. [10], implying for both these SLRs a stellar origin. We found that any considered mixing model will inevitably produce execesses of some neutron-rich isotopes (especially ^{107}Pd, see Fig. 90.1). This is due to the excess of neutrons produced by the ^{13}C neutron source, which spoils the previous positive indications by Wasserburg et al. [1]. Subsequently, we applied the same method to test the effects of a possible late contamination by a Core-Collapse Supernova (CCSN). For this purpose, we adopted nucleosynthesis yields from the MS models by Limongi and Chieffi [11], including the effects of rotation during the hydrostatic evolution and a full computation of explosive phases. As illustrated in Fig. 90.2a, a solution is not possible. Both ^{53}Mn and ^{60}Fe are over-

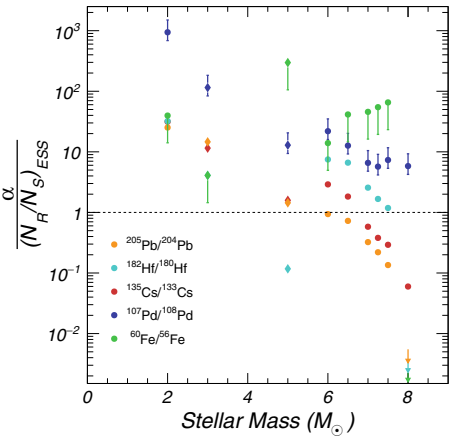

Fig. 90.1 Prediction for heavy SLRs from AGB stars using two different physical models for Deep Mixing description. In the plot, dots indicate the models of [8, 9], while diamonds those of [2, 6, 7]. Some error bars cannot be seen due to the logarithmic scale

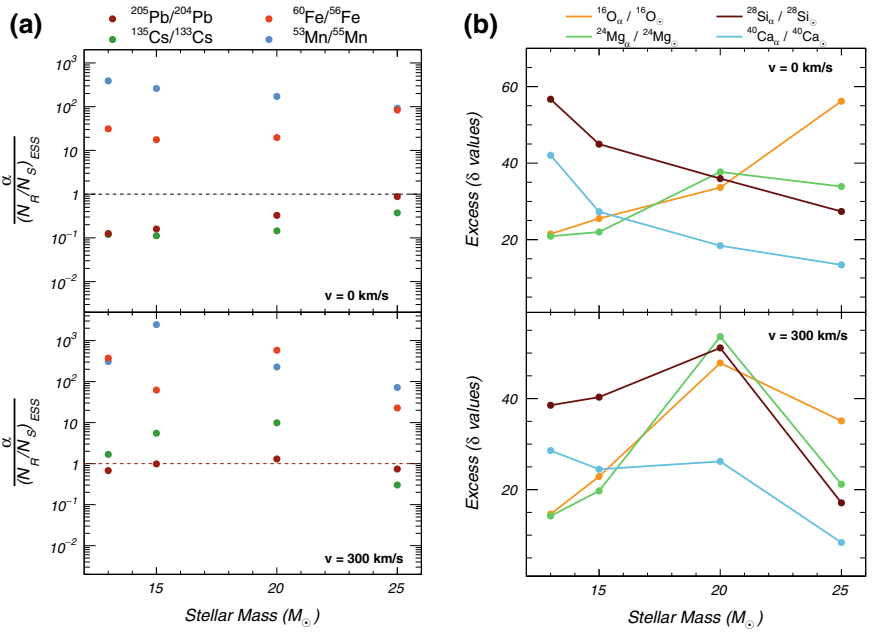

Fig. 90.2 **a** Predictions for SLRs from a late contamination by a CCSN in the mass range 13–25 $M_\odot$ and for different initial equatorial velocities. **b** Values of the excesses introduced on α-rich isotopes of major stable elements by the CCSN models discussed in the text

produced by two orders of magnitude. While for ^{53}Mn one might invoke special models with an ad-hoc mass cut [12], an unsolved problem emerges by considering the inhomogeneous addition of CCSN contributions to other nuclei. This always implies large, unobserved excesses on stable isotopes (see Fig. 90.2b).

Therefore, the possibility that a single, nearby evolved star be at the origin of ESS radioactivities meets serious problems both for an IMS and a MS source. In this last case, to avoid unobserved excesses on stable nuclei one should dilute more extensively, as in scenarios of the mixing and homogeneization of a pre-solar molecular cloud. This however would deplete ^{41}Ca ($\tau = 0.15$ Myr) completely. One possibility still open is that the contamination came from a Super-AGB star, where the ^{13}C n-source might not be active, avoiding the overproduction of ^{107}Pd. An alternative might also be found in the most massive among IMSs (7–8 $M_\odot$) if Hot Bottom Burning yields were remarkably different from what is currently available in the literature (see [2] for further details).

References

1. G.J. Wasserburg et al., NuPhA **777**, 5 (2006). https://doi.org/10.1016/j.nuclphysa.2005.07.015
2. D. Vescovi, M. Busso et al., ApJ **863**, 115 (2018). https://doi.org/10.3847/1538-4357/aad191
3. Goriely et al., PhRvL **111**, 242502 (2013). https://doi.org/10.1103/PhysRevLett.111.242502
4. R. Trappitsch et al., ApJL **857**, L15 (2018). https://doi.org/10.3847/2041-8213/aabba9
5. P.A. Sossi et al., NatAs **1**, 0055 (2017). https://doi.org/10.1038/s41550-017-0055
6. O. Trippella, M. Busso, S. Palmerini et al., ApJ **818**, 125 (2016). https://doi.org/10.3847/0004-637X/818/2/125
7. S. Palmerini, O. Trippella et al., GeCoA **221**, 21 (2018). https://doi.org/10.1016/j.gca.2017.05.030
8. S. Cristallo et al., ApJS **197**, 17 (2011). https://doi.org/10.1088/0067-0049/197/2/17
9. S. Cristallo et al., ApJS **219**, 40 (2015). https://doi.org/10.1088/0067-0049/219/2/40
10. S. Sahijpal et al., Nature **391**, 559 (1998). https://doi.org/10.1038/35325
11. M. Limongi, A. Chieffi, ApJS **237**, 13 (2018). https://doi.org/10.3847/1538-4365/aacb24
12. B.S. Meyer, D.D. Clayton, SSRv **92**, 133 (2000). https://doi.org/10.1023/A:1005282825778

Chapter 91
On the Measurements of the Beam Characteristics of Low-Energy Accelerator

Shuo Wang, Kuang Li, Shiwei Xu, Shaobo Ma, Han Chen, Xiaodong Tang, Jun Su and Yangping Shen

Abstract A new 400 kV accelerator, with high current based on an ECR source, will be installed into China JinPing underground Laboratory (CJPL) for the study of Nuclear Astrophysics (JUNA). The beam characteristics of the accelerator will be determined by several well-known resonance and non-resonance reactions. Due to the new accelerator still being under operation at CIAE, the resonance reaction of ^{27}Al(p,γ)^{28}Si and non-resonance ^{12}C(p,γ)^{13}N were studied at the 320 kV high-voltage platform of Institute of Modern Physics in Lanzhou, China. The energy spread of proton beam is about 1.0 keV and the long-term energy stability of proton beam is better than $\pm$200 eV during 4 h measurement.

91.1 Introduction

China JinPing underground Laboratory (CJPL) is located at the middle portions of the 17.5 km JinPing tunnels in Sichuan province, southwest China, which has approximately 2400 m of marble and sandstone above it and is currently the world's deepest underground laboratory with horizontal access [1–3]. The cosmic ray muon flux, $2.0 \pm 0.4 \times 10^{-10}$/(cm^2 s) [4–6], is about 2 orders of magnitude lower than that in Gran Sasso [7, 8]. Jinping Underground experiment for Nuclear Astrophysics project (JUNA), as one of the major research programs in CJPL-II, aims to direct measurement of (α,γ), (α,n), (p,γ) and (p,α) reactions involved in stellar hydrogen and helium hydrostatic burning [9–11].

A new 400 kV accelerator with high stability and high intensity will be placed in A1 experiment hall of CJPL-II. The ECR ion source is expected to delivered 12 emA

S. Wang (✉)
Shandong Provincial Key Laboratory of Optical Astronomy and Solar-Terrestrial Environment, Institute of Space Science, Shandong University, Weihai 264209, China
e-mail: wangshuo_wh@sdu.edu.cn

K. Li · S. Xu · S. Ma · H. Chen · X. Tang
Institute of Modern Physics, Lanzhou 730000, China

J. Su · Y. Shen
Department of Nuclear Physics, China Institute of Atomic Energy, Beijing 102413, China

A. Formicola et al. (eds.), *Nuclei in the Cosmos XV*, Springer
Proceedings in Physics 219, https://doi.org/10.1007/978-3-030-13876-9_91

proton, 6 emA He^+ and 2.5 emA He^{2+} [9], while the radio-frequency ions source of LUNA II 400 kV accelerator provides ion beams of 1mA hydrogen (75% H^+) and 500 μA He^+ [7]. Accelerator construction is already finished, the machine is now operating at CIAE and it will be transported to CJPL in the middle of 2019.

91.2 Experimental Setup and Results

Currently, the JUNA 400 kV accelerator is still not ready for the experiment, the testing experiments for $^{12}C(p,\gamma)^{13}N$, $^{27}Al(p,\gamma)^{28}Si$ and $^{24}Mg(p,\gamma)^{25}Al$ reactions were performed at 320 kV high-voltage platform, IMP Lanzhou [12]. The schematic diagram of the experimental setup is shown in Fig. 91.1. A High Purity Ge-detector with 70% efficiency (compared to a 3″ × 3″ NaI crystal) was placed at 0° with respect to the beam axis at a distance d = 35 mm from the target. The observed energy resolution was ΔE_γ = 3.0 keV at E_γ = 1.33 MeV.

The $^{12}C(p,\gamma)^{13}N$ reaction has been used as an alternative method to determine the absolute proton energy over a wide energy range, due to the smooth cross section of this reaction. The energy of the incident proton beam E_p can be calculated by the energy of γ-ray from $^{12}C(p,\gamma)^{13}N$ reaction:

$$E_\gamma = Q + (12/13)E_p + \Delta E_{DC}(0°) - \Delta E_R \tag{91.1}$$

with Q = 1943.5±0.3 keV [13], ΔE_{DC} (0°): the Doppler shift at θ_γ = 0°, and ΔE_R: the nuclear recoil. A thick C target (2 mm) was bombarded by proton beam with

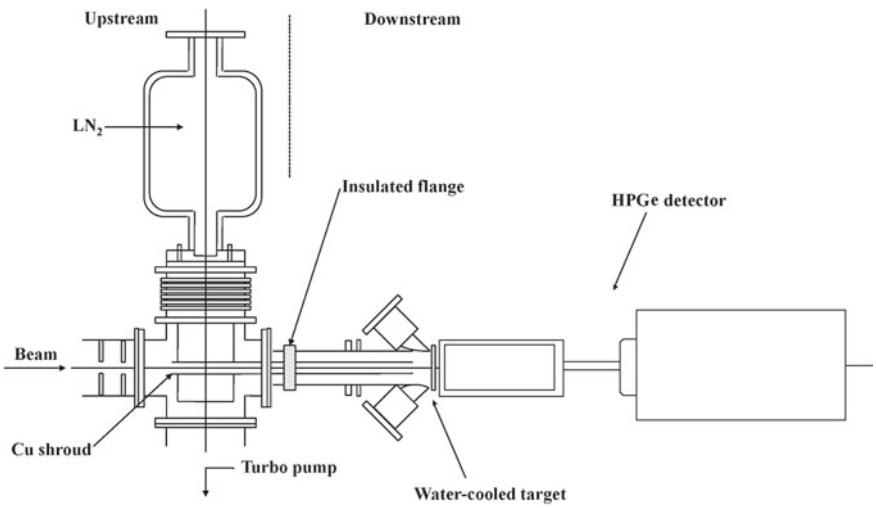

Fig. 91.1 Experimental setup at 320 kV high-voltage platform

energies 250, 260 and 290 keV, and the γ-ray spectra are shown in Fig. 91.2. A plateau of the capture transition was observed and three background γ-ray peaks were used for the energy calibration.

The yield curve of the 223 keV resonance of ^{27}Al(p,γ)^{28}Si reaction is shown in Fig. 91.3, where the data points are fitted by an error function. An experimental

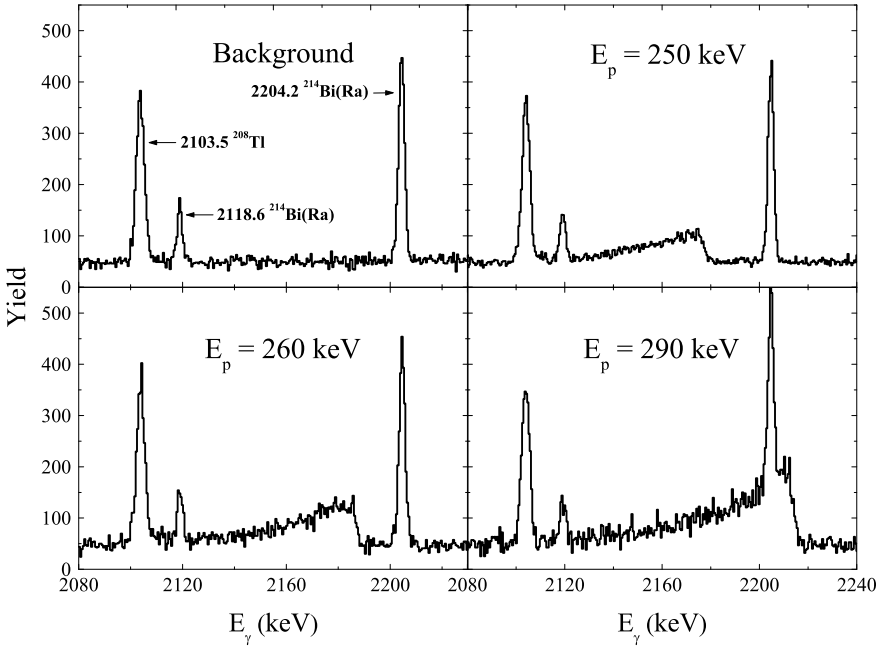

Fig. 91.2 γ-ray spectra at proton beam energies 250, 260, 290 keV and background

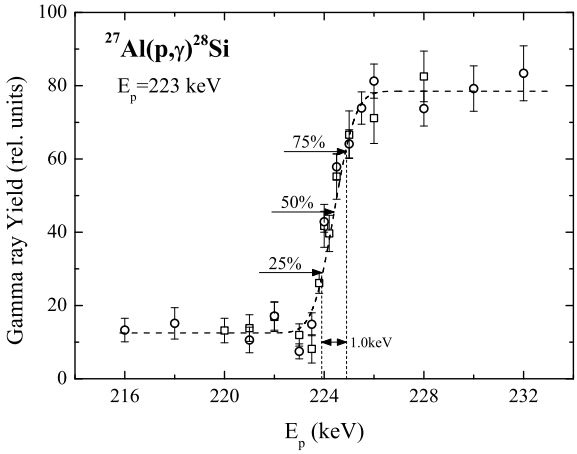

Fig. 91.3 Tricket-target yield curve of the 223 keV resonance of ^{27}Al(p,γ)^{28}Si. The circle and square points show the data at different measurement time. The dashed line through the data points is an error function

energy spread of 1.0 keV is deduced from the 25 and 75% points and the resonance energy of 224.4 keV is determined by the 50% point, which has about 1.4 keV shift from the literature [14]. Due to the steep slope of the yield curve in Fig. 91.3 near the resonance energy (50% yield point), the long-term energy stability of the accelerator is determined to be better than ±200 eV during 4 h measurement.

References

1. H.S. Chen, Science **62**, 4 (2010)
2. J.P. Cheng, S.Y. Wu, Q. Yue, M.B. Shen, Physics **40**(3), 149 (2011)
3. J.M. Li, X.D. Ji, W. Haxton, J.S.Y. Wang, Phys. Proc. **61**, 576 (2014)
4. Y.C. Wu, X.Q. Hao, Q. Yue et al., Chin. Phys. C **37**, 086001 (2013)
5. Z. Zeng, J. Su, H. Ma et al., J Radioanal Nucl. Chem. **301**, 443 (2014)
6. Z.M. Zeng, H. Gong, Q. Yue, J.M. Li, Nucl. Instr. Meth. A **804**, 108 (2015)
7. A. Formicola et al., Nucl. Instr. Meth. A **507**, 609 (2003)
8. H. Constantini et al., Rep. Prog. Phys. **972**(8), 086301 (2009)
9. W.P. Liu, Z.H. Li, J.J. He, X.D. Tang et al., Sci. China-Phys. Meth. Astron. **59**, 642001 (2016)
10. Z.H. Li, J. Su, Y.J. Li et al., Sci. China-Phys. Meth. Astron. **58**, 082002 (2015)
11. J.J. He, S.W. Xu, S.B. Ma et al., Sci. China-Phys. Meth. Astron. **59**, 652001 (2016)
12. X. Ma, et al., J. Phys.:Conf. Ser. **163**, 012104 (2009)
13. F. Ajzenber-Selove, Nucl. Phys. A **523**, 1 (1991)
14. T. Freye, H. Lorenz-Wirzba, B. Cleff et al., Z. Physik A **281**, 211 (1977)

Chapter 92
The Nuclear Physics Uncertainty on Kilonova Heating Rates and the Role of Fission

Y. L. Zhu, T. Sprouse, M. R. Mumpower, N. Vassh, R. Surman and G. C. McLaughlin

Abstract The detection of an electromagnetic counterpart to GW170817 suggests that r-process elements are produced in neutron star mergers. This electromagnetic counterpart has been modeled as a kilonova, which is a light curve thought to be powered mainly from the radioactive decay of heavy elements formed. We investigate uncertainties on the nuclear heating from the nuclear physics inputs of nucleosynthesis simulations. Using 12 theoritical mass models in regions where experimental mass measurements are unavailable, we find that the uncertainty in the total nuclear heating rate is a factor of a few. The β-decay is the dominating heating channel at about 1 day after merger for all 12 mass models. The energy contribution from fission are not neglectable at around one day.

92.1 Introduction

The detection of an electromagnetic counterpart to GW170817 [1] suggests that r-process elements are produced in neutron star mergers. This electromagnetic counterpart has been modeled as a kilonova, which is a light curve thought to be powered mainly from the radioactive decay of heavy elements formed. This heating rate is therefore dependent on nuclear physics properties, such as Q-values and reaction rates, that are as yet unmeasured. A joint effort of nuclear physicists, atomic physicists and astrophysicists is required to understand this event [2].

Y. L. Zhu (✉) · G. C. McLaughlin
Department of Physics, North Carolina State University, Raleigh, NC 27695, USA
e-mail: zhuygln@gmail.com

T. Sprouse · N. Vassh · R. Surman
Department of Physics, University of Notre Dame, Notre Dame, IN 46556, USA

M. R. Mumpower
Theoretical Division, Los Alamos National Laboratory, Los Alamos, NM 87545, USA

A. Formicola et al. (eds.), *Nuclei in the Cosmos XV*, Springer
Proceedings in Physics 219, https://doi.org/10.1007/978-3-030-13876-9_92

92.2 Objective

We consider the r-process in neutron-rich merger ejecta, with a focus on the heating rates from freshly synthesized r-process material. We investigate uncertainties in the nuclear physics inputs to kilonova calculations and examine in particular the role of heating from different reaction channels. We go beyond pervious work [3] on uncertainties by considering a larger variety of mass models.

92.3 Method

We choose an astrophysical trajectory from the 1.4 to 1.4 $M_{\odot}$ neutron star merger simulations in [4] with the initial electron fraction of Ye = 0.03488. We use the Portable Routines for Integrated nucleoSynthesis Modeling (PRISM) reaction network developed jointly at the University of Notre Dame and Los Alamos National Laboratory. All relevant nuclear reaction channels such as charged particle reactions, neutron capture, photodissociation, β-decay, and delayed neutron emission are included in our nucleosynthesis calculations. For the fission channels, we include neutron-induced fission, β-delayed fission and spontaneous fission. We use 12 mass models, FRDM2012 [5], DZ33 [6], HFB21 [7], HFB22, HFB23, HFB24, HFB25 [8], HFB27 [9], UNEDF1 [10], SLY4 [11], KTUY05 [12], WS3V6 [13]. When available, experimental data is used for masses [14] and decay properties from NUBASE2016 [15]. For the calculation with each different mass model, we use self-consistent Q-values of β-decay rates, and separation energies for neutron capture rates. Furthemore, the thermodynamical trajectories are calculated self-consistantly with nuclear re-heating. We estimate the heating rates from the reaction rate and Q-value of each nuclear reaction.

92.4 Results

The total heating rate band of all mass models and the one with FRDM2012 is shown in the left panel of Fig. 92.1.

At a time from 1 to 100 days, when the kilonova is powered by nuclear heating, the spread in the heating rate can be a factor of 2–3. As in the right panel of Fig. 92.1, we show the fraction of the heating which comes from the reaction channels, α-decay, β-decay, neutron-induced fission, β-delayed fission and spontaneous fission. The nuclear heating is dominated by β-decay for all mass models studied here. The fraction of heating from fission is nonnegligible [16]. Since the thermalization from fission products is much more efficient than the α-decay and β-decay [3], the contribution from fission cannot be neglected.

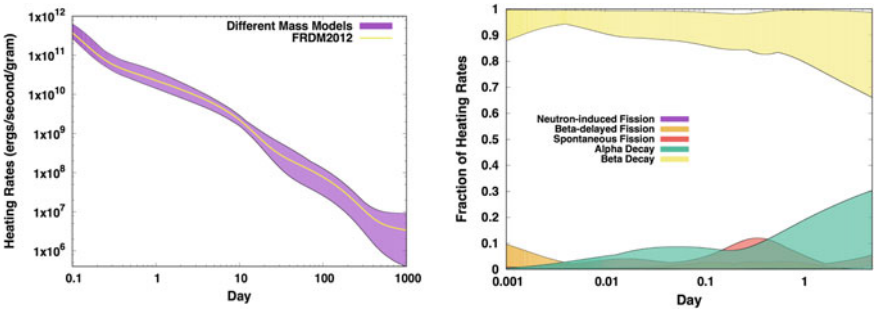

Fig. 92.1 Left: the total heating rate range of 12 mass models up to 1000 days after merger. Right: the range of fraction of heating rates from each reaction channels in nucleosynthesis calculations

92.5 Conclusion

We find that the uncertainty in the total nuclear heating rate from nuclear mass models is a factor of a few to an order of magnitude. We consider different nuclear heating channels in the nucleosynthesis simulations and analyze their roles in the process of nuclear heating. We found that beta-decay dominates the nuclear heating while fission and alpha decay are nonnegligible.

References

1. LIGO Scientific Collaboration and Virgo Collaboration, GW170817: Observation of Gravitational Waves from a Binary Neutron Star Inspiral. Phys. Rev. Lett. **119**(16), 161101 (2017)
2. A. Aprahamian, R. Surman, A. Frebel, G. C. McLaughlin, A. Arcones, A. B. Balantekin, J. Barnes et al, FRIB and the GW170817 Kilonova. arXiv preprint arXiv:1809.00703 (2018)
3. Jennifer Barnes, Daniel Kasen, Wu Meng-Ru, Gabriel Martínez-Pinedo, Radioactivity and Thermalization in the Ejecta of Compact Object Mergers and Their Impact on. Astrophys. J. **829**(2), 110 (2016)
4. O. Korobkin, S. Rosswog, A. Arcones, C. Winteler, On the astrophysical robustness of the neutron star merger r-process. MNRAS **426**(3), 1940–1949 (2012)
5. P. Möller, A.J. Sierk, T. Ichikawa, H. Sagawa, Nuclear ground-state masses and deformations: FRDM(2012). At. Data Nucl. Data Tables **109–110**, 1–204 (2016)
6. J. Duflo, A.P. Zuker, Microscopic mass formulas. Phys. Rev. C **52**(1), R23–R27 (1995)
7. S. Goriely, N. Chamel, and J. M. Pearson. Further explorations of Skyrme-Hartree-Fock-Bogoliubov mass formulas. XII. Stiffness and stability of neutron-star matter. *Phys. Rev. C*, 82(3):035804, 2010
8. Goriely, Stéphane, N. Chamel, J.M. Pearson, Further explorations of Skyrme-Hartree-Fock-Bogoliubov mass formulas. XIII. The 2012 atomic mass evaluation and the symmetry coefficient. Phys. Rev. **C88**(2), 024308 (2013)
9. Goriely, Stéphane, R. Capote, Uncertainties of mass extrapolations in Hartree-Fock-Bogoliubov mass models. Phys. Rev. **C89**(5), 054318 (2014)
10. M. Kortelainen, J. McDonnell, W. Nazarewicz, P.-G. Reinhard, J. Sarich, N. Schunck, M.V. Stoitsov, S.M. Wild, Nuclear energy density optimization: Large deformations. Phys. Rev. C **85**(2), 024304 (2012)

11. E. Chabanat, P. Bonche, P. Haensel, J. Meyer, and R. Schaeffer. A Skyrme parametrization from subnuclear to neutron star densities Part II. Nuclei far from stabilities. *Nucl. Phys. A*, 635(1):231–256, 1998
12. Hiroyuki Koura, Takahiro Tachibana, Masahiro Uno, Masami Yamada, Nuclidic Mass Formula on a Spherical Basis with an Improved Even-Odd Term. Prog. Theor. Phys. **113**(2), 305–325 (2005)
13. Min Liu, Ning Wang, Yangge Deng, Wu Xizhen, Further improvements on a global nuclear mass model. Phys. Rev. C **84**(1), 014333 (2011)
14. Meng Wang, G. Audi, F. G. Kondev, W. J. Huang, S. Naimi, and Xing Xu. The AME2016 atomic mass evaluation (II). Tables, graphs and references. *Chin. Phys. C*, 41(3):030003, 2017
15. G. Audi, F. G. Kondev, Meng Wang, W. J. Huang, and S. Naimi. The NUBASE2016 evaluation of nuclear properties. *Chin. Phys. C*, 41(3):030001, 2017
16. Y. Zhu, R.T. Wollaeger, N. Vassh, R. Surman, T.M. Sprouse, M.R. Mumpower, P. Möller, G.C. McLaughlin, O. Korobkin, T. Kawano et al., Californium-254 and Kilonova Light Curves. ApJL. **863**(2), L23 (2018). Aug